Reconfigurable Intelligent Surfaces for 6G and Beyond Wireless Networks

Edited by
Agbotiname Lucky Imoize
Vinoth Babu Kumaravelu
Dinh-Thuan Do

IEEE Press
WILEY

Reconfigurable Intelligent Surfaces for 6G and Beyond Wireless Networks

IEEE Press
445 Hoes Lane
Piscataway, NJ 08854

Reconfigurable Intelligent Surfaces for 6G and Beyond Wireless Networks

Edited by

Agbotiname Lucky Imoize
University of Lagos
Nigeria

Vinoth Babu Kumaravelu
Vellore Institute of Technology
India

Dinh-Thuan Do
University of Mount Union
Alliance
USA

IEEE*Press*
WILEY

Published by John Wiley & Sons, Inc., Hoboken, New Jersey.
Published simultaneously in Canada.

The manufacturer's authorized representative according to the EU General Product Safety Regulation is Wiley-VCH GmbH, Boschstr. 12, 69469 Weinheim, Germany,
e-mail: Product_Safety@wiley.com.

Library of Congress Cataloging-in-Publication Data Applied for:

Hardback ISBN: 9781394250110

Cover Design: Wiley
Cover Image: © ArtSpace0714/Shutterstock

Set in 9.5/12.5pt STIXTwoText by Straive, Chennai, India

In loving memory of my late sister, Sarah Afebuame (Née Imoize).

Agbotiname Lucky Imoize

To my lovely wife, Dr. Arthi Murugadass, for her unwavering support and inspiration, and to my beloved daughters, Keshika Sruthi V. A. and Akshara V. A., for bringing endless joy and meaning to my life.

Vinoth Babu Kumaravelu

In memory of my parents, Do Tan and Tran Thi Bich Nga.

Dinh-Thuan Do

Contents

About the Editors

Agbotiname Lucky Imoize received his Bachelors in Engineering (Honours) in Electrical and Electronics Engineering from Ambrose Alli University, Nigeria, in 2008, and MSc degree in the same field from the University of Lagos in 2012. He is a lecturer in the Department of Electrical and Electronics Engineering at the University of Lagos, Nigeria. Before joining the University of Lagos, he was a lecturer at Bells University of Technology, Nigeria. He has been a research scholar at the Ruhr University Bochum, Germany, under the sponsorship of the Nigerian Petroleum Technology Development Fund (PTDF) and the German Academic Exchange Service (DAAD) through the Nigerian-German Postgraduate Program. From 2017 to 2018, he was a Fulbright Fellow, conducting as a visiting scholar at the Wireless@VT Laboratory, Bradley Department of Electrical and Computer Engineering, Virginia Tech., USA, under the supervision of Professor R. Michael Buehrer. He worked as a Core Network Products Manager at ZTE, Nigeria, and a Network Switching Subsystem Engineer at Globacom, Nigeria. His research interests include 6G wireless communications, wireless security systems, and artificial intelligence. He is the vice chair of the IEEE Communication Society Nigeria chapter, a registered engineer with the Council for the Regulation of Engineering in Nigeria, and a member of the Nigerian Society of Engineers. He is a senior member of IEEE.

Vinoth Babu Kumaravelu is presently working as a professor in the Department of Communication Engineering, School of Electronics Engineering, Vellore Institute of Technology, Vellore, Tamil Nadu, India. In 2014, he received his PhD in MIMO-OFDM-based wireless communication from the Vellore Institute of Technology. In 2009, he graduated with an MTech in Communication Engineering from the same institution. During his MTech degree, he won a gold medal. He was also awarded merit scholarships twice during his master's degree at Vellore Institute of Technology for securing high grades. His areas of interest are wireless communications, digital communications, and signal processing, including spatial modulation, RIS, NOMA, wireless sensor networks, the Internet of Things, device-to-device communication, small cells, and vehicular ad hoc networks. He is the author of the books *Communication Engineering* and *Digital Communications*, published by Magnus Publications, India. He has been a guest editor for special issues in prestigious journals, including those published by Wiley and the Frontiers. He has successfully guided six PhD students and is currently mentoring four others in their doctoral research. He is a Senior Member of IEEE and an active member of the IEEE Communications Society.

Dinh-Thuan Do is an assistant professor in the School of Engineering at the University of Mount Union, Alliance, Ohio, USA. He was a research scientist at the Electrical Engineering Department, University of Colorado Denver, Denver, USA. Also, he was formerly a research scientist in the Department of Electrical and Computer Engineering at the University of Texas at Austin, USA. Prior to joining the University of Texas at Austin, he was an assistant professor at Asia University in Taiwan and a research assistant professor at Ton Duc Thang University in Vietnam. His research interests include signal processing in wireless communications networks, nonorthogonal multiple access, full-duplex transmission, and reconfigurable intelligent surfaces (RIS). He received the Golden Globe Award from the Vietnam Ministry of Science and Technology in 2015 (awarded to the top ten excellent scientists nationwide). He is currently serving as an Editor of Computer Communications, Associate Editor of EURASIP Journal on Wireless Communications and Networking, Associate Editor of Electronics, Associate Editor of ICT Express, and Editor of KSII Transactions on Internet and Information Systems. His publications include over 100 SCIE/SCI-indexed journal articles and over 40 international conference papers. Additionally, he is the author of two textbooks and six book chapters, and he holds a PhD degree in Communications Engineering from Vietnam National University (VNU-HCMC), Vietnam. He is a senior member of IEEE.

About the Contributors

Taufik Abrão SM'12, SM-SBrT received the BS, MSc, and PhD degrees in electrical engineering from the Polytechnic School of the University of São Paulo, São Paulo, Brazil, in 1992, 1996, and 2001, respectively. Since March 1997, he has been with the Communications Group, Department of Electrical Engineering, Londrina State University, Paraná, Brazil, where he is currently an Associate Professor in Telecommunications and the Head of the Telecomm. & Signal Processing Lab. In 2018, he was with the Connectivity section, Aalborg University as a Guest Researcher, and with the Southampton Wireless Research Group in 2012 as an Academic Visitor. He has served as Associate Editor for the IEEE Transactions on Vehicular Technology, the IEEE Systems Journal, the IEEE Access, the IEEE Communication Surveys & Tutorials, the AEUe-Elsevier, the IET Signal Processing, and JCIS-SBrT, and as Executive Editor of the ETT-Wiley (2016–2021) journal. His current research interests include communications systems, especially M-MIMO, XL-MIMO, RIS-aided communication, optimization methods, machine learning, scheduling, estimation, resource allocation, and random access protocols.

Abel García Barrientos (IEEE, senior member) was born in Tenancingo, Tlaxcala, Mexico, in 1979. He received the Licenciatura degree in Electronics from the Autonomous University of Puebla, Mexico, in 2000, and MSc and PhD degrees in Electronics from the National Institute for Astrophysics, Optics, and Electronics (INAOE), Tonantzintla, Puebla, in 2003 and 2006, respectively. Since 2007, he has been a researcher at the Mechatronics Department at the Polytechnic University of Pachuca, Mexico. In 2009, he was a post-doctoral fellow at the Micro- and Nano-Systems Laboratory at McMaster University, Ontario, Canada. In 2010, he was a post-doctoral fellow at the Advanced Materials and Device Analysis group of Institute for Microelectronics, Technische Universitat Wien, and in the summer of 2013, he was a visiting professor in the School of Physics & Astronomy at the University of Nottingham, UK. Since 2016, he has been a full-time professor, level VI, in the Faculty of Science at the Universidad Autonoma de San Luis Potosi. His

scientific interests include device simulation, semiconductor device modeling, high-frequency electronics, and nanoelectronics. He has been a member of SNI-Mexico from 2008 until 2022, level II. He is a fellow of the Mexican Academy of Science, the IEEE-Hidalgo Subsection (Mexico), and he is also a member of the IEEE.

Nivetha Baskar received her Bachelor's degree in Electronics and Communication Engineering and Master's degree in Applied Electronics from the Anna University, Chennai, Tamil Nadu, India, in (2014-2018) and (2018-2020), respectively. She is currently a research scholar doing her Ph.D. in the Department of Communication Engineering, School of Electronics Engineering, at Vellore Institute of Technology, Vellore, Tamil Nadu, India. Her research interests include wireless communication, massive MIMO, resource allocation, and interference management.

Mehmet Bilim received his BSc, MSc, and PhD degrees in Electrical and Electronics Engineering from Erciyes University, Turkey, in 2010, 2012, and 2018, respectively. Currently, he is an associate professor in the Department of Electrical and Electronics Engineering at Niğde Ömer Halisdemir University, Turkey. He teaches courses in wireless communications, and his current research interests include spread spectrum communications, multiuser communications, multiple access techniques, wireless networks, millimeter wave communications, digital communications, fading channels, cooperative diversity, and applications of neural networks to communication systems. He was a recipient of the PhD Research Fellowships from the Scientific and Technological Research Council of Turkey (TUBITAK). He is also the author for more than 30 papers in major conferences and journals. He is a reviewer for IEEE, Elsevier, Wiley, Springer, and IET journals. Dr. Bilim currently serves as an editor of Frontiers in Communications and Networks.

Suganthi Evangeline Chakkaravarthy is an accomplished academic and researcher currently serving as an Associate Professor in the Department of Electronics and Communication Engineering at Sri Eshwar College of Engineering. She earned her PhD in Wireless Communications from Vellore Institute of Technology, Vellore, in 2022, following her ME from Coimbatore Institute of Technology in 2012 and her BE from C. Abdul Hakeem College of Engineering and Technology in 2010. Her primary research interests encompass advanced areas such as wireless communications, vehicular ad hoc networks (VANETs), blockchain technology, and the Internet of Things (IoT). She is an IEEE member.

Vinoth Kumar Chandra Babu received the Master's degree in Communication Engineering from the PSG College of Technology, Coimbatore, Tamil Nadu, India, in 2012. He is currently pursuing his PhD in the Department of Communication Engineering, School of Electronics Engineering, at Vellore Institute of Technology, Vellore, Tamil Nadu, India. He has also participated in various conferences, such as the International Conference on Vision Towards Emerging Trends in Communication and Networking (ViTECoN 2019) and the International Conference on Microelectronic Devices, Circuits and Systems (ICMDCS), organized by Vellore Institute of Technology. His research interests include blockchain and wireless communications.

Francisco Rubén Castillo-Soria (Member, IEEE) received a Bachelor in Communications and Electronics and an M.S. degree in Telecommunications Engineering from the National Polytechnic Institute in Mexico City, Mexico, in 1999 and 2004, respectively. He received the Doctor of Science degree in Electronics and Telecommunications from the Center for Scientific Research and Higher Education of Ensenada (CICESE), Mexico, in 2015. Since 2017, he has been an Associate Professor at the Faculty of Sciences of the Autonomous University of San Luis Potosí, Mexico. His research interests include MIMO wireless communications, signal processing, spatial/index modulation, MBM, and AI for multiuser MIMO systems.

Sunil Chinnadurai received his M.S. in Electronics and Communication Engineering from the Mid Sweden University, Sweden, in 2012, and the PhD. in Electronics and Communication Engineering from Chonbuk National University, South Korea, in 2018. He was with the Signal Intelligence Research Center, Hanyang University, Seoul, South Korea, for a year, as a Postdoctoral Research Scientist. Since March 2019, he has been an Assistant Professor with SRM University AP, Amaravati, Andhra Pradesh, India. He has published many papers in reputed journals and conferences. His research interests include information theory, convex optimization, mathematical analysis, hyperspectral image processing, and optimization of signal processing algorithms for physical-layer wireless communication systems. He received the Best Paper Award at the 24th MSPT International Symposium in 2016.

Wilson de Souza Junior received both the B.S. and M.Sc. degrees in Electrical Engineering from the State University of Londrina (UEL), Paraná, Brazil, in 2021 and 2023, respectively. Currently, he is actively pursuing his PhD degree at UEL, with a primary focus on research areas on resource allocation for RIS-assisted massive MIMO, XL-MIMO, and NOMA. Beyond this, his research interests extend to optimization theory and the application of machine learning

in emerging technologies, encompassing ISAC, cooperative communication, relaying, symbiotic systems, SWIPT for URLLC and mMTC scenarios, all within the context of 5G and beyond 5G communication networks.

José Alberto del Puerto-Flores received his MSc and PhD degrees in Electrical Engineering with a specialization in Telecommunications from CINVESTAV-IPN, Guadalajara, Mexico, in 2014 and 2019, respectively. He is currently a research professor at Universidad Panamericana, Guadalajara campus. His research interests include signal and image processing, digital wireless communications, SISO and MIMO system design, channel estimation, linear and nonlinear data detection, channel estimation for vehicular communications, and modeling and simulation of nonstationary mobile wireless channels, as well as neural networks and AI-based algorithms.

Unwana Macaulay Ekpe received his BE degree in Electrical and Electronic Engineering from the University of Uyo, Nigeria, in 2004. He was awarded the M Sc degree in Satellite Communications Engineering and the PhD in Electronic Engineering by the University of Surrey, Guildford, United Kingdom, in 2017 and 2012, respectively. Dr. Ekpe started his academic career in 2006 as a graduate assistant at the Akwa Ibom State University, Ikot Akpaden, Nigeria. He was promoted to senior lecturer in 2016 and headed the Department of Electrical and Electronic Engineering from October 2018 to September 2022. He is now an associate professor at Akwa Ibom State University and a visiting senior lecturer at the Department of Electrical and Computer Engineering, Makerere University, Kampala, Uganda. Dr. Ekpe's research interests include optimization of land-mobile communication networks, virtualization of sixth-generation nonterrestrial networks, and grid integration of renewable energy resources. Dr. Ekpe has supervised and graduated over 60 postgraduate and undergraduate students and has won several research grant awards. He has authored two book chapters and over 20 technical articles in peer-reviewed international journals and conference proceedings.

Vishnu Vardhan Gudla is currently working as a 5G physical layer expert in Comms., Media & Tech Unit, L&T Technology Services, Bangalore. He has completed his M.Tech and Ph.D. in the field of wireless communication at Vellore Institute of Technology, Vellore. His doctoral research focused on exploring the potential technologies for next-generation wireless communication networks, with a particular emphasis on developing spectral and energy-efficient index/spatial modulation-based MIMO and massive MIMO systems for the next-generation networks. During his doctoral studies, he acquired a Senior

Research Fellowship (SRF) from the Council of Scientific and Industrial Research (CSIR), India from April 2019 to April 2021. He has four years of Teaching Experience and four years of Research Experience. His current research focus includes developing novel physical layer algorithmic solutions for beyond 5G and 6G technologies such as orthogonal time and frequency modulation (OTFS), integrated sensing and communication (ISAC), reconfigurable intelligent surfaces (RIS), non-orthogonal multiple access (NOMA), and machine learning for wireless applications.

Velmurugan Periyakarupan Gurusamy Sivabalan (Senior Member, IEEE) received B.E. degree in Electronics and Communication Engineering from Tamil Nadu College of Engineering, Coimbatore, India in 2002, M.E. degree in Applied Electronics from Kumaraguru College of Technology, Coimbatore in 2007 and the Ph.D. degree in Information and Communication Engineering from Anna University, in 2015. He is currently an Associate Professor in the Department of Electronics and Communication, Thiagarajar College of Engineering, Madurai. His research interests include Signal Processing for Wireless Communication, Reconfigurable Intelligent Surface, Radar Signal Processing, Convex Optimization and Software Defined Radio based analytics.

Carlos Adrián Gutiérrez Diaz de León received his BE. degree in Electronics and Digital Communication Systems from the Universidad Autónoma de Aguascalientes, Mexico, in 2002; Advanced Studies Diploma in Signal Processing and Communication Theory from the Universidad Politecnica de Cataluña, Spain, in 2005; MS degree in Electronics and Telecommunications from CICESE, Mexico, in 2006; and PhD in Mobile Communication Systems from the University of Agder, Norway, in 2009. From 2009 to 2011, he was with the School of Engineering, Universidad Panamericana, Aguascalientes, Mexico. Since January 2012, he has been with the Faculty of Sciences, Universidad Autonoma de San Luis Potosi, México. His research interests include modeling, simulation, and measurement of wireless channels; antenna design; electromagnetic wave propagation; vehicular communications; and radio sensing for vehicular applications and human activity recognition. Dr. Gutierrez has also served as an expert evaluator for the European Commission and CONACYT (Mexico); an associate editor for the *IEEE Open Journal of Vehicular Technology*, the *IEEE Vehicular Technology Magazine*; and a guest editor for several international journals. His publications received three best paper awards. He is a member of the Mexican National System of Researchers (level II), the Technical Committee on Propagation of the IEEE Vehicular Technology Society (VTS), and the Chair of the Propagation and Channel Modeling Theory Subcommittee of the IEEE VTS.

Kien Ho is a physics student at Chu Van An High School, Vietnam, and has been involved in various STEM initiatives. He is pursuing research in the fields such as computer security and machine learning.

Roilhi Frajo Ibarra-Hernández is a postdoctoral researcher at the Faculty of Sciences of the Autonomous University of San Luis Potosi, specializing in machine learning for the enhancement of wireless communication systems. His current research project focuses on developing deep learning models for next-generation wireless networks and signal processing, more specifically, the enhancement and signal detection of systems aided by reconfigurable intelligent surfaces (RIS).

Gaurav Jaiswal has been a Software Test Validation Engineer at NXP Semiconductor, Pune, since November 2020. Previously, he worked as a Validation and Integration Engineer at Qualcomm, Chennai, from May 2018 to October 2020. He holds an MTech in Communication Engineering from Vellore Institute of Technology, Vellore, and a BE in Electronics and Communication Engineering from IIST, Indore. His areas of interest include playing table tennis, volleyball, swimming, and Wi-Fi technology.

Thiruvengadam Sundarrajan Jayaraman (Senior Member, IEEE) received his BE in Electronics and Communication Engineering from the Thiagarajar College of Engineering, Madurai, India, in 1991; his ME in Applied Electronics from the College of Engineering, Guindy, Chennai, India, in 1994; and his PhD from Madurai Kamaraj University, Madurai, in 2005. From January 2008 to December 2008, he was a Visiting Associate Professor in the Department of Electrical Engineering, Stanford University, Stanford, CA, USA, under a Postdoctoral Fellowship from the Department of Science and Technology, Government of India. He is currently a Professor and Dean (Academics) in the Department of Electronics and Communication Engineering, Thiagarajar College of Engineering. His research interests include statistical signal processing, MIMO wireless communications, reconfigurable intelligent surface, and near field communication.

Helen Sheeba John Kennedy received her M.E. in Applied Electronics and her B.E. in Electronics and Communication Engineering from the Thanthai Periyar Government Institute of Technology, Vellore, Tamil Nadu, India. She is currently pursuing her Ph.D. in the Department of Communication Engineering, School of Electronics Engineering, Vellore Institute of Technology, Vellore, Tamil Nadu, India. Her research interests include reconfigurable intelligent surfaces, non-orthogonal multiple access and its variants, machine learning for wireless networks, and cooperative communication.

Yasin Kabalcı received his BSc and PhD degrees in Electrical and Electronics Engineering from Erciyes University, Turkiye, in 2009 and 2015, respectively. He is currently a full professor and the head of the Telecommunication Division as well as the head of the Modern Communication Systems Research Group, Department of Electrical and Electronics Engineering, Niğde Ömer Halisdemir University, Turkiye. His research interests include 5G and beyond communication systems, mmWave communications, power-line communication systems, error-correcting codes, smart grids, smart grid communications, remote monitoring, IoT, and optimization methods.

Nuri Kapucu received his BSc, MSc, and PhD degrees in Electrical and Electronics Engineering from Erciyes University, Türkiye, in 2010, 2012, and 2017, respectively. From 2011 to 2018, he was a research assistant in the Department of Electrical and Electronics Engineering at Erciyes University. Currently, he is an associate professor in the Department of Electrical and Electronics Engineering at Hitit University. His current research interests include performance analysis over fading channels, reconfigurable intelligent surfaces, cooperative communications, millimeter-wave communications, and analysis of modulation schemes. He serves as a reviewer for IEEE, Elsevier, Wiley, Springer, and IET journals, and he is currently a review editor for Frontiers in Communications and Networks.

Tuan Minh La is an active member of the Society of Vietnamese Young Scholars and conducts research with the WICOM lab at the University of Mount Union, Ohio, USA. His research interests include Reconfigurable Intelligent Surfaces, Tiny Machine Learning (Tiny ML), and the Internet of Things (IoT).

Sharon Macias-Velasquez received her DSc in Industrial Engineering from the Autonomous University of Baja California, Mexico, in 2020. She is currently a postdoctoral researcher in the Mechanical and Electrical Engineering department at the Faculty of Engineering of Autonomous University of de San Luis Potosi, Mexico. Dr. Macias is a member of the National System of Researchers in México. Her research interests include cognitive ergonomics, virtual reality, human–computer interaction, and communication systems.

José Carlos Marinello Filho received his BS and MS degree in Electrical Engineering (the first with Summa Cum Laude) from Londrina State University, PR, Brazil, in Dec. 2012 and Sept. 2014, respectively, and his PhD from Polytechnic School of São Paulo University, São Paulo, Brazil, in Aug. 2018. From 2015 to 2019, he was an Assistant Professor with Londrina State University, and, since 2019, he has been an Adjunct Professor with Federal University of Technology PR, Cornálio Procápio, Brazil. His research interests include signal processing

and wireless communications, especially massive MIMO/XL-MIMO precoding/decoding techniques, acquisition of channel-state information, multicarrier modulation, cross-layer optimization of MIMO/OFDM systems, interference management in 5G, massive machine type communications, and random access protocols for crowded networks. He has been serving as Associate Editor for the SBrT Journal of Communications and Information Systems since 2019.

Arthi Murugadass is presently working as an Associate Professor Grade 2 in the School of Computer Science and Engineering, Vellore Institute of Technology, Chennai, Tamil Nadu, India. She completed her PhD from the Vellore Institute of Technology, Vellore, India, in 2017, and her ME (CSE) and BE (CSE) from Anna University, Chennai, India, in 2012 and 2010, respectively. She has 14 SCI, 39 Scopus indexed, and 25 international and national conference publications and 4 book chapter publications. She is one of the authors of the books *Communication Engineering* and *Digital Communications*, published by Magnus Publications. She is an AWS-certified cloud practitioner. She has delivered invited talks and guest lectures on various latest domain topics. She is a reviewer in various reputed journals like MDPI, Springer, and Hindawi. She has more than 13 years of teaching and research experience. She has experience in different administrative roles as the head of the department, NBA coordinator, and BoS member. She is presently working in the areas of data science, blockchain technology, machine learning, and heterogeneous wireless networks.

Hieu Tri Nguyen is a high school student at Nguyen Sieu High School, located in Hanoi, Vietnam. As a young scholar, he is passionate about computational data science and electronics engineering.

Minh Dang Nguyen is currently an active member of the Society of Vietnamese Young Scholars. He is pursuing research topics in cutting-edge fields such as reconfigurable intelligent surfaces (RIS), machine learning (ML), and artificial intelligence (AI).

Rafael Augusto Pedriali received his BS degree in Electrical Engineering from the State University of Maringá (2015), followed by a Master's (2019) and a PhD (2023) in Electrical Engineering from the School of Electrical and Computer Engineering (FEEC) at the State University of Campinas, UNICAMP. He is currently a postdoctoral researcher in the joint graduate program in Electrical Engineering at the State University of Londrina (UEL) and the Federal Technological University of Paraná, Cornélio Procópio campus. Additionally, he is an assistant professor at UEL, focusing on telecommunications-related subjects in the Electrical Engineering program. In his field of research, he possesses extensive expertise in mobile

radio channels, massive MIMO technology, RIS and ISAC systems, linear and nonlinear optimization, and machine learning.

Khoi Nguyen Phan is a student at the British International School, Ho Chi Minh City. He is currently pursuing research in multimodel machine learning, specifically those involving reinforcement learning, and is a runner of an AI bootcamp in Vietnam. He has contributed to multiple open-source coding projects in the past.

Mukkara Prasanna Kumar received his BTech degree in Electronics and Communication Engineering from Yogi Vemana University, Kadapa, in 2018. He completed his MTech in Electronics and Communication Engineering at Jawaharlal Nehru Technological University Ananthapuramu College of Engineering, Ananthapuramu, in 2021. He is currently pursuing his PhD under the supervision of Dr. Sunil Chinnadurai in the Department of Electronics and Communication Engineering, SRM University, Amaravathi, India. He worked as an assistant professor for a year at S.V. College of Engineering, Andhra Pradesh. His research interests include wireless communications, 5G, massive MIMO, IRS, NOMA, and machine learning.

Minh Tuan Pham is currently an active member of the Vietnamese Young Scholars Community. He is pursuing research in computer science, deep learning and Internet of Things (IoT), with a particular focus on artificial intelligence (AI).

Narushan Pillay received his MSc Engineering (cum laude) and PhD degrees in Wireless Communications from the University of KwaZulu-Natal, Durban, South Africa, in 2008 and 2012, respectively. Since 2009, he has been with the University of KwaZulu-Natal. Previously, he was with the Council of Scientific and Industrial Research (CSIR), Defence, Peace, Safety, and Security (DPSS), South Africa. He supervised several MSc Engineering and PhD students. His research interests include physical wireless communications, including spectrum sensing for cognitive radio and MIMO systems. He has published several papers in well-known journals in the area of research. He is a National Research Foundation (NRF) Rated Researcher in South Africa.

Arjun Chakravarthi Pogaku was born in India. He received his master's degree from Asia University, Taiwan, where he is currently pursuing his PhD in the Department of Computer Science and Information Engineering. He is currently a member of the WICOM Laboratory, Asia University, which is led by Dr. Thuan. His research interest includes wireless and satellite communications.

Vetriveeran Rajamani received his PhD degree in Electronics Engineering from Chonbuk National University, South Korea, in 2018. He received his ME in VLSI Design and BE in ECE from Anna University, Chennai, in 2013 and 2010, respectively. He is working as an associate professor in the School of Electronics Engineering (SENSE), Department of Micro and Nano Electronics, Vellore Institute of Technology, Vellore, Tamil Nadu, India. He had published various research articles in SCI/SCIE journals, international conferences, and book chapters in India/abroad. He is also an active member in several professional societies. He has been awarded the Brain Korea (BK-21) Doctoral Scholarship during the academic year 2014–2018. He was invited to give numerous guest lectures at various places in India/abroad on innovative topics. His areas of interest include modeling of memristors, analysis and design of memristive systems in electronic and neuromorphic circuits, analog/digital circuits design, wireless communication, digital signal processing, and applied electronics.

Dipinkrishnan Rayaroth received his ME in Communication Systems from Anna University, Coimbatore, Tamil Nadu, India, and his BTech in Electronics and Communication Engineering from the Cochin University of Science and Technology, Kerala, India. He is currently pursuing his PhD in the Department of Communication Engineering, School of Electronics Engineering, Vellore Institute of Technology, Vellore, Tamil Nadu, India. His research interests include NOMA, digital communications, reconfigurable intelligent surfaces, and wireless communications.

Md. Abdul Latif Sarker received his PhD degree from Chonbuk National University, Republic of Korea, in 2016. He is currently working in a senior research position at the Center for ICT & Automotive Convergence at Kyungpook National University in Korea. Dr. Sarker was a participant in many projects, such as the Brain Korea-21, a world-class university, the ministry of education science and technology project, and the Samsung R&D university program. Dr. Sarker has served as a reviewer of various international journals, including *IEEE Journal on Selected Areas in Communications, IEEE Access, IEEE System Journal, IEEE Communication Letters, IEEE Transactions on Network Science and Engineering, IEEE Transactions on Computational Social Systems, and IEEE Transactions on Vehicular Technology, ICT Express, Cluster Computing*, and so on. His main research interests include various topics in signal processing for wireless communications, millimeter wave technology, localization and sensing, reconfigurable intelligent surfaces, multisensory connected and autonomous vehicles, vehicular communication, optimization, and algorithm development.

Poongundran Selvaprabhu received his Bachelor's degree in Electronics and Communication Engineering from the Anna University, Chennai, Tamil Nadu, India, in 2009, and Master's degree in Electronics Design at Mid Sweden University, Sweden, in 2012. He completed his PhD in Wireless and Mobile Communications at Chonbuk National University, South Korea, in 2017. He worked as a postdoctoral Research Fellow in the Division of Electronics and Information Engineering at Chonbuk National University and Inha University, South Korea (2017-2018). He is currently working as an Associate Professor, Vellore Institute of Technology, Vellore, Tamil Nadu, India. Dr. Poongundran was a participant in many projects such as Brain Korea 21 (BK21), World Class University (WCU), Ministry of Education Science and Technology (MEST) project, which were funded by NRF, Republic of Korea. His main research interests include various topics in 5G wireless communications, especially interference alignment for massive MIMO, signal processing, information theory, wireless body area network (WBAN) and NOMA with a focus on energy optimization, algorithm design, and artificial intelligence (AI)-machine learning.

Anjana Babu Sujatha has completed her M.Tech in Communication Engineering from the Vellore Institute of Technology (VIT), Vellore, Tamil Nadu. She has received her B.Tech in Electronics and Communication Engineering from the LBS College of Engineering, Kasaragod, Kerala. Currently, she is pursuing her Ph.D. in the Department of Communication Engineering, School of Electronics Engineering, at VIT, Vellore. Her research interests include next-generation wireless communication techniques like reconfigurable intelligent surfaces, non-orthogonal multiple access, and millimeter-wave communication.

Ammar Summaq received his BTech degree in Electronics and Communication Engineering from Damascus University in 2010. He completed his MTech in Electronics and Communication Engineering at KIIT University in 2021. He is currently pursuing his PhD under the supervision of Dr. Sunil Chinnadurai in the Department of Electronics and Communication Engineering, SRM University, Amaravathi, India. His research interests include wireless communications, 5G, IRS, and machine learning.

Samarendra Nath Sur (Senior Member, IEEE) received his MTech in Digital Electronics and Advanced Communication from Sikkim Manipal University, in 2012, and his PhD in MIMO Signal Processing from the National Institute of Technology (NIT), Durgapur, in 2019. Since 2008, he has been associated with the Sikkim Manipal Institute of Technology, India, where he is currently an Assistant Professor (SG) in the Department of Electronics and Communication

Engineering. He has published over 120 SCI/Scopus-indexed international journals and conference papers. His current research interests include wireless communications, non-orthogonal multiple access (NOMA), energy harvesting (EH), intelligent reflecting surface (IRS), the Internet of Things (IoT) remote sensing, and radar image/signal processing (soft computing). He is a member of the IEEE-IoT and Institution of Engineers, India (IEI). He is also serving as an Associate Editor for *International Journal on Smart Sensing and Intelligent Systems* (S2IS) (SCOPUS, ESCI). Additionally, he had the privilege of serving as the Guest Editor for topical collections and special issues in reputable journals published by Springer Nature, MDPI, and Hindawi.

Dang Ngoc Thien Nguyen is currently an active member in the Society of Vietnamese Young Scholars. He is pursuing research topics of cutting-edge fields such as reconfigurable intelligent surfaces, machine learning (ML), and the Internet of Things (IoT). He earned third place in a Science Research Competition and recently co-led the first AI/ML Bootcamp in Vietnam.

Vetrivel Chelian Thirumavalavan is an R&D Systems Simulation Engineer at Nokia in Bangalore. He holds a PhD in Wireless Signal Processing and specializes in analyzing the spatial correlation of signals in Intelligent Reflecting Surfaces (IRS) for 6G and beyond. His current research focuses on developing algorithms for 6G Over-the-Air (OTA) and Radio Unit (RU) applications on user devices. He is an expert in wireless channel models, particularly in massive MIMO systems and conducts performance analyses of complete wireless communication systems. His current research involves AI/ML-based channel modeling and holographic radio beamforming, contributing to the advancement of 6G and future wireless technologies.

Huu Quy Tran (Member, IEEE) received his MS in Electronics Engineering from Ho Chi Minh City University of Technology and Education (HCMUTE), Vietnam, in 2010. He has been working as a Lecturer in the Faculty of Electronics Technology, Industrial University of Ho Chi Minh City (IUH), Vietnam. He obtained his doctorate from the Faculty of Electrical and Electronics Engineering at HCMUTE, Vietnam. His research interests include wireless communications, non-orthogonal multiple access (NOMA), energy harvesting (EH), wireless cooperative relaying networks, heterogeneous networks (HetNet), cloud radio access networks (C-RAN), unmanned aerial vehicles (UAVs), reconfigurable intelligent surfaces (RIS), short-packet communication (SPC), and Internet of Things (IoT). His ORCID is https://orcid.org/0000-0001-7636-4378 (Email: tranquyhuu@iuh.edu.vn and Google Scholar: https://scholar.google.com/citations?user=kWwo2MgAAAAJ&hl=e).

Hung Gia Truong is a student at HUS High School for Gifted Students in Vietnam. He is pursuing his research at the forefront of fields such as reconfigurable intelligent surfaces, machine learning, and the Internet of Things.

Vivek Menon Unnikrishnan completed his Ph.D. in the Department of Communication Engineering, School of Electronics Engineering, at the Vellore Institute of Technology, Vellore, Tamil Nadu, India, in 2024. He also received his master's degree in communication engineering from the Vellore Institute of Technology, Vellore, Tamil Nadu, India, in 2019. He is a senior research fellow in the Department of Engineering "Enzo Ferrari", University of Modena and Reggio Emilia, Modena, Italy. He has also participated in various conferences such as the International Conference on Vision Towards Emerging Trends in Communication and Networking (ViTECoN 2019), International Conference on Microelectronic Devices, Circuits and Systems (ICMDCS), organized by the Vellore Institute of Technology, Vellore, Tamil Nadu, India. His main research interests include interference alignment in wireless communication systems, interference management in massive MIMO communication systems, reconfigurable intelligent surfaces, blockchain, and the Internet of Things.

Rajeshkumar Venkatesan received his BE in Electronics and Communication Engineering from the Anna University affiliated institution, Tamil Nadu, India, in 2009; his MTech in Communication Systems from the Sona College of Technology (Autonomous), affiliated with Anna University, Tamil Nadu, India, in 2011; and his PhD from the Department of Electronics and Communication Engineering, National Institute of Technology, Trichy, India, in 2015. He has 13 years of teaching experience at reputed engineering colleges in India. From 2012 to 2015, he was a research scholar at the National Institute of Technology, Trichy, India, and received a fellowship from MHRD, India. He is presently working as a Professor Grade I at the Vellore Institute of Technology, Vellore, India. His current research interests include the development of multiple-input multiple-output antennas, various applications of substrate-integrated waveguide techniques in antenna design, metamaterial antennas, fractal antennas, and frequency-selective surfaces for shielding applications. Dr. Rajeshkumar received various awards and honors including IETE Life and Board of Studies memberships in various autonomous engineering institutions, and he serves as a reviewer in various reputed journals. He has authored more than 50 papers in reputed journals and conferences.

Preface

The fast-growing need to satisfy billions of mobile subscribers calls for the deployment of advanced wireless communication techniques to achieve the desired quality of service. Reconfigurable intelligent surfaces (RIS) are currently being explored to ameliorate several issues in wireless networks. RIS comprises passive elements that require limited active antennas at the base station (BS) to achieve energy efficiency and spectral gains. RIS, a key enabler for 6G wireless networks, has enormous potential to address signal loss between the transmitter and the receiver. RIS can be deployed to enhance the reliability of wireless systems in 6G and beyond. Additionally, RIS can be employed to mitigate interference in wireless communication systems. RIS supports simultaneous wireless information and power transfer and enhances security at the physical layer. Compared to relay-assisted technologies, RIS offers low cost and high efficiency. However, the computational complexity issue in RIS-assisted wireless networks design is still an issue that needs to be addressed holistically. In order to address this issue, among others, there is a need for a book that investigates the characteristics, benefits, and limitations of RIS deployment in advanced wireless communication systems.

The book analyzes the design and applications of RIS in 6G and beyond. In particular, the book considers the application of RIS, aiding efficient wireless signal transmission from the base station to the mobile station, considering several practical constraints. The book is a high-quality reference to practitioners, industry and academic researchers, scientists, and engineers in the fields of wireless communications and networking, information theory, signal processing, 5G and 6G networks, antennas design, sensing and localization, channel modeling and propagation measurement, reconfigurable intelligent surfaces, ICTs, and others. Additionally, graduate and senior undergraduate students will find the book very useful for courses within the broad aspects of wireless communications. Finally, the book is structured into 17 chapters collected from industry experts, world-class academics, and researchers, resulting in a diverse and high-quality reference for the readers.

The editors specially thank the reviewers of the original book proposal for their constructive suggestions. Special thanks to all authors of the chapters for their insightful contributions. Many thanks to the reviewers, and editorial assistants at Wiley and IEEE Press for their cooperation and support.

Agbotiname Lucky Imoize
Department of Electrical and Electronics Engineering, University of Lagos, Nigeria

Vinoth Babu Kumaravelu
Vellore Institute of Technology, Vellore, Tamil Nadu, India

Dinh-Thuan Do
University of Mount Union, Ohio, USA

Acknowledgments

I sincerely express my profound gratitude to God for His divine wisdom and faithfulness in editing this book. The book would not have been possible without the support of the Department of Electrical Engineering and Information Technology, Institute of Digital Communication, Ruhr University Bochum, Germany, and the University of Lagos, Nigeria. I wholeheartedly acknowledge the sponsorship from the Nigerian Petroleum Technology Development Fund (PTDF) and the German Academic Exchange Service (DAAD) through the Nigerian-German Postgraduate Program. Additionally, I am indebted to the Deeper Life Bible Church, Essen Region, North Rhine-Westphalia, Germany, for their unwavering support. Special thanks to my beloved wife, Kelly, and our sons, Lucius, Luke, Lucas, and Luther. Lastly, I sincerely thank the editorial team at WILEY-IEEE Press for their support.

Agbotiname Lucky Imoize
Gelsenkirchen, North Rhine-Westphalia, Germany

I would like to express my sincere thanks to the leadership of Vellore Institute of Technology, Vellore, Tamil Nadu, India—Dr. G. Viswanathan, Chancellor; Mr. Sankar Viswanathan, Vice President; Dr. Sekar Viswanathan, Vice President; Dr. G. V. Selvam, Vice President; Dr. Sandhya Pentareddy, Executive Director; and Ms. Kadhambari S. Viswanathan, Assistant Vice President—for their unwavering support and encouragement throughout this endeavor. I extend my heartfelt gratitude to my dedicated research team for their invaluable support and contributions to this book. I am especially thankful to Dr. G. Ramachandra Reddy, Agbotiname Lucky Imoize, Dr. Arthi Murugadass, Dr. Suganthi Evangeline Chakkaravarthy, Dr. Vishnu Vardhan Gudla, Dr. Poongundran Selvaprabhu, Dr. Rajeshkumar Venkatesan, Dr. Sunil Chinnadurai, Ms. Helen Sheeba John Kennedy, Mr. Dipinkrishnan Rayaroth,

Mr. Gaurav Jaiswal, Mrs. Anjana Babu Sujatha, Dr. Narushan Pillay, Dr. Thiruvengadam Sundarrajan Jayaraman, Dr. Velmurugan Periyakarupan Gurusamy Sivabalan, Dr. Francisco R. Castillo Soria, Dr. Samarendra Nath Sur, Dr. Vetrivel Chelian Thirumavalavan, Dr. Dinh-Thuan Do, Dr. Mehmet Bilim, Dr. Vivek Menon U, Dr. Md. Abdul Latif Sarker, and Dr. Vetriveeran Rajamani. Their consistent encouragement, technical insights, and collaborative spirit have been crucial in developing this work.

Vinoth Babu Kumaravelu
Vellore, Tamil Nadu, India

I sincerely express my profound gratitude to my colleagues, scholars, scientists, and students. This work would not have been possible without the generous support of the Benton School of Engineering, University of Mount Union, USA. I am especially grateful for the mentorship and resources from the University of Texas at Austin and the University of Colorado Denver, where I worked and collaborated with wonderful advisors and colleagues. The creative ideas of Tri Academy students enabled me to conduct this project. Tri Academy provided a dynamic platform for academic exploration and mentorship, while its training programs offered hands-on lessons to guide students pursuing research topics for deploying 6G wireless communications. These initiatives empowered young minds to apply cutting-edge technology to real-world challenges, laying the foundation for the ideas shared in this book. I also extend heartfelt appreciation to my family and friends for their encouragement throughout this journey. Special thanks to my beloved wife, Vo Thi Hai Chau, and my sons, Tin Phuc Do and Tri Phuc Do. Lastly, I thank the editorial team at WILEY-IEEE Press for their professionalism and continued support.

Dinh-Thuan Do
North Canton, Ohio, USA

Introduction

The book, reconfigurable intelligent surfaces (RIS) for 6G and Beyond Wireless Networks sheds light on the design, modeling, and deployment of energy-efficient reconfigurable intelligent surfaces (RISs) to address several network issues, such as interference, pathloss, delay, traffic outage, among others. The book presents advanced signal-processing algorithms to enable RIS applications in realistic environments. Additionally, the book introduces advanced mathematical tools and machine learning (ML) algorithms to critically analyze RIS dynamics in evolving wireless environments. Furthermore, the book provides industry personnel, researchers, and academics with new insights into the real-world scenarios of the technological development, implementation, application, benefits, and challenges of RIS deployment in advanced wireless communication systems. The book is presented in 17 chapters outlined as follows.

Chapter 1 introduces RISs as a key element in shaping future wireless communication systems such as 6G and beyond. While 5G focuses on enhancing transmitter and receiver intelligence, 6G explores RIS to customize wireless propagation environments, offering benefits like extended coverage and improved system performance. Passive RIS enhances indoor coverage economically, while active RIS offers more control in outdoor settings, albeit with higher resource requirements. However, the task of optimizing baseband processing algorithms in wideband environments is not just a challenge but a complex task that can be quite daunting. Overcoming these challenges is crucial to fully harnessing RIS's potential in diverse deployment scenarios. To this end, the chapter explores RIS in wireless communication systems, examining both narrowband and wideband environments. Additionally, the study establishes analytical upper bounds for bit error rate (BER) using probability density function (PDF) and moment generating function (MGF) methods and validated via Monte Carlo simulations, especially in high signal-to-noise ratio (SNR) scenarios. Last, the chapter examines the effect of discrete phase shifters in place of ideal continuous phase shifters, owing to practical constraints.

Chapter 2 buttresses the fact that 6G wireless networks envision an immersive and interactive experience for the users, with high quality of service (QoS) demands, full-dimensional network coverage, microsecond latency, and high spectral and energy efficiency. RIS-assisted communication is the key enabling technology that has the potential to meet these demands, with the capability of controlled signal reflection through which the data rate is maximized. RIS helps to reduce multiple reflections of the signal, which leads to minimum latency. RIS has gained significant attention in recent years due to its potential to revolutionize various fields, including the Internet of Things, vehicular ad-hoc networks, device-to-device communications, simultaneous wireless information and power transfer protocol, unmanned aerial vehicles (UAVs), and military applications. Specifically, the chapter explores the various active and passive RIS applications in these domains and highlights their potential use cases. RIS deployment in a real-time environment, cost-effective fabrication, and scalability concerns are some of the challenges that need to be addressed. In addition, the chapter reviews RIS's potential use cases and applications to assist 6G communication functionalities. Last, the chapter elaborates on recent developments, challenges, and future research directions in RIS-empowered wireless communication systems.

Chapter 3 describes RISs as candidate enablers for the envisioned 6G technology due to their ability to manipulate electromagnetic waves in real time, enhancing cell coverage and prevent recurring blockages, and interference. This manipulative feature of RIS is especially important for 6G, where high data rates, low latency, and massive device connectivity are expected to be the norm. Specifically, the chapter presents a comprehensive examination of the RIS architecture, hardware design, operational modes, and frequency bands that are relevant to various duplexing techniques. The chapter also conducts an electromagnetic analysis of RIS-assisted networks, establishing a mathematical model to characterize the gain of both transmit and receive units. The analysis includes understanding how the RIS surface affects the propagation, reflection, and scattering of electromagnetic waves in its vicinity. The chapter also involves characterizing the electromagnetic properties of the surface materials and structures, such as their impedance, phase response, and radiation pattern. Additionally, the chapter models the channel characteristics and reflection coefficients of individual elements within the RIS. Furthermore, the chapter investigates the impact of spatial correlation and mutual coupling on the performance of RIS and explores potential mitigation approaches. Last, the expressions for average error probability under spatially correlated conditions are derived, accounting for various diversity factors.

Chapter 4 analyzes massive MIMO (M-MIMO) systems assisted by RISs, providing insights on the performance and computational complexity via extensive Monte-Carlo simulations, considering multiuser uplink (UL) scenarios. Such analyses on RIS-aided M-MIMO communication systems scenarios have potential applications for the next generations of mobile communication systems, such

as beyond 5G and 6G, which demand new electromagnetic spectrum under high millimeter-wave (mmWave) frequencies. The RIS-aided M-MIMO systems are configured with active beamforming combiners/precoders and the use of optimization methods on the N RIS element phase shift by deploying passive beamforming (PBF) and Naive local search (NLS) low-complexity quasi-optimal methods to improve metrics such as system signal-to-interference-plus-noise ratio (SINR), spectral efficiency (SE), and outage probability (OP). The key numeric results address metrics related to the QoS of the wireless communication system, operating under different types of fading channels considered, such as Rayleigh, Rice, Nakagami-m, α–μ, and κ–μ. The potential relevance is to show how these diverse channel propagation conditions impact the system performance, providing a comprehensive understanding of network behavior in different environments. This insight is crucial for optimizing wireless communication systems to ensure robustness and QoS delivery across different channel and system configurations. Additionally, the chapter strategically defines geometric configurations with well-defined positions for mobile users, a base station (BS), and an RIS panel. Two scenarios are explored; known and deterministic user equipment (UEs) localization and random UE positions. Both communication links offer insightful analyses as well as a comparison of signal reception quality between the UEs and the BS when the signal path is partially and totally obstructed.

Chapter 5 focuses on integrating RISs into wireless communication systems and its associated challenges. In practice, the task can be even more challenging when dealing with multiple users connected to a system sharing spectrum, time, or power resources. Specifically, the chapter explores the challenges of integrating the RIS into multiuser (MU) downlink transmission systems. The efficiency and applicability of RIS-assisted multiple-input single-output (MISO) and multiple-input multiple-output (MIMO) schemes are analyzed in terms of BER performance and the complexity of the algorithms and techniques utilized. Likewise, the effects of the different wireless propagation channel models are analyzed, and several approaches of blind RISs and optimization algorithms are presented. Simulation results show up to 37 dB gain in BER curves using N-RIS surfaces when the system has SE = 12 bp cu/user, 32 Tx antennas, and 8 users with 4 Rx antennas. These outcomes validate an increase in performance by adopting N-RIS surfaces and optimization techniques for adequate phase searching. In addition, the chapter presented frameworks that apply ML algorithms to improve the overall system performance, including estimation of channel state information (CSI), beamforming applications, federated learning (FL), and demodulation applications. Finally, the chapter sheds light on trends and open research areas in this exciting domain.

Chapter 6 delves into the critical aspects of optimizing energy efficiency (EE) in active RIS-assisted massive MIMO (M-MIMO) wireless communication systems.

A comprehensive and unified theoretical framework was developed to analyze the boundaries of EE within M-MIMO systems integrated with active RIS while adhering to practical constraints. The study focuses on a formulated EE optimization problem aiming to maximize the EE for active RIS-assisted M-MIMO communication systems. The goal is strategically finding the number of active RIS elements for outperforming the EE attainable by an entirely passive RIS. Besides, the proposed novel solution has been tailored to the innovative EE optimization problem. The formulation and solution design take into account analytical optimization techniques, such as Lagrangian dual transform (LDT) and fractional programming (FP), facilitating the effective implementation of RIS-aided M-MIMO applications in real-world settings. In particular, key results show that the proposed algorithm can provide up to 120% higher EE compared to the entirely passive RIS. Besides, it was found that the active RIS can operate with lower than half of the reflecting elements for the entirely passive RIS. Finally, because active RIS achieves the complete utilization of amplification power available, it should be equipped with a reasonable number of reflecting elements above $N = 49$.

Chapter 7 beams a torchlight on an intelligent reflecting surface (IRS), an exciting novel technology for future wireless communication networks, achieving energy and spectrum efficiency. In particular, an IRS consists of passive elements responsible for manipulating incoming signals, introducing an additional degree of freedom to enhance system performance, further improved with suitable phase optimization techniques. However, channel estimation becomes more challenging when employing an IRS, with channel estimation overhead being a key parameter that impacts system complexity and performance, and one way to resolve this issue is to exploit the element grouping technique. To this end, the chapter presents IRS element grouping schemes and considers the UL rate maximization challenge using the IRS. Specifically, the study utilizes the grouping of IRS-reflecting elements to analyze system performance and presents a comparative analysis between the system with and without optimization. Numerical findings indicate that an IRS with an element grouping scheme has tremendous potential to significantly enhance the capacity performance of the investigated wireless communication system.

In Chapter 8, RIS-assisted wireless communication is examined as a possible contender for next-generation networks due to its lower implementation cost and end-to-end system performance. RIS can increase the signal-to-noise ratio (SNR) by controlling the reflection and scattering properties of incoming signals. Non-orthogonal multiple access (NOMA), which assigns various power levels to different users, can provide the huge connectivity and lower latency requirements of next-generation networks. The majority of works assume RIS in between the transmitter–receiver propagation environment. However, due to the reduced received signal level at the RIS, it may not be possible to fully exploit the associated benefits. As a result, the idea of RIS as an access point

(AP) has been presented, in which the RIS is placed at the source and capable of producing phase for both constellation mapping and channel pre-compensation. In particular, RIS-AP-NOMA is presented, combining the benefits of both RIS and NOMA. For both smart and blind transmissions, analytical average bit error rate (ABER) and outage expressions are derived, assuming a two-user downlink scenario. In addition, numerical simulations are used to validate the performance of the system. The proposed smart RIS-AP-NOMA system for user 1 achieves the target outage with a significant SNR gain of ∼58 dB and the target ABER with a gain of ∼25 dB when compared with the conventional NOMA. Similarly, for user 2, the proposed system achieves the target outage with an SNR gain of ∼58 dB and the target ABER with an SNR gain of ∼31 dB.

Chapter 9 provides detailed explanations of the combined use of RIS structures with NOMA, spatial modulation, small cells, massive multiple-input multiple-output (MIMO), mmWave communication, visible light communication, terahertz communication, UAVs, and more. The characteristics, advantages, and evaluations in terms of system performance of these system structures are elaborated. Additionally, the chapter offers a comprehensive examination of some theoretical assessment metrics in communication systems, including OP, average bit error probability, and capacity analyses, and their valuable applications in RIS structures.

Chapter 10 emphasizes the promise of 6G wireless networks in revolutionizing the landscape of the Internet of Things (IoT), expanding the horizons of wireless communication, and ushering in a new era of IoT applications with unprecedented performance and reliability. However, a crucial requirement in this domain is the need for precise positioning and localization of IoT devices, which is a fundamental necessity for a plethora of applications. Nevertheless, the existing positioning and localization methods used in 6G-IoT pose several challenges due to blockages of the line-of-sight signals, interference, and difficulties arising from multipath propagation, which results in new requirements for positioning and localization. These fundamental necessities for precise positioning and localization can be fulfilled with an RIS, a potential candidate technology for future 6G wireless communication. Thus, integrating RIS in the IoT can enhance the accuracy of positioning while offering the added benefits of being economical and energy efficient. To this end, the chapter examines the role of RIS-assisted 6G-IoT networks in wireless positioning and localization. Then, the fundamental localization principles and the RIS-aided localization algorithms are explored. Moreover, the state-of-the-art research on positioning and localization, comprising RIS-assisted mmWave positioning systems, RIS for indoor, near-field, outdoor, and far-field localization, and RIS for terahertz communication, is elaborated in detail. Finally, the chapter concludes by discussing the potential challenges and future research directions of RIS-assisted 6G-IoT for wireless positioning and localization.

Chapter 11 delves into the multifaceted landscape of privacy and security issues associated with RIS deployments. Privacy concerns stem from the manipulation of wireless signals, raising issues of data leakage, location privacy, user profiling, and surveillance. In parallel, security challenges encompass unauthorized access, data tampering, signal jamming, physical infrastructure vulnerabilities, and regulatory compliance issues. Addressing these issues requires robust encryption, authentication mechanisms, intrusion detection, rigorous privacy and security regulations adherence. The chapter outlines a comprehensive strategy for various attacks and threats, ensuring data confidentiality, integrity, and availability in RIS-enabled networks. Additionally, the chapter covers physical layer security for RIS-assisted networks. Incorporating physical layer security measures into RIS deployments enhances the confidentiality and integrity of wireless communication, making it more resilient against eavesdropping and unauthorized access. Furthermore, the chapter identifies multiple challenges for future research to fully utilize the benefits of the IRS in physical layer security and covert communications. Finally, the chapter offers insights into the evolving domain of RIS, shedding light on the imperative need to balance its transformative potential with protecting individual privacy and system security.

Chapter 12 explores how the integration of RIS in wireless communication systems holds tremendous promise for revolutionizing connectivity by offering scalability, cost-efficiency, and energy neutrality. However, navigating the complexities of dynamic environments poses significant challenges for power control in RIS-empowered wireless networks. The chapter projects a method that involves implementing a cooperative deep reinforcement learning (DRL) system with two interconnected networks, DRL-M and DRL-S referred to as Deep Reinforcement Learning Master and Slave DRL (M-S), aiming to optimize system performance and energy efficiency. RL-M optimizes system performance by adjusting transmit beamforming and phase shift. The results show that increasing the transmit power (from 0 dB to 10 dB to 20 dB) leads to a proportional increase in the average reward, reaching approximately values of (2.5, 4.8, 7.8). The average reward serves as feedback for the DRL-S network, assisting it to intelligently manage power transmission to adapt to changing environmental conditions. This is achieved by leveraging the reward feedback from DRL-M, facilitating dynamic adjustment of power transmission based on variations in these rewards, either increasing or decreasing power transmission accordingly. The chapter contributes to advancing RIS-integrated wireless systems with enhanced power control capabilities, offering a robust solution to address the challenges of power control in RIS-enabled wireless systems operating in dynamic environments.

Chapter 13 examines the emergence of the IRS as a transformative technology in a new era of intelligent and efficient wireless networks. IRS can manipulate radio waves, which means they can help to improve communication in terms

of coverage, capacity, and energy efficiency. IRS can overcome obstacles such as signal blockage, pathloss, and interference, improving communication reliability and performance. IRS can adaptively reconfigure the wireless propagation environment according to changing conditions. IRS can adjust its reflective properties dynamically in real time, optimizing signal propagation based on user location and channel conditions. The work points out that propagation measurements are essential for understanding signal propagation processes and describing wireless channel behavior. These measurements involve collecting data on signal strength, fading, delay spread, and other channel parameters in various environments. Channel modeling techniques aim to represent wireless channel behavior in mathematical models accurately. These models incorporate factors such as pathloss, multipath fading, shadowing, and interference to simulate the propagation of electromagnetic waves in different scenarios. Wireless channels are inherently non-stationary, evolving unpredictably in response to environmental changes. This unpredictability poses a significant challenge for propagation measurements, which aim to characterize the behavior of wireless channels over time and space. Overcoming these challenges requires integrating IRS into 6G wireless communication systems, which promises to make a big difference in performance. Thus, the chapter comprehensively reviews the propagation measurements and channel modeling techniques in 6G wireless communication, focusing on the concept of an IRS.

Chapter 14 describes RIS as a promising technology with the potential to enable 6G wireless networks. These metasurfaces are energy efficient, enhancing overall system performance, and expand signal coverage, especially in Sub-6GHz and mmWave networks. Although RIS-based networks are proving to be a vital element in achieving better and faster wireless systems, there are certain optimizations to be made such as enhancing energy efficiency. This required the merging of ML to assist RIS-based techniques; specifically, deep reinforcement learning (DRL) algorithms, to process information more effectively and accurately. The chapter investigates the composition of DRL and presents a few works on its applications. The chapter closes off with a summary of the methods and future directions for the system examined.

Chapter 15 examines physical layer security (PLS) for RIS-aided wireless communication systems. Physical layer security is an important technique that guarantees information-theoretic security regardless of the computational capability of eavesdropping, covered security, and privacy protection, as fundamental requirements. The NOMA as a transmission technique supports higher SE. The RIS technology is envisioned promising due to their abilities in enhancing communication from key aspects. The chapter presents different approaches of RIS, NOMA securing the most favorable environment and asylum for the Internet of Things. As a result, RIS-aided PLS design solutions appeared promising within

various approaches and system models. Furthermore, RIS-aided NOMA network, a significant approach of RIS-aided PLS model, showed decent mathematical statistic, and further certificated the potential of the presented design.

Chapter 16 highlights the building blocks of RIS, being metamaterials, metasurfaces and their control mechanisms. Specifically, the supporting technologies for deploying RIS in terrestrial and non-terrestrial wireless communication systems are presented. To ensure that the variables used are consistent for both environments, the free space pathloss model is presented before detailing a complete geometry-based system model suitable for the environments. Using these models, the architecture for implementing RIS-empowered terrestrial communication systems enhanced by MIMO and Orthogonal Frequency Division Multiplexing (OFDM) techniques in the terrestrial environment is presented. For the non-terrestrial environment, RIS-empowered aerial networks comprising UAVs, and high-altitude platforms (HAPs) are highlighted. Additionally, architectures involving satellites are presented followed by a multi-layered integrated RIS-empowered system involving both terrestrial and non-terrestrial components. The chapter concludes by presenting lessons learned and discusses future research directions.

Chapter 17 concludes the book, highlighting that energy efficiency will remain a key criterion in order to evaluate the feasibility of deploying any wireless system in 6G and beyond. The study shows that the expected increase in the number of devices that use the network in the 5G and beyond underscores the critical need for enhanced network architectures to support burgeoning demands. RIS has emerged as promising for the next generation of wireless communication technology, and it is being well-perceived by both researchers and engineers, owing to their considerable potential. The chapter presents a summary of existing literature, encompassing energy efficiency evaluations and optimization techniques in RIS systems. The analysis not only deepens the understanding of methodologies for measuring energy efficiency but also sheds light on strategies for optimizing RIS systems. Finally, the chapter reviews the current methods of determining RIS energy consumption and optimizing the systems. The authors conclude that the findings could help future researchers make informed decisions when evaluating and designing RIS-aided wireless systems.

The Editors

Agbotiname Lucky Imoize
Vinoth Babu Kumaravelu
Dinh-Thuan Do

1

Reconfigurable Intelligent Surfaces-Assisted Wireless Communication Systems: Baseband Processing Perspective

Thiruvengadam Sundarrajan Jayaraman[1], Velmurugan Periyakarupan Gurusamy Sivabalan[1], Vinoth Babu Kumaravelu[2], Agbotiname Lucky Imoize[3,4], and Helen Sheeba John Kennedy[2]

[1] *Department of Electronics and Communication Engineering, Thiagarajar College of Engineering, Madurai, India*
[2] *Department of Communication Engineering, School of Electronics Engineering, Vellore Institute of Technology, Vellore, India*
[3] *Department of Electrical and Electronics Engineering, Faculty of Engineering, University of Lagos, Lagos, Nigeria*
[4] *Department of Electrical Engineering and Information Technology, Ruhr University, Bochum, Germany*

1.1 Introduction

Operating within the millimeter-wave (mmWave) spectrum of frequency range (FR2; 24.25–52.6 GHz) in 5G wireless communication encounters obstacles such as buildings and atmospheric conditions, which can impede or scatter its signals. A primary hurdle in utilizing 5G for data transfer lies in its limited ability to transmit over extended distances. An emerging solution to address these challenges is the implementation of reconfigurable intelligent surfaces (RISs), also known as intelligent reflecting surfaces (IRSs), heralded as a revolutionary paradigm for the evolution of wireless communication in the next-generation [1–5]. It finds a way in shaping the future of wireless communication networks, especially within the context of 6G networks. RISs dynamically reorganize the propagation environment to improve both capacity and coverage. The functioning of RIS relies on a straightforward principle: introducing a finite, adjustable time delay to the incoming wave at the reflective elements.

RIS is a passive device made up of meta-materials that can be easily tuned. A few commonly used meta-material structures, namely, split-ring resonator, squared structure, single-ring structure, and bow resonator, are shown in Figure 1.1 [6]. The gap in the meta-material reflecting unit and its unique design allow the engineers to control the reflection parameters of the reflected signal. RIS does not

Reconfigurable Intelligent Surfaces for 6G and Beyond Wireless Networks, First Edition.
Edited by Agbotiname Lucky Imoize, Vinoth Babu Kumaravelu, and Dinh-Thuan Do.

Figure 1.1 Common meta-material reflecting unit designs:. (a) split-ring resonator, (b) squared structure, (c) single-ring structure, and (d) bow tie resonators.

require a dedicated energy source. It can be easily deployed in indoor spaces, and any surface can be converted using RIS. Another merit of RIS is that it is neither affected by receiver noise nor amplifies the latter due to its passive characteristics. The principle behind RIS arrays is simple: By estimating the phases of incoming waves, the RIS elements are adjusted to provide a suitable received signal's phase component [7–9]. Ideally, this operation facilitates the entire reflected wave to be in phase, which leads to the up fade of the signal due to constructive interference of the multiple signals reflected from each individual RIS element. As per the theory, doubling the number of reflecting elements improves yields ∼6 dB improvement in the received signal-to-noise ratio (SNR). The RIS-based model is shown in Figure 1.2 [10].

Each reflecting element is controlled individually by field programmable gate array (FPGA) controller. By altering the states of individual elements to ON and OFF using PIN diodes, control over the reflection parameters of RIS can be achieved as desired. In the OFF state, RIS elements behave as simple reflectors without beamforming capabilities. However, through the manipulation of these switches, desired amplitudes and phase shifts can be attained to optimize multiuser communications effectively.

Fabrication of RIS and employing it to assist in wireless communication is a multidisciplinary project might bridge radio frequency (RF) and wireless engineers over a common goal. Fabrication challenges include electromagnetic (EM) functionalities like absorption, steering, and control aspects of RIS. Wireless aspect analysis of RIS includes channel sounding through RIS and data acquisition to develop a statistical channel model. Using a software defined radio to transmit the modulated signal, the data rate and error rate can be analyzed for the developed statistical channel model.

1.1.1 Key Contributions

This chapter presents several noteworthy contributions, including:

- To provide a comprehensive overview of RIS in wireless communication systems.

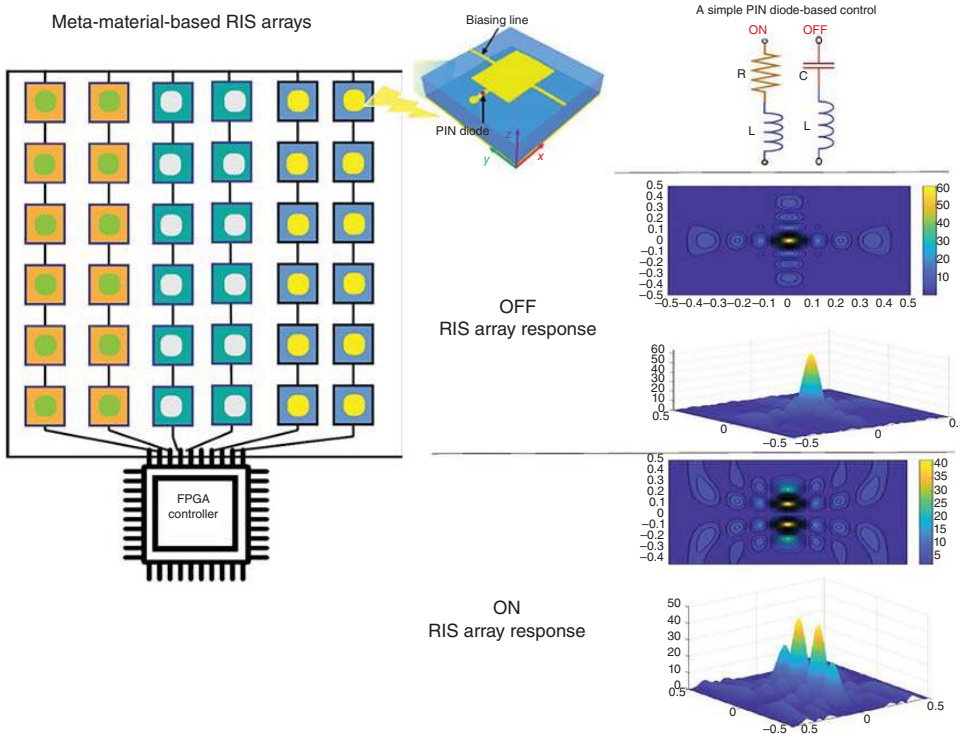

Figure 1.2 RIS model.

- To characterize the signals that are encountered in RIS-assisted wireless communication system in narrowband and wideband environments.
- To analyze bit error rate (BER) and outage performance of RIS-assisted wireless communication systems.
- To analyze the impact of discrete phase shifters in BER performance of RIS-aided transmissions.

1.1.2 Organization

Section 1.2 presents an overview of existing literature surveys that focus on the analysis of outages and BER in wireless environments assisted by RIS. It also explores the impact of discrete phase shifters and the integration of RIS with other technologies. Section 1.3 presents the comprehensive overview on the basic principles of RIS and its use-case scenarios. Section 1.4 describes the characterization of RIS-assisted wireless communication systems. The BER and outage analysis are carried out for two different configuration of RIS, namely, narrowband and wideband. Further, trade-off in using discrete phase shifter in the place of continuous phase shifter is also discussed. Results and discussion are provided in Section 1.5. Conclusion and future direction of RIS is described in Section 1.6.

1.2 Related Work

This section offers a synopsis of prior literature reviews that concentrate on BER and outage analyses within RIS-supported wireless environments. Numerous studies have explored the performance of RIS in wireless communication systems, particularly in terms of outage probability and BER. These analyses are essential for understanding the reliability and error rates associated with RIS-assisted transmissions across various scenarios.

When evaluating the effectiveness of systems, employing practical discrete phase shifters in RIS compared to those utilizing ideal continuous phase shifters. Several factors contribute to the observed decline in performance. These include quantization errors, inaccuracies in beamforming, challenges in channel estimation, and increased system complexity and overhead. While discrete phase shifters offer cost and hardware simplicity advantages over continuous ones, their limited resolution and associated constraints lead to performance deterioration compared to the ideal continuous phase shifter setup in RIS-based communication systems. Achieving a balance between performance, complexity, and cost becomes crucial when deploying RIS with discrete phase shifters. Researchers in this area investigate how discrete phase shifter degrades BER and outage probability in RIS-enhanced setups.

Furthermore, the convergence of RIS technology with other communication technologies has garnered significant attention. Studies have examined the synergies between RIS and techniques such as massive Multiple Input Multiple Output (MIMO), beamforming, and cognitive radio. This exploration aims to harness the combined benefits of RIS and other technologies to further enhance wireless communication performance, coverage, and efficiency.

By synthesizing findings from various literature surveys, a comprehensive understanding of the outage and BER characteristics of RIS-assisted wireless environments is attained. These surveys shed light on the impact of utilizing discrete phase shifters in optimizing RIS deployments and advancing the state-of-the-art in wireless communication systems. Understanding the outage and BER behavior in RIS-enabled environments is crucial for designing efficient communication systems. Moreover, insights into the influence of discrete phase shifters offer valuable guidance for practitioners aiming to leverage RIS technology effectively, leading to enhanced performance and resource utilization in wireless networks.

1.2.1 BER Analysis of RIS-aided Systems

Nemati et al. [11] suggested a novel RIS-aided ambient orthogonal frequency division multiplexing (OFDM) subcarriers paradigm for the coverage improvement of short-distance Internet of Things (IoT) applications. The suggested model enhances BER performance compared to conventional OFDM techniques. By using the unique spectrum structure of OFDM and compensating for phase distortion, the RIS improves data rate and signal quality. An iterative approach for deciding RIS element phase shifts and precoder matrix for access points utilizing OFDM links in sub-tera hertz (THz) and mmWave bands is discussed by Velez et al. [12]. This study evaluates the BER of the single-link performance between the transmitter and the user. The RIS elements increase communication efficiency by reducing BER at the user, leading to improved throughput and expanded coverage area.

In Li et al. [13], RIS-based phase shift keying (PSK) signaling transmission strategy for wideband wireless communications systems is discussed. The RIS elements are adjusted based on the transmitted PSK symbols to provide distinct cyclically delayed versions of the incident signal for multipath diversity. The BER performance is examined, and a practical channel estimator is established. The suggested model offers a reduced computational complexity and enhanced spectral efficiency. Chapala and Zafaruddin [14] investigated the influence of RIS elements on the performance of THz wireless transmissions. The average BER and outage probability are used to analyze the diversity order. According to simulation results, RIS dramatically enhances THz wireless transmission performance.

1.2.2 Outage Analysis of RIS-aided Systems

For the RIS-assisted THz system, exact expressions for outage probability are discussed by Du et al. [15]. According to the numerical findings, RIS has the potential to notably enhance the THz communications system's performance by substantially decreasing propagation and molecular absorption losses. Zhou et al. [16] presented a RIS installation and beamforming design to improve system reliability in wideband mmWave systems with random obstructions.

Du et al. [17] validated performance measures such as outage probability and average BER for strong connections in RIS-aided mmWave communications. They solved an optimization problem at the RIS with robust beamforming techniques that rely on blockage probability to reduce system outage probability. The results show that the RIS-assisted system offers better performance than the amplify and forward (AF) relay system even with fewer reflecting elements. Additionally, the RIS-assisted system achieves similar performance with less transmit power. Qin et al. [18] suggested an indoor RIS deployment method that considers human obstruction to reduce the outage probability in indoor environments in wideband mmWave communication. An algorithm for calculating RIS locations is described for both single and multiple RIS installations. Properly implementing RIS can considerably decrease indoor communication loss and the outage probability.

1.2.3 Impact of Discrete Phase Shifter on RIS-aided Systems

Traditional studies use continuous phase shifters for RIS, which can be expensive and challenging to implement due to hardware limitations. Instead, using discrete phase shifts with finite resolution is suggested, as it can reduce signaling overheads and energy consumption during channel acquisition [19]. You et al. [20] explored the balance between spectral efficiency and energy efficiency in a multiuser MIMO uplink (UL) system bolstered by RIS with discrete phase shifters. This study delves into the joint optimization of precoding and beamforming matrices at users and RIS, respectively, to maximize resource efficiency.

The discrete RIS phases are formed through an iterative mean square error minimization approach, as outlined in [21]. Pala et al. [22] demonstrated that the disparity in sum rate performance between continuous and 1-bit discrete phase shifters is minimal. Furthermore, Dai et al. [23] successfully implemented an RIS prototype at 28 GHz using a two-bit discrete phase shifter. While several studies have compared continuous and discrete phase shifters, there is a need for further examination of the impact of discrete phase shifters on metrics such as BER and outage performance. Such analysis would prove valuable for the design and practical deployment of 6G wireless communication systems.

1.2.4 Convergence of RIS with Other Technologies

In Aziz and Girici [24], an analytical model for path loss in the THz range is presented for RIS-aided unmanned aerial vehicle (UAV) systems. The authors investigate the installation and configuration of UAV-based RIS in a THz band environment, taking into account various parameters such as absorption loss, blockage probability, far-field limitations, and RIS elements. The study provides a detailed discussion of the design of UAV-based RIS in the THz band.

Chrysologou et al. [25] investigated the performance of RIS-aided non-orthogonal multiple access (NOMA) in the THz band. They analyze the outage probability and diversity order. According to the simulation results, the NOMA technique outperforms the conventional orthogonal multiple access (OMA) techniques. Li et al. [26] examined UL transmission strategy and channel estimation design for high-mobility scenarios in RIS-assisted Orthogonal Time Frequency Space (OTFS) systems, proposing an effective transmission strategy to minimize channel training overhead in real-time setup. The suggested method utilizes a low-complexity approach, which makes it suitable for effective communication in high-Doppler channels.

1.3 Comprehensive Overview of RIS

Conventional wireless communication systems operate within frequency bands ranging from a few hundred MHz to a few GHz. The preference for these bands was driven by their favorable propagation characteristics and the cost-effective implementation of efficient transceivers. Although the extensive spectrum within the mmWave range (30–100 GHz) was traditionally considered unsuitable for outdoor environments, recent extensive measurement campaigns have shed light on its potential. Especially when utilized alongside directional high-gain antenna arrays, mmWave bands have attracted considerable attention, prompting a reassessment of their feasibility in wireless communication systems.

All practical channels, which are either wireline (telephone and coaxial channels) or wireless (cellular and satellite), are constrained with finite bandwidth. These finite bandwidth channels are characterized by frequency response and impulse response. The pulse shaping filter generates pulse shapes whose spectrum fits into the channel frequency response. If the spectrum of the generated pulse shapes is not fitting into the frequency response of the channel, it creates an important impairment of digital communication called distortion or Inter Symbol Interference (ISI) [27]. The baseband model of a digital communication system over finite bandwidth channel is shown in Figure 1.3.

The impulse responses of the transmit filter, channel, and receive filters are $g_T(t)$, $c(t)$, and $g_R(t)$, respectively. $w(t)$ is modeled as Zero Mean Circularly Symmetric

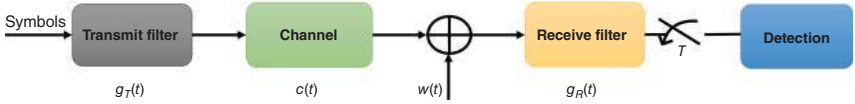

Figure 1.3 Baseband model of digital communication system in finite bandwidth channel.

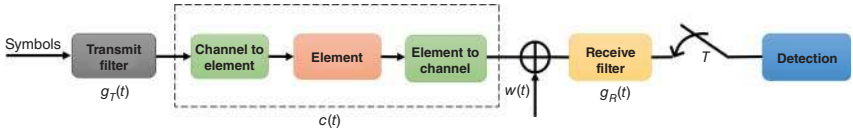

Figure 1.4 Baseband model of digital communication system in RIS supported wireless medium.

Complex Gaussian (ZMCSCG) random process. It is also to be referred as Additive White Gaussian Noise (AWGN) with power spectral density of N_0. The receive filter is a matched filter that is sampled at symbol rate to deliver the sufficient statistic y_k to the decision device. The baseband model of a digital communication system over an RIS-supported wireless medium is shown in Figure 1.4.

1.3.1 RIS

The RIS-assisted wireless communication system is shown in Figure 1.5. In a densely populated urban area, the challenge of providing consistent and

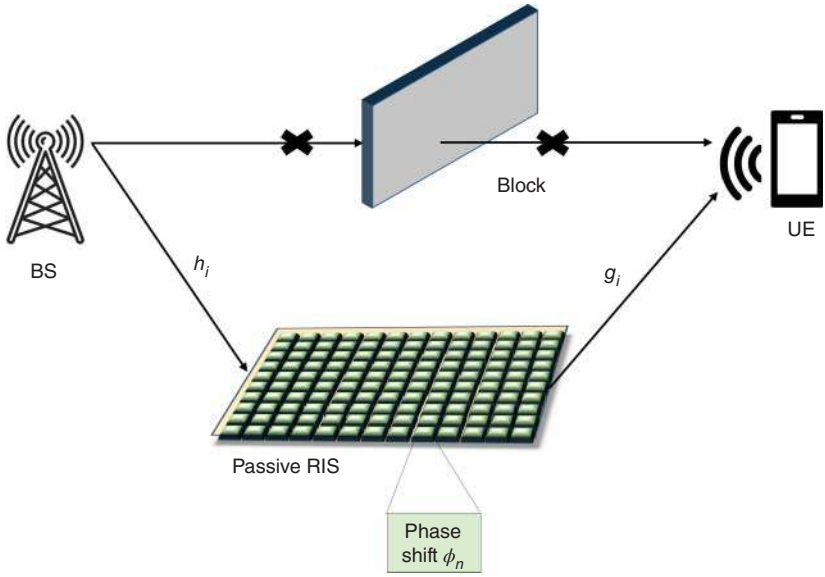

Figure 1.5 RIS-supported wireless communication system.

high-quality wireless connectivity is exacerbated by the presence of high-rise buildings, which create signal shadows and dead zones.

Traditional solutions, such as increasing the number of base stations (BS) or using decode and forward (DF) and AF relaying system, are often limited by practical constraints like cost, space, and regulatory issues. The deployment of RIS is a novel and efficient solution to these challenges. An RIS is installed on the façade of strategically chosen buildings to act as a smart reflector that can dynamically adjust the propagation environment. The RIS panels receive signals from the BS and intelligently reflect them toward the user equipment (UE), significantly improving signal strength and quality in this previously shadowed area. As the user demand fluctuates throughout the day, the RIS system dynamically adjusts, ensuring optimal service during peak hours and conserving resources when demand is lower. The smart reflection capabilities of the RIS help to mitigate interference, enhancing the overall network performance for users within its coverage area. A use-case scenario of RIS in an outdoor environment is shown in Figure 1.6.

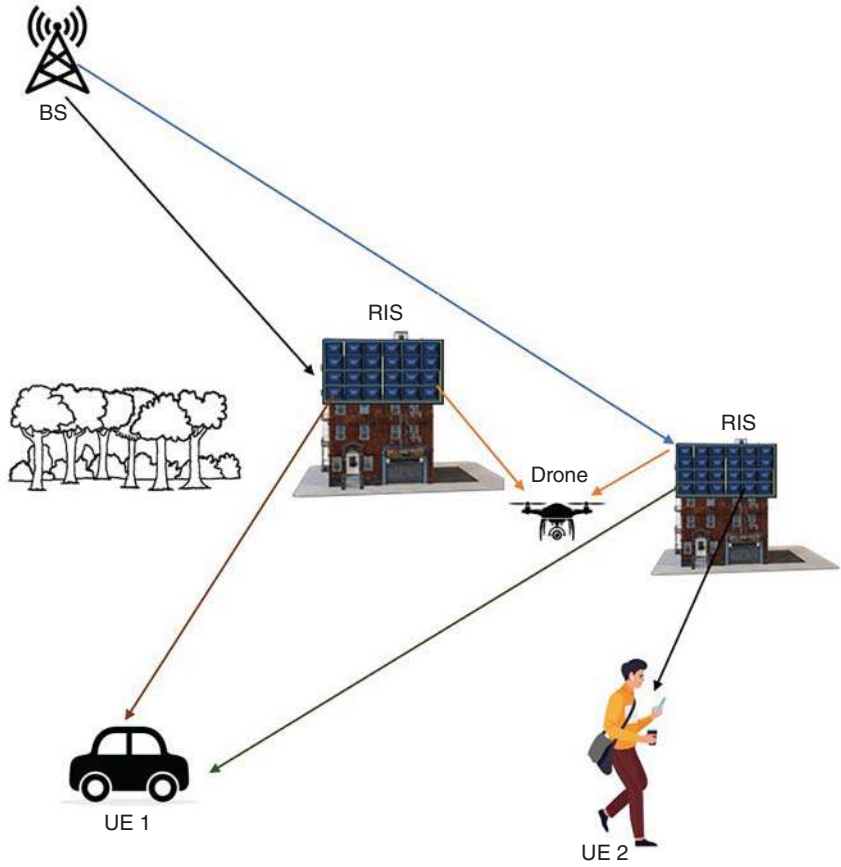

Figure 1.6 Use-case scenario of RIS in outdoor environment.

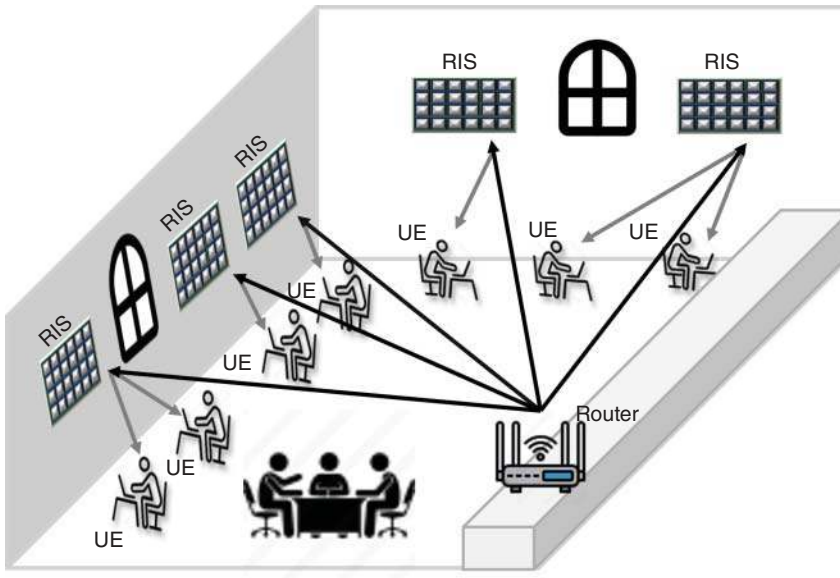

Figure 1.7 Use-case scenario of RIS in indoor environment.

Within a modern office building, maintaining reliable wireless connectivity is crucial for productivity and efficiency. However, typical office layouts with cubicles, meeting rooms, and corridors often present challenges such as signal attenuation, interference, and dead zones. To address these issues, the deployment of RIS offers a sophisticated solution for indoor wireless optimization. The scenario unfolds within a multistory office building occupied by various companies and departments. The building is equipped with standard Wi-Fi infrastructure, but users frequently encounter connectivity issues, especially in certain areas such as conference rooms and remote corners of the building. RIS panels are strategically placed throughout the building's interior to enhance wireless coverage and performance. A use-case scenario of RIS in an indoor environment is shown in Figure 1.7.

RIS operates on a fundamental principle of introducing a finite controllable time delay to incoming waves on the reflecting elements. This time delay in the time domain translates to phase shifts in the frequency domain. The impact of time delay differs between narrowband and wideband systems. The key differences are highlighted below [28]:

Narrowband Systems

- In narrowband systems, the time delay uniformly affects the phase shift of the signal across the entire frequency band.

- Since the signal operates within a narrow frequency range, it is assumed to travel at a constant speed regardless of frequency.
- Consequently, the signal experiences a consistent phase shift as it traverses the channel, irrespective of its frequency.

Wideband Systems

- In wideband systems, the time delay induces varying phase shifts across the frequency spectrum.
- Wideband signals span a broader frequency range, and at the subcarrier level, different frequencies lead to disparate phase shifts.
- This phenomenon, known as dispersive propagation, results in signals experiencing distinct phase shifts at different subcarrier frequencies.

1.4 Characterization of RIS

In this section, the BER and outage performance of RIS-assisted wireless communication systems are analyzed by developing a theoretical framework. The analytical expressions for BER are derived in two different approaches, namely, moment-generating function (MGF) and probability density function (PDF). The BER analysis is also carried out for the RIS system with discrete phase shifter. The upper bound analytical BER expressions are verified using Monte Carlo simulations. Similarly, the analytical expressions are also derived for the outage probability and verified using Monte Carlo simulations.

1.4.1 BER Analysis of RIS-assisted Narrowband Systems

Assume that the transmit symbol s has unit average energy and is drawn from a scalar constellation. Let $\mathbf{h} = \left[h_1, h_2, \ldots, h_N\right]^T$ represent the baseband equivalent flat fading channel coefficients between the transmitter and ith element of RIS. In phasor form, each element of the $N \times 1$ channel vector $\mathbf{h}$ is defined as $h_i = \alpha_i e^{j\theta_i}$, $i = 1, 2, \ldots, N$. Let $\mathbf{g} = \left[g_1, g_2, \ldots, g_N\right]^T$ represent baseband equivalent flat fading channel coefficients between the ith RIS element and the receiver. In phasor form, each element of the $N \times 1$ channel vector $\mathbf{g}$ is defined as $g_i = \beta_i e^{j\psi_i}$, $i = 1, 2, \ldots, N$. The channel coefficients $h_i, i = 1, 2, \ldots, N$ and $g_i, i = 1, 2 \ldots, N$ are modeled as independent and identically distributed (IID) ZMCSCG random variables with unit variance. The magnitude of channel coefficients $\mid h_i \mid = \alpha_i, i = 1, 2, \ldots, N$ and $\mid g_i \mid = \beta_i, i = 1, 2, \ldots, N$ are IID Rayleigh distributed random variables. The α_i and β_i are positive real with mean $\sqrt{\pi/2}$ and variance $\left(\frac{4-\pi}{2}\right)$ [29].

The adjustable phase shifts induced at ith RIS element is represented as $\phi_i, i = 1, 2 \ldots, N$. In matrix form, it is represented as $\Phi = diag\left[e^{j\phi_1}, e^{j\phi_1}, \ldots, e^{j\phi_N}\right]$.

The received signal is given in (1.1).

$$y = \sqrt{E_s}\mathbf{g}^{\mathbf{T}}\mathbf{\Phi}\mathbf{h}s + w \tag{1.1}$$

where E_s is the symbol energy at the transmitter, w is the AWGN modeled as ZMCSCG variable with variance N_0. The instantaneous SNR at the receiver is given in (1.2).

$$\eta = \frac{|\sum_{i=1}^{N} \alpha_i \beta_i e^{j(\phi_i - \theta_i - \psi_i)}|^2 E_s}{N_0} \tag{1.2}$$

It is assumed that phase shifts θ_i and ψ_i between the transmitter and RIS and RIS and receiver, respectively, are known. Then, the ith element of RIS can be configured such that $\phi_i = \theta_i + \psi_i, i = 1, 2 \ldots, N$. The maximum instantaneous SNR is given in (1.3).

$$\eta_{\max} = \frac{|\sum_{i=1}^{N} \alpha_i \beta_i|^2 E_s}{N_0} \tag{1.3}$$

Let the average SNR at the receiver be $\rho = \frac{E_s}{N_0}$. The maximum instantaneous SNR is rewritten as in (1.4).

$$\eta_{\max} = |\sum_{i=1}^{N} \alpha_i \beta_i|^2 \rho \tag{1.4}$$

Since α_i and β_i are independent and positive real with mean $\sqrt{\pi/2}$ and variance $\left(\frac{4-\pi}{2}\right)$, the mean and variance of $\alpha_i\beta_i, i = 1, 2, \ldots, N$ are given in (1.5) and (1.6) [29].

$$E[\alpha_i \beta_i] = \frac{\pi}{2}, i = 1, 2 \ldots, N \tag{1.5}$$

$$Var[\alpha_i \beta_i] = 4\left[1 - \frac{\pi^2}{16}\right], i = 1, 2 \ldots, N \tag{1.6}$$

When the number of reflecting elements N is large in RIS, the term $|\sum_{i=1}^{N} \alpha_i \beta_i|$ can be modeled as a Gaussian random variable with mean $\frac{N\pi}{2}$ and variance $4N\left[1 - \frac{\pi^2}{16}\right]$ according to the central limit theorem.

1.4.1.1 Moment-Generating Function Approach

Let X be a Gaussian distributed random variable with zero mean and unit variance and $f_X(x)$ be the PDF of X. It is defined as in (1.7).

$$f_X(x) = \frac{1}{\sqrt{(2\pi)}} e^{\frac{-x^2}{2}} \tag{1.7}$$

The MGF of X is defined as in (1.8) [29].

$$M_X(s) = M_X\left[e^{sx}\right] = \int_{-\infty}^{\infty} e^{sx} f_X(x) dx \tag{1.8}$$

Then, $\left(X+\mu_x\right)^2$ has a noncentral Chi-squared distribution with one degree of freedom. Now, the MGF of $\left(X+\mu_x\right)^2$ is given in (1.9).

$$M_X\left[e^{s(x+\mu_x)^2}\right]=\int_{-\infty}^{\infty}e^{s(x+\mu_x)^2}f_X(x)dx \tag{1.9}$$

Substituting (1.7) in (1.9), the MGF of $(X+\mu_x)$ is written as in (1.10).

$$M_X\left[e^{s(x+\mu_x)^2}\right]=\frac{1}{\sqrt{2\pi}}\int_{-\infty}^{\infty}e^{s(x+\mu_x)^2}e^{\frac{-x^2}{2}}dx \tag{1.10}$$

Simplifying this, the MGF of $\left(X+\mu_x\right)^2$ is derived as in (1.11).

$$M_X\left[e^{s(x+\mu_x)^2}\right]=(1-2s)^{-\frac{1}{2}}e^{\left(\frac{\mu_x^2 s}{1-2s}\right)} \tag{1.11}$$

Since the term $\sum_{i=1}^{N}\alpha_i\beta_i$ is modeled as Gaussian distributed, error probability can be expressed in the form of Q-function at the given channel condition. The average error probability is expressed as in (1.12) [30].

$$\widetilde{P}_e=\int_0^{\infty}Q\left(a\sqrt{\gamma}\right)f_\gamma(\gamma)d\gamma \tag{1.12}$$

where a is a constant depends on the modulation scheme. For Binary Phase Shift Keying (BPSK), $a=\sqrt{2}$. $f_\gamma(\gamma)$ is the PDF of γ. The MGF of γ is expressed as in (1.13).

$$M_\gamma(s)=\int_0^{\infty}e^{\gamma s}f_\gamma(\gamma)d\gamma \tag{1.13}$$

In alternate form, for the M-PSK modulation scheme, $Q\left(a\sqrt{\gamma}\right)$ is expressed as in (1.14) [30].

$$Q\left(a\sqrt{\gamma}\right)=\frac{1}{\pi}\int_0^{\frac{(M-1)\pi}{M}}e^{\left(\frac{-a^2\gamma}{2\sin^2\theta}\right)}d\theta \tag{1.14}$$

Substituting (1.14) in (1.12), the average probability of error (APE) is expressed as in (1.15).

$$\widetilde{P}_e=\frac{1}{\pi}\int_0^{\infty}\int_0^{\frac{(M-1)\pi}{M}}e^{\left(\frac{-a^2\gamma}{2\sin^2\theta}\right)}f_\gamma(\gamma)d\gamma d\theta \tag{1.15}$$

Comparing (1.13) and (1.15), the APE for M-PSK modulation scheme is defined as in (1.16).

$$\widetilde{P}_e=\frac{1}{\pi}\int_0^{\frac{(M-1)\pi}{M}}M_\gamma\left(\frac{-a^2\gamma}{2\sin^2\theta}\right)d\theta \tag{1.16}$$

Let $A = |\sum_{i=1}^{N} \alpha_i \beta_i|$, then $\left(A + \mu_A\right)$ is noncentral Chi-square distributed with mean μ_A and has one degree of freedom. The MGF of $\left(A + \mu_A\right)^2$ is defined as in (1.17).

$$M_{(A+\mu_A)^2}(s) = \frac{1}{\sqrt{(1-2s)}} e^{\frac{\mu_A^2 s}{1-2s}} \tag{1.17}$$

The variance of A is $\frac{N(16-\pi^2)}{4}$. Considering this, the MGF $M_\gamma\left(\frac{-a^2\gamma}{2\sin^2\theta}\right)$ is written as in (1.18).

$$M_\gamma\left(\frac{-a^2\gamma}{2\sin^2\theta}\right) = M_{(A+\mu_A)^2}\left(\frac{-N(16-\pi^2)}{4\sin^2\theta}\right) \tag{1.18}$$

substituting (1.18) in (1.16), and by using the approach in [31], the APE for M-PSK signaling is expressed as in (1.19).

$$\widetilde{P}_e = \frac{1}{\pi}\int_0^{\frac{(M-1)\pi}{M}} \left[\frac{1}{1+\left[\frac{N(16-\pi^2)\gamma}{8\sin^2\theta}\right]}\right]^{\frac{1}{2}} e^{\left(\frac{-\left(\frac{N^2\pi^2\gamma}{16\sin^2\theta}\right)}{1+\frac{N(16-\pi^2)\gamma}{8\sin^2\theta}}\right)} d\theta \tag{1.19}$$

For BPSK $M = 2$, then APE is expressed as in (1.20).

$$\widetilde{P}_e = \frac{1}{\pi}\int_0^{\frac{\pi}{2}} \left[\frac{1}{1+\left[\frac{N(16-\pi^2)\gamma}{8\sin^2\theta}\right]}\right]^{\frac{1}{2}} e^{\left(\frac{\frac{-N^2\pi^2\gamma}{16\sin^2\theta}}{1+\frac{N(16-\pi^2)\gamma}{8\sin^2\theta}}\right)} d\theta \tag{1.20}$$

In (1.20), the error probability is maximum at $\theta = \frac{\pi}{2}$. Hence, the upper bound of error probability is given in (1.21). is okay as given or else it can be changed to "≤" (globally in this chapter)

$$\widetilde{P}_e \leq \frac{1}{2}\left[\frac{1}{1+\frac{N(16-\pi^2)E_b}{8N_0}}\right] \frac{1}{2} e^{\left(\frac{\frac{-N^2\pi^2E_b}{16N_0}}{1+\frac{N(16-\pi^2)E_b}{8N_0}}\right)} \tag{1.21}$$

1.4.1.2 PDF Approach

Let $X = |\sum_{i=1}^{N} \alpha_i \beta_i|$. Since $X > 0$, the tight approximation for the PDF of the random variable X can be obtained using the Laguerre series. It is defined as in (1.22) [32].

$$f_X(x) = \sum_{n=0}^{\infty} b_n e^{-x} x^\alpha L_n^\alpha(x) \tag{1.22}$$

where $Ł_n^{\alpha}(x)$ is the generalized Laguerre polynomials and they are orthogonal to each other in the interval $[0, \infty)$. It is defined as in (1.23).

$$L_n^{(\alpha)}(x) = e^x \frac{x^{-\alpha} d^n}{n! dx^n} \left[e^{-x} x^{n+\alpha}\right], \alpha > -1 \tag{1.23}$$

The coefficients b_n are defined as in (1.24).

$$b_n = \frac{1}{\Gamma(\alpha+1)} \int_0^{\infty} L_n^{\alpha}(x) f_X(x) dx \tag{1.24}$$

where $\Gamma(x)$ is the Gamma function. Since the higher order coefficients of b_n have more complex expressions, the values of α and β are chosen such that higher order coefficients are zero. It results is $\alpha = \frac{(E[X])^2}{Var[X]} - 1$ and $\beta = \frac{Var[X]}{E[X]}$. Using (1.24), $b_0 =$ is determined as $b_0 = \frac{1}{\Gamma(\alpha+1)}$. The PDF of X is defined using the Laguerre series as in (1.25).

$$f_X(x) = \frac{1}{\beta \Gamma(\alpha+1)} \left(\frac{x}{\beta}\right)^{\alpha} e^{\left(-\frac{x}{\beta}\right)} \tag{1.25}$$

$\alpha = \frac{(E[X])^2}{Var[X]} - 1 = \frac{(N+1)\pi^2 - 16}{16 - \pi^2}$ and $\beta = \frac{Var[X]}{E[X]} = \frac{16-\pi^2}{2\pi}$. The degrees of freedom of this pdf is $\frac{\alpha+1}{2} = \frac{N}{2} \frac{\pi^2}{(16-\pi^2)}$. It implies that the RIS-assisted wireless systems has the diversity gain of $\frac{N}{2} \frac{\pi^2}{(16-\pi^2)}$ compared to the diversity gain of 1 in single input single output (SISO) link.

Assuming maximum likelihood (ML) symbol detection at the receiver, the symbol error probability is given in (1.26) [33].

$$P_e = N_e Q\left(\sqrt{\frac{\eta_{\max} d_{\min}^2}{2}}\right) \tag{1.26}$$

where N_e is the number of nearest neighbors and $d_{\min}$ is the minimum Euclidean distance in the scalar constellation from which the symbol s is drawn. Applying Chernoff inequality $Q(x) \leq e^{\left(-\frac{x^2}{2}\right)}$, the upper bound average symbol error probability (ASEP) is given in (1.27).

$$P_e \leq N_e e^{\left(-\frac{\eta_{\max} d_{\min}^2}{4}\right)} \tag{1.27}$$

Substituting for $\eta_{\max}$, the ASEP is given in (1.28).

$$P_e \leq N_e e^{\left(-\frac{|\sum_{i=1}^{N} \alpha_i \beta_i|^2 \rho d_{\min}^2}{4}\right)} \tag{1.28}$$

The symbol error probability, averaged over $|\sum_{i=1}^{N} \alpha_i \beta_i|^2$ is given in (1.29).

$$\overline{P_e} \leq N_e \prod_{i=1}^{\frac{N}{2}\frac{\pi^2}{(16-\pi^2)}} \left[\frac{1}{1 + \frac{\rho d_{\min}^2}{4}}\right] \tag{1.29}$$

At high SNR (ρ), it can be approximated as in (1.30).

$$\overline{P_e} \leq N_e \left(\rho \frac{d_{\min}^2 (16 - \pi^2)}{2N\pi^2} \right)^{-\frac{N}{2} \frac{\pi^2}{(16-\pi^2)}} \tag{1.30}$$

The array gain of the system is calculated by finding the mean of the instantaneous SNR $\eta_{\max}$ is given in (1.31).

$$\begin{aligned} E\left[\eta_{\max}\right] &= E\left[X^2 \rho\right] \\ &= \rho E[X^2] \\ &= \rho \int_0^\infty x^2 f_X(x) dx \\ &= \frac{\rho}{\beta^{\alpha+1} \Gamma(\alpha+1)} \int_0^\infty x^{\alpha+2} exp\left(-\frac{x}{b}\right) dx \end{aligned} \tag{1.31}$$

By using [34], Eq. (1.31) can be simplified as in (1.32).

$$E\left[\eta_{\max}\right] = \frac{\beta^2 \Gamma(\alpha+1)}{\Gamma(\alpha+1)} \rho \tag{1.32}$$

It implies that array gain of the system is $\frac{\beta^2 \Gamma(\alpha+1)}{\Gamma(\alpha+1)}$, as the average SNR is enhanced by the factor of $\frac{\beta^2 \Gamma(\alpha+1)}{\Gamma(\alpha+1)}$ over the standard SISO link.
The APE for BPSK modulation in a SISO system is given in (1.33) [35].

$$P_e = Q\left(\sqrt{\frac{2E_b}{N_0}}\right) = Q\left(\sqrt{2\rho}\right) \tag{1.33}$$

The APE for BPSK modulation in single input multiple output (SIMO) with M_R receive antenna is given in (1.34) [36, 37].

$$P_e \leq \prod_{i=1}^{M_R} \frac{1}{1+\rho} \tag{1.34}$$

In case of RIS-assisted wireless communication system, the APE for BPSK modulation with N element in RIS is given in (1.35).

$$\overline{P_e} \leq N_e \left(\rho \frac{2(16 - \pi^2)}{N\pi^2} \right)^{-\frac{N}{2} \frac{\pi^2}{(16-\pi^2)}} \tag{1.35}$$

As $N \gg M_R$, the ASEP is much lower than the SIMO environment with maximal ratio combining (MRC).

1.4.1.3 BER Analysis of RIS-assisted Narrowband System with Discrete Phase Shifter

In practical implementations, complete phase compensation $\phi_i = \theta_i + \psi_i$ is not feasible due to hardware limitations. Hence, discrete phase shifters are employed

at each element of RIS. However, the performance of the system is degraded due to the phase quantization error. Discrete phase shifters offer easier implementation and lower cost [38, 39].

The number of bits to represent discrete phase shift levels is represented by b. The 2^b possible discrete phase shifts that can be introduced at each element of the RIS is listed in the set is given as in (1.36).

$$\vartheta = \left[e^{\vartheta_1}, \ldots, e^{\vartheta_i}, \ldots, e^{\vartheta_N}\right]^T = \left[0, \frac{2\pi}{2^b}, \ldots, \frac{2\pi}{2^b}(2^b - 1)\right] \tag{1.36}$$

The phase shifts are equally spaced in the interval $[0, 2\pi)$. The variance of ideal RIS is reduced by factor of $\xi(b)$ due to discrete phase shifter in RIS, and it is given in (1.37) [34].

$$\xi(b) = 0.5\left(1 + \Theta(b+1) - 2\Theta\left(\frac{\pi}{4}\right)\right) \tag{1.37}$$

where

$$\Theta(b) = \left(\frac{\sin(2^{-b}\pi)}{(2^{-b}\pi)}\right) \tag{1.38}$$

The resultant mean $E[X]$ and variance $Var[X]$ of the RIS system with discrete phase shifter are given in (1.39) and (1.40).

$$\mu_b = E[X]\Theta(b) = \frac{N\pi}{2}\Theta(b) \tag{1.39}$$

$$\sigma_b^2 = Var[X]\xi(b) = \frac{N(16 - \pi^2)}{4}\xi(b) \tag{1.40}$$

The values of $\Theta(b)$ and $\xi(b)$ for different values of b are listed in Table 1.1. Now, the MGF of instantaneous SNR in Eq. (1.11) is rewritten as in (1.41).

$$M_X\left[e^{s(x+\mu_x)^2}\right] = \left(1 - 2s\sigma_b^2\right)^{-\frac{1}{2}} e^{\left(\frac{\mu_x^2 s\mu_b}{1-2s\sigma_b^2}\right)} \tag{1.41}$$

Table 1.1 Mean and variance factors $\Theta(b)$, $\xi(b)$.

b	$\Theta(b)$	$\xi(b)$
1	0.636	0.451
2	0.902	0.281
3	0.974	0.231
4	0.993	0.219
5 and above	0.999	0.215

Similarly, the upper bound of APE for BPSK modulation when discrete phase shifter is employed in RIS is given in (1.42).

$$\widetilde{P}_e \leq \frac{1}{2}\left[\frac{1}{1+\frac{N(16-\pi^2)\sigma_b^2 E_b}{8N_0}}\right]^{\frac{1}{2}} e^{\left(\frac{\frac{-N^2\pi^2 E_b \mu_b^2}{16N_0}}{1+\frac{N(16-\pi^2)\sigma_b^2 E_b}{8N_0}}\right)} \tag{1.42}$$

Whether the phase shifting is done discretely or continuously, the underlying statistical distribution of the channel response $|\sum_{i=1}^{N}\alpha_i\beta_i|$ remains unchanged. However, the influence on the distribution parameters, such as mean and variance, of the channel response can indeed vary based on b. When a discrete phase shifter is used, the phase of the transmitted signal is quantized into a finite number of levels determined by b. As b increases, the resolution of the phase quantization increases, allowing for finer adjustments in the phase of the transmitted signal. For example, increasing b in the discrete phase shifter can lead to a narrower distribution of the channel response around its mean, effectively reducing variance. Similarly, it can also affect the mean value of the channel response, as more precise phase adjustments can lead to better alignment with the receiver's expectations.

1.4.2 Outage Probability Analysis

The outage probability of a RIS-assisted narrowband wireless system, with the bandwidth of B Hz, at the bit rate of R_b bits/s is defined as in (1.43) [40].

$$P_{out}(R_b) = P[C < R_b] \tag{1.43}$$

where C is the capacity of the AWGN system, defined as in (1.44).

$$C = B\log_2\left(1+\frac{E_s}{N_0 B}\right) \text{ bits/s} \tag{1.44}$$

For convenience, let us represent the rate of transmission of data in bits/s/Hz. Then, the capacity can be represented as in (1.45).

$$C = \log_2\left(1+\gamma_{inst}\right) \text{ bits/s/Hz} \tag{1.45}$$

where $\gamma_{inst} = \frac{|\sum_{i=1}^{N}\alpha_i\beta_i|^2 E_s}{N_0} = \frac{X^2 E_s}{N_0}$ represents the instantaneous SNR of the overall system from the transmitter to receiver. Then, the outage probability at R_b bits/s/Hz can be written as in (1.46).

$$\begin{aligned} P_{out}(R_b) &= P\left[\gamma_{inst} < 2^{R_b}-1\right] \\ &= \int_0^{2^{R_b}-1} f_{\gamma_{inst}}(\gamma)\, d\gamma \end{aligned} \tag{1.46}$$

where $f_{\gamma_{inst}}(\gamma)$ is the pdf of γ_{inst}. The cumulative distribution function (CDF) of γ_{inst} can be written as in (1.47).

$$f_{\gamma_{inst}}(\gamma) = \sum_{i=1}^{n} \frac{f_X(x_i)}{|g'(x_i)|} \tag{1.47}$$

where x_i is ith root of the transformation equation is given in (1.48).

$$\gamma = g(x) = \frac{X^2 E_s}{N_0} \tag{1.48}$$

In this case, only one root $x_1 = \sqrt{\frac{\gamma N_0}{E_s}}$ is feasible. Using (1.48), the PDF of γ_{inst} is written as in (1.49).

$$f_{\gamma_{inst}}(\gamma) = \frac{f_X\left(\sqrt{\frac{\gamma N_0}{E_s}}\right)}{2\left(\sqrt{\frac{\gamma E_s}{N_0}}\right)} \tag{1.49}$$

For convenience, let $\rho = \frac{E_s}{N_0}$, then it can be simply written as in (1.50).

$$f_{\gamma_{inst}}(\gamma) = \frac{f_X\left(\sqrt{\frac{\gamma}{\rho}}\right)}{2\sqrt{\gamma\rho}} \tag{1.50}$$

Using (1.25), the PDF of $f_{inst}(\gamma)$ is defined as in (1.51).

$$f_{inst}(\gamma) = \frac{1}{2(\beta+1)\Gamma(\alpha+1)\rho^{\frac{\alpha+\beta}{2}}} \gamma^{\frac{\alpha-1}{2}} e^{\left(-\frac{1}{\beta}\sqrt{\frac{\gamma}{\rho}}\right)} \tag{1.51}$$

Substituting (1.51) in (1.47), the outage probability of RIS-assisted narrowband system is given in (1.52) [41].

$$P_{out}(R_b) = \frac{\gamma\left(\alpha+1, \frac{1}{\beta}\sqrt{\frac{2^{R_b}-1}{\rho}}\right)}{\Gamma(\alpha+1)} \tag{1.52}$$

1.4.3 BER Analysis of RIS-assisted Wideband Systems

In wideband system, the transmitter-ith RIS element-receiver channel has multiple paths and frequency selectivity. Multiple carriers are employed for the higher rate to counteract the frequency selectivity of the wideband channel. Assume that a sequence of data symbols $s\left[l\right], l = 0, 1, 2, \ldots$ drawn from a unit energy scalar constellation is to be transmitted. Let $h_i(t) = g_T(t) * c(t) * g_R(t)$ be the overall

impulse response as depicted in Figure 1.4. Considering that, there are L resolved paths in the overall channel, the received signal is given in (1.53) [42].

$$y(t) = \sum_{i=1}^{N} \left[h_i(t) * \sum_{l=0}^{L-1} \sqrt{E_s} s[l] \delta \left[t - lT_s \right] \right] + w(t) \tag{1.53}$$

where $*$ represent convolution, E_s is symbol energy, T_s is symbol duration and $n(t)$ is ZMCSCG with variance N_0. After convolving, the received signal is written as in (1.54).

$$y(t) = \sqrt{E_s} \sum_{i=1}^{N} \sum_{l=0}^{L-1} s[l] h_i \left(t - lT_s \right) + w[t] \tag{1.54}$$

If the received signal $y(t)$ is sampled at $\left(kT_s + \Delta \right)$, then the discrete-time sampled signal model at the kth symbol is given in (1.55).

$$y(k) = \sqrt{E_s} \sum_{i=1}^{N} \sum_{l=k-(L-1)}^{0} s[l] h_i \left[k - l \right] + w[k] \tag{1.55}$$

Combining the effect of impulse responses over all N reflecting elements as $h[k]$, it is simply written as in (1.56).

$$y(k) = \sqrt{E_s} \sum_{l=k-(L-1)}^{0} s[l] h \left[k - l \right] + w[k] \tag{1.56}$$

In alternate form, it is written as in (1.57).

$$y(k) = \sqrt{E_s} \sum_{l=0}^{L-1} h[l] s \left[k - l \right] + w[k] \tag{1.57}$$

1.4.3.1 RIS for OFDM-based Systems

Assume that the block of data symbol sequence $s[k], k = 0, 1, \ldots K-1$ is to be transmitted. In $(N \times 1)$ vector form, it is represented as $\mathbf{s} = [s[0], s[1], \ldots, s[K-1]]^T$. The N-point Inverse Discrete Fourier Transform (IDFT) of the data symbol sequence is given in (1.58) [42].

$$\tilde{s}[n] = \frac{1}{\sqrt{K}} \sum_{k=0}^{K-1} s[k] e^{j\frac{2\pi}{K}nk}, n = 0, 1, \ldots, K-1 \tag{1.58}$$

To eliminate ISI, a new sequences $x[n]$ is formed by appending the last $(L-1)$ samples of the sequence $\tilde{s}[n], n = 0, 1, \ldots, K-1$ as prefix to the original sequence $\tilde{s}[n], n = 0, 1, \ldots, K-1$. The new sequence $x(n)$ of length $K + L - 1$ is given in (1.59).

$$x[n] = [\tilde{s}[K-L+1], \ldots, \tilde{s}[K-1], \tilde{s}[0], \tilde{s}[1], \ldots, \tilde{s}[K-1]] \tag{1.59}$$

At the receiver, after removing cyclic prefix and computing N-point Discrete Fourier Transform (DFT), the received signal for the kth transmitted symbol is given in (1.60).

$$Y[k] = \sqrt{E_s}H[k]s[k] + n[k], k = 0, 1, \dots, K-1 \tag{1.60}$$

where $H(k)$ is the frequency response of the overall channel impulse response sequence $h[0], h[1], \dots, h[L-1]$, which is given in (1.61).

$$H[k] = \frac{1}{\sqrt{K}} \sum_{k=0}^{K-1} h[n] e^{-j\frac{2\pi}{K}nk}, n = 0, 1, \dots, K-1 \tag{1.61}$$

From (1.61), it is observed that the wideband frequency selective fading channel can be divided into K narrowband flat fading channels. Each narrowband channel occupies the bandwidth of $\frac{B}{K}$ Hz. Thus, in this case, $K + L - 1$ symbols are transmitted in one symbol duration. $L - 1$ is the length of cyclic prefix. The capacity or maximum data rate of the RIS system is expressed as in (1.62).

$$C = \max_{\sum_{n=0}^{N-1} \gamma_n^{opt} = K} \frac{1}{K + L - 1} \sum_{n=0}^{K-1} \log_2 \left(1 + \frac{E_s \gamma_n^{opt} |H_n|^2}{N_0} \right) \text{ bits/s/Hz} \tag{1.62}$$

where γ_n^{opt} is the optimal power allocated to the nth subcarrier. It is determined as in (1.63).

$$\gamma_n^{opt} = \max \left(\mu - \frac{N_0}{E_s |H_k|^2} \right) \tag{1.63}$$

where μ is a constant and can be determined using "waterpouring" algorithm.

The major challenge is how to configure RIS in a wideband environment. As the RIS is to be configured for K sub-carriers at the same time, this problem is theoretically and practicably intractable. Attempts have been made to solve this problem using heuristic techniques, namely, successive convex approximation (SCA), semidefinite relaxation (SDR), and strongest tap maximization (STM) in time domain. Further, with the use of In STM, the RIS configuration is optimized for single channel tap rather than one that is optimized for single subcarrier. The frequency selective channel with K sub-carriers is transformed to time domain using IDFT with M taps. From the M taps, the tap contributes highest energy is chosen as the strongest tap in configuring the RIS.

1.5 Results and Discussions

The performance metrics for the RIS-assisted wireless communication system are evaluated by BER and outage probability. To enhance comprehension regarding

the advantages of RIS in wireless communication systems, a foundational simulation has been conducted to analyze the probability of error (PE) in an AWGN environment for SISO and SIMO systems. This analysis is presented graphically in Figure 1.8, illustrating the relationship between SNR and PE. The simulation parameters are provided in Table 1.2, and the simulations were carried out using MATLAB R2021a.

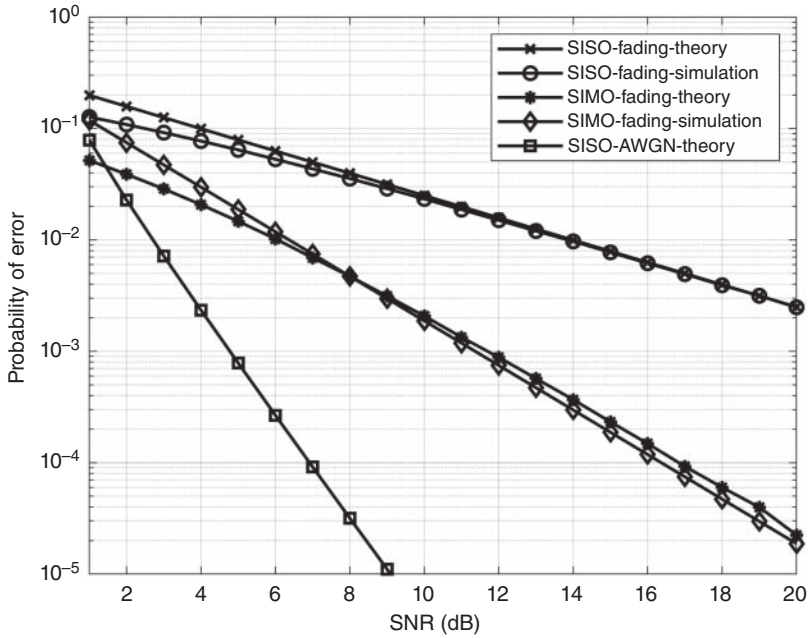

Figure 1.8 Comparison of the PE performance of SISO, SIMO systems under flat fading with SISO system under AWGN.

Table 1.2 Simulation parameters.

Parameters	Values
Modulation	BPSK
Channel	Uncorrelated Rayleigh flat fading
Number of iterations	10^6
M_T	1
M_R	2, 4
N	16, 32, and 64
b	1, 2, and 3

It is observed that in an AWGN environment ~3 dB SNR is sufficient to obtain the PE of 10^{-2}. The same error performance is achieved in a SISO system with flat fading environment with an SNR of 14 dB. This is due to multipath fading and destructive interference, which leads to deep fading in the system. In the SIMO system under the flat fading scenario, multiple receiver antennas $(M_R = 2)$ is used, which eventually results in diversity gain of M_R. This gives an improvement of ~8 dB SNR to achieve the same PE. As M_R increased in the SIMO system, the PE performance is improvised at the cost of RF chains at the receiver, and it will be closer to the performance of SISO under the AWGN channel.

In Figure 1.9, the upper bound error probability performance of SIMO flat fading system without RIS is compared with SISO flat fading system with RIS. The upper bound error probability for SIMO system is evaluated for different receiver antenna configurations of $M_R = 2, 4, 8$, and 16. The increase in the number of receiving antenna M_R of the SIMO system results with minimum improvement in SNR gain. But RIS-aided SISO system with smaller N, results in significant SNR gain over increasing number of receiving antenna M_R. It is observed that, at high SNR region, upper bound analytical expression using PDF approach and simulation results are closer to each other for $N = 16$. For the target PE of 10^{-4}, SIMO flat fading system with $M_R = 16$ requires ~−1 dB of SNR whereas RIS-aided

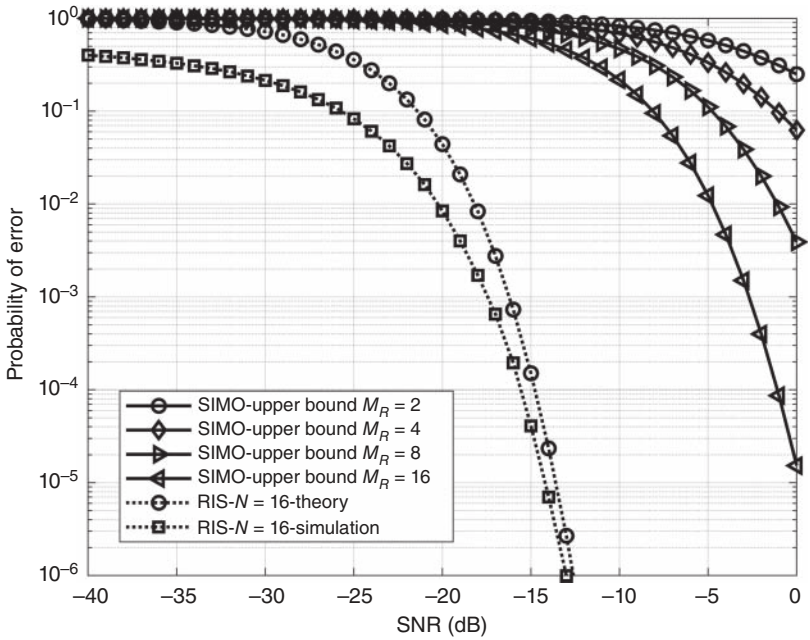

Figure 1.9 Comparison of the upper bound PE performance between SIMO flat fading system without RIS and SISO flat fading system with RIS.

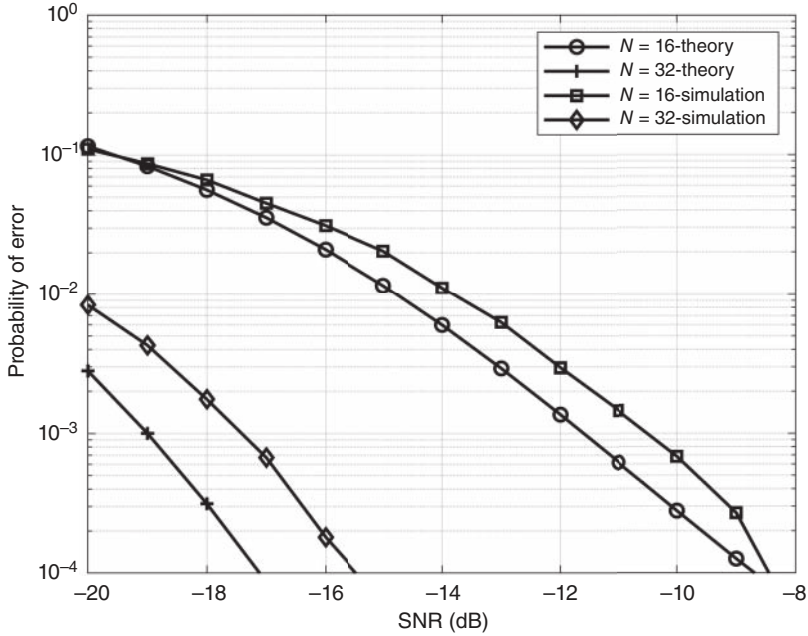

Figure 1.10 MGF approach-based APE for different values of N in RIS.

SISO system with $N = 16$ requires only ~ -14.76 dB of SNR results in ~ 13.76 dB gain. It is observed that lower PE can be attained at negative SNR regions. The PE for RIS-assisted SISO system with different values of N is shown in Figure 1.10. In this figure, analytical PE expression using MGF is compared with Monte Carlo simulation. These two results closely match with each other. As N increases, the SNR gain also increases. To attain the target PE of 10^{-4}, an RIS-aided SISO system with $N = 16$ requires ~ -9 dB of SNR and with $N = 32$ requires -17 dB of SNR.

In Figure 1.11, the PE performance of simulated RIS-aided SISO system is compared with the analytical upper bound PDF approach by varying N. From the figure, it is observed that the increase in N decreases the PE. At low SNR, the simulation results have deviation with the upper bound. As the SNR increases, the simulation results match the upper bound for all N. For the target PE of 10^{-5}, $N = 64, 32$ and 8 requires ~ -6.49 dB, ~ -13.8 dB and ~ -20.17 dB of SNR. As N doubles, ~ 6.3 dB to ~ 7.3 dB of gain is achieved.

The PE performance between the continuous and discrete phase shifter RIS for $N = 16$ is shown in Figure 1.12. It is clear that the increase in SNR is reflected in the enhanced PE performance. From (1.36), the increase in b increases the performance and nearly meets the P_e of the continuous phase shifters. For the PE of

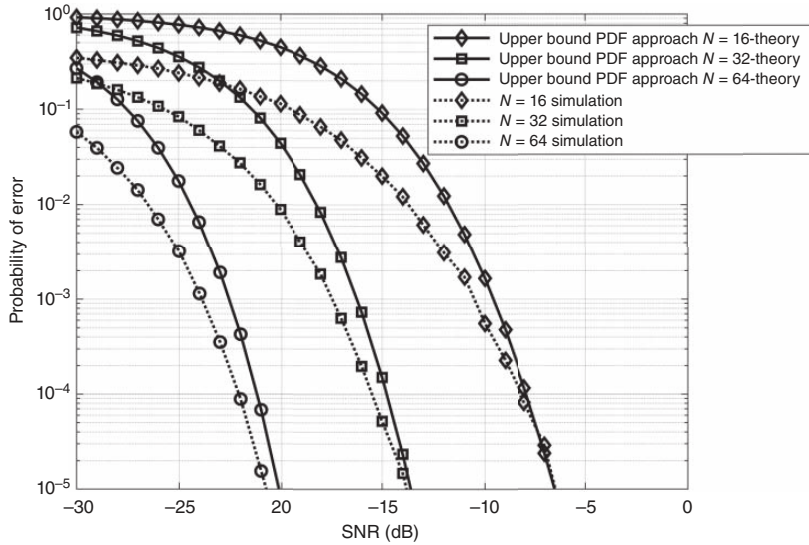

Figure 1.11 PDF approach-based APE for different values of N in RIS.

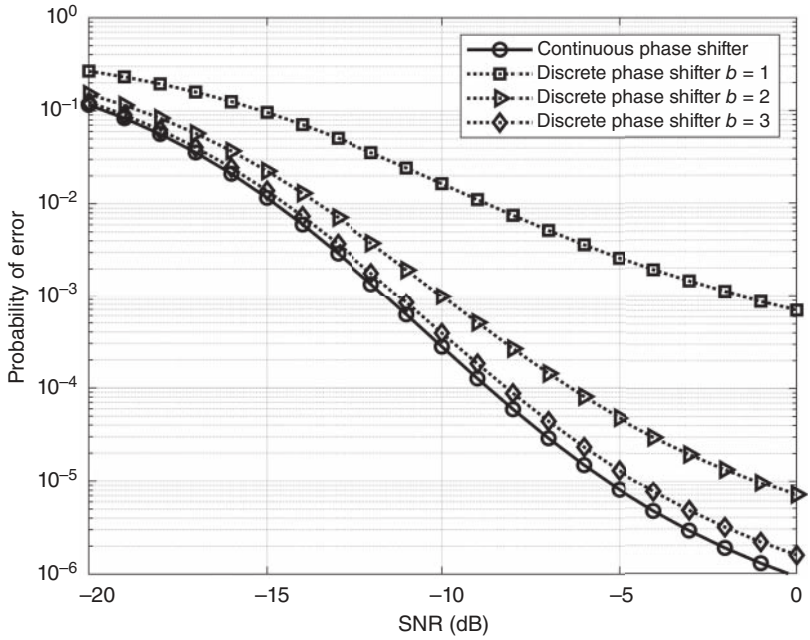

Figure 1.12 PE performance comparison between the continuous and discrete phase shifter RIS.

10^{-4}, a discrete phase shifter with $b = 1$ requires ~10 dB of SNR. As increasing the number of bits to $b = 2$ and $b = 3$ requires only ~−6.42 dB and ~−8.13 dB of SNR. The continuous phase shifter reached the PE of 10^{-4} at ~−8.52 dB of SNR. The discrete phase shifter with $b = 3$ can reach the PE performance of continuous phase shifter with the 0.39 dB of difference. Only with eight levels or phase angles does the performance of discrete phase shifters reach the continuous phase shifters with infinite angles. The impact of b on the performance of the discrete phase shifter to attain PE = 10^{-4} is presented in Table 1.3.

Table 1.3 Impact of b on the performance of the discrete phase shifter to attain PE = 10^{-4}.

b	Required SNR (dB)	Performance loss (dB)
1	~10	~18.52
2	~−6.42	~2.1
3	~−8.13	~0.39

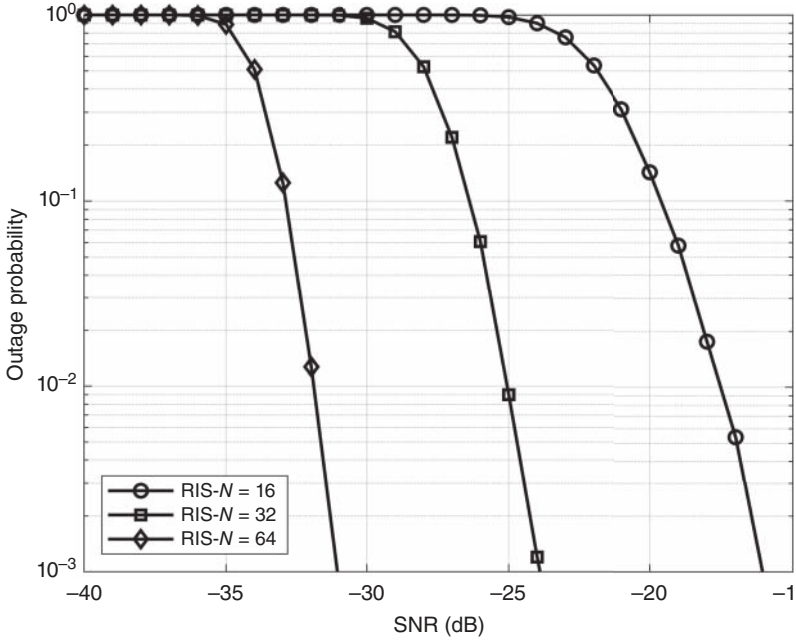

Figure 1.13 Outage performance of RIS-aided SISO system under varying N.

The outage performance of the RIS-assisted SISO system under varying N is shown in Figure 1.13. RIS integration results in the enhancement of outage performance even at the negative SNR region. From the figure, it is evident that the increase in N results in decrease in the outage. For the target outage of 10^{-3}, $N = 64, 32$ and 16 requires ~ -16 dB, ~ -23.89 dB and ~ -31.07 dB of SNR, which shows a significant gain in terms of SNR.

1.6 Conclusion and Future Directions

This book chapter provides a thorough examination of RIS in wireless communication systems, offering detailed insights into various aspects. It begins by delving into the time domain signal characterization of narrowband environments within RIS, analyzing and deriving both diversity gain and array gain achieved. Additionally, it presents an analytical upper bound for BER in RIS, employing two approaches: PDF and MGF. Notably, Monte Carlo simulations corroborate the analytical findings, particularly in high-SNR regimes. This chapter also explores the time domain signal characterization of wideband environments in RIS. Furthermore, it investigates the practical implications of discrete phase shifters compared to ideal continuous phase shifters.

Looking ahead, the chapter outlines promising directions for RIS advancement, emphasizing the development of sophisticated algorithms for optimizing beamforming, channel estimation, and resource allocation. It underscores the integration of artificial intelligence and machine learning to enhance adaptability to dynamic wireless environments and improve energy efficiency. Additionally, it suggests exploring RIS applications in higher frequency bands like mmWave and THz for enhanced data transmission capabilities. Moreover, the chapter highlights the importance of addressing practical challenges such as hardware design, scalability, and standardization efforts to foster interoperability across diverse systems.

References

1 Basar, E., Di Renzo, M., De Rosny, J. et al. (2019). Wireless communications through reconfigurable intelligent surfaces. *IEEE Access* 7: 116753–116773.

2 Björnson, E., Wymeersch, H., Matthiesen, B. et al. (2022). Reconfigurable intelligent surfaces: a signal processing perspective with wireless applications. *IEEE Signal Processing Magazine* 39 (2): 135–158.

3 Björnson, E. and Demir, Ö.T. (2024). *Introduction to Multiple Antenna Communications and Reconfigurable Surfaces*. Boston-Delft: Now Publishers, Inc. https://doi.org/10.1561/9781638283157.

4 Imoize, A.L., Obakhena, H.I., Anyasi, F.I. et al. (2022). Reconfigurable intelligent surfaces enabling 6G wireless communication systems: use cases and technical considerations. *2022 5th Information Technology for Education and Development (ITED)*, 1–7. IEEE.

5 Rivetti, S., Demir, O.T., Bjornson, E., and Skoglund, M. (2024). Malicious reconfigurable intelligent surfaces: how impactful can destructive beamforming be? *IEEE Wireless Communications Letters* 13 (7): 1918–1922.

6 Imran, M.A., Mohjazi, L., Bariah, L. et al. (2023). *Intelligent Reconfigurable Surfaces (IRS) for Prospective 6G Wireless Networks*. Wiley.

7 Kumaravelu, V.B., Imoize, A.L., Castillo Soria, F.R. et al. (2023). RIS-assisted fixed NOMA: outage probability analysis and transmit power optimization. *Future Internet* 15 (8): 249.

8 Rajak, S., Muniraj, I., Selvaprabhu, P. et al. (2023). A novel energy efficient IRS-relay network for ITS with Nakagami-m fading channels. *ICT Express* 10 (3): 507–512.

9 Van Nguyen, M.-S., Do, D.-T., Tin, P.T. et al. (2024). Full duplex reconfigurable intelligent surfaces system relying on NOMA and wireless power transfer. *Wireless Networks* 30 (4): 2127–2142.

10 Pei, X., Yin, H., Tan, L. et al. (2021). RIS-aided wireless communications: prototyping, adaptive beamforming, and indoor/outdoor field trials. *IEEE Transactions on Communications* 69 (12): 8627–8640. https://doi.org/10.1109/TCOMM.2021.3116151.

11 Nemati, M., Ding, J., and Choi, J. (2020). Short-range ambient backscatter communication using reconfigurable intelligent surfaces. *2020 IEEE Wireless Communications and Networking Conference (WCNC)*, 1–6. IEEE.

12 Velez, V., Pavia, J.P., Souto, N. et al. (2023). Performance assessment of a RIS-empowered post-5G/6G network operating at the mmWave/THz bands. *IEEE Access* 11: 49625–49638.

13 Li, Q., Wen, M., Basar, E. et al. (2023). Channel estimation and multipath diversity reception for RIS-empowered broadband wireless systems based on cyclic-prefixed single-carrier transmission. *IEEE Transactions on Wireless Communications* 22 (8): 5145–5156.

14 Chapala, V.K. and Zafaruddin, S.M. (2021). Exact analysis of RIS-aided THz wireless systems over α-μ fading with pointing errors. *IEEE Communications Letters* 25 (11): 3508–3512.

15 Du, H., Zhang, J., Guan, K. et al. (2022). Performance and optimization of reconfigurable intelligent surface aided THz communications. *IEEE Transactions on Communications* 70 (5): 3575–3593.

16 Zhou, G., Pan, C., Ren, H. et al. (2022). Fairness-oriented multiple RIS-aided mmWave transmission: stochastic optimization methods. *IEEE Transactions on Signal Processing* 70: 1402–1417.

17 Du, H., Zhang, J., Cheng, J., and Ai, B. (2021). Millimeter wave communications with reconfigurable intelligent surfaces: performance analysis and optimization. *IEEE Transactions on Communications* 69 (4): 2752–2768.

18 Qin, H., Liu, Z., and Yang, C. (2022). Indoor mm-wave coverage enhancement: reconfigurable intelligent surface deployment strategy based on human mobility model. *IEEE Communications Letters* 26 (10): 2475–2479.

19 Xiong, J., You, L., Ng, D.W.K. et al. (2020). Energy efficiency and spectral efficiency tradeoff in RIS-aided multiuser MIMO uplink systems. *GLOBECOM 2020-2020 IEEE Global Communications Conference*, 1–6. IEEE.

20 You, L., Xiong, J., Ng, D.W.K. et al. (2020). Energy efficiency and spectral efficiency tradeoff in RIS-aided multiuser MIMO uplink transmission. *IEEE Transactions on Signal Processing* 69: 1407–1421.

21 Wu, Q. and Zhang, R. (2019). Beamforming optimization for wireless network aided by intelligent reflecting surface with discrete phase shifts. *IEEE Transactions on Communications* 68 (3): 1838–1851.

22 Pala, S., Taghizadeh, O., Katwe, M. et al. (2024). Secure RIS-assisted hybrid beamforming design with low-resolution phase shifters. *IEEE Transactions on*

Wireless Communications 23 (8): 10198–10212. https://doi.org/10.1109/TWC.2024.3370372.

23 Dai, L., Wang, B., Wang, M. et al. (2020). Reconfigurable intelligent surface-based wireless communications: antenna design, prototyping, and experimental results. *IEEE Access* 8: 45913–45923.

24 Aziz, R. and Girici, T. (2022). Deployment of a UAV-mounted intelligent reflecting surface in the THz band. *2022 International Balkan Conference on Communications and Networking (BalkanCom)*, 168–172. IEEE.

25 Chrysologou, A.P., Boulogeorgos, A.-A.A., and Chatzidiamantis, N.D. (2023). When THz-NOMA meets holographic reconfigurable intelligent surfaces. *IEEE Communications Letters* 27 (9): 2516–2520.

26 Li, M., Zhang, S., Ge, Y. et al. (2022). Joint channel estimation and data detection for hybrid RIS aided millimeter wave OTFS systems. *IEEE Transactions on Communications* 70 (10): 6832–6848.

27 Lee, E.A. and Messerschmitt, D.G. (2012). *Digital Communication*. Springer Science & Business Media.

28 Li, R., Sun, S., and Tao, M. (2023). Ergodic achievable rate maximization of RIS-assisted millimeter-wave MIMO-OFDM communication systems. *IEEE Transactions on Wireless Communications* 22 (3): 2171–2184. https://doi.org/10.1109/TWC.2022.3210227.

29 Thirumavalavan, V.C. and Jayaraman, T.S. (2020). BER analysis of reconfigurable intelligent surface assisted downlink power domain NOMA system. *2020 International Conference on COMmunication Systems & NETworkS (COMSNETS)*, 519–522. https://doi.org/10.1109/COMSNETS48256.2020.9027303.

30 Simon, M.K. and Alouini, M.-S. (2008). Digital communications over fading channels (M.K. Simon and M.S. Alouini; 2005) [book review]. *IEEE Transactions on Information Theory* 54 (7): 3369–3370.

31 Craig, J.W. (1991). A new, simple and exact result for calculating the probability of error for two-dimensional signal constellations. *MILCOM 91 - Conference Record*, volume 2, 571–575. https://doi.org/10.1109/MILCOM.1991.258319.

32 Primak, S., Kontorovich, V., and Lyandres, V. (2005). *Stochastic Methods and Their Applications to Communications: Stochastic Differential Equations Approach*. Wiley.

33 Paulraj, A., Nabar, R., and Gore, D. (2003). *Introduction to Space-Time Wireless Communications*. Cambridge University Press.

34 Gradshteyn, I.S. and Ryzhik, I.M. (2014). *Table of Integrals, Series, and Products*. Academic Press.

35 Haykin, S. (2008). *Communication Systems*. Wiley.

36 Jagannatham, A.K. (2015). *Principles of Modern Wireless Communication Systems*. McGraw-Hill Education.

37 Tse, D. and Viswanath, P. (2005). *Fundamentals of Wireless Communication*. Cambridge University Press.

38 Velmurugan, P.G.S., Thiruvengadam, S.J., Kumaravelu, V.B. et al. (2023). Performance analysis of full duplex bidirectional machine type communication system using IRS with discrete phase shifter. *Applied Sciences* 13 (12): 7128.

39 Thirumavalavan, S.J.T.V.C. and Hariharan, A.B.R. (2022). BER analysis of tightly packed planar RIS system using the level of spatial correlation and discrete phase shifter. *Transactions on Emerging Telecommunications Technologies* 33 (11): 1–15.

40 Kumaravelu, V.B., Imoize, A.L., Castillo Soria, F.R. et al. (2022). Outage probability analysis and transmit power optimization for blind-reconfigurable intelligent surface-assisted non-orthogonal multiple access uplink. *Sustainability* 14 (20): 13188.

41 Boulogeorgos, A.-A.A. and Alexiou, A. (2020). Performance analysis of reconfigurable intelligent surface-assisted wireless systems and comparison with relaying. *IEEE Access* 8: 94463–94483.

42 Cho, Y.S., Kim, J., Yang, W.Y., and Kang, C.G. (2010). *MIMO-OFDM Wireless Communications with MATLAB*. Wiley.

2

Emerging Applications and Potential Use Cases of Reconfigurable Intelligent Surfaces in Wireless Communication Systems

Helen Sheeba John Kennedy[1], Anjana Babu Sujatha[1], Suganthi Evangeline Chakkaravarthy[2], Dipinkrishnan Rayaroth[1], Vinoth Babu Kumaravelu[1], Narushan Pillay[3], Arthi Murugadass[4], and Vishnu Vardhan Gudla[5]

[1] *Department of Communication Engineering, School of Electronics Engineering, Vellore Institute of Technology, Vellore, India*
[2] *Department of Electronics and Communication Engineering, Sri Eshwar College of Engineering, Coimbatore, India*
[3] *School of Engineering, University of KwaZulu-Natal, Durban, South Africa*
[4] *School of Computer Science and Engineering, Vellore Institute of Technology, Chennai, India*
[5] *Physical Layer Expert, Comms., Media & Tech Unit, L&T Technology Services, Bangalore, India*

2.1 Introduction

Reconfigurable intelligent surface (RIS) or intelligent reflective surface (IRS) is an emerging technology that enhances and manipulates electro-magnetic (EM) waves using semi-passive or active elements in the communication chain of the next-generation networks. The deployment of RIS in the next-generation wireless networks results in signal strengthening, which boosts coverage, mitigates blockage, and improves coverage in low-quality signal regions [1]. RIS is a network node that can be configured semi-dynamically or dynamically by a controller. This turns the wireless environment between the transmitter and user equipment (UE) from passive to programmable, as shown in Figure 2.1.

By strategically positioning RIS, the system can greatly enhance its energy efficiency (EE). The adaptive reflection ability of active RIS (ARIS) minimizes energy consumption and maximizes spectral efficiency (SE). These features of ARIS play a vital role in the quality of service (QoS) of different applications. The deployment of multiple RIS provides the potential for minimizing blocking probability in challenging environments like tunnels, pipes, and other applications, where the presence of obstacles degrades the signal quality. An RIS can adjust the propagation

Reconfigurable Intelligent Surfaces for 6G and Beyond Wireless Networks, First Edition.
Edited by Agbotiname Lucky Imoize, Vinoth Babu Kumaravelu, and Dinh-Thuan Do.

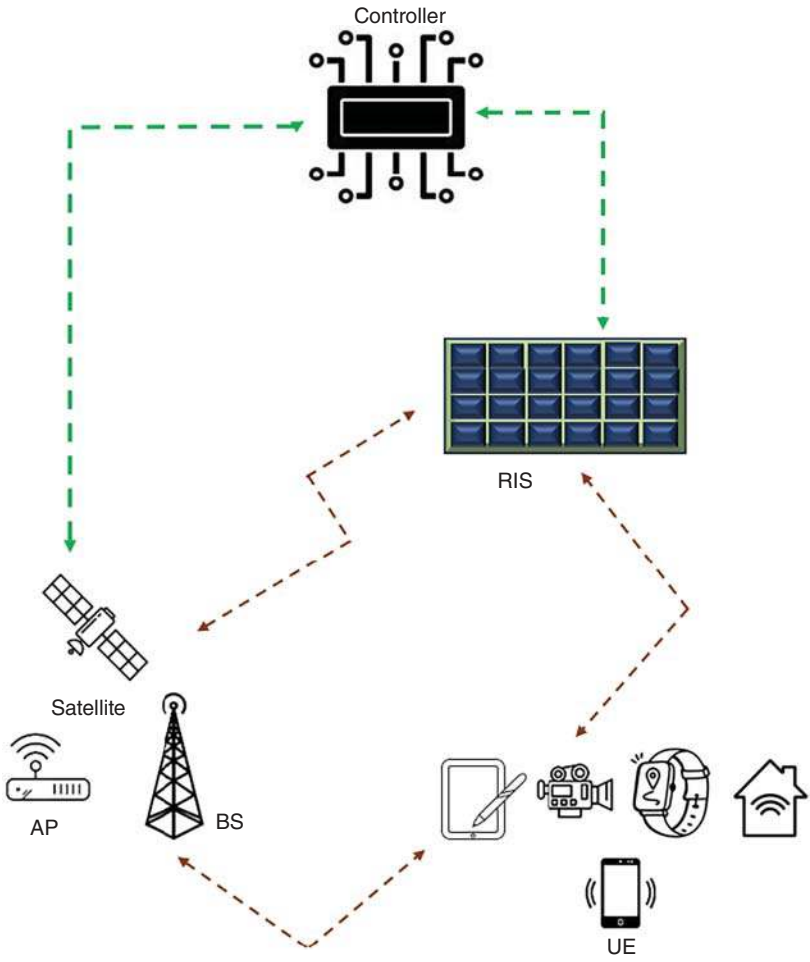

Figure 2.1 RIS-a new network node in the communication chain.

angle, optimizing the signal paths and beamforming, thereby reducing the blockages. It ensures reliable communication even in complex scenarios like cell-free networks, where the multiplicative fading effect (MFE) degrades the signal quality. The future network must provide seamless connectivity to vehicles with up to 1000 km/h speeds. RIS can marginally mitigate the end-to-end transmission delay in such systems by enhancing the performance of wireless networks.

RIS is a promising technology that can help transform the wireless environment into a smart wireless environment, meeting the requirements of fifth-generation (5G) and beyond (5GB) networks. RIS can be used to enhance SE, improve

physical layer security (PLS), increase location accuracy, improve coverage, manage beams, and enhance EE. These use cases enable a wide range of applications for next-generation networks.

The EE and beamforming properties of RIS can substantially support the wide range of potential applications across various fields of next-generation networks, such as Internet of things (IoT) applications, unmanned aerial vehicles (UAV) communication, smart environments, PLS, simultaneous wireless information and power transfer (SWIPT) protocols, IoT-based mobile edge computing, device-to-device (D2D) systems, vehicular ad hoc networks (VANET) applications, hybrid terrestrial and satellite communication, and so on [2]. These applications demonstrate the versatility and potential of RIS in various domains, from telecommunications and networking to healthcare and beyond.

2.1.1 Key Contributions

The substantial contribution of the work is listed as follows:

- The chapter examines RIS's application and its integration with various advanced technologies such as IoT, UAV, PLS, D2D, VANET, and hybrid technologies.
- The chapter discusses various use cases of RIS, such as coverage enhancement, SE enhancement, improving PLS and localization accuracy, beam management, EE enhancement, and energy-efficient cell-free network.
- A detailed study of prior works is provided in this chapter, alongside a discussion of how integration improves various parameters such as EE, SE, and total capacity.
- A detailed discussion of research challenges associated with cutting-edge technologies while integrating RIS is presented. Additionally, the work provides insights into upcoming trends in this area.

2.1.2 Organization

RIS is considered a crucial technology in developing sixth-generation (6G) wireless networks. In recent times, RIS has gained considerable attention as a fundamental component, which contributes high support for data rate demands with a low cost of implementation for next-generation wireless systems. The proposed chapter about RIS is organized as follows: Section 2.1 provides a concise introduction to the chapter. A thorough explanation of use cases involving RIS technology is provided in Section 2.2. Section 2.3 of the chapter explores the application of RIS for future networks. The challenges encountered while introducing RIS and the research trends associated with the applications are discussed in Section 2.4. Finally, the chapter concludes with Section 2.5.

2.2 Use Cases of RIS

RIS emerges as a prospective technology poised to revolutionize the wireless landscape, aligning seamlessly with the demands of 5G and 5GB networks. Its applications extend to elevating SE, fortifying the PLS, refining localization accuracy, expanding coverage, beam management, and augmenting EE. These diverse applications unlock a plethora of possibilities for advanced network functionalities, marking a significant stride toward the next era of wireless communication. This section details the requirements and prior works on RIS-aided use cases.

2.2.1 Coverage Improvement

For 6G networks, one of the essential necessities is offering users wider and more efficient coverage. The evolution of 6G will expand coverage from 2D to 3D globally. Merely 10% of the entire planet can be covered by 5G, whereas 6G is anticipated to cover 99% of the entire planet. Space-, air-, ground-, and marine-linked communication networks will enable 6G to acquire worldwide coverage [3].

When the signal is transmitted through air, there may be reflection, scattering, and diffraction of the signal due to the obstacles between the base stations (BS) and the receiver. Therefore, propagation losses increase and the coverage reduces. Increasing the number of BSs to enhance coverage is a costly and ineffective solution. RIS is gaining significant attention in communication because of its potential for enhancing coverage. A smart radio environment can be created by incorporating RIS in the communication chain.

In Figure 2.2, line-of-sight (LoS) propagation is impossible due to a building blockage between the BS and the user. By using RIS, the signal can be reflected

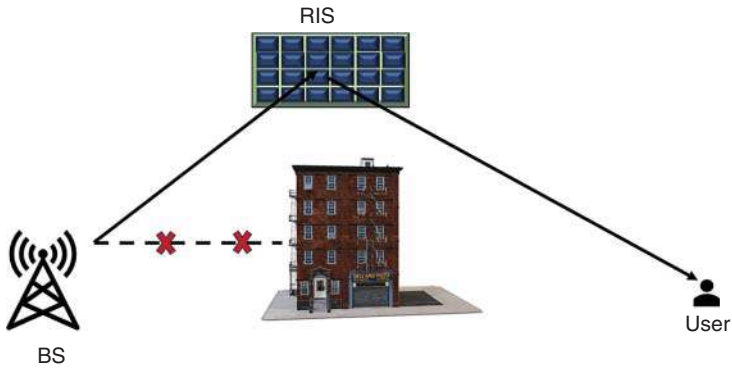

Figure 2.2 RIS-assisted communication for coverage enhancement.

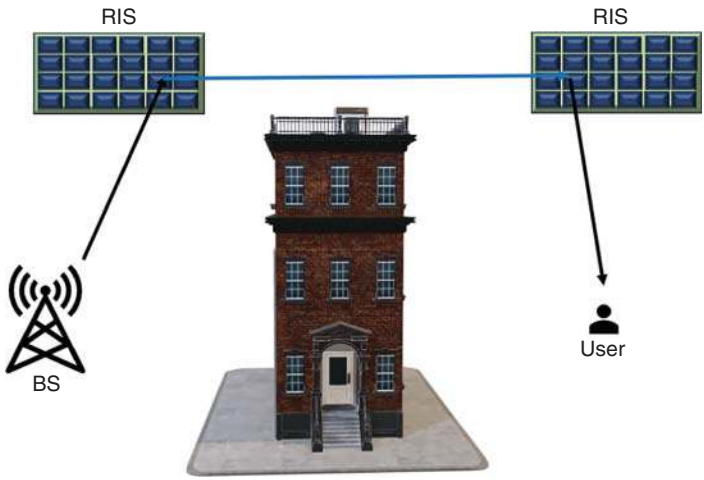

Figure 2.3 Coverage extension by cascading RIS.

to the user. Hence, blockage issues can be resolved, and coverage also increases. The RIS can be deployed in the walls and windows of buildings, vehicles, and anywhere where the signal coverage needs to be increased. The deployment of RIS is cost-effective compared to the BS installation. Figure 2.3 depicts a frequently occurring variation of the blockage problem. Additional RIS can be set up in a cascaded way for coverage extension to prevent significant penetration loss created by obstructions.

Sang et al. [4] fabricated RIS and conducted a field test on its effectiveness in improving coverage in urban environments' existing 5G commercial mobile networks. The outcomes of field test trials reveal that there is a significant improvement in the coverage and throughput by incorporating RIS in the communication chain. To enhance the coverage and remove the coverage blind spots, RIS can be placed in irregular terrains in UAV-based communication. To maximize the coverage, Savkin et al. [5] suggested a new algorithm for UAV-based BSs. One of the main factors enabling the 5GB cellular networks to accomplish high data rates is the utilization of millimeter wave (mmWave) bandwidth. However, mmWave signals suffer from large path loss, restricting their usage. Nemati et al. [6] analyzed the coverage enhancement possibilities of RIS in mmWave communication. The analytical results show that, regarding mmWave coverage enhancement, installing RIS is more effective than installing new BSs with more active antennas. Tapio et al. [7] analyzed the performance improvement offered by RIS using a link-level simulator that adheres to 5G-new radio (NR) standards. To optimize the orientation of RIS and maximize cell coverage, Zeng et al. [8] suggested an algorithm for solving the RIS deployment optimization problem with the objective of achieving optimal coverage.

2.2.2 Beam Management

Beam management is a commonly employed technique to reduce signal propagation losses during wireless transmission in wireless communication systems. To deliver higher data rates, 5GB networks require multiple antennas. Beamforming techniques are becoming more complicated due to signal processing complexity. Cellular systems are moving toward higher carrier frequencies. As a result, the crucial tasks of beam management, such as beam alignment, tracking, and recovery, will become difficult [9].

Beamforming is the most significant use case for RIS. By varying the phases of its reflecting parts, RIS can beamform messages in the direction of the intended user. RIS can beam form signals either based on constructive reflection or destructive reflection; based on that, it can be classified as energy-focusing and energy-nulling, which are explained in this Section [10].

2.2.2.1 Energy-Focusing Use Cases

In Figure 2.4, the depicted scenario illustrates the energy-focusing application of RIS. In this use case, as the signal travels from the BS to the user via the LoS path, it undergoes reflection through the RIS. Through the manipulation of the phase of the reflector elements, the two signals are strategically combined, leading to constructive interference and focus toward the targeted user. Consequently, this results in an enhancement of the received signal strength. These energy-focusing use cases can be used in applications where signal strength needs to be increased.

2.2.2.2 Energy-Nulling Use Cases

Figure 2.5 depicts the energy-nulling use cases of RIS, which is based on destructive reflection. If the transmitter sends a signal that is not meant for a particular user, it is possible to adjust the phase of the reflector elements in RIS. This adjustment allows for the addition of a LoS signal and an RIS reflected signal to destructively interfere, effectively creating a zero signal that will be received by the user.

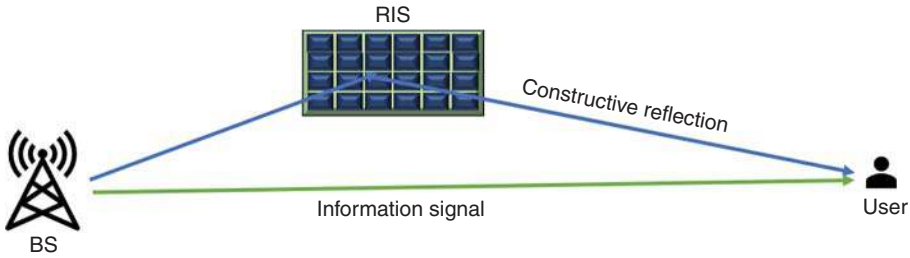

Figure 2.4 Energy-focusing use cases of RIS.

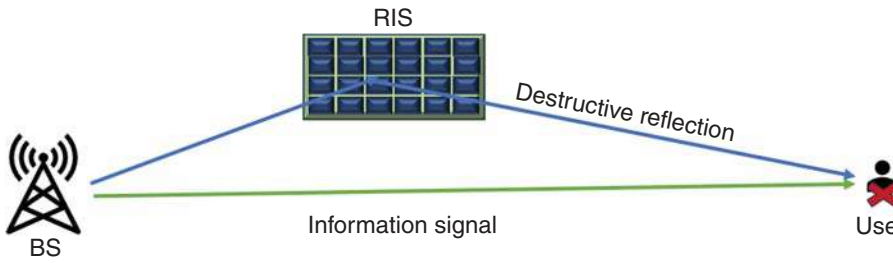

Figure 2.5 Energy-nulling use cases of RIS.

The beam training issue in RIS-assisted wideband terahertz (THz) communication systems is analyzed by Chen et al. [11]. An analytical beam training framework is suggested to increase the beam training accuracy in broadband communication. To generate different beam patterns while considering the hardware constraints of RIS, Rahal et al. [12] suggested an optimizing method for the design of RIS. For RIS-aided integrated sensing systems such as radar, reflection pattern design and transmit beamforming have a significant role in target detection [13]. Jiang et al. [14] developed a machine learning algorithm for RIS to select optimal beams between the user and BS based on the existing wireless data. The suggested method can estimate the optimal beams, and the RIS beam selection solution may achieve near-optimal attainable rates with a large reduction in beam training overhead.

2.2.3 SE Enhancement

6G networks are poised to bring about ground-breaking breakthroughs in wireless technology. With the increasing demands of modern connectivity, SE has become even more crucial in the vast domain of 6G. The use of available spectrum to transfer data at high rates is measured by a basic statistic called SE. With ultra-high-definition content and huge data traffic supported by 6G, SE is essential to meeting the growing need for faster and more seamless connectivity. Higher data rates, optimal spectrum utilization, and improved user experiences are all made possible by SE. Nevertheless, this frequently leads to increased energy usage.

On the other hand, giving EE priority saves energy but may result in decreased data rates. In fact, to ensure continuous connectivity, effective resource utilization, and future-proof technology, 6G systems need creative ways to manage this trade-off. Although 5G brought multiple input-multiple output (MIMO) technology, 6G's increasing performance requirements are greater than what 5G MIMO can handle. In the realm of 6G networks, the anticipated significance of full-duplex (FD) and MIMO capabilities at the BS is expected to be heightened.

These capabilities are foreseen to be pivotal contributors to achieving larger data rates, reduced latency, and enhanced SE and EE [15].

Through long-distance power loss compensation, RISs can reconfigure the wireless propagation environment. By passively reflecting the incoming radio signals, BSs and mobile users can establish virtual LoS relationships. Significant throughput enhancements are observed, particularly in scenarios where obstacles, like tall buildings, impede the LoS connection between BSs and users. The strategic deployment and design of RISs have the potential to establish a software-defined wireless environment. This intelligent setup has the capability to enhance the signal-to-interference-plus-noise ratio (SINR) received [16]. Figure 2.6 illustrates the application of RIS in conjunction with MIMO for multiplexing and interference management. The utilization of RIS in tandem with MIMO systems presents an innovative strategy for elevating the performance of wireless communication. RIS can augment spatial multiplexing through intelligent signal reflection and redirection, generating additional virtual channels and enhancing overall SE. Integrating MIMO and RIS concurrently optimizes signal coverage, mitigates dead zones, and overall improves the reliability of wireless communication.

Strong channel correlation between the transmitter and receiver antennas in wireless networks reduces the number of eigen-channels available for simultaneous data transfer. The channel correlation issue can be resolved by implementing RIS. Multiple access using RIS is presented in Figure 2.7. Utilizing RIS involves strategically reflecting and redirecting signals to establish separate spatial channels for individual users. This spatial multiplexing feature enables multiple users to utilize the same frequency band, thereby improving SE simultaneously.

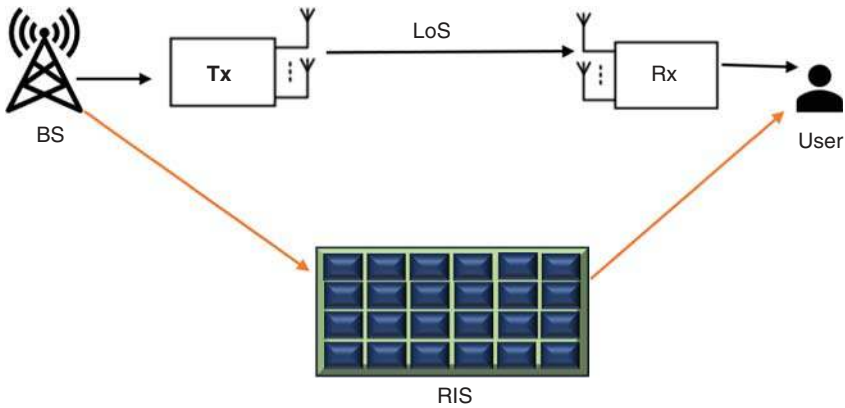

Figure 2.6 Multiplexing and interference management using RIS in conjunction with MIMO.

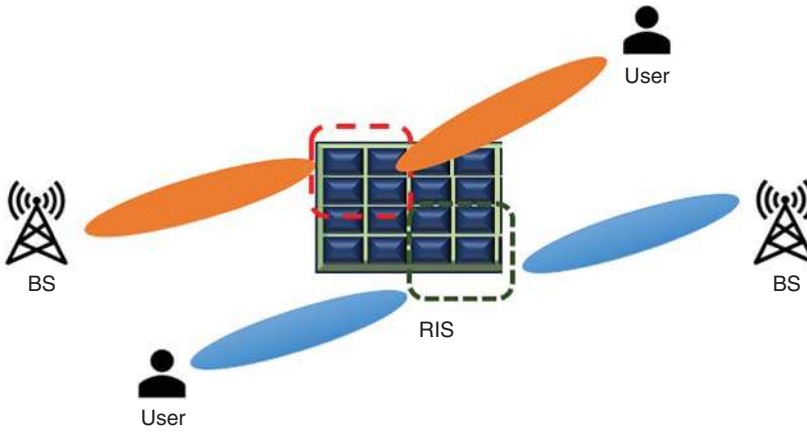

Figure 2.7 Multiple access using RIS.

The dynamic adjustment of phase and amplitude in RIS elements facilitates adaptive beamforming, accommodating multiple users. Communication networks can achieve greater SE and advantages in spatial multiplexing with more eigen-channels. Specifically, the enhanced coverage brought about by the greater received signal power also results in an increase in SE.

The combination of RISs with FD-MIMO has the ability to completely transform communication networks in the 6G future, meeting growing demand and providing several benefits like

- **Improved SE and EE**: RIS-aided FD-MIMO maximizes SINR with minimum route loss which improves SE and EE. In FD-MIMO, less energy is used, requiring fewer resources overall.
- **Increased coverage and capacity**: By overcoming limitations, RIS enables reflection to target sites, which enhances capacity and coverage. The same frequency range of FD-MIMO further enhances capacity and allows higher data rates.
- **Flexibility and adaptability**: In response to user demands and channel conditions, FD-MIMO adjusts the number of antennas and transmission power, while RIS's reconfigurability enables beamforming.
- **Improved user experience**: By utilizing the advantages of both technologies, it is possible to support several users at once, guaranteeing support for strong user without sacrificing SE and EE.

The performance of RIS-assisted systems has been the subject of numerous initiatives focused on improving network coverage, outage probability, SE, and EE. A substantial amount of research was devoted to improving the system's SE. For instance, a study by Abeywickrama et al. [17] examined how to maximize

the throughput of a single-user multiple input-single output (MISO) system. Conventional orthogonal multiple access (OMA), non-OMA (NOMA), and space division multiple access (SDMA) provide better SE and coverage capability in RIS-aided networks, especially when direct links between communicating nodes are absent [18, 19]. Yu et al. [20] suggested a method to maximize SE in an RIS-assisted MISO system. Research has been conducted on improving the SE in wireless networks with RIS-assisted FD communication. The findings demonstrated that FD technology with the same spatial dimension quadruples the SE compared to half-duplex [21–23].

2.2.4 EE Enhancement

The upcoming 6G networks are expected to provide faster speeds and greater capabilities than 5G. However, if these networks are not managed properly, they may lead to higher energy usage. In 5G, massive MIMO (mMIMO) antennas result in high energy consumption due to the large number of antennas and the need for individual radio frequency (RF) chains for signal processing, which increases system complexity. For this reason, 6G is expected to be 10 times more energy efficient than 5G.

RIS, a technology that manipulates the propagation of EM waves, has the potential to increase the EE of next-generation networks significantly. By adjusting the phase of its elements, RIS can steer signals toward the desired user, concentrating energy and reducing the need for higher transmission power. This beamforming capability has a great impact on energy consumption reduction. RIS does not require any external power source, as it consists of passive reflector elements, thus consuming much less energy than relays. Overall, RIS is a promising technology to improve the efficiency of wireless networks [24]. To enhance EE, RIS can be utilized for energy harvesting, WPT, and reducing exposure to EM field (EMF).

2.2.4.1 Energy Harvesting

5G networks require more energy to function due to their high data throughput and low latency demands. However, this energy requirement can be met sustainably by using energy harvesting technologies. One such technology is RF energy harvesting, which involves converting ambient RF signals from wireless fidelity (Wi-Fi), cellular communications, and radio and television broadcasts into electrical power. Devices on 5G networks that consume less energy, such as sensor nodes and IoT devices, usually require external batteries to function. However, energy harvesting techniques can replace these batteries, resulting in energy-efficient transmission and reception of signals.

RIS is particularly promising for creating self-sustaining wireless networks. RIS can improve the efficiency of both information and energy transfer, as radio waves can carry both. By harvesting energy from ambient RF signals, RIS can function without the need for external power sources. This is especially useful in

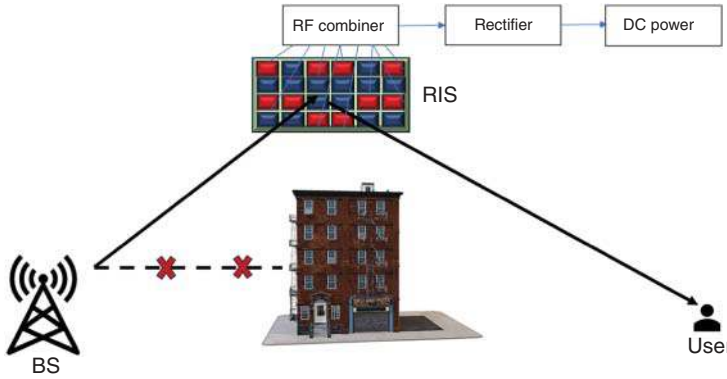

Figure 2.8 Energy harvesting using RIS.

remote locations where providing an external power source is challenging and expensive. An energy harvesting scenario using RIS is depicted in Figure 2.8, where RIS elements reflect toward the user, while others are dedicated to energy harvesting. In Figure 2.8, the user experiences blockage due to the building. Thus, the user is dependent on the RIS's reflected path. The BS sends the signal carrying information, which is reflected off the surface of the RIS. Part of the RIS elements harvest the energy with the simple RF circuitry, and the remaining elements reflect the signal to the desired user.

2.2.4.2 WPT

In today's wireless era, wireless devices are on the rise. However, their short battery life can be a problem as these devices often need to be frequently charged or replaced. This can be costly or challenging in certain situations. WPT has the potential to provide wireless energy to a large number of devices, thereby eliminating the need for battery replacement. This, in turn, can extend the battery life of battery-powered devices.

RIS technology has the ability to enable WPT. A WPT scenario using RIS is illustrated in Figure 2.9. Here, an RIS can facilitate the power transfer between the BSs

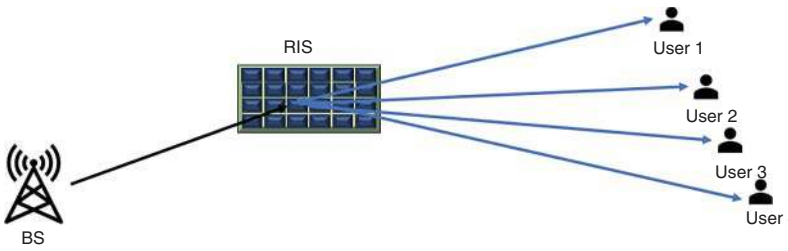

Figure 2.9 WPT using RIS.

and users when the signals between the transmitters are obstructed. This means that users can receive both the information signal and energy collected by RIS. WPT increases the EE and reduces the transmission power.

2.2.4.3 Reducing EMF Exposure

Future wireless networks must consider the rising impact of EM pollution. The implementation of 5G communication networks has raised health concerns due to the exposure to EMF radiation. When many BSs are deployed for coverage enhancement, it generates more signals and increases the EMF radiation. Although coverage can be enhanced by increasing the number of BSs, it also increases EM radiation.

However, the effective use of RIS significantly reduces the emission of EM radiation. RIS can control the EM environment and adjust the phase of the reflecting signal toward a particular user. Therefore, the beamforming property of RIS reduces unwanted EMF radiations, making it an excellent system for 5G communication systems. Ntontin et al. [25] suggested a power consumption and energy harvesting model for the RIS system by analyzing its power consumption. They suggested an effective solution to the most efficient RIS deployment problem by adjusting its components' phase and amplitude responses to maximize the signal-to-noise ratio (SNR) while harvesting enough energy for the system to function. The RIS can assist backscatter transmitters to improve the efficiency of cooperative ambient backscatter communications. In an RIS-assisted cooperative ambient backscatter communications system, the RIS with an energy harvesting circuit can reflect the signal and also gather wireless energy [26]. When IoT devices require harvesting energy, they might need to collect energy from RF signals of nearby BSs. Ahmed et al. [27] suggested a solution to reduce the amount of energy RIS panels use for the active and passive components of IoT systems. The energy harvested by the transmissions powers RIS panels. The features of signal reflection and amplification in ARIS require much energy, whereas passive RIS (PRIS) uses less energy because of its signal reflection properties.

Ren et al. [28] analyzed the benefits of implementing RIS in the WPT system and suggested an effective RIS-aided WPT strategy. RIS can significantly improve the EE of WPT systems using many ground sensors that UAVs enable [29]. Yin et al. [30] optimized the connectivity of RIS-assisted networks by considering EMF radiation limits and suggesting a power-efficient algorithm to reduce EMF exposure by 14% compared to the system without the RIS and increase the connectivity by 20%.

2.2.5 Improving PLS

The heterogeneous nodes of the 6G network range in size from macro to nanoscale [31]. It comprises an ultradense network (UDN) that handles applications

requiring high data rates and extremely dense traffic. Security must be included in the network design to use these services. Therefore, PLS can be the first defense line for certifying wireless communications confidentiality. The research community's focus has shifted to 6G physical layer technologies, such as RIS. RIS is a novel idea that offers a different transmission method and allows incident signal amplitude, phase, and frequency to be adjusted.

The uncontrolled dissemination of private information caused by the unpredictable nature of wireless propagation channels is one of the elements affecting communication system security. Using RIS, creating a controlled and intelligent wireless propagation environment that efficiently prevents eavesdroppers from intercepting sensitive signals and enhanced communication system security is possible. Without RIS, as shown in an example scenario in Figure 2.10, data delivered to a UE can readily be leaked to listeners through reflections from surfaces like walls and ceilings. Redirecting reflections to a "trusted region" is one way RIS might address this issue and improve communication security by minimizing data leakage to possible eavesdroppers.

Similar to various technologies with substantial potential for wireless applications, RIS can also be exploited for malicious purposes. For instance, an unauthorized party might deploy an RIS with the intention of leveraging its capability to establish a secure wireless link with a legitimate system. This could enable the eavesdropper to intercept and decode data that has been legitimately transmitted. In these circumstances, adopting just artificial noise (AN) broadcast by the legitimate system might not be able to ensure confidentiality, making a genuine RIS equally necessary.

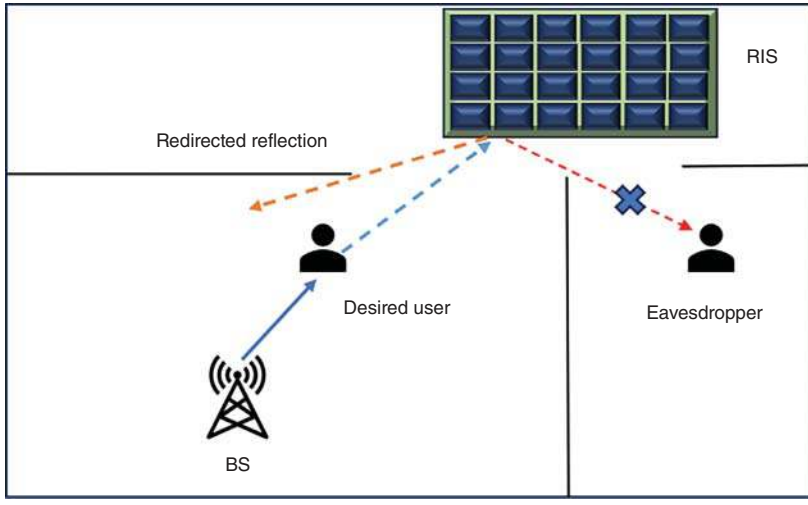

Figure 2.10 RIS for secure communication.

Secrecy capacity (SC) is a key criterion assessed in PLS; it represents the fundamental bound of secure communications. In Zhou et al. [32], Yu et al. [33], and Cui et al. [34], RIS-assisted secrecy communications were examined. Active transmit and passive reflect beamforming are collaboratively developed to improve the achievable SC, utilizing various optimization strategies. Additionally, Guan et al. [35] and Feng et al. [36] examined AN, which may be employed in RIS-assisted secure communication as a transmit jammer. They demonstrated how this design enhances the network SC. The PLS can be obtained by integrating RIS with the system, and it results in better performance in the following dimensions:

- **Secure signal beamforming and reflection**: RIS has the ability to modify the environment's signal beamforming and reflection dynamically. Adjusting signal routes makes it possible to create secure communication zones where it is more difficult for eavesdroppers to intercept or tamper with the communication.
- **Enhanced signal confidentiality**: By reducing the signal strength in undesired directions, RIS can be utilized to foster ideal propagation conditions for the targeted communication channel. This aids in preserving the confidentiality of the transmitted information.
- **Decreased susceptibility to interception**: Due to its ability to regulate signal pathways and reflections, RIS makes the communication environment more dynamic and unpredictable, making it more difficult for potential eavesdroppers to intercept messages.
- **Energy-efficient security**: Energy-efficient security solutions may benefit from using RIS. RIS can assist in lowering the communication system's overall energy usage while preserving a high level of security by optimizing signal pathways and reflections.

In the simple design of RIS-aided PLS, the transmitter sends signals to the receiver through an insecure communication link. The RIS is strategically placed to take advantage of the unique features of the propagation channel. By limiting the information of the secret messages that the eavesdropper can extract, the RIS can prevent eavesdropping. This can be achieved by either degrading the eavesdropper or improving the SINR at the receiver. RIS-assisted PLS solutions have proven more successful in difficult situations than traditional MIMO techniques [37–42]. This could apply in cases where the eavesdropper/jammer is situated closer to the transmitter, has more antenna (or better channel conditions) than the receiver, or has a higher secrecy rate need. Under such circumstances, both spatial beamforming and PLS with larger antenna arrays might be unsuccessful in terms of providing enough secrecy gain.

2.2.6 Improving Localization Accuracy

One crucial element in ensuring smooth network connectivity is device localization. Localization information ensures reliable multi-hop connectivity, specifically in sensor networks. Likewise, effective network design and real-time resource distribution rely on location data to improve connection quality. The applications like, industrial IoT (IIoT), intelligent transportation systems (ITS), SWIPT, location-aware systems, radar, robot localization, and extended reality, are developed based on the increasing demand and societal advancements. Traditional wireless communication systems already offer positioning services. Nevertheless, the location, LoS availability, and BS count restrict the accuracy. Implementing RIS is less expensive and more versatile than implementing BS. Employing RIS, communication networks can achieve greater spatial precision of placement and resolution. The use of RIS can also increase the indoor scenario's placement accuracy. Figure 2.11 depicts the process of attaining localization accuracy using RIS. RIS's dynamic adaptation of the phase and amplitude of reflected signals facilitates the creation of focused beams. Steering these beams toward the designated device, RIS plays a key role in enhancing signal strength and directionality, thereby contributing to heightened precision in localization. Strategic placement of RIS can be leveraged to improve SNR at the receiver, a critical factor for precise signal detection in localization systems.

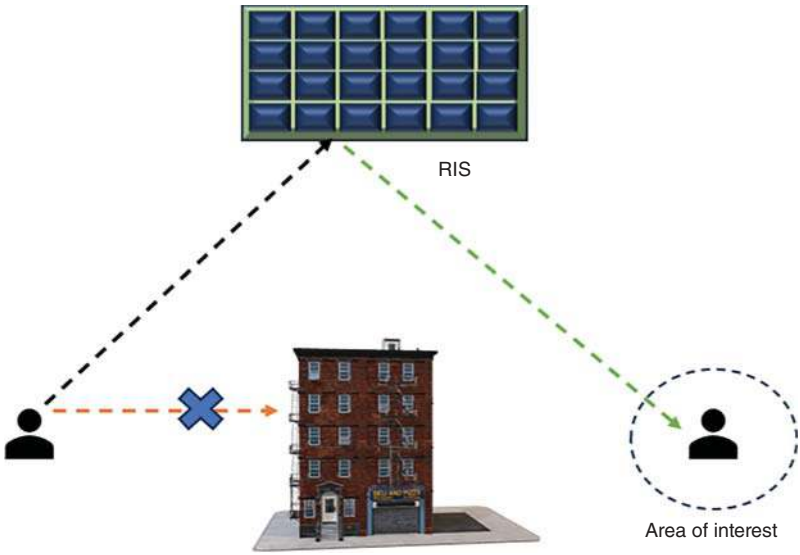

Figure 2.11 Localization accuracy using RIS.

Numerous investigations have been carried out, and various approaches have been proposed in recent years to enhance localization accuracy. RIS offers an additional degree of latitude in this regard to enhance the localization data. A platform like this can be utilized both indoors and outdoors. This encourages the researchers to investigate RIS's potential for localization. Elzanaty et al. [43] have shown that using RIS can greatly enhance the position and orientation error bounds. Additionally, it enhanced multiuser localization by utilizing IRS to boost signal strength [44].

In addition to measuring signal intensity, time delay can also be used, as discussed by Wymeersch and Denis [45]. By maximizing the phase distribution for the RIS elements and their selection, the authors have successfully optimized the position error bounds in this instance. Moreover, the RIS can be used as a lens or reflector for localization and sensing applications. Similar reports can be found for RIS-aided sensing [46] and RIS-aided localization [47–49]. In Hu et al. [49], the effects of RIS size, RIS deployment tactics, and associated impairments are covered. In Alegría and Rusek [48], it is reported how RIS quantization affects localization performance. Abu-Shaban et al. [47] have illustrated the potential applications of RIS in 3D localization.

2.2.7 Energy-efficient Cell-free Network

The cell-free network has become increasingly appealing in the context of 5G without cell boundaries [50]. It has much potential for use in next-generation indoor hotspot environments, such as subways, train stations, hospitals, and retail centers. Furthermore, cell-free networks perform especially well in high-mobility situations without incurring changeover costs, such as automobile networks [51]. Despite the aforementioned benefits, deploying many access points (APs) in a standard cell-free network produces high power consumption for both hardware and transmit power, lowering EE. This is one issue that needs to be resolved in future networks.

RIS has emerged as a potentially useful technology in recent times for overcoming barriers, boosting channel capacity, and enhancing EE in various situations, including secure communications [52, 53]. Cell-free networks use PRIS to minimize power usage, but the double-fading effect limits the data rate. To enhance the EE in cell-free networks and mitigate fading effects, hybrid RISs with active elements that can amplify the incident signal could replace some of the APs.

Future wireless networks will require very high data rates, so energy consumption has become a major worry. Numerous energy-saving techniques have been developed to guarantee sustainable and environmentally friendly

wireless networks. Deploying RIS can greatly improve network performance regarding coverage and data rates; in the RIS-assisted scenario, fewer BSs and less transmit power from the BSs would be needed to reach a required coverage or data rate target. Compared to relay solutions, RIS-assisted deployments can be a compelling way to improve network efficiency and performance while consuming less energy. Similarly, RIS deployment can enhance user EE when considering the uplink transfer that the RIS facilitates. The system model for the cell-free RIS network is given in Figure 2.12. In the context of a hybrid RIS-aided cell-free network, the deliberate deployment of RIS elements is coordinated with cell-free APs. The integration of RIS with cell-free communication is designed to capitalize on the unique advantages of both technologies, aiming for enhanced overall performance. Within the cell-free framework, where multiple APs may serve a user, the strategic use of RIS assists in alleviating inter-cell interference, thereby contributing to improved network performance.

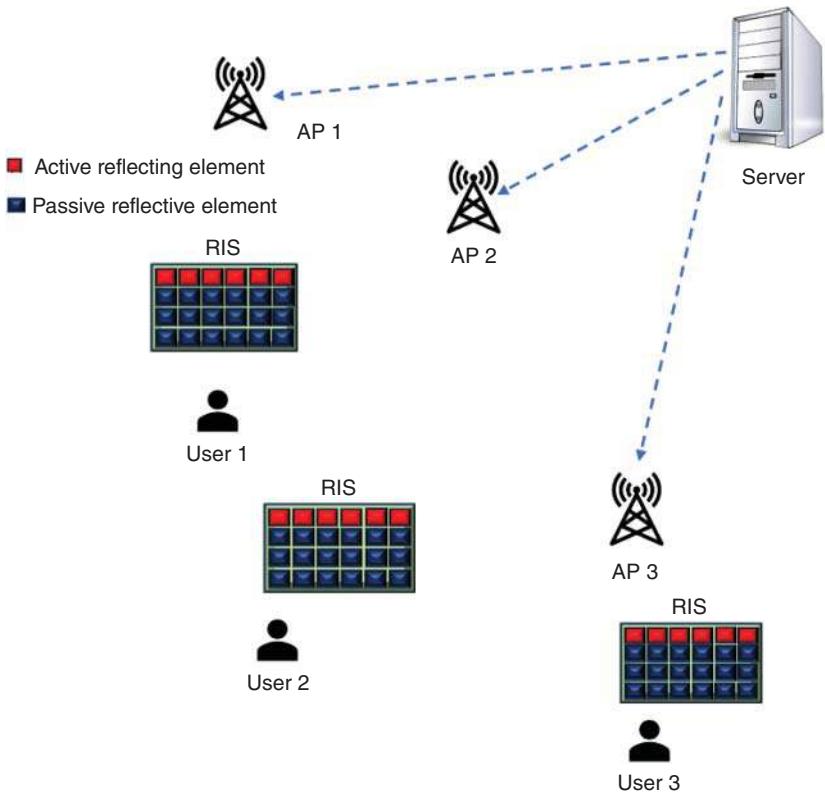

Figure 2.12 Hybrid RIS-aided cell-free network.

RIS hardware architectures are categorized into four groups based on their ability to control the impinging signal: hybrid, active, passive, and semi-active. With its almost passive or passive components, a PRIS can function without a dedicated power source, allowing for enormous connections with low power consumption and lower complexity. On the other hand, power amplifiers (PAs), signal processors, and RF circuits may be included in an ARIS or semi-ARIS.

The kind and resolution of each reflective element in an RIS determines how much power it uses in the main. The power consumption of passive and ARIS is intended to be lower than that of conventional alternatives like micro-BSs or relays. A novel approach for indoor and outdoor radio access networks that incorporates RIS will aid in lowering the network's power usage. In particular, RIS-assisted networks require fewer BSs to cover a given region.

RIS has been employed not only to improve system capacity but also to provide low power consumption. Additionally, RIS has been incorporated into cell-free networks to take the position of some APs [54–56]. However, because of the MFE, it is practically difficult to reach the optimum capacity improvements. RIS offers extraordinarily significant path loss in the cascaded channels. Considering this, Zhang et al. [57] have developed a novel RIS structure called ARIS, in which RF chains and PAs are arranged in conjunction with active reflecting parts to mitigate the severe fading impact. On the other hand, the ARIS uses more power and produces thermal noise and non-negligible self-interference.

Hybrid RIS architecture has been presented by Nguyen et al. [58], Yigit et al. [59], and Nguyen et al. [60], taking into account the trade-off between power consumption and the signal amplification effect. Only a few reflecting elements in this architecture are active, which results in less effective noise and transmit power than in ARIS but a much stronger signal than in full RIS. With reasonable cost and power consumption, a hybrid RIS offers a dependable and sustainable solution for wireless network architecture.

2.3 RIS Applications

The EE and beamforming capabilities inherent in RIS present substantial support for a diverse array of applications within the realms of next-generation networks. These applications span a wide range of fields, including IoT applications, communication for UAVs, smart environments, PLS, SWIPT protocols, IoT-based mobile edge computing, D2D systems, VANET, and hybrid terrestrial and satellite communication. This section provides an overview of the requirements for RIS-aided applications and prior works in this area.

2.3.1 RIS-aided IoT Applications

The IoT revolutionizes various industries by enabling innovative applications and services. Key uses include smart infrastructure management, industrial automation, smart cities, healthcare monitoring and telemedicine, smart homes, environmental monitoring and agriculture, supply chain management and logistics, and energy management [61, 62]. IoT devices enable infrastructure monitoring, optimizing production processes, and improving efficiency [63]. Smart cities connect urban systems, improving quality of life. Healthcare monitoring and telemedicine use IoT devices for remote patient monitoring and chronic disease management [64]. Smart homes can be controlled remotely via smartphone apps or voice commands. Environmental monitoring and agriculture use IoT sensors to collect data on air quality, water quality, soil moisture, weather conditions, and crop health. Supply chain management and logistics use IoT for real-time tracking and monitoring of goods. In conclusion, IoT plays a transformative role in next-generation networks, enabling innovative applications and services across various industries and improving efficiency, productivity, sustainability, and quality of life.

Figure 2.13 illustrates IoT applications that are assisted by RIS. In IoT applications, current methods relying on Wi-Fi or Bluetooth have limited connections, leading to interference, reduced throughput, and congestion when scaled up. Inadequacy in the signal coverage can result in security threats and privacy risks. IoT devices are vulnerable to harsh or outdoor environments with varying weather conditions, terrain obstacles, and EM interference. Most of the IoT devices are battery-driven. Connectivity issues arise due to limited power consumption by IoT devices during transmissions and receptions.

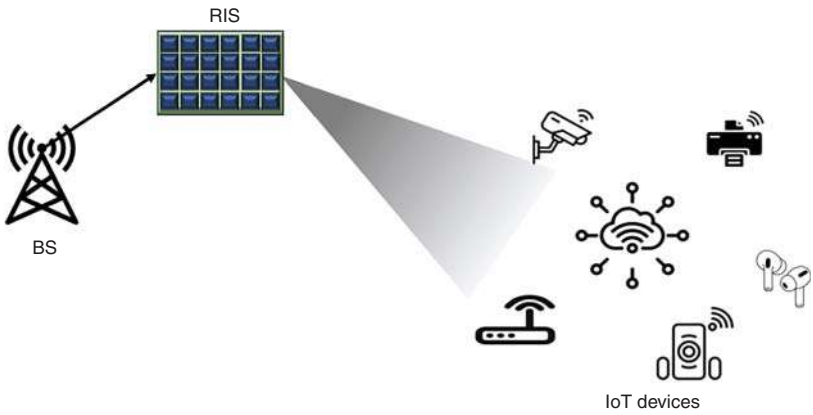

Figure 2.13 RIS-aided IoT applications.

2.3.1.1 Advantages of RIS in the IoT Applications

- **Strong connectivity**: RIS optimizes signal propagation and mitigates interference and connectivity issues, such as weak signals, dead zones, and signal blockages, which support the reliability and coverage of IoT networks [65].
- **Congestion control**: RIS dynamically controls the signal reflections and refractions, interference, and performance degradation due to congestion in IoT applications and overcome packet loss, reduced throughput, and high latency.
- **Enhanced coverage**: RIS deployment enhances signal propagation and extends coverage in IoT applications to achieve adequate coverage in specific locations. Also, RIS adaptively adjusts signal propagation and compensates for environmental effects [66].
- **Optimal power consumption**: RIS optimizes signal transmission and reception and maintains connectivity, leading to longer battery life in IoT devices.
- **Scalability and flexibility**: RIS dynamically adapts to changing network conditions and user requirements. Deploying and managing large-scale IoT deployments with RIS gives IoT solutions efficient signal optimization, scalability, and flexibility.

These highlight the importance of RIS in overcoming various challenges associated with wireless connectivity and enhancing the performance, reliability, and security of IoT applications.

In Niu et al. [67], researchers investigated secure communication in an IoT network using a combination of an ARIS-based transmitter and a PRIS in order to enhance user secrecy. This research aims to create and refine phase angle compensations, beamforming, and power allocation to maximize the weighted sum secrecy rate. Additionally, the researchers also extended the scheme to solve secrecy energy maximization problems. The results of the simulation demonstrate the effectiveness of the suggested scheme. Another work, Sagir et al. [68] discussed the usage of RISs as cooperative relay systems to enhance wireless communication performance in IoT networks. The paper presents novel cooperative RIS (CRIS) models that use deep neural networks (DNN)-CRIS in order to enhance cooperative communications and optimize the RIS phase. The authors have demonstrated that the models preserve modest system complexity and exhibit good bit error rate (BER) performance, even in high-noise conditions. Chu et al. [69] characterized the relationship between primary and cognitive networks using a Stackelberg game in cognitive IoT systems. The suggested scheme demonstrated superiority in numerical results, focusing on unlocking the potential of RISs in IoT. According to Zhang et al. [70], RIS-assisted placement is recommended for numerous IoT devices in location-based IoT services. The technique takes advantage of user-to-BS direct connection signals that

are reflected through the RIS. Propagation delay can be estimated using the triangulation-based positioning framework. By optimizing the multi-antenna BS and RIS, the total transmission power can be reduced. Numerical findings indicate that decimeter-based localization provides a considerable power gain and precision with low power consumption when compared to unoptimized RIS-assisted localization.

2.3.2 RIS-aided D2D Communication

RIS-aided D2D communication uses RIS to improve the efficiency and reliability of direct communication between devices. By optimizing signal paths, minimizing interference, and controlling reflections, this approach reduces energy consumption and latency, opening up new opportunities for proximity-based services, collaborative applications, and better connectivity in densely populated environments [71]. It enables direct communication between nearby devices without the need for an intermediate network infrastructure. However, D2D applications may face several limitations, such as limitations in usability range, poor interference, and blockage management. Most of the D2D communication depends on LoS which is practically not realizable [72].

Figure 2.14 illustrates how RIS integration with D2D communication enhances the coverage area. In this scenario, a device sends and receives information to and from another device via RIS. This suppresses the limited range, interference and signal blockage, LoS dependence, spectrum congestion, power consumption, security and privacy concerns, scalability, and reliability in conventional D2D applications. In crowded wireless environments, interference and signal blockage due to other devices or physical obstacles can be observed in D2D communication. However, enhanced RIS-aided D2D links can improve performance and connectivity, especially in urban or outdoor environments. The RIS system overcomes the issue of obstacles and obstructions encountered in traditional D2D links that are dependent on LoS. Spectrum is effectively utilized in RIS-assisted D2D links, which results in improved throughput and reduced latency.

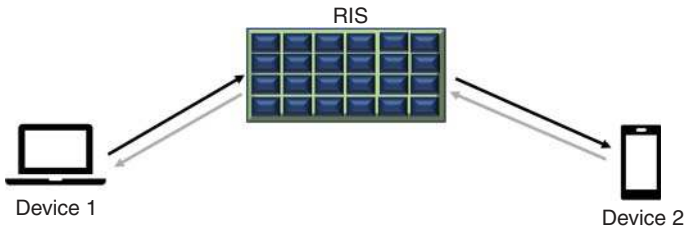

Figure 2.14 RIS-aided D2D communication.

Zhao et al. [73] use Nakagami-*m* fading to derive closed-form outage and data rate expressions for RIS-assisted D2D communication. In Zhao et al. [73], the system model discusses both the underlay and overlay modes. The theoretical expressions derived are verified using simulations. A noval active elements selection approach for a hybrid RIS-assisted D2D communication system is suggested by Mu et al. [74]. To connect to PAs and passively reflect incident signals, they selected a subset of RIS elements. The sum capacity is maximized by designing the active elements selection (AES) matrix, beamforming matrix of RIS, and D2D transmission power.

In their study, Selim and Tomasin [75] evaluate how well an RIS-aided NOMA system works for D2D transmissions. They provide approximate closed-form expressions for the outage probability of devices connected to the RIS-aided NOMA system. In addition, they calculate the ergodic data rate of each device using a fixed power allocation and verify their expressions through simulations.

An optimized sum capacity for an RIS-assisted D2D multicast system using a hypergraph is presented by Li and Zhu [76]. The maximum sum capacity is obtained by optimizing channel reuse coefficients and active and passive beamforming. A new block coordinate descent algorithm is designed, and simulation results show the suggested hypergraph method can improve sum capacity efficiently.

2.3.3 RIS-aided VANET Applications

ITS and autonomous driving are cutting-edge technologies for 6G wireless networks, enabling improved traffic effectiveness, road safety, economy of fuel usage, and daily travel management. However, the dynamic nature of wireless propagation environments, especially with fast-moving vehicles, makes transmission links unstable [10, 77, 78]. RIS can address this by improving channel conditions through intelligent signal reflections and enhancing coverage and communication efficiency. To fully utilize RISs in ITS, resource management and vehicular scheduling must be optimized. RISs can improve VANETs' coverage area and capacity in next-generation networks. However, their dynamic links are unreliable due to variable SNR and fading effects. Software-controlled configuration of reflecting surfaces provides additional control of phase shifts and reflection angles, enhancing received signal strength and removing channel fading. In Figure 2.15, RIS placement in building walls enables vehicle-to-vehicle (V2V) communication that results in highly directed beams and strengthens the connection between vehicles.

2.3.3.1 Advantages of RIS-aided VANET Applications

- The limitation in coverage and connectivity in V2V and vehicle-to-infrastructure (V2I) due to changes in topology and shadowing effect can be overcome by

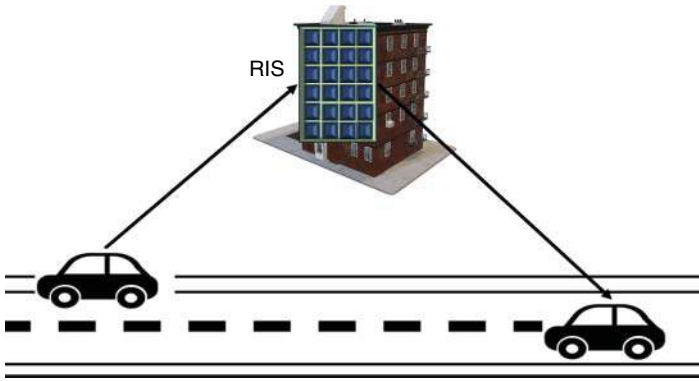

Figure 2.15 RIS-aided VANETs.

integrating RIS in the vehicle or environment. RIS-aided V2V or V2I results in large-range coverage with ubiquitous connectivity [77].

- RIS-aided VANETs are effective even under vulnerable fading channels [79]. It is more effective in multipath propagation, especially in urban canyons and areas with high-rise buildings, resulting in reliable communication links and enhanced data transmission rates.
- Effective spectrum usage is obtained with enhanced network capacity.
- RIS-aided VANETs are more flexible and scalable than the conventional VANETs. With many vehicles and diverse applications, it is easy to maintain reliable communication and efficient resources. Integration of RIS results in efficient bandwidth usage and tackles mobility issues.
- Deploying and maintaining RIS-aided infrastructure for VANETs, including roadside units (RSUs) and communication infrastructure, is cost-effective.

Integration of RIS leads to innovative solutions for VANETs, improving reliability, coverage, scalability, and efficiency through network protocols, resource management strategies, interference mitigation techniques, and security mechanisms.

A recent survey conducted by Chen et al. [80] offers extensive insight into the use of RIS technology in vehicular communication systems. The survey covers various aspects such as RIS-enabled channel modeling, beamforming techniques, resource allocation (RA) strategies, interference mitigation, etc. The article discusses practical considerations, such as hardware implementation, scalability, and regulatory challenges, associated with deploying RIS in vehicular environments. The authors also discuss the emerging applications of RIS technology, such as cooperative sensing and localization, and highlight future research directions for leveraging RIS in dynamic vehicular environments. Alsenwi et al. [81] have conducted research on the use of RIS to address the limitations in mmWave

communications. These surfaces are designed to reflect mmWave signals to vehicles that experience obstructions in direct connections. An optimization problem is formulated under stochastic obstructions to improvise the precoding matrix and RIS phase angles. The authors have developed a solution by utilizing a decomposition and relaxation-based optimization algorithm and a learning-based method. Extensive simulations have been conducted to validate the efficacy of the algorithms.

2.3.4 RIS-aided UAV Applications

In next-generation networks, UAVs will address the increasing demand for high data rates and ubiquitous connectivity. UAVs are expected to serve as airborne platforms, providing extended coverage, enhanced capacity, and faster deployment facilities in areas with limited or no existing infrastructure. With their ability to rapidly navigate and adapt to dynamic environments, UAVs will support various applications, including emergency communication, disaster recovery, surveillance, and IoT connectivity [10]. Furthermore, because of their small coverage areas, fuel efficacy, environmental vulnerabilities, and inefficient bandwidth usage, UAVs outfitted with cutting-edge communication technologies like 5GB will find it difficult to facilitate adaptable and effective network deployments. This will disrupt future networks' seamless connectivity and user experiences [82].

RIS-aided UAV applications leverage the combined capabilities of RIS and UAVs to enable a wide range of innovative functionalities and it is illustrated in Figure 2.16. In Figure 2.16, the direct link between the UAV and the BS may be weak and distorted. However, the RIS-dependent link to the UAV enables an array of reflections that provide strong and extended coverage for UAVs.

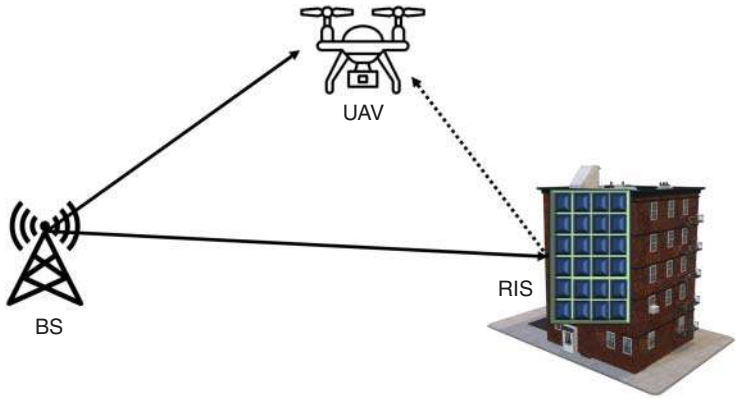

Figure 2.16 RIS-aided UAVs.

These applications encompass various domains such as wireless communication, surveillance, disaster management, agriculture, and infrastructure inspection. RIS surfaces are deployed strategically to manipulate EM waves, which helps to enhance signal coverage, improve communication reliability, and enable precise beamforming for UAVs equipped with communication or sensing payloads. By dynamically adjusting signal propagation, RIS-aided UAVs can establish and maintain connectivity in challenging environments, such as urban canyons or remote areas with limited infrastructure. RIS-aided UAVs can be useful in surveillance and monitoring tasks. They can make use of the reflective properties of RIS surfaces to extend the sensing range, thereby facilitating data collection in complex terrains or obstructed environments. By directing sensors to specific areas of interest, RIS-aided UAVs can optimize data acquisition, improving the efficiency and effectiveness of monitoring operations in agricultural applications. In conclusion, RIS-aided UAVs have the potential to address various challenges and create new opportunities across multiple sectors [83].

In Hu et al. [84], a deep learning (DL) framework for trajectory planning and jamming rejection is discussed. The algorithms offer reliable resistance against jamming and demonstrate robustness against different jammer locations. This algorithm is used to learn UAV trajectory and RIS configuration. Yang et al. [85] suggested an RIS-aided UAV scheme to enhance the coverage and performance of UAV communication systems. The RIS is deployed on a building to reflect signals from the terrestrial source to the UAV, relaying the decoded messages to the destination. The statistical distribution of the RIS-assisted terrestrial-to-areal links is modeled, analytical expressions for outage and BER are derived, and simulations validate the effectiveness of RIS integration. Yang et al. [86] investigated the efficiency of a UAV system assisted by RIS. In this configuration, the RIS is situated on the UAV to reflect signals to terrestrial users, with a specific emphasis on probability density functions (PDFs) of instantaneous SNR. The study derived analytical expressions for outage probability, average BER, and sum rate, supplementing the findings with numerical results to validate the analysis. In Abualhayja'a et al. [87], the performance limits of a multi-hop RIS-aided UAV system are analyzed. The analytical expressions for SNR, outage probability, and BER under statistical RIS channels are given. Under various fading conditions, the analysis shows that strategically placing required RIS elements can enhance UAV communications performance. RIS effectively adapts to various channels and device locations, enhancing performance in various locations.

2.3.5 RIS-aided SWIPT Protocols

SWIPT, is crucial for sustainable and energy-efficient wireless communication systems. It enables devices to decode information and collect energy from incoming

signals, improving network efficiency and battery life. SWIPT is especially important for powering sensor networks, IoT devices, and low-power devices, reducing dependency on conventional power sources and supporting applications like smart infrastructure and remote sensing [88].

Due to direct communication lines, SWIPT systems have limits with regard to power transfer, spatial coverage, and energy harvesting efficiency. Additionally, they might encounter more interference and poorer signal quality, which could undermine system dependability. Furthermore, their low adaptability in dynamic situations impedes the simultaneous optimization of information decoding and energy harvesting. Figure 2.17 illustrates the SWIPT-enabled RIS communication under blockage and provides extended coverage. Figure 2.17 describes the RIS-aided SWIPT for multiuser systems. In this scenario, users experience significant shadowing, so they rely on RIS-assisted transmission. The users harvest a portion of the energy (ψ) from the reflected signal from RIS, while the remaining energy ($1 - \psi$) is used for information decoding. The harvested energy provides extended battery usage for the users.

RIS-assisted SWIPT systems can provide advantages in wireless communication networks. With RIS integration, enhanced signal focusing, beamforming, spatial coverage, and energy harvesting efficiency can be observed. RIS's configurability allows dynamic signal reflection and refraction optimization, mitigating interference and improving signal quality. RIS-assisted SWIPT systems also enable adaptability in dynamic environments, optimizing information decoding and energy harvesting, contributing to network efficiency and sustainability.

In Zhang et al. [89], RIS-aided SWIPT networks with rate-splitting multiple access (RSMA) are explored. It suggests a deep reinforcement learning-based approach for optimizing power allocation and discrete phase shifts. This approach outperforms traditional SWIPT-only methods and enhances energy and information transmission. Simulation results show the suggested system achieves enhanced energy EE with RSMA. The application of RIS in SWIPT with

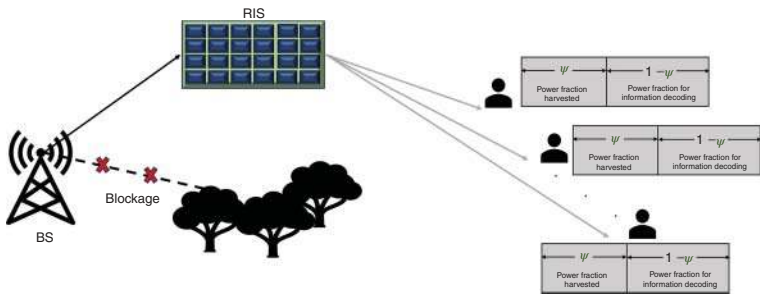

Figure 2.17 RIS-aided SWIPT.

multi-antenna AP systems is discussed by Yang and Zhang [90]. By employing sorting and iterative optimization methods to simplify the objective function, the authors developed two solutions for optimal and nonideal channels. They effectively resolve the issue under ideal boundary and Karush–Kuhn–Tucker conditions, demonstrating a potential method for next-generation networks. Yaswanth et al. [91] explore an ARIS framework for improving SWIPT system performance under imperfect channel conditions. It suggests that joint beamforming design can reduce transmit power by ∼60% compared to PRIS while maintaining QoS requirements, and it is validated using simulations.

The study by Yaswanth et al. [92] addressed the SWIPT-enabled RIS-assisted MIMO communication network, emphasizing active and passive beaming optimization matrix and power reduction. It suggests computationally efficient algorithms and uses mean square error and alternating optimization techniques to simplify the problem. The impact of imperfect channel conditions is also discussed.

2.4 Challenges and Research Trends

RIS introduces several kinds of challenges that need to be addressed according to the service demands of users. This section outlines critical prospects for future research that are essential to realizing the full potential of RISs in 6G networks.

2.4.1 RIS-aided THz Communication

With its ultrawide bandwidth, THz communication is considered a potential option for 6G communication. However, due to its ultrahigh frequency, THz transmission may experience significant signal distortion and communication disruptions, affecting coverage performance. To address this issue, RIS can be applied to THz communication, which can help improve coverage performance. However, significant challenges associated with RIS-assisted THz communication need to be addressed to fully utilize the special THz propagation features in the RIS-assisted network.

2.4.2 Aerial RIS-aided System

An airborne RIS carried by a UAV or a balloon can provide full-space reflections, enabling it to serve a comparatively higher number of users than a ground RIS fixed at a site [82]. The aerial RIS is less susceptible to blockages and can benefit from LoS channel conditions. The high mobile UAVs can further expand the coverage of the aerial RIS. However, the aerial RIS presents other challenges, such as 3D positioning and channel estimation, that must be addressed.

2.4.3 RIS-assisted PLS

The RIS can improve PLS by manipulating the signal. This is done by simultaneously enhancing the signal beam directed toward the intended user and suppressing the beam directed toward the undesired user. However, obtaining accurate channel information from an interferer to the RIS and the BS in real-world scenarios is challenging. Therefore, a complex channel information and beamforming design is required for RIS-aided PLS under imprecise channel state information.

2.4.4 RIS-aided Optical Wireless Communication

Optical wireless communication (OWC) is a cost-effective option for high data rate applications in the next generation, thanks to its comparatively less hardware complexity. However, it requires LoS between the transceivers to function properly. To address this issue, RIS can be used to guide the optical beam in the right direction, thus reducing LoS obstructions. By integrating RIS and OWC, it becomes possible to enable a wide range of applications for both indoor and outdoor environments.

2.4.5 RIS-assisted mMIMO Network

MIMO technology has been extended to mMIMO, which helps to increase SE and transmission gain significantly. However, the main hurdles in the practical deployment of mMIMO systems are their high power and hardware costs. To overcome these challenges, RIS can be integrated with mMIMO to achieve the necessary performance improvements in an economical and energy-efficient way. For optimal performance, it is essential to investigate low-complexity methods for beamforming and RA for RIS-aided mMIMO systems.

2.4.6 Joint Optimization of the Number of Elements and Phase Shifts

The number of elements and the phase shifts control the beamforming of reflected signals. Optimizing these parameters minimizes system energy consumption, aligning with sustainable wireless concepts. Due to the larger elements, channel coefficients increase significantly. This results in path diversity, but it is challenging to select the optimal channel and estimate it accurately in this scenario.

2.4.7 Optimal Deployment of RIS

Deploying a meta-surface in a proper location is also considered a bottleneck, especially in the system, where multiple obstacles are present. It is treated

as a primary concern in mmWave applications where LoS communication plays a major role. Placing multiple RISs in a multi-hop signal propagation scenario increases beam-routing complexity. Most research considers this to be a multi-objective optimization problem. The investigation of the size and arrangement of elements within an RIS constitutes a research direction that holds significance in communication scenarios characterized by constrained spaces, such as pipes or tunnels. Researchers use the ray tracing method to identify the propagation mechanism of RIS and for multi-hop beam-routing. Transparent ARIS (TARIS) is an evolving work that boosts the aesthetics of the environment.

2.4.8 Selection of Type of RIS

The research trends in RIS show rapid advancements in every dimension. Element with a dynamic role as either active or passive is one among them; PRIS only reflects the signal where as ARIS amplifies and reflects the signal. This dual nature provides the freedom of mode selection and results in an energy-efficient system [93, 94]. Simultaneous transmission and reflection RIS (STAR–RIS) is one of the primary research areas focusing on coverage improvement [95, 96]. Programmable RIS is another research area where RIS can adaptively decide signals' reflection angle and beam-routing.

2.5 Conclusions

Emerging applications and potential use cases of RIS in wireless communication systems are explored in this chapter. Various use cases are discussed in detail. Integration of RIS with the existing communication chain is easily realizable and results in extended coverage; the large RIS elements on the surface produce highly focused beams in which the phase angles are controlled. The significance of energy-focusing and energy-nulling characteristics of RIS is highlighted based on the desired and interfering user. The description of EE enhancement with RIS is given, and the EMF exposure reduction using RIS is detailed. The key features of RIS that support 6G applications, such as PLS, localization accuracy, and EE cell-free networks are discussed in detail. Furthermore, the significant applications such as IoT networks, UAV communication, D2D, and VANET are discussed, and the significance of the integration of RIS with the existing applications is highlighted. Finally, the chapter is directed to the research trends and challenges associated with the various technologies, such as mMIMO, THz communication, OWC, etc. Based on the requirements and applications, the selection of PRIS, ARIS, and STAR–RIS deployment is suggested in the chapter.

References

1 Das, S.K., Benkhelifa, F., Sun, Y. et al. (2023). Comprehensive review on ml-based RIS-enhanced IoT systems: basics, research progress and future challenges. *Computer Networks* 224: 109581.

2 Khalid, W., Rehman, M.A.U., Van Chien, T. et al. (2023). Reconfigurable intelligent surface for physical layer security in 6G-IoT: designs, issues, and advances. *IEEE Internet of Things Journal* 11 (2): 3599–3613.

3 Wang, C.-X., You, X., Gao, X. et al. (2023). On the road to 6G: visions, requirements, key technologies and testbeds. *IEEE Communications Surveys & Tutorials* 25 (2): 905–974.

4 Sang, J., Yuan, Y., Tang, W. et al. (2022). Coverage enhancement by deploying RIS in 5G commercial mobile networks: field trials. *IEEE Wireless Communications* 31 (1): 172–180.

5 Savkin, A.V., Huang, C., and Ni, W. (2022). On-demand deployment of aerial base stations for coverage enhancement in reconfigurable intelligent surface-assisted cellular networks on uneven terrains. *IEEE Communications Letters* 27 (2): 666–670.

6 Nemati, M., Park, J., and Choi, J. (2020). RIS-assisted coverage enhancement in millimeter-wave cellular networks. *IEEE Access* 8: 188171–188185.

7 Tapio, V., Shojaeifard, A., Hemadeh, I. et al. (2021). Reconfigurable intelligent surface for 5G NR uplink coverage enhancement. *2021 IEEE 94th Vehicular Technology Conference (VTC2021-Fall)*, 1–5. IEEE.

8 Zeng, S., Zhang, H., Di, B. et al. (2020). Reconfigurable intelligent surface (RIS) assisted wireless coverage extension: RIS orientation and location optimization. *IEEE Communications Letters* 25 (1): 269–273.

9 da Silva Brilhante, D., Manjarres, J.C., Moreira, R. et al. (2023). A literature survey on AI-aided beamforming and beam management for 5G and 6G systems. *Sensors* 23 (9): 4359. https://doi.org/10.3390/s23094359.

10 Evangeline, S., Lenin, A., and Kumaravelu, V.B. (2023). Blockchain system for secure and efficient UAV-to-vehicle communication in smart cities. *International Journal of Electronics and Telecommunications* 69 (1): 133–138.

11 Chen, Y., Tan, J., Hao, M. et al. (2023). Accurate beam training for RIS-assisted wideband terahertz communication. *IEEE Transactions on Communications* 71 (12): 7425–7440.

12 Rahal, M., Denis, B., Keykhosravi, K. et al. (2023). Performance of RIS-aided near-field localization under beams approximation from real hardware characterization. *EURASIP Journal on Wireless Communications and Networking* 2023 (1): 86.

13 Sankar, R.S.P., Chepuri, S.P., and Eldar, Y.C. (2023). Beamforming in integrated sensing and communication systems with reconfigurable intelligent surfaces. *IEEE Transactions on Wireless Communications* 23 (5): 4017–4031.

14 Jiang, S., Hindy, A., and Alkhateeb, A. (2023). Sensing aided reconfigurable intelligent surfaces for 3GPP 5G transparent operation. *IEEE Transactions on Communications* 71 (11): 6348–6362.

15 Van Nguyen, M.-S., Do, D.-T., Tin, P.T. et al. (2024). Full duplex reconfigurable intelligent surfaces system relying on NOMA and wireless power transfer. *Wireless Networks* 30 (4): 1–16.

16 Kumaravelu, V.B., Imoize, A.L., Castillo Soria, F.R. et al. (2023). RIS-assisted fixed NOMA: outage probability analysis and transmit power optimization. *Future Internet* 15 (8): 249.

17 Abeywickrama, S., Zhang, R., Wu, Q., and Yuen, C. (2020). Intelligent reflecting surface: practical phase shift model and beamforming optimization. *IEEE Transactions on Communications* 68 (9): 5849–5863.

18 Fang, F., Xu, Y., Pham, Q.-V., and Ding, Z. (2020). Energy-efficient design of IRS-NOMA networks. *IEEE Transactions on Vehicular Technology* 69 (11): 14088–14092.

19 Zeng, M., Li, X., Li, G. et al. (2020). Sum rate maximization for IRS-assisted uplink NOMA. *IEEE Communications Letters* 25 (1): 234–238.

20 Yu, X., Xu, D., and Schober, R. (2019). MISO wireless communication systems via intelligent reflecting surfaces. *2019 IEEE/CIC International Conference on Communications in China (ICCC)*, 735–740. IEEE.

21 Katwe, M., Singh, K., Sharma, P.K. et al. (2021). Dynamic user clustering and optimal power allocation in UAV-assisted full-duplex hybrid NOMA system. *IEEE Transactions on Wireless Communications* 21 (4): 2573–2590.

22 Singh, S.K., Agrawal, K., Singh, K. et al. (2022). NOMA enhanced hybrid RIS-UAV-assisted full-duplex communication system with imperfect SIC and CSI. *IEEE Transactions on Communications* 70 (11): 7609–7627.

23 Velmurugan, P.G.S., Thiruvengadam, S.J., Kumaravelu, V.B. et al. (2023). Performance analysis of full duplex bidirectional machine type communication system using IRS with discrete phase shifter. *Applied Sciences* 13 (12): 7128.

24 Di Renzo, M., Ntontin, K., Song, J. et al. (2020). Reconfigurable intelligent surfaces vs. relaying: differences, similarities, and performance comparison. *IEEE Open Journal of the Communications Society* 1: 798–807.

25 Ntontin, K., Boulogeorgos, A.-A.A., Björnson, E. et al. (2022). Autonomous reconfigurable intelligent surfaces through wireless energy harvesting. *2022 IEEE 95th Vehicular Technology Conference:(VTC2022-Spring)*, 1–6. IEEE.

26 Ma, H., Zhang, H., Zhang, N. et al. (2022). Reconfigurable intelligent surface with energy harvesting assisted cooperative ambient backscatter communications. *IEEE Wireless Communications Letters* 11 (6): 1283–1287.

27 Ahmed, S., Kamal, A.E., and Selim, M.Y. (2021). Adding active elements to reconfigurable intelligent surfaces to enhance energy harvesting for IoT devices. *MILCOM 2021-2021 IEEE Military Communications Conference (MILCOM)*, 297–302. IEEE.

28 Ren, H., Chen, Z., Hu, G. et al. (2023). Transmission design for active RIS-aided simultaneous wireless information and power transfer. *IEEE Wireless Communications Letters* 12 (4): 600–604.

29 Ren, H., Zhang, Z., Peng, Z. et al. (2022). Energy minimization in RIS-assisted UAV-enabled wireless power transfer systems. *IEEE Internet of Things Journal* 10 (7): 5794–5809.

30 Yin, B., Joseph, W., and Deruyck, M. (2023). RIS-aided mmWave network planning towards connectivity enhancement and minimal electromagnetic field exposure. *IEEE Access* 11: 115911–115923.

31 Murugadass, A. and Pachiyappan, A. (2017). Fuzzy logic based coverage and cost effective placement of serving nodes for 4G and beyond cellular networks. *Wireless Communications and Mobile Computing* 2017 (1): 8086204.

32 Zhou, G., Pan, C., Ren, H. et al. (2021). Secure wireless communication in RIS-aided MISO system with hardware impairments. *IEEE Wireless Communications Letters* 10 (6): 1309–1313.

33 Yu, X., Xu, D., Sun, Y. et al. (2020). Robust and secure wireless communications via intelligent reflecting surfaces. *IEEE Journal on Selected Areas in Communications* 38 (11): 2637–2652.

34 Cui, M., Zhang, G., and Zhang, R. (2019). Secure wireless communication via intelligent reflecting surface. *IEEE Wireless Communications Letters* 8 (5): 1410–1414.

35 Guan, X., Wu, Q., and Zhang, R. (2020). Intelligent reflecting surface assisted secrecy communication: is artificial noise helpful or not? *IEEE Wireless Communications Letters* 9 (6): 778–782.

36 Feng, B., Wu, Y., Zheng, M. et al. (2020). Large intelligent surface aided physical layer security transmission. *IEEE Transactions on Signal Processing* 68: 5276–5291.

37 Gu, X., Duan, W., Zhang, G. et al. (2022). Physical layer security for RIS-aided wireless communications with uncertain eavesdropper distributions. *IEEE Systems Journal* 17 (1): 848–859.

38 Han, Y., Li, N., Liu, Y. et al. (2022). Artificial noise aided secure NOMA communications in STAR-RIS networks. *IEEE Wireless Communications Letters* 11 (6): 1191–1195.

39 Sun, Y., An, K., Zhu, Y. et al. (2022). Energy-efficient hybrid beamforming for multilayer RIS-assisted secure integrated terrestrial-aerial networks. *IEEE Transactions on Communications* 70 (6): 4189–4210.

40 Thien, H.T., Tuan, P.-V., and Koo, I. (2022). A secure-transmission maximization scheme for SWIPT systems assisted by an intelligent reflecting surface and deep learning. *IEEE Access* 10: 31851–31867.

41 Wang, W., Liu, X., Tang, J. et al. (2021). Beamforming and jamming optimization for IRS-aided secure NOMA networks. *IEEE Transactions on Wireless Communications* 21 (3): 1557–1569.

42 Xu, S., Liu, J., and Cao, Y. (2021). Intelligent reflecting surface empowered physical-layer security: signal cancellation or jamming? *IEEE Internet of Things Journal* 9 (2): 1265–1275.

43 Elzanaty, A., Guerra, A., Guidi, F., and Alouini, M.-S. (2021). Reconfigurable intelligent surfaces for localization: position and orientation error bounds. *IEEE Transactions on Signal Processing* 69: 5386–5402.

44 Zhang, H., Hu, J., Zhang, H. et al. (2020). MetaRadar: indoor localization by reconfigurable metamaterials. *IEEE Transactions on Mobile Computing* 21 (8): 2895–2908.

45 Wymeersch, H. and Denis, B. (2020). Beyond 5G wireless localization with reconfigurable intelligent surfaces. *ICC 2020-2020 IEEE International Conference on Communications (ICC)*, 1–6. IEEE.

46 Hu, J., Zhang, H., Di, B. et al. (2020). Reconfigurable intelligent surface based RF sensing: design, optimization, and implementation. *IEEE Journal on Selected Areas in Communications* 38 (11): 2700–2716.

47 Abu-Shaban, Z., Keykhosravi, K., Keskin, M.F. et al. (2021). Near-field localization with a reconfigurable intelligent surface acting as lens. *ICC 2021-IEEE International Conference on Communications*, 1–6. IEEE.

48 Alegría, J.V. and Rusek, F. (2019). Cramér-Rao lower bounds for positioning with large intelligent surfaces using quantized amplitude and phase. *2019 53rd Asilomar Conference on Signals, Systems, and Computers*, 10–14. IEEE.

49 Hu, S., Rusek, F., and Edfors, O. (2018). Beyond massive MIMO: the potential of positioning with large intelligent surfaces. *IEEE Transactions on Signal Processing* 66 (7): 1761–1774.

50 Nayebi, E., Ashikhmin, A., Marzetta, T.L., and Yang, H. (2015). Cell-free massive MIMO systems. *2015 49th Asilomar Conference on Signals, Systems and Computers*, 695–699. IEEE.

51 Giordani, M., Polese, M., Mezzavilla, M. et al. (2020). Toward 6G networks: use cases and technologies. *IEEE Communications Magazine* 58 (3): 55–61.

52 Huang, C., Zappone, A., Alexandropoulos, G.C. et al. (2019). Reconfigurable intelligent surfaces for energy efficiency in wireless communication. *IEEE Transactions on Wireless Communications* 18 (8): 4157–4170.

53 Yang, Z., Chen, M., Saad, W. et al. (2021). Energy-efficient wireless communications with distributed reconfigurable intelligent surfaces. *IEEE Transactions on Wireless Communications* 21 (1): 665–679.

54 Zhang, Y., Di, B., Zhang, H. et al. (2021). Beyond cell-free MIMO: energy efficient reconfigurable intelligent surface aided cell-free MIMO communications. *IEEE Transactions on Cognitive Communications and Networking* 7 (2): 412–426.

55 Al-Nahhas, B., Obeed, M., Chaaban, A., and Hossain, M.J. (2021). RIS-aided cell-free massive MIMO: performance analysis and competitiveness. *2021 IEEE International Conference on Communications Workshops (ICC Workshops)*, 1–6. IEEE.

56 Zhang, Z. and Dai, L. (2021). A joint precoding framework for wideband reconfigurable intelligent surface-aided cell-free network. *IEEE Transactions on Signal Processing* 69: 4085–4101.

57 Zhang, Z., Dai, L., Chen, X. et al. (2022). Active RIS vs. passive RIS: which will prevail in 6G? *IEEE Transactions on Communications* 71 (3): 1707–1725.

58 Nguyen, N.T., Vu, Q.-D., Lee, K., and Juntti, M. (2022). Hybrid relay-reflecting intelligent surface-assisted wireless communications. *IEEE Transactions on Vehicular Technology* 71 (6): 6228–6244.

59 Yigit, Z., Basar, E., Wen, M., and Altunbas, I. (2022). Hybrid reflection modulation. *IEEE Transactions on Wireless Communications* 22 (6): 4106–4116.

60 Nguyen, N.T., Vu, Q.-D., Lee, K., and Juntti, M. (2021). Spectral efficiency optimization for hybrid relay-reflecting intelligent surface. *2021 IEEE International Conference on Communications Workshops (ICC Workshops)*, 1–6. IEEE.

61 John, A., Rajput, A., and Babu, K.V. (2017). Energy saving cluster head selection in wireless sensor networks for Internet of Things applications. *2017 International Conference on Communication and Signal Processing (ICCSP)*, 0034–0038. IEEE.

62 Rajput, A. and Kumaravelu, V.B. (2019). Scalable and sustainable wireless sensor networks for agricultural application of Internet of Things using fuzzy c-means algorithm. *Sustainable Computing: Informatics and Systems* 22: 62–74.

63 Ramaneti, K., Mohanty, N., and Kumaravelu, V.B. (2021). IoT based 2D indoor navigation system using BLE beacons and Dijkstra's algorithm. *2021 12th International Conference on Computing Communication and Networking Technologies (ICCCNT)*, 1–6. IEEE.

64 Selvaprabhu, P., Chinnadurai, S., Tamilarasan, I. et al. (2022). Priority-based resource allocation and energy harvesting for WBAN smart health. *Wireless Communications and Mobile Computing* 2022 (1): 8294149.

65 Tekbıyık, K., Kurt, G.K., and Yanikomeroglu, H. (2021). Energy-efficient RIS-assisted satellites for IoT networks. *IEEE Internet of Things Journal* 9 (16): 14891–14899.

66 Hassouna, S., Jamshed, M.A., Rains, J. et al. (2023). A survey on reconfigurable intelligent surfaces: wireless communication perspective. *IET Communications* 17 (5): 497–537.

67 Niu, H., Lin, Z., Chu, Z. et al. (2022). Joint beamforming design for secure RIS-assisted IoT networks. *IEEE Internet of Things Journal* 10 (2): 1628–1641.

68 Sagir, B., Aydin, E., and Ilhan, H. (2023). Deep-learning assisted IoT based RIS for cooperative communications. *IEEE Internet of Things Journal* 10 (12): 10471–10483.

69 Chu, Z., Xiao, P., Mi, D. et al. (2020). Intelligent reflecting surfaces enabled cognitive Internet of Things based on practical pathloss model. *China Communications* 17 (12): 1–16.

70 Zhang, J., Zheng, Z., Fei, Z., and Han, Z. (2022). Energy-efficient multiuser localization in the RIS-assisted IoT networks. *IEEE Internet of Things Journal* 9 (20): 20651–20665.

71 Subramani, M., Kumaravelu, V.B., and Murugadass, A. (2021). Fuzzy logic-based handover requirement analysis and access network selection for device-to-device communication. *Journal of Circuits, Systems and Computers* 30 (01): 2150009.

72 Subramani, M. and Kumaravelu, V.B. (2020). A fuzzy based vertical handover network selection scheme. *Indonesian Journal of Electrical Engineering and Computer Science* 17 (1): 324–330.

73 Zhao, H., Liu, Y., Ni, Y. et al. (2023). Performance analysis of RIS-assisted D2D communication under Nakagami-m fading. *IEEE Transactions on Vehicular Technology* 73 (1): 1447–1452.

74 Mu, G., Zhang, P., Hou, Y. et al. (2023). Efficient active elements selection algorithm for hybrid RIS-assisted D2D communication system. *IEEE Communications Letters* 28 (2): 377–381.

75 Selim, M.M. and Tomasin, S. (2024). Performance analysis of RIS-assisted downlink NOMA wireless systems under D2D interference. *Digital Signal Processing* 144: 104269.

76 Li, J. and Zhu, X. (2024). Sum-rate optimization algorithms for RIS aided D2D multicast system based on hypergraph. *IEEE Wireless Communications Letters* 13 (5): 1330–1334.

77 Evangeline, C.S. and Kumaravelu, V.B. (2022). A two-phase fuzzy based access network selection scheme for vehicular ad hoc networks. *Peer-to-Peer Networking and Applications* 15 (1): 107–133.

78 Rajak, S., Muniraj, I., Selvaprabhu, P. et al. (2023). A novel energy efficient IRS-relay network for ITS with Nakagami-m fading channels. *ICT Express* 10 (3): 507–512.

79 Kumaravelu, V.B., Selvaprabhu, P., Han, D.S. et al. (2023). Blind reconfigurable intelligent surface-aided fixed non-orthogonal multiple access for intelligent

vehicular networks. *EURASIP Journal on Wireless Communications and Networking* 2023 (1): 83.

80 Chen, Y., Wang, Y., Zhang, J. et al. (2022). Reconfigurable intelligent surface (RIS)-aided vehicular networks: their protocols, resource allocation, and performance. *IEEE Vehicular Technology Magazine* 17 (2): 26–36.

81 Alsenwi, M., Abolhasan, M., and Lipman, J. (2022). Intelligent and reliable millimeter wave communications for RIS-aided vehicular networks. *IEEE Transactions on Intelligent Transportation Systems* 23 (11): 21582–21592.

82 Kumaravelu, V.B., Jadhav, H.K., BS, A. et al. (2022). Unmanned aerial vehicle-assisted reconfigurable intelligent surface for energy efficient and reliable communication. In: *Unmanned Aerial Vehicle Cellular Communications* (ed. A.L. Imoize, S.M.N. Islam, T. Poongodi, et al.), 173–201. Cham: Springer International Publishing. https://doi.org/10.1007/978-3-031-08395-2_8.

83 Pogaku, A.C., Do, D.-T., Lee, B.M., and Nguyen, N.D. (2022). UAV-assisted RIS for future wireless communications: a survey on optimization and performance analysis. *IEEE Access* 10: 16320–16336.

84 Hu, S., Yuan, X., Ni, W. et al. (2023). RIS-assisted jamming rejection and path planning for UAV-borne IoT platform: a new deep reinforcement learning framework. *IEEE Internet of Things Journal* 10 (22): 20162–20173.

85 Yang, L., Meng, F., Zhang, J. et al. (2020). On the performance of RIS-assisted dual-hop UAV communication systems. *IEEE Transactions on Vehicular Technology* 69 (9): 10385–10390.

86 Yang, L., Li, P., Meng, F., and Yu, S. (2022). Performance analysis of RIS-assisted UAV communication systems. *IEEE Transactions on Vehicular Technology* 71 (8): 9078–9082.

87 Abualhayja'a, M., Centeno, A., Mohjazi, L. et al. (2023). Exploiting multi-hop RIS-assisted UAV communications: performance analysis. *IEEE Communications Letters* 28 (1): 133–137.

88 Zhang, G., Lu, Y., Lin, Y. et al. (2023). AoI minimization in RIS-aided SWIPT systems. *IEEE Transactions on Vehicular Technology* 73 (2): 2895–2900.

89 Zhang, R., Xiong, K., Lu, Y. et al. (2023). Energy efficiency maximization in RIS-assisted SWIPT networks with RSMA: a PPO-based approach. *IEEE Journal on Selected Areas in Communications* 41 (5): 1413–1430.

90 Yang, Z. and Zhang, Y. (2021). Optimal SWIPT in RIS-aided MIMO networks. *IEEE Access* 9: 112552–112560.

91 Yaswanth, J., Katwe, M., Singh, K. et al. (2023). Robust beamforming design for active-RIS aided MIMO SWIPT communication system: a power minimization approach. *IEEE Transactions on Wireless Communications* 23 (5): 4767–4785.

92 Yaswanth, J., Singh, S.K., Singh, K., and Flanagan, M.F. (2023). Energy-efficient beamforming design for RIS-aided MIMO downlink communication with SWIPT. *IEEE Transactions on Green Communications and Networking* 7 (3): 1164–1180.

93 Liao, C., Wang, F., Han, G. et al. (2023). Beamforming design for hybrid active-passive RIS assisted integrated sensing and communications. *IEEE Communications Letters* 27 (11): 2938–2942.

94 Rihan, M., Zappone, A., Buzzi, S. et al. (2023). Passive vs. active reconfigurable intelligent surfaces for integrated sensing and communication: challenges and opportunities. *IEEE Network* 38 (3): 218–226.

95 Liu, Z., Li, X., Ji, H. et al. (2023). Toward STAR-RIS-empowered integrated sensing and communications: joint active and passive beamforming design. *IEEE Transactions on Vehicular Technology* 72 (12): 15991–16005.

96 Papazafeiropoulos, A., Ge, H., Kourtessis, P. et al. (2024). Two-timescale design for active STAR-RIS aided massive MIMO systems. *IEEE Transactions on Vehicular Technology* 73 (7): 10118–10134.

3

Reconfigurable Intelligent Surfaces for 6G: A Comprehensive Overview and Electromagnetic Analysis

Suganthi Evangeline Chakkaravarthy[1], Dipinkrishnan Rayaroth[2], Vinoth Babu Kumaravelu[2], Thiruvengadam Sundarrajan Jayaraman[3], Velmurugan Periyakarupan Gurusamy Sivabalan[3], Vetrivel Chelian Thirumavalavan[4], Rajeshkumar Venkatesan[2], Arthi Murugadass[5], and Agbotiname Lucky Imoize[6,7]

[1] *Department of Electronics and Communication Engineering, Sri Eshwar College of Engineering, Coimbatore, Tamil Nadu, India*
[2] *Department of Communication Engineering, School of Electronics Engineering, Vellore Institute of Technology, Vellore, Tamil Nadu, India*
[3] *Department of Electronics and Communication Engineering, Thiagarajar College of Engineering, Madurai, Tamil Nadu, India*
[4] *Nokia Mobile Networks, Bangalore, Karnataka, India*
[5] *School of Computer Science and Engineering, Vellore Institute of Technology, Chennai, Tamil Nadu, India*
[6] *Department of Electrical and Electronics Engineering, Faculty of Engineering, University of Lagos, Akoka, Lagos, Nigeria*
[7] *Department of Electrical Engineering and Information Technology, Ruhr University, Bochum, Germany*

3.1 Introduction

Global use of fifth-generation (5G) networks, which are engineered to satisfy international mobile telecommunications (IMT)-2020 requirements, is increasing. High-performance networks with distributed intelligence to the edge and end-to-end automated coordination to meet individual user needs are now possible thanks to a combination of new network capabilities associated with the 5G core, an advanced wireless system built upon the 5G-new radio (NR) interface, and a new architecture utilizing cloud-native approach [1]. The goal of 5G's evolution and many of its characteristics is to make 5G networks future-proof as the industry moves forward and research into potential sixth-generation (6G) systems is being conducted worldwide. The key requirements for 6G are a higher data rate of 1 TB/s with a peak spectral efficiency of 60 b/s/Hz. It also should encompass ubiquitous 3D coverage, resilience, security, and sustainability.

Reconfigurable Intelligent Surfaces for 6G and Beyond Wireless Networks, First Edition.
Edited by Agbotiname Lucky Imoize, Vinoth Babu Kumaravelu, and Dinh-Thuan Do.

Many interesting technologies have the potential to enable 6G. One such technology is reconfigurable intelligent surfaces (RISs), which aims to partially control the channel for better coverage and data rate gains. RIS is a two-dimensional grid of antennas/reflectors which are reconfigurable in nature. The RIS controller controls the RIS antennas/reflectors. The RIS system is almost passive (i.e., the signal is not amplified or regenerated); the only power consumed is the one by the RIS controller. The RIS system increases coverage, and it can be placed on building facades, billboards, underground ceilings, train stations, and airports [2–6].

RISs are a promising hardware-based transmission technique that has the potential to artificially alter wireless propagation environments. Several discrete, flexible parts implanted on a flat surface, each with sub-wavelength dimensions, reflect incident electromagnetic (EM) waves. The RIS uses an intelligent RIS controller to modify the signal phases and/or amplitudes, increasing the degrees of freedom (DoF) of wireless channels, improving signal propagation, and enabling sophisticated wireless functions [7–9]. Section 3.2 delves into an in-depth exploration of RIS, offering a comprehensive overview of its functionality and capabilities.

3.1.1 Related Work

RIS introduces an innovative method to enhance signal quality within tunnels and pipes, particularly in the presence of obstacles, making it a pivotal solution in this domain [10]. The authors suggest using RIS in tunnels to counter the ray-blocking issue caused by obstacles. The closed-form expression of blocking probability with single and multiple RIS is derived. The number of elements and placement points of RIS are iteratively changed, and the corresponding blocking probability is plotted. The results are analyzed for multiple obstacle scenarios, showcasing the unique superiority of the suggested model over the scheme without the RIS.

Mei and Zhang [11] suggested a distributed model for beam training that carries significant practical implications. This model enhances the end-to-end gain for active RIS (ARIS) and passive RIS (PRIS)-based systems with a multi-hop routing approach. By strategically placing ARIS and PRIS in multiple locations in a system with obstacles, path diversity is provided. The suggested cooperative beamforming model addresses the challenge of dealing with many channel coefficients, and a routing control approach has been adapted to optimize the channel selection, making it a highly relevant solution for real-world scenarios.

Zheng et al. [12] suggested a channel estimation scheme in a multiuser multiple input-multiple output (MIMO) system embedded with two RIS arrays. They employ a rigorous methodology where the mean squared error (MSE) corresponding to the system's transmit power and phase is analyzed for different reflection models. The system's performance is then evaluated, providing a robust

and reliable assessment of the suggested model. Addressing the hurdle of attaining the necessary data rates for users, especially given the constraints imposed by the quantity of RIS elements and the power levels achieved via amplification by ARIS, presents a formidable challenge. In Fu and Zhang [13], the authors focused on improving user rates by strategically placing ARIS and PRIS between a single transmitter and a receiver which is particularly noteworthy. The optimal positioning of ARIS, determined to achieve a design with minimum complexity, yielded compelling results. The study found that even with lower power levels of amplification (less than ∼12 dBm) placing ARIS between the transmitter and PRIS led to superior performance.

The PRIS phenomenon causes a double path loss due to an additional reflection point in the network. This leads to weaker signal strength, higher power consumption, and lower energy efficiency (EE). Peng et al. [14] introduced an ARIS solution to mitigate this problem in a mobile edge computing (MEC) network. The suggested method optimizes the reflection parameter, complexity of computation, and resource allocation scheme to improve latency. The performance improvement is measured by comparing the usage of PRIS and ARIS.

The role of ARIS in signal amplification, while leading to a marginal increase in energy utilization, is a crucial aspect to consider. In Ma et al. [15], the authors' introduction of an innovative optimization approach to circumvent the adverse effect on EE is particularly noteworthy. The derivation of a reflection matrix by introducing ARIS in the system, where beamforming and EE are included for forming the optimization problem, represents a novel approach. The complexity of the suggested procedure is further reduced by introducing a quadratic transform method in the defined fractional transform approach. The iterative approach investigated the EE of the system corresponding to user location and power, and the results surpassed those of conventional approaches, highlighting the potential impact of this research.

Signal attenuation in a simultaneous wireless information and power transfer (SWIPT) system is addressed by Gao et al. [16], and the deployment of ARIS is utilized to mitigate the path loss. An optimization algorithm is introduced for sum rate maximization through ARIS positioning and phase shift control. Chen [17] discussed RIS-aided system, in which the elements can act either in a passive or active mode according to user demand. The suggested work with a minimum power budget achieves a marginal increase in EE. The phase shift, mode, and beamforming introduced by RIS are considered together for optimization, which uses a cross-entropy approach based on probability learning.

The introduction of RIS in millimeter wave (mmWave)-based wireless systems for vehicular communication is discussed by Alsenwi et al. [18]. Obstacles in the network marginally degrade the signals of this application, which can be mitigated by controlling the phase shifts of the reflected signals. An optimization

framework for precoding and the dynamic tuning of phase shifts are performed using a learning method. The suggested method improves the data rate and reliability, which is analyzed using simulation results. Zeng et al. [19] introduced a fairness-guaranteed ARIS-aided wireless power transfer (WPT) system by developing an optimization framework for sum-throughput enhancement. Different beamforming methods are adapted to optimize the trade-off between fairness and complexity. The suggested system gains marginal improvement in EE and coverage compared to PRIS-based systems.

In mmWave applications, user devices often face severe path loss in indoor environments due to the limited available power budget. Feng and Zhao [20] suggested a solution to this problem by using transparent ARIS (TARIS) made of glass material in the mmWave system. TARIS can be placed as doors or windows, improving both the aesthetics and achievable rate of the system. Results show that the TARIS scheme provides a slight improvement in EE compared to PRIS.

The application of RIS in a cell-free network is studied by Wang and Peng [21]. The multiplicative fading effect (MFE) is a challenge faced in the network when introducing RIS. It is resolved by replacing it with ARIS. The system enhances EE by optimizing beamforming and power allocation. The result shows that the work successfully enhances the EE of the user even with poor channel conditions. Mei et al. [22] suggested a resource allocation optimization approach for multiple RIS-based WPT systems. The dynamic method for beam routing reduces the required power budget. In Li et al. [23], the ray tracing method is utilized to study the propagation characteristics of RIS materials in the mmWave network. The author suggests an optimization approach to minimize the RIS elements corresponding to the user's rate demands by jointly optimizing the location of RIS, signal phase shift, and time slots in an indoor environment.

Mao et al. [24] suggested a sustainable ARIS-assisted wireless network for low-power Internet of things (IoT) applications. ARIS enhances the simultaneous transfer of power and information through the Dinkelbach-type optimization of time slots, reflection parameters, and transmit power. Zou et al. [25] suggested a machine learning (ML) approach to improve the quality of service (QoS) of the RIS-aided nonorthogonal multiple access (NOMA)-based IoT system. Power allocation and phase shift optimization are performed to enhance the QoS of the system with minimum transmit power. A reinforcement learning method is applied and compared with deep learning (DL) techniques in terms of throughput.

Singh et al. [26] discussed an unmanned aerial vehicle (UAV)-based relay system in which RIS materials are mounted. Rate splitting multiple access (RSMA) is adapted to attain the system's spectral efficiency demand. The heuristic optimization method considered UAV positioning, signal phase shifts, and RSMA parameters. Rejection of jamming signals is considered as a use-case of RIS. In Hu et al. [27], multiple RIS-embedded UAV-assisted IoT system is

considered, where the trajectory and signal phase shifts are decided using the DL approach. The hybrid domain multiple access (HDMA) for RIS-assisted visible light communication (VLC) is discussed by Yu et al. [28]. The interference introduced by the multiple LEDs in the system is mitigated by employing RIS, which performs transmission and reflection. Here, phase shift optimization is performed to improve the system's capacity. Simultaneously transmitting and reflecting (STAR)–RIS is the upgraded version of RIS, which provides maximum coverage for radio signals in every direction. Maraqa et al. [29] discussed the application of STAR–RIS in an RSMA-based VLC system to improve the sum rate. Multiple obstacles are considered to optimize positioning and phase shift.

3.1.2 Key Contributions

The following are the significant contributions of this chapter:

- A comprehensive overview of RIS's architecture, hardware design, operational modes, and frequency bands suitable for different duplexing are presented.
- An EM analysis of RIS is carried out, which offers a mathematical model representing the gain of both transmit and receiving units. The channel and reflection coefficient of each element within the RIS are also modeled.
- The effects of mutual coupling and spatial correlation on the performance of RIS are also examined, while also exploring mitigation strategies. The expressions for average error probability under spatially correlated conditions are derived, considering various diversity factors.

3.1.3 Organization

To construct 6G wireless networks, RIS is seen to be an essential technology. In recent years, RIS has garnered much attention as a key element that helps next-generation wireless systems support high data rate needs at an inexpensive installation cost. The suggested structure for this chapter is as follows: The chapter is succinctly introduced in Section 3.1. A comprehensive synopsis of the RIS is in Section 3.2. Section 3.3 of the chapter examines the EM analysis of RIS. The impact of mutual coupling and spatial correlation are analyzed in Sections 3.4 and 3.5, respectively. The simulation results are discussed in Section 3.6, and the chapter concludes in Section 3.7.

3.2 Overview of RIS

This section provides an extensive examination of RIS, covering its structure, hardware design, operating modes, frequency of operation, and duplexing modes.

3.2.1 Structure

RIS is an affordable and energy-efficient technology that can be implemented mainly with passive components. RIS can be integrated into any surface and can take any shape. The structure of RIS can vary depending on factors such as cost, design, integration, and form factor.

3.2.1.1 Metamaterial

A novel class of synthetic materials known as metamaterials has been developed, with a microstructure designed to display special EM characteristics not seen in nature and previously thought to be physically impossible [30]. Atoms make up the periodic structure of any material that may be found in nature. An artificial periodic structure is made and grafted onto a host material to form metamaterials. The constituent elements of this manufactured periodic structure are larger than the atoms of the host material. This size difference results in overcoming the host material's inherent reaction to the entering EM pulse. As a result, the penetration, reflection loss, and reflection angle that occur are unique to the artificial structure rather than the host material's atomic structure.

Metamaterials with artificially created periodic structures can be composed of semiconductors, metals, or polymers. When an EM wave interacts with a metamaterial, its wavelength must be significantly smaller than the size of the "meta-atom," which is a periodic structural pattern that repeats. This is required because the incoming wave must see the periodic structure uniformly.

Each of the N pieces that make up an RIS is a tiny antenna that passively reradiates after receiving information with a time delay that can be adjusted. In narrowband transmissions, a phase shift is equivalent to this delay. The scattered waves accumulate constructively at the receiver, provided that the phase shifts are appropriately controlled. This idea is comparable to traditional beamforming, in which a specific radiation pattern is assigned to each component. However, the accumulation of phase shifts between the scattered waves determines the areas of constructive interference.

3.2.1.2 Reflect Array

The most basic version of a RIS is a dynamic reflect array, which consists of programmable omnidirectional antennas that can be modified dynamically to backscatter/phase shift the incident signals. Using a 2D planar type of metamaterial with a dynamically tunable metasurface has demonstrated strong abilities to manipulate EM waves, making it a more complex approach. By utilizing the metasurface implementation, an RIS unit can scatter/phase shift the signal, control polarization, and function as an anomalous mirror with a programmable reflection angle. Previous designs of metasurfaces were predicated

on fixed, predetermined designs of meta-atoms that could not be altered after they were fabricated.

Subsequent designs, however, rely on semiconductor components that may be modified in practice to alter the meta-atom structure beneath the surface and, consequently, the metasurface's EM behavior. Integrating mechanical, electrical, or thermally tunable components allow for this reconfigurability. Electrically tunable metasurfaces can be produced at low cost using well-understood semiconductor technologies, and by adding varactor diodes or liquid crystals within the meta-atoms, they can be tuned quickly enough to adjust to the time-varying channel.

3.2.2 Hardware Design

The most recent RIS hardware architectures and a few suggested fabrication techniques are discussed in this section. The most notable feature of the RIS is its ability to fully shape and control the EM response of environmental objects dispersed throughout the network, thereby making the environment controllable compared to the transceiver technologies currently in use in wireless networks.

3.2.2.1 Passive RIS

The PRIS is built using EM materials. RIS can be inexpensively deployed in various locations, including buildings, movable walls, platforms, billboards, highway poles, glasses, and pedestrian apparel [31]. By considering power losses over long distances, the RIS can modify the conditions for wireless transmission. RIS can create a virtual line of sight (LoS) between the base station (BS) and the user equipment (UE) by passively reflecting the received signals. The input–output relationship of i th element of a PRIS is given by (3.1):

$$y_i = \mu_i e^{j\eta_i} s_i \tag{3.1}$$

where s_i and y_i are incoming and outgoing signals, $\eta_i \in [0, 2\pi)$ is the controllable phase and $\mu_i \in [0,1]$ is the amplitude of ith RIS element. Figure 3.1 depicts PRIS technology that enhances wireless communication by reflecting and manipulating incident signals, improving signal quality, and coverage.

RIS does not require a power amplifier because, unlike traditional relays it may modify the phase of input signal [32]. This indicates that using RIS is far more economical and environmentally beneficial than using traditional relays. Full-duplex (FD) and full-band transmission are also possible with RIS, as EM waves are only reflected. PRIS offers a dependable reflection link alongside a direct link for signal transfer. There is always a double fading effect on this reflection link in addition to having much large-scale fading. PRISs can only provide a limited capacity in many cases when the direct link is strong. The corresponding path loss of a

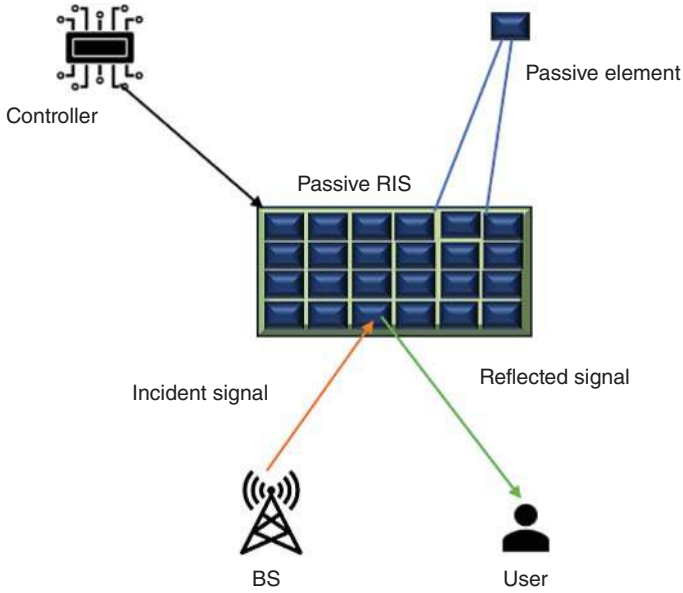

Figure 3.1 PRIS.

transmitter-RIS-receiver link is the product, as opposed to the total path losses, in contrast to a direct link [33]. Signals from the relatively long reflection link affect power loss more if the fading coefficient is higher than the shorter direct link. This implies that there is little to no difference between a system with and one without RIS.

3.2.2.2 Active RIS

One of the main performance bottlenecks of PRIS is its "multiplicative fading" effect; as a potential remedy, ARIS was proposed by Zhang et al. [34], You and Zhang [35], and Long et al. [36]. ARIS, like PRIS, allows for adjustable phase-shift reflection of incident signals. Compared to PRIS, which just reflects incident signals, ARIS can further augment the reflected impulses. The ith element of an ARIS's input–output relationship is:

$$y_i = \mu_i e^{j\eta_i} s_i + \mu_i e^{j\eta_i} \omega_i \tag{3.2}$$

where $\omega_i \sim C\mathcal{N}(0, \sigma_i^2)$ is the input noise amplified by the ith RIS unit and $\mu_i > 1$. Figure 3.2 presents the structure of ARIS that optimizes wireless communication through real-time control and adaptive signal modulation, enhancing performance and efficiency. ARIS's hardware architecture differs from PRIS's [37]. In an ARIS, phase shift circuits and reflection-type amplifiers are employed to increase the received signal power. The power needs of ARIS cannot be disregarded, as

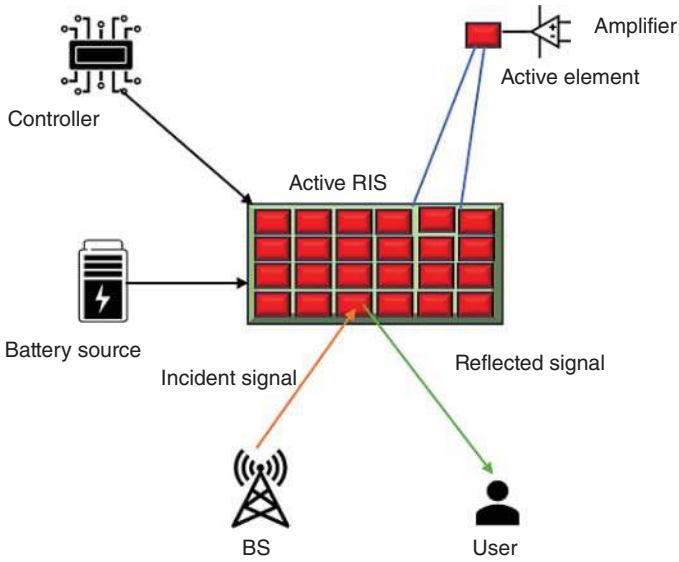

Figure 3.2 ARIS.

they can be comparable to those of the amplifiers of BS, owing to the possibility that ARIS-assisted systems may use a lot more power overall than PRIS-assisted systems [38]. Because ARIS provides an amplification gain and converts the multiplicative fading into an additive form, it is therefore more effective. The performance may be enhanced via a hybrid architecture that combines active and PRIS components. It may be difficult for an off-grid RIS to power its active components. Research on an ARIS is desirable since we anticipate it to be more economical and effective than an amplify-and-forward relay [39]. Although both PRIS and ARIS offer 180° coverage, their usefulness is limited because users may really be on both sides of the RIS.

3.2.2.3 Hybrid RIS

A hybrid RIS or STAR–RIS or intelligent omni surfaces (IOSs) may sense and reflect a portion of its impinging signal [40, 41]. The transmitted signal from the ith element of a hybrid RIS is

$$y_i^t = \mu_i^t e^{j\eta_i^t} s_i \tag{3.3}$$

The reflected signal from the ith element of a hybrid RIS is

$$y_i^r = \mu_i^r e^{j\eta_i^r} s_i \tag{3.4}$$

where $\mu_i^t, \mu_i^r \in [0,1]$, $\mu_i^{t^2} + \mu_i^{r^2} = 1$, and $\eta_l^t, \eta_i^r \in [0, 2\pi)$. To offer 360° coverage, STAR–RIS can be installed inside a wall or in the middle of the communication

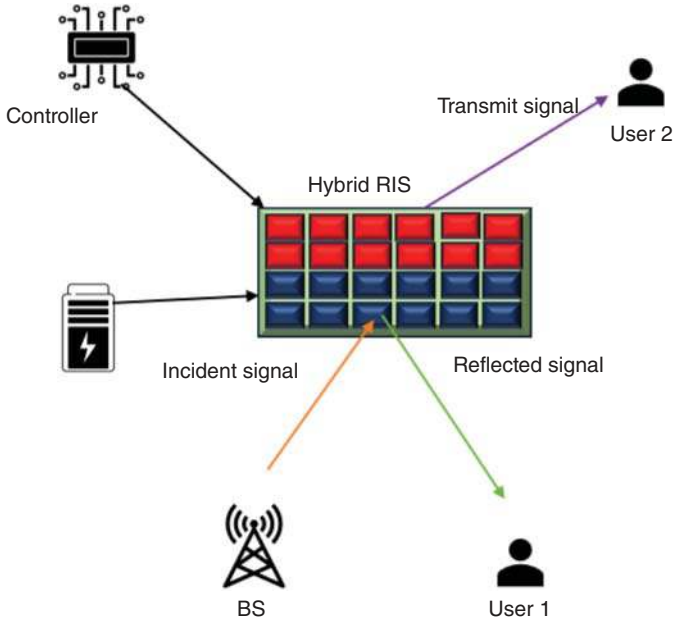

Figure 3.3 Hybrid RIS.

space. Without substantially compromising the benefits of PRIS's increased coverage and EE, hybrid RIS can improve coherent communications significantly. A hybrid RIS can be implemented by loading a surface with a varactor, which alters the capacitance of the surface based on an external DC signal. The reflected wave's phase can be altered by the fluctuating capacitance. By changing the phase, the hybrid RIS can direct the reflected wave in the desired direction. The hybrid RIS arrangement is shown in Figure 3.3.

3.2.2.4 Contiguous RIS

Contiguous RISs combine numerous small components into a compact space to generate a transceiver aperture that is spatially continuous [42, 43]. Utilizing holography methodology, it becomes feasible to capture an EM field generated by a signal source when scattered from objects. As a result, a contiguous RIS can create a spatially continuous transceiver aperture, which is useful for many applications. Figure 3.4 presents the internal structure of contiguous RIS, which ensures seamless adaptability in wireless environments through ongoing adjustments, fostering sustained signal enhancement and communication optimization.

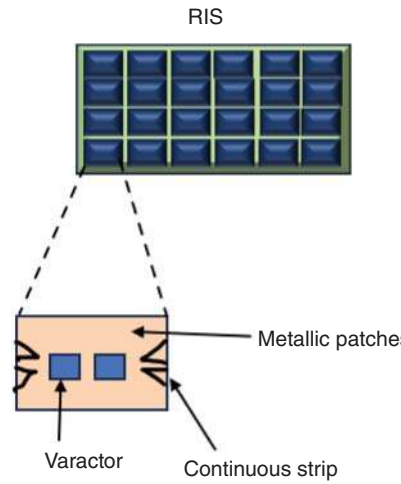

Figure 3.4 Contiguous RIS.

3.2.2.5 Discrete RIS

Several discrete unit cells constructed of low-power software-tunable metamaterials often make up a discrete RIS [43–47]. Liquid crystals, microelectromechanical systems (MEMSs), electromechanical switches, etc., can be used to electrically alter the EM properties of the unit cells in addition to commonly used electrical components. Comparing this construction to a traditional multi-antenna antenna array reveals significant differences. Liaskos et al. [48] designed a surface with electronically adjustable reflection properties using discrete meta-atoms. As previously noted, the discrete surface is active, which is based on photonic antenna arrays. From an implementation and hardware standpoint, discrete RISs differ significantly from contiguous RISs [49, 50]. Figure 3.5 illustrates the layered structure of discrete RIS.

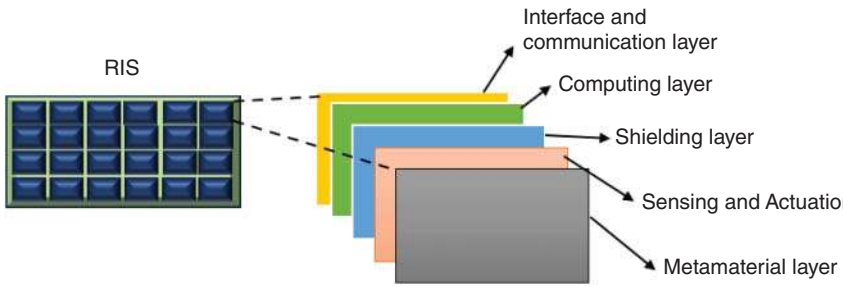

Figure 3.5 Discrete RIS.

3.2.3 Operating Modes

This section discusses about the various operating modes of RIS and its significance.

3.2.3.1 Reflection Mode

The reflective PRIS consumes very little power [51]. Their main purpose is to leverage the surface's ability to change the reflection properties of elements, allowing for programmable alteration of incoming EM waves across various capabilities. For accurate beamforming, precise control over the reflected EM field is required. This can be accomplished with sub-wavelength meta-atoms, however, they will unavoidably have well-defined grey-scale-tunable EM properties and significant mutual coupling. The reflection mode with opaque RIS substrate is depicted in Figure 3.6.

In settings with rich scattering, wave energy is evenly distributed throughout the wireless medium. The results from ray pandemonium suggest that the RIS can be affected by rays coming from any direction rather than just one clearly defined orientation. Instead of using directional beams, the goal is to manipulate as many ray trajectories as possible. This manipulation has two goals: efficiently directing the field and modifying those rays to produce constructive interference at a specific location. These manipulations can be efficiently performed by RIS equipped with half-wavelength-sized meta-atoms, which permit the control of more rays with a fixed amount of electrical components (e.g., PIN diodes). When in reflection mode, RIS can be used to enhance capacity, reduce interference, and function as a reflector in the surrounding area.

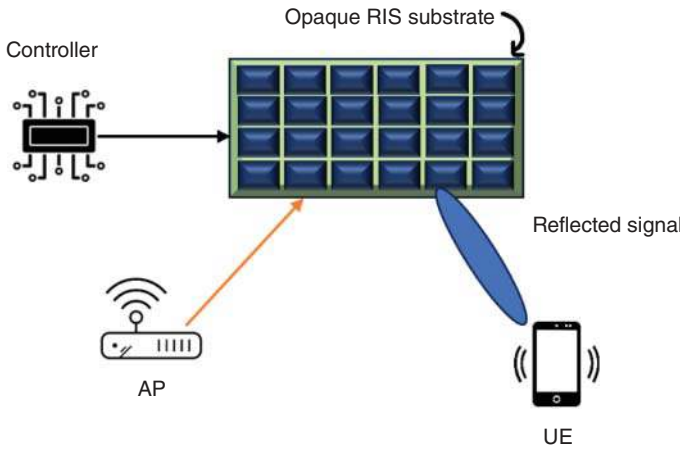

Figure 3.6 Reflective mode of RIS.

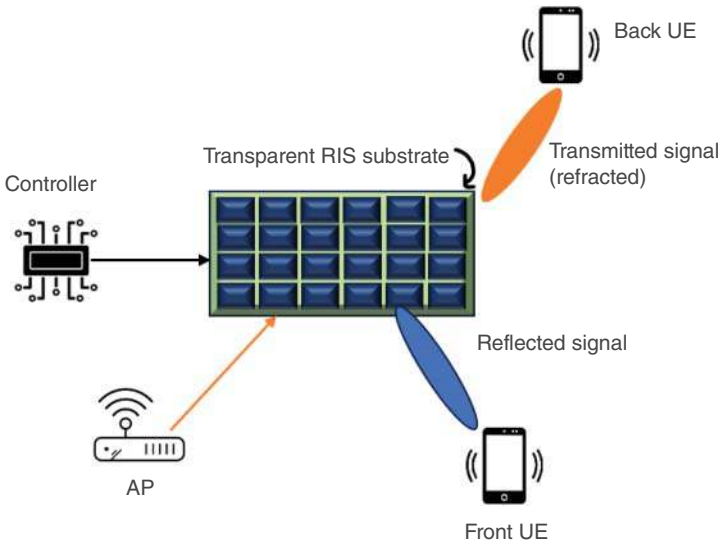

Figure 3.7 Refraction mode of RIS.

3.2.3.2 Refraction Mode

By changing their phase, EM waves that incident on the RIS can be refracted to different target directions using the refraction mode. The working of RIS with transparent substrate in refracted mode is given in Figure 3.7. A notable contrast between the refraction and reflection modes lies in the lack of a shielding layer within the RIS panel. This absence permits EM waves to traverse through the panel. An example where refraction mode can be used is when transitioning from an outdoor to an indoor environment. The RIS will be used as window glasses to focus incident EM radiation onto various target areas, hence improving coverage for particular locations within the building.

3.2.3.3 Absorption Mode

A radio wave with a specific center frequency and bandwidth can ideally be fully absorbed when it is in the absorption mode, which is characterized by the absence of reflection waves. Since the absorption mode of RIS generates little to no output waves, industries involved in information security, privacy, and interference reduction may find value in it. Using RIS to block EM radiation on a building's façade is one typical use-case. By doing this, EM radiation from various interior or exterior locations would be isolated. To prevent the incident wave from passing through building walls, the RIS plane will absorb it. The capacity of the RIS to switch between the absorption or refraction or reflection modes is determined by the bias voltage.

3.2.3.4 Backscattering Mode

In the event that an RIS is in backscattering mode, its reflected wave ought to include a broad region rather than a specific area. The effective area and gain need to be balanced in order to provide broad-angle blind spot coverage. Backscattering mode operation is also possible for PRIS, which is designed to reflect an incoming EM signal in a desired direction.

3.2.3.5 Transmitting Mode

Integrating an RIS with the transmitting mode of a radio transmitter aids in shaping the emitted radio wave [51]. The transmitting mode of RIS with unmodulated carrier input along with data source is presented in Figure 3.8. Recently, dynamic metasurface antennas (DMAs) have been suggested as an effective way to realize extremely large antenna arrays. DMAs process both broadcast and received signals in the analog domain and have the ability to adjust beams. They use less complicated transceiver technology and operate in a dynamically programmable manner. Additionally, DMA-based systems require less power and cost than conventional antenna arrays, eliminating the need for active phase shifters and/or complex corporate feed.

3.2.3.6 Receiving Mode

When in receiving mode, an RIS can receive and process radio signals. To achieve this, each RIS element or group of parts can have waveguides that steer incoming radio signals toward reception gear. This reception gear can include

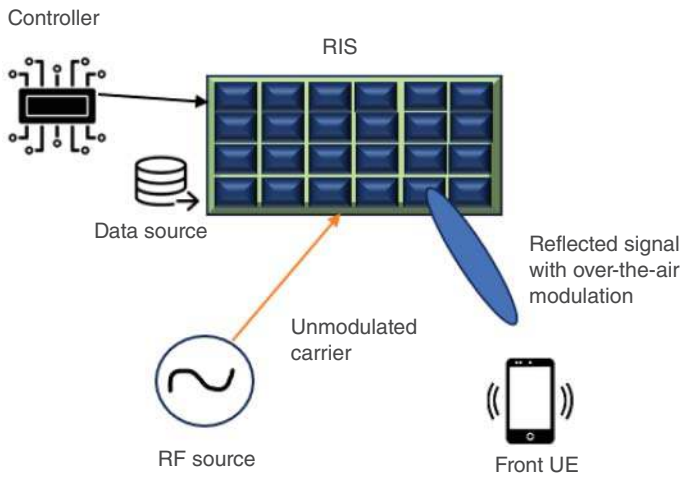

Figure 3.8 Transmitting mode of RIS.

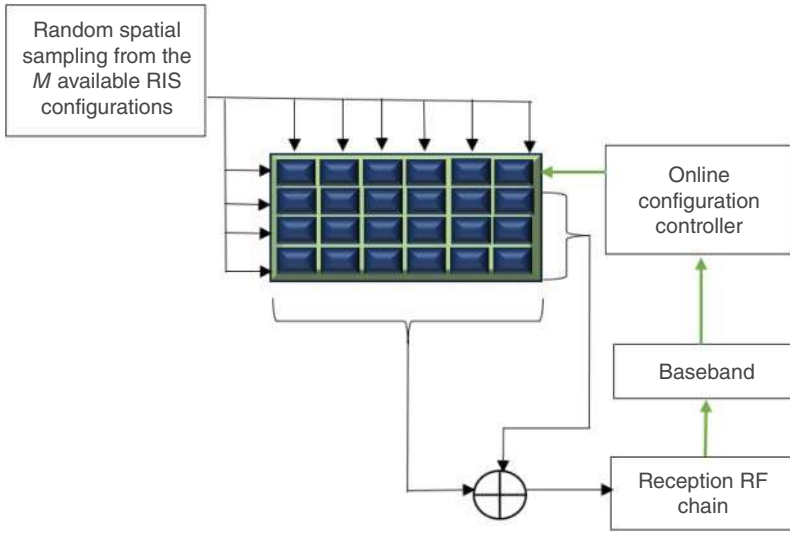

Figure 3.9 Receiving mode of RIS.

an analog-to-digital converter, a mixer that down-converts the signal from radio frequency (RF) to baseband, and a low-noise amplifier, among other things.

As depicted in Figure 3.9, a training EM signal interacts with the components of the RIS, and the received signal in the RF domain is influenced by M phase configurations of the RIS, which are chosen randomly via a spatial sampling unit. With substantially fewer RF chains-even just one-than the number of RIS elements, signal reception at the RIS is made possible by this collection of spatially random analog mixed copies of the impinging radio signals. This facilitates the application of channel estimate approaches based on compressive sensing.

3.2.4 Operating Frequency

RISs are devices that work on RF. Depending on the requirements and application, RIS can be configured to operate over different frequency bands. Generally, RIS operates within the part of the EM spectrum reserved for wireless communication [52].

3.2.4.1 Frequency Range 1 (FR1)

The frequency range below 6 GHz, also referred to as FR1, is commonly used for 5G and previous generations of wireless communication. This range includes various frequency bands such as 1.8 GHz, 2.1 GHz, 2.3 GHz, 2.4 GHz, 2.5 GHz, 3.5 GHz, and more. The use of FR1 enables wide-area coverage, making it a popular choice for cellular communication.

3.2.4.2 Frequency Range 2 (FR2)

To support mmWave installations for 5G-NR, RIS can be engineered for mmWave frequency bands (FR2) over 24 GHz [53]. Due to their potential for directional communication and large data rates, mmWave frequencies are highly intriguing for RIS applications.

3.2.4.3 Terahertz (THz)

THz is a range of frequencies that spans from 100 GHz to 10 THz. Researchers are exploring the potential of THz communication for high-speed data transfer and applications such as high-capacity wireless networks and imaging [54]. Although it is not commonly used for mainstream wireless communication, THz technology shows promise for the future.

3.2.4.4 Unlicensed Bands

Unlicensed bands are frequency bands that can be used without a special license from regulatory bodies [55, 56]. The 2.4 and 5 GHz bands are commonly used for wireless-fidelity (Wi-Fi) transmission. The 60 GHz frequency, also known as the V-band, is used for high-data-rate communication applications such as Wireless Gigabit (WiGig) and other short-range transmissions.

3.2.4.5 Custom Frequency Bands

RIS can be configured to operate within custom frequency bands depending on the specific requirements and use-cases. This is particularly useful when the application necessitates a specific frequency range for optimization.

3.2.5 Duplexing Modes

RIS plays a crucial role in facilitating communication between transmitters and receivers using different duplexing modes. The duplexing mode determines the division of the communication channel into downlink (DL) and uplink (UL), thereby enabling smooth and efficient communication.

3.2.5.1 Time-Division Duplexing (TDD)

The communication channel is split into alternating time slots when using TDD for UL and DL broadcasts. RIS can dynamically modify its reflective characteristics to optimize the channel for both directions. The reciprocity-constrained mode and the reciprocity-non-constrained mode are the two conceivable TDD modes. For most RIS hardware implementations, channel reciprocity can be preserved.

Reciprocity, however, might not always be maintained depending on how the RIS is designed.

In a reciprocity-constrained mode of operation, it is imperative to adjust the phase shifts of the RIS units to reflect UL/DL toward BS/UE in order to maintain channel reciprocity. Because of this, BS/UE can use the same corresponding beams to broadcast DL/UL and receive UL/DL. Conversely, the reciprocity-non-constrained mode might not require channel reciprocity. As a result, the RIS phase shifts can be configured separately from the UE/BS UL/DL beams. The two scenarios of the reciprocity-constrained and reciprocity-non-constrained modes are illustrated in Figures 3.10 and 3.11.

3.2.5.2 Frequency-Division Duplexing (FDD)

FDD divides UL and DL broadcasts using distinct frequency bands. RIS optimizes reflections for efficient communication in both directions. Figure 3.12 illustrates FDD transmission aided by RIS.

3.2.5.3 Hybrid Duplexing

Hybrid duplexing is a technique that combines elements of both TDD and FDD to provide more flexibility in how frequency and time resources are utilized. With an adaptive approach, the RIS in such a system can modify its characteristics according to the particular combinations of time and frequency.

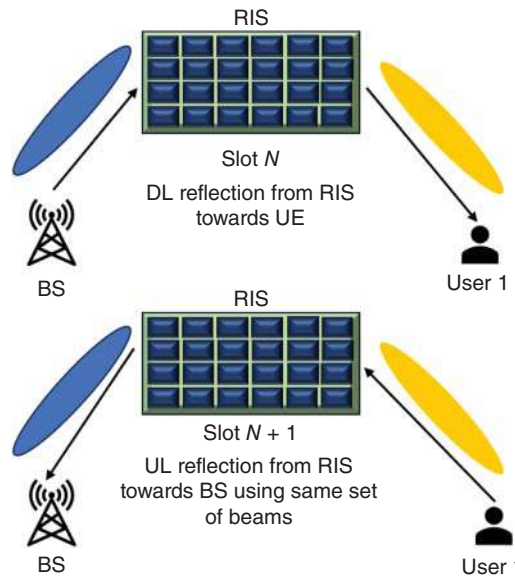

Figure 3.10 A scenario of TDD communication employing the same set of phase shifts for UL and DL at RIS and a reciprocity-constrained mode at UE.

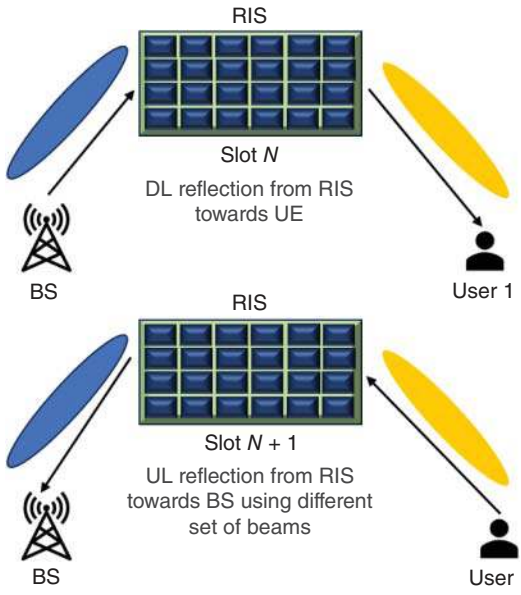

Figure 3.11 A scenario of TDD communication using a separate set of phase shifts for UL and DL at RIS and a reciprocity-non-constrained mode at UE.

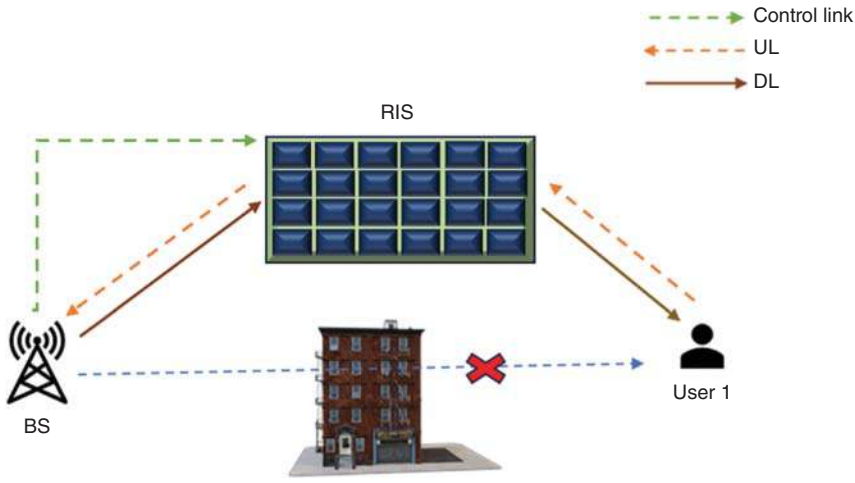

Figure 3.12 RIS-aided FDD transmission.

3.2.5.4 Full-Duplex (FD)

Simultaneously, transmitting and receiving are possible with FD communication on the same frequency. In FD systems, RIS can help reduce self-interference, which enhances simultaneous bidirectional communication performance overall [6, 9, 57, 58]. An illustration of FD mode RIS communicating with one BS and two UEs is shown in Figure 3.13.

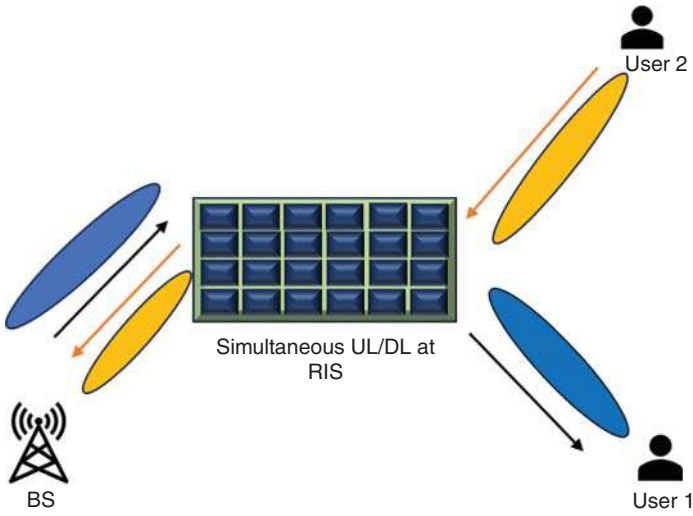

Figure 3.13 A scenario of the FD mode at RIS.

3.2.5.5 Dynamic Duplexing with RIS

RIS technology enhances duplexing's adaptability by continuously adjusting its reflecting properties based on communication requirements. This means that RIS can adapt to changing channel conditions by optimizing reflections to enhance signal quality during UL or DL transmission.

3.3 EM Analysis of RIS

Let us consider a communication system aided by RIS in which there is an obstructed LoS path between the UE and the BS, as depicted in Figure 3.14. Compared to sub-6 GHz bands, mmWave technology has substantially fewer multipaths because of its high transmission frequency. The RIS with N units is positioned on the y–z plane of a Cartesian coordinate system. We assume that the bottom left corner of the RIS aligns with the origin of the coordinate system. A uniform planar array (UPA) with N_C columns and N_R rows is used to model the RIS. Each element has an area of $A_u = S_r \times S_c$, where the horizontal and vertical spacing between elements are denoted by S_r and S_c, respectively. For every reflecting element, H_u is the gain and $G(\upsilon, \phi)$ is the radiation pattern of normalized power. Here, υ is the zenith angle and ϕ is the azimuth angle, respectively.

$G_i^t = G\left(\upsilon_i^t, \phi_i^t\right)$ is the radiation pattern of normalized power from the ith reflecting unit of the RIS to BS and $G_i^r = G\left(\upsilon_i^r, \phi_i^r\right)$ is the radiation pattern of normalized power from the ith reflecting unit of the RIS to the UE. Here, $\upsilon_i^t, \phi_i^t, \upsilon_i^r$, and ϕ_i^r are

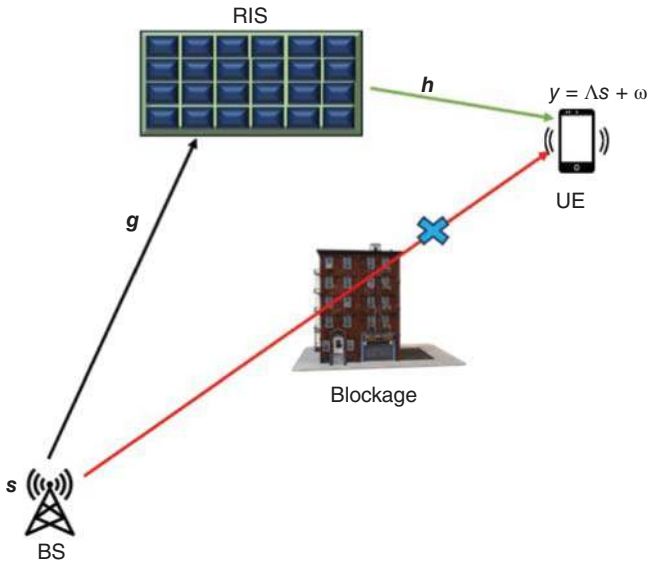

Figure 3.14 RIS-aided wireless transmission.

the respective zenith and azimuth angles. The vectors $\eta = \left[\eta_1, \eta_2, \ldots, \eta_i, \ldots, \eta_N\right]$, $\eta_i \in [0, 2\pi)$, and $\mu = \left[\mu_1, \mu_2, \ldots, \mu_i, \ldots, \mu_N\right]$, $\mu_i \in [0, 1]$ denotes phase shift and amplitude of RIS's reflection coefficient. The reflection coefficients of the RIS, denoted by $\Phi \in \mathbb{C}^{N\times 1}$ is expressed as,

$$\begin{aligned}\Phi &= \left[\phi_1, \ldots, \phi_N\right]^T \\ &= [\mu_1 e^{j\eta_1}, \ldots, \mu_i \mathrm{e}^{\mathrm{j}\eta_i}, \ldots, \mu_N e^{j\eta_N}]^T\end{aligned} \tag{3.5}$$

where $\phi_i = \mu_i e^{j\eta_i}$ is the reflection co-efficient of the ith reflecting unit.

Cui et al. [59] focused predominantly on LoS connections, which are notably more robust compared to other multipath elements within the mmWave spectrum, linking the transceivers and the RIS. They posit a scenario where the UE and the BS each possess a single antenna, maintaining broad applicability. However, the suggested methodology readily lends itself to accommodating scenarios involving multiple antennas for both the BS and UE. The channel between the ith reflecting component and the BS is characterized as per (3.6) [59].

$$g_i = \sqrt{\frac{A_u G_i^{tx} G_i^t}{4\pi l_{t,i}^2}}\, e^{\frac{-j2\pi l_{t,i}}{\lambda}} \tag{3.6}$$

Here, λ is the wavelength, $G_i^{tx} = G^{tx}\left(\upsilon_i^{tx}, \phi_i^{tx}\right)$ is the transmit antenna's radiation pattern from the BS to the ith RIS unit. υ_i^{tx} and ϕ_i^{tx} are the respective zenith and azimuth angles, and $l_{t,i}$ is the distance between the BS and the ith RIS component.

The channel vector between BS and the RIS, $\mathbf{g} \in \mathbb{C}^{N\times 1}$ is expressed as,

$$\begin{aligned}\mathbf{g} &= \left[g_1, \ldots, g_N\right]^T \\ &= \left[\sqrt{\frac{A_u G_1^{tx} G_1^t}{4\pi l_{t,1}^2}}\, e^{\frac{-j2\pi l_{t,1}}{\lambda}}, \ldots\ldots, \sqrt{\frac{A_u G_N^{tx} G_N^t}{4\pi l_{t,N}^2}}\, e^{\frac{-j2\pi l_{t,N}}{\lambda}}\right]^T\end{aligned} \tag{3.7}$$

The channel for ith RIS unit to UE is expressed as,

$$h_i = \sqrt{\frac{A_r\, G_i^{rx} G_i^r}{4\pi l_{r,i}^2}}\, e^{\frac{-j2\pi\, l_{r,i}}{\lambda}} \tag{3.8}$$

Here, A_r is the receiving antenna aperture, $G_i^{rx} = G^{rx}\left(\upsilon_i^{rx}, \phi_i^{rx}\right)$ is the normalized radiation pattern of the UE antenna to the RIS's ith reflecting unit. υ_i^{rx} and ϕ_i^{rx} are the zenith and azimuth angles of UE, and $l_{r,i}$ is the distance between the UE and RIS's ith reflecting unit.

Based on (3.8), the LoS component between the UE and the RIS is expressed as:

$$\begin{aligned}\mathbf{h} &= \left[h_1, \ldots, h_N\right]^T \\ &= \left[\sqrt{\frac{A_r\, G_1^{rx} G_1^r}{4\pi l_{r,1}^2}}\, e^{\frac{-j2\pi\, l_{r,1}}{\lambda}}, \ldots\ldots, \sqrt{\frac{A_r\, G_N^{rx} G_N^r}{4\pi l_{r,N}^2}}\, e^{\frac{-j2\pi\, l_{r,N}}{\lambda}}\right]^T\end{aligned} \tag{3.9}$$

From (3.7) and (3.9), the cascaded BS-RIS-UE channel is presented as:

$$\begin{aligned}\omega &= \left(\left(\sqrt{H_r}\boldsymbol{h}\right) \odot \left(\sqrt{H_t}\mathbf{g}\right)\right)^T \left(\sqrt{H_u}\,\Phi\right) \\ &= \sqrt{H_r H_u H_t}(\boldsymbol{h} \odot \mathbf{g})^T\, \Phi \\ &= \frac{\sqrt{H_r H_u H_t A_r A_u}}{4\pi} \sum_{i=1}^{N} \frac{\sqrt{\tilde{G}}\phi_i}{l_{t,i}\, l_{r,i}} e^{\frac{-j2\pi(l_{t,i}\, +\, l_{r,i})}{\lambda}}\end{aligned} \tag{3.10}$$

Here, H_t and H_r denote transmit and receive antenna gain and $\tilde{G} = G_i^{tx} G_i^t G_i^{rx} G_i^r$ is the effect of normalized radiation pattern on the received signal.

The signal received at the UE is

$$y = \Lambda s + \omega \tag{3.11}$$

where s is the BS's transmitted signal and $\omega \sim C\mathcal{N}\,(0, N_o)$ is the noise at the UE with variance N_o.

Substituting (3.10) in (3.11) gives

$$= s\frac{\sqrt{H_r H_u H_t A_r A_u}}{4\pi} \sum_{i=1}^{N} \frac{\sqrt{\tilde{G}}\phi_i}{l_{t,i}\, l_{r,i}} e^{\frac{-j2\pi(l_{t,i}\, +\, l_{r,i})}{\lambda}} + \omega \tag{3.12}$$

To maximize the strength of the UE's received signal power P_s, the reflection coefficient vector $\boldsymbol{\Phi}$ is generated using the estimated channel state information (CSI). The problem can be formulated as:

$$\check{\boldsymbol{\Phi}} = \underset{\boldsymbol{\Phi}}{argmax} \left\{ |(\boldsymbol{h} \odot \boldsymbol{g})^T \boldsymbol{\Phi}|^2 \right\} \tag{3.13}$$

For perfect CSI, the optimal reflection coefficient of the ith unit is

$$\check{\Phi}_i = \frac{h_i^* g_i^*}{|h_i g_i|}, \; i = 1, \ldots, N \tag{3.14}$$

The process of estimating CSI is challenging because of the numerous RIS units and the absence of signal processing at RIS.

3.4 Impact of Mutual Coupling in RIS

This section highlights the impact of mutual coupling in the design considerations for RIS. Mutual coupling refers to the unintended interactions among individual RIS elements inherent to RIS technology. Although each component is designed to manipulate radio waves independently, their proximity to one another can impact their EM behavior [60]. Mutual coupling significantly affects the performance of communication and localization systems and algorithmic design considerations [61].

The EM emissions from one element can alter the reflection characteristics of neighboring elements that are in close proximity. This interference disrupts the intended reflection pattern and can also impact the directivity of the system. Furthermore, signal quality deteriorates due to undesirable reflections and leakage between elements. Designing a model becomes more complex based on factors such as the number of radiating elements, the precision required, and the computational resources available. This coupling phenomenon results in notable energy losses, ultimately diminishing system efficiency.

Mutual coupling links the impedance of one element with that of its neighbors. To achieve more consistent and reliable RIS performance, it is crucial to anticipate and address the effects of mutual coupling during the design phase, employing advanced modeling and simulation tools [62]. While increasing the spacing between elements can reduce mutual coupling, space limitations may make this impractical. Various strategies can be implemented to mitigate mutual coupling, such as incorporating isolation structures between elements or utilizing metamaterial designs. Utilizing more precise models that accurately account for mutual coupling can optimize RIS design and configuration, minimizing its adverse impact on performance. By carefully designing the RIS layout to increase spacing between elements and selecting appropriate metamaterials, the effects of mutual coupling can be mitigated.

3.5 Impact of Spatial Correlation in RIS

In the realm of wireless communication, spatial correlation refers to the similarity in fading behaviors among different antenna elements due to their proximity to each other in space. The correlation among the elements of the RIS can significantly influence the overall performance of the system. Intense spatial correlation can lead to coherent signal cancellation or merging at the receiver, potentially affecting the signal's amplitude and quality upon reception. Additionally, the operating frequency plays a crucial role in spatial correlation. Higher frequencies, characterized by shorter wavelengths and less spatial variation, tend to exhibit higher correlations. Spatial correlation influences various aspects of RIS performance, including channel modeling, beamforming, diversity, and channel estimation.

Understanding spatial correlation is essential for developing effective signal-processing techniques and configuring RIS setups. This knowledge serves as the foundation for channel modeling in THz and mmWave communication [63]. The channel model relies on factors such as the dimensions of the RIS surface, operating frequency, spacing between RIS elements, as well as correlation matrices, path loss, and fading effects. Geographical correlation enables RIS elements to concentrate and steer incoming signals. However, the closely coupled nature of RIS elements, akin to a single large reflective surface, can limit beamforming accuracy [64]. When RIS elements exhibit high spatial correlation due to similar properties, the overall diversity of the received signal is diminished (Liu et al., 2023) [65]. This reduction in signal diversity adversely affects the system's ability to combat channel fading [66].

Introducing randomness into the placement of RIS elements can effectively reduce spatial correlation within signal paths, as suggested by Sun and Yan [67]. Moreover, incorporating metamaterials and engineered materials with specific EM properties into RIS design offers control over spatial correlation, as suggested by Shamsuri Agus et al. [68]. Adaptive algorithms capable of correcting reflection phase shifts can also influence spatial coherence, as noted by Tu et al. [69]. Additionally, techniques such as geographic filtering and precoding can be employed to mitigate the effects of correlation and further enhance RIS system performance.

3.5.1 Performance Analysis of RIS-Assisted Wireless Communication Systems with Spatial Correlation

The RIS-assisted communication system with spatial correlation is shown in Figure 3.15. The N RIS elements are tightly packed and arranged in the planar rectangular structure with R rows and C columns. There is no direct path between the source and destination. Both the source and destination is assumed to have single antennas. The spacing between the elements in rows and columns are

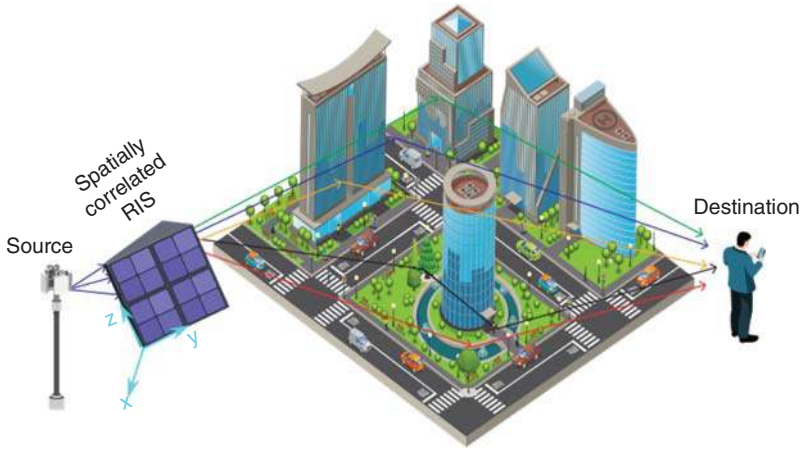

Figure 3.15 Spatial correlation in RIS-assisted communication.

represented by S_r and S_c, respectively. It implies that the area of the planar rectangular structure is $A_R = NS_rS_c$. Assume that, the RIS structure is in y–z plane with azimuth angle ϕ and elevation angle θ. The RIS structure has N_R meta surface elements in each row and N_C meta surface elements in each column and $N = N_RN_C$. Then, the two dimensional position vector of ith RIS reflecting meta surface element is given by,

$$\mathbf{u}_i[y_i, z_i] = \left[mod(i-1, N_R)S_r, \lfloor (i-1)/N_R \rfloor S_c\right] \tag{3.15}$$

The array response vector of the RIS structure is given by,

$$\mathbf{a}(\phi, \theta) = \left[1, exp\left(j\frac{2\pi}{\lambda}[\cos(\theta)\cos(\phi), \sin(\theta)]\mathbf{u}_2^T\right), \ldots, \right.$$
$$\left. \exp\left(j\frac{2\pi}{\lambda}[\cos(\theta)\cos(\phi), \sin(\theta)]\mathbf{u}_N^T\right)\right]. \tag{3.16}$$

The spatial correlation is introduced in the RIS planar structure when the reflecting elements in the RIS are tightly packed. The spatial correlation between the array response vectors of ith and jth elements is given by,

$$\mathbf{R}_{ij} = E[\mathbf{a}(\phi_i, \theta_i)\,\mathbf{a}^H(\phi, \theta)] = \sin c\left(\frac{2||\mathbf{u_i} - \mathbf{u_j}||}{\lambda}\right),$$
$$i = 1, 2, \ldots, N; j = 1, 2, \ldots, N. \tag{3.17}$$

The spatial correlation coefficient values are shown in Figures 3.16–3.18 for inter-element spacing of $0.04\lambda, 0.1\lambda, 0.5\lambda$, respectively, between the reflecting elements in the RIS structure. Substituting equation (3.17), the correlation matrix

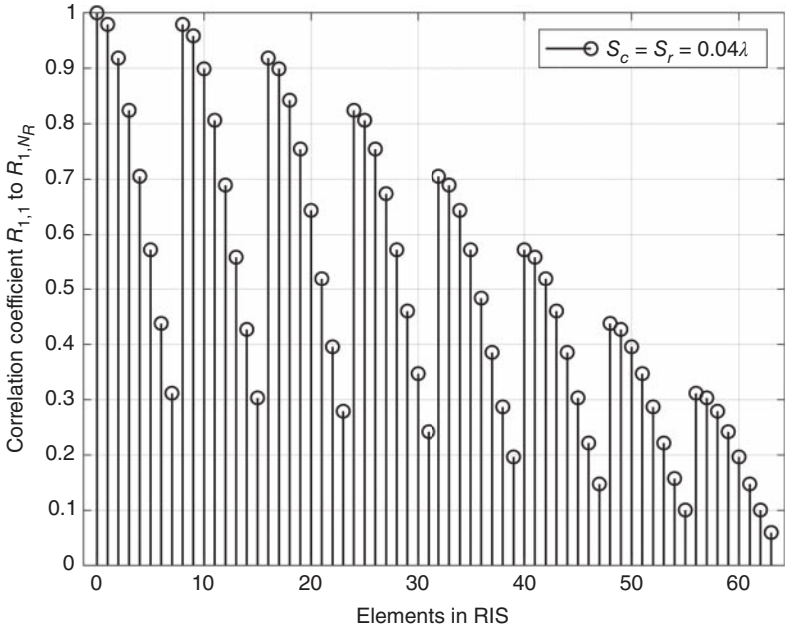

Figure 3.16 Spatial correlation coefficient values of RIS with $N = 64$ and element spacing of 0.04λ.

is given by,

$$\mathbf{R} = \begin{bmatrix} 1 & R_{1,2} & R_{1,3} & \cdots & R_{1,N_R} \\ R_{2,1} & 1 & R_{2,3} & \cdots & R_{2,N_R} \\ \vdots & \vdots & \vdots & \cdots & \vdots \\ R_{N_R,1} & \cdots & \cdots & \cdots & 1 \end{bmatrix} \tag{3.18}$$

The level of spatial correlation in the RIS structure is determined by the diversity factor of $\mathbf{R}$, which is given by,

$$D(\mathbf{R}) = \frac{[tr(\mathbf{R})]^2}{tr(\mathbf{R}^2)} = \frac{[tr(\mathbf{R})]^2}{\|\mathbf{R}\|_F^2} \tag{3.19}$$

If the RIS structure has no spatial correlation, then the diversity factor is maximum at N. The diversity factor is unity for full spatial correlation among the RIS elements in the structure. The channel between the source and destination has P resolvable independent paths and the channel coefficients $h_i, i = 1, 2, \ldots, P$ are independent and identically distributed. It implies that there is no spatial correlation in the channel between the source and destination. Then, the channel impulse

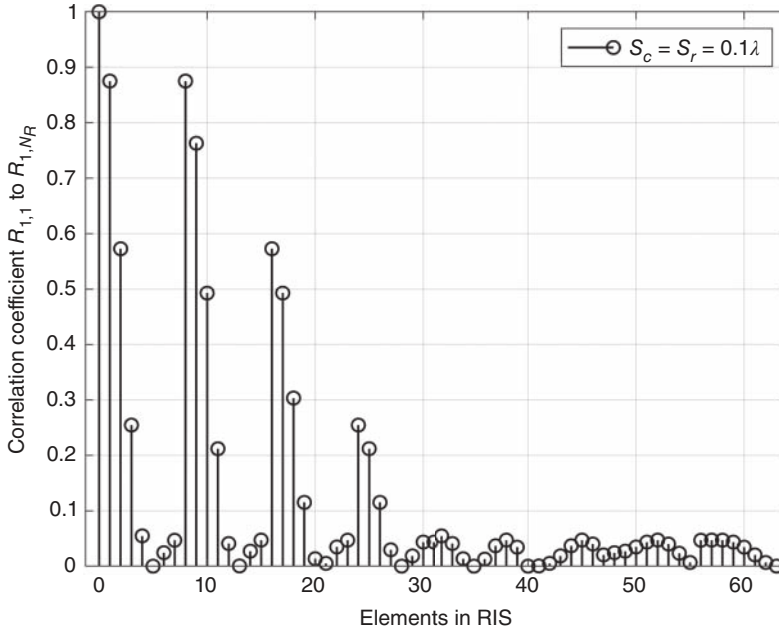

Figure 3.17 Spatial correlation coefficient values of RIS with $N = 64$ and element spacing of 0.1λ.

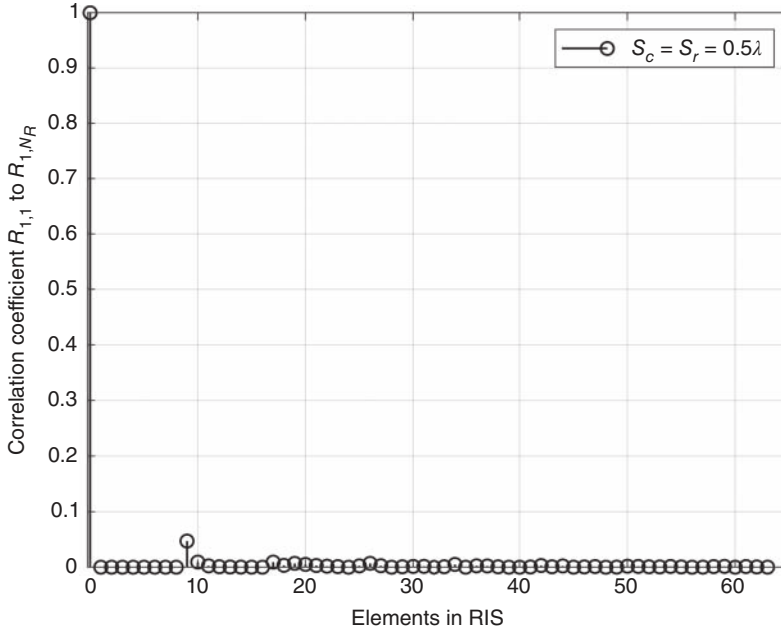

Figure 3.18 Spatial correlation coefficient values of RIS with $N = 64$ and element spacing of 0.5λ.

response is defined as,

$$\mathbf{h} = \frac{1}{\sqrt{p}} \sum_{i=1}^{P} h_i \mathbf{a}(\phi_i, \theta_i) \tag{3.20}$$

The $N \times 1$ channel impulse response vector between the N elements of RIS structure and destination is given by,

$$\mathbf{h} = \left[\alpha_1 e^{j\xi_1}, \ldots, \alpha_N e^{j\xi_N}\right]^T \tag{3.21}$$

The magnitude components $\alpha_i, i = 1, 2, \ldots, N$ are modeled as Rayleigh distributed with mean $\frac{\sqrt{S_c S_r \pi}}{2}$ and variance $S_c S_r \left(\frac{4-\pi}{4}\right)$. Assume that the transmit symbol s has unit average energy and drawn from scalar constellation at the source. The receive signal at the destination is given by,

$$y = \sqrt{E_s}\mathbf{h}^T \Phi s + w \tag{3.22}$$

where E_s is the symbol energy at the source. $\mathbf{\Phi}$ is a $N \times 1$ vector represents the phase shift introduced at the RIS elements.

$$\mathbf{\Phi} = \left[\Phi_1^T, \Phi_2^T, \ldots, \Phi_{N_R}^T\right]^T \tag{3.23}$$

Let Φ_i be the $Nc \times 1$ vector represents the phase shift introduced by the RIS elements in the ith row of the RIS planar structure,

$$\Phi_i = \left[e^{j\eta(i-1)N_R+1}, \ldots, e^{j\eta(i-1)N_R+N_C}\right]^T, i = 1, 2, \ldots, N_R \tag{3.24}$$

Let $\rho = \frac{E_s}{N_0}$. The instantaneous signal-to-noise ratio (SNR) is given by,

$$\gamma = \frac{E_s \left|\sum_{i=1}^{N} \alpha_i e^{j(\xi_i - \eta_i)}\right|^2}{N_0} = \rho \left|\sum_{i=1}^{N} \alpha_i e^{j(\xi_i - \eta_i)}\right|^2 \tag{3.25}$$

Let $A = |\sum_{i=1}^{N} \alpha_i e^{j(\xi_i - \eta_i)}|$. When the inter-element spacing is $\frac{\lambda}{2}$ in the RIS structure, the diversity factor $D(\mathbf{R}) = N$ if the elements are arranged as uniform linear array (ULA). According to central limit theorem (CLT), A is modeled as Gaussian distributed with mean $\mu = N\frac{\sqrt{S_c \pi}}{2}$ and variance $\sigma^2 = NS_c\left(\frac{4-\pi}{4}\right)$. However, in the planar structure with inter-element spacing of $\frac{\lambda}{2}$, the diversity factor $D(\mathbf{R})$ is less than N. In planar structure, when N is large, A can be modeled as Gaussian distributed random variable with mean $\mu = N\frac{\sqrt{S_c S_r \pi}}{2}$ and variance $\sigma^2 = \left(\mathbf{1}_N \mathbf{R} \mathbf{1}_N^T\right) S_c S_r \left(\frac{4-\pi}{4}\right)$, where $\mathbf{1}_N$ is $N \times 1$ ones vector. This is applicable only when the number of independent summands or diversity factor $D(\mathbf{R}) \geq 8$.

In the presence of spatial correlation in RIS structure, the diversity factor $D(\mathbf{R})$ decreases as the correlation level increases. In Thirumavalavan et al. [70], it is experimentally analyzed and proved that A can be modeled as Rician distributed when $6 \leq D(\mathbf{R}) < 8$, as log-normal distributed when $1.25 \leq D(\mathbf{R}) < 6$ and as

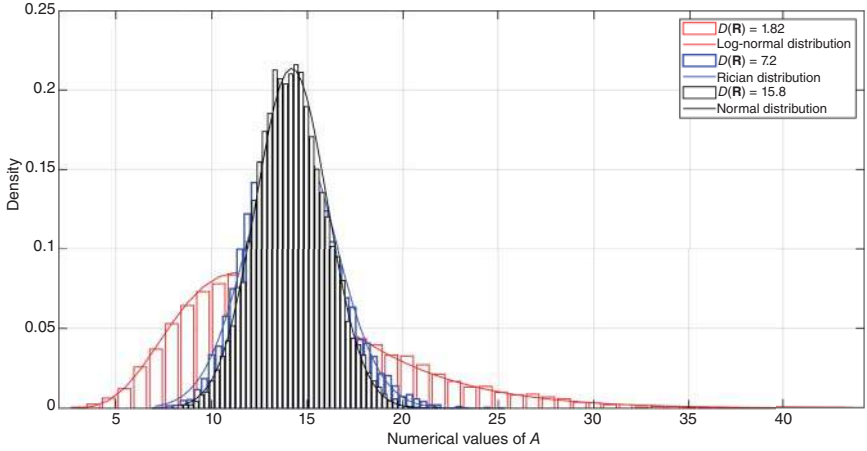

Figure 3.19 Distribution density fit for $N = 16$ and $S_r = S_c = 0.075$.

Rayleigh distributed when $1 \leq D(\mathbf{R}) < 1.25$. The distribution density fit for $N_R = N_C = 4$ is shown in Figure 3.19.

If the RIS phase shifts are adjusted perfectly, the maximum instantaneous SNR is given by (3.26), with reference to (3.25).

$$\gamma_{\max} = \rho \left| \sum_{i=1}^{N} \alpha_i \right|^2 = \rho B \tag{3.26}$$

3.5.1.1 Probability of Error Analysis When Diversity Factor ($D(\mathbf{R}) > 8$)

When $D(R) \geq 8$, B is Gaussian distributed and hence B^2 is modeled as non-central Chi-square distribution with one degree of freedom.

Assuming maximum likelihood (ML) symbol detection at the receiver, the symbol error probability is given by:

$$P_e = N_e Q\left(\sqrt{\frac{\gamma_{\max} d_{\min}^2}{2}}\right) \tag{3.27}$$

where N_e is the number of nearest neighbors and $d_{\min}$ is the minimum Euclidean distance in the scalar constellation from which the symbol s is drawn. Using (3.26), the average error probability is given by,

$$\widetilde{P}_e = \int_0^{\infty} N_e Q\left(\sqrt{\frac{\rho B d_{\min}^2}{2}}\right) f_B(b) db \tag{3.28}$$

The moment generating function (MGF) of the random variable B with mean μ and variance σ^2 is given by,

$$M_B(s) = \left[\frac{1}{1-2s\sigma^2}\right]^{\frac{1}{2}} \exp\left(\frac{s\mu^2}{1-2s\sigma^2}\right) \tag{3.29}$$

Using alternate expression for Q function and the definition of the MGF, the average error probability of M-ary PSK system is written as,

$$\overline{P_e} = \frac{N_e}{\pi}\int_0^{\frac{(M-1)\pi}{M}} M_B\left(\frac{-d_{\min}^2\rho}{2\sin^2\theta}\right)d\theta \tag{3.30}$$

Using (3.29), the MGF $M_B\left(\frac{-d_{\min}^2\rho}{2\sin^2\theta}\right)$ is given by,

$$M_B\left(\frac{-d_{\min}^2\rho}{2\sin^2\theta}\right) = \left[\frac{1}{1+\frac{d_{\min}^2\sigma^2\rho}{\sin^2\theta}}\right]^{\frac{1}{2}} \exp\left(\frac{\frac{-d_{\min}^2\mu^2\rho}{2\sin^2\theta}}{1+\frac{d_{\min}^2\sigma^2\rho}{\sin^2\theta}}\right) \tag{3.31}$$

Substituting for (3.31) and the values of μ and σ^2, the average error probability for M-PSK system is given by,

$$\overline{P}_e = \frac{N_e}{\pi}\int_0^{\frac{(M-1)\pi}{M}} \left[\frac{1}{1+\left(\frac{2d_{\min}^2\left(\mathbf{1_N}\mathbf{R}\mathbf{1_N^T}\right)S_cS_r(4-\pi)\rho}{4\sin^2\theta}\right)}\right]^{\frac{1}{2}} \exp\left(\frac{\frac{-N^2d_{\min}^2S_cS_r\pi\rho}{4\sin^2\theta}}{1+\frac{2d_{\min}^2\left(\mathbf{1_N}\mathbf{R}\mathbf{1_N^T}\right)S_cS_r(4-\pi)\rho}{4\sin^2\theta}}\right)d\theta \tag{3.32}$$

For BPSK, $M=2$, $N_e=1$, and $d_{\min}=2$. The maximum error occurs at $\theta=\frac{\pi}{2}$. Hence, the upper bound average error probability of BPSK system is given by,

$$\overline{P}_e \le \frac{1}{\pi}\int_0^{\frac{\pi}{2}} \left[\frac{1}{1+2\left(\mathbf{1_N}\mathbf{R}\mathbf{1_N^T}\right)S_cS_r(4-\pi)\rho}\right]^{\frac{1}{2}} \exp\left(\frac{-N^2S_cS_r\pi\rho}{1+2\left(\mathbf{1_N}\mathbf{R}\mathbf{1_N^T}\right)S_cS_r(4-\pi)\rho}\right)d\theta. \tag{3.33}$$

The upper bound error probability is given by,

$$\overline{P}_e \leq \frac{1}{2}\left[\frac{1}{1+2\left(\mathbf{1_N R 1_N^T}\right)S_c S_r(4-\pi)\rho}\right]^{\frac{1}{2}} \exp\left(\frac{-N^2 S_c S_r \pi\rho}{1+2\left(\mathbf{1_N R 1_N^T}\right)S_c S_r(4-\pi)\rho}\right). \tag{3.34}$$

3.5.1.2 Probability of Error Analysis When Diversity Factor ($1 \leq D(\mathbf{R}) < 1.25$)

In this case, A is fit to Rayleigh distribution. Then, the instantaneous SNR $\gamma_{\max} = \rho B$ is modeled as exponential distribution. The probability density function (PDF) of B is defined as,

$$f_B(b) = \frac{1}{\overline{b}}\exp\left(-\frac{b}{\overline{b}}\right) \tag{3.35}$$

where $\overline{b}$ is average SNR. The MGF of B is determined as,

$$M_B(s) = \int_0^\infty f_B(b)\exp(-bs)db = \frac{1}{1-s\overline{b}} \tag{3.36}$$

If the probability of error of the system is $N_e Q\left(\sqrt{\frac{\gamma d_{\min}^2}{2}}\right) = N_e Q\left(\sqrt{\frac{\rho B d_{\min}^2}{2}}\right)$ then, the average probability of error is given by,

$$\overline{P}_e = \frac{N_e}{\pi}\int_0^{\frac{(M-1)\pi}{M}} M_B\left(-\frac{d_{\min}^2\rho}{4\sin^2\theta}\right)d\theta \tag{3.37}$$

Substituting (3.36), the average error probability of M-PSK system is given by,

$$\overline{P}_e = \frac{N_e}{\pi}\int_0^{\frac{(M-1)\pi}{M}} \left(1+\frac{\overline{b}d_{\min}^2\rho}{4\sin^2\theta}\right)^{-1} d\theta \tag{3.38}$$

For BPSK system, $M = 2, N_e = 1, d_{\min} = 2, \overline{b} = \frac{N^2\pi}{\left(\mathbf{1_N R 1_N^T}\right)(4-\pi)}$, then the average probability of error is given by,

$$\overline{P}_e = \frac{1}{2}\left(1-\sqrt{\frac{N^2\pi\rho}{N^2\pi\rho+\left(\mathbf{1_N R 1_N^T}\right)(4-\pi)}}\right) \tag{3.39}$$

3.5.1.3 Probability of Error Analysis When Diversity Factor ($1.25 \leq D(\mathbf{R}) < 6$)

In this case, A is log-normal distributed with mean $\mu_A = \frac{N\sqrt{S_c S_r}}{2}$ and variance $\sigma_A^2 = \left(\mathbf{1_N R 1_N^T}\right)S_c S_r\left(\frac{(4-\pi)}{4}\right)$. The corresponding PDF is given by,

$$f_A(a) = \frac{10}{\ln(10)\sqrt{2\pi}a\sigma_A}\exp\left(-\frac{\left(10\log_{10}a - 10\log_{10}\mu_A\right)^2}{20\log_{10}\sigma_A^2}\right) \tag{3.40}$$

The instantaneous SNR is given by,

$$\gamma = \frac{E_s}{N_0} A^2 = \rho A^2 = \rho B \tag{3.41}$$

By probability theory, $A^2 = B$ is also log-normal distributed with mean μ_B and variance σ_B^2 are as follows,

$$\begin{aligned} \mu_B &= \exp\left(2\mu_A + \sigma_A^2\right) \\ \sigma_B^2 &= \exp\left(2\mu_A + \sigma_A^2\right)\left[\exp(\sigma_A^2) - 1\right] \end{aligned} \tag{3.42}$$

The PDF of B is given by,

$$f_A(a) = \frac{10}{\ln(10)\sqrt{2\pi} b \sigma_B} \exp\left(-\frac{\left(10\log_{10} b - 10\log_{10}\mu_B\right)^2}{20\log_{10}\sigma_B^2}\right) \tag{3.43}$$

If the probability of error of the system is $N_e Q\left(\frac{b\rho d_{\min}^2}{2}\right)$, then the average error probability is given by,

$$\overline{P}_e = N_e \int_0^\infty Q\left(\frac{b\rho d_{\min}^2}{2}\right) f_B(b) db \tag{3.44}$$

This integral can be expressed using Gauss–Hermite quadrature integration [71, 72] and can be evaluated using MATLAB.

3.6 Results and Discussion

In this section, we delve into an EM analysis of RIS via simulations, probing the influence of spatial correlation on the average probability of error performance.

Figure 3.20 represents the geometrical structure of a single RIS cell. The design comprises a dipole antenna with a frequency of 7.125 GHz (an upper 6 GHz band, which is a licensed band of 5G-NR FR1). A reflector behind the antenna can control the RIS's periodicity by adjusting the width. The antenna tilt angle is adjusted so the dipole becomes horizontal relative to the ground.

Figure 3.21 shows a rectangular array of RIS elements with dimensions 10×10. Each cell in the meta-surface contains an antenna and reflector, with the horizontal bowtie antenna functioning as an exciter and the reflector enhancing directivity and gain. The spacing and dimensions of elements are designed based on the wavelength of incident signals.

Figure 3.22 demonstrates the structure of infinite RIS. Instead of placing many RIS elements, an approximation method for the infinite array concept is used for simulation. The periodic Green's function is used for the implementation, and the accuracy of results depends on the number of terms. In the design, receiver directions are modified for specifying the scan angles.

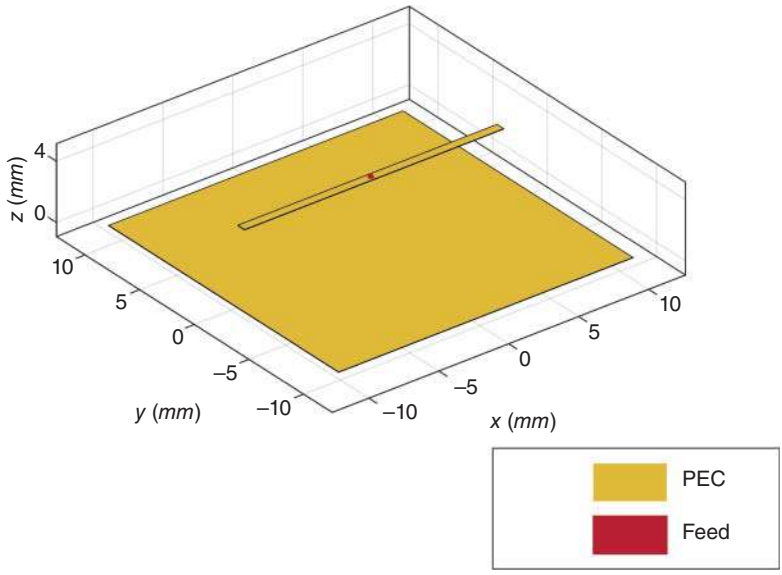

Figure 3.20 Geometrical structure of a single RIS cell.

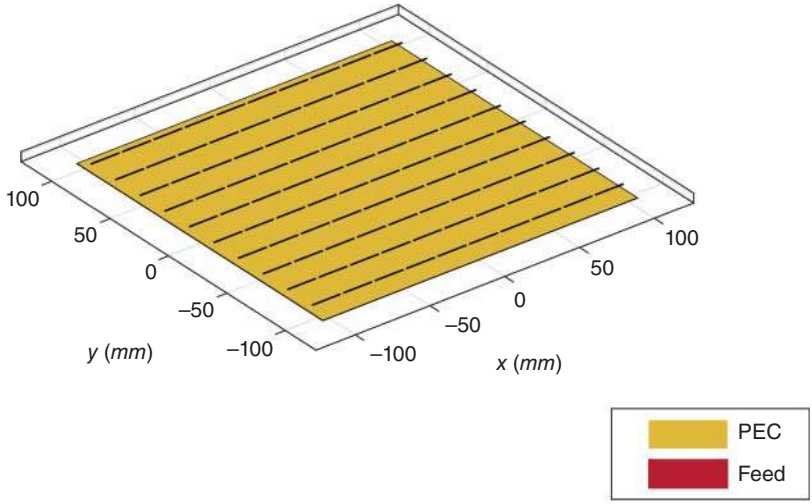

Figure 3.21 Finite RIS.

Figure 3.23 demonstrates the relation between the magnitude of the RIS reflection coefficient and the incident angle of signals. The RIS antennas are excited for the plane waves for the simulation, and the corresponding direction and polarization adjustments are performed. The incidence angle is varied between −30°

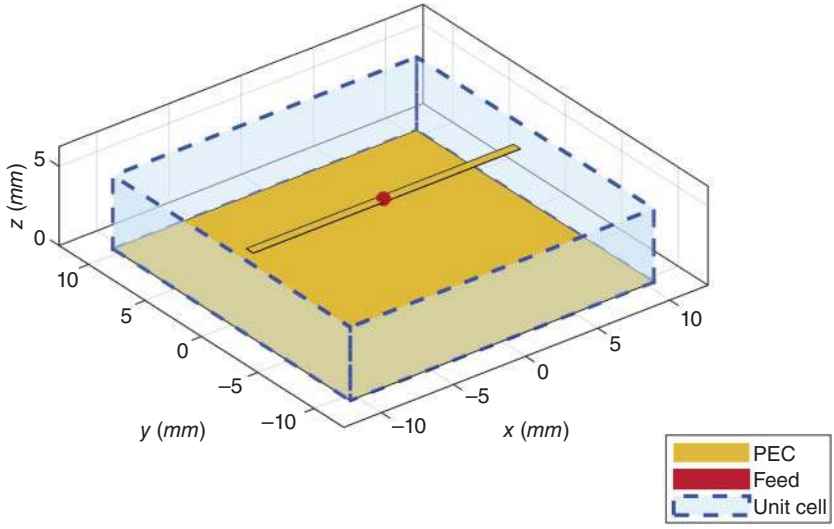

Figure 3.22 Infinite RIS.

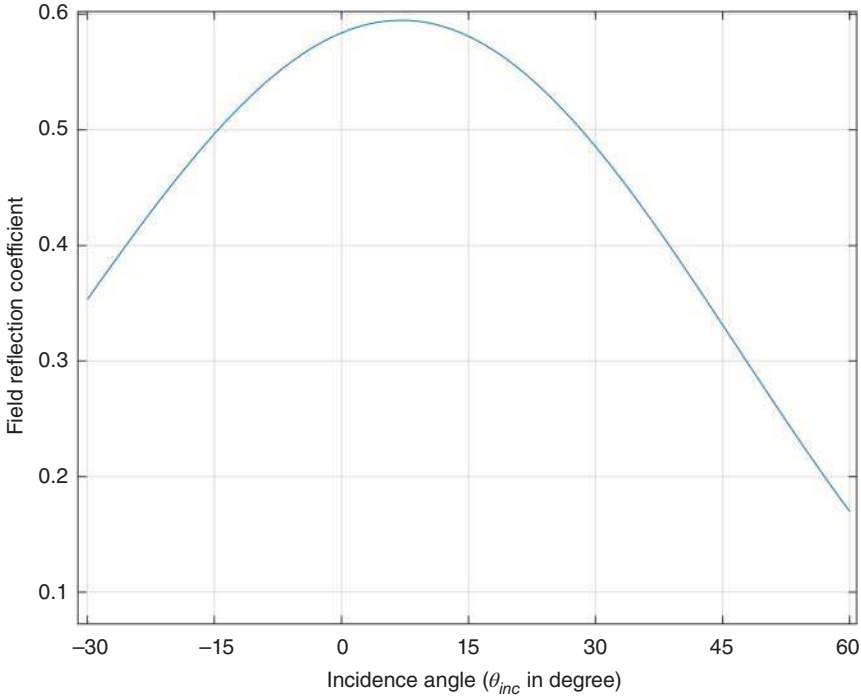

Figure 3.23 Reflection coefficient magnitude against incidence angle.

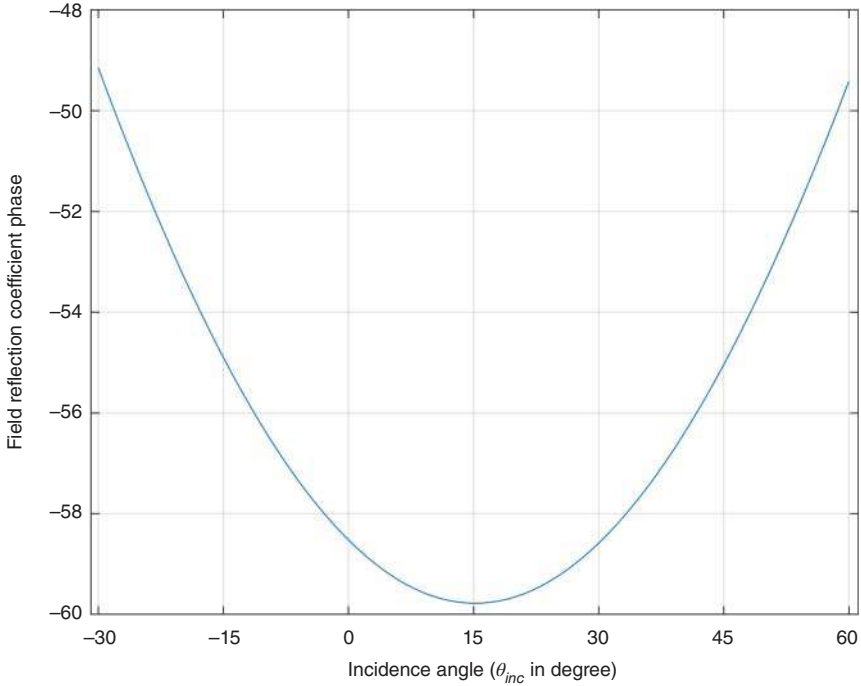

Figure 3.24 Reflection coefficient phase against incidence angle.

and $+60^{\circ}$ for the calculation. Results show that at $\theta_{inc} \approx 8^{\circ}$, the system has the maximum reflection coefficient ≈ 0.5948.

Figure 3.24 demonstrates the relation between the phase of the RIS reflection coefficient and the incident angle of signals. The result follows a parabolic shape in which the phase of the reflection coefficient varies from $\approx -30^{\circ}$ to $\approx 60^{\circ}$.

The average probability of error with $N = 64, 8 \times 8$ planar RIS with inter-element spacing of $S_c = S_r = 0.5\lambda, 0.3\lambda, 0.2\lambda, 0.1\lambda, 0.04\lambda$ is shown in Figure 3.25. It is observed that as inter-element spacing in the RIS element decreases, the SNR requirement for achieving desired probability of error increases. For example, the minimum SNR requirement for $\overline{P}_e = 10^{-4}$ are -26 dB, -21 dB, -16 dB, and -3 dB with the inter-element spacing of $S_c = S_r = 0.5\lambda, 0.3\lambda, 0.2\lambda, 0.1\lambda$, respectively. The average probability of error with $N = 16, 4 \times 4$ and $N = 64, 8 \times 8$ planar RIS with different diversity factors is shown in Figure 3.26. The attainment of a BER of 10^{-4} necessitates an SNR of approximately -26 dB for the planar 8×8 RIS setup with a diversity factor of 63.5. Conversely, for the same planar configuration, reducing the spacing between RIS elements leads to a reduced SNR requirement, with approximately -16 dB SNR

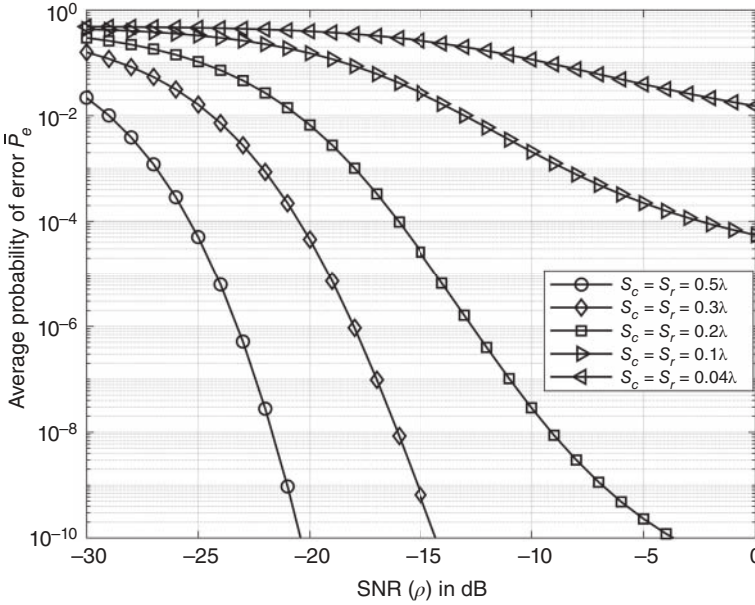

Figure 3.25 Probability of error for 8×8 planar RIS with various inter-element spacing.

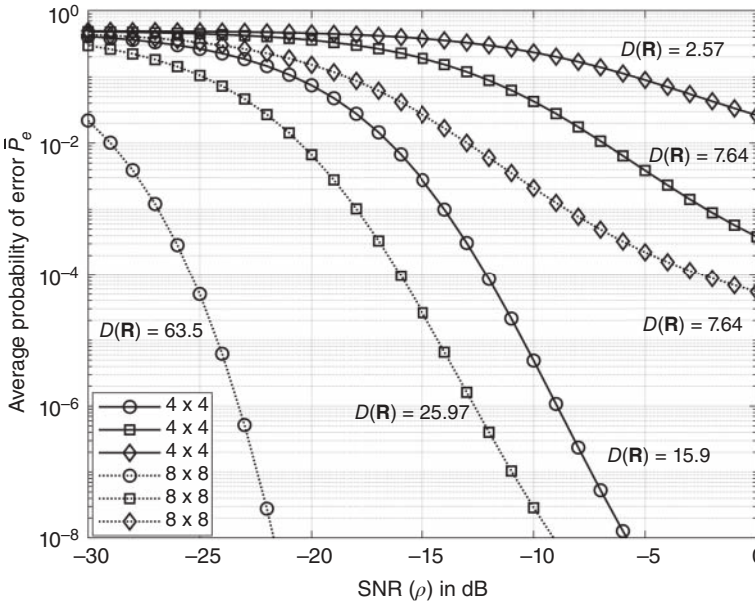

Figure 3.26 Probability of error for 4×4 planar RIS with Diversity factor ($D(\mathbf{R})$).

needed for a diversity factor of 25.97, and a further decrease to about −3 dB SNR for a diversity factor of 7.64. This trend is consistent across the planar 4×4 RIS geometry as well.

3.7 Conclusions

This chapter offers a thorough exploration of the architecture, hardware design, operational modes, and frequency bands pertinent to a variety of duplexing techniques within RIS. Moreover, it delves into an EM analysis of RIS a pivotal aspect involving the intricate study of EM wave interactions with the surface and its constituent elements. This analysis encompasses understanding how the RIS influences EM wave propagation, reflection, and scattering in its vicinity. It also entails the detailed characterization of the EM properties of the surface materials and structures, including their impedance, phase response, and radiation pattern. Additionally, the chapter presents a mathematical model that characterizes the gain of both transmit and receive units within the RIS setup. This model serves to elucidate the performance capabilities of the RIS in manipulating EM signals. Furthermore, the chapter extends its analysis to model the channel characteristics and reflection coefficients of individual elements within the RIS, providing insights into signal behavior and interaction dynamics.

Moreover, it investigates the effects of mutual coupling and spatial correlation on the performance of RIS. The derived expressions for average error probability under spatial correlation conditions demonstrate a clear trend: error rates escalate with increasing spatial correlation. These factors are crucial in shaping signal propagation and reception within the RIS environment. The chapter not only identifies these potential challenges but also explores mitigation strategies to optimize RIS performance under various operating conditions. By comprehensively addressing these aspects, the chapter contributes to a deeper understanding of RIS functionality and its implications for next-generation wireless communication systems.

The analysis of EM waves in RISs holds great promise for advancing our understanding and use of this transformative technology in various domains. This includes advanced modeling, optimization algorithms, material innovation, experimental validation, integration with artificial intelligence and ML, identifying cross-disciplinary applications, standardization, and regularization. Overall, the future scope of EM analysis of RISs is vast and multifaceted, offering numerous opportunities for innovation, collaboration, and societal impact across a wide range of applications.

References

1 Imoize, A.L., Adedeji, O., Tandiya, N., and Shetty, S. (2021). 6G enabled smart infrastructure for sustainable society: opportunities, challenges, and research roadmap. *Sensors* 21 (5): 1709.

2 Castillo-Soria, F.R., Del Puerto-Flores, J.A., Azurdia-Meza, C.A. et al. (2023). Precoding for RIS-assisted multi-user MIMO-DQSM transmission systems. *Future Internet* 15 (9): 299.

3 Kumaravelu, V.B., Imoize, A.L., Castillo Soria, F.R. et al. (2023). RIS-assisted fixed NOMA: outage probability analysis and transmit power optimization. *Future Internet* 15 (8): 249.

4 Kumaravelu, V.B., Selvaprabhu, P., Han, D.S. et al. (2023). Blind reconfigurable intelligent surface-aided fixed non-orthogonal multiple access for intelligent vehicular networks. *EURASIP Journal on Wireless Communications and Networking* 2023 (1): 83.

5 Rajak, S., Muniraj, I., Selvaprabhu, P. et al. (2023). A novel energy efficient IRS-relay network for ITS with Nakagami-m fading channels. *ICT Express* 10 (3): 507–512.

6 Van Nguyen, M.S., Do, D.T., Tin, P.T. et al. (2024). Full duplex reconfigurable intelligent surfaces system relying on NOMA and wireless power transfer. *Wireless Networks* 30: 2127–2142.

7 Jadhav, H.K. and Kumaravelu, V.B. (2022). Blind RIS aided ordered NOMA: design, probability of outage analysis and transmit power optimization. *Symmetry* 14 (11): 2266.

8 Kumaravelu, V.B., Imoize, A.L., Castillo Soria, F.R. et al. (2022). Outage probability analysis and transmit power optimization for blind-reconfigurable intelligent surface-assisted non-orthogonal multiple access uplink. *Sustainability* 14 (20): 13188.

9 Velmurugan, P.G.S., Thiruvengadam, S.J., Kumaravelu, V.B. et al. (2023). Performance analysis of full duplex bidirectional machine type communication system using IRS with discrete phase shifter. *Applied Sciences* 13 (12): 7128.

10 Chen, C. and Pan, C. (2021). Blocking probability in obstructed tunnels with reconfigurable intelligent surface. *IEEE Communications Letters* 26 (2): 458–462.

11 Mei, W. and Zhang, R. (2021). Distributed beam training for intelligent reflecting surface enabled multi-hop routing. *IEEE Wireless Communications Letters* 10 (11): 2489–2493.

12 Zheng, B., You, C., and Zhang, R. (2021). Efficient channel estimation for double-IRS aided multi-user MIMO system. *IEEE Transactions on Communications* 69 (6): 3818–3832.

13 Fu, M. and Zhang, R. (2022). Active and passive IRS jointly aided communication: deployment design and achievable rate. *IEEE Wireless Communications Letters* 12 (2): 302–306.

14 Peng, Z., Weng, R., Zhang, Z. et al. (2022). Active reconfigurable intelligent surface for mobile edge computing. *IEEE Wireless Communications Letters* 11 (12): 2482–2486.

15 Ma, Y., Li, M., Liu, Y. et al. (2022). Active reconfigurable intelligent surface for energy efficiency in MU-MISO systems. *IEEE Transactions on Vehicular Technology* 72 (3): 4103–4107.

16 Gao, Y., Wu, Q., Zhang, G. et al. (2022). Beamforming optimization for active intelligent reflecting surface-aided SWIPT. *IEEE Transactions on Wireless Communications* 22 (1): 362–378.

17 Chen, J.-C. (2022). Capacity improvement for intelligent reflecting surface-assisted wireless systems with a small portion of active elements. *IEEE Access* 10: 100438–100445.

18 Alsenwi, M., Abolhasan, M., and Lipman, J. (2022). Intelligent and reliable millimeter wave communications for RIS-aided vehicular networks. *IEEE Transactions on Intelligent Transportation Systems* 23 (11): 21582–21592.

19 Zeng, P., Qiao, D., Wu, Q., and Wu, Y. (2022). Throughput maximization for active intelligent reflecting surface-aided wireless powered communications. *IEEE Wireless Communications Letters* 11 (5): 992–996.

20 Feng, H. and Zhao, Y. (2023). Active RIS-assisted mmWave indoor signal enhancement based on transparent RIS. *arXiv preprint arXiv:2305.09228*.

21 Wang, Y. and Peng, J. (2023). Energy efficiency fairness of active reconfigurable intelligent surfaces-aided cell-free network. *IEEE Access* 11: 5884–5893.

22 Mei, W., Chen, Z., and Zhang, R. (2023). Joint beam routing and resource allocation optimization for multi-IRS-reflection wireless power transfer. *arXiv preprint arXiv:2307.08548*.

23 Li, Z., Topal, O.A., Demir, Ö.T. et al. (2023). mmWave coverage extension using reconfigurable intelligent surfaces in indoor dense spaces. *ICC 2023-IEEE International Conference on Communications*, 5805–5810. IEEE.

24 Mao, S., Liu, L., and Shao, C. (2023). Energy-efficient scheduling for active RIS-assisted self-sustainable wireless powered IoT networks in smart societies. *Sustainable Cities and Society* 95: 104559.

25 Zou, Y., Liu, Y., Mu, X. et al. (2023). Machine learning in RIS-assisted NOMA IoT networks. *IEEE Internet of Things Journal*.

26 Singh, S.K., Agrawal, K., Singh, K. et al. (2023). RSMA for hybrid RIS-UAV-aided full-duplex communications with finite blocklength codes under imperfect SIC. *IEEE Transactions on Wireless Communications* 22 (9): 5957–5975.

27 Hu, S., Yuan, X., Ni, W. et al. (2023). RIS-assisted jamming rejection and path planning for UAV-borne IoT platform: a new deep reinforcement learning framework. *IEEE Internet of Things Journal* 10 (22): 20162–20173.

28 Yu, L., Lv, X., Qian, J. et al. (2023). Design and analysis of HDMA-assisted visible light communication system based on transmitting and reflecting RIS. *2023 8th International Conference on Computer and Communication Systems (ICCCS)*, 515–520. IEEE.

29 Maraqa, O., Aboagye, S., and Ngatched, T.M.N. (2023). Optical STAR-RIS-aided VLC systems: RSMA versus NOMA. *IEEE Open Journal of the Communications Society* 5: 430–441.

30 Rhee, J.Y., Yoo, Y.J., Kim, K.W. et al. (2014). Metamaterial-based perfect absorbers. *Journal of Electromagnetic Waves and Applications* 28 (13): 1541–1580.

31 Liu, Y., Liu, X., Mu, X. et al. (2021). Reconfigurable intelligent surfaces: principles and opportunities. *IEEE Communications Surveys & Tutorials* 23 (3): 1546–1577.

32 Basar, E., Di Renzo, M., De Rosny, J. et al. (2019). Wireless communications through reconfigurable intelligent surfaces. *IEEE Access* 7: 116753–116773.

33 Najafi, M., Jamali, V., Schober, R., and Poor, H.V. (2020). Physics-based modeling and scalable optimization of large intelligent reflecting surfaces. *IEEE Transactions on Communications* 69 (4): 2673–2691.

34 Zhang, Z., Dai, L., Chen, X. et al. (2022). Active RIS vs. passive RIS: which will prevail in 6G? *IEEE Transactions on Communications* 71 (3): 1707–1725.

35 You, C. and Zhang, R. (2021). Wireless communication aided by intelligent reflecting surface: active or passive? *IEEE Wireless Communications Letters* 10 (12): 2659–2663.

36 Long, R., Liang, Y.-C., Pei, Y., and Larsson, E.G. (2021). Active reconfigurable intelligent surface-aided wireless communications. *IEEE Transactions on Wireless Communications* 20 (8): 4962–4975.

37 Lončar, J. and Šipuš, Z. (2020). Challenges in design of power-amplifying active metasurfaces. *2020 International Symposium ELMAR*, 9–12. IEEE.

38 Zhi, K., Pan, C., Ren, H. et al. (2022). Active RIS versus passive RIS: which is superior with the same power budget? *IEEE Communications Letters* 26 (5): 1150–1154.

39 Long, W., Chen, R., Moretti, M. et al. (2021). A promising technology for 6G wireless networks: intelligent reflecting surface. *Journal of Communications and Information Networks* 6 (1): 1–16.

40 Liu, Y., Mu, X., Xu, J. et al. (2021). STAR: simultaneous transmission and reflection for 360° coverage by intelligent surfaces. *IEEE Wireless Communications* 28 (6): 102–109.

41 Schroeder, R., He, J., and Juntti, M. (2021). Passive RIS vs. hybrid RIS: a comparative study on channel estimation. *2021 IEEE 93rd Vehicular Technology Conference (VTC2021-Spring)*, 1–7. IEEE.

42 Pizzo, A., Marzetta, T.L., and Sanguinetti, L. (2020). Spatially-stationary model for holographic MIMO small-scale fading. *IEEE Journal on Selected Areas in Communications* 38 (9): 1964–1979.

43 Yurduseven, O., Marks, D.L., Fromenteze, T., and Smith, D.R. (2018). Dynamically reconfigurable holographic metasurface aperture for a mills-cross monochromatic microwave camera. *Optics Express* 26 (5): 5281–5291.

44 Huang, C., Zappone, A., Alexandropoulos, G.C. et al. (2019). Reconfigurable intelligent surfaces for energy efficiency in wireless communication. *IEEE Transactions on Wireless Communications* 18 (8): 4157–4170.

45 Kaina, N., Dupré, M., Lerosey, G., and Fink, M. (2014). Shaping complex microwave fields in reverberating media with binary tunable metasurfaces. *Scientific Reports* 4 (1): 6693.

46 Di Renzo, M., Debbah, M., Phan-Huy, D.-T. et al. (2019). Smart radio environments empowered by reconfigurable AI meta-surfaces: an idea whose time has come. *EURASIP Journal on Wireless Communications and Networking* 2019 (1): 1–20.

47 Shlezinger, N., Dicker, O., Eldar, Y.C. et al. (2019). Dynamic metasurface antennas for uplink massive MIMO systems. *IEEE Transactions on Communications* 67 (10): 6829–6843.

48 Liaskos, C., Nie, S., Tsioliaridou, A. et al. (2018). A new wireless communication paradigm through software-controlled metasurfaces. *IEEE Communications Magazine* 56 (9): 162–169.

49 Huang, C., Hu, S., Alexandropoulos, G.C. et al. (2020). Holographic MIMO surfaces for 6G wireless networks: opportunities, challenges, and trends. *IEEE Wireless Communications* 27 (5): 118–125.

50 Jian, M., Alexandropoulos, G.C., Basar, E. et al. (2022). Reconfigurable intelligent surfaces for wireless communications: overview of hardware designs, channel models, and estimation techniques. *Intelligent and Converged Networks* 3 (1): 1–32.

51 Basar, E. and Poor, H.V. (2021). Present and future of reconfigurable intelligent surface-empowered communications [perspectives]. *IEEE Signal Processing Magazine* 38 (6): 146–152.

52 Cui, Z., Zhang, P., and Pollin, S. (2023). 6G wireless communications in 7-24 GHz band: opportunities, techniques, and challenges. *arXiv preprint arXiv:2310.06425*.

53 da Silva, L.G., Alexandre, L.C., Xiao, P., and Cerqueira, A. (2023). RIS development and implementation in a mm-Waves 5G-NR system towards 6G. *IEEE Wireless Communications Letters* 13 (3): 736–740.

54 Su, X., He, R., Ai, B. et al. (2024). Channel estimation for RIS assisted THz systems with beam split. *IEEE Communications Letters* 28 (3): 637–641.

55 Naaz, F., Nauman, A., Khurshaid, T., and Kim, S.-W. (2024). Empowering the vehicular network with RIS technology: a state-of-the-art review. *Sensors* 24 (2): 337.

56 Shen, L.-H., Feng, K.-T., Lee, T.-S. et al. (2024). AI-enabled unmanned vehicle-assisted reconfigurable intelligent surfaces: deployment, prototyping, experiments, and opportunities. *IEEE Network* 38 (6): 289–299.

57 Elhattab, M., Arfaoui, M.A., Assi, C., and Ghrayeb, A. (2021). Reconfigurable intelligent surface enabled full-duplex/half-duplex cooperative non-orthogonal multiple access. *IEEE Transactions on Wireless Communications* 21 (5): 3349–3364.

58 Guo, B., Sun, C., and Tao, M. (2021). Two-way passive beamforming design for RIS-aided FDD communication systems. *2021 IEEE Wireless Communications and Networking Conference (WCNC)*, 1–6. IEEE.

59 Cui, Y., Yin, H., Tan, L., and Di Renzo, M. (2022). A 3D positioning-based channel estimation method for RIS-aided mmWave communications. *arXiv preprint arXiv:2203.14636*.

60 Qian, X. and Di Renzo, M. (2021). Mutual coupling and unit cell aware optimization for reconfigurable intelligent surfaces. *IEEE Wireless Communications Letters* 10 (6): 1183–1187.

61 Abrardo, A., Dardari, D., Di Renzo, M., and Qian, X. (2021). MIMO interference channels assisted by reconfigurable intelligent surfaces: mutual coupling aware sum-rate optimization based on a mutual impedance channel model. *IEEE Wireless Communications Letters* 10 (12): 2624–2628.

62 Hassouna, S., Jamshed, M.A., Rains, J. et al. (2023). A survey on reconfigurable intelligent surfaces: wireless communication perspective. *IET Communications* 17 (5): 497–537.

63 Fu, X., Peng, R., Liu, G. et al. (2022). Channel modeling for RIS-assisted 6G communications. *Electronics* 11 (19): 2977.

64 Papazafeiropoulos, A., Ngo, H.Q., Kourtessis, P., and Chatzinotas, S. (2023). STAR-RIS assisted cell-free massive MIMO system under spatially-correlated channels. *IEEE Transactions on Vehicular Technology* 73 (3): 3932–3948.

65 Liu, Z., Zhang, J., Wang, Z. et al. (2023). Cell-Free Massive MIMO with Mixed Resolution: ADCS and I/Q Imbalance Over Rician Spatially Correlated Channels. *IEEE Transactions on Vehicular Technology* 72 (7): 9567–9572.

66 Fang, W., Liang, X., Bao, X. et al. (2022). Channel estimation for a RIS-assisted MU-MIMO system using one-bit ADCs over spatially correlated channels.

2022 IEEE/CIC International Conference on Communications in China (ICCC), 690–695. IEEE.

67 Sun, S. and Yan, H. (2021). Small-scale spatial-temporal correlation and degrees of freedom for reconfigurable intelligent surfaces. *IEEE Wireless Communications Letters* 10 (12): 2698–2702.

68 Shamsuri Agus, A.N.S., Sabapathy, T., Jusoh, M. et al. (2022). Combined RIS and EBG surfaces inspired meta-wearable textile MIMO antenna using Viscose-Wool felt. *Polymers* 14 (10): 1989.

69 Tu, X., Fang, H., Zhang, Y. et al. (2023). RIS-assisted spatially correlated cell-free massive MIMO system. *2023 IEEE/CIC International Conference on Communications in China (ICCC)*, 1–6. IEEE.

70 Thirumavalavan, V.C., Hariharan, A.B.R., and Thiruvengadam, S.J. (2022). BER analysis of tightly packed planar RIS system using the level of spatial correlation and discrete phase shifter. *Transactions on Emerging Telecommunications Technologies* 33 (11): e4596.

71 Shao, T.S., Chen, T.C., and Frank, R.M. (1964). Tables of zeros and Gaussian weights of certain associated Laguerre polynomials and the related generalized Hermite polynomials. *Mathematics of Computation* 18 (88): 598–616.

72 Simon, M.K. and Alouini, M.-S. (2008). Digital communications over fading channels (M.K. Simon and M.S. Alouini; 2005) [book review]. *IEEE Transactions on Information Theory* 54 (7): 3369–3370.

4

Spectral Efficiency and Rate Fairness for RIS-Aided Multiuser Massive MIMO System

*Rafael Augusto Pedriali, Wilson de Souza Junior, and Taufik Abrão**

Department of Electrical Engineering, State University of Londrina (UEL), Londrina, Paraná, Brazil

4.1 Introduction

Wireless communication has evolved rapidly over the past few decades, with new technologies and standards aimed at improving spectral efficiency (SE), data rates, and quality of service (QoS). With the advent of fifth-generation (5G) networks and the beyond-5G (B5G) and sixth-generation (6G) networks, there is a need for innovative solutions that can meet the growing demands for connectivity. One of the promising technologies in this scenario is the reconfigurable intelligent surface (RIS), which has the potential to transform the propagation environment into an ally to improve the performance of the communication system.

RIS are flat surfaces composed of passive elements that can reflect radio waves in a controlled manner, changing the phase and amplitude of the reflected signal. This ability to shape radio waves enables the optimization of the wireless communication scenario, improves SE, and providing significant gains in terms of data rates and QoS. Moreover, RIS can be integrated into existing networks, offering a low-cost solution to enhance the performance of 5G and 6G networks. One of the main challenges in 5G and 6G networks is using millimeter-wave (mm-Wave) frequencies and beyond, which can provide higher data rates and capacity compared to lower frequencies. However, these higher frequencies are more susceptible to blockage and absorption by obstacles such as buildings, vehicles, trees, and others. This significantly degrades the signal quality and, consequently deteriorates the communication link between users and the base

*This work was supported in part by the National Council for Scientific and Technological Development (CNPq) of Brazil, Grants: 405301/2021-9 and 310681/2019-7, in part by the Coordination of Superior Level Staff Improvement (CAPES), Grant: 88887.847039/2023-00, and by Londrina State University (UEL), Brazil.

Reconfigurable Intelligent Surfaces for 6G and Beyond Wireless Networks, First Edition.
Edited by Agbotiname Lucky Imoize, Vinoth Babu Kumaravelu, and Dinh-Thuan Do.

station (BS). Additionally, electromagnetic theory establishes that an increase in carrier frequency correlates with an enhanced attenuation of electromagnetic waves. Consequently, this underscores that mmWave frequencies exhibit shorter propagation ranges than those transmitted at sub-6 GHz frequencies. The RIS technology application can play a crucial role in mitigating these challenges by intelligently reflecting and shaping the radio waves, thereby improving the propagation environment and ensuring a reliable communication link, even in the presence of obstacles [1, 2].

4.1.1 Related Work

Wireless communications have marked a significant leap with RIS technologies, promising enhanced data rates and signal quality by manipulating electromagnetic waves across N RIS elements. Thus, we review several studies exploring optimization problems to maximize QoS, showcasing RIS technology's broad applicability and potential. The work [3, 4] studies applications with the passive beamforming (PBF) optimization on the N RIS elements. de Souza Junior and Abrao [3] presents the performance RIS-assisted cooperative non-orthogonal multiple access (NOMA) systems. It focuses on systems where two users are paired, with RIS phases optimized to enhance the signal for a device at the cell center, acting as a full-duplex relay to assist a device at the cell edge. The work [4] proposes schemes closed form solution's performance while offering much lower computational complexity. This makes the schemes particularly suitable for real scenarios where the scalability and optimality of RIS configurations are crucial. The paper's contributions offer a general framework for configuring RIS elements efficiently, improving the deployment of RIS in future wireless networks to meet the increasing demand for high data rates. In contrast, the work [5] delves into the development and evaluation of a joint optimization strategy for beamforming RIS phases and power allocation aimed at maximizing the minimum signal-to-interference-plus-noise ratio (SINR) in an uplink (UL) communication system augmented by RIS, i.e., a conventional max–min optimization problem. Similarly, the [6] applies max -min strategies on a system's downlink (DL) scenario, specifically highlighting the performance of STAR-RIS-assisted M-MIMO systems under hardware impairments. The work [7] presents a comprehensive study on enhancing the performance of multiuser multiple-input single-output (MISO) wireless communication systems by applying RIS. The study focuses on optimizing all users' weighted sum rate (WSR) by jointly designing the beamforming at the access point and the phase adjustments of the RIS elements. The proposed problem enables the manipulation of electromagnetic waves, offering a promising approach to achieving a programmable wireless environment. Table 4.1 compares recent works with the topics discussed in this chapter, highlighting differences in channel and carrier considerations and the proposed optimization problems.

Table 4.1 Related work that addresses current open issues in channel conditions, with optimization problems for QoS in wireless communication systems.

References	Channel	Carrier	Optimization problem	Observations
de Souza Junior and Abrao [3]	Nakagami-m	Sub-6 GHz	PBF	This work offers an insightful overview of the Nakagami-m channel with optimal PBF on the N RIS elements within cooperative NOMA systems.
Sun et al. [4]	Generic (not specified)	Generic (not specified)	PBF	This work presents analytical solutions to optimization problems. However, it lacks specific carrier details, and the channel information is described broadly without detailing potential statistical channel conditions.
Subhash et al. [5]	Rice	mmWave	Max–min problem	Provide an interesting overview of RIS with mmWave carrier and a closed-form formulations, but limited to Rice channel.
Papazafeiropoulos et al. [6]	Rayleigh	Sub-6 GHz	Max–min problem	Offers an interesting overview of STAR-RIS, including analytical formulations, yet its scope is limited to Rayleigh channels and sub-6 GHz carrier frequencies.
Guo et al. [7]	Rayleigh and Rice	Generic (not specified)	Sum rate problem	This work aims to address the analytical formulation of the N RIS elements to maximize the weighted sum rate (WSR) in a MISO multiuser DL scenario. However, details regarding carrier frequencies, as well as near-field and far-field conditions, are not provided.
This Chapter	Rayleigh, Rice, Nakagami-m, α–μ, and κ–μ	Sub-6 GHz and mmWave	PBF, Max–min and sum rate problems	Our work offers a comprehensive overview of various channel conditions, employing both sub-6 GHz and mmWave carrier conditions, and conducting a thorough comparison among the optimization techniques discussed in the literature, alongside the naive local search (NLS) method, to address the max–min and sum rate problems.

4.1.2 Contributions

This book chapter delves into the analysis of Massive MIMO (M-MIMO) systems assisted by RIS, focusing on performance and computational complexity through extensive simulations in multiuser UL scenarios. It highlights the potential of RIS-aided M-MIMO systems for future generations of wireless mobile communications systems, exploring various fading channels, multiuser combiners/precoders, and optimization methods to enhance reliability and coverage, impacting the SINR, SE, and outage probability (OP). It also details strategies for positioning user equipment in static and dynamic configurations for its subsequent analysis. In this manner, we integrate several well-established concepts from the literature to offer a thorough and valuable analysis, paving the way for novel results, studies, and insights for the RIS-aided M-MIMO communication systems. Table 4.2 summarizes our key findings results discussed in Section 4.4, incorporating insights and observations.

4.1.3 Organization

This chapter is organized into five key sections that comprehensively cover various aspects of RIS-aided M-MIMO systems. Section 4.2 related reviews M-MIMO concepts and technologies, emphasizing their important role in current and future wireless networks. Besides, we revisit the concepts of active beamforming and outline the understanding of near-field and far-field regions, their transition, and their applications in wireless communication systems. Next, we explore various statistical channel models applied in analyzing and designing wireless communication systems, such as Rayleigh, Rice, Nakagami-m κ–μ, and α–μ distributions. We summarize recent studies on applying RIS to enhance massive multiuser MIMO systems, showcasing the state-of-the-art technology in this rapidly evolving field.

Section 4.3 describes the system setup for RIS-aided M-MIMO communication systems, encompassing the BS, the RIS, and multiple UEs with a single antenna sharing the channel. We then discuss performance metrics related to QoS, such as SINR, SE, and OP, used to evaluate the RIS-aided M-MIMO systems. This section also covers the search mechanisms employed to identify optimal configurations of RIS elements, aiming to maximize system performance. Furthermore, we address the optimization problems formulated within this section, which are designed to enhance the QoS performance.

In Section 4.4, both the dynamic and static scenarios are explored. Within such scenarios, four analyses are conducted, offering deep insights into RIS-aided M-MIMO channel modeling and with different carrier frequencies (including sub-6 GHz and mmWave), and the strategies employed through optimization

Table 4.2 The key summarized results and observations of this chapter, comprising channel models, optimization problems, and carrier frequencies for RIS-Aided M-MIMO systems.

Scenario	Channel model UEs-RIS	Optimization problem	Carrier frequency	Description
Dynamic UEs positions	Rayleigh	PBF, NLS	1 GHz	An example demonstrating the efficient operation of RIS-aided M-MIMO systems with dynamical UEs positions, using sub-6 GHz carriers and considering the lower bound channel conditions.
Dynamic, with different channels	Rayleigh, Rice, Nakagami-m, α–μ, and κ–μ	PBF	1 GHz	The first results introducing the statistical α–μ and κ–μ channel models for RIS-aided M-MIMO systems.
Static, with UEs uniformly distributed	Rayleigh	PBF, NLS	60 GHz	A specific example illustrating enhanced QoS through sum rate optimization compared to the max–min optimization approach. Additionally, demonstrate how the highest carrier damages the QoS with the distance.
Static, with UEs equally spaced from RIS but with different angles	Rayleigh	PBF, NLS	30 GHz	An example demonstrating the efficient operation of RIS-aided M-MIMO systems with static and equally spaced UEs positions relative to RIS, as well as using mmWave carriers and considering the lower bound channel conditions.

problems to enhance the QoS performance. The analyses described include dynamic scenarios, dynamic scenarios with different channel models, static scenarios with UEs uniformly distributed, and static scenarios with UEs equally spaced from RIS but with different angles. Each setup provides a unique perspective on the system's efficacy under varying conditions.

Finally, Section 4.5 concludes the chapter by synthesizing the findings, and highlighting the enhancement in wireless communication systems' performance due to RIS deployment. This section discusses the challenges and opportunities in optimizing RIS-aided M-MIMO systems, the adaptability of RIS technology to various user configurations, and its potential to meet diverse communication needs efficiently. Moreover, it offers insights into the proposed model's limitations and outlines future research directions, including exploring new steering vectors, addressing different multipath channels, and optimizing energy efficiency.

4.2 Fundamental Concepts

This section delves into the core concepts, physical theories, statistical channels, and technological properties well documented in the literature. Our presentation of these topics will be thorough, methodically structured, and interrelated to ensure they collectively enhance understanding. Our objective is to furnish a holistic and valuable resource for researchers and professionals in the field, thereby deepening theoretical and practical insights into RIS technology. The subjects in this section include active beamforming techniques, the principles and practical implementation of near-field communication channels, the examination and utilization of statistical channel models, and an overview of RIS technology, including its operational modes and system models.

4.2.1 MIMO

MIMO stands for multiple input multiple output, a wireless technology whose central development was in the third generation with the promise to improve the communication performance of wireless communications systems significantly. Here's a brief explanation of this technology.

The MIMO system involves multiple antennas at both the transmitter and receiver of a wireless communication system. The core idea is to increase the capacity of a radio link using multiple antennas in the transmitter and receiver. Additionally, MIMO systems allow the transmission of multiple data streams simultaneously over the same radio frequency channel. This can significantly increase the network's data throughput without additional bandwidth or

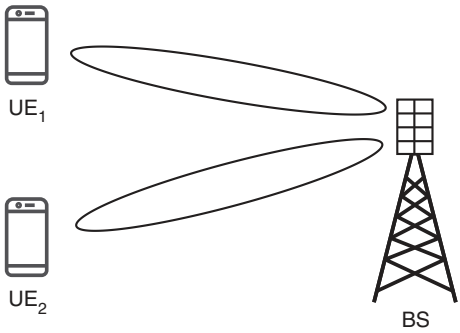

Figure 4.1 MIMO system. Source: The Authors.

increased transmit power. It enhances the reliability of wireless communications by providing multiple paths for data to reach its destination, reducing the likelihood of dropouts or signal degradation.

This technology allows the systems to utilize two main techniques: spatial diversity and spatial multiplexing. The first improves signal robustness by sending redundant data across different paths. On the other hand, spatial multiplexing increases channel capacity by transmitting different data streams on different antennas simultaneously.

Figure 4.1 illustrates two UEs and a BS with multiple antennas sharing the channel in a communication system. This configuration is technically known as MIMO systems, which involves the use of multiple antennas at both the transmitter and receiver ends [8].

To summarize, MIMO represents a significant advancement in wireless communication technology. It allows more data to be transmitted at higher speeds and with greater reliability, making it a foundational technology in modern wireless infrastructure.

4.2.1.1 Massive MIMO

The evolution to M-MIMO was an extension of MIMO, addressing new technologies and techniques. The M-MIMO is mainly envisioned for advanced 5G networks and beyond. Its ability to handle numerous simultaneous connections robustly makes it ideal for densely populated urban areas and applications requiring high data throughput and capacity.

Figure 4.2 illustrates an M-MIMO system with k UEs sharing the channel with one BS with multiple antennas.

In essence, the M-MIMO is a wireless technology that involves equipping BS with many antennas so that multiple users can share the channel simultaneously. This setup increases several wireless communications systems'

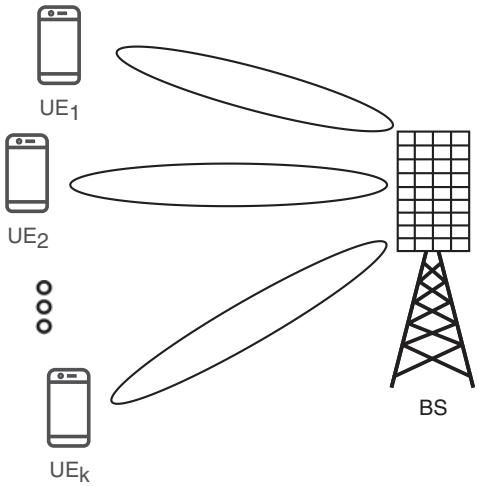

Figure 4.2 M-MIMO system. Source: The Authors.

spectral and energy efficiency, significantly improving data throughput and connection reliability.

Technical aspects of M-MIMO systems use simple linear processing techniques like matched filter (MF) precoding and combining, which become increasingly effective as the number of antennas grows. The technology leverages the large number of degrees of freedom provided by the massive antenna arrays for efficient signal processing. At the heart of M-MIMO are the large antenna arrays. Unlike conventional MIMO, which may use a handful of antennas, M-MIMO can employ hundreds of antennas at a single BS. This allows for simultaneous communication with many users, enhancing the network's capacity. Another critical feature of M-MIMO is that user devices, like smartphones, tablets, or other wireless devices, are typically equipped with a single antenna. This practical and cost-effective setup makes it well-suited for most mobile devices. The core of this chapter is to explore scenarios with spectrum sharing with Beamforming techniques presented in Section 4.2.1.3.

Therefore, using many antennas increases the throughput and capacity, but the system's complexity also grows significantly. This leads to higher costs, power consumption, and more sophisticated signal processing requirements [9].

4.2.1.2 Particular Cases

In this chapter, the system under simulation exemplifies a distinct category within M-MIMO systems, emphasizing the single input multiple output (SIMO) multiuser UL system and MISO multiuser DL system. Their respective setup is presented below.

In an SIMO multiuser UL system, each user (or device) has a single antenna (single input), while the BS has multiple antennas (multiple outputs). This configuration is typical in UL scenarios, where multiple users transmit signals to a single BS. The BS uses multiple antennas to receive these signals, potentially employing techniques like diversity reception to enhance signal quality.

Conversely, in the MISO multiuser DL system, the BS uses its multiple antennas (multiple inputs) to transmit signals to users, each of whom has a single antenna (single output). This is a typical DL scenario. Here, techniques like beamforming are often used to improve transmission efficiency and signal quality for each user [9].

Additionally, it is paramount to note that the system model presented in this paper have also the RIS added aiming to reflect the signal between the BS and devices, and the complete setup device-RIS-BS is given in Section 4.3.1.

4.2.1.3 Beamforming

Beamforming is an advanced technique that shapes the radiation patterns of an antenna array by effectively consolidating signals toward targeted users while simultaneously nullifying signals from unwanted directions [10]. It involves the intelligent combination of signals from multiple antennas to form a focused beam toward the intended user. This process utilizes finite impulse response (FIR) filters, which are advantageous due to their adaptive weight adjustment capabilities, enabling optimal beamforming configurations. When applied in extensive MIMO systems, beamforming brings several key benefits. These include significantly improved aspects, such as better SE and energy efficiency, heightened security within the system, and suitability for use in mmWave frequency bands. These aspects are detailed as follows:

- **Improving SE:** In M-MIMO systems, beamforming enhances SE through carefully controlling UL and DL signals, using training sequence information, and improving signal quality. This is achieved by deploying large arrays of beamforming antenna elements at BSs, combined with coherent precoding and detector processing;
- **Improving energy efficiency:** The beamforming technique applied in M-MIMO systems can contribute to energy savings by reducing the power needed to send signals to specific users, thus reducing power consumption. This aspect of energy efficiency is crucial for future wireless communication systems. Additionally, beamforming techniques can optimize the efficiency of antenna elements in M-MIMO systems, improving power consumption and performance. This optimization ensures that the energy efficiency remains consistent regardless of the number of active antenna elements, leading

to cost-effective and energy-efficient solutions. Optimizing beamforming techniques, including power control, is essential to minimize power usage at BSs;

- **Improving system security:** The application of beamforming in M-MIMO systems also enhances system security. This improvement comes from the ability of beamforming to focus signals directly to specific users while minimizing leakage to other users. This focused transmission reduces the risk of eavesdropping and mitigates the potential for interference with other devices. As a result, beamforming is a critical factor in securing wireless communication systems, particularly in environments where security and privacy are paramount;
- **Suitability for mm-Wave frequencies:** The applicability of beamforming in mmWave frequency bands is a significant advantage. This technology is particularly suited for mmWave bands because it can combat the high path loss typically associated with these frequencies. Beamforming achieves this by directing concentrated energy toward specific users, enhancing signal strength and reliability. This property makes beam forming an integral part of the deployment strategies for next-generation wireless networks operating in mmWave bands.

4.2.1.4 Adaptive Beamforming

Adaptive beamforming techniques allow the system to dynamically adjust the beam pattern based on user location and channel conditions, particularly in the realms of wireless communications and radar systems. The "adaptive" aspect of beamforming comes into play when the system automatically adjusts the phase and amplitude of signals at each antenna element. This adjustment is based on real-time assessments of the incoming signals in the environment.

This technique offers significant advantages, particularly in environments where signal conditions are constantly changing. By dynamically adjusting the array's pattern, adaptive beamforming enhances the signal-to-noise ratio (SNR) and signal-to-interference-plus-noise ratio (SINR), improving overall signal quality and making the system more efficient and reliable. This is especially beneficial in wireless communication networks and radar systems, where maintaining signal clarity and strength is crucial.

Certain fundamental beamforming techniques in M-MIMO systems, such as MF, zero forcing (ZF), and minimum mean square error (MMSE), are important for signal processing in multiuser contexts. They are crucial for BS on reception, employing combiners, and on transmission, using precoders. These methods enable the BS to effectively handle the intricacies of simultaneously catering to multiple users, thereby enhancing signal quality and reducing interference. The details of these beamforming techniques are outlined as follows [10].

Matched Filter The MF beamforming technique utilized in receivers is maximum ratio combining (MRC). It aims to achieve the highest attainable SNR for a single-user setup. For multiusers setups, the MRC operates by amplifying the signal from a specific antenna while reducing interference from other antennas. This method's strength lies in its straightforward signal processing at the BS, coupled with the optimization of SNR or SINR, which is particularly beneficial in systems where prioritizing a single user is crucial. On the other hand, the disadvantage arises in scenarios where multiple users are also crucial to the system. In such cases, this technique falls short of adequately mitigating interference effects for all users.

The maximum ratio transmission (MRT) share the same principle of MRC. However, it is applied to the DL signal transmission in wireless communication systems. Its primary goal is to maximize the SNR at the receiving device. This is achieved by calibrating the phase and amplitude of signals transmitted from the BS's antennas. Such adjustments ensure that, upon reaching the receiver, these signals combine to amplify the desired signal significantly.

In both cases, the technique employs the expression in Eq. (4.1) for beamforming:

$$\mathbf{W_{MF}} = \mathbf{H}^H \tag{4.1}$$

in which $\mathbf{H}$ is the channel and is a complex array, and $(\cdot)^H$ is the Hermitian operation.

Zero Forcing The ZF plays a significant role in M-MIMO systems, particularly in the realms of combiners and precoders. The ZF technique is centered on completely eliminating the multiuser interference. In the context of precoding, this is achieved by estimating the orthogonal complement of interference between users. It involves tailoring the transmitted signals so that, upon reception, the interference among signals intended for different users is entirely eliminated.

In the realm of combiners, ZF assumes a comparable role, albeit in a reverse manner. In this scenario, the technique processes the signals received at the BS from various users. ZF functions to segregate these signals with the aim of reducing or completely nullifying the interference among them. By identifying and counteracting the interference observed across different users' channels, ZF facilitates the clearer extraction of each signal, free from distortion induced by other concurrent signals. This enhancement markedly elevates the quality of the received signal for each user in multiuser settings.

In both the ZF combiner and precoder, the expression for beamforming is represented by the pseudo-inverse of the channel matrix, expressed in Eq. (4.2)

$$\mathbf{W}_{ZF} = \mathbf{H}\,(\mathbf{H}\mathbf{H}^H)^{-1} \tag{4.2}$$

in which $(.)^{-1}$ corresponds to the inverse matrix operation.

Minimum Mean Square Error This technique applies in combiners and precoders and minimizes the mean squared error between the transmitted and estimated signals. The MMSE approach considers both interference and noise, aiming to find an optimal balance between them for a more accurate signal estimation. This objective is achieved using Eq. (4.3),

$$\mathbf{W}_{MMSE} = \mathbf{H}(\mathbf{H}\mathbf{H}^H + \sigma^2\mathbf{I})^{-1} \tag{4.3}$$

in which σ^2 is the noise variance and $\mathbf{I}$ is the eye matrix. Be aware that for the matrix operation to be valid, the dimension of I must match with a dimension of $\mathbf{H}\mathbf{H}^H$.

4.2.2 Near-Field and Far-Field Communication

In the realm of 6G communication technologies, understanding the behavior of electromagnetic fields around antennas becomes increasingly critical, especially as we move towards employing larger antenna arrays and higher frequencies. This shift necessitates a deeper exploration of the near-field and far-field regions, concepts fundamental to antenna theory but taking on new significance in the context of 6G's advancements [11].

Historically, the division between near-field and far-field regions was determined by the Rayleigh distance, a formula derived from the antenna's physical dimensions and the wavelength of the electromagnetic waves it emits. This distance helps us predict whether the electromagnetic wavefront is located in the near-field or far-field region. In the near-field region, the strength of electromagnetic interactions changes rapidly with distance, characterized by spherical waves. In contrast, in the far-field region, the electromagnetic field becomes more uniform and predictable, with propagation in the form of planar waves.

The Rayleigh distance (d_r), calculated as $d_r = \frac{2D^2}{\lambda}$, in which D represents the diameter of the antenna aperture or the size of the radiating element. It also serves as a key metric for differentiating between the near-field and far-field regions, highlighting its importance in electromagnetic wave propagation. Additionally, the channel phase error caused by the far-field approximation can not exceed $\frac{\pi}{8} = 22.5°$.

Figure 4.3 illustrates a BS array transmitting signals represented by waves. The spherical waves within the Rayleigh distance adheres to a power density distribution that follows spherical coordinates. Conversely, the planar waves, deemed far from the BS, are characterized by a simplified planar wavefront transmission model.

The transition between the near-field and far-field regions is not abrupt but gradual, complicating efforts to define where one ends and the other begins precisely. Researchers have proposed various metrics to characterize this transition, looking

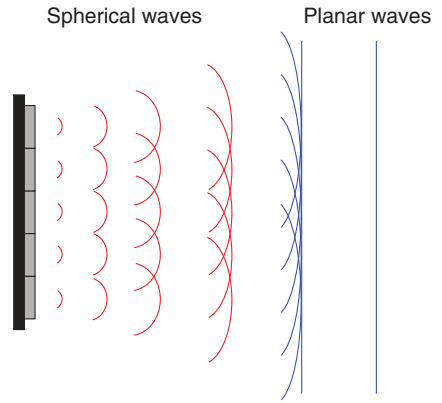

Figure 4.3 The propagation of spherical waves becoming planar after the Rayleigh distance. Source: The Authors.

at phase and channel gain errors. These efforts reflect the growing recognition of the near-field's importance in 6G communication systems, where traditional far-field models and assumptions may no longer apply. With earlier generations of wireless technology, from 1G to 5G, the focus was predominantly on the far-field region. This was because the physical size of antenna arrays and the frequencies used resulted in a near-field region that was relatively small, often extending only a few meters or less from the antenna. This made far-field assumptions sufficient for most communication system designs, as the complex interactions in the near-field had minimal impact on the network's overall performance.

However, the landscape changes dramatically with 6G. Using extremely large antenna arrays and frequencies in the tens or hundreds of GHz range significantly expand the near-field region, sometimes to hundreds of meters. This expansion is not trivial, as the properties of the electromagnetic field in the near-field region can drastically affect how signals are transmitted and received, introducing new challenges and opportunities for system design.

Understanding and addressing the complexities of near-field communication in 6G networks requires a new system design and modeling approach. It calls for innovative research to develop methods that accurately account for the unique properties of the near-field, ensuring that the next generation of wireless networks can fully leverage the potential of these advanced technologies.

Exploring this domain and understanding these concepts is essential in B5G wireless communications. The differentiation between near-field and far-field, previously considered, now holds significant practical relevance for developing and functioning state-of-the-art networks. Therefore, this subsection delves into the technique of near-field communication using a uniform linear array (ULA), highlighting its technique application settings [11].

4.2.2.1 The Steering Vector for MISO System

Consider a communication between a device and a BS with N antenna elements. The steering vector expression describes the near-field channel model applied to MISO systems as:

$$\mathbf{sv}_n\left(\mathbf{r}, \mathbf{s}_n\right) = e^{-i\frac{2\pi}{\lambda}\left\|\mathbf{r}-\mathbf{s}_n\right\|} \tag{4.4}$$

rewriting Eq. (4.4) in vector form

$$\mathbf{sv}\left(\mathbf{s}_n, \mathbf{r}\right) = \left[e^{-i\frac{2\pi}{\lambda}\left\|\mathbf{r}-\mathbf{s}_{-\tilde{N}}\right\|}, e^{-i\frac{2\pi}{\lambda}\left\|\mathbf{r}-\mathbf{s}_{-\tilde{N}+1}\right\|}, e^{-i\frac{2\pi}{\lambda}\left\|\mathbf{r}-\mathbf{s}_{-\tilde{N}+2}\right\|}, \ldots, e^{-i\frac{2\pi}{\lambda}\left\|\mathbf{r}-\mathbf{s}_{\tilde{N}}\right\|}\right] \tag{4.5}$$

In this context, $\left\|\mathbf{r}-\mathbf{s}_n\right\|$ represents a vector operation denoting the distance from the device to the nth element of the array. Consequently, this value can be accurately determined using vector operations in Cartesian coordinates as:

$$\mathbf{r}-\mathbf{s}_n = \left(\mathbf{r}_x - \mathbf{s}_n, \mathbf{r}_y\right) \tag{4.6}$$

where $\mathbf{s}_n$ represents the distance from the nth element of the array to its center, defined as $\mathbf{s}_n = \frac{\lambda}{2}n$, with $n \in [-\tilde{N}, \tilde{N}]$ and $N = 2\tilde{N}+1$.

Figure 4.4 provides a geometric representation of a wireless communication setup, in which a gray line denotes the distance between a user's device and a specific antenna element within a BS array. The length of this gray line symbolizes the direct path distance, which is a crucial factor in calculating the steering vector between a single antenna device and a BS array.

We assume that $\mathbf{s}_n$ is aligned parallel to the x-axis. The term $\mathbf{r}_x$ denotes the projection of $\mathbf{r}$ onto the x-axis, while $\mathbf{r}_y$ represents the projection of $\mathbf{r}$ onto

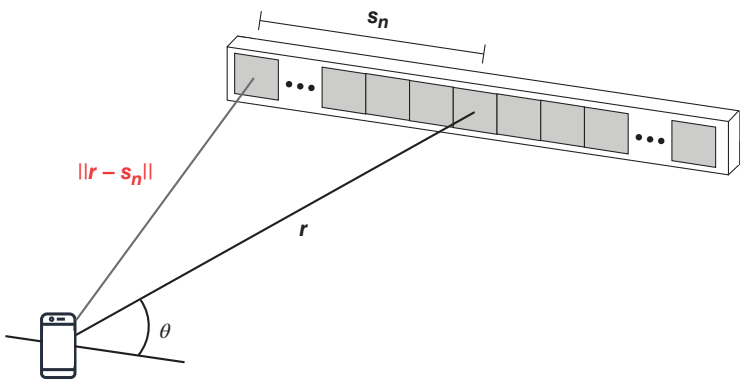

Figure 4.4 A gray line depicting the distance between a device and an element from a BS array. Source: The Authors.

the y-axis, which is perpendicular to the array axis, thus

$$\mathbf{r} - \mathbf{s}_n = \left(r\cos(\theta) - \frac{\lambda n}{2}, r\sin(\theta) \right) \tag{4.7}$$

Applying the norm property in Eq. (4.7),

$$\|\mathbf{r} - \mathbf{s}_n\| = \sqrt{\left(r\cos(\theta) - \frac{\lambda n}{2} \right)^2 + (r\sin(\theta))^2} \tag{4.8}$$

simplifying,

$$\|\mathbf{r} - \mathbf{s}_n\| = \sqrt{\frac{\lambda^2 n^2}{4} - nr\cos(\theta) + r^2} \tag{4.9}$$

Thus, the near-field channel model vector for MISO systems can be generated by distance provided in Eq. (4.9) into the vector presented in Eq. (4.5).

Additionally, it is essential to note that the far-field model is essentially a particular case of the near-field model, offering a more straightforward approximation. However, in our simulation, we utilized the more general case of near-field communication, representing both near-field and far-field communications.

4.2.2.2 The Steering Vector for MIMO System

Consider a communication between two arrays similar to the following figure. Both array has $M = 2\tilde{M} + 1$ and $N = 2\tilde{N} + 1$ antennas elements, respectively. Figure 4.5 provides a geometric representation of a wireless communication setup, in which a gray line denotes the distance between a device array with N elements and a BS array with M elements. The length of this gray line symbolizes the direct path: the steering vector between two arrays.

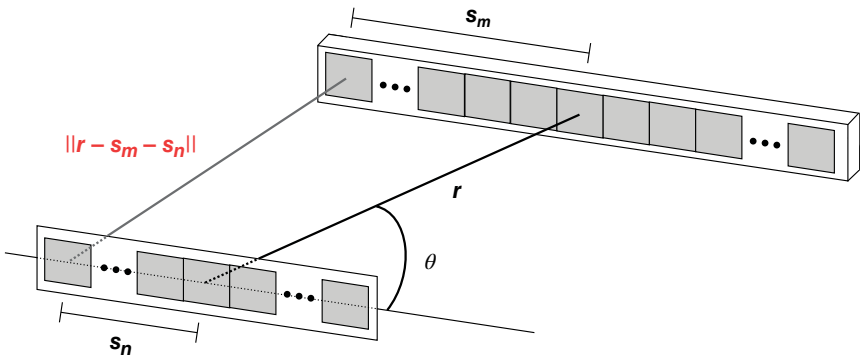

Figure 4.5 A gray line depicting the distance between two elements from parallel arrays. Source: The Authors.

In this case, the near-field channel model applied to MIMO systems is described by the steering vector $\mathbf{sv}_{m,n}\left(\mathbf{r}, \mathbf{s}_m, \mathbf{s}_n\right) \in \mathbb{C}^{M\times N}$ expression as:

$$\mathbf{sv}_{m,n}\left(\mathbf{r}, \mathbf{s}_m, \mathbf{s}_n\right) = e^{-i\frac{2\pi}{\lambda}\left\|\mathbf{r}-\mathbf{s}_m-\mathbf{s}_n\right\|} \tag{4.10}$$

Rewriting Eq. (4.10) in matrix form as:

$$\begin{aligned}&\mathbf{sv}\left(\mathbf{r}, \mathbf{s}_m, \mathbf{s}_n\right)\\ &= \begin{bmatrix} e^{-i\frac{2\pi}{\lambda}\left\|-\mathbf{s}_{-\tilde{M}}-\mathbf{s}_{-\tilde{N}}+\mathbf{r}\right\|} & e^{-i\frac{(2\pi)}{\lambda}\left\|-\mathbf{s}_{-\tilde{M}}-\mathbf{s}_{-\tilde{N}+1}+\mathbf{r}\right\|} & \ldots & e^{-i\frac{2\pi}{\lambda}\left\|-\mathbf{s}_{-\tilde{M}}-\mathbf{s}_{\tilde{N}}+\mathbf{r}\right\|} \\ e^{-i\frac{2\pi}{\lambda}\left\|-\mathbf{s}_{-\tilde{M}+1}-\mathbf{s}_{-\tilde{N}}+\mathbf{r}\right\|} & e^{-i\frac{(2\pi)}{\lambda}\left\|-\mathbf{s}_{-\tilde{M}+1}-\mathbf{s}_{-\tilde{N}+1}+\mathbf{r}\right\|} & \ldots & e^{-i\frac{2\pi}{\lambda}\left\|-\mathbf{s}_{-\tilde{M}+1}-\mathbf{s}_{\tilde{N}}+\mathbf{r}\right\|} \\ e^{-i\frac{2\pi}{\lambda}\left\|-\mathbf{s}_{-\tilde{M}+2}-\mathbf{s}_{-\tilde{N}}+\mathbf{r}\right\|} & e^{-i\frac{(2\pi)}{\lambda}\left\|-\mathbf{s}_{-\tilde{M}+2}-\mathbf{s}_{-\tilde{N}+1}+\mathbf{r}\right\|} & \ldots & e^{-i\frac{2\pi}{\lambda}\left\|-\mathbf{s}_{-\tilde{M}+2}-\mathbf{s}_{\tilde{N}}+\mathbf{r}\right\|} \\ \ldots & & \ldots & \\ e^{-i\frac{2\pi}{\lambda}\left\|-s_{\tilde{M}}-s_{-\tilde{N}}+\mathbf{r}\right\|} & e^{-i\frac{(2\pi)}{\lambda}\left\|-s_{\tilde{M}}-s_{-\tilde{N}+1}+\mathbf{r}\right\|} & \ldots & e^{-i\frac{2\pi}{\lambda}\left\|-s_{\tilde{M}}-s_{\tilde{N}}+\mathbf{r}\right\|} \end{bmatrix}\end{aligned} \tag{4.11}$$

in which $\left\|\mathbf{r}-\mathbf{s}_m-\mathbf{s}_n\right\|$ represents a vector operation denoting the distance from the mth element of one array to the nth element of the other array. Consequently, this value can be accurately determined using vector operations in Cartesian coordinates, as demonstrated by:

$$\mathbf{r}-\mathbf{s}_m-\mathbf{s}_n = \left(-\mathbf{s}_m-\mathbf{s}_n+\mathbf{r}_x, \mathbf{r}_y\right) \tag{4.12}$$

where $\mathbf{s}_m$ represents the distance from the mth element of its array to its center array, defined as $\mathbf{s}_m = \frac{\lambda}{2}m$, with $m \in [-\tilde{M}, \tilde{M}]$. We assume that $\mathbf{s}_m$ is aligned parallel to $\mathbf{s}_n$ and to the x-axis. The term $\mathbf{r}_x$ denotes the projection of $\mathbf{r}$ onto the x-axis, while $\mathbf{r}_y$ represents the projection of $\mathbf{r}$ onto the y-axis, which is perpendicular to the array axis, thus

$$\mathbf{r}-\mathbf{s}_m-\mathbf{s}_n = \left(-\frac{\lambda m}{2}-\frac{\lambda n}{2}+r\cos(\theta), r\sin(\theta)\right) \tag{4.13}$$

Applying the norm property in Eq. (4.13),

$$\left\|\mathbf{r}-\mathbf{s}_m-\mathbf{s}_n\right\| = \sqrt{\left(-\frac{\lambda m}{2}-\frac{\lambda n}{2}+r\cos(\theta)\right)^2+(r\sin(\theta))^2} \tag{4.14}$$

simplifying

$$\left\|\mathbf{r}-\mathbf{s}_m-\mathbf{s}_n\right\| = \sqrt{\frac{1}{4}\lambda^2(m+n)^2-\lambda r\cos(\theta)(m+n)+r^2} \tag{4.15}$$

Thus, the near-field channel model matrix for MIMO systems can be generated by applying the distance provided in Eq. (4.15) into each element in the matrix presented in Eq. (4.11).

4.2.3 Channel Models

This section examines various multipath fading models extensively acknowledged and researched in mobile communications literature. These models play a

crucial role in comprehending and simulating signal behavior in environments filled with numerous obstacles and reflectors, typical of urban and indoor settings. The discussion will highlight prominent models such as Rayleigh, Rice, Nakagami-m, κ–μ, and α–μ. Our analysis will explore their mathematical foundations and particular scenarios.

4.2.3.1 Rayleigh

The Rayleigh fading model represents one of the simplest and most common approaches for statistical mobile radio channel models. It characterizes the signal envelope, which emerges from the propagation of in-phase and quadrature signals. These signals follow Gaussian distributions and form clusters of scattered signals. Such scattering results from diverse reflections, diffractions, and interactions with various environmental objects. Consequently, the signal undergoes random fluctuations, arriving at the receiver at distinct times with varying amplitudes and phases. The physical representation of this model is given by:

$$R = X + jY \tag{4.16}$$

in which R is a random variable (RV) of the signal envelope, X and Y are RVs mutually independent Gaussian processes with zero mean $E(X) = E(Y) = 0$, the variance is equal to $\mathrm{Var}(X) = \mathrm{Var}(Y) = \sigma^2$, and $j = \sqrt{-1}$ is the imaginary unit. Also, the complex samples of the Rayleigh distribution can be similarly derived using a complex representation, expressed as:

$$R = \sqrt{X^2 + Y^2}\, \exp(j\,\phi) \tag{4.17}$$

in which $\phi = \mathrm{atan2} = \mathrm{atan2}(X, Y)$, and atan2(.,.) is the arc-tangent between two arguments.

The Rayleigh distribution models the fading effect in a non-line-of-sight (NLoS) communication channel. As a signal propagates from a transmitter to a receiver, it may experience reflections, diffractions, and dispersions caused by various environmental obstacles, like buildings and trees. Consequently, this leads to multiple pathways for the radio waves to arrive at the receiver. Its probability density function (PDF) is specified by,

$$f_R(r) = \frac{r}{\sigma^2} \exp\left(-\frac{r^2}{2\sigma^2}\right) \qquad r \geq 0 \tag{4.18}$$

Additionally, it's crucial to note σ does not represent the variance of the Rayleigh distribution; instead, it signifies the variance of the original Gaussian distribution, and its value can be found by $\sigma = \hat{r}^2/2$, with $\hat{r}$ the root means square (RMS) value of samples [12].

4.2.3.2 Rice

Contrasting with the Rayleigh fading model, which assumes a scenario with many indirect paths, the Rice fading or Rician distribution includes a line-of-sight (LoS) component where the direct path is more significant and dominant than the scattering signals. This distribution is particularly relevant when there is a clear direct signal between the transmitter and receiver, common in open or semi-open environments. The physical representation of Rice is:

$$R = (X + k) + jY \tag{4.19}$$

in which X and Y follow Gaussian distribution and k is a constant related to the envelope of the dominant signal. Also, the complex samples of the Rice distribution can be similarly derived using the Eq. (4.20):

$$R = \sqrt{(X + k)^2 + Y^2}\, \exp(j\phi) \tag{4.20}$$

in which $\phi = \text{atan2}(X + k, Y)$.

In the literature, an alternative method for generating samples of a Ricean channel can be used and is presented in Eq. (4.21). This approach incorporates both NLoS ($\tilde{h}$) and LoS ($\overline{h}$) components. The Rician factor, denoted as ϵ_k, quantifies the relative contributions of the NLoS and LoS components within the Rician model,

$$h = \left(\sqrt{\frac{\epsilon_k}{\epsilon_k + 1}} \overline{h}_{n,k} + \sqrt{\frac{1}{\epsilon_k + 1}} \tilde{h}_{n,k} \right) \tag{4.21}$$

Both RVs in Eqs. (4.20) and (4.21) for generating Rician fading samples are align with the PDF distribution, as presented in Eq. (4.22),

$$f(r) = \frac{r}{\sigma^2} \exp\left(-\frac{r^2 + k^2}{2\sigma^2} \right) I_0\left(\frac{r\nu}{\sigma^2} \right) \tag{4.22}$$

in which $I_0(.)$ is the modified Bessel function of the first type and order zero [12].

4.2.3.3 Nakagami-*m*

First introduced by Minoru Nakagami in 1943, this model arose from experimental research on fast fading with high frequency. It characterizes an environment with multiple multipath clusters in a setting where direct LoS is not available. In this model, the signal components are distinguished by their random phases and propagation delays.

The Nakagami-m distribution's physical model is depicted by integrating m components in phase (X) and quadrature (Y). This is illustrated by the physical representation given in (4.23).

$$R = \sum_{i=1}^{m} \left(X_i + jY_i \right) \tag{4.23}$$

where X_i and Y_i are mutually independent Gaussian processes with zero mean $E(X) = E(Y) = 0$ and variance equal to $\mathrm{Var}(X) = \mathrm{Var}(Y) = \sigma^2$. Additionally, the complex samples of the Nakagami-m distribution can be similarly derived using the complex representation

$$R = \sqrt{\sum_{i=1}^{m} \left(X_i^2 + Y_i^2\right)} \exp(j\phi) \tag{4.24}$$

in which $\phi = \mathrm{atan2}\left(\sum_{i=1}^{m} X_i, \sum_{i=1}^{m} Y_i\right)$.

The PDF of the Nakagami-m is derived from the moment-generating function of its in-phase and quadrature components, considering the presence of m multipath clusters. Thus, the PDF of Nakagami-m corresponds to Eq. (4.25)

$$f_R(r) = \frac{2m^m r^{2m-1}}{\Gamma(m)\Omega^m} \exp\left(-\frac{m r^2}{\Omega}\right) \qquad r \geq 0 \tag{4.25}$$

in which $\Gamma(.)$ is the Gamma function [[13], Eq. 6.1.1], $\Omega = \hat{r}^2$, and m representing the actual extent of the number of multipath clusters. Considering $m = 1$, the Nakagami-m distribution reduces to the Rayleigh distribution [14].

4.2.3.4 $\kappa-\mu$

The $\kappa-\mu$ distribution was introduced by Yacoub, which considered a general fading model composed of multiple clusters of signals propagating in a non-homogeneous environment with a dominant component. It's assumed that the scattered waves possess equal powers, supplemented by a dominant component. Additionally, the phases of these scattered waves are random and exhibit similar time delays.

Equation (4.26) provides the physical model of the signal envelope in terms of its phase and quadrature components,

$$R = \sum_{i=1}^{n} \left(X_i + p_i\right) + j\sum_{i=1}^{n} \left(Y_i + q_i\right) \tag{4.26}$$

in which X_i and Y_i are Gaussian processes with zero mean and variance σ^2, n is the number of multipath clusters, the elements p_i and q_i are the mean phase values and quadrature for each cluster. Additionally, an alternative complex representation of the signal envelope is provided as:

$$R = \sqrt{\sum_{i=1}^{n} \left(X_i + p_i\right)^2 + \sum_{i=1}^{n} \left(Y_i + q_i\right)^2} \exp(j\,\phi) \tag{4.27}$$

in which $\phi = \mathrm{atan2}\left(\sum_{i=1}^{m} \left(X_i + p_i\right), \sum_{i=1}^{m} \left(Y_i + q_i\right)\right)$.

The PDF of κ–μ distribution is expressed by Eq. (4.28),

$$f_R(r) = \frac{2\mu\,(\kappa+1)^{\frac{\mu+1}{2}}\, r^{\mu}}{\kappa^{\frac{\mu-1}{2}}\,\exp(\kappa\mu)\,\hat{r}^{\mu+1}}\,\exp\left(-\frac{(\kappa+1)\mu r^2}{\hat{r}^2}\right) I_{\mu-1}\left(2\mu\sqrt{\kappa(\kappa+1)}\frac{r}{\hat{r}}\right) \tag{4.28}$$

in which $\hat{r}$ is the RMS value of the κ–μ samples, κ is defined by the ratio between the total power of the dominant components and the power of the dispersed waves and μ represents the real extent of the number of multipath clusters propagating in a non-homogeneous environment. This physical parameters of the distribution are defined by:

$$\begin{aligned}\kappa &= \frac{d^2}{2n\sigma^2}\\ \mu &= \frac{E^2(W)}{\mathrm{Var}(W)}\frac{(2\kappa+1)}{(\kappa+1)^2}\end{aligned} \tag{4.29}$$

The κ–μ distribution is a more general fading model used in wireless communications, encompassing traditional distributions like Rayleigh, Rice, and Nakagami-m. The Nakagami-m can be represented by setting $\kappa \to 0$ and μ equals to m parameter from Nakagami-m. The Rice distribution is a particular case of κ–μ when the fading environment has a dominant LoS component ($\mu = 1$). Rayleigh is another specific case from κ–μ when setting $\mu = 1$ and $\kappa \to 0$. In summary, while Rayleigh, Rice, and Nakagami-m distributions are specific to certain types of fading environments, the κ–μ distribution offers a unified framework with adjustable parameters to model a broader range of scenarios, from purely NLoS to strong LoS conditions. This adaptability makes κ–μ a valuable tool in the analysis and design of wireless communication systems [15].

4.2.3.5 α–μ

This distribution reflects a more comprehensive channel model, accounting for μ as the actual number of multipath clusters with equal powers propagating within a non-homogeneous environment. In this model, channel nonlinearity is characterized by the α parameter. Furthermore, in any cluster of this model, the phases of the dispersed waves are random and have similar time delays but with a relative difference between the delay times of different clusters.

In the α–μ model, the signal envelope is depicted as a nonlinear function, determined by the magnitude of the aggregated multipath clusters, which are influenced by environmental nonlinearity. Consequently, its physical representation can be described by (4.30):

$$R^{\alpha} = \sum_{i=1}^{n}\left(X_i^2 + Y_i^2\right) \tag{4.30}$$

in which n is the number of multipath clusters, X_i and Y_i are Gaussian processes, with zero mean, variance: $\mathrm{Var}(X) = \mathrm{Var}(Y) = \hat{r}^{\alpha}/2n$, and the envelope mean value for the α–μ distribution, is characterized as $\hat{r} = \sqrt[\alpha]{E(R^{\alpha})}$. Also, the complex samples of the α–μ distribution can be similarly derived using the complex representation

$$R = \left(\sum_{i=1}^{n} \left(X_i^2 + Y_i^2 \right) \right)^{\frac{1}{\alpha}} \exp(j\phi) \tag{4.31}$$

The PDF of the α–μ distribution is expressed by the Eq. (4.32),

$$f_R(r) = \frac{\alpha \mu^{\mu} r^{\alpha\mu - 1}}{\Gamma(\mu)\, \hat{r}^{\alpha\mu}} \exp\left[-\mu \left(\frac{r}{\hat{r}} \right)^{\alpha} \right] \tag{4.32}$$

Additionally, the α–μ distribution is a versatile fading model, capturing various channel characteristics through physical parameters α and μ adjustments. It can even fits traditional distributions by assigning particular values to these parameters. For instance, setting $\alpha = 2$ and $\mu = m$ yields the Nakagami-m distribution, while the Rayleigh distribution emerges when $\alpha = 2$ and $\mu = 1$ [16].

4.2.4 RIS-Aided Multiuser M-MIMO

In this section, we delve into the details of RIS technology and explore possible application scenarios where it can be effectively integrated with M-MIMO technology. We will examine how these two advanced technologies can complement each other, enhancing the performance and efficiency of wireless communication systems.

4.2.4.1 RIS

The advent of RIS technology enables the programming, control, and reconfiguration of radio wave propagation in wireless communications. This is achieved through cost-effective passive or active reflector units, which enhance signal reconfiguration but may increase energy-efficient consumption. RIS is rapidly gaining recognition as a promising technology for boosting the capacity and coverage of wireless networks. This is particularly pertinent to developing 6G communication networks, which hold the potential for groundbreaking applications, including ultra-massive wireless connectivity, high data rates, exceptional reliability, and significantly reduced latency [17].

The project involves assembling metamaterials or arrangements in a format that consists of passive or active components. These can be conveniently installed in various structures, including building facades, internal walls, aerial platforms, roadside billboards, and even indoor settings, as referenced in [18]. This versatility is primarily due to its cost-effectiveness.

Its principal function is to reconfigure the wireless propagation environment, compensating for power loss over long distances and improving throughput, especially in scenarios where the data link occurs in NLoS. They are more energy-efficient and environmentally friendly than traditional relay systems, such as amplification and relay and decoding systems [17]. Furthermore, RISs support Full Duplex transmission without internal interference and full-band reflection of electromagnetic waves [18].

Moreover, these devices can function in far and near-field regions, performing tasks like anomalous reflection and beamforming. Consequently, the steering vector concepts and techniques commonly utilized in M-MIMO systems also apply to RIS. Anomalous reflection changes the course of a plane wave in a different direction. In contrast, beamforming transforms a plane wave into a specific wavefront by concentrating energy towards a particular direction or point.

In Section 4.2.4.2, we will discuss a RIS-aided M-MIMO communication system technology, focusing on configurations suitable for UL and DL operations.

4.2.4.2 Uplink and Downlink System Model

Consider a system of RIS, BS, and users as depicted in Figure 4.6. The illustration depicts a RIS-aided M-MIMO communication system in (a) UL mode and (b) DL mode. The link between the RIS and the BS typically involves a LoS link, as both positions are well-defined. Consequently, a Rice channel model is most commonly employed under these conditions. Conversely, the users' positions may be entirely random, and various objects and walls surrounding the UE location can introduce different types of interference. This variability suggests that a range of statistical channel models could be applicable to the link between the UEs and the RIS.

Figure 4.6a shows the UL mode, the users UE_1, UE_2, and UE_3 transmitting signals to the RIS, characterized by an array of controllable elements which reflected the to the BS. Such a configuration is strategically composed to intercept and smartly reconfigure the incoming signal paths from the UEs for enhanced reception at the BS. This advanced system design highlights using RIS to improve signal strength and quality by optimizing the propagation environment in UL wireless communications. Conversely, Figure 4.6b shows an RIS-aided M-MIMO communication system in DL mode, the BS transmitting signals to RIS, characterized by an array of controllable elements that reflected the signals to users UE_1, UE_2, and UE_3. This configuration is strategically composed to intercept and smartly reconfigure the incoming signal paths from the BS for enhanced reception at the UE. This advanced system design highlights the use of RIS to improve signal strength and quality by optimizing the propagation environment in DL wireless communications.

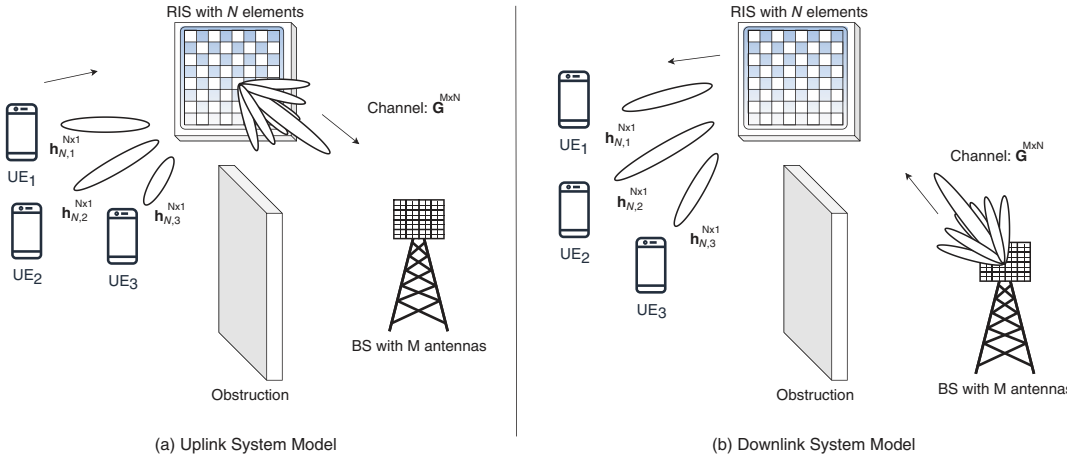

Figure 4.6 Representations of RIS-aided M-MIMO communication systems. (a) operating in UL mode and (b) in DL mode. Source: The Authors.

It is also important to note that the direct link between users and the BS often encounters obstructions (indicated by the block), which can partially or completely degrade the direct communication quality between them. The channels $\mathbf{G}$ and $\mathbf{h}_{n,k}$ are more thoroughly described in Section 4.3.1.

A general UL system can be analyzed with UE_i with $i \in \{1, 2, 3, ..., K\}$ represents the ith users up to K user, equipped with a single antenna. The RIS comprises N reflecting elements, while the BS comprises M antennas. During operation, data transmission begins simultaneously from the users; it travels through the radio channel in the direction of the RIS, where it is then reflected toward the BS via another radio channel. The radio channels utilized can be any of those mentioned in Section 4.2.3. Key details of this configuration include a transmitted signal power of approximately 0.1 W, as referenced in [19]. Each RIS element is configured to reflect the propagated signal toward the BS, aiming to maximize the SINR and, consequently, the SE for all users simultaneously. Furthermore, the BS employs one of the combiner techniques outlined in Section 4.2.1.4 to improve the transmitted signals. This approach is also aimed at enhancing the system's SINR and SE.

A general DL configuration maintains the same setup for the user, RIS, and BS. The critical difference lies in the direction of transmission, which originates from the BS and passes through the channel toward the RIS, where its N elements optimize the signals. Then, the signals are directed toward the users. Additionally, in this operational mode, the BS transmits signals with a power of approximately 10 W, as detailed in [19]. At the transmission's outset, the BS fine-tunes the phase of each signal transmitted by its M antennas using a predefined precoder. These signals then travel through the channel to the N elements of the RIS, reflecting the data toward the users.

4.3 Methodology

In this section, we provide a detailed description of the methodology to set up the system model for RIS-aided M-MIMO communication systems and provide simulations and results using all the approach concepts outlined in this chapter.

4.3.1 System Model

In a typical UL RIS-aided communication system, similar to Figure 4.6a, we model a BS equipped with M antennas, an RIS with N reflecting elements, and K single-antenna UEs. We assume the RIS is strategically placed to maintain a direct LoS connection with the BS, allowing us to calculate the path loss for this sub-channel exclusively. For the UEs–RIS link, we consider various multipath

fading models to account for partial obstructions, including from people, trees, or objects that might interfere with signal propagation. Additionally, we assume a complete obstruction scenario for the UEs–RIS communication link. Therefore, we can express the received signal at the BS as:

$$\mathbf{y} = \mathbf{G}\boldsymbol{\Theta}\mathbf{H}^{H}\mathbf{x} + \boldsymbol{\sigma}_n^2 \tag{4.33}$$

in which $\mathbf{G} \in \mathbb{C}^{M\times N}$ is the channel matrix for the RIS–BS link, whose matrix representation is given in Eq. (4.34). $\boldsymbol{\Theta} \in \mathbb{C}^{N\times N}$ is the phase-shift of N RIS elements, its matrix representation is given in Eq. (4.36). $\mathbf{H} = (\mathbf{h}_{n,1}, \mathbf{h}_{n,2}, \mathbf{h}_{n,3}, ..., \mathbf{h}_{n,K})^T \in \mathbb{C}^{K\times N}$ is the channel matrix for UEs–RIS link, its matrix representation is given in Eq. (4.37). The operator $(.)^H$ represents the Hermitian or conjugate transpose of a complex matrix. Also, $\mathbf{x} \in \mathbb{C}^{K\times 1}$ denotes the simultaneously transmitted signal from K users, and $\boldsymbol{\sigma}^2 \sim \mathcal{CN}(0, 1)$ is the vector of samples of additive white Gaussian noise (AWGN).

$$\mathbf{G} = \begin{bmatrix} g_{1,1} & g_{1,2} & \cdots & g_{1,N} \\ g_{2,1} & g_{2,2} & \cdots & g_{2,N} \\ \vdots & \vdots & \ddots & \vdots \\ g_{M,1} & g_{M,2} & \cdots & g_{M,N} \end{bmatrix} \tag{4.34}$$

the elements $g_{m,n}$ of the RIS–BS LoS channel matrix $\mathbf{G}$ are given in Eq. (4.35) and are described by the path loss coefficients $L_{m,n}^{\text{LOS}}$, with samples of Rice channel model ($r_{m,n}$) as described in Section 4.2.3.2 and the near-field channel model ($sv_{m,n}$) described in Section 4.2.2,

$$\mathbf{g}_{m,n} = \sqrt{L_{m,n}^{\text{LOS}}}\, r_{m,n}\, sv_{m,n} \tag{4.35}$$

in which $L_{m,n}^{\text{LOS}} = \frac{G_m \lambda^2}{(4\pi b_{m,n})^2}$, with G_m representing the gain of the mth antenna, and $b_{m,n}$ denoting the distance between the nth antenna on the RIS and the mth antenna on the BS.

The matrix $\boldsymbol{\Theta}$ is the RIS phase shifts matrix,

$$\boldsymbol{\Theta} = \text{diag}\left(\begin{bmatrix} \beta_1 e^{j\theta_1} & \cdots & \beta_N e^{j\theta_N} \end{bmatrix}\right) \tag{4.36}$$

in which $\beta_i \in [0, 1]$ with $i = 1, 2, ..., N$ is the reflection amplitude of the RIS elements, representing full reflection, and $\beta_i = 0$ indicates complete absorption. In this work, we assumed $\beta_i = 1,\ \forall n$, *i.e.*, the RIS is assumed to be entirely passive. The $\beta_i \in [0, 2\pi]$ with $i = 1, 2, ..., N$ is the phase response of ith RIS element.

The channel model between UE_k and RIS is described by:

$$\mathbf{H} = \begin{bmatrix} h_{1,1} & h_{1,2} & \cdots & h_{1,K} \\ h_{2,1} & h_{2,2} & \cdots & h_{2,K} \\ \vdots & \vdots & \ddots & \vdots \\ h_{N,1} & h_{N,2} & \cdots & h_{N,K} \end{bmatrix} \tag{4.37}$$

the elements $h_{k,n}$ of the UEs–RIS channel matrix $\mathbf{G}$ are given in Eq. (4.38) and are described by the path loss coefficients $L_{n,k}^{\text{LOS}}$, with any kind of multipath channel model ($r_{n,k}$) described in Section 4.2.3 and the near-field channel model described in Section 4.2.2,

$$\mathbf{h}_{n,k} = \sqrt{L_{n,k}^{\text{LOS}}}\, r_{n,k}\, sv_{n,k} \tag{4.38}$$

The channel $\mathbf{H}$ can be generated under two distinct scenarios: (i) in the first scenario, we consider a static position for the UE_i; (ii) in the second scenario, a dynamic position for the UE_i was considered. Numerical simulation results with respective analyses are provided in Section 4.4 for both scenarios.

In the Monte Carlo simulations, the channel matrix $\mathbf{G}$ samples are generated obeying the line-of-sight (LoS) condition, with both the RIS and BS positions being fixed and well-defined. This setup makes the Rice fading an ideal choice for channel $\mathbf{G}$. However, in the communication between UE_i and the RIS (regardless of whether the users are in a static or dynamic position), the signal might experience blockages, multipath propagation, or nonlinear environments. Therefore, we assume the $\mathbf{H}$ channel matrix is subject to various multipath fading effects.

4.3.2 Metrics

In this section, we delve into the details to learn and calculate important QoS metrics, such as SINR, SE, and OP.

4.3.2.1 Signal-to-Interference-Plus-Noise Ratio

The SINR is a fundamental concept for telecommunications systems that quantifies the quality of a wireless communication link. It is a measure that compares the level of a desired signal to the level of background noise and interference. This concept can be address in the Eq. (4.39) [9],

$$SINR_k = \frac{P_{signal}}{P_{interf} + \sigma_n^2} \tag{4.39}$$

in which σ_n^2 is the noise power, P_{signal} is the desired signal power for user k and P_{interf} is the interference power. Thus, this expression can be expanded by,

$$SINR_k = \frac{\left|\left(\mathbf{G}^{\mathbf{H}}\boldsymbol{\Theta}\mathbf{h}_k\right)\mathbf{w}_k\right|^2}{\sum_{i=1,i\neq k}^{K}\left|\left(\mathbf{G}^{H}\boldsymbol{\Theta}\mathbf{h}_i\right)\mathbf{w}_i\right|^2 + \sigma_n^2} \tag{4.40}$$

in which $\mathbf{h}_k \in \mathbb{C}^{1\times N}$ corresponds to the communication channel between the RIS and the kth user and $\mathbf{w}_k \in \mathbb{C}^{1\times M}$ is the beamforming vector for user k.

The noise power in communication systems is calculated using the fundamental formula for a communication channel, succinctly represented in Eq. (4.41):

$$\sigma_n^2 = 10^{\frac{N_0}{10}-3} BW \tag{4.41}$$

in which N_0 is the noise power spectral density, it is typically set at -204 dBm/Hz, reflecting the standard thermal noise level at an ideal ambient temperature of approximately 17 °C. The parameter BW denotes the bandwidth in Hertz (Hz). The term 10^{-3} is used to convert the noise power from decibel-milliwatts (dBm) to Watts, aligning with the convention in communication theory, as detailed by Haykin [20].

4.3.2.2 Spectral Efficiency

The SE of a communication system, given in Eq. (4.42), is defined as the capacity for data transmission per unit of bandwidth, measured in bits per second per Hertz (bits/s/Hz). This concept is closely tied to Shannon's formula, which describes the maximum theoretical capacity of a communication channel

$$SE = \frac{C}{B} = \log_2(1 + SINR) \qquad \left[\frac{\text{bits/s}}{\text{Hz}}\right] \tag{4.42}$$

in which, C is the channel capacity, B is the bandwidth [20].

Enhancing SE is a primary goal in RIS-aided systems. However, energy efficiency emerges as another critical aspect closely related to SE and implementations in RIS and BS. This necessitates distinct optimization strategies, though they can be adapted and implemented in conjunction with the provided metrics for SE.

4.3.2.3 Outage Probability

The OP (P_{out}) represents the probability of service disruption due to the failure to maintain a minimum SNR or SINR at the receiver's input. This metric serves as a crucial index for assessing the robustness of mobile telecommunication systems against noise and interference. It is considered an important complement to Cumulative distribution function (CDF) and has garnered considerable attention in academic research as [12]. This metric can be measured in Eq. (4.43) and quantified as the probability that the SINR falls below a specified threshold,

$$P_{out} = P[SINR_{mc,k} \leq \gamma_{\text{th}}] \tag{4.43}$$

in which $SINR_{mc,k}$ denotes a sample of the SINR from the Monte Carlo simulations, with $mc \in [1, \text{MC}]$ whose MC represents the total number of Monte Carlo iterations, for user k and γ_{th} is the threshold for the SINR that ensures the QoS is maintained [21].

4.3.3 Optimization Problems

In the context of RIS-aided M-MIMO systems communications the literature has delved into optimization strategies to finely tune the N phase shift elements of RIS, targeting a holistic enhancement of the network's communication efficiency. Key optimization challenges in this realm include the Max–SINR, which focuses on maximizing the SINR, the WSR metric, and the max–min SINR, which prioritizes equitable service across users. Typically, these optimization efforts have yielded solutions that cater to the optimal performance for the kth individual user. The challenge emerges when the goal shifts toward optimizing the performance for all users concurrently. The core issue lies in the fact that an optimal solution for one user may fall when applied to the network collectively, thereby degrading from the system's overall efficiency. This limitation is frequently cited as the main gap in RIS technology. The issue of joint optimization, considering all users simultaneously, remains an open problem in the literature. The inherent complexity of this issue arises from the need to balance individual gains with the collective performance of the system, a challenge that has not yet been fully overcome and which stands out as an active research frontier in the area of wireless communications.

Futheremore, the issues explored in this section are well formulated for M-MIMO systems and readily adaptable to include RIS technology. We elaborate on the methodology and practical implementation of each problem via computer simulations. The discussed scenarios can accommodate both static and dynamic user configurations.

4.3.3.1 Max SINR_k

In this optimization challenge, we deploy an optimal approach that iteratively evaluates the performance of three optimum combining techniques (MF, ZF, and MMSE) alongside the optimal passive beamforming strategy within the RIS elements. Therefore, we introduce the following problem for discussion on this topic:

$$\begin{aligned} \max_{\boldsymbol{\Theta}} \quad & SINR_k \\ \text{s.t.} \quad & \left|\theta_n\right| = 1, \forall n \in \{1, \ldots, N\} \end{aligned} \tag{4.44}$$

in which p_k means the transmission power assigned to user k. The UL scenarios involving multiple users with different channel configurations, p_k can differ among users. The term $p_{max,k}$ specifies the maximal transmission power permissible for user k, serving as a ceiling determined by regulatory standards, hardware limitations, or design criteria. This constraint aims to ensure safe and effective data reception at the BS amid concurrent transmissions from various K users.

In this problem, the objective function is $SINR_k$, with constraints set by $\left|\theta_n\right| = 1$. The decision variables in question are p_k, $\boldsymbol{\Theta}$, and $\mathbf{w}_k$. The desired solutions comprise the optimal combiners: MF, ZF, and MMSE, along with the optimal $\boldsymbol{\Theta}$ as

determined by Eq. (4.47). The detailed algorithm for this approach is documented in the code in Algorithm 4.3.

4.3.3.2 Weighted Sum Rate Metric

This problem is a conventional optimization problem within wireless communication systems [7]. The aim is to modify the RIS phase coefficients ($\boldsymbol{\Theta}$) and the combiners to optimize the WSR of all K users in the system, prioritizing those deemed most important. Thus, this optimization approach is recommended for scenarios involving stationary user positions. Therefore, we introduce the following problem for discussion on this topic:

$$\begin{aligned} \max_{\boldsymbol{\Theta}} \quad & \sum_{k=1}^{K} \omega \log_2(1 + SINR_k) \\ \text{s.t.} \quad & \left|\theta_n\right| = 1, \forall n \in \{1, \ldots, N\} \end{aligned} \tag{4.45}$$

in which $\omega = (\omega_1, \omega_2, ..., \omega_K)$ represents the weights assigned to K users, whose values are determined based on their respective priority levels.

We address a WSR optimization challenge within an RIS-aided M-MIMO communication system, considering the UL scenario. The goal is to maximize the objective function $\sum_{k=1}^{K} \omega_k \log_2(1 + SINR_k)$, subject to the constraint $\left|\theta_n\right| = 1$.

Additionally, we employ the NLS strategy to identify the optimal $\boldsymbol{\Theta} = (\theta_1, \theta_2, ..., \theta_N)$ common for all users. Algorithm 4.1 presents the pseudocode detailing the implemented methodology.

The algorithm initiates by allocating random values of $\exp(j\,\phi)$, with $\phi \in (0, 2\pi)$ in all elements of $\boldsymbol{\Theta}$. In the initial loop, we experiment on REPEAT times to achieve an optimal search outcome by averaging the results across these iterations. A random ordering sequence is generated inside this loop for the N elements of $\boldsymbol{\Theta}$ in the RIS, ensuring uniqueness in each L_2 iteration. Subsequently, in loop L_3, we choose a specific position θ_{l_2} to conduct a phase sweep using $\exp(j\,l_3)$, incrementing l_3 by small amounts within the range from 0 to 2π, effectively setting $\theta_{l_2} = \exp(j\,l_3)$. This step involves computing and updating the composite channel (comprising both the physical channel and the RIS element phase shifts) with its optimal combiner. Finally, loop L_4 is responsible for calculating the SINR for all users based on the current $\boldsymbol{\Theta}$ configuration and its corresponding combiner $\mathbf{w}_k$.

With these results, we can calculate the first sum of rates and obtain a value for $\mathrm{SR}_{l_3}(\mathbf{w}_k, \boldsymbol{\Theta})$. Although it's uncertain if this is the maximum value, we arrange it for subsequent evaluation.

In the L_3 loop, we continue to adjust $\theta_{l_2} = \exp(j\,l_3)$, aiming to update $\boldsymbol{\Theta}$, $\mathbf{H}_c$, and $\mathbf{w}_k$, alongside recalculating the SINR for all users and the sum rate $\mathrm{SR}l_3(\mathbf{w}_k, \boldsymbol{\Theta})$, arranging these values for future comparison. This process repeats until we've passed through all possible increments within the L_3 loop.

Completing loop L_3, we return to loop L_2 and we are able to analyze and find the θ_{l_2} that has the highest value of the sum rate $\mathrm{SR}_{l_3}(\mathbf{w}, \boldsymbol{\Theta})$.

Algorithm 4.1 Pseudocode for the weighted sum rate optimization with NLS search method.

```
% Algorithm for Weighted Sum Rate Optimization
Initialize the N elements of Θ by exp(jϕ) with ϕ ∈ (0, 2π);
for iteration l1 from 1 to REPEAT: % loop L1
    Create a random sequence of N elements and store in RandomOrder vector;
    for each n element index, from 1 to N: % loop L2
        Select the RIS element as l2=randomOrder(n);
        for phase shift l3 in increments of 0.1 radians from 0 to 2π: % Phase
            adjustment loop L3
            Set θ_l2 to exp(jl3);
            Updated composite channel H_c as G^H Diag(Θ)H;
            Optimize the combiner w_k using MMSE and H_c;
            for each user l4 from 1 to K:% Loop L4
                Calculate and record the SINR_l4 over users
            end
            Compute and record SR_l3 = Σ_{l4=1}^{K} ω_k log2(1 + SINR_l4);
        end
        Identify the phase shift l3 yielding the highest SR_l3, and define θ_l2
            as exp(jl3(optimal));
        Recompute H_c using the optimum Θ;
        Recompute w_k using the optimum H_c;
        Evaluate SINR_{Θ,i} on each user i = 1, 2, 3, ... , K;
    end
Compute the average SINR_{Θ,i} over users: SINR_Θ =mean(SINR_{Θ,i});
Compute the average SINR_Θ over l1 iterations: SINR=mean(SINR_Θ);
```

This process ensures the selection of the most effective phase shift configuration for the RIS element at position l_2. Subsequently, we return to the L_2 loop start, which selects the next $\boldsymbol{\Theta}$ element in the random ordering sequence. This same optimization process is then applied to refine the phase shift angle at this new position of θ_{l_2}. This search and optimization cycle is repeated within the L_2 loop for all $\boldsymbol{\Theta}$ elements until each one is optimized. Upon completing the L_2 loop, we arrive at the optimized configuration, $\boldsymbol{\Theta}_{opt}$.

4.3.3.3 Max–Min SINR

This problem is formulated in Eq. (4.46) representing a classic optimization challenge in RIS-aided M-MIMO communication systems [5, 6]. The goal is to enhance the lowest SINR ratio among the users, adopting a max–min strategy. Such an approach guarantees equitable service quality by improving the SINR for the user

experiencing the poorest channel.

$$\begin{aligned} &\max_{\boldsymbol{\Theta}} \quad \min_{k} \quad SINR_k \\ &\text{s.t.} \quad \left|\theta_n\right| = 1, \forall n \in \{1, \ldots, N\} \end{aligned} \tag{4.46}$$

The problem is maximizing the minimum SINR for k users in an RIS-aided M-MIMO communication system, focusing on the UL scenario. The objective function is to maximize the minimum SINR across all users, denoted as $\min_k SINR_k$. The constraint include the phase shift condition $\left|\theta_n\right| = 1$.

For this method, we employ the NLS strategy to determine the optimal common phase shift set $\boldsymbol{\Theta} = (\theta_1, \theta_2, ..., \theta_N)$ applicable to the N RIS elements to cover all users simultaneously. The associated pseudocode is described in Algorithm 4.2 and is deployed along this chapter.

Algorithm 4.2 Pseudocode for the max–min SINR optimization with NLS search method.

% Algorithm for Max-Min SINR Optimization
Initialize the N elements of $\boldsymbol{\Theta}$ by $\exp(j\phi)$ with $\phi \in (0, 2\pi)$;
for iteration l_1 from 1 to REPEAT: % loop L_1
    Create a random sequence of N elements and store in RandomOrder vector;
    for each n element index, from 1 to N: % loop L_2
        Select the RIS element as l_2=randomOrder(n);
        for phase shift l_3 in increments of 0.1 radians from 0 to 2π: % Phase adjustment loop L_3
            Set θ_{l_2} to $\exp(jl_3)$;
            Updated composite channel $\mathbf{H}_c$ as $\mathbf{G}^H \text{Diag}(\boldsymbol{\Theta})\mathbf{H}$;
            Optimize the combiner $\mathbf{w}_k$ using MMSE and $\mathbf{H}_c$;
            for each user l_4 from 1 to K:% Loop L_4
                Calculate and record the SINR_{l_4} over users
            end
            Among the SINRs of users, identify which one has the lowest value and store its value in a vector SINR_{min};
        end
        Among the minimum SINR values stored in SINR_{min} vector, identify the argument that results in the highest SINR. Once selected, store it in $\theta_{opt}(l_2)$, which is considered the optimal phase shift;
        Recompute $\mathbf{H}_c$ using the optimum $\boldsymbol{\Theta}$;
        Recompute $\mathbf{w}_k$ using the optimum $\mathbf{H}_c$;
        Evaluate $\text{SINR}_{\boldsymbol{\Theta},i}$ on each user $i = 1, 2, 3, ..., K$;
    end
Compute the average $\text{SINR}_{\boldsymbol{\Theta},i}$ over users: SINR_{Θ} =mean($\text{SINR}_{\boldsymbol{\Theta},i}$);
Compute the average $\text{SINR}_{\boldsymbol{\Theta}}$ over l_1 iterations: SINR=mean($\text{SINR}_{\boldsymbol{\Theta}}$);

This algorithm initiates by assigning random phase values $\exp(j\phi)$, whose $\phi \in (0, 2\pi)$ for all $\boldsymbol{\Theta}$ elements. The process begins with a loop, denoted as L_1, whose experiment is conducted on REPEAT times. A random ordering sequence is generated inside this loop for the N elements of $\boldsymbol{\Theta}$ in the RIS, ensuring uniqueness in each L_2 iteration. Subsequently, in loop L_3, we choose a specific position θ_{l_2} to conduct a phase sweep using $\exp(j\,l_3)$, incrementing l_3 by small amounts within the range from 0 to 2π, effectively setting $\theta_{l_2} = \exp(j\,l_3)$. This step involves computing and updating the composite channel (comprising both the physical channel and the RIS element phase shifts) with its optimal combiner. Finally, loop L_4 is responsible for calculating the SINR for all users based on the current $\boldsymbol{\Theta}$ configuration and its corresponding combiner $\mathbf{w}_k$.

Upon completing loop L_4, we assess the SINR of all users to identify the one with the lowest SINR and store this value in the SINR_{min} vector for later comparison. Moving forward, we proceed to the second iteration of loop L_3, in which a slight increase in the phase shift l_3 is applied, followed by a recalculation of the composite channel and its specific combiner. This initiates another cycle through loop L_4 to recalculate the SINR for all users based on this new configuration. Subsequently, we once again determine the user with the lowest SINR among all and store this value in the $SINR_{min}$ vector for future comparison. This search mechanism repeats until all increments in loop L_3 have been completed.

After completing the L_3 loop, we undertake a fresh comparison to identify the configuration of θ_{l_2} with the highest SINR from all minimum values stored in the $SINR_{min}$ vector. This process ensures the selection of the most effective phase shift configuration for the RIS element at position l_2. Subsequently, we return back to the L_2 loop start, which selects the next $\boldsymbol{\Theta}$ element in the random ordering sequence. This same optimization process is then applied to refine the phase shift angle at this new position of θ_{l_2}. This search and optimization cycle is repeated within the L_2 loop for all $\boldsymbol{\Theta}$ elements until each one is optimized. Upon completing the L_2 loop, we arrive at the optimized configuration, $\boldsymbol{\Theta}_{opt}$.

Finally, the L_1 loop repeats the entire algorithm detailed previously to guarantee the average in its iterations and ensure that the search is optimal.

4.3.4 Search Mechanisms

In this section, we present two phase-shift-search methodologies which have been utilized to solve the stated optimization problems in Sections 4.3.4.1 and 4.3.4.2, respectively referred to as PBF optimization and Naive Local Search (NLS). These strategies are essential for addressing issues within the RIS-aided M-MIMO communication system and boosting data communication efficiency and performance.

4.3.4.1 Passive Beamforming Optimization Method

This optimization approach is suitable for both static and dynamic user configurations. However, for simplicity, we will focus on a static scenario. In Algorithm 4.3, we introduce the PBF pseudocode.

In this example, we detail the pseudocode presented in Algorithm 4.3, which utilizes the PBF optimization technique to achieve our objective. Assuming K users are positioned statically, with the channel matrix samples $\mathbf{G}$ and $\mathbf{H}$ predetermined. The procedure begins with a loop, denoted L_1. Then random values of $\exp(j\,\phi)$, with $\phi \in (0, 2\pi)$, are assigned to every element of $\mathbf{\Theta}_k$ for all N RIS element positions, denoted as $\mathbf{\Theta}_k = (\theta_{k,1}, \theta_{k,2}, ..., \theta_{k,N})$. Inside this loop, we iterate over $\mathbf{\Theta}_k$ for $k = 1, 2, ..., K$, aiming to identify its optimal configuration since each user k benefits from a unique optimal passive beamforming setup. Importantly, only one configuration can be active at any given time for all users, meaning a unique RIS setup with N elements must be shared among all users. This implies that while $\mathbf{\Theta}_1$ may be the optimal solution for user 1, it might not be optimal for other users. For convenience and to facilitate easy comparison of the strategies applied in this chapter, we calculate the mean SINR over the optimal $\mathbf{\Theta}_i$ for all users.

In the second loop (L_2), we implement the process to find the optimal passive beamforming for user k. The loop continues until the SINR for the kth user reaches

Algorithm 4.3 Pseudocode for optimizing $\mathbf{\Theta}$ through passive beamforming (PBF).

```
% Optimal search strategy through passive beamforming
for each user k from 1 to K; % Loop L1, over K users
    Θ is initialized with a vector of N elements having random phase shifts
      exp(jϕ), with ϕ ~ U(0, 2π);
    Initialize SINR_k = 0 and SINR_comp = 1;
    while (|SINR_k - SINR_comp| ≥ 10^-3) % Convergence loop L2
        SINR_comp = SINR_k;
        Compute the effective channel H_c as G^H Diag(Θ_k)H;
        Update the combining vector w_k based on H_c, using MMSE, ZF, or MRC
          techniques;
        Adjust Θ_k to: Θ_k = exp[−j arg(w_k^H G^H Diag(H_k))];
        Update H_c and w_k;
        Recalculate SINR_k;
    end
    With the optimized Θ_k to user k:
    Compute SINR_i over i = 1, 2, 3, ..., K users
    Calculate SINR_Θk = mean(SINR_i)
end
Compute the average SINR, SINR_avg = mean(SINR_Θk)
```

a point where the absolute difference between the current SINR and the SINR from the previous iteration (denoted as $SINR_{comp}$) falls below 10^{-3}, serving as our stopping criterion. This maximizes the received signal for the kth user.

During each interact in L_2 loop, the $\mathbf{\Theta}$ matrix containing the N elements in the RIS with the phase shift are iteratively refined to find the optimal RIS angle for the user k, which is described by the Eq. (4.47)

$$\mathbf{\Theta}_k = \exp[-j \arg(\mathbf{w}_k^H \mathbf{G}^H \text{ Diag}(\mathbf{H}_k))] \tag{4.47}$$

This optimal solution has been documented across numerous studies in the literature [3, 4]. The solution presented in Eq. (4.47) is justified by the fact that, in communication between transmitting and receiving terminals, the phase shift among signals at the receiving terminals, induced by the channels can degrade the quality of the communication link. Therefore, to enhance the detection of the received signal, it is necessary to adjust the signal phases across the N elements of the RIS. This adjustment begins with channel estimation, enabling the configuration of the N RIS elements to align with the estimated channels according to the analytical result described in Eq. (4.47). Through this process, a coherent phase shift is applied, optimizing the power received at the terminal. However, it is important to highlight this approach is optimally suited for individual users and less so for multiple users. Identifying an optimal configuration that benefits all users remains an unresolved challenge in the literature.

Therefore, we utilize the Eq. (4.47) to provide combining technique to ascertain the value of the received signal. The purpose of the L_2 loop is to iteratively refine $\mathbf{\Theta}_k$ and its corresponding combiner $\mathbf{w}_k$, ensuring the iterative maximization of $SINR_k$.

In deploying RIS-aided M-MIMO systems, the challenge extends beyond the theoretical formulation of determining the N optimal RIS phases for solely the kth user. A pivotal concern is how the BS can realistically estimate the channels $\mathbf{G}$ and $\mathbf{H}_k$. The accuracy of these estimations is paramount as it directly influences the system's robustness and overall performance. To avoid this obstacle, the BS employs pilot sequences that are known at transmitting and receiving antennas. The information received by the antenna is then decoded to approximate the channels. This approach necessitates not just an extra interval for the transmission of these pilot sequences but also allocates substantial time for the data processing of the received signals. Although this strategy facilitates the estimation of the channels, it imposes an additional operational time for processing the received pilot. This method, despite making it possible to estimate channels, introduces an additional operational cost and delay in the system, affecting the system's efficiency in real-world applications.

An alternative solution to the traditional necessity for processing and decoding channels to optimize the N elements of RIS involves the employment of the NLS technique. Distinct from conventional PBF, the NLS focuses on directly

identifying the optimal phase angle by comparing the achievable SINR as the RIS elements undergo phase scanning. This method eliminates the requirement of channel decoding, significantly reducing the complexity and time required for optimal configuration. The technique operates on the phase sweep of the N RIS elements and makes adjustments until the setup that maximizes the SINR for the given scenario is in question. Once this optimal configuration is determined, it is deemed the most suitable for the particular context.

To evaluate the complexity of the PBF code, given in Algorithm 4.3, it is essential to analyze the loops and operations it encompasses, which can be classified as:

- **Loop L_1:** Iterates over each user K, ranging from 1 to K. This introduces a complexity factor of $\mathcal{O}(K)$.
- **Loop L_2:** Inside the loop L1, include variable initialization, operations, and an internal convergence loop (L_2), which typically converges quickly (in about $C = 3$ or 4 iterations), contributing minimal complexity to the overall process. Thus, this loop has a low complexity but must be considered and given by $\mathcal{O}(C)$.
- **Composite channel calculation:** Calculating the composite channel ($H_c = \mathbf{G}^H \text{ Diag}(\mathbf{\Theta}_k)\mathbf{H}$) involves matrix multiplication, which introduces a dominant complexity term of $\mathcal{O}(MN^2)$.

Consequently, the overall computational dominant complexity of such an algorithm is expressed as $\mathcal{O}(KCMN^2)$, reflecting the interaction between the loops and operations within the pseudocode.

4.3.4.2 Naive Local Search Method

The NLS is an optimization technique designed to find near-optimal solutions for complex problems where computing the absolute optimum is computationally impractical. Functioning as a heuristic approach, NLS methodically enhances an initial solution by making minor, incremental adjustments, thereby seeking a better solution within a constrained local search area.

This technique involves iterative fine-tuning, specifically by making minor modifications to the angles of decision variables ($\mathbf{\Theta}$), to improve the optimization outcome and identify a viable optimal solution. Beyond adjusting $\mathbf{\Theta}$, the method further includes alterations to additional simulation parameters to ensure the optimal adjustment of $\mathbf{\Theta}$, detailed as follows.

1) The L_1 loop iterates over l_1, aiming to replicate the experiment and compute the mean value;
2) The L_2 loop through all N elements of Θ within the RIS, which are randomly arranged in l_2;
3) The L_3 loop proceeds through l_3, adjusting the phase shift in the RIS from 0 to 2π; and

4) The L_4 loop iterates over all users in l_4, tasked with calculating each user's SINR. This calculation considers the positioning of RIS elements as specified in l_2 and the phase shift defined by $\exp(jl_3)$.

The full implementation of this technique, along with its algorithmic details, are outlined in Sections 4.3.3.2 and 4.3.3.3.

To evaluate the complexity of the NLS method, it is essential to analyze the loops and operations it encompasses.

- **Loop L_1 (repeat):** The complexity depends on the repetition count (R), making the loop's execution complexity $\mathcal{O}(R)$.
- **Loop L_2 (Element selection):** This loop cycles through N elements, elevating the cumulative complexity to $\mathcal{O}(R \times N)$.
- **Loop L_3 (Phase adjustment):** For each element N, this loop increments in steps of 0.1 radians from 0 to 2π, resulting in $\lfloor \frac{2\pi}{0.1} \rfloor$ iterations for each element. Given this is a constant, denoted as P, the complexity for each iteration of L_3 is $\mathcal{O}(P)$.
- **Composite channel calculation:** Calculating the composite channel ($H_c = \mathbf{G}^H \text{Diag}(\mathbf{\Theta}_k)\mathbf{H}$) involves matrix multiplication, which introduces a dominant complexity term of $\mathcal{O}(MN^2)$.

Consequently, the aggregate dominant complexity term in this algorithm is $\mathcal{O}(RPMN^3)$, for both max–min and sum rate optimization problems.

When comparing these two assessments' complexity, it becomes evident that the complexity of the PBF method is lower than that of the NLS. This observation aligns with other findings in the literature, as seen in references [6] and [7], which report similar levels of numerical complexity with the dominant complexity of $\mathcal{O}(KM^3)$ and $\mathcal{O}(I_0 I_\lambda I_w KM^3)$ respectively, in which I_0, I_λ, and I_w are loops iteration algorithms.

4.4 Numerical Results

As explained in Section 4.2.2, the far-field model is essentially a particular case of the near-field model, offering a more straightforward approximation. Our simulation was conducted under spherical wave propagation conditions. Therefore, there is no need to perform far-field approximations, since the spherical wave equation remains valid for higher distances used in the cases discussed. Furthermore, the calculations discussed do not represent increases in computational complexity.

Additionally, in scenarios where signal spectrum sharing is utilized, every user is allocated the same transmission power. Without employing any network-sharing strategies and ignoring path loss effects, the interference power can achieve

up to $K-1$ times the power of the target user's signal. Consequently, the implementation of optimization and beamforming techniques becomes crucial to ensure the system's optimal performance. In every simulation conducted, we illustrate the analysis of each scenario with three important graphs: SINR in dB, SE, and OP. Those three indicators are essential in assessing the signal's quality and the communication's efficacy. However, for simplicity across all simulations, we standardize the transmission power for every user at $p_k = 100\,\text{mW}$. The combiner utilizes the optimal solutions found in the literature, such as MRC, ZF, and MMSE, with the specific combiner used, indicated inside the figures. Additionally, in the implementations over the sum rate strategics, we consider all K users to hold equal priority, hence setting $\boldsymbol{\omega}_i = 1$ for all $i = 1, 2, ..., K$.

Starting with SINR in dB, it's interesting to recognize a value around 1.2 dB because it is sufficient for differentiating the signal of interest from the surrounding interference and noise. This differentiation is possible because the signal of interest's power significantly exceeds the combined powers of interference and noise. For robust and dependable communication, a higher SINR is advisable to provide an extra buffer against fluctuations in signal quality, thus ensuring uninterrupted communication. This buffer is vital to enhancing transmission quality and ensuring a seamless experience for the user.

Regarding SE, this metric measures the effective use of the frequency spectrum for information transmission. Improving SE signifies a more efficient use of the spectrum resources, leading to more effective communication. It's worth noting that SE is closely linked to SINR, as presented in Eq. (4.42).

Finally, OP offers insights into the telecommunications system's reliability and service quality. Technically, elevated P_{out} values suggest a higher likelihood of transmission errors or failures, potentially causing service interruptions or significant drops in system performance. Hence, minimizing OP is critical for achieving an optimal transmission rate.

4.4.1 Dynamic Scenario

The simulation parameters for the proposed scenario configuration are outlined in Table 4.3. Additionally, a sample of 20 random UE positions from the Monte Carlo simulations in the system is depicted in Figure 4.7.

The proposed scenario evaluates the metrics for SINR in dB, depicted in Figure 4.8; SE shown in Figure 4.9; and OP, illustrated in Figure 4.10. Furthermore, we demonstrate our work focuses on the sub 6 GHz band within a UL system, utilizing a comparatively narrow range bandwidth. This approach emphasizes energy efficiency for users, which is particularly beneficial over long distances where the system's operational effectiveness is critical. Notably, users are situated randomly and may be in motion within the delimited region.

Table 4.3 System parameters and configurations of RIS-aided M-MIMO systems with devices in dynamic environments.

Parameter	Value
MC simulation	1000 realizations
Carrier freq.	1 GHz
BW	20 MHz
N	41 RIS passive elements
M	65 BS antennas
K	from 1 up to 20 mobile terminals (MTs)
Transmit power per MT	$p_k = 100$ [mW]
RIS position	RIS centered at (0,0) with element spacing of $\lambda/2$
BS position	BS centered at (106, −106) with antennas spacing of $\lambda/2$
UEs positions	Random
Cell area	150×120 [m]
G channel	Rice, (Rice Factor $\epsilon_k = 3$)
H channel	Rayleigh

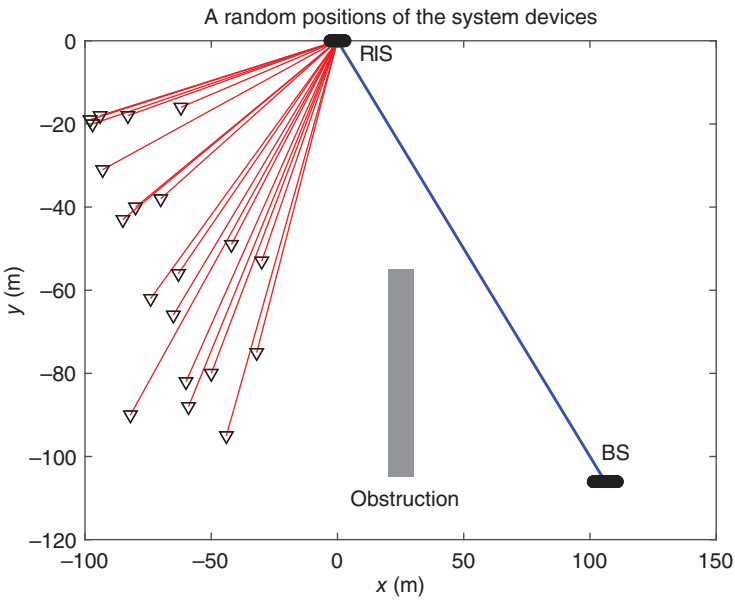

Figure 4.7 An RIS-aided M-MIMO communication system with random user positions and fixed BS and RIS positions. Source: The Authors.

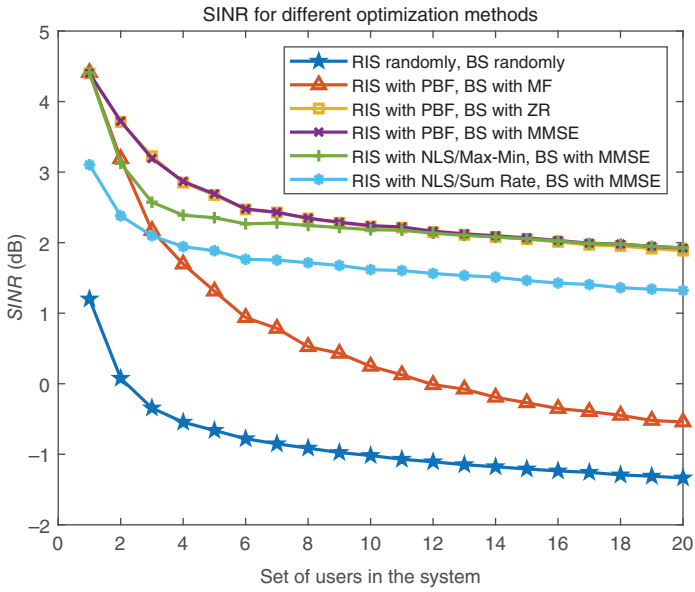

Figure 4.8 Comparison of different optimization techniques, demonstrating the SINR metric in dB against a set of users in random positions. Source: The Authors.

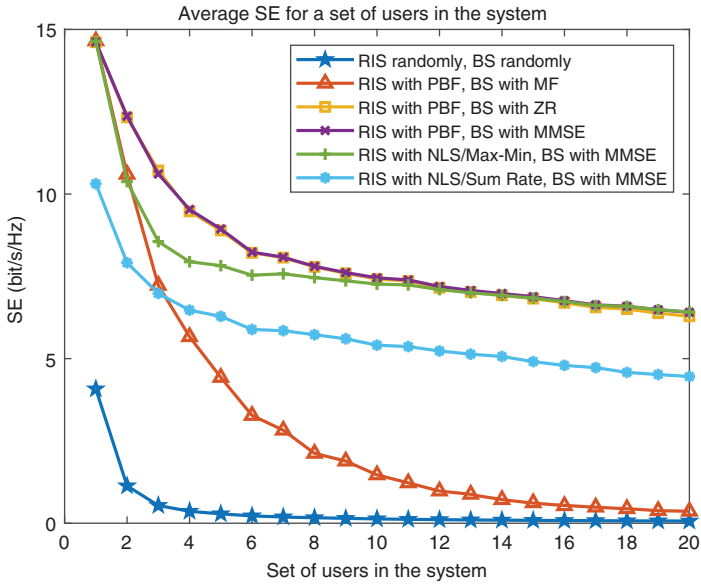

Figure 4.9 Comparison of different optimization techniques, revealing the average SE against a set of users in random positions. Source: The Authors.

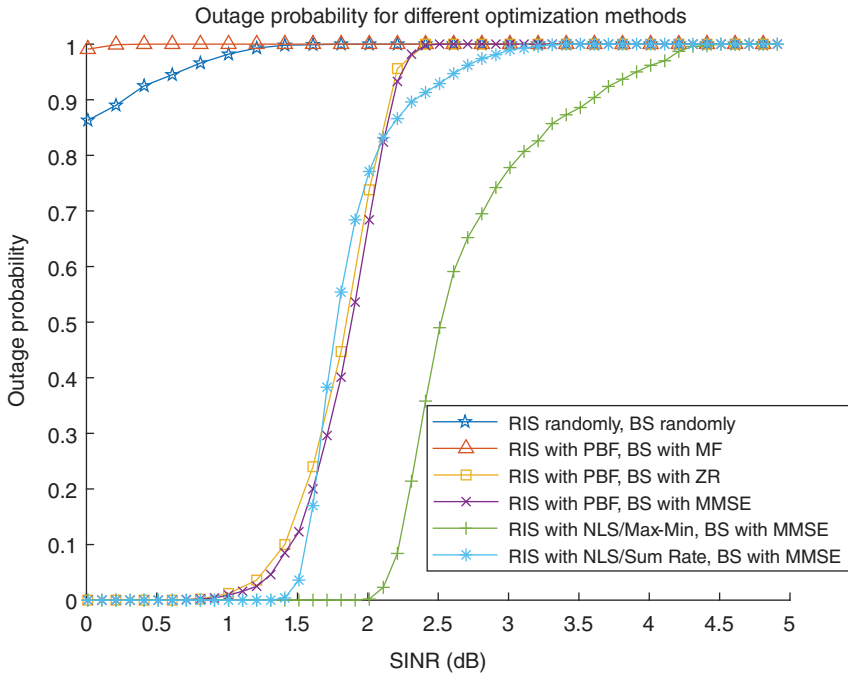

Figure 4.10 Comparison of different optimization techniques, demonstrating the OP against a set of users in random positions. Source: The Authors.

The decision to analyze this particular carrier stems from the variability of user locations across a broad and extended region, over a hundred meters from the BS and obstructions in the direct link. The random UEs positions are allocated inside a square region delimited between −100 to 0 m in x-axis and −100 to −15 in y-axis. This aspect underscores the simulation's ability to align with theoretical and practical understandings of carrier frequency path loss and telecommunication channel behaviors, consistent with electromagnetic theory, whose attenuation factor of the electromagnetic wave increases as the signal frequency becomes higher. The simulation also demonstrates its adaptability to address the PBF optimization and NLS with max–min and sum rate the optimization strategies introduced in this chapter.

Our analysis further delves into various optimization methods, as evidenced by the trends depicted in the graphs. It's observed that, on average, the combination of PBF at the RIS and active beamforming at the BS yields superior outcomes in terms of capacity, SINR, and OP. This is particularly true when employing MMSE and ZF combiners, whereas using an MF combiner is deemed optimal solely for individual users. Moreover, the increase in the user count and a marked decline in signal quality are noted, mirroring the simulation results.

In this dynamic scenario, optimization through NLS on RIS elements shows impressive results, particularly with the max–min technique, which closely approaches the optimal model. In contrast, the sum rate technique lags in performance compared to max–min, as it is more applicable to scenarios with static users with different priority conditions, aiming to maximize the priority user SINR.

We highlight that when evaluating the optimization techniques across random configurations of RIS elements and BS antennas, it becomes apparent that the system's lower bounds performance (in terms of SINR, SE, and OP) is reached under these random conditions. These observations are demonstrated by the curves in Figures 4.8–4.10.

Figures 4.8 and 4.9 illustrate that the QoS for only one user is optimal due to the absence of interference. However, as the number of users increases, a deteriorated QoS is noticeable, attributed to the rise in power interference. Despite these challenges, the deployed techniques continue to yield satisfactory outcomes for the collectively utilized network. Another interesting detail observed is the same SE and SINR convergence values for a single user applying PBF (with MF, ZF, and MMSE) and NLS with max–min strategies.

4.4.2 Dynamic Scenario with Different Channels

Figures 4.11–4.13 take into account the PBF optimization on RIS and MMSE combiner on the BS. The Ricean channel model from RIS to BS and feature variations with multipath channels from the UEs to RIS, as detailed in their respective legends. In addition, Table 4.4 outlines the simulation parameters for the proposed scenario configuration, and a sample of 20 random UEs positions from the Monte Carlo simulations in the system can also be depicted in Figure 4.7.

Figures 4.11–4.13 demonstrate that variations in channel parameters significantly affect the quality of the metrics. Thus, we provide a refined analysis over those different channel conditions.

The parameter m of Nakagami-m and μ from α–μ and κ–μ represent the exact relationship of the number of multipath clusters. Throughout the curves shown, we observe the variation of this parameter during signal transmission from the user to the RIS. These statistical channels may vary randomly, particularly in dynamic scenarios where users are located randomly, such as in urban areas filled with buildings, vehicles, and trees, all of which contribute to multipath signal propagation. It's also demonstrated that increasing multipath clusters enhances the communication system's quality making the scenario more deterministic.

Analyzing the κ–μ channel, we know it is a generalized form of the Rice distribution, and the ratio of the dominant signal to scattered waves in each multipath cluster is quantified by the κ parameter. The graphs show that a higher κ correlates with improved system quality and makes the scenario more deterministic.

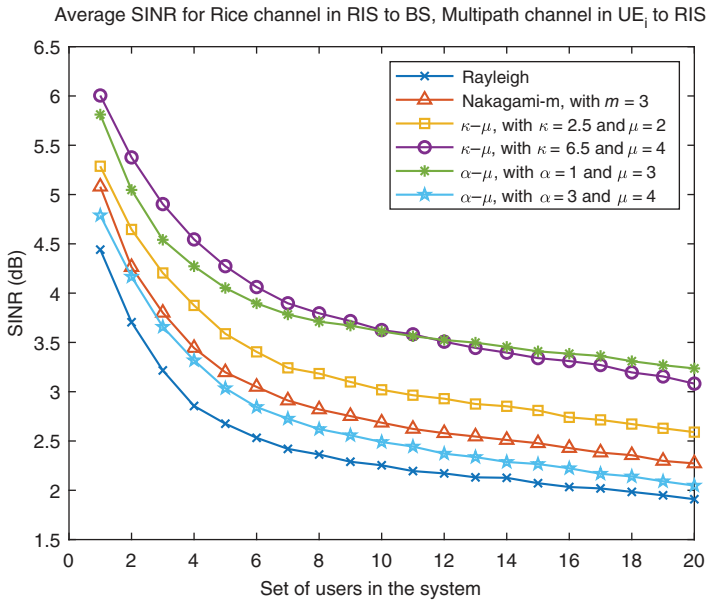

Figure 4.11 Comparison of an RIS-aided M-MIMO communication system with random user positions and demonstrating the SINR in dB under different channel conditions. Source: The Authors.

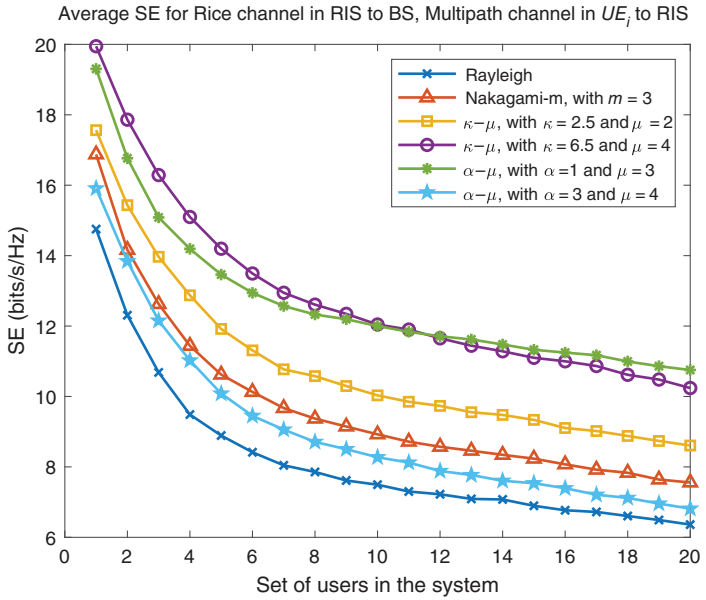

Figure 4.12 Comparison of an RIS-aided M-MIMO communication system with random user positions and demonstrating the average SE under different channel conditions. Source: The Authors.

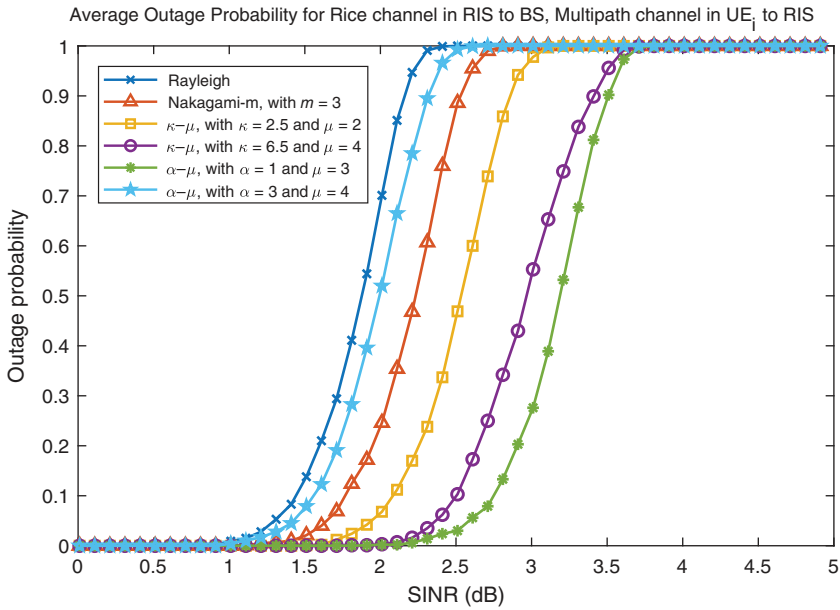

Figure 4.13 Comparison of an RIS-aided M-MIMO communication system with random user positions and demonstrating the OP under different channel conditions. Source: The Authors.

Table 4.4 System parameters and configurations of RIS-aided M-MIMO systems with devices in dynamic environments and with different channel conditions.

Parameters	**Value**
MC simulation	1000 realizations
Carrier	1 GHz
BW	20 MHz
N	41
M	65
K	from 1 up to 20 MTs
Transmit power per MT	$p_k = 100$ [mW]
RIS position	RIS centered at (0,0) with element spacing of $\lambda/2$
BS position	BS centered at $(106, -106)$ with antennas spacing of $\lambda/2$
UEs positions	Random
Cell area	150×120 [m]
G channel	Rice (Rice Factor $\epsilon_k = 3$)
H channel	Multipath

The α–μ channel is analogous to the Nakagami-m channel for $\alpha = 2$. The α parameter, although infrequently observed in practice, does manifest under specific conditions, such as in environments with air density fluctuations or high ionization levels. Here, variations in α are noticeable, with the distribution indicating that α is affected by environmental nonlinearity and signal attenuation levels, resulting in varied Nakagami-m conditions where $\alpha \neq 2$. A higher α value indicates reduced signal attenuation during channel transmission, as seen in the graph curves for $\alpha > 2$ and $\alpha < 2$.

In the Rayleigh distribution, the signal is scattered with a NLoS. It can be inferred that the Rayleigh distribution represents the lower bound of quality performance for those channel communications (except the α–μ channel at a very high α).

Thus, by simulating other scenarios with the Rayleigh channel as the lower bound quality performance benchmark, we conclude that more deterministic statistical channel conditions enhance communication quality and improve communication outcomes.

4.4.3 Static Scenario, with UEs Uniformly Distributed

The simulation parameters for a static scenario composed by UEs uniformly distributed equally spaced on x axes are outlined in Table 4.5, and its configuration can be depicted in Figure 4.14.

Table 4.5 System parameters and configurations of RIS-aided M-MIMO systems with devices in static and uniformly spaced distributed.

Parameters	Value
MC simulation	150 realizations
Carrier	60 GHz
BW	50 MHz
N	201
M	305
K	5 MTs
Transmit power per MT	$p_k = 100\,[\text{mW}]$
RIS position	RIS centered at (0,0) with element spacing of $\lambda/2$
BS position	BS centered at (7.7,6.4) with antennas spacing of $\lambda/2$
UEs positions	$(-10,-10), (-8,-10), (-6,-10), (-4,-10), (-2,-10)$
G channel	Rice (Rice Factor $\epsilon_k = 3$)
H channel	Rayleigh

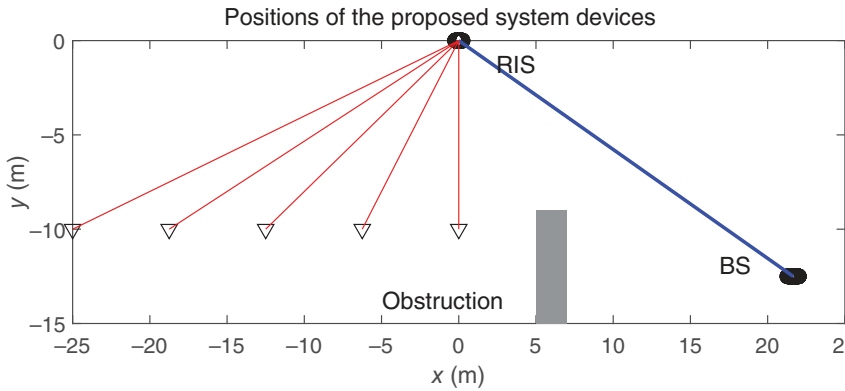

Figure 4.14 An RIS-aided M-MIMO communication system featuring fixed and strategically placed of users, RIS and BS. Source: The Authors.

In this setup, we implement a RIS-aided M-MIMO communication system utilizing a millimeter wave carrier at a frequency of 60 GHz. According to electromagnetic wave theory, the attenuation factor of a wave increases with its frequency. The simulations reveal that device distances are significantly shorter than those achievable with sub 6 GHz carriers. This highlights another advantage of RIS technology: it extends communication range besides circumventing obstacles. As observed in the provided Figures 4.15–4.17 the users positioned farther away don't achieve the same efficiency in SE, SINR, and OP as those nearer to the source. Nevertheless, they are still able to maintain basic communication with the BS through the use of active and passive beamforming techniques.

We also note that our analysis involves a Rayleigh channel (considered the upper bound). An enhancement in SE would be evident in channels with more deterministic properties.

An additional insight is the superior performance of sum rate in this static setup. In such user configurations, the max–min function's priority is to boost the SE of the furthest user, often at the expense of quality for others. Conversely, with the sum rate, the furthest user is deprioritized to enhance the general quality for users closer to the source.

4.4.4 Static Scenario, with UEs Equally Spaced from RIS but with Different Angles

In this scenario, the user positions users are equidistant from the RIS, differing only in their departure angles while employing a uniform carrier frequency of 30 GHz. The simulation parameters for a static scenario configuration are outlined in Table 4.6, and its configuration can be depicted in Figure 4.18.

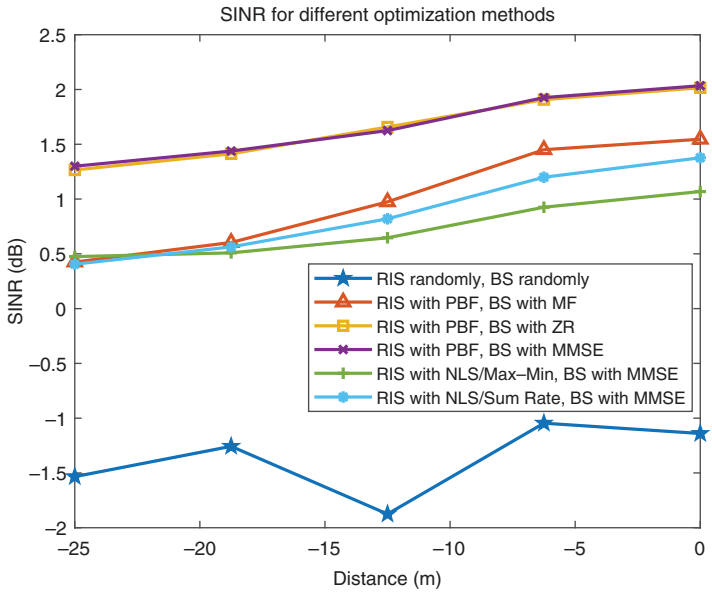

Figure 4.15 Comparison of different optimization techniques, demonstrating the SINR in dB against users strategically positioned in the system. Source: The Authors.

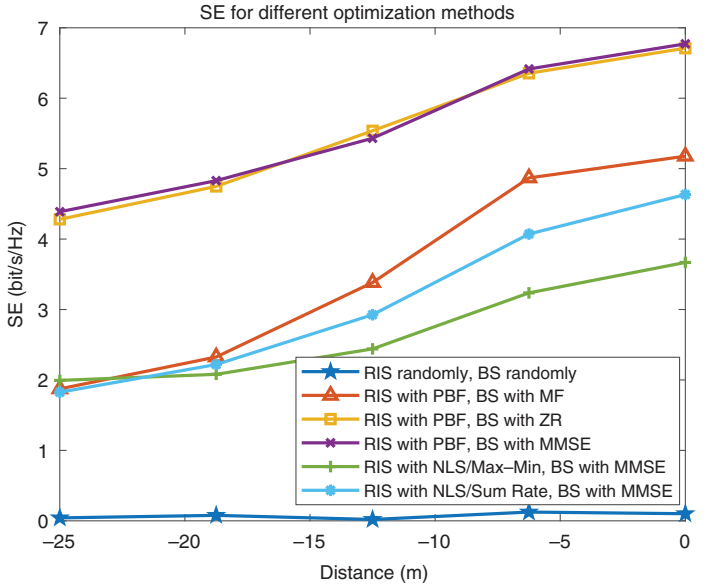

Figure 4.16 Comparison of different optimization techniques, demonstrating the average SE against users strategically positioned in the system. Source: The Authors.

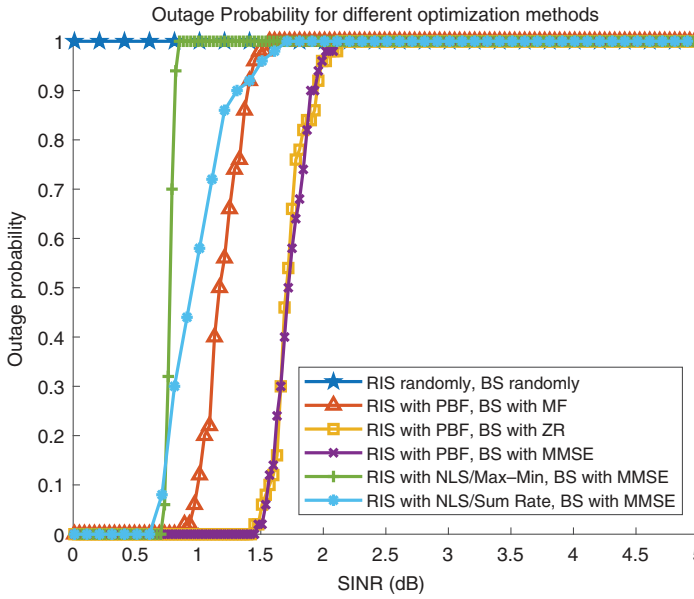

Figure 4.17 Comparison of different optimization techniques, demonstrating the OP against users strategically positioned in the system. Source: The Authors.

Table 4.6 System parameters and configurations of RIS-aided M-MIMO systems with devices in static and uniformly distributed by angle and all with the same distance from RIS.

Parameters	**Value**
MC simulation	150 realizations
Carrier	30 GHz
BW	50 MHz
N	201
M	305
K	5 MTs
Transmit power per MT	$p_k = 100\,[\text{mW}]$
RIS position	RIS centered at (0,0) with element spacing of $\lambda/2$
BS position	BS centered at (7.7,6.4) with antennas spacing of $\lambda/2$
UEs positions	$(-7,-34)$ $(-16.5,-30.9)$ $(-24.7,-24.7)$ $(-30.9,-16.5)$ $(-34,-7)$
$\mathbf{G}$ channel	Rice (Rice Factor $\epsilon_k = 3$)
$\mathbf{H}$ channel	Rayleigh

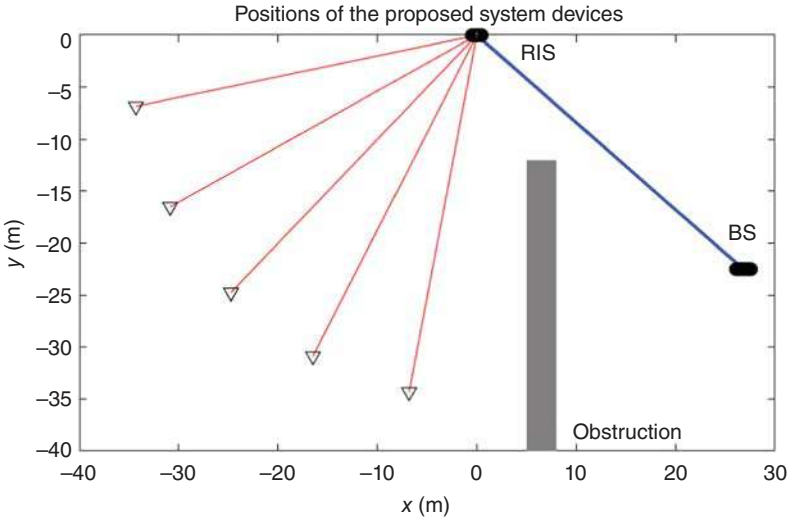

Figure 4.18 An RIS-aided M-MIMO communication system featuring fixed and strategically placed users, RIS and BS. Source: The Authors.

Our observations reveal that thanks to the optimization techniques applied, capacity remains consistent across all users under reasonable conditions, given their equal distances from the RIS.

As expected, reducing the carrier frequency to 30 GHz effectively expands the range of the telecommunications system. This is observed in the simulation results, which show an improvement in SE as presented in Figure 4.19 and SINR in Figure 4.20, also indicate a reduced OP, as demonstrated in Figure 4.21.

It's pertinent to reiterate that our discussion involves a Rayleigh channel (considered the upper bound) from users to RIS. Nevertheless, transitioning to more deterministic channels would enhance communication quality.

Across all scenarios examined in Sections 4.4.1, 4.4.2, 4.4.3, and 4.4.4, it was found that PBF with MMSE outperformed the NLS method, leading us to regard it as the more robust method. For the NLS technique, we conducted experiments with progressively increasing phase swap resolution (the increments $l_3 \rightarrow 0$), which enhanced the SINR but at the cost of significantly increased computational demand. This implementation appears to approximate the process of an exhaustive search. Despite that, the simulation with $l_3 = 0.1$ achieved SINR values approximately 90% similar to those found in exhaustive searches. Therefore, employing a $l_3 = 0.1$ not only ensures precision but also enhances robustness in solving for results more efficiently than using a $l_3 \rightarrow 0$ reducing processing time substantially.

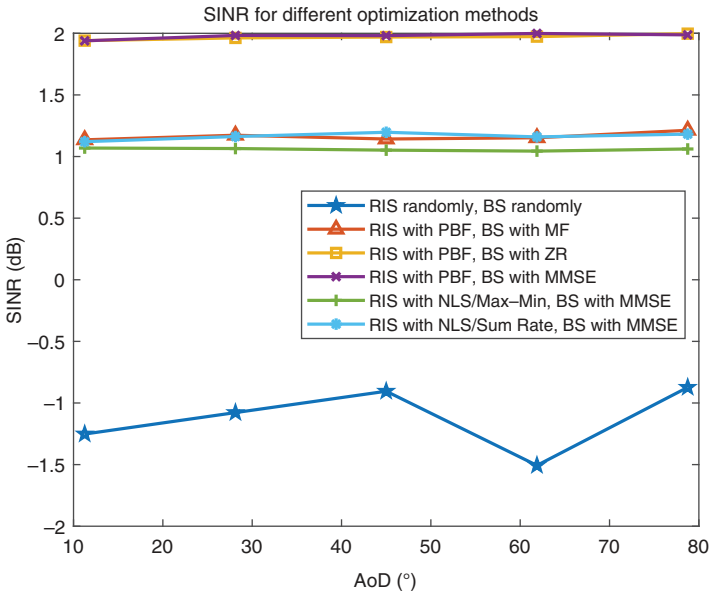

Figure 4.19 Comparison of different optimization techniques, demonstrating the SINR in dB against users strategically positioned in the system. Source: The Authors.

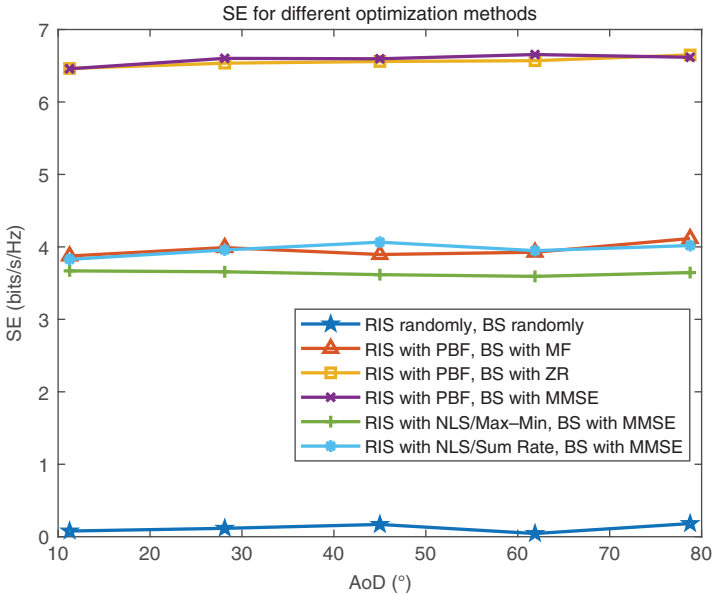

Figure 4.20 Comparison of different optimization techniques, demonstrating the average SE against users strategically positioned in the system. Source: The Authors.

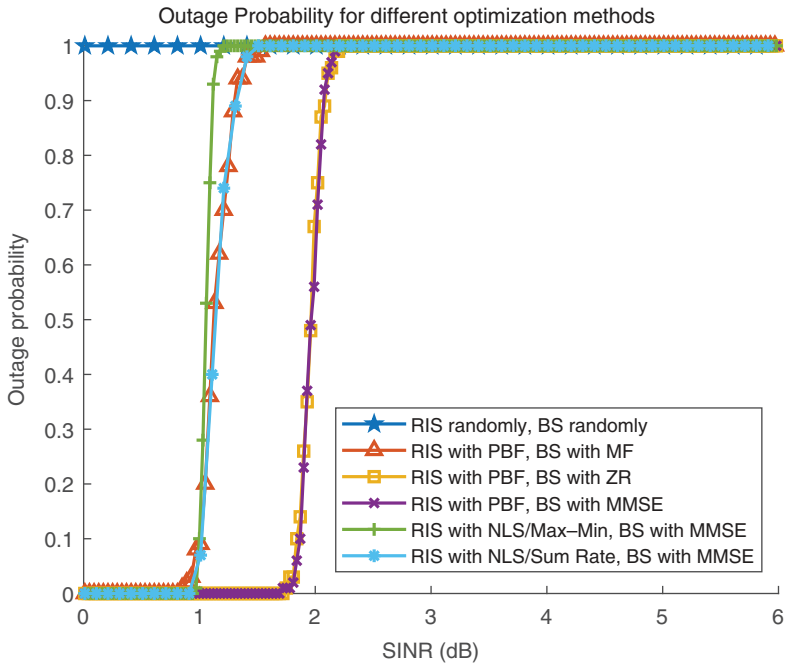

Figure 4.21 Comparison of different optimization techniques, demonstrating the OP against users strategically positioned in the system. Source: The Authors.

4.5 Conclusions

Based on the comprehensive analysis and numerical results discussed throughout the chapter, it was demonstrated that deploying RIS-aided M-MIMO communications systems significantly enhances wireless communication systems' performance, in terms of SINR, SE, and OP. This chapter evaluates three optimization problem challenges, precisely, the SINR maximization, the WSR maximization, and the minimum SINR maximization across users, each demonstrating the pivotal role of RIS in improving channel reliability, SE, reducing OP, and ensuring equitable QoS (fairness) across users.

The dynamic and static scenarios analyzed highlight the adaptability of RIS technology to diverse user configurations and mobility patterns, underscoring its potential to meet varying communication demands efficiently. The successful application of techniques like PBF and the NLS, particularly in dynamic environments, showcases the capability of RIS to optimize the communication channel in real time, catering to both stationary and moving users.

Furthermore, the chapter delves into the impact of different channel conditions, including Rayleigh, Rice, Nakagami-m, α–μ, and κ–μ on the system's

performance. It demonstrates how RIS can mitigate adverse effects, such as signal fading and path loss, ensuring robust and reliable communication even in challenging environments.

4.5.1 Limitations of the Proposed Model

The limitations of the models examined are listed as:

- The adoption of ULAs for both the RIS elements and BS antennas has confined the investigation into the two-dimensional network configuration. This approach inadvertently omits the exploration of three-dimensional systems, thus presenting a limited analysis of network patterns.
- The study could benefit from incorporating analyses on the Weibull, η–μ channel, and also a class of composite fading models. Including these models is suggested as they offer the capability to represent a broader range of channel conditions through adjustments to the channel parameters, thereby enhancing the robustness of the analysis.
- It is proposed to reconsider the assumption that the obstruction of the direct link between the BS and the UEs unequivocally precludes the direct path. Instead, it is advised to incorporate the partially obstructed direct path into the calculations, which could yield a more nuanced understanding of the network's performance under various environmental conditions.
- While the analysis concerning the communication channel between the BS and the RIS exclusively contemplated a Rice channel, extending this examination to include other channel models is recommended. This expansion would facilitate a more holistic understanding of the communication dynamics and potentially uncover additional insights into the system's operational efficacy.
- Traditional channel estimation methods require a dedicated interval for the transmission of pilot sequences, along with a substantial amount of time allocated for processing the received signals. This approach introduces an additional layer of operational delay and cost. The simulation does not account for this extension in operational timelines, which affects the system's applicability in real world.
- The proposed analysis considers constant power allocation for the users and utilizes known linear precodings. The expansion for power allocation and precoding optimization cover extensive potential gains.

4.5.2 Lessons Learned

The key contributions provided in this chapter are highlighted as:

- A detailed implementation of general statistical channel models (Rayleigh, Rice, Nakagami-m, α–μ, and κ–μ) applied to M-MIMO systems. The models can simulate the behavior of wireless channels in these systems, with many antennas for

transmission and reception, thereby enhancing communication reliability and data rates.

- The chapter provides a complete description of the implementation of steering vector channel models in conjunction with the statistical channel. This approach allows the adaptive modification of the antenna array's directionality to improve signal reception and transmission quality, particularly in diverse environmental conditions.
- The implementation of RIS devices incorporates optimization techniques for its elements. This involves adjusting the RIS's elements to enhance the communication channel's efficiency, contributing to more adaptive and efficient wireless communication networks.
- A comprehensive analysis is conducted on applying optimization methods to solve problems related to RIS elements, aiming to enhance the QoS. This enhancement is achieved through using two distinct methods: PBF and NLS, along with strategies such as the sum rate and max–min techniques. These methods provide fine-tuning and adjust the configuration of RIS elements. They ensure optimal signal enhancement and interference reduction by manipulating electromagnetic waves, thus improving signal propagation and reception.
- The simulations and analyses are conducted using a system model that accommodates various setups, including static or dynamic UEs positions, diverse channel conditions, and multiple carrier frequencies. This comprehensive examination thoroughly assesses the system's performance across various real-world scenarios. By exploring these different configurations, the study contributes to developing more efficient and reliable systems, guiding the design of robust wireless communication systems.

4.5.3 Future Scope

Future research directions aim to address and bridge previously identified limitations and gaps. The proposed enhancements include:

- A detailed implementation of the steering vector for the uniform planar array (UPA) to model a three-dimensional channel accurately. This approach would also involve using planar elements in both the BS and RIS structures, thereby enriching the dimensional analysis of the network.
- The exploration and incorporation of more comprehensive channel models. This entails applying generalized channel models to both the communication link between the BS and the RIS and the link between the RIS and the UEs to ensure a more extensive examination of channel dynamics.

- Including the direct communication link between users and the BS in the analysis aims to provide a more holistic view of the network's performance by considering all possible communication pathways.
- As a proposal, including a new class of optimization problems surrounding SE and energy efficiency (EE) to improve the QoS in RIS-aided MIMO systems.
- Addressing the unaccounted operational delays and costs associated with pilot transmission and signal processing for enhancing the efficiency and real-world viability of RIS-aided M-MIMO systems.
- We will consider new methodologies with lower complexity and promising results for phase-shift optimization. Additionally, we will take into account power allocation and precoding optimization as well.

In conclusion, the insights garnered from this chapter are invaluable to the field, offering potential solutions and guiding principles for future research. Future applications could explore new steering vectors in UPA and other RIS configurations, addressing diverse multipath channels, shadowing, or composite channels, with open issues not examined in this chapter. Additionally, further optimization problems, including those involving energy efficiency, present significant opportunities for advancement. Thus, as the demand for wireless communication continues to grow, the novel perspectives and methodologies presented here will undoubtedly inspire further innovations, paving the way for more efficient, scalable, and flexible communication systems. This chapter contributes to the academic community and holds significant implications for the practical development of next-generation wireless networks.

References

1 Wang, C.-X., Huang, J., Wang, H. et al. (2020). 6G wireless channel measurements and models: trends and challenges. *IEEE Vehicular Technology Magazine* 15 (4): 22–32.

2 Zhu, X., Chen, W., Li, Z. et al. (2023). RIS-aided spatial scattering modulation for mmWave MIMO transmissions. *IEEE Transactions on Communications* 71 (12): 7378–7392.

3 de Souza Junior, W. and Abrao, T. (2022). RIS-aided cooperative FD-SWIPT-NOMA outage performance in Nakagami-m channels. *arXiv: 2204.01900*.

4 Sun, Q., Liu, H., Yan, S. et al. (2023). Joint receive and passive beamforming optimization for RIS-assisted uplink RSMA systems. *IEEE Wireless Communications Letters* 12 (7): 1204–1208.

5 Subhash, A., Kammoun, A., Elzanaty, A. et al. (2023). Max-min SINR optimization for RIS-aided uplink communications with green constraints. *IEEE Wireless Communications Letters* 12 (6): 942–946.

6 Papazafeiropoulos, A., Kourtessis, P., and Chatzinotas, S. (2023). Max-min SINR analysis of STAR-RIS assisted massive MIMO systems with hardware impairments. *IEEE Transactions on Wireless Communications* 23 (5): 4255–4268.

7 Guo, H., Liang, Y.-C., Chen, J., and Larsson, E.G. (2020). Weighted sum-rate maximization for reconfigurable intelligent surface aided wireless networks. *IEEE Transactions on Wireless Communications* 19 (5): 3064–3076.

8 Chiani, M., Win, M.Z., and Shin, H. (2010). MIMO networks: the effects of interference. *IEEE Transactions on Information Theory* 56 (1): 336–349.

9 Björnson, E., Hoydis, J., and Sanguinetti, L. (2018). *Massive MIMO Networks: Spectral, Energy, and Hardware Efficiency*, Foundations and Trends in Signal Processing. Now Publishers. https://books.google.com.br/books?id=ekHYswEACAAJ.

10 Ali, E., Ismail, M., Nordin, R., and Abdulah, N.F. (2017). Beamforming techniques for massive MIMO systems in 5G: overview, classification, and trends for future research. *Frontiers of Information Technology & Electronic Engineering* 18: 753–772.

11 Liu, Y., Wang, Z., Xu, J. et al. (2023). Near-field communications: a tutorial review. *IEEE Open Journal of the Communications Society* 4: 1999–2049.

12 Yacoub, M. (1993). *Foundations of Mobile Radio Engineering*. CRC Press.

13 Abramowitz, M. and Stegun, I. (1972). *Handbook of Mathematical Functions with Formulas, Graphs, and Mathematical Tables*, A Wiley-Interscience Publication. Wiley.

14 Yacoub, M.D., Bautista, J.E.V., and de Rezende Guedes, L.G. (1999). On higher order statistics of the Nakagami-m distribution. *IEEE Transactions on Vehicular Technology* 48 (3): 790–794.

15 Yacoub, M.D. (2007). The κ-μ distribution and the n-μ distribution. *IEEE Antennas and Propagation Magazine* 49 (1): 68–81.

16 Yacoub, M.D. (2007). The α-μ distribution: a physical fading model for the Stacy distribution. *IEEE Transactions on Vehicular Technology* 56 (1): 27–34.

17 Yuan, X., Zhang, Y.-J.A., Shi, Y. et al. (2021). Reconfigurable-intelligent-surface empowered wireless communications: challenges and opportunities. *IEEE Wireless Communications* 28 (2): 136–143.

18 Zhi, K., Pan, C., Ren, H., and Wang, K. (2022). Power scaling law analysis and phase shift optimization of RIS-aided massive MIMO systems with statistical CSI. *IEEE Transactions on Communications* 70 (5): 3558–3574.

19 Report ITU-R M.2412-0 (2017). Guidelines for Evaluation of Radio Interface Technologies for IMT-2020. Geneva: International Telecommunication Union. https://www.itu.int/dms_pub/itu-r/opb/rep/R-REP-M.2412-2017-PDF-E.pdf (accessed 16 December 2024).

20 Haykin, S. (2008). *Communication Systems*, 3e. Wiley India Pvt. Limited. https://books.google.com.br/books?id=Q4iWOkVEonMC (accessed 16 December 2024).

21 Ding, Q. and Jing, Y. (2018). Outage probability analysis and resolution profile design for massive MIMO uplink with mixed-ADC. *IEEE Transactions on Wireless Communications* 17 (9): 6293–6306.

5

Performance Optimization of Multiple RIS-Assisted Multiuser MIMO Communication Systems

Francisco Rubén Castillo Soria[1], Roilhi Frajo Ibarra-Hernández[1], Carlos Adrián Gutiérrez Diaz de León[1], Abel García Barrientos[1], Sharon Macias-Velasquez[2], and José Alberto del Puerto-Flores[3]

[1] *Faculty of Science, Universidad Autonoma de San Luis Potosi (UASLP), S.L.P., Mexico*
[2] *Faculty of Engineering, Universidad Autonoma de San Luis Potosi (UASLP), S.L.P, Mexico*
[3] *Facultad de Ingeniería, Universidad Panamericana, Álvaro del Portillo 49, Zapopan 45010, Mexico*

5.1 Introduction

The 6th generation of wireless communication systems requires high data transmission rates to interconnect different sources efficiently. Higher speed rates and high quality of service are two persistent claims in the design of modern mobile communication systems. An improved throughput, latency, availability, energy efficiency, and cost-efficiency emerged from novel mobile applications such as Industry 4.0, vehicular communication, and the Internet of Things (IoT). Two of the key technologies considered in 6G for higher data transmission rates are the use of electromagnetic waves in the THz band, also known as mmWave communications, and the increase in the number of antennas or massive multiple input-multiple output (MIMO) [1]. One of the most promising technologies for realizing the 6G vision is reconfigurable intelligent surfaces (RISs). The RIS is a two-dimensional surface composed of controllable elements made of low-cost passive components that can be designed to change the phases of the incoming signals so that they are received coherently by the user, resulting in a channel that can be controlled to exploit the diversity gains where the energy of the transmitted signals is utilized more efficiently. Recent investigations have demonstrated that RISs can improve the system performance with significant energy savings [2]. Due to the aforementioned properties, RIS can be exploited to assist communication systems applications such as power transfer, physical layer security, unnamed aerial vehicles communication, IoT, and sensor networks, among others. Based

Reconfigurable Intelligent Surfaces for 6G and Beyond Wireless Networks, First Edition.
Edited by Agbotiname Lucky Imoize, Vinoth Babu Kumaravelu, and Dinh-Thuan Do.

on the nomenclature for MIMO systems, RIS-assisted multiuser (MU) systems can be classified as:

- **RIS-MU-single input-single output (SISO) systems**: Formed by a single Tx antenna and multiple users equipped with a single Rx antenna.
- **RIS-MU-multiple input-single output (MISO) systems**: Formed by a transmitter with multiple antennas and multiple receiving users equipped with a single Rx antenna.
- **RIS-MU-single input-multiple output (SIMO) systems**: Formed by a transmitter with a single antenna and multiple receiving users equipped with multiple Rx antennas.
- **RIS-MU-MIMO systems**: Formed by a transmitter with multiple antennas and multiple receiving users with multiple Rx antennas each.
- **N-RIS-MU-MIMO systems**: If multiple RISs are used working in parallel, the system is referred to as an N-RIS.

The design of a RIS-assisted MIMO downlink transmission system can be addressed as an optimization problem that considers the design of a precoding or beamforming matrix at the transmitter (Tx) in the base station (BS) and the phase shifts of the mirrors at the RIS. However, this approach can be challenging even for systems with single-antenna users and a single RIS [3, 4]. If multiple RISs are considered in a multiuser (MU) scenario, with single-antenna users (MISO), the design of the phase shift vector in the RISs barely improves the bit error rate (BER) performance of the system [5]. In this case, multiple receive (Rx) antennas can exploit diversity to improve the system's BER performance. Alternatively, different RISs can be utilized for different users [6]. The system design with a single RIS and multiple users using multiple Rx antennas has been recently addressed [7]. In this scenario, linear precoding can precancel the interference produced by the MIMO broadcast channel [8]. Also, precoding techniques can be used along with space-orthogonal schemes to improve the multi-RIS-aided MU-MIMO system [9]. In this case, the solution is focused on a zero-interference criterion, and the MU interference is canceled regardless of the RIS phase shifts. The most complex scenario uses multiple parallel RIS to assist several users with multiple Rx antennas (MU-MIMO). Due to the interference caused by multiple links in the system, the system's efficiency and complexity could be challenged in this case.

A promising alternative to solve the problems above in RIS-assisted MU-MIMO systems is machine learning (ML) technology. ML methods have been proposed as an effective alternative for optimizing RIS-assisted communication systems. This technique is particularly applied when the computational complexity increases due to a fast increase in the number of users and the interference produced by its interactions [10]. Section 5.6 discusses some artificial intelligence (AI) algorithms for RIS-assisted communication systems. Section 5.6 addresses

some open problems and future trends in RIS-assisted communications where ML algorithms and some learning algorithms can be applied.

5.1.1 Contributions

The integration of multiple RIS to MU-MIMO systems is expected to boost coverage, connectivity, and energy efficiency. The BER performance and complexity of several novel proposals are analyzed in this chapter. Also, we shed light on the future challenges and opportunities in this complex system. The main contributions of this chapter are listed below:

- Exhaustive Monte Carlo simulation results for the BER performance and complexity of the N-RIS-assisted MU-MIMO system are presented. Blind-RIS and optimized-RIS approaches are considered.
- A channel with spatial correlation and channel state information (CSI) errors is considered to show the effect of these channel impairments on the system.
- AI-based algorithms are analyzed and discussed as an alternative to deal with the system's high complexity. Future trends and opportunities in this novel research topic are also discussed.

5.1.2 Organization

The rest of the chapter is organized as follows: Section 5.2 delves into the related work. Section 5.3 introduces the N-RIS-MU-MIMO system model, including the channel model and the optimal detection technique. Section 5.4 presents the blind-RIS technique and an optimization procedure that can solve the system's interference. Section 5.5 presents the performance results of the N-RIS-assisted MU-MIMO system. Section 5.6 introduces AI as an alternative to the optimization problem. Section 5.7 presents future trends and opportunities in N-RIS-assisted MU-MIMO systems. Finally, Section 5.8 concludes the chapter.

5.2 Related Work

The design of RIS-assisted wireless communication systems can be analyzed using the classification of systems given in the introduction. From the simplest scenario using only one RIS and an SISO scheme up to the more complex system that uses multiple RIS and multiple users under MIMO configurations. Table 5.1 shows a summary of related works that adopt these different schemes to optimize the resources of RIS-aided systems. In particular, this chapter focuses on Multiple RIS-assisted MU-MIMO systems. In Bai et al. [3] and Jiang et al. [4], algorithms are proposed to incorporate RIS in an MU-MISO scenario.

Table 5.1 Related approaches for optimization of RIS-aided systems using MISO, MIMO, single-RIS, and multi-RIS configurations.

References	Contributions	Remarks
Bai et al. [3]	Improvement of the reliability of RIS-assisted systems by using hybrid phase and code modulation (HPCM)	RIS in MU-MISO outperforms in BER calculation applying HPCM
Jiang et al. [4]	Joint design of user scheduling and phase-shift design for multi-RIS MU-MISO	RIS shift phase design by an ergodic spectral sum optimization metric
Yan et al. [5]	Beamforming and information transfer for MU-MIMO RIS	Extension from single to multi-RIS phase optimization by sample average approximation
Jung et al. [6]	Resource allocation algorithm to jointly consider user scheduling and power control	Users are labeled according to the BS connection, direct or through the RIS
Xu et al. [7]	Optimization for MU-MIMO multi-RIS system considering the MSE gain for each user	Use of precoders to cancel the interference and MSE based optimization of all users
Semmler et al. [8]	Sum rate maximization of RIS-aided MU-MIMO system using linear precoding	The linear precoder cancels in parallel the interference among users to increase the sum-rate
Ning et al. [9]	Design of space-orthogonal scheme to eliminate interferences in an MU-MIMO multi-RIS system	Interference is eliminated regardless of the RIS phase shift design
Souto and Silva [11]	Joint precoding optimization and rate maximization based on the monotone accelerated proximal for a multi-RIS system	The use of multiple RIS surfaces in parallel substantially impacts the overall system enhancement
Yu et al. [12]	Phase shift optimization based on semidefinite relaxation and gauss randomization for MU-MIMO multi-RIS systems	Two optimization algorithms proposed for both continuous and discrete phase shift designs

The MISO configuration is extended to the multiple RIS cases in [5], which shows that the design of the phase shift vector in the RISs barely improves the BER performance of the system. Since each user is optimized with a different combination of the phase shift vector, optimizing a group of users results in a suboptimal solution. Different RISs can be allocated to different users [6] to overcome this drawback. Xu et al. [7] and Semmler et al. [8] analyzes the problem of using a single RIS in a multiuser scenario with multiple Rx antennas (MIMO). In this case, a precoding technique can cancel the interference. Precoding schemes can also be used with space-orthogonal coding to improve the MU-MIMO system [9]. Souto and Silva [11] propose a monotone accelerated proximal gradient (mAPG) method that includes an extrapolation to improve the algorithm's convergence. Souto and Silva [11] show that combining multiple RISs can be an effective solution to improve the performance of the system. Previously proposed systems show the effectiveness of using RIS in MU-MIMO systems. The most complex scenario uses multiple parallel RIS to assist an MU-MIMO system. This configuration increases the system's complexity, and as shown in [5], the system's design needs to be approached carefully to optimize all system components. In that sense, ML algorithms could represent a promising alternative for an effective solution to this problem. Souto and Silva [11] introduced an iterative algorithm grounded in the monotone accelerated proximal gradient (mAPG) method, which incorporates an extrapolation step to enhance convergence speed. Moreover, the algorithm includes variable monitoring mechanisms to ensure adequate descent. The findings in [11] indicate that amalgamating multiple RIS panels can notably enhance achievable rates. These previously proposed systems clearly show the effectiveness of using RIS to assist MU-MIMO systems. The RIS improves the wireless system's overall performance and extends the coverage area. Even when a discrete phase shift is considered [12].

5.3 N-RIS-assisted MU-MIMO System Model

Figure 5.1 shows the N-RIS-assisted MU-MIMO general system model. The BS is equipped with N_t Tx antennas. The reception comprises K users or mobile stations (MSs) with N_r antennas. The system uses N RISs with N_s mirrors to reflect the signals. The end-to-end configuration is defined as a $(K \cdot N_r) \times (N \cdot N_s) \times N_t$ N-RIS-assisted MU-MIMO downlink transmission system. The channel matrix between the nth RIS and the kth MS is defined as $\boldsymbol{H}_{n,k} \in \mathbb{C}^{N_r \times N_s}$, $n \in \{1, 2, \dots, N\}, k \in \{1, 2, \dots, K\}$, the channel matrix between the BS and the kth user that does not propagate through the RISs is defined as $\boldsymbol{H}_k^{DP} \in \mathbb{C}^{N_r \times N_t}$, $k \in \{1, 2, \dots, K\}$, and the channel matrix between the BS and the nth RIS is defined as $\boldsymbol{G}_n \in \mathbb{C}^{N_s \times N_t}, n \in \{1, 2, \dots, N\}$.

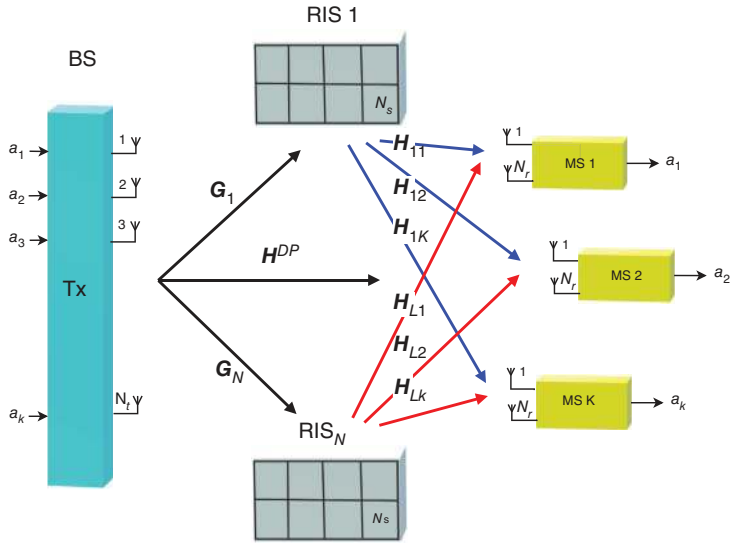

Figure 5.1 N-RIS assisted MU-MIMO downlink transmission system.

Let us consider a precoding matrix $\boldsymbol{W}_k \in \mathbb{C}^{N_t \times N_r}$ for the kth user. Then, the precoded transmission vector for the kth user is $\boldsymbol{W}_k \boldsymbol{x}_k, \in \mathbb{C}^{N_t \times 1}, k \in \{1, 2, \ldots, K\}$. The precoding matrix $\boldsymbol{W}_k$ expands the transmission vector to a vector of size N_t. The vector of transmitted signals considering K users is

$$\boldsymbol{t}_{\boldsymbol{x}} = \sum_{k=1}^{K} \boldsymbol{t}_{\boldsymbol{x}}^{(k)} \tag{5.1}$$

As shown in Figure 5.1, from the BS to the MSs, the transmitted signals $\boldsymbol{t}_{\boldsymbol{x}}$ go through N RISs and also go through a path that does not use RIS to reach their destination.

5.3.1 Transmission/Reception

The signal received for the kth user coming from all RISs, and the direct path is:

$$\begin{aligned} \boldsymbol{y}_k = & \sqrt{\gamma_k}\boldsymbol{H}_{1,k}\Theta_1\boldsymbol{G}_1\boldsymbol{t}_{\boldsymbol{x}} + \sqrt{\gamma_k}\boldsymbol{H}_{2,k}\Theta_2\boldsymbol{G}_2\boldsymbol{t}_{\boldsymbol{x}} + \cdots \\ & + \sqrt{\gamma_k}\boldsymbol{H}_{l,k}\Theta_l\boldsymbol{G}_l\boldsymbol{t}_{\boldsymbol{x}} + \cdots + \sqrt{\gamma_k}\boldsymbol{H}_{L,k}\Theta_L\boldsymbol{G}_L\boldsymbol{t}_{\boldsymbol{x}} \\ & + \sqrt{\gamma_k}\boldsymbol{H}_k^{DP}\boldsymbol{t}_{\boldsymbol{x}} + \boldsymbol{n}_k \end{aligned} \tag{5.2}$$

where Θ_l is the lth phase shift matrix, defined as $\Theta_l = \text{diag}(e^{j\theta_{l,1}}, e^{j\theta_{l,2}}, \ldots, e^{j\theta_{l,N_s}})$. Here, $\theta_{l,i}$ denotes the phase shift of the ith reflecting element of the lth RIS and $\boldsymbol{n}_k \in \mathbb{C}^{N_r \times 1}$ is the noise. The noise samples are assumed to be independent and identically distributed (i.i.d.) with $\mathcal{CN}(0, \sigma^2)$. Furthermore, $\sqrt{\gamma_k}$ is the

signal-to-noise ratio (SNR). Finally, the received signal for the kth user can be written as:

$$\boldsymbol{y}_k = \sqrt{\gamma_k}\left(\sum_{l=1}^{N}\boldsymbol{H}_{l,k}\Theta_l\boldsymbol{G}_l + \boldsymbol{H}_k^{DP}\right)\boldsymbol{t}_{\boldsymbol{x}} + \boldsymbol{n}_k \tag{5.3}$$

Let us consider an equivalent matrix $\boldsymbol{H}_k^{Eq} \in \mathbb{C}^{N_r \times N_t}$ defined as:

$$\boldsymbol{H}_k^{Eq} = \sum_{l=1}^{N}\boldsymbol{H}_{l,k}\Theta_l\boldsymbol{G}_l + \boldsymbol{H}_k^{DP} \tag{5.4}$$

There exist K different equivalent matrices that contain the information of all the N RISs in the system and the link that does not pass through the RISs. The signal received by the kth user or MS is rewritten as:

$$\boldsymbol{y}_k = \sqrt{\gamma_k}\boldsymbol{H}_k^{Eq}\boldsymbol{t}_{\boldsymbol{x}} + \boldsymbol{n}_k \tag{5.5}$$

5.3.2 Channel Model

The distance between the Tx or Rx antennas can cause a correlation effect in the wireless channel. As a result, the systems suffer from diversity losses. The spatial correlation also exists among the mirrors in the RIS, affecting the system's overall performance. In this work, the effects of the spatially correlated channel are evaluated by a standard method known as the Kronecker model. The spatially correlated MIMO channel is modeled as [13]

$$\boldsymbol{H}^{[corr]} = \boldsymbol{R}_r^{1/2}\boldsymbol{H}^{[w]}\boldsymbol{R}_t^{1/2} \tag{5.6}$$

where $\boldsymbol{H}^{[w]}$ is defined as a quasi-static Rayleigh fading channel with i.i.d. complex Gaussian random variables elements $\mathcal{CN}(0,1)$. The matrices $\boldsymbol{R}_r$ and $\boldsymbol{R}_t$ represent the receive and transmit correlation matrices, respectively. The correlation matrices are formulated using the exponential model, as described in [13]

$$\boldsymbol{R}_t = \begin{bmatrix} 1 & \rho_t & \rho_t^2 & \cdots & \rho_t^{(N_t-1)} \\ \rho_t & 1 & \rho_t & & \rho_t^{(N_t-2)} \\ \rho_t^2 & \rho_t & 1 & & \vdots \\ \vdots & & & \ddots & \\ \rho_t^{(N_t-1)} & \rho_t^{(N_t-2)} & & & 1 \end{bmatrix} \tag{5.7}$$

$$\boldsymbol{R}_r = \begin{bmatrix} 1 & \rho_r & \rho_r^2 & \cdots & \rho_r^{(N_r-1)} \\ \rho_r & 1 & \rho_r & & \rho_r^{(N_r-2)} \\ \rho_r^2 & \rho_r & 1 & & \vdots \\ \vdots & & & \ddots & \\ \rho_r^{(N_r-1)} & \rho_r^{(N_r-2)} & & & 1 \end{bmatrix} \tag{5.8}$$

where ρ_t and ρ_r are the correlation coefficients between adjacent antennas at the transmitter and receiver sides, respectively. The estimated channel $\hat{\mathbf{H}}$ in the reception is modeled as [14]

$$\hat{\mathbf{H}}_k = \mathbf{H}_k^{[corr]} + \mathbf{E}_h \tag{5.9}$$

where $\mathbf{E}_h \in \mathbb{C}^{N_r \times N_t}$ is the channel estimation error matrix, which is independent of $\mathbf{H}_k^{[corr]}$ and has complex Gaussian elements $\mathcal{CN}(0, \sigma_e^2)$. Therefore, $\hat{\mathbf{H}}_k$ has a modified distribution of $\mathcal{CN}(0, 1 + \sigma_e^2)$.

5.3.3 Detection

The maximum likelihood criterion (MLC) is used as a reference in detection. The MLC compares the Euclidean distance between the received signal and all possible noiseless received signals. For the analyzed N-RIS-MU-MIMO system, the MLC is written as [15]

$$\hat{\boldsymbol{x}}_k = \underset{\mathbf{x}_k \in \boldsymbol{D}}{\operatorname{argmin}} \| \boldsymbol{y}_k - \sqrt{\gamma_k} \boldsymbol{H}_k^{Eq} \boldsymbol{W}_k \boldsymbol{D} \|_F^2 \tag{5.10}$$

where the matrix $\boldsymbol{D} \in \mathbb{C}^{Nr \times 2^m}$ is the complete set of noiseless quadrature amplitude modulation (QAM) signals at the reception.

5.4 Blind RISs and Optimized Transmission

RIS-assisted systems have gained significant attention due to their capacity to enhance system performance through optimized utilization of radiated energy. However, a notable drawback of RIS-based systems lies in the precise control required over the phases and amplitudes of impinging signals within the RIS. Typically, achieving this control necessitates an additional control unit within the RIS. Nonetheless, this poses a challenge, particularly when the RIS is at a considerable distance from the transmitter or BS.

5.4.1 Blind RISs

This section describes the precoding technique used to precancel the interference caused by multiple users and multiple RISs under simultaneous signal transmissions. Figure 5.2 shows the block diagram of a precoding technique for the analyzed RIS-assisted MU-MIMO system. The received signal by the kth user can be rewritten as [15]:

$$\boldsymbol{y}_k = \sqrt{\gamma_k} \boldsymbol{H}_k^{Eq} \sum_{k=1}^{K} \boldsymbol{W}_k \boldsymbol{x}_k + \boldsymbol{n}_k \tag{5.11}$$

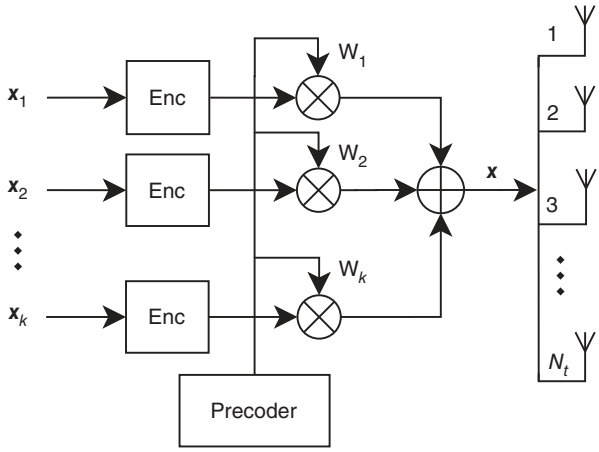

Figure 5.2 Precoding for N-RIS-MU-MIMO systems.

which can be also expressed as:

$$\boldsymbol{y}_k = \sqrt{\gamma_k}\boldsymbol{H}_k^{Eq}\boldsymbol{W}_k\boldsymbol{x}_k + \sqrt{\gamma_k}\boldsymbol{H}_k^{Eq}\sum_{i=1,i\neq k}^{K}\boldsymbol{W}_i\boldsymbol{x}_i + \boldsymbol{n}_k \tag{5.12}$$

the first term is the signal sent to the kth user or MS, the second is the interference produced by the other users, and the third is the noise at the reception. The complete system has the following matrix representation:

$$\begin{bmatrix}\boldsymbol{y}_1\\ \boldsymbol{y}_2\\ \vdots\\ \boldsymbol{y}_K\end{bmatrix} = \begin{bmatrix}\boldsymbol{H}_1^{Eq} & \cdots & \boldsymbol{H}_1^{Eq}\\ \boldsymbol{H}_2^{Eq} & \cdots & \boldsymbol{H}_2^{Eq}\\ \vdots & \ddots & \vdots\\ \boldsymbol{H}_K^{Eq} & \cdots & \boldsymbol{H}_K^{Eq}\end{bmatrix}\begin{bmatrix}\boldsymbol{W}_1\boldsymbol{x}_1\\ \boldsymbol{W}_2\boldsymbol{x}_2\\ \vdots\\ \boldsymbol{W}_K\boldsymbol{x}_K\end{bmatrix} + \begin{bmatrix}\boldsymbol{n}_1\\ \boldsymbol{n}_2\\ \vdots\\ \boldsymbol{n}_K\end{bmatrix}, \tag{5.13}$$

where $\sqrt{\gamma_k} = 1$ for simplicity. To remove the interference term, a precoding technique based on block diagonalization (BD) is utilized [16]. The required condition is $\boldsymbol{H}_k^{Eq}\boldsymbol{W}_i = \boldsymbol{0}, \forall i \neq k$, which can be written as:

$$\overline{\boldsymbol{H}}_k^{Eq}\boldsymbol{W}_k = \boldsymbol{0}, \quad k = 1, 2, \ldots, K \tag{5.14}$$

where $\overline{\boldsymbol{H}}_k^{Eq}$ contains all user matrices in the system except that of the kth user, which can be expressed as:

$$\overline{\boldsymbol{H}}_k^{Eq} = \left[(\boldsymbol{H}_1^{Eq})^H, \ldots, (\boldsymbol{H}_{k-1}^{Eq})^H, (\boldsymbol{H}_{k+1}^{Eq})^H, \ldots, (\boldsymbol{H}_K^{Eq})^H\right]^H \tag{5.15}$$

For example, for $K = 4$ users in the system, the following auxiliary matrices can be obtained:

$$\overline{\boldsymbol{H}}_1^{Eq} = \left[(\boldsymbol{H}_2^{Eq})^H, (\boldsymbol{H}_3^{Eq})^H, (\boldsymbol{H}_4^{Eq})^H\right]^H$$
$$\overline{\boldsymbol{H}}_2^{Eq} = \left[(\boldsymbol{H}_1^{Eq})^H, (\boldsymbol{H}_3^{Eq})^H, (\boldsymbol{H}_4^{Eq})^H\right]^H$$
$$\overline{\boldsymbol{H}}_3^{Eq} = \left[(\boldsymbol{H}_1^{Eq})^H, (\boldsymbol{H}_2^{Eq})^H, (\boldsymbol{H}_4^{Eq})^H\right]^H$$
$$\overline{\boldsymbol{H}}_4^{Eq} = \left[(\boldsymbol{H}_1^{Eq})^H, (\boldsymbol{H}_2^{Eq})^H, (\boldsymbol{H}_3^{Eq})^H\right]^H$$

The precoding matrices are obtained decomposing $\overline{\boldsymbol{H}}_k^{Eq}$ into its singular values as [15]:

$$\overline{\boldsymbol{H}}_k^{Eq} = \boldsymbol{U}_k \left[\Sigma_k, \boldsymbol{0}\right] \left[\boldsymbol{V}_k^{(1)} \boldsymbol{V}_k^{(0)}\right]^H \tag{5.16}$$

where $\boldsymbol{U}_k$ is a unitary matrix, Σ_k is a diagonal matrix containing the non-negative singular values of $\overline{\boldsymbol{H}}_k^{\text{Eq}}$, $\boldsymbol{0}$ is an all-zero matrix, $\boldsymbol{V}_k^{(0)}$ contains vectors corresponding to the zero singular values and $\boldsymbol{V}_k^{(1)}$ contains vectors corresponding to the nonzero singular values. The matrix $\boldsymbol{V}_k^{(0)}$ contains the last N_r columns of $\boldsymbol{V}_k$, which form an orthogonal basis that is in the null space of $\overline{\boldsymbol{H}}_k^{\text{Eq}}$. Therefore, $\boldsymbol{V}_k^{(0)}$ can be used as the precoding matrix $\boldsymbol{W}_k$. The precoding matrices are obtained as:

$$\boldsymbol{W}_k = \boldsymbol{V}_k(:, N_t - N_r + 1, N_t - N_r + 2, \ldots, N_t) \tag{5.17}$$

where $(:)$ represents all the rows in the matrix $\boldsymbol{V}_k$. The received signal can be rewritten as an interference-free signal as:

$$\boldsymbol{y}_k = \sqrt{\gamma_k} \boldsymbol{H}_k^{Eq} \boldsymbol{W}_k \boldsymbol{x}_k + \boldsymbol{n}_k \tag{5.18}$$

The complete system can be represented as:

$$\begin{bmatrix} \boldsymbol{y}_1 \\ \boldsymbol{y}_2 \\ \vdots \\ \boldsymbol{y}_K \end{bmatrix} = \begin{bmatrix} \boldsymbol{H}_1^{Eq} \boldsymbol{W}_1 & \cdots & \boldsymbol{0} \\ \boldsymbol{0} & \cdots & \boldsymbol{0} \\ \vdots & \ddots & \vdots \\ \boldsymbol{0} & \cdots & \boldsymbol{H}_K^{Eq} \boldsymbol{W}_K \end{bmatrix} \begin{bmatrix} \boldsymbol{x}_1 \\ \boldsymbol{x}_2 \\ \vdots \\ \boldsymbol{x}_K \end{bmatrix} + \begin{bmatrix} \boldsymbol{n}_1 \\ \boldsymbol{n}_2 \\ \vdots \\ \boldsymbol{n}_K \end{bmatrix}. \tag{5.19}$$

The blind RIS technique described here guarantees interference-free signals at the destination regardless of the phases in the multiple RISs. In the next section, a suboptimal optimization algorithm is investigated to improve the performance of the system.

The matrices $\mathbf{G}_l$ and $\boldsymbol{\Theta}_l$ in Eq. (5.3) can be adjusted to control the impinging signal amplitude and phase through the RIS elements, respectively. One of the most important RIS communications advantages is called *beamforming*. Beamforming enhances RIS communications by allowing the control of the signal reflection

toward a desired direction to improve the transmission quality. There are two main approaches for RIS beamforming:

- **Active beamforming**: Requires additional *active* components or circuits to manipulate the amplitude and phase of RIS-impinging signals. Although the signal adjustments are implemented in real time, the power consumption and system complexity increase.
- **Passive beamforming**: Here, the system relies on exploiting the properties of RIS rather than adding additional electronic circuits. These systems are less complex than active beamforming, consuming less power.

Several approaches develop a *hybrid beamforming* by combining the active and passive designs [17, 18]. In practice, RIS is usually designed to have a large number of reflecting elements. Thus, it will be more effective to implement discrete amplitude/phase shift levels that require only a small number of control bits for each element. For instance, reflecting-absorbing for amplitude control and 0–π for phase shift control. The cost of phase shift control is higher than amplitude control [18] since the optimal phase shift solutions should align all the reflected signals by the RIS despite their strength with the signal transmitted from the BS. The alignment produces a coherent combined signal that maximizes the received signal power at the user device.

5.4.2 Optimization

Optimization includes the search for the appropriate phases in the RIS that lead to better system performance. The first approximation is to systematically change the phases of the RIS and compare the complete system's performance. A better solution could be based on an optimization function such as the signal plus interference-to-noise ratio (SINR). Genetic algorithms (GAs) and other AI-based techniques have recently been used to address this nondeterministic polynomial time (NP-hard) problem. The optimization problem can be seen as the maximization of the SINR function for the kth user defined as:

$$SINR_k = \frac{|\boldsymbol{H}_k^{Eq}\boldsymbol{W}_k\boldsymbol{x}_k|^2}{|\boldsymbol{H}_k^{Eq}\sum_{i=1,i\neq k}^{K}\boldsymbol{W}_i\boldsymbol{x}_i|^2+\boldsymbol{\sigma}_n^2} \tag{5.20}$$

where $\boldsymbol{H}_k^{Eq}=\sum_{l=1}^{L}\boldsymbol{H}_{l,k}\Theta_l\boldsymbol{G}_l+\boldsymbol{H}_k^{DP}$, and Θ_l is the phase shift matrix of the lth RIS that contains in its diagonal the phase shift vector $\boldsymbol{\phi}_l=\{\phi^{(1)},\phi^{(2)},\ldots,\phi^{(N_s)}\}$. The algorithm looks for the phases ϕ_l that maximize the SINR function. The optimization procedure can be formulated as

$$\begin{aligned} & \Phi^{\text{subopt}} = \max(SINR_k) \\ \text{s.t.} \quad & C_1 : \ \phi^{(i)} \in [0, 2\pi] \forall i \in \{1, 2, \ldots, N_s\}, \\ & C_2 : \ \mathbb{E}[\|\boldsymbol{t_x}^H \boldsymbol{t_x}\|] = K \\ & C_3 : \ |\phi^{(i)}| = 1 \end{aligned} \tag{5.21}$$

Considering several users ($K > 1$), the optimization algorithm seeks for

$$\Phi^{\text{subopt}} = \max(\boldsymbol{\psi}) \tag{5.22}$$

where $\boldsymbol{\psi} = f(\phi_1, \phi_2, \ldots, \phi_j), 1 < j \leq K$, is a concatenated SINR function. Section 5.6 discusses the main AI-based strategies to deal with this complex problem.

5.5 System Performance Results

To measure the BER system performance, we conduct exhaustive simulations. Simulations were carried out using MATLAB. The first scenario considers only the blind RISs where the phases in the RIS are not modified, i.e., $\Theta = \boldsymbol{I}$. The second scenario considers an optimization procedure using a stochastic search. The stochastic search seeks the phases in the RISs that maximize the SINR. First a $(4 \cdot 2) \times (N \cdot 32) \times 8$ configuration with SE = 8 bpcu/user is utilized. Second, a $(8 \cdot 4) \times (N \cdot 32) \times 32$ configuration with SE = 12 bpcu/user is used. The N-RIS-MU-MIMO system uses 16-QAM and spatial multiplexing (SMux) for the first configuration to get a SE = 8 bpcu/user. The second configuration uses 8-QAM to get a SE = 12 bpcu/user. Evaluations are carried out for $1 \leq N \leq 8$ RISs, where each RIS is equipped with 32 mirrors. A similar system that does not use RISs is evaluated as a reference. For simulations, a normalized transmission energy per user, i.e., $\mathbb{E}[\|\boldsymbol{t_x}^H \boldsymbol{t_x}\|] = K$ is considered. Table 5.2 enlists all the different parameters to configure the different scenarios for the simulations conducted in this work. In addition, Figure 5.3 illustrates in a flowchart the processes involved in conducting simulations, where each level of SNR γ_k is updated as well as a certain number of Monte Carlo channel realizations.

5.5.1 BER Performance Results

Figure 5.4 shows a BER performance comparison for a different number of RISs. Blind and optimization search approaches. SE = 8 bpcu/user, 8 Tx antennas, and 4 users with 2 Rx antennas. Results show that the N-RIS system has up to 30 dB gains compared with a similar system that does not use RIS. The optimization procedure improves up to 8 dB the performance of the systems.

Figure 5.5 shows a BER performance comparison for a different number of RISs. Blind and optimization search approaches. SE = 12 bpcu/user, 32 Tx antennas, and

Table 5.2 Simulation parameters for the different RIS scenarios considered in this work.

Parameter	Value
SNR γ_k	$[-10, 30]$ dB
Number of Tx antennas Nt	8, 32
Number of user equipment (UE) K	4, 8
Number of UE antennas N	2, 4
Number of RIS surfaces N	1, 2, 4, 8
Number of RIS reflectors Ns	32
Modulation $\mathbf{x}_k$	16-QAM
Channel fading $\mathbf{H}_k^{Eq}$	Rayleigh
Channel spatial correlation ρ	$\rho = 0.7$

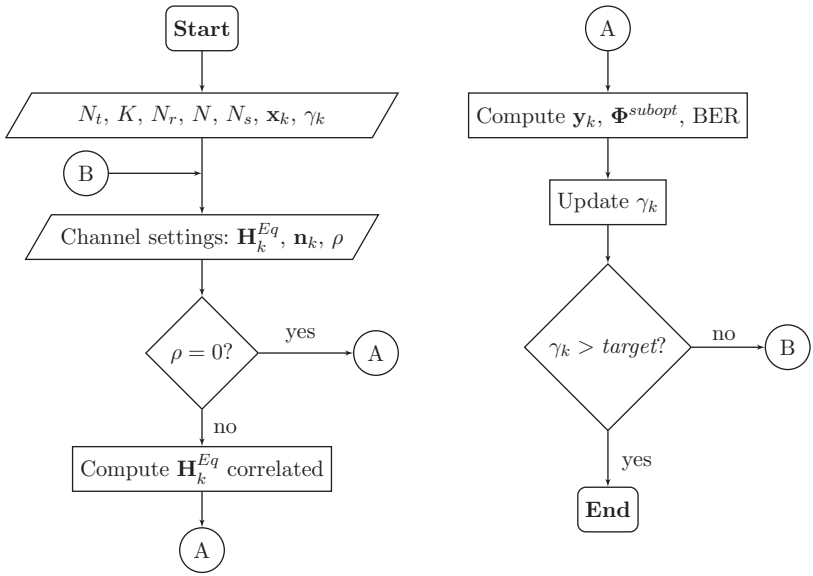

Figure 5.3 The flowchart with all processes involved in conducting the experiments for different RIS-aided system configurations.

8 users with 4 Rx antennas. Results show that the N-RIS system has up to 37 dB gains compared with a similar system that does not use RIS. In this case, the optimization procedure improves only 2 dB in the BER performance.

Figure 5.6 shows a BER performance comparison for a different number of RISs. SE = 8 bpcu/user, 8 Tx antennas, and 4 users with 2 Rx antennas. A channel with

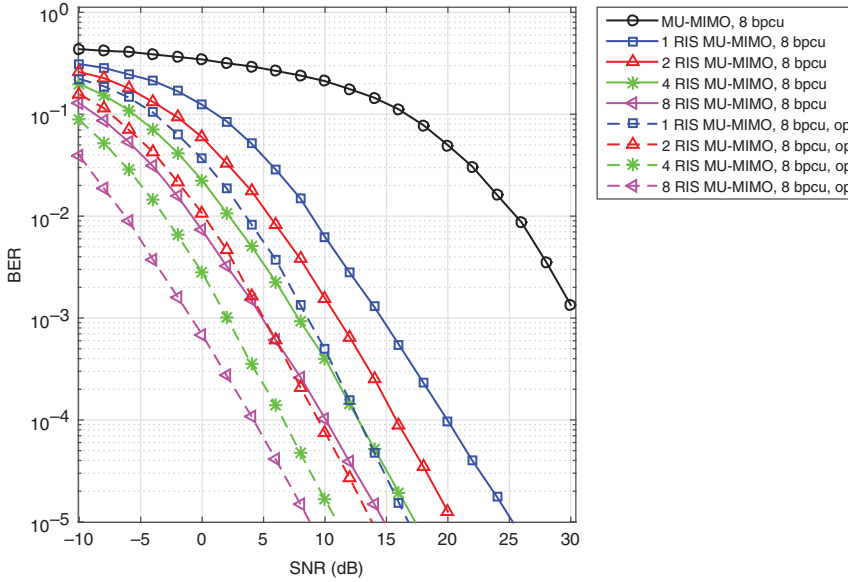

Figure 5.4 N-RIS-MU-MIMO, BER performance comparison for a different number of RISs. Blind and optimized approaches. SE = 8 bps/user, 8 Tx antennas, and 4 users with 2 Rx antennas.

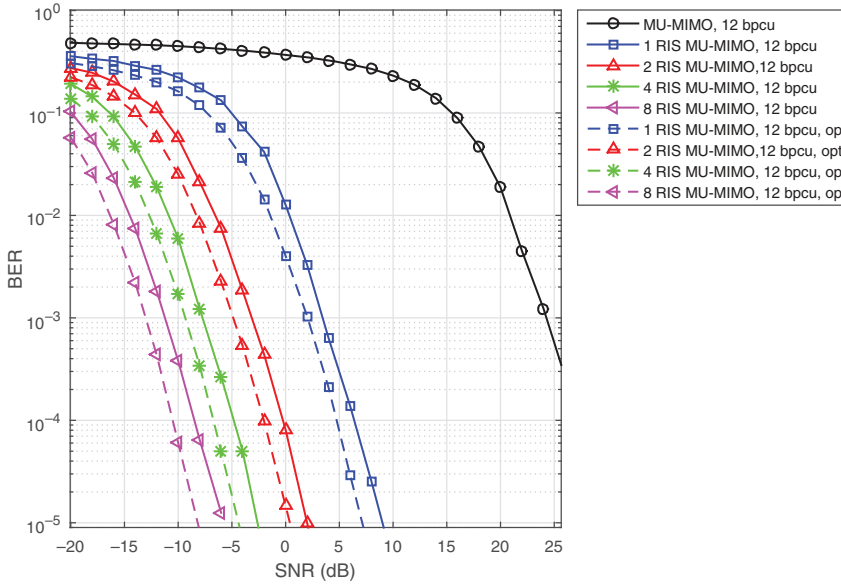

Figure 5.5 N-RIS-MU-MIMO, BER performance comparison for a different number of RISs. Blind-RIS and optimized-RIS approaches. SE = 12 bpcu/user, 32 Tx antennas, and 8 users with 4 Rx antennas.

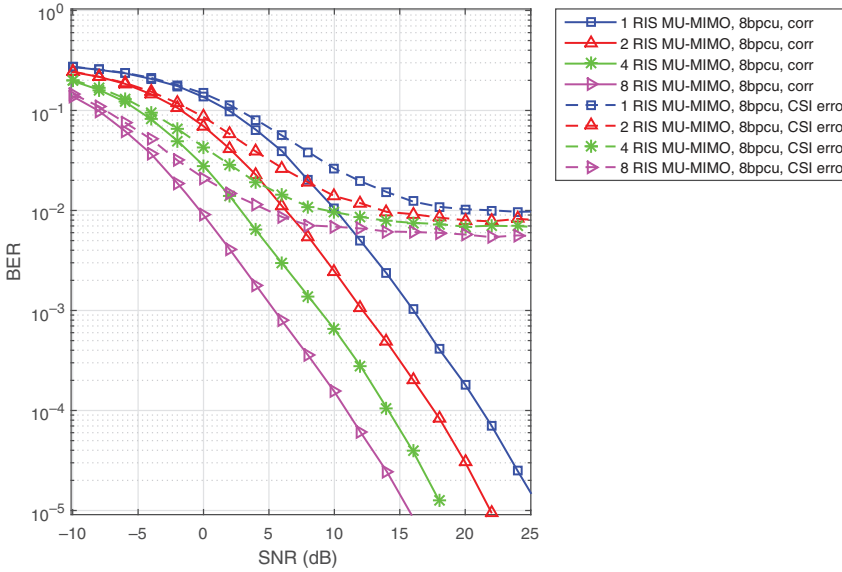

Figure 5.6 N-RIS-MU-MIMO, BER performance comparison for a different number of RISs considering spatial correlation and CSI errors plus correlation. SE = 8 bpcu/user, 8 Tx antennas, and 4 users with 2 Rx antennas.

spatial correlation $\rho = 0.7$ and CSI errors of 2% plus correlation is considered. Results show that spatial correlation has losses of 7 dB. When spatial correlation plus CSI errors are considered, the system presents poor BER performance since it has a floor noticeable at 10 dB.

Figure 5.7 shows a BER performance comparison for a different number of RISs. SE = 12 bpcu/user, 32 Tx antennas, and 8 users with 4 Rx antennas. A channel with spatial correlation $\rho = 0.7$ and CSI errors of 2% plus correlation is considered. In this case, the system with spatial correlation has losses of 20 dB. When spatial correlation plus CSI errors are considered, the system presents very poor BER performance. Table 5.3 summarizes all the obtained results from the conducted simulations previously described. The first column enlists the parameters set for each configuration scenario, and the first column compares the obtained gains when the system includes a RIS surface. We noticed that the highest gain in BER performance is presented in the third-row scenario, where the system achieves a 37 dB gain compared with an equivalent system that does not include an RIS surface. On the other hand, the worst case was presented when a spatial correlation in the channel of $\rho = 2$ was considered and an $SE = 12$ bpcu/user, presenting 20 dB of losses. It is important to notice that most of the frameworks in the literature consider reporting the system performance in terms of an achievable gain like sum rate or MSE rather than BER, which is our case.

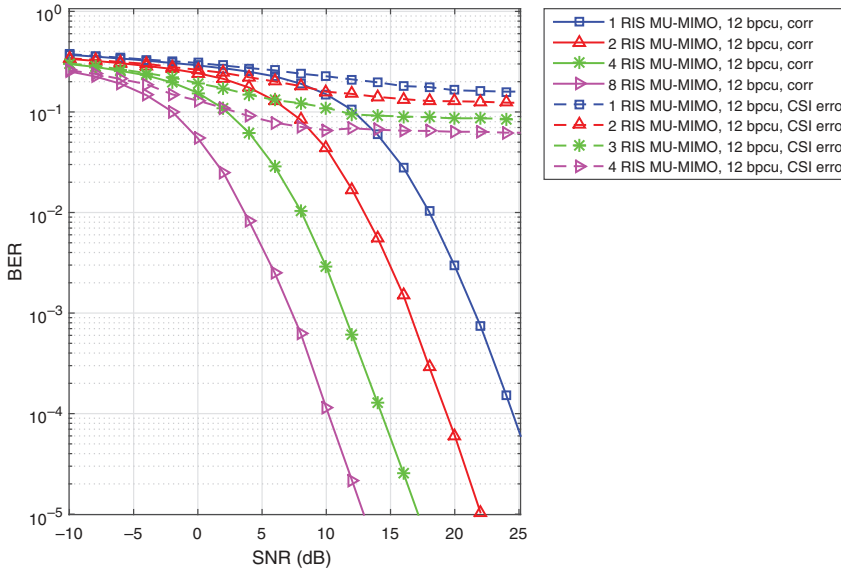

Figure 5.7 N-RIS-MU-MIMO, BER performance comparison for a different number of RISs considering spatial correlation and CSI errors plus correlation. SE = 12 bpcu/user, 32 Tx antennas, and 8 users with 4 Rx antennas.

Table 5.3 Simulation results obtained from the different multi-RIS system configurations.

Parameters	Results
$SE = 8$ bpcu/user, $N_t = 8$,	30 dB gain No RIS,
$K = 4, N_r = 2$	8 dB gain RIS
$SE = 12$ bpcu/user, $N_t = 32$,	37 dB gain No RIS,
$K = 8, N_r = 4$	2 dB gain RIS
$SE = 8$ bpcu/user, $N_t = 8$,	7 dB losses,
$K = 4, N_r = 2, \rho = 0.7$	floor: 10^{-2}
$SE = 12$ bpcu/user, $N_t = 32$,	20 dB losses
$K = 8, N_r = 4, \rho = 0.7$	floor: 10^{-1}

5.5.2 Detection Complexity

To compare the proposed and the baseline systems' detection complexity (η), we count the total number of floating-point operations (*flops*) required to solve the ML criterion. For real additions, multiplications, and comparisons, 1 *flop* is carried out. For complex additions and multiplications, 2 and 6 *flops* are carried out,

Table 5.4 Detection complexity.

Operation	Complexity
$\mathbf{Q}_k = \mathbf{H}_k\mathbf{W}_k$	$8N_r^2N_s$
$\mathbf{Q}_k\mathbf{D}$	$8N_r^2 2^m$
Subtractions	$2N_r 2^m$
$\|\cdot\|_F^2$	$3N_r 2^m$
Maximum ratio combining (MRC)	$2N_r 2^m$
Ordering	$2(2^m)$
$\mathbf{Q} = \mathbf{H}_k\mathbf{G}$	$8N_rN_sN_t$
$\mathbf{P} = \mathbf{Q}\mathbf{Z}_k^{Eq}$	$8N_r^2N_t$
$\mathbf{PD}$	$8N_r^2 2^m$

Source: Castillo-Soria et al. [15].

respectively, while subtractions and divisions take the same number as additions and multiplications, respectively [15]. A complex matrix multiplication of $m \times n$ and $n \times p$ requires $8mnp$ *flops*. The lattice of the ML detector can be written as $\boldsymbol{G}_k = \boldsymbol{H}_k^{Eq}\boldsymbol{W}_k\boldsymbol{D}$, where the matrix $\boldsymbol{D} \in \mathbb{C}^{N_r \times 2^m}$ is composed by all possible combinations of transmitted symbols.

The multiplication of $\boldsymbol{H}_k^{Eq}\boldsymbol{W}_k$ has a complexity cost of $8N_tN_r^2$*flops* and generates a square matrix of dimensions $N_r \times N_r$. The multiplication of this matrix by the matrix $\boldsymbol{D}$ has a complexity cost of $8N_r^2 2^m$*flops*. Therefore, the matrix $\mathbf{G}_k$ has a complexity of $8N_r^2(N_t + 2^m)$*flops*. The differences have a complexity of $2(2^m)N_r$*flops*. Obtaining the magnitude has a complexity cost of $3N_r 2^m$*flops*. The combiner has a complexity cost of $2(N_r - 1)2^m$*flops*, and finding the minimum value has a complexity of $2(2^m)$*flops*. Adding all these results, the detection complexity of the N-RIS-MU-MIMO-system is (Table 5.4)

$$\eta = 8N_r^2N_t + 8N_r^2 2^m + 7N_r 2^m \quad flops \tag{5.23}$$

5.5.3 Limitations of the Proposed Model and Alternative Solutions

Thanks to signal processing, a precoding technique can be applied to solve the interference problem generated by multiple users and multiple RISs on the downlink transmission system. As expected, as RISs are added, a better system BER performance is obtained. Mainly, thanks to the precoding, considerable gains can be obtained in the system without requiring large amounts of processing in the RISs. However, some limitations were imposed by the model used. First, perfect CSI knowledge is assumed. When a more realistic channel model is used, the performance can drop abruptly. Therefore, it is necessary to extend the studies to consider more realistic channel models. Secondly, the utilized interference

cancellation model is based on a BD scheme. This scheme imposes some conditions on the dimensions of the channels. That is, the number of transmitting antennas required should equal the number of antennas on the receivers. This can be a limiting factor in the design of practical systems. A possible solution could be using strategies such as "dirty paper coding" (DPC) that relax these restrictions and which has also shown good performance in MU systems. Finally, the optimal design of the system must be reviewed again. Although the proposed system shows significant gains compared to a system without RIS, effective combining precoding and optimization techniques is still an open research area. Results show that the addition of seeking the optimal phases in the RIS is a complex procedure that barely improves the BER performance in a MU–MIMO scenario. Therefore, the following questions remain unanswered: What aspects of the system can be managed deterministically? What aspects of the system can be conveniently optimized by artificial intelligence? How should the system be modeled for better BER performance and greater spectral and energy efficiency? These are some unknowns that will direct future research in the area.

5.6 Artificial Intelligence in RIS-assisted MU-MIMO Systems

AI indeed revolutionizes technology applications and communication systems. 5G/6G systems requirements reside on lower latency, availability, energy, and cost efficiency for novel mobile communications as well as for IoT and vehicular network applications. More specifically, some ML and deep learning (DL) frameworks have been developed for RIS-aided wireless communication systems, which are presented in this section. We present a comparative analysis for AI–RIS applications comprising the details about the ML algorithms required, the type of network architecture in the case of DL, and the type of data source for the training stage. We divide our comparative study according to the type of research problem stated for each framework, having the following issues:

- Estimation of CSI applications
- Beamforming applications
- Federated learning applications
- Demodulation applications

This section also describes the source database used for training the DL algorithms if available to the research community. Applications on signal demodulation on RIS systems are also enlisted, where researchers explored diverse architectures for decoding the information signal using neural network (NN) architectures. ML applications on RIS also cover other research problems; however, this is an evolving field with ongoing research and development.

5.6.1 Estimation of CSI Applications

CSI estimation consists of calculating a matrix that represents the channel state having as input a pilot signal known at the receiver at different channel realizations. Then, selecting an ML algorithm, an optimizer, an activation function, and a mean squared error (MSE) based loss function, the CSI is obtained. Matrices naturally give the realizations of the channel of MU systems, so DL is the principal choice among reported frameworks in literature to develop ML–CSI estimation applications for RIS-aided communications. The loss function of the DL algorithm is one of its main components and computes the distance between the actual CSI and the estimated output. The DL approaches for channel estimation on RIS-aided wireless systems reported in the literature adopt the loss function according to the MSE and its variations, such as the minimum MSE (MMSE) and the least MSE (LMSE), among others. The optimizer is another important component of the DL algorithm; it adjusts the model parameters (for instance, the weights of neurons) and rebuilds the model according to the neuron activation function. Channel estimation for RIS-aided communications is one of the most challenging tasks since there is a direct association between the channel and the transmission failure [19]; when performing channel estimation, it involves an improvement in the phase-shift selection at RIS [20]. DL approaches can effectively reduce RIS hardware's complexity in estimating CSI. Figure 5.8 depicts a diagram for the process of CSI estimation for wireless systems aided by multi-RIS. As mentioned before, the matrices of pilot signals and the matrix of channel realizations are used as inputs to feed an ML algorithm (first of the settings) and then create a model for channel estimation. Since the ML algorithm requires certain parameters for training, the most important settings shown in Figure 5.8 are the loss function based on MSE, the optimizer to address the finding of the minimal value of the loss function, and the activation of neurons. Finally, the output will be the estimated matrices of CSI.

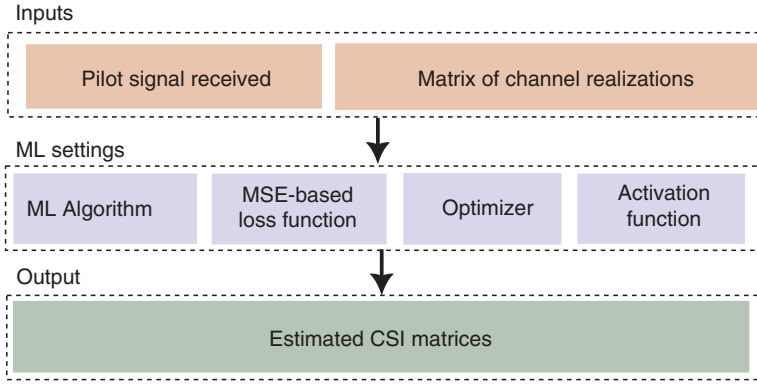

Figure 5.8 ML-based CSI estimation procedure for RIS communication systems.

Elbir et al. [21] introduced a DL approach for CIS in RIS surfaces. In this work, the DL model uses pilot signals that arrive at the receiver (UE device) as input. The training data consists of synthetic channel simulations, where RIS elements were controlled at ON/OFF states, making pairs of input–output for several channel realizations. The input data comes from both direct and cascaded channels, and the deep neural network (DNN) output consists of a vectorized form of channel matrices. This approach does not need re-training when the user changes its location to 4°. The network architecture consists of two convolutional neural networks (CNNs), each composed of nine layers.

The application reported by Taha et al. [22] proposes a two-phase system consisting of learning and prediction stages. The first stage consists of an exhaustive search from the RIS to collect a dataset for the DL model; here, the model learns the mapping between the input channel vector to output an achievable rate vector from the beamforming with the highest rate reflected from the transmitted data. For the second stage, the DL model makes an inference from the estimated sampled channel to a beamforming vector. The model architecture is an adapted neural network with a variable number of layers, ReLU as an activation function, and training data generated from the publicly available DeepMIMO dataset [23].

Applications such as [24] consist of a DL-based CSI detector called *DeepRIS*. It estimates the channel fading and phase angles from the received signal. The training stage of the model was offline, using synthetic channel realizations and randomly generated bit streams. The output estimated by the model is the transmitted symbol. Its architecture consists of an artificial neural network whose number of layers is variable and fully connected.

As seen before, MU precoding for downlink in RIS-aided communications enhances the received signal quality by eliminating the interference caused by users and other involved RIS surfaces transmitting simultaneously. Wu et al. [25] propose an architecture of a reflective network with linear layers where the line of sight (LOS) patterns between the BS and UEs are blocked. The CSI is estimated at the BS using the NN with pilot inputs and feedback signaling overhead.

5.6.2 Beamforming Applications

Another research problem to enhance RIS communications is beamforming, which consists of estimating the values of matrices $\boldsymbol{G}_l$ and Θ_l to improve the quality of transmission according to the $SINR_k$ function defined in Eq. (5.20). As in CSI, ML-based approaches are considered training data to send pilot signals and channel realizations for this issue. Figure 5.9 depicts the entire process followed in ML-based beamforming approaches for RIS-aided wireless systems. As shown in Figure 5.9, this procedure is similar to CSI estimation since input data for training consists of pilot signals or channel realizations. However, the ML

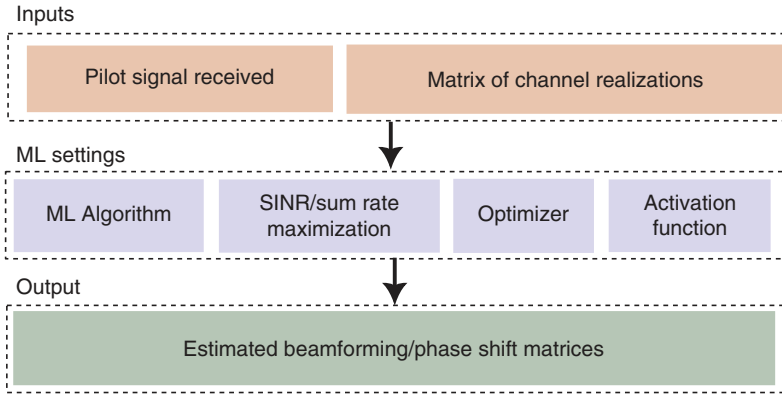

Figure 5.9 Scheme for ML-based beamforming estimation procedure for RIS communication systems.

settings, such as the type of algorithm, network architecture, hyperparameters, optimizer, and activation function, are chosen to satisfy the optimization problem of $SINR_k$ maximization.

Most research frameworks in the literature generate synthetic channel realizations to train the ML algorithms for beamforming. Most reported research uses DL schemes. However, deep reinforcement learning (DRL) has recently been applied to beamforming to avoid using a training dataset. In DRL-based beamforming, the matrices of channel realizations are considered as the environment for the state-space building. The agent is designed at the transmitter and performs actions through the RIS surface, where each action aims to optimize the phase shift and beamforming matrices at each channel realization. The $SINR_k$ or sum rate[1] is chosen as the instant reward since the optimization problem is subject to maximize this magnitude. Figure 5.10 illustrates the process of beamforming optimization for RIS-aided wireless systems supported by DRL. Here, it is defined as a set called action $\mathbf{A}(t)$, where matrices $\mathbf{G}_k(t)$ and $\mathbf{\Phi}_k(t)$ for each time interval t are collected. The state stands for the collection over time t of channel matrices $\mathbf{H}_{l,k}(t)$, $\mathbf{H}_k^{DP}(t)$, $\mathbf{H}_k^{EQ}$ and the action in the last time interval $\mathbf{A}(t-1)$. The agent modifies the action to maximize the instant-cumulative reward $\mathbf{R}(t)$, designed according to the *SINR*.

The application developed by Taha et al. [22] consists of a novel RIS architecture, where only a few elements are active, and the remaining majority are passive. The RIS surface learns to interact optimally with the incident signal at the active elements. The synthetic channel realizations dataset is Deep-MIMO [23], choosing an outdoor ray-tracing scenario. The authors selected a multilayer perception

1 The sum rate is defined as $R_k = 1 + \log_2(SINR_k)$.

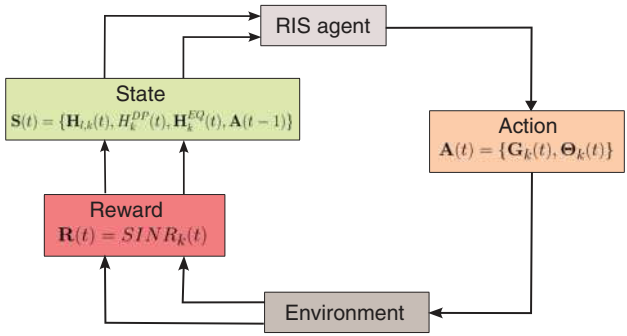

Figure 5.10 Deep-reinforcement learning scheme for beamforming in RIS-aided communication systems.

for the DL architecture with a variable number of fully connected layers, a ReLU activation function at the output, and MSE as a loss function.

Özdoğan and Björnson [26], developed a DL approach for the phase configuration of an RIS–MIMO system. The authors used a two-network architecture, where the first has the CSI estimation as a task, and the second network predicts the optimum phases and beamforming vectors online. The inputs are pilot sequences. The first neural network (NN) architecture consists of three fully connected hidden layers, a standard scaler to preprocess units, an Adam optimizer, and a ReLU activation function. For the second NN, the architecture consists of 4 fully connected layers: Adam optimizer and ReLU activation. The training pilot signals were synthetically generated.

Gao et al. [27] developed an unsupervised learning solution to make real-time predictions of phase shifts online, maintaining a desired rate performance. This architecture consists of five fully connected layers with a variable number of neurons, ReLU activation, batch normalization, and Adam optimizer. Training data was generated by synthetic channel realizations, which had previously normalized it.

Jiang et al. [28] developed a DL architecture of two NNs to optimize the signal processing functions at RIS. The first NN is located at the BS and maps the transmitted bit stream to the transmitted signal modulation and beamforming. The second DNN is located at the user device, where the received signal is combined and demodulated at the UE to the estimated soft bit stream. The beamforming optimization is designed to achieve the lowest BER, so the network is trained once. This application can simultaneously optimize the BS, RIS, and UE device weights. The architecture of both BS and UE networks consists of three fully connected layers with ReLU activation at the output. The UE NN uses

a Xavier initialization and Adam optimizer. This approach suggests a kind of transfer-learning algorithm for beamforming.

Huang et al. [29] reported a scheme based on DRL for beamforming in RIS-aided wireless systems. Here, the authors performed the optimization using the deep deterministic policy gradient (DDPG) algorithm for the joint design of the beamforming and phase shift matrices at the RIS surface. The sum-rate metric was used as the instant reward for the agent training. The architecture consists of two NNs; the actor and the critic networks. The number of units in each network corresponds to the number of users and antennas at the BS and RIS elements.

Motivated by this approach, Saglam et al. [30] developed a beamforming optimization strategy under imperfect CSI and hardware impairments. This approach uses the DRL's soft-actor-critic (SAC) algorithm to optimize the beamforming design and phase shift matrices to maximize the sum rate as a reward. The SAC architecture consists of two NNs called Q-networks and one-third of the NN called the policy network. Adam optimization and tanh activation were used for the output layer, and ReLU was used for the hidden layers.

The proposed framework by Wang and Zhang [31] is considered a model-free design to configure the reflections on RIS-aided communications. This DRL approach does not require sub-channels CSI and operates through a MIMO scheme. The architecture consists of a double deep Q-network to perform a real-time phase control, composed of four layers with 128 units each, Adam optimization, and a mean-squared error loss function.

The DRL-based beamforming applications have been used for the enhancement of the 3D trajectory and phase shift design of unnamed aerial vehicles (UAVs) communications aided by RIS. Mei et al. [32] performed a joint optimization of the phase shifts and UAV trajectory by applying the DDPG and deep deterministic Q-Network (DDQN) algorithms. Here, the optimal phase shift of the RIS is considered according to the UAV mobility. The architecture consists of NNs with 30 neurons and two layers, applying Adam optimization and a ReLU activation function. For the state space, the authors considered the channel realizations and the locations of the UAVs.

Peng and Wang [33] application consists of a scheme for energy harvesting that contributes to the resource allocation and convex optimization of phase shifts in a UAV–RIS system. The soft-max deep double deterministic policy gradient (SD3) was used as the algorithm for optimization. It consists of two *critic* networks where the reward was calculated regarding the harvested energy. For the state space, the equivalent channels from the BS to the UAV–RIS surface, the distance between the UAV elements and meta-surface, the location of the meta-surfaces, and the position of each UAV antenna were considered. In contrast, the action space consists of the phase shifts at the RIS elements, the transmit power to each UAV, and the scheduling variable.

5.6.3 Federated Learning Applications

Federated learning (FL) is an approach where the training of ML models is *decentralized*. The privacy-sensitive data can be stored locally on each MS device when using FL, avoiding transmission over the wireless communication channel. Each MS device performs local training using each local dataset. In the BS, the model updates are joined in a global model by performing an *aggregation* process. The N RIS surfaces aid the system in controlling the phase shifts and amplitude of each element, modifying the wireless channels between the BS and the MS devices. The RIS-aided FL system achieves better performance in terms of hardware cost and energy consumption than traditional MIMO systems. Figure 5.11 illustrates an FL scheme aided by N RIS surfaces. In this scheme, each device considers its local dataset as well as the ML model trained by this dataset. Then, each UE link sends this information to each of the K RIS surfaces, where the aggregation model at the base station controls the phase shifts and amplitudes of all RIS surfaces by training a global model.

Wang et al. [34] application consists of a joint optimization of the device selection, the aggregation beamformer at the BS, and the phase shifts at the RIS via FL. The optimization approach aims to maximize the number of devices participating in the model aggregation under MSE requirements. The framework is divided into two steps. For the first step, the sparsity is considered for device selection, and then, the maximum feasible device is found by solving a series of MSE minimization problems. For the second step, an alternating optimization framework is applied to design the aggregation of beamformers at the BS efficiently. The model is based on an over-the-air computation (AirComp) strategy [35].

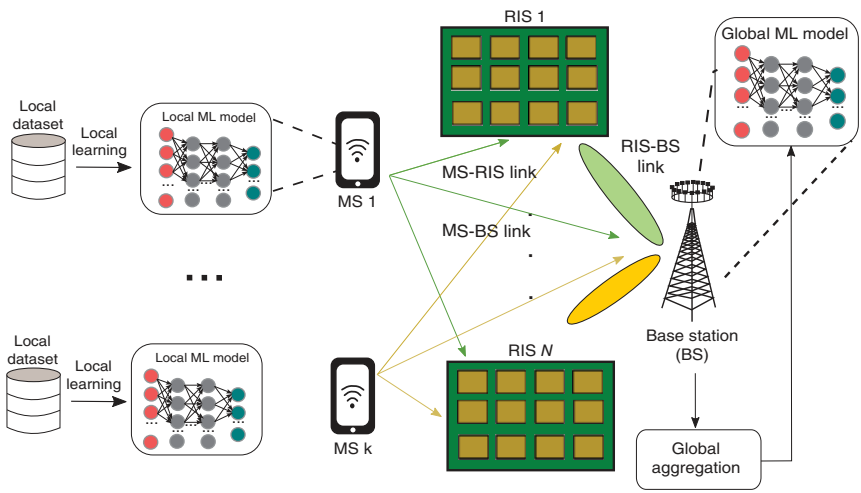

Figure 5.11 Scheme of federated learning in multiple RIS MU-MIMO communication systems.

The AirComp strategy can be used offline to enhance RIS–FL schemes. Zhao et al. [36] propose a Lyapunov framework for the sequential decomposition of the look-ahead information. Then, the authors use a block coordinate descent (BCD) algorithm for the phase shift tunning decoupled at the transceiver. Finally, an RIS with a discrete shift constraint is implemented practically with an element-wise successive refinement algorithm with low complexity.

Zhao et al. [37] conducted research to study the computation and communication of the resource allocation of an FL in an RIS-aided communication system to minimize the training latency. They propose a technique called block coordinate descend for alternate optimization of variables. The user selection and power allocation are optimized using a majorize–minimization algorithm. This application obtains the RIS phase shift using semidefinite relaxation (SDR) and Gaussian minimization.

The local training and data processing in each MS device performed by FL is an efficient solution for IoT applications. The RIS integration to FL significantly enhances IoT networks' energy efficiency to avoid extra huge operating expenses [38]. One of the approaches for FL–RIS-aided IoT applications is resource allocation. Zhang and Mao [39] addressed the energy constraint that limits the interaction between the central server and each IoT device by using an iterative resource allocation algorithm. The approach reduces energy consumption when the local training and uploading are jointly performed.

FL has been applied in RIS-aided UAV communications. Liu et al. [40] propose an FL solution using AirComp for ubiquitous network coverage under privacy and low latency requirements. The goal is the minimization of the worst-case MSE by the joint optimization of the RIS phase shifts and the noise factor for noise suppression using the transmitted power of the UAVs and the UAV trajectory.

5.6.4 ML for Signal Decoding in RIS-assisted Communications

Due to their capacity to control the propagation environment, RIS surfaces can improve wireless capacity and coverage. However, for the overall efficiency of RIS-aided wireless systems, the decrease in transmission error depends on the optimal decoding of the received signal at the MS device. Applications on signal decoding based on ML for RIS communication have been developed to enhance the system's overall performance. This section presents several revised approaches for decoding the information signals considering only one RIS surface.

Sejan et al. [41] propose the demodulation of an orthogonal frequency division multiplexing (OFDM) signal transmitted through an RIS-aided MIMO system. The demodulation scheme is based on a CNN. The training data is considered the transmitted data at the BS and is also used to test the model. Authors consider the Saleh–Valenzuela model for the generation of Rayleigh fading channels. The network architecture considers a CNN with two hidden

layers, an Adam optimization, and a ReLU activation function. The BER and symbol error rate (SER) metrics calculate the performance evaluation.

Rahman et al. [42] application consists of a signal detection scheme for a RIS-assisted wireless system. The signal is decoded using a hybrid CNN–gated recurrent unit (GRU) architecture. The network is trained with synthetic OFDM data offline. For the model evaluation, the BER and SER metrics were calculated. The CNN architecture comprises 64 filters of size 3×3 and a pooling layer. The GRU architecture consists of four layers using a tanh activation in the hidden layers and a sigmoid activation at the output layer, which shows the probability of belonging to one of the classes or symbols. Motivated by these results [43], developed improvements on this DL-signal detection system for RIS communications by applying two long-short memory networks (LSTM) connected to receive inputs in forward and backward directions. To train the bi-LSTM proposed architecture, authors feed the network with Monte–Carlo simulations of Saleh–Valenzuela channel realizations and OFDM–quadrature phase shift keying (QPSK) modulated signals. The system performance is measured in terms of SER, achieving a 9 dB gain compared to least squares (LS) and least mean squares (LMS) approaches for channel estimation. In terms of DL hyperparameters, the choice was 100 epochs, 0.01 as the learning rate, batch size of 1000, and Adam optimizer. Figure 5.12 shows the obtained results, where CP stands for the cyclic prefix for OFDM.

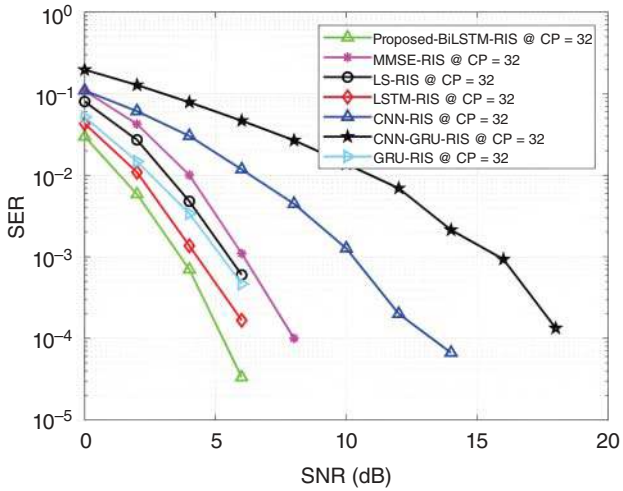

Figure 5.12 SER performance for DL-based detection schemes in RIS communications reported by Rahman et al. [43]. The proposed Bi-LSTM model outperforms achieving a 9 dB gain compared to LS and LMS approaches for channel estimation. Source: Adapted from Rahman et al. [43].

5.7 Future Trends, Challenges, and Opportunities

The use of RIS in wireless systems shows potential due to its capabilities to enhance performance in high data rate networks, low latency, and spectral efficiency. ML, additionally, has been presented as a promising technology for improving RIS networks in various tasks. However, ML applications to RIS communications are a relatively nascent research area, and consequently, several open research issues to address can be enlisted.

- **Lack of databases**: The majority of the reported applications in the literature are supervised learning approaches that require the use of labeled data for model training, the model performance depends on data. However, we can find a few authors that collected physical measurements to train ML algorithms for RIS-aided wireless network enhancement [44].
- **Sharing the source code**: The design of ML models can be strengthened when the results are open to the research community. Findings can be validated and verified when the source code of the reported framework in the literature is available online. Since research on ML approaches for RIS communications is a recent area, its faster progress to develop new algorithms and technologies can be ensured by having open source initiatives.
- **Deployment of ML models for RIS communications**: The dynamic conditions given by wireless communications require a constant updating of ML models since most of them have been trained offline. The quick variation of channel conditions demands the monitoring and updating of ML models. Another critical issue for the ML model's deployment is the hyperparameter tuning. The effectiveness of a model is improved when the parameters have been appropriately adjusted (such as the number of layers, neurons, optimizer function, loss, etc.).
- **Exploration of new learning approaches**: Most ML applications for RIS systems are based on DL. However, some researchers started to incorporate reinforcement learning (RL) and FL as well. Nonetheless, other learning algorithms could appropriately fit the enhancement of RIS communications, such as transfer learning to address the data efficiency and the carbon footprint for environmental sustainability, as well as the generalizations of models. The distributed machine learning area can also be applied to RIS-aided networks since here is possible to exchange the model parameters and calculated gradients among nodes without the coordination or synchronization techniques [45].
- **Extreme machine learning (ELM)**: This paradigm offers faster training and a reduced number of hyperparameters compared to most DL approaches. The tuning is more uncomplicated and straightforward [46]. Due to hardware

constraints, ELM can particularly fit RIS-based IoT applications since devices have fewer memory resources than conventional schemes.

- **Transformer architectures for 6G**: transformers are the core architecture for the emerging large language models (LLMs), popularized recently with the release of the open AI's Chat generative pre-training transformer (GPT) application. Transformers have recently been applied to the design of 6G intelligent networks due to their self-attention layers. The potential benefits of transformers can address some challenges for 6G networks [47].

5.8 Conclusion

The implementation of RIS surfaces emerges as a promising technology for the next generation of wireless networks due to its channel management and control capabilities, so the ML applications on RIS can conduct further research to impact the system's performance. In this chapter, the performance of the N-RIS-assisted MU-MIMO downlink transmission system has been presented. The RISs improve the wireless system's overall performance and extend the coverage area. For simulations, two scenarios and two configurations with different SEs were considered. The first scenario was blind RISs where the phases in the RIS are not modified, i.e., $\theta = I$. For the second scenario, a stochastic search was incorporated to seek the phases in the RISs that maximize the SINR. Results show that the systems have important BER performance gains compared to a similar system that does not use RISs. Results also show that the systems transmitting with higher SEs have a better BER performance. This can be explained by the higher number of Rx antennas utilized in the SE = 12 bpcu/user configuration. However, the spatial correlation and CSI errors can severely affect this system. In this chapter, a review of ML applications for RIS-aided communication systems was also provided, most of which were solved by ML strategies. The sequel discussed several open research problems and future trends in applying ML algorithms to RIS-assisted MU-MIMO systems. Although ML offers potential benefits for the enhancement that can outperform conventional RIS communication schemes, there is ongoing research and remaining open challenges in training larger and more realistic wireless scenarios and the interpretability of the ML-trained models. For this reason, our future work will explore the optimal way of incorporating ML models for the phase shift optimization of MU-MIMO communication schemes assisted by multiple RIS surfaces.

References

1 Li, J., Dang, S., Wen, M. et al. (2023). Index modulation multiple access for 6G communications: principles, applications, and challenges. *IEEE Network* 37 (1): 52–60. https://doi.org/10.1109/MNET.002.2200433.

2 Di Renzo, M., Ntontin, K., Song, J. et al. (2020). Reconfigurable intelligent surfaces vs. relaying: differences, similarities, and performance comparison. *IEEE Open Journal of the Communications Society* 1: 798–807.

3 Bai, S., Li, Q., and Cai, D. (2023). Reconfigurable intelligent surface-based hybrid phase and code modulation for symbiotic radio. *China Communications* 20 (10): 30–42. https://doi.org/10.23919/JCC.fa.2022-0829.202310.

4 Jiang, L., Li, X., Matthaiou, M., and Jin, S. (2023). Joint user scheduling and phase shift design for RIS assisted multi-cell MISO systems. *IEEE Wireless Communications Letters* 12 (3): 431–435. https://doi.org/10.1109/LWC.2022.3229441.

5 Yan, W., Yuan, X., He, Z.-Q., and Kuai, X. (2020). Passive beamforming and information transfer design for reconfigurable intelligent surfaces aided multiuser MIMO systems. *IEEE Journal on Selected Areas in Communications* 38 (8): 1793–1808. https://doi.org/10.1109/JSAC.2020.3000811.

6 Jung, M., Saad, W., Debbah, M., and Hong, C.S. (2021). On the optimality of reconfigurable intelligent surfaces (RISs): passive beamforming, modulation, and resource allocation. *IEEE Transactions on Wireless Communications* 20 (7): 4347–4363. https://doi.org/10.1109/TWC.2021.3058366.

7 Xu, K., Gong, S., Cui, M. et al. (2022). Statistically robust transceiver design for multi-RIS assisted multi-user MIMO systems. *IEEE Communications Letters* 26 (6): 1428–1432. https://doi.org/10.1109/LCOMM.2022.3157127.

8 Semmler, D., Joham, M., and Utschick, W. (2022). Linear precoding in the intelligent reflecting surface assisted MIMO broadcast channel. *2022 IEEE 23rd International Workshop on Signal Processing Advances in Wireless Communication (SPAWC)*, 1–5. https://doi.org/10.1109/SPAWC51304.2022.9833988.

9 Ning, B., Wang, P., Li, L. et al. (2022). Multi-IRS-aided multi-user MIMO in mmWave/THz communications: a space-orthogonal scheme. *IEEE Transactions on Communications* 70 (12): 8138–8152. https://doi.org/10.1109/TCOMM.2022.3216344.

10 Faisal, K.M. and Choi, W. (2022). Machine learning approaches for reconfigurable intelligent surfaces: a survey. *IEEE Access* 10: 27343–27367.

11 Souto, N. and Silva, J.C. (2023). Joint beamforming algorithm for multi-stream MIMO systems assisted by multiple reconfigurable intelligent surfaces. *IEEE Open Journal of the Communications Society* 4: 1317–1333. https://doi.org/10.1109/OJCOMS.2023.3282671.

12 Yu, Z., Han, Y., Matthaiou, M. et al. (2022). Statistical CSI-based design for RIS-assisted communication systems. *IEEE Wireless Communications Letters* 11 (10): 2115–2119. https://doi.org/10.1109/LWC.2022.3194192.

13 Yu, K., Bengtsson, M., Ottersten, B. et al. (2002). A wideband statistical model for NLOS indoor MIMO channels. *Proceedings of IEEE 55th Vehicular Technology Conference*, volume 1, 370–374, Birmingham, AL, USA (6–9 May 2002). https://doi.org/10.1109/VTC.2002.1002729.

14 Basar, E., Aygolu, U., Panayirci, E., and Poor, H.V. (2012). Performance of spatial modulation in the presence of channel estimation errors. *IEEE Communications Letters* 16 (2): 176–179.

15 Castillo-Soria, F.R., Del Puerto-Flores, J.A., Azurdia-Meza, C.A. et al. (2023). Precoding for RIS-assisted multi-user MIMO-DQSM transmission systems. *Future Internet* 15 (9): 299. https://doi.org/10.3390/fi15090299.

16 Castillo-Soria, F.R., Basar, E., Cortez, J., and Cardenas-Juarez, M. (2020). Quadrature spatial modulation based multiuser MIMO transmission system. *IET Communications* 14 (7): 1147–1154. https://doi.org/10.1049/iet-com.2019.0573.

17 Lyu, J. and Zhang, R. (2021). Hybrid active/passive wireless network aided by intelligent reflecting surface: system modeling and performance analysis. *IEEE Transactions on Wireless Communications* 20 (11): 7196–7212.

18 Wu, Q., Zhang, S., Zheng, B. et al. (2021). Intelligent reflecting surface-aided wireless communications: a tutorial. *IEEE Transactions on Communications* 69 (5): 3313–3351.

19 Sun, R., Wang, W., Chen, L. et al. (2021). Diagnosis of intelligent reflecting surface in millimeter-wave communication systems. *IEEE Transactions on Wireless Communications* 21 (6): 3921–3934.

20 Demir, Ö.T. and Björnson, E. (2022). Is channel estimation necessary to select phase-shifts for RIS-assisted massive MIMO? *IEEE Transactions on Wireless Communications* 21 (11): 9537–9552.

21 Elbir, A.M., Papazafeiropoulos, A., Kourtessis, P., and Chatzinotas, S. (2020). Deep channel learning for large intelligent surfaces aided mm-Wave massive MIMO systems. *IEEE Wireless Communications Letters* 9 (9): 1447–1451.

22 Taha, A., Alrabeiah, M., and Alkhateeb, A. (2019). Deep learning for large intelligent surfaces in millimeter wave and massive MIMO systems. *2019 IEEE Global Communications Conference (GLOBECOM)*, 1–6. IEEE.

23 Alkhateeb, A. (2019). DeepMIMO: a generic deep learning dataset for millimeter wave and massive MIMO applications. *ArXiv*, abs/1902.06435. https://arxiv.org/abs/1902.06435.

24 Khan, S., Khan, K.S., Haider, N., and Shin, S.Y. (2019). Deep-learning-aided detection for reconfigurable intelligent surfaces. *arXiv preprint arXiv:1910.09136*.

25 Wu, M., Gao, Z., Huang, Y. et al. (2023). Deep learning-based rate-splitting multiple access for reconfigurable intelligent surface-aided tera-hertz massive MIMO. *IEEE Journal on Selected Areas in Communications* 41 (5): 1431–1451.

26 Özdoğan, Ö. and Björnson, E. (2020). Deep learning-based phase reconfiguration for intelligent reflecting surfaces. *2020 54th Asilomar Conference on Signals, Systems, and Computers*, 707–711. IEEE.

27 Gao, J., Zhong, C., Chen, X. et al. (2020). Unsupervised learning for passive beamforming. *IEEE Communications Letters* 24 (5): 1052–1056.

28 Jiang, H., Dai, L., Hao, M., and MacKenzie, R. (2022). End-to-end learning for RIS-aided communication systems. *IEEE Transactions on Vehicular Technology* 71 (6): 6778–6783.

29 Huang, C., Mo, R., and Yuen, C. (2020). Reconfigurable intelligent surface assisted multiuser MISO systems exploiting deep reinforcement learning. *IEEE Journal on Selected Areas in Communications* 38 (8): 1839–1850.

30 Saglam, B., Gurgunoglu, D., and Kozat, S.S. (2022). Deep reinforcement learning based joint downlink beamforming and RIS configuration in RIS-aided MU-MISO systems under hardware impairments and imperfect CSI. *arXiv preprint arXiv:2211.09702*.

31 Wang, W. and Zhang, W. (2022). Intelligent reflecting surface configurations for smart radio using deep reinforcement learning. *IEEE Journal on Selected Areas in Communications* 40 (8): 2335–2346.

32 Mei, H., Yang, K., Liu, Q., and Wang, K. (2022). 3D-trajectory and phase-shift design for RIS-assisted UAV systems using deep reinforcement learning. *IEEE Transactions on Vehicular Technology* 71 (3): 3020–3029.

33 Peng, H. and Wang, L.-C. (2023). Energy harvesting reconfigurable intelligent surface for UAV based on robust deep reinforcement learning. *IEEE Transactions on Wireless Communications* 22 (10): 6826–6838.

34 Wang, Z., Qiu, J., Zhou, Y. et al. (2021). Federated learning via intelligent reflecting surface. *IEEE Transactions on Wireless Communications* 21 (2): 808–822.

35 Wang, Z., Zhao, Y., Zhou, Y. et al. (2022). Over-the-air computation: foundations, technologies, and applications. *arXiv preprint arXiv:2210.10524*.

36 Zhao, Y., Wu, Q., Chen, W. et al. (2023). Performance-oriented design for intelligent reflecting surface assisted federated learning. *IEEE Transactions on Communications* 71 (9): 5228–5243.

37 Zhao, L., Xu, H., Wang, J. et al. (2022). Computation–communication resource allocation for federated learning system with intelligent reflecting surfaces. *Arabian Journal for Science and Engineering* (8): 1–7.

38 Ni, W., Liu, Y., Yang, Z. et al. (2021). Federated learning in multi-RIS-aided systems. *IEEE Internet of Things Journal* 9 (12): 9608–9624.

39 Zhang, T. and Mao, S. (2021). Energy-efficient federated learning with intelligent reflecting surface. *IEEE Transactions on Green Communications and Networking* 6 (2): 845–858.

40 Liu, H., Yuan, X., and Zhang, Y.-J.A. (2021). Reconfigurable intelligent surface enabled federated learning: a unified communication-learning design approach. *IEEE Transactions on Wireless Communications* 20 (11): 7595–7609.

41 Sejan, M.A.S., Rahman, M.H., and Song, H.-K. (2022). Demod-CNN: a robust deep learning approach for intelligent reflecting surface-assisted multiuser MIMO communication. *Sensors* 22 (16): 5971.

42 Rahman, M.H., Sejan, M.A.S., Aziz, M.A. et al. (2023). Deep convolutional and recurrent neural-network-based optimal decoding for RIS-assisted MIMO communication. *Mathematics* 11 (15): 3397.

43 Rahman, M.H., Sejan, M.A.S., Aziz, M.A. et al. (2023). Deep learning based improved cascaded channel estimation and signal detection for reconfigurable intelligent surfaces-assisted MU-MISO systems. *IEEE Transactions on Green Communications and Networking* 7 (3): 1515–1527.

44 Tewes, S., Heinrichs, M., Weinberger, K. et al. (2023). A comprehensive dataset of RIS-based channel measurements in the 5GHz band. *2023 IEEE 97th Vehicular Technology Conference (VTC2023-Spring)*, 1–5. IEEE.

45 Asad, M., Moustafa, A., and Ito, T. (2021). Federated learning versus classical machine learning: a convergence comparison. *arXiv preprint arXiv:2107.10976*.

46 Huang, G.-B., Zhu, Q.-Y., and Siew, C.-K. (2004). Extreme learning machine: a new learning scheme of feedforward neural networks. *2004 IEEE International Joint Conference on Neural Networks (IEEE Cat. No. 04CH37541)*, volume 2, 985–990. IEEE.

47 Wang, Y., Gao, Z., Zheng, D. et al. (2022). Transformer-empowered 6G intelligent networks: from massive MIMO processing to semantic communication. *IEEE Wireless Communications* 30 (6): 127–135.

6

Analytical Phase Shift and Amplitude Element Optimization for Energy-Efficient Active RIS-Aided Massive MIMO Systems

Wilson de Souza Junior[1], *José Carlos Marinello Filho*[2], *and Taufik Abrão*[1]

[1] *Electrical Engineering Department, Londrina State University, Brazil, Londrina, Paraná, Brazil*
[2] *Electrical Engineering Department, UTFPR, Cornélio Procópio, Paraná, Brazil*

6.1 Introduction

The expansion of the fifth generation (5G) wireless networks has increased worldwide incentive and development efforts in the research field, resulting in an intensified exploration of possibilities offered by the Beyond-5G (B5G) wireless networks. Envisioned to be denoted by its exceptional data-driven capabilities and global connectivity, B5G is expected to provide a wide range of applications and services that will reshape communication systems. These innovations can be achieved across diverse domains, such as extended reality (XR), holographic communications, etc., promising to redefine the technological scenario. The advent of B5G will bring a high quantity of new services and elevate existing ones to higher levels. However, given this aim, integrating such technologies becomes essential to encourage the deployment of these services and confirm their optimal functioning in the technological scenario. Essentially, the commercialization of B5G will demand an intense embrace of state-of-the-art technologies, signaling a paradigm shift in our perception of the potential of wireless communication networks.

Among all emerging technologies, reconfigurable intelligent surface (RIS) stands out as one of the most promising recent enabling techniques poised to impact future communication systems, extending beyond the 5G and sixth generation (6G). RIS has the potential to significantly enhance transmission capabilities by establishing a "virtual" re-configurable/reprogrammable communication link. Essentially, the RIS is a thin planar surface consisting of a massive number of low-cost reflecting elements composed of meta-materials to reconfigure and redirect the impinging signal by changing its electromagnetic properties (phase and/or magnitude) [1], so that, the reflected signal can be

Reconfigurable Intelligent Surfaces for 6G and Beyond Wireless Networks, First Edition.
Edited by Agbotiname Lucky Imoize, Vinoth Babu Kumaravelu, and Dinh-Thuan Do.

focused towards a specific direction with a specific gain. The electromagnetic characteristics of incoming waves are modified by leveraging electronic components like PIN diodes or radio frequency (RF) switches embedded within the RIS panel. Adjusting the impedance of PIN diodes or fine-tuning the RF switch enables manipulation of the reflection and magnitude of the impinging waves, respectively. This dynamic fine-tuning aids in augmenting specific performance metrics. Hence, RIS holds great promise owing to its ability to control the wireless environment in a software-defined manner dynamically and its potential to alleviate certain inherent challenges. The distinct advantages of RIS arrays can be succinctly summarized as follows [2]:

- Easiness in implementation;
- Enhancement of spectral efficiency (SE) and energy efficiency (EE);
- Sustainability; and
- Compatibility.

Given these characteristics, RIS is a promising solution for addressing various challenges. In addition, when compared to conventional relaying techniques like Amplify-and-Forward (AF) and Decode-and-Forward (DF), RIS offers numerous advantages. It presents a cost-effective yet highly efficient solution that optimizes both the system's EE and SE, as well as other metrics. However, as with any nascent technology, introducing RIS brings new applications and challenges. Particularly in the communications and signal processing fields, issues such as optimizing phase shifts of scattering elements and acquiring channel information for additional links introduced by RIS deployment are paramount and must be tackled efficiently.

Various architectural variants for the RIS have been introduced to enhance its effectiveness. These variations aim to improve performance significantly, offering innovative solutions to overcome challenges and elevating the effectiveness of GLSS-supported communication systems. Among them, we can mention the active RIS structure, which is an alternative for providing better conditions for the double-fading attenuation link. In active RIS, each resource efficiency (RE) is bolstered by a series of active-load impedances, allowing the active RIS to function as a dynamic reflector. In this way, it not only reflects incoming signals but also applies power amplification to them. An exciting advantage of the active RIS elements is their capability to estimate the channel between the transmitter-RIS in downlink (DL) and uplink (UL) at the RIS side [3]. Besides, since the active RIS can amplify the incident signal, fewer reflecting elements are required to achieve the same signal-to-noise ratio (SNR) at the receiver when compared with the conventional entirely passive RIS [4]. However, evaluating the EE for the entirely passive RIS versus active RIS is a critical problem that should be further investigated.

Conversely, the proliferation of massive MIMO (M-MIMO) technology, characterized by the deployment of an extensive array of transmit/receiver antennas at the base station (BS), plays a pivotal role in enhancing the SE of the system. This technology is instrumental in efficiently accommodating multiples user's equipments (UEs) by leveraging the same physical resources. This strategic utilization enhances the SE and optimizes the resource utilization, exemplifying the versatility and efficiency of M-MIMO in contemporary wireless communication systems.

Besides the technologies mentioned above, a promising technology in future communications networks is the millimeter-wave (mmWave) technology. It emerges as a strategic pivotal solution in addressing the evolving connectivity demands. Operating within the high-frequency spectrum, typically from 30 to 100 GHz, mmWave technology presents a promising solution capable of supplying characteristics such as the utilization of higher bandwidth for contemporary communication networks. Furthermore, with the large arrays, the near-field emerges, enabling the beam focusing instead of the traditional beam steering for far-field communications [5–7].

However, the implementation of these higher-frequency systems, which often entails the use of large-scale arrays at the BS or the RIS, introduces inherent complexities in both passive and active beamforming, demanding low-complexity, approximate yet efficient solutions for accurate channel estimation and RIS configuration. The joint operation of RIS, M-MIMO, and mmWave technologies emerges as key enablers for future communication systems. Expected to play central roles in the upcoming generation of wireless networks, these technologies are designed to support high data rates and accommodate a substantial number of connected UEs, operating with expanded array sizes. In response to this evolution, there is a fundamental growth to prioritize the system's EE, measured in bits-per-Joule,[1] as a crucial performance metric. The focus on EE emphasizes developing sustainable communication systems, especially as efficient energy utilization becomes a global concern across various fields, including telecommunications. In function of alarming levels of climate change, there is an urgent need to limit global warming to 1.5° above the preindustrial mark [8]. Within this context, developing the next-generation telecommunication standard, often referred to as B5G or 6G, assumes particular importance. It aims to establish a highly energy-efficient system that meets expected requirements, such as a peak throughput of 1 [Tbps] and latency in the order of microseconds [9]. This forward-looking approach aligns with the broader goal of enabling technological advancements that meet the requirements necessary in terms of performance and actively contribute to the sustainability challenges of our time.

1 Alternatively, Joule-per-bit.

In light of these challenges, developing pioneering strategies that enhance EE and facilitate the intricate processes of channel estimation and configuration for large-scale array systems is of paramount importance. This chapter focuses on addressing these challenges with innovative approaches and practical solutions tailored to the modern network's infrastructures.

6.1.1 Contributions of the Chapter

The contributions of this book chapter lie in analyzing the RIS-assisted M-MIMO scenario, which will become essential components of future communication systems. Specifically, the aim is to devise a solution that effectively optimizes the signal amplification of active RIS concerning the EE, envisaging the determination of the number of active RIS elements that outperforms entirely passive RIS. To elaborate further, in this chapter, we systematically:

- Propose a comprehensive optimization methodology for system EE maximization, focusing on the deployment of specific optimization tools, including convex optimization procedures, to reduce the computational complexity and aim the application of the algorithm in a real-world scenario;
- We have introduced an algorithm with low complexity and promising performance. In this algorithm, we develop a way of calculating both the angle-phase shift and the amplitude of each RIS element in a closed-form manner;
- Optimize the phase and amplitude of the active RIS in a sustainable perspective, i.e., the phase and amplitude that result in the power consumption necessary to obtain high-performance gains sufficient to outperform the passive RIS;
- Investigate the number of RIS active elements to be selected that surpasses the EE performance of the entirely passive RIS within the system EE optimization framework and different configurations/scenarios parameters.

6.1.2 Organization

The remainder of this book chapter is organized into seven sections. These sections are meticulously structured to comprehensively explore the various aspects of the RIS-assisted M-MIMO system. In Section 6.2, we summarize the related works; while in Section 6.3, we present the groundwork by formulating a general system model that effectively captures the key aspects associated with the integration of the active RIS into the M-MIMO systems. Also, we explore the SE and EE definitions and present the coupling power consumption model for RIS-assisted M-MIMO systems. In Section 6.4, we review the definitions, features, and concepts of some fundamental techniques for addressing our intended problem, such as fractional programming (FP) techniques and sum-of-ratio techniques. Moving forward, in Section 6.5, we meticulously present the defined problem formulation, emphasizing its relevance and significance in contemporary real-world

applications. The motivations and justifications for adopting this particular problem are thoroughly expounded, shedding light on the challenges and opportunities that emphasize its importance in modern communication systems. Section 6.6 provides a complete and detailed description of our proposed solution for the EE problem in active RIS-assisted M-MIMO systems. Section 6.7 presents numerical results, accompanied by an extensive and in-depth discussion on the effectiveness, efficiency, and potential of the proposed technique. The section also includes a relevant debate about the advantages/drawbacks of the active RIS structure in contrast to the entirely passive RIS within the context of EE.

Finally, in Section 6.8, we provide a relevant and comprehensive discussion that encapsulates our perspective on the problem-solving approach adopted throughout this chapter and the obtained insights. Our analysis and conclusions are framed within the broader context of the current state of the art, aiming to provide valuable insights and potential directions for future research.

6.2 Related Works

An extensive number of works including [10–27] have studied the RIS deployment impact in M-MIMO systems under different objectives, such as: maximizing the weigthed sum-rate (WSR) [10, 11], maximizing the sum-rate (SR) [12], maximizing the EE [13–15], RIS-assisted sensing [16, 17], minimizing the total transmit power [18], maximizing the minimum rate [19, 20], for interference nulling [21, 22], and active RIS [23–27].

The above-cited studies demonstrate the immense potential and versatility of RIS within wireless systems. The work in [10] investigates the weighted SR maximization. It uses a convex optimization approach to design the BS precoding matrix and the RIS-phase shift for the passive RIS. The paper proposes two different techniques for the analyzed problem. The proposed optimization method utilizes FP techniques aiming at the problem of "convexation." Besides, a block coordinate descent (BCD) method is used to optimize sequentially the BS precoding matrix and the RIS phase shift, where analytical methods and *Riemannian* conjugate gradient have been utilized. The proposed method is available under two scenarios: perfect and imperfect channel estimation. Numerical simulations confirm the effectiveness and efficiency of the proposed method.

The work in [11] suggests that by attempting to reduce intercell interference, the weighted SR in RIS-aided DL multicell could be maximized. Hence, to achieve this aim, Pan et al. [11] jointly optimizes the active precoding matrices at BSs and the phase shifts at the RIS subject to each BSâ's power constraint and unit modulus constraint, respectively. In this case, the optimization problem does not consider any Quality of Service (QoS) restriction, e.g., a minimum rate requirement for the users. As a result, this solution tends to maximize the rate of users with better channel conditions.

In [12], the authors investigated the ergodic rate of an RIS-assisted M-MIMO system. The authors derive a closed-form lower bound expression for the system ergodic rate by applying random matrix theory. The derived bound reveals tightness over several system and channel parameters. Besides, it is promising since the statistical channel state information (CSI) optimization can be deployed based on this bound. It is helpful to alleviate the channel estimation burden since it matches the expected results very well. Besides, they provided a gradient-ascent method to optimize the RIS angle phase-shift given maximizing the system SR.

The EE maximization problem is addressed in [13] by considering UL multiuser single-antenna devices and Multiple-input single-output (MISO) RIS-aided systems. The joint optimization involves the transmit power at users, phase shift at the RIS, and combining matrix at BS receiver. The proposed BCD iterative procedure can handle one variable during each iteration while the others are held fixed. Numerical results indicate that the proposed scheme outperforms baselines that jointly optimize two of three variables.

In [14], the joint number of antennas, power allocation, and passive RIS reflecting coefficients optimization for EE maximization with statistical CSI is studied. Analytical techniques have been applied in view of maximizing the EE with low overhead for channel estimation. EE problem has been maximized with a low-complexity algorithm, where the power allocation, RIS phase shift, and the number of active antennas at BS have been optimized based on closed-form expressions, utilizing the BCD method. The method was demonstrated to be promising, outperforming the gradient ascend methodology for passive RIS reflecting coefficients optimization with statistical CSI.

In [15], the authors also analyzed the EE in RIS-assisted systems. In this study, the EE maximization has been analyzed under joint optimization of power consumption for both RIS and BS. The authors proposed an innovative power consumption model on the RIS by considering the ON and OFF state of the RIS unit reflecting element, matching further precisely with the real-world behavior of physical components. The paper also proposes low-complexity and practical algorithms, for which the simulation has proved promising results.

In [16], the authors studied the integrated sensing and communication (ISAC) system for a double RIS-assisted system. The research primarily addresses the challenge of mutual interference between the radar and communication functionalities by leveraging a joint optimization approach for beamforming and radar operations. To manage the complexity of the solution, the authors introduce a -based approach and a BCD algorithm. These methods effectively reduce computational complexity, offering practical and efficient solutions for real-world implementation. Moreover, the work presented in [17] addresses the challenges of a sensing-assisted multiuser mmWave system. The study focuses on optimizing the channel sensing duration for each UE to enhance the overall system SR.

By effectively managing the sensing duration, the research aims to improve the performance of the mmWave system, offering potential advancements for future wireless communication technologies.

In [18], the phase shift and BS beamforming optimization techniques have been proposed given minimizing the UL transmit power in an RIS-aided Internet of Things (IoT) network. The proposed technique was promising since it can reduce to about half of the UL transmit power over the conventional scheme without RIS. The methodology exploits the product *Riemannian manifold* structure of the sets of unit-modulus phase shifts and unit-norm beamforming vectors. Besides, the *manifold* method converts the nonconvex UL transmit power minimization problem into an unconstrained problem and then finds the optimal solution over the product *Riemannian manifold*.

In [19], the focus was on the study of the maximum–minimum rate problem. The research delved into the joint optimization of transmit and passive beamforming, considering the uncertainty of UEs locations. To address this challenge, the authors proposed an alternating optimization approach combined with sucessive convex approximation (SCA) technique and a double loop penalty algorithm.

In the research paper [20], the authors demonstrated that the nonconvex max –min rate problem in RIS-assisted multiuser communication systems can be reformulated into a second order conic programming (SOCP) problem. They also explored the application of semi-defined relaxation (SDR) and SCA techniques to optimize the passive and active beamforming for the system under consideration.

In [21], the RIS structure is deployed aiming at interference nulling, where an alternating projection method is utilized. This method can converge for a solution that eliminates the interference. However, the number of elements for achieving this goal can vary according to some parameters, such as the number of served UEs. Besides, the authors also explored the `max-min` rate problem. The numerical results are promising since the proposed procedure achieves high performance with low complexity. Adhering to a similar approach, the authors in [22] proposed a method to determine the angles for two distinct passive RISs, aiming to achieve complete orthogonalization of channels between UEs and thereby nulling interference. The investigation delves specifically into both diagonal and beyond-diagonal RISs, employing a *manifold*-based algorithm to find the angles for both RISs, adhering to the unitary matrix constraint essential for achieving complete orthogonalization of channels between the UEs. Notably, the study highlights that signal amplification is unnecessary for achieving orthogonalization. Furthermore, the paper introduces an efficient channel estimation method to complement the proposed approach.

Recent works (2022–2024) addressing RE (EE and SE trade-off optimization) in active RIS-aided M-MIMO systems are summarized in Table 6.1. Our previous related works and contributions on the RE optimization, EE and SE in M-MIMO

Table 6.1 Recent works addressing Resource Efficiency (EE and SE) and related open issues in active RIS-aided M-MIMO systems.

Setup (year)	Contributions	Problem	Method	References
M-MIMO and double active RIS (2024)	SR maximization for an ISAC system with practical constraints is studied. Design of the radarâ's beamforming vector and the active RISsâ' reflecting coefficient matrices. A penalty dual decomposition is proposed jointly with Lagrangian and BCD framework. Findings: double active RIS setup achieves higher rates than entirely passive single RIS setup and entirely passive double RIS setup.	SR maximization for double active RIS setup	By utilizing the FP technique, the problem is decomposed in a more feasible form; thus, the penalty dual decomposition is applied. In order to solve each sub-problem, with respect to radar and communication beamforming and both active RIS reflecting coefficient matrices. The BCD method is applied jointly with the Lagrangian dual method.	[23]
M-MIMO and active RIS (2022)	The power saving on BS is studied in this work, where an active RIS is considered to assist the communication system. The authors consider that the UEs can exploit the PS to decode information and harvest energy. Besides, a realistic piecewise nonlinear EH model is considered. An algorithm is proposed in view of optimizing the beamforming at the BS, PS ratios, and the RIS reflecting coefficients.	Transmit power minimization for active RIS setup	The algorithm proposed utilized the BCD method given optimizing the variables. For the BS beamforming and PS ratios, the SDR and SCA are applied to find a solution. For solving the active RIS reflection coefficient, SDP method is applied, where a penalty-based method is applied for achieving a rank-one solution.	[24]

M-MIMO and active RIS (2023)	The signal model of active RIS, considering the amplification of the incident signal and accounting for the non-negligible thermal noise introduced by the active elements has been proposed. Besides, the SR maximization problem for an active RIS is solved, considering practical factors expected to be present in practical systems.	SR maximization under active RIS	A low-complexity algorithm based on FP technique is proposed aiming at maximizing the system SR for an active RIS-aided M-MIMO system. The algorithm shows promising results in all considered scenarios, i.e., with suppression of self-interference and without suppression of self-interference imposed by the active RIS.	[25]
ISAC and active RIS (2023)	The authors analyzed the active RIS within an ISAC scenario. The paper specifically investigates the EE of the system under practical system power budgets, considering constraints on user communication QoS and sensing SNR.	EE maximization under ISAC-assisted active RIS	An algorithm is proposed based on Rayleigh quotient optimization approach, SDR, and the MM framework. The numerical results demonstrated that the active RIS can outperform the entirely passive RIS in both SE and EE for RIS-assisted ISAC systems.	[26]
M-MIMO and active RIS (2023)	The deployment of an active RIS, focusing on enhancing the security of communication systems, is studied. Their findings highlight the potential of active RIS to mitigate the double-fading effect by amplifying the incident signal, by increasing EE and security compared to passive RISs.	EE maximization and transmit power minimization for active RIS	To minimize the transmit power and maximize EE, the authors proposed a penalty-based *alternating minimization* algorithm for optimizing the beamforming in both the RIS and BS.	[27]

(Continued)

Table 6.1 (Continued)

Setup (year)	Contributions	Problem	Method	References
M-MIMO and active RIS (2024)	Consistent analysis of an active RIS scenario considering the practical hardware limitations of amplifiers by providing an accurate amplification model. Both the joint transmit-beamforming and active RIS reflection beamforming are optimized in this scenario.	SR maximization under active RIS	The FP, MM, and BCD are applied given solving the complex problem. The proposed algorithm demonstrates the effectiveness compared to the entirely passive RIS.	[37]
M-MIMO and active RIS (2024)	Both amplitude and phase of an active RIS is optimized analytically by using fractional programming techniques. We derive closed-form solutions differently from other works in the literature. This innovative approach has significant appeal since it can reduce complexity remarkably. Besides, the number of elements of active RIS is analyzed given matching the performance of entirely passive RIS.	EE maximization under **active** RIS setups	Based on FP optimization technique, a low-complexity with closed-form solutions-based algorithm is proposed for maximizing the EE of active RIS operating in multiuser scenarios under realistic constraints. The algorithm presented a substantial reduction in the complexity when compared with the SDR solution.	**This work**

systems aided or not by RIS include: [14, 28–36]. In this chapter, we propose to deploy the FP methodology to solve the phase-shift and amplification coefficients of an active RIS aiming at EE maximization problem considering the context of the DL RIS-aided multiuser M-MIMO systems.

6.3 General System Model for RIS-aided M-MIMO

We start the section by describing the general model for M-MIMO systems assisted by an RIS setup considered. This system model is conceived to cover a diverse range of practical scenarios. Subsequently, we present the models for the DL-received baseband signals. Built such a model, we finish the section by formulating expressions for SE and EE within the specified RIS-aided M-MIMO scenarios. The notation deployed in this chapter is entirely outlined in Table 6.2.

Let a DL RIS-assisted M-MIMO scenario where the direct link between the BS and UEs is entirely obstructed, Figure 6.1. In this setup, K single-antenna UEs are served by the BS equipped with M elements through an RIS comprising N elements, as illustrated in Figure 6.2. Additionally, we assume a dedicated connection between the RIS and the BS, facilitated by a programmable controller. This arrangement empowers the BS to oversee both the phase-shifts and amplitude coefficients of the RIS. Moreover, we assume that the time required for RIS amplitude/phase configuration is shorter than the channel coherence time. Hence, at the onset of each time slot, the BS must appropriately configure the RIS for its operation. Let us denote $\boldsymbol{H}_1$ the channel from the BS to the RIS and $\boldsymbol{H}_2$ as the channel from the RIS to the UEs. The cascaded channel between the BS and UEs via the RIS can be expressed as $\boldsymbol{H} = \left[\boldsymbol{h}_1, \boldsymbol{h}_2, \ldots, \boldsymbol{h}_K\right]$ more specifically, denoted as:

$$\boldsymbol{h}_k = \boldsymbol{H}_1 \boldsymbol{\Phi} \boldsymbol{h}_{2,k}, \quad \forall k \in \mathcal{K} \tag{6.1}$$

where $\boldsymbol{\Phi} = \text{diag}(\boldsymbol{v}) \in \mathbb{C}^{N \times N}$, with $\boldsymbol{v} = [v_1^*, v_2^*, \ldots, v_N^*]^H \in \mathbb{C}^{N \times 1}$, being $v_n = \alpha_n e^{j\theta_n} \in \mathbb{C}$ the phase-shift and amplitude applied by the nth element of the RIS, with

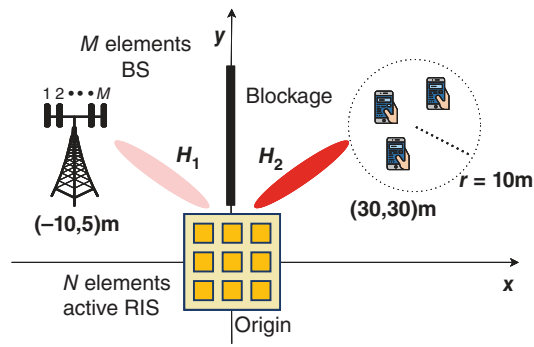

Figure 6.1 The simulated RIS-aided K-user M-MIMO communication scenario, with M-antenna BS and N-element RIS.

Table 6.2 List of notation and symbols for the RIS-aided M-MIMO scenario.

Symbol	Description
$M \in \mathbb{Z}_+$	Number of BS antennas
$K \in \mathbb{Z}_+$	Number of UEs
$N \in \mathbb{Z}_+$	Number of total RIS elements
$N_{pas} \in \mathbb{Z}_+$	Number of total passive RIS elements
$N_{act} \in \mathbb{Z}_+$	Number of total active RIS elements
$\mathcal{K} = \{1, 2, \dots, K\}$	UEs set
$\mathcal{N} = \{1, 2, \dots, N\}$	RISs elements set
$\mathcal{N}_a = \{1, 2, \dots, N_{act}\}$	RISs active elements set
$\mathcal{N}_p = \{1, 2, \dots, N_{pas}\}$	RISs passive elements set
$\lambda > 0$	Carrier wavelength
$\beta_1 \in \mathbb{R}$	Large-scale fading coefficient of the channel from BS to RIS
$\beta_{2,k} \in \mathbb{R}$	Large-scale fading coefficient of the channel from RIS to kth UE
$\boldsymbol{H} \in \mathbb{C}^{M \times K}$	Cascaded channel matrix of the BS and UEs through RIS
$\boldsymbol{H}_1 \in \mathbb{C}^{M \times N}$	Channel between the BS and RIS
$\overline{\boldsymbol{H}}_1 \in \mathbb{C}^{M \times N}$	LoS component of the BS and RIS channel
$\widetilde{\boldsymbol{H}}_1 \in \mathbb{C}^{M \times N}$	Multipath component of the BS and RIS channel
$\boldsymbol{H}_2 \in \mathbb{C}^{N \times K}$	Channel between the RIS and UEs
$\overline{\boldsymbol{H}}_2 \in \mathbb{C}^{N \times K}$	LoS component of the RIS and UEs channel
$\widetilde{\boldsymbol{H}}_2 \in \mathbb{C}^{N \times K}$	Multipath component of the RIS and UEs channel
$\boldsymbol{v} \in \mathbb{C}^N$	RIS amplitude/phase-shift vector
$\boldsymbol{\Phi} \in \mathbb{C}^{N \times N}$	RIS amplitude/phase-shift diagonal matrix
$\kappa_1 \in [0, \infty)$	Rician κ-factor for RIS and BS channel
$\kappa_{2,k} \in [0, \infty)$	Rician κ-factor for RIS and kth UE
$p_k \in \mathbb{R}^+$	Power designated to the kth UE
$\boldsymbol{W} \in \mathbb{C}^{M \times K}$	Precoding matrix
$s_k \in \mathbb{C}$	Information symbol intended to the kth UE
$n_k \in \mathbb{C}$	AWGN sample at the kth UE
$\boldsymbol{z} \in \mathbb{C}^{N \times 1}$	AWGN sample vector at the RIS
$\alpha_n \in \mathbb{R}_+$	Amplitude value of nth element of RIS
$\theta_n \in [0, 2\pi)$	Phase-shift value of nth element of RIS
$\alpha_{\max} \in \mathbb{R}_+^*$	Maximum amplitude provided by the RIS
$P_{\max}^{RIS} \in \mathbb{R}_+$	Maximum amplification power of RIS

Source: The Authors.

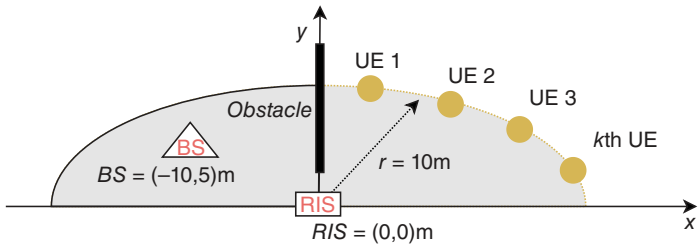

Figure 6.2 The adopted RIS-aided K-user M-MIMO communication simplified two-dimensional scenario.

$\alpha_n \in [0, \alpha_{\max}]$ and $\theta_n \in [0, 2\pi)$. The BS uses a precoding matrix $\boldsymbol{W} = [\boldsymbol{w}_1, \boldsymbol{w}_2, \ldots, \boldsymbol{w}_K] \in \mathbb{C}^{M \times K}$, with $||\boldsymbol{w}_k||^2 = p_k \in \mathbb{R}^+$, in view of beamforming the signal toward the UEs, where p_k is the power allocated for the kth UE served. Here, for simplicity, we adopt maximum ratio (MR) precoding with equal power allocation (EPA).

Utilizing the system model explained above, the DL baseband transmitted signal $\boldsymbol{x} \in \mathbb{C}^{M \times 1}$ can be written as:

$$\boldsymbol{x} = \sum_{k=1}^{K} \boldsymbol{w}_k s_k \tag{6.2}$$

where s_k is the symbol intended to the kth UE, with $\mathbb{E}[|s_k|^2] = 1$. While the received signal by the kth UE is given as:

$$y_k = \boldsymbol{w}_k^H \boldsymbol{h}_k s_k + \sum_{j=1, j \neq K}^{K} \boldsymbol{w}_j^H \boldsymbol{h}_k s_k + \boldsymbol{h}_{2,k}^H \boldsymbol{\Phi} \boldsymbol{z} + n_k \tag{6.3}$$

in which $n_k \in \mathbb{C}$ is the AWGN sample at the kth UE, following $n_k \sim \mathcal{CN}(0, \sigma^2)$, $\forall k \in \mathcal{K}$, and $\mathbf{z} \in \mathbb{C}^{N \times 1}$ is the AWGN at the RIS, with $\mathbf{z} \sim \mathcal{CN}(\mathbf{0}_N, \sigma_{RIS}^2 \mathbf{I}_N)$.

6.3.1 RIS-aided M-MIMO Channel Modeling

The RIS takes the form of a thin uniform squared planar array (USPA), featuring $N = N_h \times N_v$ total elements, where $N_h = N_v = \sqrt{N}$ elements in the horizontal and vertical directions, with $\sqrt{N}$ being a positive integer ($\sqrt{N} \in \mathbb{Z}_+$). Furthermore, the elements are vertically and horizontally equally spaced with spacing d_R. Besides, the BS is assumed to be equipped with a uniform linear array (ULA) of M total elements disposed in the x axis, *i.e.*, parallel to the RIS.

In the channel model for RIS-aided M-MIMO, we make the assumption of far-field wavefront propagation regime between the BS and the RIS panels, as well as between the RIS and the UEs, i.e., the planar wavefront is assumed in both links.

6.3.1.1 BS–RIS Link

To be more specific, we establish the channel between the BS and the RIS based on the Rician-fading model, given by [38–40]:

$$\boldsymbol{H}_1 = \sqrt{\frac{\beta_1 \kappa_1}{\kappa_1 + 1}} \overline{\boldsymbol{H}}_1 + \sqrt{\frac{\beta_1}{\kappa_1 + 1}} \widetilde{\boldsymbol{H}}_1 \tag{6.4}$$

where $\overline{\boldsymbol{H}}_1 \in \mathbb{C}^{M \times N}$ corresponds to the deterministic LoS channel component, $\widetilde{\boldsymbol{H}}_1 \in \mathbb{C}^{M \times N}$ to the Rayleigh-fading multipath component, $\kappa_1 \geq 0$ denotes the Rician κ-factor, and β_1 is the large-scale fading coefficient for this link specifically. The large-scale fading coefficient is given by:

$$\beta_1 = \frac{\beta_0}{d_{BR}^{\lambda_{BR}}} \tag{6.5}$$

in which β_0 is the path loss at a reference distance of 1 m, d_{BR}, and λ_{BR} is the distance and the path-loss exponent between the BS and RIS, respectively. The deterministic LoS component can be given through the steering vector of a two-dimensional uniform planar array (UPA). Let us consider the RIS centered in the origin of the Cartesian coordinates; therefore, each column of LoS channel matrix $\overline{\boldsymbol{H}}_1$ is given as:

$$\overline{\boldsymbol{H}}_1 = \boldsymbol{a}_B(\vartheta_B)\boldsymbol{a}_R(\vartheta_R, \varphi_R)^H \tag{6.6}$$

where ϑ_B is the azimuthal angle of departure (AoD) of the signal departing from the BS toward the RIS, and ϑ_R and φ_R are the azimuthal and elevation angle of arrival (AoA) at the RIS from the BS. The array response vector of the BS ULA and of the RIS UPA, are defined, respectively, as:

$$\boldsymbol{a}_B(\vartheta_B) = \left[1, e^{j\pi \frac{2d_B}{\lambda} \sin \vartheta_B}, \ldots, e^{j(M-1)\pi \frac{2d_B}{\lambda} \sin \vartheta_B}\right]^H \tag{6.7}$$

$$\begin{aligned} \boldsymbol{a}_R(\vartheta_R, \varphi_R) = &\left[1, e^{j\pi \frac{2d_R}{\lambda} \sin \vartheta_R \cos \varphi_R}, \ldots, e^{j(\sqrt{N}-1)\pi \frac{2d_R}{\lambda} \sin \vartheta_R \cos \varphi_R}\right]^H \\ &\otimes \left[1, e^{j\pi \frac{2d_R}{\lambda} \sin \varphi_R}, \ldots, e^{j(\sqrt{N}-1)\pi \frac{2d_R}{\lambda} \sin \varphi_R}\right]^H \end{aligned} \tag{6.8}$$

with d_B being the distance between the antenna elements at the BS. Moreover, the multipath component follows an uncorrelated Rayleigh distribution such that $\tilde{\mathbf{h}}_{1,i} \sim \mathcal{CN}(\mathbf{0}_N, \mathbf{I}_N)$, $\forall i \in \{1, \ldots, M\}$, with $\tilde{\mathbf{h}}_{1,i}$ being the ith column of matrix $\tilde{\mathbf{H}}_1$.

6.3.1.2 RIS–UE Link

The link between the RIS and UEs, $\boldsymbol{H}_2 = [\boldsymbol{h}_{2,1}\, \boldsymbol{h}_{2,2}\, \ldots\, \boldsymbol{h}_{2,K}]$, is also assumed to be Rician fading and given as:

$$\boldsymbol{h}_{2,k} = \sqrt{\frac{\beta_{2,k}\kappa_{2,k}}{\kappa_{2,k} + 1}} \overline{\boldsymbol{h}}_{2,k} + \sqrt{\frac{\beta_{2,k}}{\kappa_{2,k} + 1}} \widetilde{\boldsymbol{h}}_{2,k}, \quad \forall k \in \mathcal{K} \tag{6.9}$$

where $\overline{\mathbf{h}}_{2,k} \in \mathbb{C}^{N\times 1}$ corresponds to the deterministic LoS channel component between the RIS and the kth UE, $\widetilde{\boldsymbol{h}}_{2,k} \in \mathbb{C}^{N\times 1}$ to the Rayleigh-fading multipath component between RIS and kth UE, and $\kappa_{2,k}$ denotes the Rician κ-factor for this same link, with $\kappa_{2,k} \geq 0\ \forall k \in \mathcal{K}$. Besides, $\beta_{2,k}$ corresponds to the large-scale fading from the RIS to the kth UE, given as:

$$\beta_{2,k} = \frac{\beta_0}{d_{RU,k}^{\lambda_{RU}}} \tag{6.10}$$

with $d_{RU,k}$ being the distance between the RIS and kth UE, and λ_{RU} the path loss exponent between the RIS and UEs.

6.3.1.3 LoS Component

Similar to the BS and RIS channel model, the deterministic LoS component $\overline{\boldsymbol{h}}_{2,k}$ can be given by the steering vector:

$$\begin{aligned}\overline{\boldsymbol{h}}_{2,k} &= \boldsymbol{a}_{R,k}(\vartheta_{R,k}, \varphi_{R,k}) \\ &= \left[1, e^{j\pi \frac{2d_R}{\lambda} \sin\vartheta_R \cos\varphi_R}, \ldots, e^{j(\sqrt{N}-1)\pi \frac{2d_R}{\lambda} \sin\vartheta_R \cos\varphi_R}\right]^H \\ &\quad \otimes \left[1, e^{j\pi \frac{2d_R}{\lambda} \sin\varphi_R}, \ldots, e^{j(\sqrt{N}-1)\pi \frac{2d_R}{\lambda} \sin\varphi_R}\right]^H\end{aligned} \tag{6.11}$$

6.3.2 SE and EE Formulation in RIS-Assisted M-MIMO

In this subsection, we introduce two critical and crucial performance metrics for analyzing the performance of communication systems. We initiate the discussion with the concept of SE and then expand into EE.

6.3.2.1 Spectral Efficiency

To assess the wireless system performance, it is crucial to evaluate the capacity for transmitting bits per second per Hertz, namely as SE. This fundamental metric measures the efficiency of information transmission through a channel. The SE reflects the average number of bits transmitted per channel use across varying fading conditions, serving as a standard metric for evaluating communication system capabilities. Since for the RIS-assisted systems, the channel is a generalization of the conventional M-MIMO systems, the SE can be equally represented as the following:

$$SE_k = \log_2(1 + SINR_k), \qquad \left[\frac{\text{bit}}{\text{s} \cdot \text{Hz}}\right] \tag{6.12}$$

where the signal-to-interference-plus-noise ratio (SINR) of the kth UE, $SINR_k$, can be expressed as:

$$SINR_k = \frac{|\boldsymbol{w}_k^H \mathbf{h}_k|^2}{\sum_{j=1, j\neq K}^{K} |\boldsymbol{w}_j \mathbf{h}_k|^2 + |\boldsymbol{z}^H \boldsymbol{\Phi} \boldsymbol{h}_{2,k}|^2 + |n_k|^2} \tag{6.13}$$

Finally, we can define the system's normalized SR as the following:

$$R = \sum_{k=1}^{K} \log_2 \left(1 + \frac{|\boldsymbol{w}_k^H \mathbf{h}_k|^2}{\sum_{j=1, j\neq K}^{K} |\boldsymbol{w}_j \mathbf{h}_k|^2 + |\boldsymbol{z}^H \boldsymbol{\Phi} \boldsymbol{h}_{2,k}|^2 + |n_k|^2} \right) \tag{6.14}$$

6.3.2.2 Energy Efficiency

The metric for evaluating a system's sustainable capacity is referred to as EE. This metric essentially quantifies the number of bits that can be reliably transmitted per unit of energy, expressed as:

$$\text{EE} = \frac{\text{Normalized Sum Rate [bit/s/Hz]}}{\text{System Power Consumption [W]}} = \frac{\sum_k SE_k}{P_{total}} \qquad \left[\frac{\text{bit}}{\text{Joule} \cdot \text{Hz}}\right] \tag{6.15}$$

where P_{total} is the total power consumed by the communication system as detailed in Remark 6.2 and formulated in Section 6.3.2.3.

Remark 6.1 The EE optimization as a function of the amount of transmit RF power in (6.15) involves a ratio of a convex function in the numerator and an affine function in the denominator. Hence, one can formulate the EE optimization problem as a single-ratio problem, briefly revisited in Section 6.4.2.

Remark 6.2 The power consumption for RIS-assisted M-MIMO systems requires more detailed consideration than traditional M-MIMO systems since although the RIS technology achieves low power consumption, its consumption is not entirely negligible and should be thoroughly examined. Therefore, in Section 6.3.2.3, we further detail the adopted system power consumption model.

6.3.2.3 System's Power Consumption Model

Different from most prior works, which mostly consider entirely passive RIS, here, we adopt a more practical, realistic energy consumption model by taking into account two primary components: the power consumption of the BS and the power consumption related to the active RIS. Generically, the total power consumption model can be written as:

$$P_{total} = P_{BS} + P_{RIS} \tag{6.16}$$

The power consumption at the BS is related directly to three main factors: the constant power required for BS operation, i.e., site-cooling, control signaling, load-independent power of backhaul infrastructure, baseband processor, etc; the power necessary to run the circuit components attached to each antenna, such

as converters, mixers, filters, etc; and the RF transmit power allocated to the UEs [41], resulting in:

$$P_{BS} = P_{0,BS} + MP_M + \sum_{k=1}^{K} \varrho ||\boldsymbol{w}_k||^2 \tag{6.17}$$

where ϱ denotes the inefficiency of the transmit power amplifier.

On the other hand, for the hybrid RIS, each passive component can redirect the incident signal with a desired phase shift. In contrast, the active components are implemented by both power amplifier (PA) and phase shift control (PSC), thereby achieving simultaneous tuning over the phase and amplitude of the signal. By toggling the switches ON or OFF, the hybrid RIS elements can dynamically switch between active and passive modes, adapting to the practical requirements of various applications. Moreover, the RIS needs a controller,[2] which is required for receiving the external signals, processing data, and programming, as well as configuring the RIS unit cells. Overall, the total power consumption dissipated to operate the RIS consists of three parts; (**a**) one is the static power consumption generated by the FPGA control board and drive circuits, namely, P_{CB} [42, 43]; (**b**) the power consumption by the passive and active RIS unit cells, being, the power necessary for controlling the impedance of each element via an amplifier and phase turner, in order to configure the phase/amplitude of reflection; and (**c**) the active power for RF signal amplification. Accordingly, the power consumed at the active RIS can be expressed as:

$$P_{RIS} = P_{CB} + P_{pas} + P_{act} + \varrho P_{RIS}^{out} \tag{6.18}$$

where P_{RIS}^{out} is the signal RF power that departs from the RIS, given by [44]:

$$P_{RIS}^{out} = ||\boldsymbol{\Phi z}||^2 + \sum_{k=1}^{K} ||\boldsymbol{w}_k^H \boldsymbol{H}_1 \boldsymbol{\Phi}||^2 = \text{tr}\left(\boldsymbol{Z v v}^H \boldsymbol{Z}^H\right) + \sum_{k=1}^{K} \text{tr}(\boldsymbol{U}_k \boldsymbol{v v}^H \boldsymbol{U}_k^H) \tag{6.19}$$

where $\boldsymbol{Z} \triangleq \text{diag}(\boldsymbol{z})$ and $\boldsymbol{U}_k \triangleq \text{diag}(\boldsymbol{H}_1^H \boldsymbol{w}_k)$. Thereby, the total RF power amplification at the active RIS can be expressed as:

$$\begin{aligned} P_{RIS}^{out} &= \text{tr}\left(\boldsymbol{Z v v}^H \boldsymbol{Z}^H\right) + \sum_{k=1}^{K} \text{tr}\left(\boldsymbol{U}_k \boldsymbol{v v}^H \boldsymbol{U}_k^H\right) \\ &= \text{tr}\left(\boldsymbol{v v}^H \boldsymbol{Z}^H \boldsymbol{Z}\right) + \text{tr}\left(\boldsymbol{v v}^H \sum_{k=1}^{K} \boldsymbol{U}_k^H \boldsymbol{U}_k\right) \\ &= \text{tr}\left(\boldsymbol{v v}^H \boldsymbol{Q}\right), \\ &= \boldsymbol{v}^H \boldsymbol{Q} \boldsymbol{v} \end{aligned} \tag{6.20}$$

2 The controller includes a field programmable gate array (FPGA) and drive circuits.

where

$$\boldsymbol{Q} \triangleq \boldsymbol{Z}^H \boldsymbol{Z} + \sum_{k=1}^{K} \boldsymbol{U}_k^H \boldsymbol{U}_k \tag{6.21}$$

The power consumption of the passive elements is given by $P_{pas} = N_{pas} P_c$, where P_c represents the switch and control circuit power consumption at each reflecting passive element. On the other hand, the power consumption of the active elements is given by $P_{act} = N_{act}(P_{\mathrm{DC}} + P_c)$, where P_{DC} is the DC biasing power consumption at each active elements [4]. Therefore, Eq. (6.18) also can be written as a function of $\boldsymbol{v}$ as following[3]:

$$P_{RIS} = P_{CB} + N_{pas} P_c + N_{act}(P_{\mathrm{DC}} + P_c) + \varrho \boldsymbol{v}^H \boldsymbol{Q} \boldsymbol{v} \tag{6.22}$$

A detailed discussion on the static power consumption generated by the FPGA board and drive circuits P_{CB} is found in [42, 43].

6.4 Optimization Techniques

To fully clarify the proposed optimization strategy for tackling the EE active RIS-aided M-MIMO optimization problem, it is crucial to delve into some fundamental optimization techniques that act in our proposed solution. These techniques play essential roles in our approach to addressing the investigated problem, and an entire comprehension of their concepts is crucial for carefully understanding the proposed solution. The following provides a detailed review of these techniques, including lagrangian dual transform (LDT) and fractional single and multiple-ratio problems.

6.4.1 Lagrangian Dual Transform

In addressing the challenge posed by the sum-of-logarithms problem, specific techniques prove valuable in easing the management of the optimization problem, thereby enabling the possibility of finding a closed-form, low-complexity solution. Given that communication system-related problems frequently involve logarithmic function summation, finding any solution can be exceedingly challenging as the presence of logarithmic functions hinders analytical tractability and optimization. As a result, an optimization technique introduced by Shen and Yu [45], namely, LDT leverages the Lagrangian duality to externalize the argument of logarithm functions to the outside, eliminating the dependence

3 Herein, we assume that the RIS is unable to absorb the incident power. However, it is possible to utilize energy harvesting circuits embedded at the RIS. Therefore, $P_{RIS}^{out} \geq P_{RIS}^{in}$ always hold, with the equality when $|v_n| = 1, \forall n \in \mathcal{N}$.

of the variable of interest with the logarithmic functions, resulting in easier management and analytical tractability of the problem. To further understand the LDT, let us define the following target maximization problem:

$$\underset{\mathbf{x}}{\text{maximize}} \quad \sum_{\ell=1}^{L} \log\left(1+\frac{f_\ell(\mathbf{x})}{g_\ell(\mathbf{x})}\right) \tag{6.23}$$

$$\text{subject to} \quad h_i(\mathbf{x}) \leq 0, \quad i \in \{1,\dots,I\} \tag{6.23a}$$

where $f_\ell(\mathbf{x}) : \mathbb{C}^N \to \mathbb{R}_+$ is a non-negative function, and $g_\ell(\mathbf{x}) : \mathbb{C}^N \to \mathbb{R}_+^*$ is a positive function, $\forall \ell \in \{1,\dots,L\}$. It is important to observe that the ratio $f_\ell(\mathbf{x})/g_\ell(\mathbf{x})$ can have a physical interpretation as SINR in our context. The problem (6.23) is assumed to be a non-convex problem, with a nonconvex constraint (6.23a). According to [46], the problem (6.23) can be transformed in the following equivalent problem:

$$\underset{\mathbf{x},\boldsymbol{\alpha}}{\text{maximize}} \quad \sum_{\ell=1}^{L} \log(1+\gamma_\ell) - \sum_{\ell=1}^{L}\gamma_\ell + \sum_{\ell=1}^{L}(1+\gamma_\ell)\frac{f_\ell(\mathbf{x})}{f_\ell(\mathbf{x})+g_\ell(\mathbf{x})} \tag{6.24}$$

$$\text{subject to} \quad h_i(\mathbf{x}) \leq 0, \qquad \forall i \in \{1,\dots,I\} \tag{6.24a}$$

$$\gamma_\ell \geq 0, \qquad \forall \ell \in \{1,\dots,L\} \tag{6.24b}$$

where $\boldsymbol{\gamma}^{(t)} = [\gamma_1^{(t)}, \gamma_2^{(t)}, \dots, \gamma_L^{(t)}]^T$ is an auxiliary variable, which is iteratively updated, introduced for each ratio term $f_\ell(\mathbf{x}^{(t-1)})/g_\ell(\mathbf{x}^{(t-1)})$. It's important to note that the two problems, (6.23) and (6.24), are equivalent. In other words, at the convergence, the solution $\mathbf{x}$ to (6.23) is identical to the solution to (6.24), and their respective optimal objective values are also equal [[45], III-B]. Furthermore, it is worth highlighting that, according to the Karush-Kuhn-Tucker (KKT) conditions, we can obtain the following:

$$\frac{\partial\left(\sum_{\ell=1}^{L}\log(1+\gamma_\ell^{(t+1)}) - \sum_{\ell=1}^{L}\gamma_\ell^{(t+1)} + \sum_{\ell=1}^{L}\frac{(1+\gamma_\ell^{(t+1)})f_\ell(\mathbf{x}^{(t)})}{f_\ell(\mathbf{x}^{(t)})+g_\ell(\mathbf{x}^{(t)})}\right)}{\partial\gamma_\ell} = 0 \tag{6.25}$$

$$\gamma_\ell^{\star(t+1)} = \frac{f_\ell(\mathbf{x}^{(t)})}{g_\ell(\mathbf{x}^{(t)})} \tag{6.26}$$

This equivalence allows for a seamless transition between the two problem formulations while preserving the optimality.

6.4.2 Fractional Programming

Fractional programming theory is the branch of optimization theory concerned with the properties and optimization of fractional functions, i.e., a ratio of two generally nonlinear functions. They can be found in several areas and are generically

subdivided into two classes: single-ratio problems and multiple-ratio problems. Below, we review techniques designed to address these classes and their respective solution methodologies.

6.4.2.1 Single-Ratio Problems

Many transforms deal consistently with this type of problem; the most classical is named *Dinkelbach's* Transform [45–47]. For a better understanding, let us define the following optimization problem.

$$\underset{\mathbf{x}}{\text{maximize}} \quad \frac{f(\mathbf{x})}{g(\mathbf{x})} \tag{6.27}$$

$$\text{subject to} \quad h_i(\mathbf{x}) \leq 0, \qquad \forall i \in \{1, \dots, I\} \tag{6.27a}$$

where $f(\mathbf{x}) : \mathbb{C}^N \to \mathbb{R}_+$ and $g(\mathbf{x}) : \mathbb{C}^N \to \mathbb{R}_+^*$ are nonnegative function and positive function, respectively. The conventional approach for dealing with this FP is decoupling the numerator and denominator and treating it jointly. The *Dinkelbach's* transform reformulates the single-ratio problem (6.27) as the following:

$$\underset{\mathbf{x},\eta}{\text{maximize}} \quad f(\mathbf{x}) - \eta g(\mathbf{x}) \tag{6.28}$$

$$\text{subject to} \quad h_i(\mathbf{x}) \leq 0, \qquad \forall i \in \{1, \dots, I\} \tag{6.28a}$$

where η is an auxiliary variable that is iteratively updated by:

$$\eta^{(t)} = \frac{f(\mathbf{x}^{(t-1)})}{g(\mathbf{x}^{(t-1)})} \tag{6.29}$$

where t is the iteration index.

6.4.2.2 Multiple-Ratio Problems

Although the classic *Dinkelbach's* transform [47] works well for single-ratio problems, they cannot be easily extended to the multiple-ratio problems, since for single-ratio objective functions, the optimal solution is the same for the original FP and the transformed problem, but not the value of the objective function of both. To solve the multi-ratio problem, several different techniques have been proposed, such as *Quadratic Transform* [45] and [48]. Herein, we focus on the technique developed by Jong [48]. Let us define the following multi-ratio problem:

$$\underset{\mathbf{x}}{\text{maximize}} \quad \sum_{\ell=1}^{L} \frac{f_\ell(\mathbf{x})}{g_\ell(\mathbf{x})} \tag{6.30}$$

$$\text{subject to} \quad h_i(\mathbf{x}) \leq 0, \qquad i \in \{1, \dots, I\} \tag{6.30a}$$

where $f_\ell(\mathbf{x}) : \mathbb{C}^N \to \mathbb{R}_+$ and $g_\ell(\mathbf{x}) : \mathbb{C}^N \to \mathbb{R}_+^*$, $\forall \ell \in \{1, \dots, L\}$. In [48], the authors proposed an iterative solution in order to solve problem (6.30), where the

equivalent problem can be given as:

$$\underset{\mathbf{x},\mathbf{u},\boldsymbol{\beta}}{\text{maximize}} \quad \sum_{\ell=1}^{L} u_\ell \left(f_\ell(\mathbf{x}) - \beta_\ell g_\ell(\mathbf{x})\right) \tag{6.31}$$

$$\text{subject to} \quad h_i(\mathbf{x}) \leq 0, \qquad i \in \{1, \ldots, I\} \tag{6.31a}$$

where $\mathbf{u}$ and $\boldsymbol{\beta}$ are auxiliary variables which are iteratively updated as:

$$u_\ell^{(t+1)} = \frac{1}{g_\ell(\mathbf{x}^{(t)})}, \quad \forall \ell = 1, \ldots, L \tag{6.32}$$

$$\beta_\ell^{(t+1)} = \frac{f_\ell(\mathbf{x}^{(t)})}{g_\ell(\mathbf{x}^{(t)})}, \quad \forall \ell = 1, \ldots, L \tag{6.33}$$

6.5 Problem Formulation

Given addressing all the arguments above, regarding EE exposed in Section 6.1, we formulate an optimization problem whose main objective is optimizing the reflecting coefficients of an active RIS to assess the necessary number of RIS elements that should be selected to outperform the entirely passive RIS in terms of EE. The idea is to reduce the number of operating elements in the RIS in view of reducing their power consumption while increasing the total SR by amplifying the incoming signal intended for the UEs. Hence, such an objective can be formulated as the following optimization problem, denoted as $\mathcal{P}_0$:

$$\mathcal{P}_0\colon \underset{\boldsymbol{v}}{\text{maximize}} \quad \frac{\sum_{k=1}^{K} \log_2\left(1 + \frac{|\boldsymbol{w}_k^H \boldsymbol{h}_k|^2}{\sum_{j=1, j\neq K}^{K} |\boldsymbol{w}_j \boldsymbol{h}_k|^2 + |\boldsymbol{z}^H \boldsymbol{\Phi} \boldsymbol{h}_{2,k}|^2 + |n_k|^2}\right)}{\begin{array}{l} P_{0,BS} + P_{CB} + MP_M + \varrho\left(\sum_{k=1}^{K} ||\boldsymbol{w}_k||^2 + \boldsymbol{v}^H \boldsymbol{Q} \boldsymbol{v}\right) \\ + N_{act}(P_{\text{DC}} + P_c) + N_{pas} P_c \end{array}} \tag{6.34}$$

$$\text{subject to} \quad \boldsymbol{v}^H \boldsymbol{Q} \boldsymbol{v} \leq P_{\max}^{RIS} \tag{6.34a}$$

$$|v_n| \leq \alpha_{\max}, \qquad \forall n \in \mathcal{N}_a \tag{6.34b}$$

$$|v_n| = 1, \qquad \forall n \in \mathcal{N}_p \tag{6.34c}$$

Constraint (6.34a) considers the maximum amplification of power provided by the active RIS (forward power budget at the RIS), while constraint (6.34b) considers the maximum amplitude gain imposed by each active element of the RIS, constraint (6.34c) consider the amplitude of passive elements. One should notice that problem $\mathcal{P}_0$ is more challenging and hardest to solve than the EE optimization with entirely passive RIS since the RIS configuration vector also appears in the denominator of the objective function of Eq. (6.35). In Section 6.6, we aim to develop an efficient approach to handle $\mathcal{P}_0$.

6.6 Proposed Solution

In Section 6.6.1, we introduce the proposed algorithm, namely, analytical-FP-based active beamforming design, which utilizes the FP optimization technique to obtain closed-form solutions for amplitude and phase of each active element at the RIS. Specifically, the proposed closed-form solutions for EE optimization problems incorporates auxiliary variables derived from Dilkelbach's Transform, LDT, and from the methodology outlined in [48]. This integration strategically molds the objective function into a convex form, facilitating analytical optimization approaches.

Subsequently, in Section 6.6.2, we conduct a comprehensive analysis of the algorithm's complexity. This examination provides valuable insights, emphasizing the algorithm's efficiency and suitability for real-world applications.

Finally, in Section 6.7, we present a comparative evaluation of the proposed algorithm's performance within typical RIS-aided M-MIMO channel and system scenarios. This comparative analysis validates and illustrates the algorithm's efficacy across a range of practical and diverse operating conditions.

6.6.1 Analytical-FP-Based Solution Method

Before delving directly into the problem, it is useful to establish a more concise nomenclature. Therefore, firstly, for the sake of tractability, we shall rewrite Eq. (6.13) as follows:

$$SINR_k = \frac{|\boldsymbol{w}_k^H \boldsymbol{h}_k|^2}{\sum_{j=1, j\neq K}^{K} |\boldsymbol{w}_j \boldsymbol{h}_k|^2 + |\boldsymbol{z}^H \boldsymbol{\Phi} \boldsymbol{h}_{2,k}|^2 + |n_k|^2} = \frac{\boldsymbol{v}^H \boldsymbol{A}_k \boldsymbol{v}}{\boldsymbol{v}^H \boldsymbol{B}_k \boldsymbol{v} + |n_k|^2} \tag{6.35}$$

where with few analytical manipulations, we obtain that

$$\boldsymbol{A}_k \triangleq \boldsymbol{H}_{2,k}^H \boldsymbol{H}_1^H \boldsymbol{w}_k \boldsymbol{w}_k^H \boldsymbol{H}_1 \boldsymbol{H}_{2,k} \tag{6.36}$$

$$\boldsymbol{B}_k \triangleq \boldsymbol{H}_{2,k}^H \boldsymbol{z}\boldsymbol{z}^H \boldsymbol{H}_{2,k} + \sum_{j=1, j\neq k}^{K} \boldsymbol{H}_{2,k}^H \boldsymbol{H}_1^H \boldsymbol{w}_j \boldsymbol{w}_j \boldsymbol{H}_1 \boldsymbol{H}_{2,k} \tag{6.37}$$

with $\mathbf{H}_{2,k} = \text{diag}(\mathbf{h}_{2,k})$. This manipulation enables us to effortlessly address our problem, thereby facilitating the derivation of subsequent equations. Rewriting problem given by Eq. (6.34), we have the following:

$$\begin{aligned} \mathcal{P}_0\text{: } \underset{\boldsymbol{v}}{\text{maximize}} \quad & \frac{\sum_{k=1}^{K} \log_2 \left(1 + \frac{\boldsymbol{v}^H \boldsymbol{A}_k \boldsymbol{v}}{\boldsymbol{v}^H \boldsymbol{B}_k \boldsymbol{v} + |n_k|^2}\right)}{\hat{P} + \varrho \boldsymbol{v}^H \boldsymbol{Q} \boldsymbol{v}} \\ \text{subject to} \quad & \text{(6.34a), (6.34b)} \end{aligned} \tag{6.38}$$

where we define $\hat{P} \triangleq \sum_{k=1}^{K} \varrho ||\boldsymbol{w}_k||^2 + P_{0,\mathrm{BS}} + P_{CB} + MP_{\mathrm{M}} + N_{act}(P_{\mathrm{DC}} + P_c) + N_{pas}P_c$. One can see that Problem (6.38) is a nonconvex problem.

Given proposing a new solution for $\mathcal{P}_0$, we apply some optimization transform techniques, namely, Dinkelbach transform, Lagrangian Dual transform, and Multiple-Ratio function transform, followed by our proposed analytical optimization methodology, which will be discussed through Sections 6.6.1.1–6.6.1.4.

6.6.1.1 Dinkelbach Transform

We should observe that $\mathcal{P}_0$, given by Eq. (6.38), is a single ratio problem. Therefore, a pre-processing step should be applied to the objective function before solving the optimization process due to its intractable fractional form. To decouple the numerator and denominator of Eq. (6.38), we employ the classic Dinkelbach's methodology [47]. Specifically, by introducing an auxiliary variable $\eta \in \mathbb{R}$, according to Section 6.4.2, the original problem can be equivalently reformulated as:

$$\begin{aligned} \mathcal{P}_1\colon \underset{\boldsymbol{v},\eta}{\text{maximize}} \quad & \sum_{k=1}^{K} \log_2\left(1 + \frac{\boldsymbol{v}^H \boldsymbol{A}_k \boldsymbol{v}}{\boldsymbol{v}^H \boldsymbol{B}_k \boldsymbol{v} + |n_k|^2}\right) - \eta\left(\hat{P} + \varrho \boldsymbol{v}^H \boldsymbol{Q} \boldsymbol{v}\right) \\ \text{subject to} \quad & \text{(6.34a)},\ \text{(6.34b)} \end{aligned} \tag{6.39}$$

Thus, to solve $\mathcal{P}_1$, we optimize the prime variable $\boldsymbol{v}$ and auxiliary variable η iteratively. According to Eq. (6.29), given $\boldsymbol{v}$, the optimal η can be directly obtained as:

$$\eta^{\star} = \frac{\sum_{k=1}^{K} \log_2\left(1 + \frac{\boldsymbol{v}^H \boldsymbol{A}_k \boldsymbol{v}}{\boldsymbol{v}^H \boldsymbol{B}_k \boldsymbol{v} + |n_k|^2}\right)}{\hat{P} + \varrho \boldsymbol{v}^H \mathbf{Q} \boldsymbol{v}} \tag{6.40}$$

Now, we deal with optimizing $\boldsymbol{v}$ with a given η. In this way, we should see that $\mathcal{P}_1$ is still hard to solve. Moreover, it is composed of differences between a multiple-ratio function term and a quadratic form. Therefore, aiming to externalize the optimization variable $\boldsymbol{v}$ from the log function, we utilize the LDT technique.

6.6.1.2 Lagrangian Dual Transform

Applying the LDT technique in $\mathcal{P}_1$, given by Eq. (6.39), as explained in Section 6.4.1, we can introduce the auxiliary variable $\boldsymbol{\gamma}$, and rewrite $\mathcal{P}_1$ in an equivalent way, obtaining the following optimization problem, which we denote as $\mathcal{P}_2$

$$\begin{aligned} \mathcal{P}_2\colon \underset{\boldsymbol{v},\boldsymbol{\gamma}}{\text{maximize}} \quad & \sum_{k=1}^{K} \log_2(1+\gamma_k) - \gamma_k + \frac{(1+\gamma_k)\boldsymbol{v}^H \boldsymbol{A}_k \boldsymbol{v}}{\boldsymbol{v}^H\left(\boldsymbol{A}_k + \boldsymbol{B}_k\right)\boldsymbol{v} + |n_k|^2} - \eta\left(\hat{P} + \varrho \boldsymbol{v}^H \boldsymbol{Q} \boldsymbol{v}\right) \\ \text{subject to} \quad & \text{(6.34a)}, \text{(6.34b)} \end{aligned} \tag{6.41}$$

where the γ that maximizes $\mathcal{P}_2$, accordingly to Eq. (6.26), at the ℓth iteration is given by:

$$\gamma_k^{\star} = \frac{\boldsymbol{v}^H \boldsymbol{A}_k \boldsymbol{v}}{\boldsymbol{v}^H \boldsymbol{B}_k \boldsymbol{v} + |n_k|^2}, \qquad \forall k \in \mathcal{K} \tag{6.42}$$

We now observe that $\mathcal{P}_2$, given by Eq. (6.41) is composed by a term of multiple ratio function subtracted by a quadratic term in $\boldsymbol{v}$. In view of linearize the multiple ratio function in $\mathcal{P}_2$, we apply the method described in Section 6.4.2.

6.6.1.3 Multiple-Ratio Function Transform

Because of linearizing the multiple-ratio function in $\mathcal{P}_2$, we apply the multiple-ratio function transform proposed in [48]. Therefore, by introducing the auxiliary variables, $\boldsymbol{\beta}$, and $\boldsymbol{u}$, we can recast $\mathcal{P}_2$ as the equivalent following problem, denoted as $\mathcal{P}_3$

$$\begin{aligned} \mathcal{P}_3\colon \underset{\boldsymbol{v},\boldsymbol{u},\boldsymbol{\beta}}{\text{maximize}} \quad & \sum_{k=1}^{K} \log_2\left(1+\gamma_k\right) - \gamma_k + u_k \Big[(1+\gamma_k)\boldsymbol{v}^H \boldsymbol{A}_k \boldsymbol{v} \\ & - \beta_k \left(\boldsymbol{v}^H \left(\boldsymbol{A}_k + \boldsymbol{B}_k\right)\boldsymbol{v} + |n_k|^2\right)\Big] - \eta\left(\hat{P} + \varrho \boldsymbol{v}^H \boldsymbol{Q} \boldsymbol{v}\right) \\ \text{subject to} \quad & (6.34a),\ (6.34b),\ (6.34c) \end{aligned} \tag{6.43}$$

The β_k and u_k that maximize $\mathcal{P}_3$ at the ℓth iteration can be obtained by the KKT conditions, and given accordingly to Eqs. (6.32) and (6.33) as:

$$\beta_k^{\star} = \frac{(1+\gamma_k)\boldsymbol{v}^H \boldsymbol{A}_k \boldsymbol{v}}{\boldsymbol{v}^H \left(\boldsymbol{A}_k + \boldsymbol{B}_k\right)\boldsymbol{v} + |n_k|^2}, \qquad \forall k \in \mathcal{K} \tag{6.44}$$

$$u_k^{\star} = \frac{1}{\boldsymbol{v}^H \left(\boldsymbol{A}_k + \boldsymbol{B}_k\right)\boldsymbol{v} + |n_k|^2}, \qquad \forall k \in \mathcal{K} \tag{6.45}$$

Reorganizing $\mathcal{P}_3$ in a more compact form, given $\eta, \boldsymbol{\gamma}, \boldsymbol{\beta}$, and $\boldsymbol{u}$ we arrive at the following equivalent problem which is a quadratic problem

$$\begin{aligned} \mathcal{P}_3\colon \underset{\boldsymbol{v}}{\text{maximize}} \quad & \boldsymbol{v}^H \boldsymbol{C} \boldsymbol{v} \\ \text{subject to} \quad & (6.34a),\ (6.34b),\ (6.34c) \end{aligned} \tag{6.46}$$

where the matrix $\boldsymbol{C}$ can be directly computed as the following:

$$\boldsymbol{C} = -\eta\varrho\boldsymbol{Q} + \sum_{k=1}^{K} u_k(1+\gamma_k)\boldsymbol{A}_k - u_k\beta_k\left(\boldsymbol{A}_k + \boldsymbol{B}_k\right) \tag{6.47}$$

Notice that the matrix $\boldsymbol{C} \prec \boldsymbol{0}$, if and only if $(1+\gamma_k)\boldsymbol{A}_k - \beta_k\left(\boldsymbol{A}_k - \boldsymbol{B}_k\right) \prec \boldsymbol{0}$, given that $\boldsymbol{A}_k, \boldsymbol{B}_k$, and $\boldsymbol{Q}$ are positive defined matrices. Therefore, one can conclude that $\boldsymbol{P}_3$ represents a non-convex quadratically constrained quadratic programming

(QCQP). One potential strategy to tackle $\mathcal{P}_3$, is utilizing the conventional SDR methodology, as well done in [49]. Nonetheless, in this work, we proposed a **novel closed-form solution for both phase and amplitude of each active element of RIS**, which is further explained in Section 6.6.1.4.

6.6.1.4 Proposed Analytical Methodology

To solve $\mathcal{P}_3$ efficiently and with minimal complexity, we adopt the methodology proposed by de Souza and Abrão [14], extending their closed-form solution for phase and deriving a new closed-form solution for the amplitude of each RIS active element. This methodology optimizes the nth element of $\boldsymbol{v}$ while keeping the others constant. The process is iterative and continues until the objective function converges.

Initially, we observe that $\mathcal{P}_3$ can be equivalently transformed into the following optimization problem:

$$\begin{aligned} &\underset{\boldsymbol{v}}{\text{maximize}} \;\; \boldsymbol{v}^H \boldsymbol{C} \boldsymbol{v} \equiv \underset{\boldsymbol{v}}{\text{maximize}} \; tr(\boldsymbol{C}\boldsymbol{V}), \\ &\text{subject to} \qquad (6.34a),\ (6.34b),\ rank(\boldsymbol{V}) = 1 \end{aligned} \tag{6.48}$$

with $\boldsymbol{V} = \boldsymbol{v}\boldsymbol{v}^H$, where the following constraints $rank(\boldsymbol{V}) = 1$ must be attained.

Proceeding conveniently, one can rewritten $\boldsymbol{v}$ as the following manner:

$$\boldsymbol{v} = \left[\hat{\boldsymbol{v}}_n^H,\ \alpha_n e^{-j\theta_n},\ \widetilde{\boldsymbol{v}}_n^H\right]^H \tag{6.49}$$

where $\hat{\boldsymbol{v}}_n \in \mathbb{C}^{n-1}$ and $\widetilde{\boldsymbol{v}}_n \in \mathbb{C}^{N-n}$ are, respectively, defined as $\hat{\boldsymbol{v}}_n \triangleq [\boldsymbol{v}]_{1:(n-1)}$ and $\widetilde{\boldsymbol{v}}_n \triangleq [\boldsymbol{v}]_{(n+1):N}$. This alternative notation enables us to look for the nth element of $\boldsymbol{v}$, $\alpha_n e^{j\theta_n}$. Therefore, by utilizing Eq. (6.49), one can rewrite $\boldsymbol{V}$ as:

$$\boldsymbol{V} = \boldsymbol{v}\boldsymbol{v}^H = \begin{bmatrix} \hat{\boldsymbol{v}}_n \hat{\boldsymbol{v}}_n^H & \alpha_n e^{-j\theta_n} \hat{\boldsymbol{v}}_n & \hat{\boldsymbol{v}}_n \widetilde{\boldsymbol{v}}_n^H \\ \alpha_n e^{j\theta_n} \hat{\boldsymbol{v}}_n^H & \alpha_n^2 & \alpha_n e^{j\theta_n} \widetilde{\boldsymbol{v}}_n^H \\ \widetilde{\boldsymbol{v}}_n \hat{\boldsymbol{v}}_n^H & \alpha_n e^{-j\theta_n} \widetilde{\boldsymbol{v}}_n & \widetilde{\boldsymbol{v}}_n \widetilde{\boldsymbol{v}}_n^H \end{bmatrix} \tag{6.50}$$

Following the same idea, the matrix $\boldsymbol{C}$ can be equivalently decomposed in sub-matrices and written as:

$$\boldsymbol{C} = \begin{bmatrix} \boldsymbol{C}_1 & \boldsymbol{c}_2 & \boldsymbol{C}_3 \\ \boldsymbol{c}_2^H & C_4 & \boldsymbol{c}_5 \\ \boldsymbol{C}_3^H & \boldsymbol{c}_5^H & \boldsymbol{C}_6 \end{bmatrix}, \text{ with } \begin{cases} \boldsymbol{C}_1 = [\boldsymbol{C}]_{1:(n-1),1:(n-1)} & \in \mathbb{C}^{(n-1)\times(n-1)} \\ \boldsymbol{c}_2 = [\boldsymbol{C}]_{1:(n-1),n} & \in \mathbb{C}^{(n-1)\times 1} \\ \boldsymbol{C}_3 = [\boldsymbol{C}]_{1:(n-1),(n+1):N} & \in \mathbb{C}^{(n-1)\times(N-n)} \\ C_4 = [\boldsymbol{C}]_{n,n} & \in \mathbb{C} \\ \boldsymbol{c}_5 = [\boldsymbol{C}]_{n,(n+1):N} & \in \mathbb{C}^{1\times(N-n)} \\ \boldsymbol{C}_6 = [\boldsymbol{C}]_{(n+1):N,(n+1):N} & \in \mathbb{C}^{(N-n)\times(N-n)} \end{cases} \tag{6.51}$$

Therefore, realizing the product of $\boldsymbol{CV}$ and after some basic algebraic manipulations, one obtains the following representation of $tr(\boldsymbol{CV})$:

$$\begin{aligned} tr(\boldsymbol{CV}) &= tr\left(\boldsymbol{C}_1\hat{\boldsymbol{v}}_n\hat{\boldsymbol{v}}_n^H + \alpha_n e^{j\theta_n}\boldsymbol{c}_2\hat{\boldsymbol{v}}_n^H + \boldsymbol{C}_3\widetilde{\boldsymbol{v}}_n\hat{\boldsymbol{v}}_n^H\right) \\ &\quad + tr\left(\alpha_n e^{-j\theta_n}\boldsymbol{c}_2^H\hat{\boldsymbol{v}}_n + \alpha_n^2 C_4 + \alpha_n e^{-j\theta_n}\boldsymbol{c}_5\widetilde{\boldsymbol{v}}_n\right) \\ &\quad + tr\left(\boldsymbol{C}_3^H\hat{\boldsymbol{v}}_n\widetilde{\boldsymbol{v}}_n^H + \alpha_n e^{j\theta_n}\boldsymbol{c}_5^H\widetilde{\boldsymbol{v}}_n^H + \boldsymbol{C}_6\widetilde{\boldsymbol{v}}_n\widetilde{\boldsymbol{v}}_n^H\right) \\ &= \alpha_n^2 C_4 + \alpha_n e^{-j\theta_n}\left(\boldsymbol{c}_2^H\hat{\boldsymbol{v}}_n + \boldsymbol{c}_5\widetilde{\boldsymbol{v}}_n\right) + \alpha_n e^{j\theta_n} tr\left(\boldsymbol{c}_2\hat{\boldsymbol{v}}_n^H + \boldsymbol{c}_5^H\widetilde{\boldsymbol{v}}_n^H\right) \\ &\quad + tr\left(\boldsymbol{C}_1\hat{\boldsymbol{v}}_n\hat{\boldsymbol{v}}_n^H + \boldsymbol{C}_3\widetilde{\boldsymbol{v}}_n\hat{\boldsymbol{v}}_n^H\right) + tr\left(\boldsymbol{C}_3^H\hat{\boldsymbol{v}}_n\widetilde{\boldsymbol{v}}_n^H + \boldsymbol{C}_6\widetilde{\boldsymbol{v}}_n\widetilde{\boldsymbol{v}}_n^H\right) \end{aligned} \tag{6.52}$$

Through careful manipulation of Eq. (6.52), one can separate and organize its terms, thereby illuminating a critical insight: the task of maximizing the expression $tr(\boldsymbol{CV})$ with respect to the variable $\upsilon_n = \alpha_n e^{j\theta_n}$ can be elegantly recast as follows:

$$\underset{\theta_n,\alpha_n}{\text{maximize}} \quad \alpha_n^2 C_4 + 2\alpha_n \mathbb{R}\{e^{-j\theta_n}(\boldsymbol{c}_2^H\hat{\boldsymbol{v}}_n + \boldsymbol{c}_5\widetilde{\boldsymbol{v}}_n)\} + \Pi \tag{6.53}$$

$$\text{subject to} \quad \alpha_n^2 Q_4 + 2\alpha_n \mathbb{R}\{e^{-j\theta_n}(\boldsymbol{q}_2^H\hat{\boldsymbol{v}}_n + \boldsymbol{q}_5\widetilde{\boldsymbol{v}}_n)\} + \psi \le 0 \tag{6.53a}$$

$$\alpha_n \ge 1 \tag{6.53b}$$

where, $\Pi = tr\left(\boldsymbol{C}_1\hat{\boldsymbol{v}}_n\hat{\boldsymbol{v}}_n^H + \boldsymbol{C}_3\widetilde{\boldsymbol{v}}_n\hat{\boldsymbol{v}}_n^H\right) + tr\left(\boldsymbol{C}_3^H\hat{\boldsymbol{v}}_n\widetilde{\boldsymbol{v}}_n^H + \boldsymbol{C}_6\widetilde{\boldsymbol{v}}_n\widetilde{\boldsymbol{v}}_n^H\right)$, is a constant which does not depend of α_n, and $\psi = tr\left(\boldsymbol{Q}_1\hat{\boldsymbol{v}}_n\hat{\boldsymbol{v}}_n^H + \boldsymbol{Q}_3\widetilde{\boldsymbol{v}}_n\hat{\boldsymbol{v}}_n^H\right) + tr\left(\boldsymbol{Q}_3^H\hat{\boldsymbol{v}}_n\widetilde{\boldsymbol{v}}_n^H + \boldsymbol{Q}_6\widetilde{\boldsymbol{v}}_n\widetilde{\boldsymbol{v}}_n^H\right)$ with $\boldsymbol{Q}_1, \boldsymbol{q}_2, \boldsymbol{Q}_3, \boldsymbol{q}_5$, and $\boldsymbol{Q}_6$ being defined similar to Eq. (6.51), however, for matrix $\boldsymbol{Q}$. It should be noted that Eq. (6.53a) denotes the constraint (6.34b) as a function of α_n and θ_n.

The expression (6.54) encapsulates a fundamental optimization challenge, which is crucial to our analysis. By looking specifically for υ_n, we can see that the amplitude coefficient obeys a second-order equation, while the phase coefficient can be obtained by phase canceling. This reformulation simplifies the problem-solving process and enables us to find closed-form solutions for both angle and phase variables, enabling a deeper understanding of the problem at hand. As we delve into the intricacies of this maximization task, we uncover valuable insights that contribute to decision-making and efficient resource allocation in practical scenarios with low complexity. Therefore, maximizing Eq. (6.53) regarding to θ_n and α_n can be readily obtained easily as:

$$\theta_n^\star = \angle\left(\boldsymbol{c}_2^H\hat{\boldsymbol{v}}_n + \boldsymbol{c}_5\widetilde{\boldsymbol{v}}_n\right), \ \forall n \in \mathcal{N} \quad \alpha_n^\star = -\frac{2\mathbb{R}\{e^{-j\theta_n}(\boldsymbol{c}_2^H\hat{\boldsymbol{v}}_n + \boldsymbol{c}_5\widetilde{\boldsymbol{v}}_n)\}}{C_4}, \ \forall n \in \mathcal{N}_a \tag{6.54}$$

The complete process involves sweeping through each element of the vector $\boldsymbol{v}$, $\upsilon_n = \alpha_n e^{j\theta_n}$, computing its phase and amplitude coefficients using Eq. (6.54) while keeping the others constant. This iterative process continues until the convergence of the objective function $tr(\boldsymbol{CV})$.

Based on the above derivations, the overall FP-based Amplitude/Phase Beamforming design algorithm is summarized in Algorithm 6.1. By appropriately initializing the variable $\boldsymbol{v}$ and the BS transmit power $\boldsymbol{p}$, the RIS reflection/amplification matrix $\boldsymbol{\Phi} = \text{diag}(\boldsymbol{v})$ is iteratively updated, until the EE of the RIS-aided M-MIMO system converges.

Algorithm 6.1: FP-based Amplitude/Phase Beamforming Design

Input: $\boldsymbol{p}$, $\mathbf{A}_k$, $\mathbf{B}_k$, $\forall k \in \{1, \ldots, K\}$
Set $\ell = 1$;
Set feasible value for $\boldsymbol{v}^{(\ell-1)}$;
Set $\eta^{(\ell-1)} = 0$;
repeat
  Step 1: Compute $\eta^{\star(\ell)}$ by Eq. (6.40);
  Step 2: Update $\boldsymbol{\gamma}^{\star(\ell)}$ by Eq. (6.42);
  Step 3: Compute $\boldsymbol{\beta}^{\star(\ell)}$ by Eq. (6.44);
  Step 4: Update $\boldsymbol{u}^{\star(\ell)}$ by Eq. (6.45);
  Step 5: Compute $\boldsymbol{C}^{(\ell)}$ by Eq. (6.47);
  while $\left| tr\left(\boldsymbol{C}^{(\ell)}\boldsymbol{V}^{(\ell)}\right) - tr\left(\boldsymbol{C}^{(\ell)}\boldsymbol{V}^{(\ell-1)}\right)\right| < \epsilon$ **do**
    for n $\in \mathcal{N}$ **do**
      Step 6: Compute $v_n = \alpha_n^{\star} e^{j\theta_n^{\star}}$ with $\theta_n^{\star}$ and $\alpha_n^{\star}$ based on Eq. (6.54);
    end for
  end while
  Step 7: Update $\eta^{\star(\ell)}$ by Eq. (6.40);
  Step 8: $\ell = \ell + 1$;
until $|\eta^{\star(\ell)} - \eta^{\star(\ell-1)}| < \epsilon$
Output: $\boldsymbol{v}^{\star} = [\alpha_1^{\star} e^{-j\theta_1^{\star}}, \alpha_2^{\star} e^{-j\theta_2^{\star}}, \ldots, \alpha_N^{\star} e^{-j\theta_N^{\star}}]^H$

6.6.2 Complexity

So far, we have completed the design of active RIS phase-shift matrix $\boldsymbol{\Phi}$. To clarify this scheme procedure, we summarize the main ideas of the proposed FP-based amplitude/phase beamforming design algorithm as follows. First, by fixing η, we can obtain $\boldsymbol{\gamma}$, $\boldsymbol{\beta}$, and $\boldsymbol{u}$, with closed-form expressions, and the RIS phase-shift matrix $\boldsymbol{v}$ by solving $\mathcal{P}_4$, as illustrated in Algorithm 6.1. The alternating iterating procedure is repeated among four variables until the termination condition is reached. Herein, we describe the complexity of the proposed iterative algorithm. It is known that, the complexity to update $\boldsymbol{\gamma}$, $\boldsymbol{\beta}$, and $\boldsymbol{u}$ are $\mathcal{O}(2KN^2)$, $\mathcal{O}(2KN^2)$, and $\mathcal{O}(KN^2)$, respectively. Besides, the η updating and finding the angles and phases

requires $\mathcal{O}(3KN^2)$ and $\mathcal{O}(N)$, respectively. Therefore, the overall complexity is given by $\mathcal{O}\left(\left(8LKN^2+N\right)\ln(\frac{1}{\epsilon})\right)$ Floating Point Operations (FLOPs), where L denotes the number of loop iterations.

6.7 Numerical Results

Herein, in this section, we illustrate simulation results in view to demonstrate the effectiveness of the proposed FP-based amplitude/phase beamforming design algorithm, where the active RIS amplitude/phase vector is obtained by running Algorithm 6.1. Given the proposed analytical optimization technique, we adopt the method proposed in [49] where, for reference, we solve the SDR problem via CVX solver in MATLAB.

For the simulation setup, we assume that the UEs are evenly located on the quarter-circle centered on $(x, y) = (0\text{ m}, 0\text{ m})$ of radius 10 m; the BS is located at $(-10\text{ m}, 5\text{ m})$ and the RIS is located at the origin $(0\text{ m}, 0\text{ m})$. For the BS–RIS link, we defined $\beta_0^{BR} = 10^{-3}$ and $\lambda^{BR} = 2$, while for the RIS–UEs link, we assume $\beta_0^{RU} = 1e^{-3}$ and $\lambda^{RU} = 2.5$, Figure 6.2. Unless specified otherwise, the remainder of the parameters are listed in Table 6.3. Aiming for a fair comparison, we assume the same power budget for entirely passive RIS and active RIS, where the maximum power for RIS amplification, $P_{\max}^{RIS}$, is given by $P_{\max}^{RIS} = \tau_{RIS} P_{TX}$, where $\tau_{RIS} \in [0, 1]$.

6.7.1 Efficiency of the Proposed Algorithm

Initially, in Figure 6.3, we assess and compare the EE of both active/passive RIS as a function of transmit budget power P_{TX}. For each point along the curve, we optimize the power of reflection of the active RIS array with two different methods: the analytical approach proposed in this study, denoted as "Active RIS – Analytical (prop.)," and the SDR method proposed in [49], denoted as "Active RIS–SDR [49]." For the passive RIS, we optimize the phase-shift angles using the conventional algorithm proposed in [14], denoted as "Passive RIS." Additionally, we also include the "Random RIS" as the entirely passive RIS assigned random precoding and random RIS reflecting coefficients matrix. Throughout this section, we denote the SDR, proposed method, passive RIS, and random RIS with the colors blue, red, green, and pink, respectively.

In this scenario, we consider $N = 64$ reflective elements for both passive and active RISs. Specifically for the active RIS we consider $N_{act} = 49$ and $N_{pas=15}$. The elements are randomly assigned to operate in active and passive in each MCs. We can see the importance of optimizing the phase of RIS, regardless of whether they are passive or active. Furthermore, notably, our analytical method demonstrates remarkable efficacy, especially in the low-power regime, where we can see

Table 6.3 List of simulation parameters.

Parameter	Description
$P_{\text{TX}} = [10 : 5 : 45]$ dBm	Maximum power budget at BS
$\sigma_k^2 = -95$ dBm	Noise variance at UEs, $\forall k \in \mathcal{K}$
$\sigma_{RIS}^2 = -80$ dBm	Noise variance at RIS
$K = 5$	Numbers of UEs
$M = 128$	Number of antennas at BS
$N = 64$	Number of reflecting meta-surfaces elements
$\varrho = 1.2$	Power amplifier inefficiency
$P_{0,BS} = 9$ dBW	Fixed power consumption at BS
$P_{\text{M}} = 1$ W	Power consumed by a BS transceiver chain
$P_{\text{CB}} = 4.8$ W	Power consumed by control board
$P_{DC} = 20$ dBm	DC biasing power consumption at each element
$P_c = 10$ dBm	Power of the switch and control circuit at each element
$\alpha_{\max} = 10$	Maximum amplitude gain
$\kappa_1 = 0.1$	Rician coefficient for BS–RIS link
$\kappa_{2,k} = 0.01$	Rician coefficient for RIS–UEs links, $\forall k \in \mathcal{K}$
$\tau_{RIS} = 0.2$	Coefficient for RIS amplification
$\mathcal{T} = 500$	Realizations MCs

Source: The Authors.

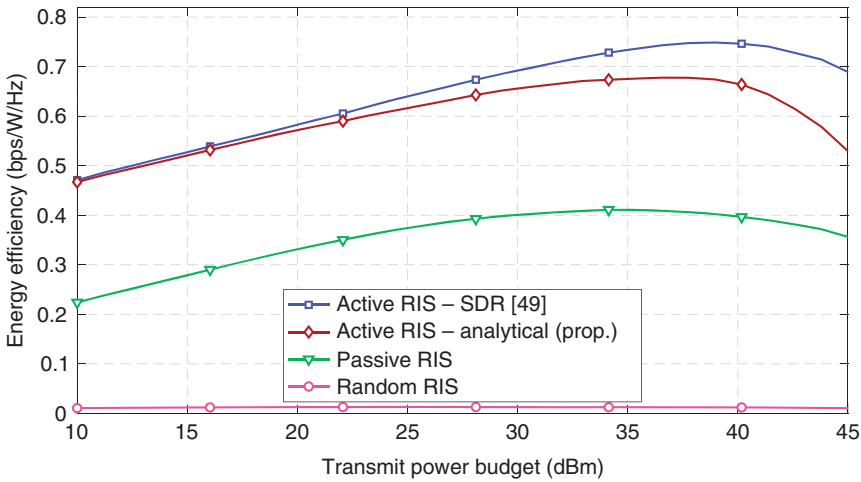

Figure 6.3 Average EE versus the transmit budget power [dBm] at the BS (P_{TX}). Performance evaluation of the proposed algorithm for the active RIS analytical versus active RIS with SDR, entirely passive RIS, and random phase shift/precoding, with $N = 64$. Here we assume $N_{act} = 49$, $N_{pas} = 15$, and $\tau_{RIS} = 0.2$.

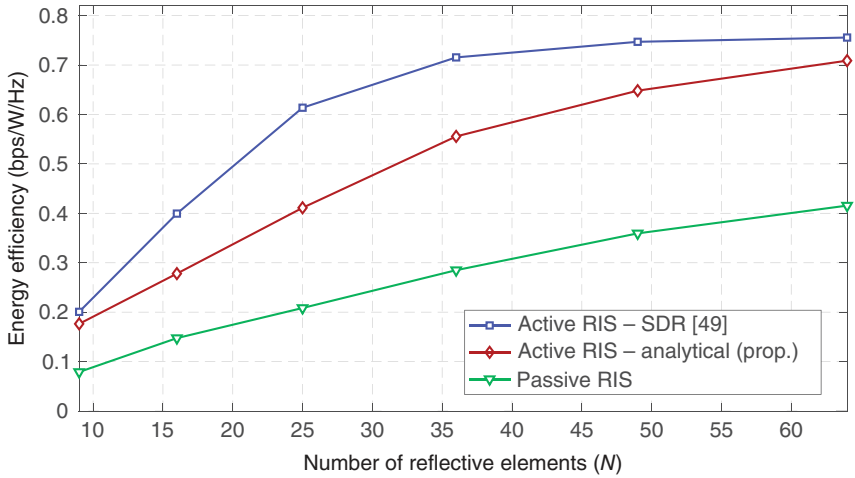

Figure 6.4 Average EE versus the total number of reflective elements at the RIS (N). Performance evaluation of the proposed algorithm for the active RIS analytical versus active RIS with SDR, and entirely passive RIS. Here we assume $N_{act} = N$, for the active RIS scenario.

that it can achieve performance very similar to the SDR method. However, as the power level escalates, one can observe an increase in the performance difference between the two methods, becoming further stressed, mainly under a high-power regime. This difference in performance will be further detailed in Section 6.7.2. Nonetheless, it is worth noticing that our analytical proposed method consistently can achieve convincing performance enhancements across all power regimes compared to the passive one.

In Figure 6.4, we plot the average EE versus the number of total elements at the RIS. Here, we consider that all elements are operating in the active mode. Notice that for low values of RIS elements, the proposed method achieves performance very close to that of the SDR method. Additionally, as the number of RIS elements increases, this performance gap widens, indicating a scenario where the proposed method exhibits inferior performance than the SDR method. However, one can see that for high RIS elements, the performance gap is interestingly decreased. This finding indicates that in more realistic scenarios, where the RIS operates with a high number of elements, the proposed method can achieve performance close to that of the SDR method, making it appealing for practical implementations due to its low complexity. Furthermore, one can see that the proposed method always achieves performance higher than the entirely passive RIS.

The cumulative density function (CDF) for the amplitude gain of the active RIS considering SDR and the proposed analytical method is depicted in Figure 6.5. Both methods satisfy the constraints (6.34b) and (6.34c), as the probability of an

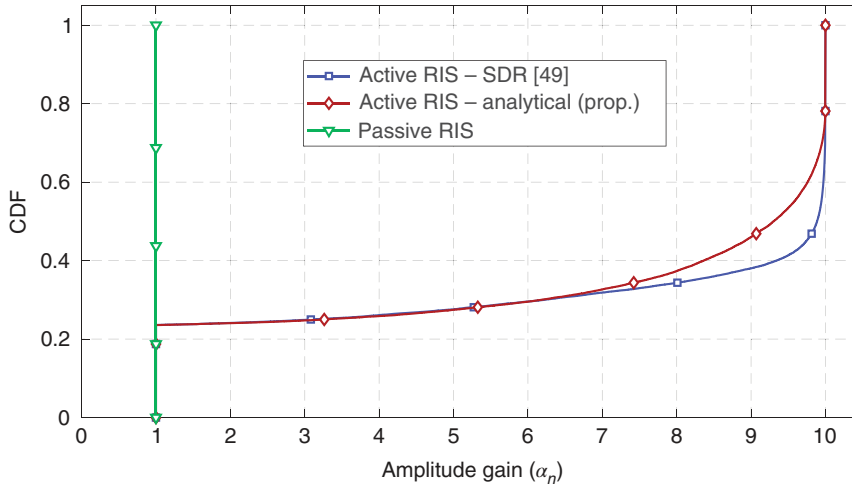

Figure 6.5 CDF of the amplitude gain (α_n) for transmit budget power of 10 dBm. Performance evaluation of the proposed algorithm for the active RIS analytical versus active RIS with SDR, and entirely passive RIS. Here we assume $N = 64$, with $N_{act} = 49$, $N_{pas} = 15$, and $\tau_{RIS} = 0.2$.

individual α_n value being lower than 1 is zero, and above α_{max} is also zero. However, it is noteworthy that the optimization policy for α_n differs between the two algorithms. While the analytical method tends to impose lower values, the SDR method opts for higher values. This discrepancy may serve as one explanation for the observed performance difference between the two algorithms. Finally, we can see that the entirely passive RIS always achieves the unitary amplitude, i.e., the probability of an amplitude gain of passive RIS being 1, is always 1 since it does not amplify the reflected signal.

Figure 6.6 illustrates how both the analytical proposed algorithm and the SDR benchmark utilize the total available power. It is important to note that the x-axis represents the total power budget. Still, the power budget at the RIS depends on the RIS amplification coefficient τ_{RIS}, meaning that $P_{\max}^{RIS} = P_{TX}\tau_{RIS}$. We observe that the SDR method consumes more power than the analytical method, consistent with the result depicted in Figure 6.5. This difference may partially explain the higher performance of the SDR method. However, other factors are at play, such as the initial solution provided for the analytical method. Here, we adopt the complete solution obtained for the entirely passive RIS. Additionally, both algorithms cannot fully utilize 100% of the available power. This limitation is due to the constraint on α_n, which we assume as $\alpha_{max} = 10$. Therefore, this constraint restricts the active RIS from utilizing the total available power. In practical scenarios, it would be beneficial to optimize the τ_{RIS} factor, as it may result in unused power.

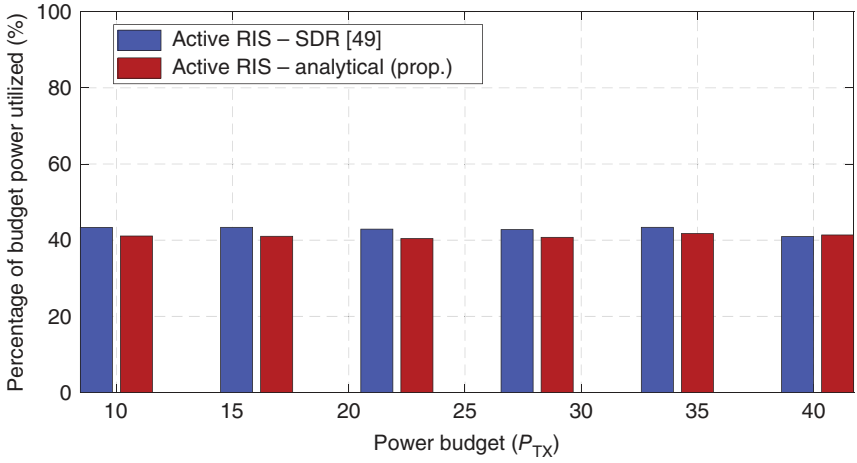

Figure 6.6 Percentage of budget power utilized versus transmit budget power. Performance evaluation of the proposed algorithm for the active RIS analytical versus active RIS with SDR.

6.7.2 Convergence and Complexity of the Proposed Algorithm

Figure 6.7 illustrates the convergence patterns of both the proposed algorithm and the benchmark method under two distinct conditions, namely $P_{\text{TX}} = \{10, 40\}$ dBm, thereby highlighting their effectiveness under each circumstance. Additionally, we provide insights into the average runtime of a single CSI realization for both methodologies. It is clear that for both scenarios, in Figure 6.7a,b, the EE initially experiences an upward trend and subsequently stabilizes with increasing iterations, demonstrating rapid convergence within 6 to 8 iterations. Furthermore, in scenario (a), we note a marginal performance gap of 3.81% between the SDR and the analytical approach, with the latter showcasing a notable 51% enhancement over the passive RIS.

Associate to it, within the same scenario, we can also see in Figure 6.7c that the average running time of the analytical compared to the SDR is highly reduced, from ≈ 5 seconds to less than 1 second constituting an 85.16% reduction. This is significant because the reduction in computational overhead highlights its practical appeal, motivating and making it conducive for real-world implementation scenarios, owing to its remarkably low complexity. Its complexity is directly related to the derived closed-form solutions given by Eq. (6.54), which can accelerate and facilitate its implementation while providing a substantial performance enhancement. We also can see that for scenario (b), the performance gap between the SDR and analytical increases, achieving 16.34%, while the obtained gain concerning the passive RIS decreases, presenting 39.70%. Nevertheless, the analytical method

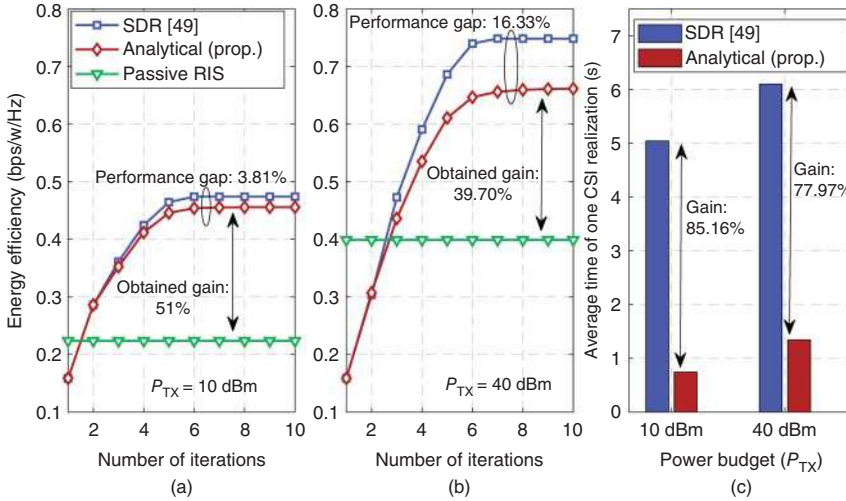

Figure 6.7 Average EE versus number of iterations for the proposed algorithm. Performance evaluation of the proposed algorithm for the active RIS for two different scenarios $P_{TX} = \{10, 40\}$ dBm. (a) $P_{TX} = 10$ dBm, (b) $P_{TX} = 40$ dBm, and (c) average running time. Furthermore, we also plot the average running time of one CSI realization for the SDR technique [49] and analytical proposed.

demonstrates an appealing runtime from ≈ 6 seconds to ≈ 1.2 seconds, constituting a 77.97% reduction in computational time.

6.8 Conclusions and Perspectives

We have examined the profound implications of optimizing the EE for active RIS scenarios, seeking to understand and find the number of elements that need to be selected for acting in active RIS because of outperforming its entirely passive RIS counterpart. By exploring various optimization techniques, we aim to provide a low-complexity solution and ensure its proximity to the optimal solution. This approach allows us to assess the effectiveness of our analytical methodology to handle complex optimization challenges.

The numerical results show that the active RIS can easily outperform the entirely passive RIS in terms of system EE, achieving a gain of about 120%. Furthermore, for typical system and channel scenarios, active RIS can operate with less than half of elements compared with the passive RIS given achieving about the same performance, enabling an operational cost reduction for physical arrays and lower channel estimation overhead for practical implementations. However, to achieve better performance in signal amplification, the active RIS needs to be equipped with a reasonable number of reflective elements, mainly in

Table 6.4 Summary of the contributions – key quantitative results and a brief comparison with the literature.

References	Contribution	Key results
This work	Joint amplitude and phase shifts analytical design for active RIS elements, aiming to maximize the EE in RIS-aided M-MIMO systems (*Sections 6.5 and 6.6*)	• achieved gains of 51% and 39.70% related to the passive RIS for transmit budget power of 10 and 40 dBm, respectively; • Presented lower performance related to the active RIS with SDR method. However, it demonstrated significantly lower complexity, achieving reductions of 85.16% and 77.97% in processing time.
Liter.	Contribution	Goal differences with this work
[23]	Sum rate maximization for double-active RIS systems	EE maximization (instead SR) for single RIS systems with practical implementation constraints.
[25]	Sum rate maximization for single-active RIS systems	EE maximization for single RIS systems under practical implementation constraints.
[27]	EE maximization and transmit power minimization for active RIS systems	EE maximization with a focus on assessing the number of active RIS elements necessary for outperforming the entirely passive RIS.

scenarios where the available power for signal amplification is high. Finally, we show how the proposed algorithm can be promising since it has required a few iterations for convergence. A summary of the key quantitative results obtained and contribution by this book chapter is provided in Table 6.4.

6.8.1 Limitations and Lessons Learned

Limitations of the proposed model can be drawn as:

- The RIS-aided M-MIMO model system could aggregate the channel estimation step, including overhead impact in both SE (numerator) and energy consumption (denominator) expressions. Then, a more complex but useful max-EE optimization problem can be formulated and solved.
- The precoding, power allocation for the UEs, the number of active/passive elements on the RIS, and RIS power budget factor τ_{RIS} could be aggregated in the EE optimization problem, becoming a more intricate and hard-to-solve problem.

Lessons learned from the investigation:

- When well configured, active RIS has the potential to impact substantially the system performance. by improving remarkably when compared with the entirely passive RIS with both random and optimized phases.
- The optimization of phases and amplitudes of RIS with closed-form solutions provide significant time reduction compared with the SDR technique while attaining reasonable performance gain related to the passive RIS.

6.8.2 Research Perspectives

In this chapter, we delved into the optimization of EE in RIS-assisted M-MIMO systems. While significant progress has been made, several crucial aspects pose open research challenges, offering promising avenues for exploration.

Our initial focus was on optimizing the RIS reflection coefficients within the framework of MR precoding with EPA. However, it is noteworthy that the precoding strategy at the BS also presents an opportunity for optimization. Considering the joint optimization of RIS and BS precoding can potentially unveil enhanced EE performance.

Moreover, our system model has assumed a far-field propagation channel. Extending and investigating the analysis of near-field propagation channels is a relevant topic for future works. This extension is particularly pertinent due to the prevalence of large aperture arrays aimed at mitigating the multiplicative path-loss effect and higher frequency operations for increased bandwidth, which inherently increase the Rayleigh distance. Notably, this has extended the range where near-field propagation dominates. Furthermore, new opportunities arise in the near-field context; for instance, the beam-focusing effect becomes a prominent phenomenon. This effect not only allows adjustment of the direction of the reflected beam but also offers the intriguing capability to control the distance within a specific angle. Developing strategies to improve the EE of RIS-assisted M-MIMO networks leveraging the beam-focusing effect for near-field scenarios is thus of significant relevance.

Additionally, the current investigation centered on a single active RIS. Extending the system model to accommodate a scenario with multiple active RIS units is a valuable avenue for future research, offering insights into the complexities and opportunities associated with such configurations.

Finally, the optimization scope can be broadened by considering the joint optimization of BS and RIS active/passive elements. By optimizing both components simultaneously, the overall EE of the system can be finely tuned for improved performance and resource utilization. These avenues highlight the richness of potential research directions in advancing the understanding and optimization of active RIS-assisted M-MIMO systems.

List of Acronyms

3-D	three-dimensional
3GPP	3rd Generation Partnership Project
5G	fifth generation
6G	sixth generation
AoA	angle of arrival
AoD	angle of departure
AS	antenna selection
AWGN	additive white gaussian noise
AF	Amplify-and-Forward
BS	base station
BCD	block coordinate descent
B5G	Beyond-5G
CSI	channel state information
CHEST	channel estimation
CDF	cumulative density function
DL	downlink
D/A	Diginal/Analog
DF	Decode-and-Forward
EE	energy efficiency
ER	ergodic rate
EH	enerhy harvesting
EPA	equal power allocation
FP	fractional programming
FET	field-effect transistor
FPGA	field programmable gate array
FLOPs	Floating Point Operations
GA	genetic algorithm
i.i.d.	independent and identically distributed
ISAC	integrated sensing and communication
IoT	Internet of Things
KKT	Karush-Kuhn-Tucker
LoS	line-of-sight
LDT	lagrangian dual transform
MIMO	multiple-input multiple-output
M-MIMO	massive MIMO
mmWave	millimeter-wave
MCs	Monte-Carlo Simulation
MISO	Multiple-input single-output
MM	majorization-minimization

MR	maximum ratio
PC	pilot contamination
PDD	penalty dual decomposition
PSO	particle swarm optimization
PS	power splitting
PA	power amplifier
PSC	phase shift control
QoS	Quality of Service
QCQP	quadratically constrained quadratic programming
RF	radio frequency
RE	resource efficiency
RIS	reconfigurable intelligent surface
SE	spectral efficiency
SINR	signal-to-interference-plus-noise ratio
SNR	signal-to-noise ratio
SCA	sucessive convex approximation
SOCP	second order conic programming
SDR	semi-defined relaxation
SFP	sequential fractional programming
SDP	semi-definite program
SR	sum-rate
TDD	time-division duplex
UE	user's equipment
UL	uplink
UPA	uniform planar array
USPA	uniform squared planar array
ULA	uniform linear array
VR	visibility region
WSR	weigthed sum-rate
XL-MIMO	extra-large scale massive MIMO
XR	extended reality
ZF	zero-forcing

References

1 Wu, Q. and Zhang, R. (2020). Towards smart and reconfigurable environment: intelligent reflecting surface aided wireless network. *IEEE Communications Magazine* 58 (1): 106–112. https://doi.org/10.1109/MCOM.001.1900107.

2 Gong, S., Lu, X., Hoang, D.T. et al. (2020). Toward smart wireless communications via intelligent reflecting surfaces: a contemporary survey. *IEEE*

Communications Surveys & Tutorials 22 (4): 2283–2314. https://doi.org/10.1109/COMST.2020.3004197.

3 Taha, A., Alrabeiah, M., and Alkhateeb, A. (2021). Enabling large intelligent surfaces with compressive sensing and deep learning. *IEEE Access* 9: 44304–44321. https://doi.org/10.1109/ACCESS.2021.3064073.

4 Long, R., Liang, Y.-C., Pei, Y., and Larsson, E.G. (2021). Active reconfigurable intelligent surface-aided wireless communications. *IEEE Transactions on Wireless Communications* 20 (8): 4962–4975. https://doi.org/10.1109/TWC.2021.3064024.

5 An, J., Yuen, C., Dai, L. et al. (2023). Toward beamfocusing-aided near-field communications: research advances, potential, and challenges. *arXiv preprint arXiv:2309.09242*.

6 Zhang, X. and Zhang, H. (2023). Hybrid reconfigurable intelligent surfaces-assisted near-field localization. *IEEE Communications Letters* 27 (1): 135–139. https://doi.org/10.1109/LCOMM.2022.3215253.

7 Wu, Z. and Dai, L. (2023). Multiple access for near-field communications: SDMA or LDMA? *IEEE Journal on Selected Areas in Communications* 41 (6): 1918–1935. https://doi.org/10.1109/JSAC.2023.3275616.

8 Ahmed, I., Shahid, M.K., Khammari, H., and Masud, M. (2021). Machine learning based beam selection with low complexity hybrid beamforming design for 5G massive MIMO systems. *IEEE Transactions on Green Communications and Networking* 5 (4): 2160–2173. https://doi.org/10.1109/TGCN.2021.3093439.

9 Huang, T., Yang, W., Wu, J. et al. (2019). A survey on green 6G network: architecture and technologies. *IEEE Access* 7: 175758–175768. https://doi.org/10.1109/ACCESS.2019.2957648.

10 Guo, H., Liang, Y.-C., Chen, J., and Larsson, E.G. (2020). Weighted sum-rate maximization for reconfigurable intelligent surface aided wireless networks. *IEEE Transactions on Wireless Communications* 19 (5): 3064–3076. https://doi.org/10.1109/TWC.2020.2970061.

11 Pan, C., Ren, H., Wang, K. et al. (2020). Multicell MIMO communications relying on intelligent reflecting surfaces. *IEEE Transactions on Wireless Communications* 19 (8): 5218–5233. https://doi.org/10.1109/TWC.2020.2990766.

12 Zhi, K., Pan, C., Ren, H., and Wang, K. (2022). Ergodic rate analysis of reconfigurable intelligent surface-aided massive MIMO systems with ZF detectors. *IEEE Communications Letters* 26 (2): 264–268. https://doi.org/10.1109/LCOMM.2021.3128904.

13 Zeng, M., Bedeer, E., Dobre, O.A. et al. (2021). Energy-efficient resource allocation for IRS-assisted multi-antenna uplink systems. *IEEE Wireless Communications Letters* 10 (6): 1261–1265. https://doi.org/10.1109/LWC.2021.3063554.

14 de Souza, W. and Abrão, T. (2023). Energy efficiency maximization for intelligent surfaces-aided massive MIMO with zero forcing. *IEEE Transactions on Green Communications and Networking* 8 (2): 802–814. https://doi.org/10.1109/TGCN.2023.3346367.

15 Li, Z., Zhang, J., Zhu, J., and Dai, L. (2023). RIS energy efficiency optimization with practical power models. *2023 International Wireless Communications and Mobile Computing (IWCMC)*, 1172–1177. https://doi.org/10.1109/IWCMC58020.2023.10183034.

16 He, Y., Cai, Y., Mao, H., and Yu, G. (2022). RIS-assisted communication radar coexistence: joint beamforming design and analysis. *IEEE Journal on Selected Areas in Communications* 40 (7): 2131–2145. https://doi.org/10.1109/JSAC.2022.3155507.

17 Kang, J., Wymeersch, H., Fischione, C. et al. (2022). Optimized switching between sensing and communication for mmWave MU-MISO systems. *2022 IEEE International Conference on Communications Workshops (ICC Workshops)*, 498–503. https://doi.org/10.1109/ICCWorkshops53468.2022.9814527.

18 Wu, J., Kim, S., and Shim, B. (2022). Energy-efficient power control and beamforming for reconfigurable intelligent surface-aided uplink IoT networks. *IEEE Transactions on Wireless Communications* 21 (12): 10162–10176. https://doi.org/10.1109/TWC.2022.3182773.

19 Ji, T., Hua, M., Li, C. et al. (2023). Robust max-min fairness transmission design for IRS-aided wireless network considering user location uncertainty. *IEEE Transactions on Communications* 71 (8): 4678–4693. https://doi.org/10.1109/TCOMM.2023.3280211.

20 Xie, H., Xu, J., and Liu, Y.-F. (2021). Max-min fairness in IRS-aided multi-cell MISO systems with joint transmit and reflective beamforming. *IEEE Transactions on Wireless Communications* 20 (2): 1379–1393. https://doi.org/10.1109/TWC.2020.3033332.

21 Jiang, T. and Yu, W. (2022). Interference nulling using reconfigurable intelligent surface. *IEEE Journal on Selected Areas in Communications* 40 (5): 1392–1406. https://doi.org/10.1109/JSAC.2022.3143220.

22 Alegría, J.V. and Rusek, F. (2022). Channel orthogonalization with reconfigurable surfaces. *2022 IEEE Globecom Workshops (GC Wkshps)*, 37–42. https://doi.org/10.1109/GCWkshps56602.2022.10008751.

23 Liu, M., Ren, H., Pan, C. et al. (2024). Joint beamforming design for double active RIS-assisted radar-communication coexistence systems. *arXiv preprint arXiv:2402.04532*.

24 Zargari, S., Hakimi, A., Tellambura, C., and Herath, S. (2022). Multiuser MISO PS-SWIPT systems: active or passive RIS? *IEEE Wireless Communications Letters* 11 (9): 1920–1924. https://doi.org/10.1109/LWC.2022.3187671.

25 Zhang, Z., Dai, L., Chen, X. et al. (2023). Active RIS vs. passive RIS: which will prevail in 6G? *IEEE Transactions on Communications* 71 (3): 1707–1725. https://doi.org/10.1109/TCOMM.2022.3231893.

26 Ye, J., Rihan, M., Zhang, P. et al. (2024). Energy efficiency optimization in active reconfigurable intelligent surface-aided integrated sensing and communication systems. *IEEE Transactions on Vehicular Technology* 1–16.

27 Lv, W., Bai, J., Yan, Q., and Wang, H.M. (2023). RIS-assisted green secure communications: active RIS or passive RIS? *IEEE Wireless Communications Letters* 12 (2): 237–241. https://doi.org/10.1109/LWC.2022.3221609.

28 de Souza, J.H.I., Marinello Filho, J.C., Amiri, A., and Abrão, T. (2023). QoS-aware user scheduling in crowded XL-MIMO systems under non-stationary multi-state LoS/NLoS channels. *IEEE Transactions on Vehicular Technology* 72 (6): 7639–7652. https://doi.org/10.1109/TVT.2023.3243488.

29 dos Santos, H.L., Marinello, J.C., Panazio, C.M., and Abrão, T. (2022). Machine learning-aided pilot and power allocation in multi-cellular massive MIMO networks. *Physical Communication* 52: 101646. https://doi.org/10.1016/j.phycom.2022.101646.

30 Marinello Filho, J.C., Brante, G., Souza, R.D., and Abrão, T. (2022). Exploring the non-overlapping visibility regions in XL-MIMO random access and scheduling. *IEEE Transactions on Wireless Communications* 21 (8): 6597–6610. https://doi.org/10.1109/TWC.2022.3151329.

31 de Souza, J.H.I., Marinello Filho, J.C., Abrão, T., and Panazio, C. (2022). Reconfigurable intelligent surfaces to enable energy-efficient IoT networks. *2022 Symposium on Internet of Things (SIoT)*, 1–4. https://doi.org/10.1109/SIoT56383.2022.10070317.

32 Marinello, J.C., Abrão, T., Amiri, A. et al. (2020). Antenna selection for improving energy efficiency in XL-MIMO systems. *IEEE Transactions on Vehicular Technology* 69 (11): 13305–13318. https://doi.org/10.1109/TVT.2020.3022708.

33 Taniguchi, L.M., de Souza, J.H.I., Guerra, D.W.M., and Abrão, T. (2021). Resource efficiency and pilot decontamination in XL-MIMO double-scattering correlated channels. *Transactions on Emerging Telecommunications Technologies* 32 (12): e4365. https://doi.org/10.1002/ett.4365.

34 Ubiali, G.A., Marinello, J.C., and Abrao, T. (2021). Energy-efficient flexible and fixed antenna selection methods for XL-MIMO systems. *AEU-International Journal of Electronics and Communications* 130: 153568.

35 Marinello Filho, J.C., Abrão, T., Hossain, E., and Mezghani, A. (2024). Reconfigurable intelligent surfaces-enabled intra-cell pilot reuse in massive MIMO systems. *IEEE Transactions on Wireless Communications* 23 (8): 9446–9459. https://doi.org/10.1109/TWC.2024.3362517.

36 Rosa, K.B. and Abrão, T. (2023). Improving the resource efficiency in massive MIMO-NOMA systems. *Journal of Network and Systems Management* 31 (4): 74.

37 Yang, Y., Lu, Z., Li, M. et al. (2024). A practical beamforming design for active RIS-assisted MU-MISO systems. *arXiv preprint arXiv:2401.03873*.

38 Wu, Q. and Zhang, R. (2019). Intelligent reflecting surface enhanced wireless network via joint active and passive beamforming. *IEEE Transactions on Wireless Communications* 18 (11): 5394–5409. https://doi.org/10.1109/TWC.2019.2936025.

39 You, C., Zheng, B., and Zhang, R. (2020). Fast beam training for IRS-assisted multiuser communications. *IEEE Wireless Communications Letters* 9 (11): 1845–1849. https://doi.org/10.1109/LWC.2020.3005980.

40 Jiang, L., Li, X., Matthaiou, M., and Jin, S. (2023). Joint user scheduling and phase shift design for RIS assisted multi-cell MISO systems. *IEEE Wireless Communications Letters* 12 (3): 431–435. https://doi.org/10.1109/LWC.2022.3229441.

41 Björnson, E., Sanguinetti, L., Hoydis, J., and Debbah, M. (2015). Optimal design of energy-efficient multi-user MIMO systems: is massive MIMO the answer? *IEEE Transactions on Wireless Communications* 14 (6): 3059–3075. https://doi.org/10.1109/TWC.2015.2400437.

42 Wang, J., Tang, W., Liang, J.C. et al. (2024). Reconfigurable intelligent surface: power consumption modeling and practical measurement validation. *IEEE Transactions on Communications* 72 (9): 5720–5734.

43 Pei, X., Yin, H., Tan, L. et al. (2021). RIS-aided wireless communications: prototyping, adaptive beamforming, and indoor/outdoor field trials. *IEEE Transactions on Communications* 69 (12): 8627–8640. https://doi.org/10.1109/tcomm.2021.3116151.

44 Fotock, R.K., Zappone, A., and Di Renzo, M. (2023). Energy efficiency in RIS-aided wireless networks: active or passive RIS? *ICC 2023-IEEE International Conference on Communications*, 2704–2709. IEEE.

45 Shen, K. and Yu, W. (2018). Fractional programming for communication systems–Part II: uplink scheduling via matching. *IEEE Transactions on Signal Processing* 66 (10): 2631–2644. https://doi.org/10.1109/TSP.2018.2812748.

46 Shen, K. and Yu, W. (2018). Fractional programming for communication systems–Part I: power control and beamforming. *IEEE Transactions on Signal Processing* 66 (10): 2616–2630. https://doi.org/10.1109/TSP.2018.2812733.

47 Dinkelbach, W. (1967). On nonlinear fractional programming. *Management Science* 133 (7): 492–498. https://doi.org/10.1287/MNSC.13.7.492.

48 Jong, Y. (2012). *An Efficient Global Optimization Algorithm for Nonlinear Sum-of-Ratios Problem*. Optimization Online.

49 Souza, W. Jr., Marinello, J.C., and Abrão, T. (2024). Energy-efficient active element selection in RIS-aided massive MIMO systems. arXiv:2402.14994v2 [cs.IT]; https://doi.org/10.48550/arXiv.2402.14994; https://arxiv.org/abs/2402.14994.

7

Element Grouping in IRS-Aided Wireless Communication System

Samarendra Nath Sur[1], Huu Quy Tran[2], and Agbotiname Lucky Imoize[3,4]

[1] *Department of Electronics and Communication Engineering, Sikkim Manipal Institute of Technology, Majitar, Sikkim Manipal University, Gangtok, India*
[2] *Faculty of Electronics Technology, Industrial University of Ho Chi Minh City, Ho Chi Minh City, Vietnam*
[3] *Department of Electrical and Electronics Engineering, Faculty of Engineering, University of Lagos, Lagos, Nigeria*
[4] *Department of Electrical Engineering and Information Technology, Institute of Digital Communication, Ruhr University, Bochum, Germany*

7.1 Introduction

Next-generation wireless communication systems, such as fifth-generation (5G) and sixth-generation (6G) are essential for achieving spectral efficiency (SE) and energy efficiency (EE) while effectively connecting billions of users. The primary objective of 6G is to deliver faster data rates, improved reliability, lower latency, and efficient secure transmission [1, 2]. The emergence of intelligent reflecting surfaces (IRSs) [3–8] technology has provided researchers with an exciting opportunity to optimize the radio channel for maximum benefits. IRS is considered a valuable tool in enhancing the energy and SE of wireless networks. The improvement discussed can be achieved through intelligent configuration of the wireless environment [9]. Each element of the IRS has a fundamental role in independently controlling the amplitude, phase frequency, and polarization of the incident signal. This control enables highly directive beamforming, which has been demonstrated to enhance signal quality and enable interference nulling. The IRS introduces a new degree of freedom by providing additional control over the propagation environment, resulting in performance improvements over traditional communication networks [7, 10]. Furthermore, the IRS offers several significant advantages, including cost-effectiveness and low-energy consumption [6, 10]. While the concept of active elements in an IRSs has been explored in various studies, including the work by the authors in [11, 12], the authors have also proposed the use of passive and active elements in IRS to enhance network performance. A basic IRS

Reconfigurable Intelligent Surfaces for 6G and Beyond Wireless Networks, First Edition.
Edited by Agbotiname Lucky Imoize, Vinoth Babu Kumaravelu, and Dinh-Thuan Do.

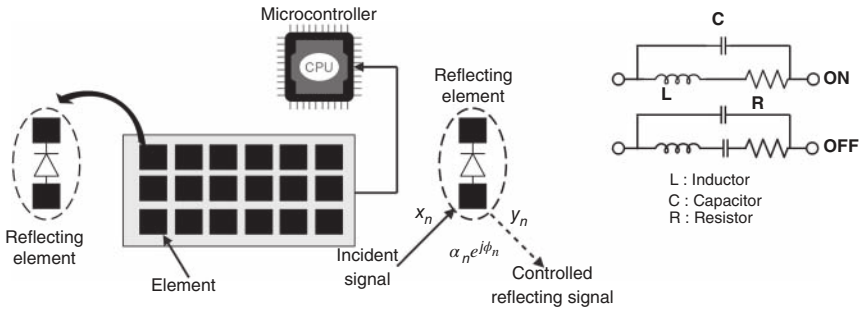

Figure 7.1 IRS basic architecture. Source: Sur et al. [14]. Reprinted with permission from Springer Nature.

architecture and equivalent circuit [13] for an individual IRS element is shown in Figure 7.1,

The surface's tunability, as depicted in Figure 7.1, is achieved by incorporating various components such as positive-intrinsic negative (PIN) diodes, varactor-tuned resonators, liquid crystals, and leveraging microelectromechanical systems (MEMS) technologies [15]. By utilizing PIN diodes as switches, the bias voltage can establish two distinct states (ON/OFF) for the IRS. When in the OFF state, the incident electromagnetic wave is absorbed, while the surface exhibits reflective properties in the ON state [16]. The IRS distinguishes itself from conventional half-duplex amplify-and-forward (AF) relays by leveraging intelligent reflection to achieve substantial beamforming gains in a full-duplex manner. Notably, the IRS accomplishes this without the need for extra energy consumption or additional time/frequency resources for signal regeneration and retransmission [8, 17].

Existing studies on the IRS typically make the assumption of having accurate channel state information (CSI) available at the base station (BS) or IRS [7, 12, 17–19]. This assumption allows for the optimization of various design parameters in order to improve the overall system performance. However, in certain scenarios, the utilization of only statistical CSI [20, 21] is sufficient for the design problem, particularly in cases where large-scale antenna array systems are deployed. Researchers can overcome design obstacles and improve performance by using statistical CSI without having to have a perfect understanding of the channel characteristics.

When it comes to IRS-aided wireless systems that require instantaneous CSI, there are two general approaches for channel acquisition that have been explored in existing research. The first approach involves the use of IRS elements that have the capability to both sense the channel and reflect signals [22, 23]. This allows for channel estimation between the IRS and the BS or users through the principles of channel reciprocity and time division duplexing (TDD) [24, 25]. Conventional

channel estimate techniques can therefore be used in this situation. It is important to keep in mind that this strategy requires more energy and has higher implementation expenses. On the other hand, the second approach assumes the utilization of purely passive IRS elements, which makes it impossible to directly obtain the individual channels of the BS–IRS and IRS–user equipment (UE) links [22, 23]. Alternative methods must be used in this situation to estimate the channel information. Researchers have been looking into a number of approaches to address this issue and acquire the required CSI in deployments of completely passive IRS units. Despite the restrictions given by the passive nature of the IRS parts, the goal is to enable effective communication and optimize system performance.

To address these challenges, a novel approach has been proposed involving the division of IRS elements into groups [17, 26]. Each group comprises of adjacent elements that are presumptively related by a similar reflection coefficient. In light of this, just the aggregated channel for each group needs to be predicted, significantly reducing the required training overhead and the complexity of the IRS coefficient design. Importantly, this scheme eliminates the need to receive radio frequency (RF) chains or additional sensors, resulting in a lower implementation cost and energy consumption. This motivates the authors to analyze the performance of an IRS-assisted wireless system with elements grouping.

To overcome these challenges, researchers have suggested a revolutionary strategy that divides the IRS elements into groups [17, 26, 27]. A common reflection coefficient is considered to be shared by each set of neighboring elements. By adopting this grouping strategy, it becomes possible to estimate only the combined channel of each group, thereby significantly reducing the required training overhead and the complexity associated with designing the IRS coefficients. One of the key advantages of this approach is that it eliminates the need for RF chains or sensors to be installed on the IRS, which leads to lower implementation costs and reduced energy consumption. This characteristic of the scheme inspired the authors to perform a comprehensive evaluation of the effectiveness of an IRS-assisted wireless system with elements grouping. By investigating the system's behavior under these conditions, the authors aim to provide key insights and understand the potential benefits and limitations of utilizing grouped IRS elements in practical deployments.

7.1.1 Contributions

The chapter encompasses various key aspects, which are outlined as follows:

- A concise overview of the IRS system, introducing its purpose and functionality. It also highlights different IRS grouping schemes.
- A comprehensive comparative analysis is presented, focusing on existing works related to the system employing IRS grouping. A comparative table is also

presented to highlight different approaches for the IRS element grouping, aim for the element grouping, and related achievements, etc. This analysis aims to focus on the necessity of IRS grouping.

- The performance analysis of the IRS system is addressed in a particular case study that is presented. In particular, the study looks into how phase optimization and element grouping affect system performance. Here, we have exploited the iterative optimization technique to find out the maximum rate corresponding to the IRS-assisted uplink network. And the impact of the phase discretization of the phase on the system performance is also evaluated.
- A numerical comparison that assesses how the system with IRS element grouping performs in comparison to both standard IRS-aided systems with random phase distribution and systems without IRS. The goal of the analysis is to identify the benefits and drawbacks of using IRS element grouping in various contexts.

7.1.2 Chapter Organization

The remaining sections of the chapter are structured as follows: Section 7.2 explores the current state of research on IRS-grouping methods. It includes a comparative analysis that looks at the similarities and differences between these strategies and provides a thorough review of the various techniques adopted. The IRS-assisted communication system is mathematically described in Section 7.3, with an emphasis on the grouping of the IRS elements. A thorough numerical study of the proposed IRS-assisted communication system is presented in Section 7.4. With the help of several numerical simulations, this analysis evaluates the system's performance and offers numerical insights into how effective it is. The chapter is concluded with Section 7.5, which summarizes the major findings.

7.2 Element Grouping

This section briefly highlights the different grouping approaches and related works.

7.2.1 Overview

This section highlights the signal processing aspect related to conventional IRS-assisted communication systems and communication systems with IRS elements grouping.

Figure 7.2 represents a downlink communication system where BS with M antennas communication with single antenna UE via IRS with N_{irs} elements. As is Figure 7.2, all the elements are directly configured to manipulate the

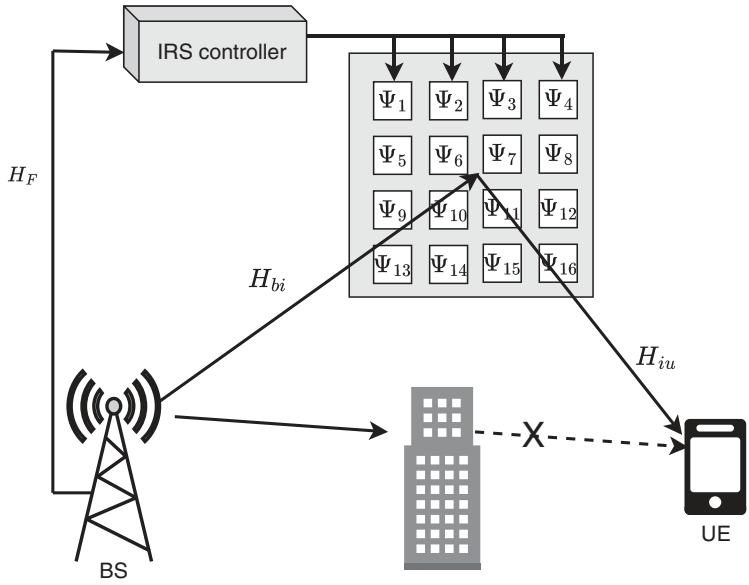

Figure 7.2 IRS-assisted communication system.

incident signal by configuring the phase of the each elements. This is basically the conventional approach without any element grouping. These phase shifts are designed at the BS and fed back to the IRS controller via the separate limited-rate feedback channel ($H_F \in \mathbb{C}$). The IRS operates in a passive manner, it lacks active receiving or transmitting capabilities and greatly depends on feedback bits denoted as b_F to execute the phase-shift values applied at each of its N_{irs} elements. These phase shifts serve to direct the reflected signal paths toward the receiver, ultimately generating a focused beampattern. For a given transmitted signal $\mathbf{s}$, the received signal can be expressed as in Eq. (7.1) [28–30],

$$\mathbf{y} = (\mathbf{H}_{bi}\boldsymbol{\Theta}\mathbf{H}_{iu})\mathbf{s} + \mathbf{n} \tag{7.1}$$

where $\mathbf{n}$ represents the overall noise vector corresponding to complex additive white Gaussian noise (AWGN) at the BS. More specifically, $\mathbf{n} = [n_1, \ldots, n_M]$ with $\sim \mathscr{CN}(0, N_0)$. And the channel between the UE and IRS is represented by $\mathbf{H_{iu}} \in \mathbb{C}^{N_{irs} \times 1}$. Furthermore, $\mathbf{H_{bi}} \in \mathbb{C}^{M \times N_{irs}}$ be the channel between BS and IRS. Each component at the IRS refracts the signals that have been received with a unique reflection coefficient. Let $\Theta = \left[\theta_1, \ldots, \theta_{N_{irs}}\right]^T \in \mathbb{C}^{N_{irs} \times 1}$ represents the IRS reflection coefficients. More specifically, each reflection coefficient can be expressed as $\theta_n = \rho_n e^{j\phi_n}$. Here, $\rho_n \in [0, 1]$ denotes the amplitude coefficient and the corresponding phase shift is $\phi_n \in [-\pi, \pi)$. As in Eq. (7.1), the effective channel

$\mathbf{H}_{eff} = \mathbf{H}_{bi}\boldsymbol{\Theta}\mathbf{H}_{iu}$. More specifically, the effective channel from the mth transmit antenna to the UE can be expressed as:

$$h_m = \sum_{n}^{N_{irs}} h_{bi\,nm}\theta_n h_{iu\,nm} \tag{7.2}$$

Therefore, collecting all h_m, the combined channel matrix $\mathbf{H}_{eff}$ can be form and can be expressed as:

$$\mathbf{H}_{eff} = \mathbf{H}_r\boldsymbol{\theta} \tag{7.3}$$

where, $\mathbf{H}_r = \mathbf{H}_{bi} \odot \mathbf{H}_{iu} \in \mathbb{C}^{M\times N_{irs}}$. Considering the system as in Figure 7.2, the optimization problem statement associated with the signal to noise ratio (SNR) maximization can be expressed as:

$$\max_{\theta} \left|\mathbf{H}_r\boldsymbol{\theta}\right|^2 \tag{7.4a}$$

$$\text{s.t. } \left|\theta_n\right| \leq 1\ \forall n \tag{7.4b}$$

The conventional method outlined above exhibits notable drawbacks, particularly in terms of challenges associated with channel estimation and feedback costs, both of which contribute to overall system overhead. These issues, in turn, result in a reduction in the achievable data rate. Consequently, the burden of overhead becomes a significant concern, necessitating in-depth examination. This concern prompted the exploration and development of the IRS element grouping as a potential solution. By addressing issues related to channel estimation, feedback costs, and overall overhead, the IRS element grouping approach aims to mitigate these challenges and enhance the efficiency of the system. It is crucial to thoroughly investigate this development to better understand its implications and benefits in optimizing data rates [17].

To address the trade-off issue associated with overhead, a method introduced in [17] stands out for significantly reducing overhead while minimizing SNR loss. The fundamental concept leverages the closely packed nature of elements in an IRS and relies on the assumption that neighboring elements exhibit high correlation. In contrast to assigning an optimized reflection coefficient to each individual IRS element, the proposed approach involves grouping nearby elements into evenly sized clusters. Each cluster shares a common reflection coefficient that is optimized for the entire group. This innovative strategy results in a notable increase in the net achievable rate, accompanied by only marginal effective SNR loss. Importantly, this method achieves these benefits with a considerably smaller overhead cost compared to approaches without grouping. Thorough exploration and understanding of this approach are crucial to appreciate its potential in mitigating overhead-related challenges while optimizing system performance. As in [17], the IRS elements are divided into D number of subgroups. It also assumed

that it could share one reflection coefficient and thereby optimize that particular subgroup. Therefore, one can easily realize that the requirement of the channel estimation and associated feedback is greatly reduced. This is due to the fact that channel estimation is required for the $\mathcal{D}$ number channel rather than N_{irs} number of channels. Therefore, the optimization problem, as in Eq. (7.4) can be rewritten as:

$$\max_{\theta^c} \left|\mathbf{H}_r''\boldsymbol{\theta}^{\mathbf{c}}\right|^2 \tag{7.5a}$$

$$\text{s.t.} \ \left|\theta_d^c\right| \leq 1 \ \forall d \tag{7.5b}$$

where $\theta^c \in \mathbb{C}^{D\times 1}$ and $\mathbf{H}_r''$ are the phase-shift vector and sub-channel matrix associated with each subchannel. In this context, the authors in [17] also addressed one important aspect related to the grouping strategy through the section on the best grouping ratio $\gamma = \mathcal{D}/N_{irs}$. Selecting the optimal grouping ratio is crucial for enhancing the achievable rate while maintaining a delicate balance between effective SNR gain and overhead. However, determining the most suitable grouping ratio presents a substantial challenge.

Subsequently in this chapter, the authors have discussed some of the basic grouping approaches that are investigated and reported.

Figure 7.3 represents a uniform IRS element grouping strategy. Here, $\mathcal{D}$ be the number of groups and a same number of IRS elements are associated with each group. Thus, the objective is to exploit the individual group to estimate the channel and figure out a common reflection coefficient corresponding to each group. The IRS reflection coefficients can be rephrased as follows by applying a common reflection coefficient to each group's constituents [17, 31]:

$$\boldsymbol{\Theta} = \theta^c \otimes 1_{G\times 1} \tag{7.6}$$

where G is the number of elements in each groups. $\theta^c = \left[\theta_1^c, \ldots, \theta_D^c\right]^T \in \mathbb{C}^{D\times 1}$ represents the reflection coefficients corresponding to the groups. Specifically, θ_d^c indicating the dth group's common reflection coefficient. Thus, the optimization problem in Eq. (7.4) can be redefine as,

$$\max_{\theta^c} \left|\mathbf{H}_r''(\theta^c \otimes 1_{G\times 1})\right|^2 \tag{7.7a}$$

$$\text{s.t.} \ \left|\theta_d^c\right| \leq 1 \ \forall d \tag{7.7b}$$

Figure 7.3 IRS elements uniform phase grouping.

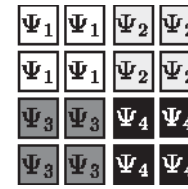

Figure 7.4 IRS elements double phase grouping.

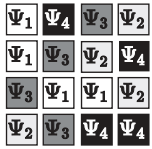

Figure 7.5 IRS elements random grouping.

In the previous strategy, it is assumed that the IRS reflection coefficients are exactly repeated for each element in the group. In the strategy, as presented in Figure 7.4, a new kernel, $\alpha \in \mathbb{C}^{G\times 1}$ is introduced and its distribution is presented in the above figure. As the amplitude is invariance to phase rotation, these two vectors can be implemented simultaneously through the Kronecker product. Thus, the optimization problem can be written as,

$$\max_{\theta^c,\alpha} \left|\mathbf{H}_r''(\theta^c \otimes \alpha)\right|^2 \tag{7.8a}$$

$$\text{s.t. } \left|\theta_d^c\right| \leq 1, \ \forall d \ \text{ and } \ \left|\alpha_g\right| = 1 \forall g (g = 1, \ldots, G) \tag{7.8b}$$

For both strategies, it is assumed that groups are made up of nearby IRS elements and of equally sized. But the effective SNR can be significantly improved by exploiting random grouping as presented in Figure 7.5. Although it enhances the feedback overhead little bits.

As in Figure 7.5, it is apparent that each element can adopt the phase shift associated with any group without being restricted by its location or the size of the group. Although it is acknowledged that there is a correlation among adjacent elements within an IRS, the introduction of dynamic sizes and locations in structuring these groups enables a flexible partitioning of elements. This approach ensures that the grouping configuration captures the coherence of optimized phases (θ^c) in a manner that is adaptable to the inherent correlations, allowing for a more nuanced and efficient utilization of the system's elements [31].

7.2.2 Related Works

Accurate phase optimization relies heavily on precise channel estimation, which becomes challenging in an IRS-assisted network due to the large number of elements that comprise an IRS. The presence of numerous elements significantly increases the number of links that necessitate estimation, thereby complicating the channel estimation process. Additionally, the passive nature of the IRS

means that channel detection at the receiver can only be achieved by probing the channel from the transmitter [32]. To address the issue of the channel estimation, researchers are exploited IRS element (or group) ON/OFF scheme [33] to have sub-optimal solution for an IRS-MISO system [34]. Extending further, the authors in [17, 26] have developed a unique transmission protocol for an orthogonal frequency division multiplexing (OFDM)-based wireless system that incorporates an IRS to successfully address the issues brought on by frequency-selective channels. The protocol makes use of the idea of grouping IRS elements, whereby nearby elements are taken to have a common reflection coefficient. As a result, the system's complexity is decreased because the estimation of each group's combined channel becomes the main focus. A practical transmission protocol combining pilot training has been devised based on this grouping mechanism to assure viability [17, 26]. The grouping mechanism can be beneficial for the interference cancellation and with the same motivation, the authors in [35] proposed IRS-based space-time block coded (STBC) transmission scheme. A primary concern arises from the fact that the channels associated with individual IRS elements cannot be guaranteed to be identical, resulting in limited access to CSI within the element-grouping scheme. The impacts of channel interference among various IRS elements have been thoroughly studied by the authors Zhang et al. [36] in order to address this difficulty. A deep learning (DL)-based network has been suggested as a means of minimizing this interference and obtaining refined partial cascaded channels. The authors have effectively expanded these fragmented cascaded channels to produce complete channels by utilizing neural networks. Furthermore, the concept of the element grouping scheme is expanded to introduce a practical modulation scheme known as IRS-based reflection pattern modulation (IRS–RPM) [37] aims to improve the efficiency of the passive beamforming and information transfer (PB IT) scheme. A subset of IRS elements inside the IRS-RPM architecture is selectively triggered to produce a focussed beam that is aimed at the desired location. Additionally, the active IRS elements' combined indices are used to subtly convey additional information about the IRS. The authors Tahir et al. [38] have exploited the idea of IRS element grouping to support multiple users in an IRS-nonorthogonal multiple access (NOMA) uplink system. Based on electromagnetic theory, the authors Mao et al. [39] have developed a realistic reflection coefficient model for the element-grouping IRS. In order to maximize the received power at the user, this practical model concentrated on exploring phase-shift optimization problems in wireless networks using IRS. The authors of Hwang et al. [40] examine the potential of an IRS element grouping scheme for intelligent beamforming optimization for an IRS-assisted full duplex relay (FDR) system. It becomes especially crucial when there exists a large number of links. Taking inspiration from the advantages of element grouping, the authors of Xu et al. [41] have applied this concept to an IRS-simultaneously

transmitting and reflecting (STAR) system. The study focuses on evaluating the performance of the IRS–STAR system under a multiuser near-field scenario. Two grouping strategies, namely, Selective element grouping (SEG) and random element grouping (REG), were employed and compared. The results indicate that SEG outperforms REG in terms of near-field channel gain in the context of an IRS–STAR setup. A study on the effectiveness of a cyclic-prefixed single-carrier (CPSC) transmission scheme using phase-shift keying (PSK) signaling for wireless communication systems that leverage IRS was recently reported by Li et al. [27]. In order to make implementation less complicated, the research focuses on using an element grouping technique. Furthermore, the authors emphasize the importance of initiating grouping based on the statistical behavior of the channel. In another related work by Wang et al. [42], the authors explore the integration of IRS in dual-function radar-communication (DFRC) systems to enhance communication capacity, sensing precision, and coverage for both radar and communication functions. The suggested method enables full-space coverage by combining a configurable single/group/fully connected architecture with a hybrid reflecting and transmitting mode. This system's major goal is to increase target detection while keeping communication quality of service (QoS) levels at acceptable levels. A comparative analysis of the work is presented in Table 7.1.

Based on the above works and the potential of the element grouping scheme to address the challenges involved in the channel estimation associated with IRS, the authors have investigated the performance of the IRS-assisted system with element grouping and phase optimization.

7.3 Mathematical Model

We consider a single-user (UE) wireless system, wherein an IRS is integrated in the system to enhance the communication link between the BS and the user. In this network, we consider the BS is consisting of uniform planer array with M antennas and single antenna UE. The overall IRS structure in presented in Figure 7.6. As in figure, all the elements (N_{irs}) of the IRS is distributed in rectangular shape with N_x and N_y elements in each row and column respectively [$N_{irs} = N_x \times N_y$].

Further we assume that G_x and G_y number of IRS elements are selected in each row and column to form the group. It is evident that $1 \leq G_x \leq N_x$ and $1 \leq G_y \leq N_y$. Her, we focus on uplink communication from the UE to BS as in Figure 7.7.

Let, $\mathbf{h_d} \in \mathbb{C}^{M\times 1}$ be the direct channel between the UE and BS. The channel between the UE and IRS is represented by $\mathbf{h_u} \in \mathbb{C}^{N_{irs}\times 1}$. Furthermore, $\mathbf{h_r} \in \mathbb{C}^{M\times N_{irs}}$ be the channel between IRS and BS. Each component at the IRS refracts the signals that have been received with a unique reflection coefficient. Let $\Theta = \left[\theta_1, \ldots, \theta_{N_{irs}}\right]^T \in \mathbb{C}^{N_{irs}\times 1}$ represents the IRS reflection coefficients. More

Table 7.1 Summary: IRS element grouping related works.

References	Year	System	Purpose of element grouping	Mechanism	Performance matrices	Achievement
Yang et al. [17]	2020	Single-user OFDM-based wireless system	To reduce the training overhead and estimation complexity	It proposed a mechanism to group the adjacent IRS elements to form a small block. Thereby estimate the combined channel of each group and consider a common reflection coefficient in the same group	Achievable rate.	The suggested methodology surpasses the arbitrary phase arrangement across all SNR ranges, even in instances of exceptionally small coherence time
Song and Guan [35]	2021	IRS-assisted extended quasiorthogonal STBC (QO-STBC) system.	To reduce interference.	In the proposed IRS-aided QO-STBC model, the authors have divided the N IRS elements into $N/4$ groups. Each group has four reflection elements to modulate the phase of the reflected signal	Bit error rate (BER).	Improved BER performance in comparison to conventional STBC-aided the IRS system
Zhang et al. [36]	2021	IRS-assisted communica-tions system with single antenna user communicate with multi-antenna access point	To reduce the pilot overhead and to reduce the interference among the IRS elements	It utilizes the pilot orthogonality to eliminate the interference among different element groups. After that a DL-based network is developed to eliminate the interference within each element group and acquire the refined partial cascaded channels. Finally an neural networks based algorithm is used to extrapolate the full cascaded channels	Normalized mean square error (NMSE).	The proposed two deep learning based networks provide significant gain compared to the conventional element-grouping method without interference elimination

(*continued*)

Table 7.1 (Continued)

References	Year	System	Purpose of element grouping	Mechanism	Performance matrices	Achievement
Lin et al. [37]	2021	IRS-assisted downlink MISO wireless communication system with reflection pattern modulation (RPM)	To maximize the average received signal power and achievable rate	The IRS adopts RPM via the combination of the ON/OFF states of the IRS groups. The idea of this scheme is to activate a subset of the IRS elements for producing a sharp beam toward the desired destination, while exploiting the index combination of the ON-state IRS elements to implicitly convey the additional information of the IRS	Outage rate, average signal power and achievable rate.	The proposed joint optimization technique with the IRS–RPM enhanced the instantaneous received signal power
Mao et al. [39]	2022	IRS-assisted communication system, where a single-antenna access point (AP) is communicating with a single-antenna user equipment	To maximize the receiver power signal at the user	It creates the group of adjacent IRS elements to form a sub-surface. Thereby estimate the combined channel of each group and consider a common reflection coefficient in the same sub-surface	Received Signal power at the user.	It proposed a practical reflection coefficient model for the element-grouping IRS from the electromagnetic theoretic perspective. And also proposed a geometry-based optimal phase control algorithm for the IRS reflection optimization to maximize the received power at the user

Hwang et al. [40]	2022	IRS assisted decode-and forward (DaF) protocol based full duplex relay (FDR) system	To improve the signal-to-interference ratio (SINR)	The reflective components within the IRS are thoughtfully organized into distinct sets, each aligning with specific criteria. Through a dedicated phase adjustment algorithm, the IRS elements are arranged into a few groups to maximize the end-to-end throughput of the FDR link	SINR	The proposed joint optimization technique improve the FDR performance
Asmoro and Shin [43]	2022	IRS grouping based index modulation (RGB-IM) assisted single input multiple output (SIMO) communication system	To improve the spectral efficiency and bit error rate (BER).	The fundamental concept revolves around partitioning the IRS into a predetermined number of distinct elements organized into group surfaces. Subsequently, user information undergoes segmentation and modulated into spatial symbol, serving as a means to activate the index associated with a particular group surface	Capacity and BER	The proposed RGB-IM outperform the conventional relay-assisted spatial modulation (SM)

(*continued*)

Table 7.1 (Continued)

References	Year	System	Purpose of element grouping	Mechanism	Performance matrices	Achievement
Xu et al. [41]	2023	IRS-assisted simultaneously transmitting and reflecting (STAR) system	To improve the channel gain and the signal coverage	Selective element grouping (SEG) and random element grouping (REG).	Channel gain and sum rate.	Under near-field scenario the SEG strategy has the best sum rate performance. And also under hybrid near- and far-field scenario, the proposed STAR–IRS significantly improved the channel gains of users and also improved the signal coverage
Cai et al. [44]	2023	IRS-assisted multiple input multiple output (MIMO) system.	To reduce the optimization complexity related to large IRS and maximize the rate	It propose a partitioning of IRS into sub-surfaces, so as to optimize the phase shifts in sub-surface levels to reduce complexity. Here, a linear phase variation structure is utilized corresponding to each sub-surface to reflect the incident signal to a desired direction. And also the sizes of sub-surfaces is adaptively adjusted based on the channel conditions	Achievable rate	It proposed a joint optimization algorithm for active and passive beamforming for the achievable rate maximization. Importantly, the passive beamforming optimization reduces to the manipulation of the sub-surface sizes, the phase gradients of sub-surfaces, and the common phase shifts of subsurfaces

Kim et al. [45]	2023	IRS-assisted multiuser-MIMO system with rate-splitting multiple access	To improve the sum rate and the energy efficiency. It also aims to reduce the complexity	The IRS elements with high channel gain are grouped in the order of user scheduling. Thereafter, the scattering matrix is optimized for each group	Sum rate	The proposed system provides high sum-rate than the conventional IRS-assisted spatial-division multiple access (SDMA) system
Awais et al. [46]	2023	IRS-assisted communication system where single antenna BS communication with single antenna user	To reduce the training overhead by sharing a reflection coefficient among a subgroup of elements at the cost of interference	The element grouping (EG), where the IRS elements are subgrouped to share a common reflection coefficient among subgroup elements with similar channel responses. And element-puncturing (EP), random grouping of elements	Normalized MSE.	It proposed a deep learning (DL)-based estimators and in collaboration with the EG. It outperformed the conventional grouping technique by mitigating the interference effectively for different noise levels
Li et al. [47]	2023	Multiuser multiple-input multiple-output (MU–MIMO) system with beyond diagonal IRS	To maximize the sum rate	It proposed a novel and unified cell-wise dynamically group-connected (CW-DGC) architecture for the IRS dynamic grouping based on the channel state information	Sum-rate	The proposed dynamically group connected IRS system out perform the group-connected cases

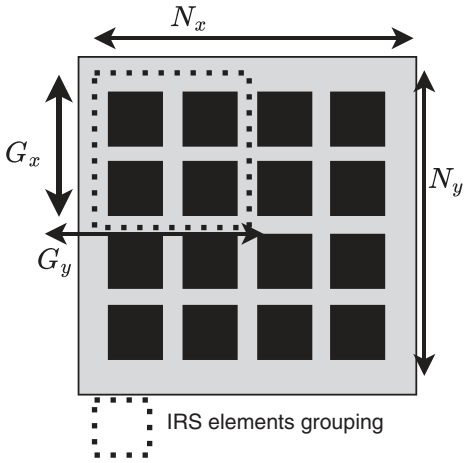

Figure 7.6 IRS elements grouping.

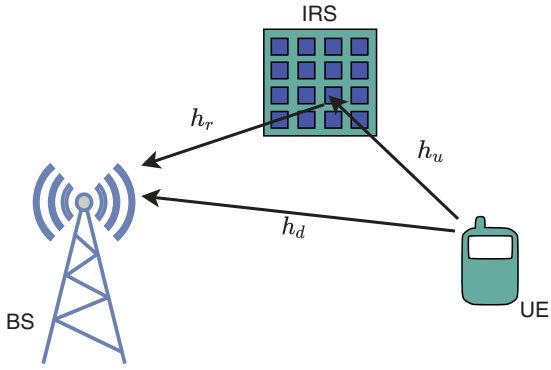

Figure 7.7 IRS-aided communication network.

specifically, each reflection coefficient cab be expressed as $\theta_n = \rho_n e^{j\phi_n}$. Here, $\rho_n \in [0, 1]$ denotes the amplitude coefficient and the corresponding phase shift is $\phi_n \in [-\pi, \pi)$. We evaluate the performance of the system under the consideration that these phase shift is discretized (with level, say, (L)) and also we presume that these phase shifts take one of the values that result from uniformly quantizing the range $[0, 2\pi]$. Thus, the discrete phase shifts can be expressed as,

$$\mathcal{F} = \{0, \Delta\theta, \ldots, (L-1)\Delta\theta\}\,;\ \Delta\theta = 2\pi/L \tag{7.9}$$

Considering the network as in Figure 7.7, the received signal at the BS can be expressed as,

$$\mathbf{y} = (\mathbf{h}_d + \mathbf{h}_r \boldsymbol{\Theta} \mathbf{h}_u)\mathbf{s} + \mathbf{n} \tag{7.10}$$

where $\mathbf{s}$ denotes the transmitted signal from the UE toward the BS. And $\mathbf{n}$ represents the overall noise vector corresponding to complex AWGN at the BS. More

specifically, $\mathbf{n} = [n_1, \ldots, n_M]$ with $\sim \mathscr{CN}(0, N_0)$. For the simplicity, the authors have considered zero forcing (ZF) to decode s. Following the formulation as in [48] the SNR cab be expressed as,

$$SNR = \frac{P_T \left\| \mathbf{h}_d + \mathbf{h}_r \boldsymbol{\Theta} \mathbf{h}_u \right\|^2}{N_0} \tag{7.11}$$

where P_T represents the transmitted power. Therefore, the achievable rate (bits/s/Hz) can be defined as follows,

$$R = \log_2 \left(1 + \frac{P_T \left\| \mathbf{h}_d + \mathbf{h}_r \boldsymbol{\Theta} \mathbf{h}_u \right\|^2}{N_0} \right) \tag{7.12}$$

The achievable rate is influenced by the IRS's reflection matrix ($\boldsymbol{\Theta}$), as shown in Eq. (7.12). Therefore, by carefully modifying $\boldsymbol{\Theta}$ matrix, higher rates ought to be attainable. In other words, through phase optimization the rate, R, can be improved significantly and in this chapter phase optimization problem for an IRS-assisted network is considered. As in Eq. (7.12), $\boldsymbol{\Theta}$ corresponds to the entire reflection matrix. But in this chapter we consider the grouping of the elements (as in Figure 7.6) to reduce the overall channel estimation overheads. Let, $\mathcal{D}$ be the number of groups and for simplicity we assume same size, i.e., same number of IRS elements, for each group. Thus, the objective is to exploit the individual group to estimate the channel and figure out a common reflection coefficient corresponding to each group. The IRS reflection coefficients can be rephrased as follows by applying a common reflection coefficient to each group's constituents [17]:

$$\boldsymbol{\Theta} = \theta^c \otimes 1_{G_{irs} \times 1} \tag{7.13}$$

where $G_{irs} = G_x G_y$ is the number of elements in each group. $\theta^c = \left[\theta_1^c, \ldots, \theta_{\mathcal{D}}^c\right]^T \in \mathbb{C}^{\mathcal{D} \times 1}$ represents the reflection coefficients corresponding to the groups. Specifically, θ_d^c indicating the dth group's common reflection coefficient.

Therefore, under the grouping scheme, the optimization problem can be defined as follows,

$$\max_{\boldsymbol{\Theta}} R \left(= \log_2 \left(1 + \frac{P_T \left\| \mathbf{h}_d + \mathbf{h}_r \boldsymbol{\Theta} \mathbf{h}_u \right\|^2}{N_0} \right) |_{\boldsymbol{\Theta} = \theta^c \otimes 1_{G_{irs} \times 1}} \right) \tag{7.14a}$$

$$\text{s.t.} \left| \theta_d^c \right| \leq 1, \ \forall d \in \mathcal{D} \tag{7.14b}$$

As presented in Eq. (7.14), we restricted our model to the phase optimization problem at the IRS. Due to discrete phase changes, the optimization problem in Eq. (7.14) is non-convex and can be solved using low-complex algorithm based on successive refinement by exploiting the channel gain [17, 49]. And also, it

is clear from Eq. (7.14) that the maximization of the channel gain leads to the maximization of R. Thus, the maximization problem Eq. (7.14) can be redefined as,

$$\max_{\boldsymbol{\Theta}} \left\| \mathbf{h}_d + \mathbf{h}_r \boldsymbol{\Theta} \mathbf{h}_u \right\|^2 \tag{7.15a}$$

$$\text{s.t.} \left| \theta_d^c \right| \leq 1, \ \forall d \in \mathcal{D} \tag{7.15b}$$

Following Wu and Zhang [49], $\mathbf{h}_r \boldsymbol{\Theta} \mathbf{h}_u$ can be expressed as $\mathbf{v}\boldsymbol{\Phi}$, where $\mathbf{v} = \left[e^{j\theta_1}, \ldots, e^{j\theta_{N_{irs}}} \right]^T$ and $\boldsymbol{\Phi} = \mathbf{h}_r diag\left(\mathbf{h}_u\right) \in \mathbb{C}^{N_{irs} \times M}$. Let, $\mathcal{B} = \boldsymbol{\Phi}^H \boldsymbol{\Phi}$ and $\check{\mathbf{h}}_d = \boldsymbol{\Phi}^H h_d$. Therefore, the channel gain can be expressed as,

$$\left\| \mathbf{h}_d + \mathbf{h}_r \boldsymbol{\Theta} \mathbf{h}_u \right\|^2 = \left\| \mathbf{h}_d + \mathbf{v}\boldsymbol{\Phi} \right\|^2 = \mathbf{v}^H \mathcal{B} \mathbf{v} + 2Re\left\{ \mathbf{v}^H \check{\mathbf{h}}_d \right\} + \left\| \mathbf{h}_d \right\|^2 \tag{7.16}$$

The channel gain maximization can be achieved through the discrete phase optimization using low-complex successive refinement algorithm [48, 49] as in Algorithm 7.1.

Algorithm 7.1: Successive refinement algorithm.

Input: $\mathbf{h}_d$;$\mathbf{h}_r$;$\mathbf{h}_u$; ε_{th};
Output: $\mathbf{v}$;R
Initialize: $\boldsymbol{\Phi} = \boldsymbol{\Phi}^0; m = 0$
Calculate: $\boldsymbol{\Phi} = \mathbf{h}_r diag\left(\mathbf{h}_u\right); \mathcal{B} = \boldsymbol{\Phi}^H \boldsymbol{\Phi}; \check{\mathbf{h}}_d = \boldsymbol{\Phi}^H h_d$.
$\mathbf{v} = exp(j\theta_i) \forall\ i = 1, \ldots, N_{irs}$; Discrete level random phases
$R^0 = \log_2 \left(1 + \frac{P_T \left\| \mathbf{h}_d + \mathbf{h}_r diag(\mathbf{v}) \mathbf{h}_u \right\|^2}{N_0} \right)$
while $\left| R^k - R^{k+1} \right| > \varepsilon_{th}$ **do**
  for $m = 1 : N_{irs}$ **do**
    $k_m = \check{\mathbf{h}}_d(m)$;
    for $i = 1 : N_{irs}$ **do**
      $k_m = k_m + \mathcal{B}(m, i)\mathbf{v}(i); \forall\ i \neq m$
    $\theta_m^* = arg\ min_{\theta \in \mathcal{F}} \left| \theta - \angle k_m \right|$
    k=k+1
  $\mathbf{v} = exp(j\theta)$
  $R^k = \log_2 \left(1 + \frac{P_T \left\| \mathbf{h}_d + \mathbf{h}_r diag(\mathbf{v}) \mathbf{h}_u \right\|^2}{N_0} \right)$

7.4 Results

We present numerical findings in this section to support our analysis and the effectiveness of the IRS grouping technique. A uniform rectangular array (URA) at the BS and a URA at the IRS along with a single antenna UE are considered in a 3D plan as in Figure 7.8. For simplicity, for both the BS and IRS, the antenna/elements

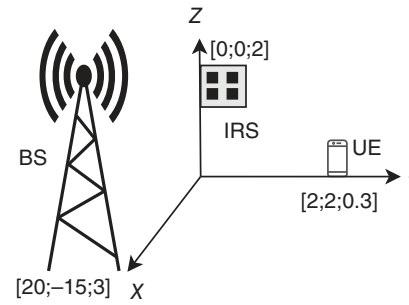

Figure 7.8 IRS-assisted network setup for simulation.

are arranged with same number of rows and columns. To make it more practical oriented, both the large-scale and small-scale fadings are considered. In the case of large scale, i.e., distance dependent fading channel, the corresponding path is modeled as $C_0 d^{-\alpha}$ where d represents the distance corresponding to each path. And also for the simulation, we consider $\alpha_{BS \to IRS} = 2.2$ and $\alpha_{IRS \to UE} = 2.8$. The Rician fading model is used for realizing the small-scale fading.

The simulation is carried out on the MATLAB platform. Following an average of more than 1000 random channel implementations, the findings are shown here.

Quantizing the phase shifts yields the effects shown in Figure 7.9. As we can observing, existing communication without IRS scarcely offers any advantages

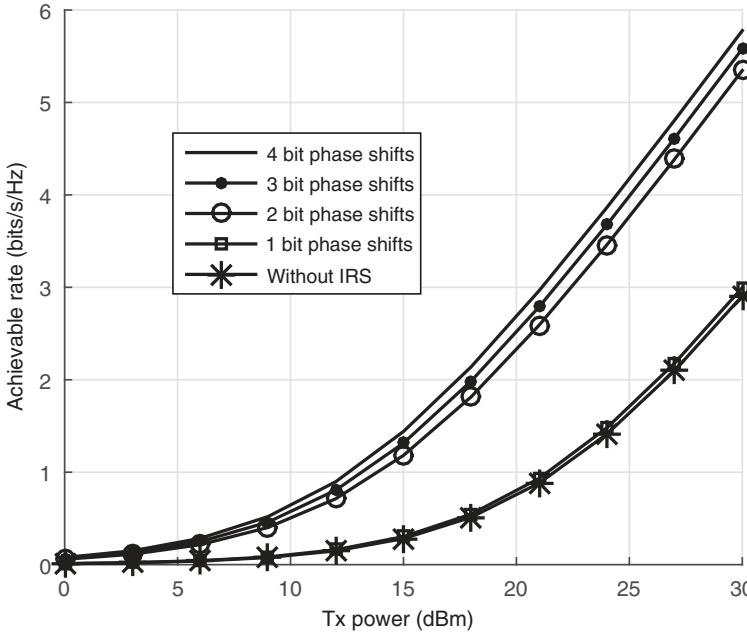

Figure 7.9 Impact of bits.

above 1-bit phase shifts. The performance of the proposed system sharply improves as the discretization level of the phase-shift values is increased to 2 bits. The performance improvement is not all that great when we further increase the number of quantization bits to 3/4. As depicted, with $P_T = 15$ dBm, the system achievable rate is $R = 0.3023$ bits/s/Hz, $R = 1.182$ bits/s/Hz, $R = 1.315$ bits/s/Hz, and $R = 1.441$ bits/s/Hz for the system with 1 bit, 2 bits, 3 bits, and 4 bits quantization respectively. Thus, we can say that even 2-bit phase shifts in IRS are enough to increase the performance of the communication system with much-reduced implementation complexity.

Figure 7.10 represents the impact of the number of IRS elements (N_{irs}) over the system performance. For this simulation, the same networks are considered as in Figure 7.8 with 4×4 antenna arrangement at the BS and full CSI. As depicted in Figure 7.11, with ($P_T = 20$ dBm) N_{irs}=36, 64, 100, 144, and 256, the achievable rates are $R = 0.9504$ bits/s/Hz, $R = 1.134$ bits/s/Hz, $R = 1.417$ bits/s/Hz, $R = 1.739$

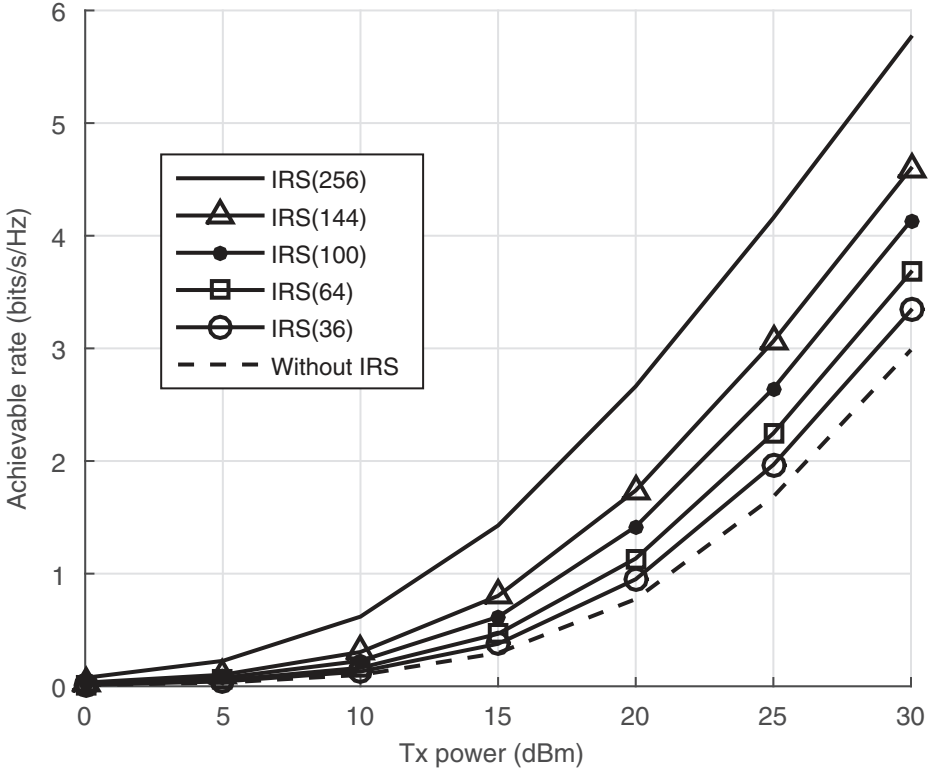

Figure 7.10 Impact of N_{irs}.

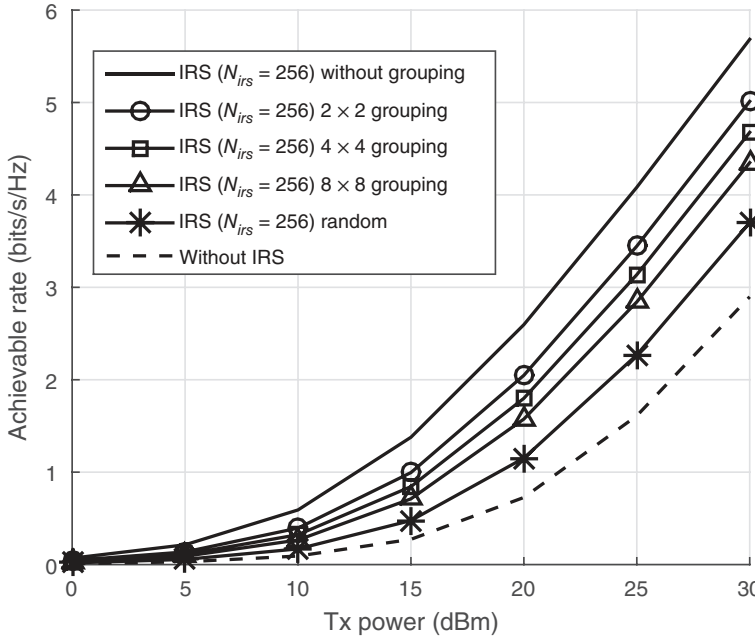

Figure 7.11 Impact of grouping.

bits/s/Hz, and $R = 2.663$ bits/s/Hz, respectively. It clearly indicates that with the increase in N_{irs}, there is a significant increase in the achievable rate (R).

The effect of IRS grouping scheme on the system performance is shown in Figure 7.10. For this analysis, we take into account of 4×4 antennas at the BS and 16×16 elements at the IRS with variable grouping size. As in the result, one can observe the decrease in the performance with the introduction in the grouping but still it is providing better performance than the system without IRS. As depicted, with $P_T = 20$ dBm, the system achievable rate is $R = 2.048$ bits/s/Hz, $R = 1.799$ bits/s/Hz, and $R = 1.575$ bits/s/Hz, when grouping size is 2×2, 4×4, and 8×8, respectively. And also, it depicts the importance of the optimization of phases. For example, with $P_T = 20$ dBm, the system with $N_{irs} = 256$ provides $R = 2.596$ bits/s/Hz and $R = 1.152$ bits/s/Hz with optimized phase and random-phase, respectively.

Figure 7.12 represents the cumulative distribution function (CDF) and probability density function (PDF) variation with the change in received power. Both the curves demonstrate the impact of IRS grouping over the achievable rate of the system and also it show that there exists a significant improvement due to the presence of the IRS.

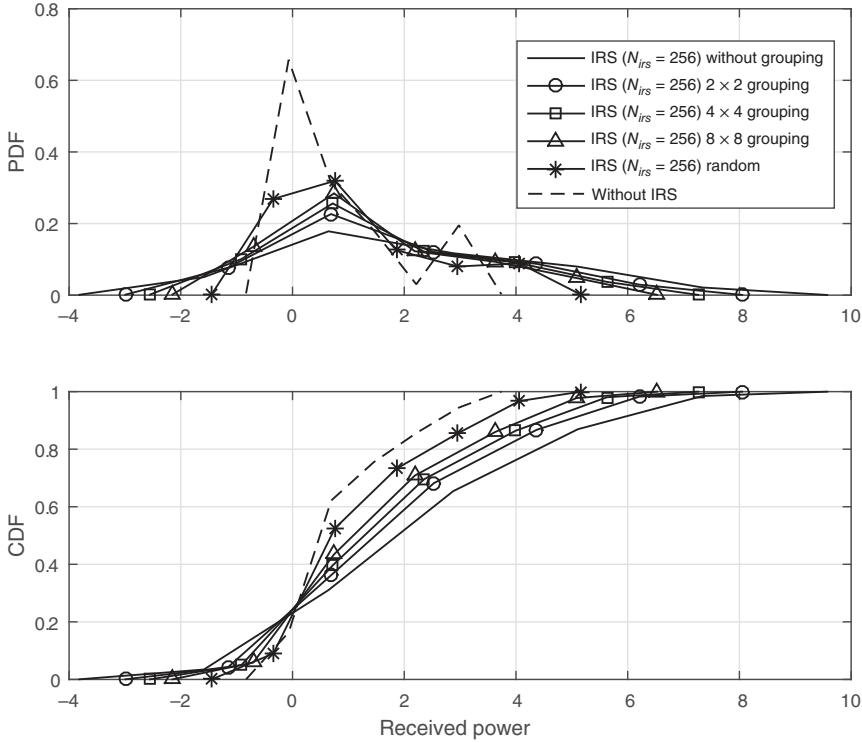

Figure 7.12 CDF and PDF variation with IRS grouping.

7.5 Conclusion and Future Scope

From the perspective of the future generation wireless communication system, the IRS is emerging as a key player. At the same time, it comes with lots of challenges, channel estimation for a large IRS system is one of them. It becomes particularly important for phase/beamformation optimization. Therefore, considering the tread-of between the performance gain and the implementation complexity, the IRS element grouping technique emerges as a promising solution. Through the numerical analysis presented in this chapter, it is clear that it improves the system's performance in comparison to the conventional system without IRS. At the same time, the system performance degrades with the increase in the group size as channels associated with individual IRS elements cannot be guaranteed to be identical, resulting in limited access to CSI within the element-grouping scheme.

In future scope, one can explore the possibility of adaptive IRS element grouping and also under multiuser scenario, intelligent group selection can be exploited.

References

1 Imoize, A.L., Adedeji, O., Tandiya, N., and Shetty, S. (2021). 6G enabled smart infrastructure for sustainable society: opportunities, challenges, and research roadmap. *Sensors* 21 (5): 1709. https://doi.org/10.3390/s21051709.

2 Imoize, A.L., Obakhena, H.I., Anyasi, F.I., and Sur, S.N. (2022). A review of energy efficiency and power control schemes in ultra-dense cell-free massive MIMO systems for sustainable 6G wireless communication. *Sustainability* 14 (17): 11100. https://doi.org/10.3390/su141711100.

3 Le, C.-B., Do, D.-T., and Sur, S.N. (2021). Reconfigurable intelligent surface (RIS)-assisted wireless systems: potentials for 6G and a case study. *Advances in Communication, Devices and Networking: Proceedings of ICCDN 2020*, 367–378. Springer Singapore. https://doi.org/10.1007/978-981-16-2911-2_39.

4 Liu, Y., Liu, X., Mu, X. et al. (2021). Reconfigurable intelligent surfaces: principles and opportunities. *IEEE Communications Surveys & Tutorials* 23 (3): 1546–1577. https://doi.org/10.1109/comst.2021.3077737.

5 Pan, C., Zhou, G., Zhi, K. et al. (2022). An overview of signal processing techniques for RIS/IRS-aided wireless systems. *IEEE Journal of Selected Topics in Signal Processing* 16 (5): 883–917. https://doi.org/10.1109/jstsp.2022.3195671.

6 Sur, S.N. and Bera, R. (2021). Intelligent reflecting surface assisted MIMO communication system: a review. *Physical Communication* 47: 101386. https://doi.org/10.1016/j.phycom.2021.101386.

7 Wu, Q. and Zhang, R. (2019). Intelligent reflecting surface enhanced wireless network via joint active and passive beamforming. *IEEE Transactions on Wireless Communications* 18 (11): 5394–5409. https://doi.org/10.1109/twc.2019.2936025.

8 Wu, Q. and Zhang, R. (2020). Towards smart and reconfigurable environment: intelligent reflecting surface aided wireless network. *IEEE Communications Magazine* 58 (1): 106–112. https://doi.org/10.1109/mcom.001.1900107.

9 Bjornson, E., Wymeersch, H., Matthiesen, B. et al. (2022). Reconfigurable intelligent surfaces: a signal processing perspective with wireless applications. *IEEE Signal Processing Magazine* 39 (2): 135–158. https://doi.org/10.1109/msp.2021.3130549.

10 Shlezinger, N., Alexandropoulos, G.C., Imani, M.F. et al. (2021). Dynamic metasurface antennas for 6G extreme massive MIMO communications. *IEEE Wireless Communications* 28 (2): 106–113. https://doi.org/10.1109/mwc.001.2000267.

11 Jung, M., Saad, W., Jang, Y. et al. (2020). Performance analysis of large intelligent surfaces (LISs): asymptotic data rate and channel hardening effects. *IEEE Transactions on Wireless Communications* 19 (3): 2052–2065. https://doi.org/10.1109/twc.2019.2961990.

12 Wu, Q., Zhang, S., Zheng, B. et al. (2021). Intelligent reflecting surface-aided wireless communications: a tutorial. *IEEE Transactions on Communications* 69 (5): 3313–3351. https://doi.org/10.1109/tcomm.2021.3051897.

13 Sur, S.N., Singh, A.K., Kandar, D. et al. (2022). Intelligent reflecting surface assisted localization: opportunities and challenges. *Electronics* 11 (9): 1411. https://doi.org/10.3390/electronics11091411.

14 Sur, S.N., Kandar, D., Imoize, A.L., and Bera, R. (2022). An overview of intelligent reflecting surface assisted UAV communication systems. In: *Unmanned Aerial Vehicle Cellular Communications*, 67–94. Springer International Publishing. https://doi.org/10.1007/978-3-031-08395-2_4.

15 Yang, H., Cao, X., Yang, F. et al. (2016). A programmable metasurface with dynamic polarization, scattering and focusing control. *Scientific Reports* 6 (1): https://doi.org/10.1038/srep35692.

16 Pérez-Adán, D., Fresnedo, Ó., González-Coma, J.P., and Castedo, L. (2021). Intelligent reflective surfaces for wireless networks: an overview of applications, approached issues, and open problems. *Electronics* 10 (19): 2345. https://doi.org/10.3390/electronics10192345.

17 Yang, Y., Zheng, B., Zhang, S., and Zhang, R. (2020). Intelligent reflecting surface meets OFDM: protocol design and rate maximization. *IEEE Transactions on Communications* 68 (7): 4522–4535. https://doi.org/10.1109/tcomm.2020.2981458.

18 Hu, J., Liang, Y.-C., Pei, Y. et al. (2023). Reconfigurable intelligent surface based uplink MU-MIMO symbiotic radio system. *IEEE Transactions on Wireless Communications* 22 (1): 423–438. https://doi.org/10.1109/twc.2022.3194910.

19 Huang, C., Zappone, A., Alexandropoulos, G.C. et al. (2019). Reconfigurable intelligent surfaces for energy efficiency in wireless communication. *IEEE Transactions on Wireless Communications* 18 (8): 4157–4170. https://doi.org/10.1109/twc.2019.2922609.

20 Chen, Y., Wang, Y., and Jiao, L. (2022). Robust transmission for reconfigurable intelligent surface aided millimeter wave vehicular communications with statistical CSI. *IEEE Transactions on Wireless Communications* 21 (2): 928–944. https://doi.org/10.1109/twc.2021.3100492.

21 Luo, C., Li, X., Jin, S., and Chen, Y. (2021). Reconfigurable intelligent surface-assisted multi-cell MISO communication systems exploiting statistical CSI. *IEEE Wireless Communications Letters* 10 (10): 2313–2317. https://doi.org/10.1109/lwc.2021.3100427.

22 Ahmed, S., Kamal, A.E., and Selim, M.Y. (2021). Adding active elements to reconfigurable intelligent surfaces to enhance energy harvesting for IoT devices. *MILCOM 2021 - 2021 IEEE Military Communications Conference (MILCOM)*. IEEE. https://doi.org/10.1109/milcom52596.2021.9653007.

23 Khoshafa, M.H., Ngatched, T.M.N., Ahmed, M.H., and Ndjiongue, A.R. (2021). Active reconfigurable intelligent surfaces-aided wireless communication system. *IEEE Communications Letters* 25 (11): 3699–3703. https://doi.org/10.1109/lcomm.2021.3110714.

24 Dajer, M., Ma, Z., Piazzi, L. et al. (2022). Reconfigurable intelligent surface: design the channel—a new opportunity for future wireless networks. *Digital Communications and Networks* 8 (2): 87–104. https://doi.org/10.1016/j.dcan.2021.11.002.

25 Tang, W., Chen, X., Chen, M.Z. et al. (2021). On channel reciprocity in reconfigurable intelligent surface assisted wireless networks. *IEEE Wireless Communications* 28 (6): 94–101. https://doi.org/10.1109/mwc.001.2100136.

26 Yang, Y., Zhang, S., and Zhang, R. (2019). IRS-enhanced OFDM: power allocation and passive array optimization. *2019 IEEE Global Communications Conference (GLOBECOM)*. IEEE. https://doi.org/10.1109/globecom38437.2019.9014204.

27 Li, H., Shen, S., Nerini, M., and Clerckx, B. (2024). Reconfigurable intelligent surfaces 2.0: beyond diagonal phase shift matrices. *IEEE Communications Magazine* 62 (3): 102–108. https://doi.org/10.1109/MCOM.001.2300019.

28 Nguyen, T.-A., Nguyen, H.-V., Do, D.-T., and Sur, S.N. (2023). *Performance Analysis of Two IRS-NOMA Users in Downlink*, 661–674. Springer Nature Singapore. ISBN 9789819919833. https://doi.org/10.1007/978-981-99-1983-3_60.

29 Sur, S.N., Singh, A.K., Kandar, D., and Bera, R. (2021). Sum-rate analysis of intelligent reflecting surface aided multi-user millimeter wave communications system. *Journal of Physics: Conference Series* 1921 (1): 012050. https://doi.org/10.1088/1742-6596/1921/1/012050.

30 Sur, S.N., Singh, A.K., Kandar, D., and Imoize, A.L. (2023). Aerial IRS-assisted wireless communication systems. *2023 10th International Conference on Signal Processing and Integrated Networks (SPIN)*. IEEE. https://doi.org/10.1109/spin57001.2023.10117437.

31 Daniel, C.J. (2022). Dynamic metasurface grouping for IRS optimization in massive MIMO communications. PhD thesis. University of Kansas.

32 Nadeem, Q.-U.-A., Alwazani, H., Kammoun, A. et al. (2020). Intelligent reflecting surface-assisted multi-user MISO communication: channel estimation and beamforming design. *IEEE Open Journal of the Communications Society* 1: 661–680. https://doi.org/10.1109/ojcoms.2020.2992791.

33 He, Z.-Q. and Yuan, X. (2020). Cascaded channel estimation for large intelligent metasurface assisted massive MIMO. *IEEE Wireless Communications Letters* 9 (2): 210–214. https://doi.org/10.1109/lwc.2019.2948632.

34 Jensen, T.L. and De Carvalho, E. (2020). An optimal channel estimation scheme for intelligent reflecting surfaces based on a minimum variance unbiased estimator. *ICASSP 2020 - 2020 IEEE International Conference on*

Acoustics, Speech and Signal Processing (ICASSP). IEEE. https://doi.org/10.1109/icassp40776.2020.9053695.

35 Song, W. and Guan, B. (2021). Reconfigurable intelligent surface-based space-time block transmission on 6G. *Wireless Communications and Mobile Computing* 2021: 1–9. https://doi.org/10.1155/2021/5569006.

36 Zhang, S., Zhang, S., Gao, F. et al. (2021). Deep learning-based RIS channel extrapolation with element-grouping. *IEEE Wireless Communications Letters* 10 (12): 2644–2648. https://doi.org/10.1109/lwc.2021.3110305.

37 Lin, S., Zheng, B., Alexandropoulos, G.C. et al. (2021). Reconfigurable intelligent surfaces with reflection pattern modulation: beamforming design and performance analysis. *IEEE Transactions on Wireless Communications* 20 (2): 741–754. https://doi.org/10.1109/twc.2020.3028198.

38 Tahir, B., Schwarz, S., and Rupp, M. (2021). Outage analysis of uplink IRS-assisted NOMA under elements splitting. *2021 IEEE 93rd Vehicular Technology Conference (VTC2021-Spring)*. IEEE. https://doi.org/10.1109/vtc2021-spring51267.2021.9449027.

39 Mao, Z., Wang, W., Xia, Q. et al. (2022). Element-grouping intelligent reflecting surface: electromagnetic-compliant model and geometry-based optimization. *IEEE Transactions on Wireless Communications* 21 (7): 5362–5376. https://doi.org/10.1109/twc.2021.3139611.

40 Hwang, D., Yang, J., Nam, S.-S., and Song, H.-K. (2022). Full duplex relaying with intelligent reflecting surface: joint beamforming and phase adjustment. *Mathematics* 10 (17): 3075. https://doi.org/10.3390/math10173075.

41 Xu, J., Mu, X., and Liu, Y. (2022). Exploiting STAR-RISs in near-field communications. *IEEE Transactions on Wireless Communications* 23 (3): 2181–2196. https://doi.org/10.1109/TWC.2023.3296191.

42 Wang, B., Li, H., Cheng, Z. et al. (2023). A dual-function radar-communication system empowered by beyond diagonal reconfigurable intelligent surface. *IEEE Transactions on Communications* https://doi.org/10.1109/TCOMM.2024.3447917.

43 Asmoro, K. and Shin, S.Y. (2022). RIS grouping based index modulation for 6G telecommunications. *IEEE Wireless Communications Letters* 11 (11): 2410–2414. https://doi.org/10.1109/lwc.2022.3205038.

44 Cai, C., Yuan, X., and Zhang, Y.-J.A. (2023). RIS partitioning based scalable beamforming design for large-scale MIMO: asymptotic analysis and optimization. *IEEE Transactions on Wireless Communications* 22 (9): 6061–6077. https://doi.org/10.1109/twc.2023.3239371.

45 Kim, M.-A., Yoo, S.-G., Kim, H.-D. et al. (2023). Group-connected impedance network of RIS-assisted rate-splitting multiple access in MU-MIMO wireless communication systems. *Sensors* 23 (8): 3934. https://doi.org/10.3390/s23083934.

46 Awais, M., Khan, M.A., and Kim, Y.H. (2023). Deep denoising and unfolding for IRS cascaded channel estimation with element-grouping. *IEEE Wireless Communications Letters* 12 (10): 1726–1730. https://doi.org/10.1109/lwc.2023.3290204.

47 Li, H., Shen, S., and Clerckx, B. (2023). A dynamic grouping strategy for beyond diagonal reconfigurable intelligent surfaces with hybrid transmitting and reflecting mode. *IEEE Transactions on Vehicular Technology* 72 (12): 16748–16753.

48 Dampahalage, D., Manosha, K.B.S., Rajatheva, N., and Latva-aho, M. (2020). Intelligent reflecting surface aided vehicular communications. *2020 IEEE Globecom Workshops (GC Wkshps*. IEEE. https://doi.org/10.1109/gcwkshps50303.2020.9367569.

49 Wu, Q. and Zhang, R. (2020). Beamforming optimization for wireless network aided by intelligent reflecting surface with discrete phase shifts. *IEEE Transactions on Communications* 68 (3): 1838–1851. https://doi.org/10.1109/tcomm.2019.2958916.

8

Reconfigurable Intelligent Surface-Empowered Non-orthogonal Multiple Access: Outage and ABER Analysis of Smart and Blind Transmissions

Vinoth Babu Kumaravelu[1], Anjana Babu Sujatha[1], Helen Sheeba John Kennedy[1], Francisco Rubén Castillo Soria[2], Dinh-Thuan Do[3], Velmurugan Periyakarupan Gurusamy Sivabalan[4], Thiruvengadam Sundarrajan Jayaraman[4], Agbotiname Lucky Imoize[5,6], Vishnu Vardhan Gudla[7], and Arthi Murugadass[8]

[1] *Department of Communication Engineering, School of Electronics Engineering, Vellore Institute of Technology, Vellore, Tamil Nadu, India*
[2] *Telecommunications Department, Faculty of Science, Autonomous University of San Luis Potosi (UASLP), San Luis Potosi, Mexico*
[3] *Brenton School of Engineering, University of Mount Union, Alliance, OH, USA*
[4] *Department of Electronics and Communication Engineering, Thiagarajar College of Engineering, Madurai, Tamil Nadu, India*
[5] *Department of Electrical and Electronics Engineering, Faculty of Engineering, University of Lagos, Lagos, Nigeria*
[6] *Department of Electrical Engineering and Information Technology, Ruhr University, Bochum, Germany*
[7] *Physical Layer Expert, Comms., Media & Tech Unit, L&T Technology Services, Bangalore, India*
[8] *School of Computer Science and Engineering, Vellore Institute of Technology, Chennai, Tamil Nadu, India*

8.1 Introduction

Because sophisticated multimedia applications are rapidly evolving, next-generation networks are required to offer improved spectral efficiency, energy efficiency, and massive connectivity [1]. Energy consumption is a challenging task for future networks due to higher data rates and massive connections. Some nations began releasing fifth-generation (5G) compatible mobile devices to the market in the first quarter of 2020 [2]. The first 5G deployment took place in 2018, and it focused on physical layer technologies such as millimeter waves and orthogonal frequency division multiplexing (OFDM). Alternative technologies, such as index modulation (IM), non-orthogonal multiple access (NOMA), less costly multiple input-multiple output (MIMO) variations, and terahertz (THz) communications have been developed by researchers all around the globe for subsequent 5G releases. The sixth-generation (6G) network is an extension of

Reconfigurable Intelligent Surfaces for 6G and Beyond Wireless Networks, First Edition.
Edited by Agbotiname Lucky Imoize, Vinoth Babu Kumaravelu, and Dinh-Thuan Do.

the 5G network, which is projected to be operational by 2030. It should be able to accommodate new user needs, applications, and use cases. 6G does not need additional bandwidth; rather, it necessitates greater bandwidth efficiency [3].

8.1.1 RIS

Electromagnetic (EM) wave transmission is affected by several uncontrollable factors such as signal attenuation due to path loss, signal absorption, reflections, and diffractions due to multipath propagation from a large number of objects [4]. As a result of uncontrollable radio environments, quality of service (QoS) and communication efficiency are significantly degraded. Recently, with advances in reconfigurable meta-surfaces, a new technology known as reconfigurable intelligent surfaces (RISs) has evolved, which can enable deterministic and programmable control over the behavior of the wireless environments.

RIS is a real-time programmable two-dimensional structure made up of meta elements. It is used to focus the EM waves towards the intended user by changing the properties of the surface. It has many use cases such as energy focusing and energy nulling to support the desired user and to nullify the signal to the undesired user, as illustrated in Figure 8.1.

The baseband signal reflected by N RIS elements is received by the user, which is given by,

$$y = \left[\sum_{i=1}^{N} p_i e^{j\phi_i} h_i\right] x + w \tag{8.1}$$

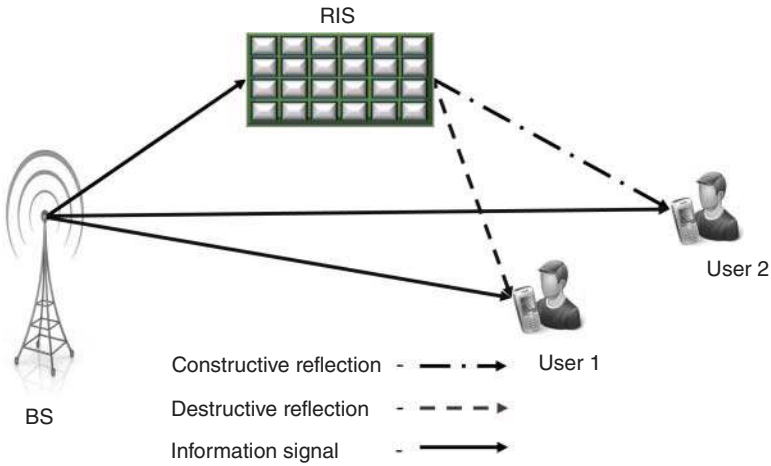

Figure 8.1 Use cases of RIS.

where $p_i \sim C\mathcal{N}(0,1)$ is the flat fading channel between AP and RIS. $h_i \sim C\mathcal{N}(0,1)$ is the flat fading channel between RIS and user. When RIS performs smart reflection $\phi_i = \angle p_i + \angle h_i, i = 1, 2, \ldots, N$. This smart transmission leads to diversity and array gains, which increases with N. However, it requires accurate knowledge of dual-hop channel. But this is not feasible every time. However, the array gain can be attained through blind transmission, where $\phi_i = 0, i = 1, 2, \ldots, N$. In (8.1), $w \sim C\mathcal{N}\left(0, N_0\right)$ is the noise added at the user end, and x is transmitted symbol with average energy, E_s.

RIS has the potential to enhance coverage ratio, spectrum, and energy efficiency [5]. It has the ability to create smart radio propagation environments. This customizes the signal propagation from the transmitter to the receiver [6]. The following distinctive aspects of RIS were noted by the authors of [7]: They do not require any energy, and the components are almost passive. They are made out of a contiguous surface that can shape an incoming wave impinging on any point. Analog-to-digital converters (ADCs), digital-to-analog converters (DACs), and power amplifiers are not used. As a result, no thermal noise is introduced or amplified. They are capable of working at any operational frequency. They are easily deployable on walls, building facades, advertisement boards, vehicle doors, human clothing, unmanned aerial vehicles (UAVs), and other surfaces. For effective beamforming, traditional MIMO involves extensive precoding and radio frequency (RF) level processing, which may be readily accomplished with the aid of RIS [7–9].

8.1.2 NOMA

Frequency division multiple access (FDMA), time division multiple access (TDMA), code division multiple access (CDMA), and orthogonal frequency division multiple access (OFDMA) are examples of traditional orthogonal multiple access (OMA) methods that cannot match the expanding service needs [10]. The notion of NOMA is introduced in 5G to overcome the massive connectivity issue. Multiple users share resources in the power-domain (PD) NOMA by distributing various power levels. When there are two users, the user 1 with good channel gain receives less power than the user 2 with low-channel gain.

In NOMA, the superimposed signal is transmitted, and at reception, by performing successive interference cancellation (SIC) users decode their own information. The superimposed signal transmitted from an AP for K number of users in the downlink is given by,

$$x_s = \sum_{k=1}^{K} \sqrt{\rho_k} x_k = \sum_{k=1}^{K} \sqrt{\beta_k E_s} x_k \tag{8.2}$$

where $\sqrt{\rho_k}$ is the power allocated to kth user and x_k is the transmitted symbol corresponding to kth user. NOMA recognizes the benefits of cooperative communication [11–15]. NOMA is extremely susceptible to hardware failures [16]. The MIMO–NOMA concept is costly to implement and demands a high level of computational complexity [17]. Furthermore, when there are a large number of users, the system's performance is limited. As a result, relying only on NOMA for massive connectivity and broad coverage is impossible.

8.1.3 Contributions

Integration of RIS with multiple access techniques is projected to boost coverage, connectivity, spectrum, and energy efficiency [18]. The analytical outage and average bit error rate (ABER) expressions for RIS-assisted NOMA for an access point (AP) scenario are derived in this chapter. The proposed system has a huge impact on energy efficiency. The important contributions of this chapter are listed below:

- A unique RIS–AP-aided downlink PD NOMA system is proposed. Based on the availability of channel information, two transmission techniques, smart and blind, have been devised for RIS-AP-NOMA.
- The analytical ABER and outage expressions are developed for both near and far users.
- Numerical simulation results are used to validate the proposed systems's performance.

8.1.4 Organization

The following is how the rest of the chapter is organized: Section 8.2 delves into the prior works. Section 8.3 introduces the RIS-AP-NOMA. Section 8.4 deduces the analytical outage and ABER expressions for smart and blind RIS-AP-NOMA. Section 8.5 simulates the analytical expressions, and Section 8.6 concludes the chapter.

8.2 Related Works

8.2.1 Prior Works on RIS

Cui et al. [19], Di Renzo and Song [20], and Tang et al. [21] demonstrated that by using software to control the reflecting components on RIS, physical characteristics such as the reflection coefficient may be modified, allowing the reflected waves to be adjusted. The use of channel state information (CSI) allows for joint transmitter, RIS, and receiver optimization [4, 22, 23]. Basar et al. [4], Basar [24],

and Di Renzo et al. [25] formulated an analytical framework for RIS-assisted point-to-point communications to measure the ABER. The channel capacity of RIS-assisted point-to-point communications is derived by Han et al. [26].

To avoid the effect of line-of-sight (LoS) blocking, a RIS-aided light fidelity (LiFi) system is presented by Abumarshoud et al. [27]. The significant issues that this entails, as well as future research areas, are also discussed. RIS-assisted quadrature reflection modulation (QRM) is suggested by Lin et al. [28], which promises to convey information without the use of extra RF chains. RIS–QRM outperforms traditional ON/OFF-based RIS systems in terms of error performance.

The RF chains, signal processing capabilities, noise, duplexing, hardware cost, and power consumption of RIS are compared to those of amplify-and-forward (AF), decode-and-forward (DF), and full-duplex (FD) relays by Pan et al. [29]. The use of RIS in millimeter wave (mmWave) systems, multicell networks, simultaneous wireless information and power transfer (SWIPT) networks, mobile edge computing networks, multicast networks, NOMA, cognitive networks, physical layer security (PLS) networks, and other areas is described.

The recent advancements in the field of RIS, as well as notable opportunities for future study are discussed by Basar and Poor [30]. The advantages and disadvantages of active, transmitter, transmissive reflective, stand-alone RISs over reflective RISs are reviewed in this paper. RIS is used to aid terahertz communications [31]. The sum rate is optimized while fulfilling the rate demands of individual users by adjusting the phase shifts of RIS.

The network-level optimization of RIS-assisted point-to-multipoint communications is investigated by Liu et al. [9]. Xu et al. [32] analyzed the PLS of RIS in terms of secrecy outage probability and secrecy rate. RIS suppresses the information leakage from eavesdroppers by passive beamforming toward desired directions. RIS can be used as a transmitter carrying extra information through phase modulation, therefore it provides secure communication.

8.2.2 Prior Works on RIS-Aided NOMA

By sharing the orthogonal resource block among numerous users, NOMA can improve the spectral efficiency of classical OMA. NOMA may not be a viable choice if the users' channel vectors are orthogonal. The NOMA is most effective when all of the users' channel vectors are pointing in the same angular direction. The wireless channel vectors of all users can be modified with the help of RIS to meet NOMA's requirements [33]. A simple RIS-assisted NOMA system is suggested in [34], where the power level of cell-edge users is enhanced to ensure better QoS. Fu et al. [33] optimized beamforming vectors at the base station (BS) and RIS phase shifts to reduce BS power consumption while maintaining the QoS requirements of each user. Here, a difference of convex optimization method is

devised that outperforms traditional methods in terms of reducing BS transmit power.

For the RIS-aided NOMA downlink scenario, a priority of design (POD) is proposed, which is capable of boosting spectral efficiency by improving the performance of the user with the best channel condition, while the remaining users use beamforming at RIS for reliability [35]. The performance of the RIS-assisted NOMA system is further assessed here by deriving closed-form expressions for outage probability, ergodic rate, spectrum efficiency, and energy efficiency. Simulation results show that NOMA with RIS-assisted optimal power allocation (PA) outperforms its OMA equivalent.

Two different RIS-aided PD NOMA systems are suggested by Chauhan et al. [36], namely, RIS partition-assisted (RISP)-quadrature NOMA (RISP-Q-NOMA) and RISP-PD-NOMA system. The in-phase and quadrature components are involved to support the odd and even users of RISP-Q-NOMA's superimposed signal, whereas in RISP-PD-NOMA, certain elements in RIS are allocated to a specific user in the system. The evaluation of these systems' performance under various scenarios reveals that RISP-Q-NOMA works better under imperfect SIC because of lower detection latency and decoding intricacy, RISP-PD-NOMA performs better under perfect SIC. Zheng et al. [37] suggested the multifunctional RIS to improve the performance of the NOMA downlink multiuser network. Multifunctional RIS can provide transmission, reflection, and amplification at the same time.

8.2.3 Prior Works on RIS-Aided NOMA with ABER and Outage Calculations

A deep deterministic policy gradient (DDPG) machine learning algorithm is used to optimize user partitioning and RIS phase shifting in an RIS-aided multiuser NOMA downlink system. When compared to a standard OMA system, simulation results show that the devised approach provides a higher sum rate [38].

To enhance user fairness and spectrum efficiency, a NOMA method with RIS partitioning is presented by Khaleel and Basar [39]. The precise and asymptotic outage probability expressions are also developed. The suggested system's performance is compared to that of traditional benchmark systems in terms of ergodic capacity, outage probability, and user fairness using simulations.

The ABER performance of simultaneously transmitting and reflecting (STAR)–RIS-supported NOMA networks are examined by Aldababsa et al. [40]. Monte Carlo simulations are used to validate the closed-form ABER equations in the circumstances of perfect and imperfect SIC. According to the results, STAR-RIS-NOMA performs better in terms of ABER than the traditional NOMA system, indicating that STAR–RIS may be a viable NOMA 2.0 option.

Kumaravelu et al. [41] suggested the RIS-assisted NOMA system, which overcomes wireless challenges in an energy efficient way. The analytical outage probability expressions for RIS-assisted NOMA are derived by considering RIS as a smart reflector (SR) and an AP, and an optimization framework is formulated for deciding PA factors to maximize the sum rate. RIS-assisted NOMA surpasses conventional NOMA in terms of outage and sum capacity. It has a ∼62% higher sum capacity than the conventional NOMA system.

Kumaravelu et al. [42] employed the RIS for the smart vehicular networks, which is implemented to assist downlink fixed-NOMA (FNOMA) system. The suggested system is evaluated for two scenarios such as RIS as SR and RIS as roadside units (RSUs). The integration of RIS outperforms traditional NOMA variants in terms of outage and throughput. The analytical outage expressions for blind RIS-assisted FNOMA are derived and observed that the suggested model outperforms the traditional NOMA variants.

Velmurugan et al. [43] suggested FD bidirectional machine-type communication (MTC) system with RIS. Instead of continuous phase shifting, discrete phase shifting in RIS is implemented, which is realizable. The ABER and outage performances with continuous and discrete phase shifting are analyzed. It is observed that the outage performance in FD mode has an SNR improvement of ∼6 dB compared to half duplex mode. The ABER performance in FD mode has an SNR improvement of ∼8 dB as the number of reflecting elements doubles in RIS. The performance of the system is limited due to the self-interference in FD and discrete phase shifts in RIS.

Thirumavalavan and Jayaraman [44] suggested an RIS-assisted PD NOMA that improves reliability by integrating the benefits of both RIS and NOMA. The suggested system's analytical ABER expressions are derived considering smart RIS with two-hop communication. The numerical simulation results are used to analyze the suggested system. It has been discovered that the suggested system outperforms the conventional NOMA system. It is assumed in this study that RIS is positioned between the transmitter and the receiver in the propagation environment. However, because of the propagation losses and fading, the signal obtained at RIS is very low. As a result, it is recommended that RIS be used near the AP or receiver. Motivated by the work of [44], we derived the ABER of RIS-AP-NOMA system in this chapter.

8.3 RIS-AP-NOMA

The idea of RIS-AP-NOMA is illustrated in Figure 8.2. A new paradigm RIS as an AP is introduced by Basar [24], where the information is transmitted by the RIS itself. RIS is made up of low-cost passive reflector elements that also serve as a

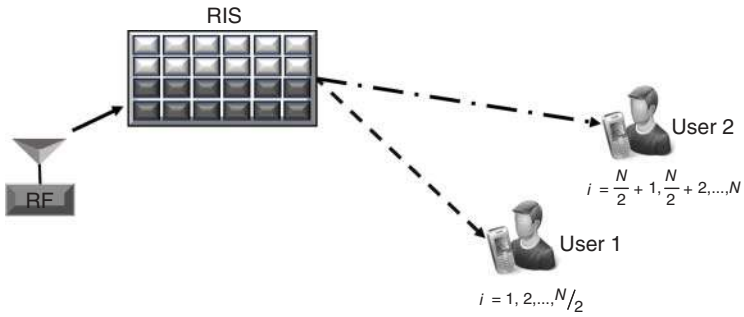

Figure 8.2 RIS-AP-NOMA system.

source. In this configuration, RIS is linked to the network through a wired connection, allowing for transmission without RF processing. RIS jointly generates the phase shifts for modulation (information-to-constellation mapping) and channel compensation. The unmodulated carrier is generated by the RF generator. The RF source is positioned closer to the RIS or on the RIS so that fading does not impair the transmission. As a result, the source-RIS channel may be omitted in this study. In [24], two alternative RIS–AP ideas, smart and blind, are implemented based on channel knowledge on RIS. The two-user PD NOMA is explored in this study. The RIS elements are split evenly between the two users ($N_1 = N_2 = N/2$). The superimposed signal is transmitted from RIS–AP, which contains the symbols of both user 1 and user 2. Usually, more power is allocated to user 2 and less power is allocated to user 1. This chapter does not address the optimal way to distribute power to users.

8.4 Analytical Model

In this section, analytical closed-form outages and ABER expressions are derived for smart and blind transmissions.

8.4.1 Smart Transmission

The channel phases between each RIS element and receiver are expected to be available at the RIS for pre-compensation in a smart transmission system. The superimposed symbol for a two-user scenario can be deduced from (8.2) as,

$$x_s = \sqrt{\rho_1} x_1 + \sqrt{\rho_2} x_2 \tag{8.3}$$

The superimposed signal contains the symbols corresponding to user 1 (x_1) and user 2 (x_2), which has a total power of E_S. $\rho_1 = \beta_1 E_s$ and $\rho_2 = \beta_2 E_s$ are the powers

allocated to user 1 and user 2, respectively. β_1 and β_2 are the NOMA PA coefficients with $\beta_1 + \beta_2 = 1, 0 \leq \beta_1, \beta_2 \leq 1$.
The received signal of user 2 is given by,

$$y_2 = \left[\sum_{i=\left(\frac{N}{2}\right)+1}^{N} h_i e^{-j\phi_i} \right] x_s + w_2 \tag{8.4}$$

where $w_2 \sim C\mathcal{N}\ \left(0, N_0\right)$ is the noise added to the user 2's signal. The channel gain between ith RIS element and the user is given by,

$$h_i = \alpha_i e^{-j\psi_i} \tag{8.5}$$

Here, α_i and ψ_i are the magnitude and phase components of h_i. For AP scenario, $\psi_i = \phi_i$. The received signal expression in (8.4) becomes:

$$y_2 = \underbrace{\left[\sum_{i=(N/2)+1}^{N} \alpha_i \right]}_{H} x_s + w_2 \tag{8.6}$$

The received signal at user 1 is given by,

$$y_1 = \left[\sum_{i=1}^{N/2} h_i e^{-j\phi_i} \right] x_s + w_1 \tag{8.7}$$

where $w_1 \sim C\mathcal{N}\ \left(0, N_0\right)$ is the noise added to the user 1's signal. Due to smart transmission, (8.7) can be written as,

$$y_1 = \underbrace{\left[\sum_{i=1}^{N/2} \alpha_i \right]}_{G} x_s + w_1 \tag{8.8}$$

8.4.1.1 Outage Probability Analysis of Smart RIS-AP-NOMA

The signal-to-interference plus noise ratio (SINR) for user 2 is:

$$\Gamma_2 = \frac{H^2 \rho_2}{H^2 \rho_1 + N_0} = \frac{H^2 \beta_2 E_s}{H^2 \beta_1 E_s + N_0} \tag{8.9}$$

The outage occurs for user 2, when

$$\log_2\left(1 + \Gamma_2\right) < \tilde{D}_2 \tag{8.10}$$

Here $\tilde{D}_2$ is the spectral efficiency demand for user 2. Substituting (8.9) in (8.10) and simplifying gives,

$$H^2 \leq \frac{D_2}{\left(\beta_2 - \beta_1 D_2\right) \kappa} \tag{8.11}$$

where $\kappa = \frac{E_s}{N_0}$ is the transmit SNR. Solving (8.11) for H

$$H \leq \underbrace{\sqrt{\frac{D_2}{\left(\beta_2 - \beta_1 D_2\right)\kappa}}}_{r_2} \tag{8.12}$$

$D_2 = 2^{\tilde{D}_2} - 1$. According to central limit theorem (CLT) for larger, $H \sim C\mathcal{N}\left(\underbrace{\frac{N_2\sqrt{\pi}}{2}}_{m_H}, \underbrace{N_2\left[1 - \frac{\pi}{4}\right]}_{\sigma_H^2}\right)$. The probability that user 2 experiences outage is given by,

$$P_2^s = \int_0^{r_2} f_H(h)\ \mathrm{dh} \tag{8.13}$$

where $f_H(h)$ is the probability density function (PDF) of H. Simplifying (8.13) results in

$$P_2^s = \frac{\sigma_H\left\{erf\left(\frac{r_2 - m_H}{\sqrt{2}\,\sigma_H}\right) + erf\left(\frac{m_H}{\sqrt{2}\,\sigma_H}\right)\right\}}{2\sigma_H} \tag{8.14}$$

The instantaneous SINR of detecting user 2's symbol at user 1 is

$$\Gamma_1^2 = \frac{G^2\beta_2 E_S}{G^2\beta_1 E_s + N_0} = \frac{G^2\beta_2\kappa}{G^2\beta_1\kappa + 1} \tag{8.15}$$

After SIC, instantaneous SNR of detecting user 1's symbol at user 1 is

$$\Gamma_1^1 = G^2\beta_1\kappa \tag{8.16}$$

The outage occurs for user 2 at user 1, when

$$\log_2(1 + \Gamma_1^2) < \tilde{D}_2 \tag{8.17}$$

Substituting (8.15) in (8.17) and simplifying for G results in

$$G \leq \sqrt{\frac{D_2}{\left(\beta_2 - \beta_1 D_2\right)\kappa}} \tag{8.18}$$

The outage occurs for user 1 at user 1, when

$$\log_2(1 + \Gamma_1^1) < \tilde{D}_1 \tag{8.19}$$

Here $\tilde{D}_1$ is the spectral efficiency demand for user 1. Substituting (8.16) in (8.19) and simplifying for G

$$G \leq \sqrt{\frac{D_1}{\beta_1 \kappa}} \tag{8.20}$$

$D_1 = 2^{\tilde{D}_1} - 1$. Combining the conditions in (8.18) and (8.20) gives the condition for which outage occurs at user 1

$$G \leq \underbrace{\max\left\{\sqrt{\frac{D_2}{(\beta_2 - \beta_1 D_2)\,\kappa}}, \sqrt{\frac{D_1}{\beta_1 \kappa}}\right\}}_{r_1} \tag{8.21}$$

As per CLT, for larger values of N, $G \sim \mathcal{CN}\left(\underbrace{\frac{N_1\sqrt{\pi}}{2}}_{m_G}, \underbrace{N_1\left[1 - \frac{\pi}{4}\right]}_{\sigma_G^2}\right)$. The probability of outage at user 1 is obtained by,

$$P_2^s = \int_0^{r_1} f_G(\mathrm{g})\ \mathrm{dg} \tag{8.22}$$

where $f_G(\mathrm{g})$ is the PDF of G. Simplifying (8.22) results in,

$$\mathrm{P}_1^s = \frac{\sigma_G\left\{erf\left(\frac{r_1 - m_G}{\sqrt{2}\sigma_G}\right) + erf\left(\frac{m_G}{\sqrt{2}\sigma_G}\right)\right\}}{2\sigma_G} \tag{8.23}$$

8.4.1.2 ABER Analysis of Smart RIS-AP-NOMA

For simplicity, interference terms are ignored in the ABER analysis. Hence, the instantaneous SNR for user 2 can be calculated using:

$$\Gamma_2 = \frac{\left|\sum_{i=(N/2)+1}^{N} \alpha_i\right|^2 E_S}{N_0} = H^2\kappa \tag{8.24}$$

The SNR of user 1 after SIC can be calculated using

$$\Gamma_1 = \frac{\left|\sum_{i=1}^{N/2} \alpha_i\right|^2 E_S}{N_0} = G^2\kappa \tag{8.25}$$

The moment generation function (MGF) of instantaneous SNR is expressed as [24]:

$$M_{\Gamma}(t) = \left(\frac{1}{1 - \frac{t(4-\pi)N\kappa}{2}}\right)^{\frac{1}{2}} \exp\left(\frac{\frac{t\pi N^2\kappa}{4}}{1 - \frac{t(4-\pi)N\kappa}{2}}\right) \tag{8.26}$$

The average symbol error probability (ASEP) for M-ary phase shift keying (PSK) modulation is obtained by [44]

$$p_e^s = \frac{1}{\pi}\int_0^{\pi(M-1)/M} M_{\Gamma}\left(-\frac{\sin^2(\pi/M)}{\sin^2\mu}\right) d\mu \tag{8.27}$$

For binary phase shift keying (BPSK), $M = 2$. Substituting (8.26) in (8.27) gives,

$$p_e^s = \frac{1}{\pi}\int_0^{\pi/2} \left(\frac{1}{1 + \frac{(4-\pi)N\kappa}{2\sin^2\mu}}\right)^{\frac{1}{2}} \exp\left(\frac{-\frac{\pi N^2\kappa}{4\sin^2\mu}}{1 + \frac{(4-\pi)N\kappa}{2\sin^2\mu}}\right) d\mu \tag{8.28}$$

The upper bound of ASEP is obtained by substituting $\mu = \pi/2$ in (8.28)

$$p_e^s = \frac{1}{2}\left(\frac{1}{1 + \frac{(4-\pi)N\kappa}{2}}\right)^{\frac{1}{2}} \exp\left(\frac{-\frac{\pi N^2\kappa}{4}}{1 + \frac{(4-\pi)N\kappa}{2}}\right) \tag{8.29}$$

The ABER of conventional NOMA user 2 with BPSK modulation is given by [45],

$$p_2(\mathrm{e}) = \frac{1}{2}\left[Q\left(\frac{\sqrt{\rho_2} + \sqrt{\rho_1/2}}{\sqrt{N_0/2}}\right) + Q\left(\frac{\sqrt{\rho_2} - \sqrt{\rho_1/2}}{\sqrt{N_0/2}}\right)\right] \tag{8.30}$$

From Eqs. (8.28) and (8.30), the expression for ABER of user 2 is obtained as in (8.31).

$$\begin{aligned} P_2^s(e) = {} & \frac{1}{2\pi}\int_0^{\pi/2} \left(\frac{1}{1 + \frac{(4-\pi)N_2\left(\sqrt{\rho_2} + \sqrt{\rho_1/2}\right)}{2\sqrt{N_0}\sin^2\mu}}\right)^{\frac{1}{2}} \exp\left(\frac{\frac{-\pi N_2^2\left(\sqrt{\rho_2} + \sqrt{\rho_1/2}\right)}{4\sqrt{N_0}\sin^2\mu}}{1 + \frac{(4-\pi)N_2\left(\sqrt{\rho_2} + \sqrt{\rho_1/2}\right)}{2\sqrt{N_0}\sin^2\mu}}\right) d\mu \\ & + \frac{1}{2\pi}\int_0^{\pi/2} \left(\frac{1}{1 + \frac{(4-\pi)N_2\left(\sqrt{\rho_2} - \sqrt{\rho_1/2}\right)}{2\sqrt{N_0}\sin^2\mu}}\right)^{\frac{1}{2}} \exp\left(\frac{\frac{-\pi N_2^2\left(\sqrt{\rho_2} - \sqrt{\rho_1/2}\right)}{4\sqrt{N_0}\sin^2\mu}}{1 + \frac{(4-\pi)N_2\left(\sqrt{\rho_2} - \sqrt{\rho_1/2}\right)}{2\sqrt{N_0}\sin^2\mu}}\right) d\mu \end{aligned} \tag{8.31}$$

The ABER of conventional NOMA user 1 after SIC is given by [45],

$$p_1(e) = \frac{1}{4}\left[Q\left(\sqrt{\frac{\rho_1}{N_0}}\right)\left\{4 - Q\left(\sqrt{\frac{\left(\sqrt{2\rho_2}+\sqrt{\rho_1}\right)^2}{N_0}}\right) - Q\left(\sqrt{\frac{\left(\sqrt{2\rho_2}-\sqrt{\rho_1}\right)^2}{N_0}}\right)\right\} - Q\left(\sqrt{\frac{\left(\sqrt{2\rho_2}+\sqrt{\rho_1}\right)^2}{N_0}}\right)\right] \tag{8.32}$$

Near users are likely to employ quadrature phase shift keying (QPSK) modulation due to improved channel gain. From Eqs. (8.28) and (8.32), the expression for ABER of user 1 is obtained as in (8.33).

$$P_1^s(e) = \frac{1}{4\pi}\left[\xi\left\{4 - \zeta - \psi\right\} - \zeta\right] \tag{8.33}$$

where,

$$\xi = \int_0^{\pi/2}\left(\frac{1}{1+\frac{(4-\pi)N_1\rho_1}{2\sqrt{N_0}\sin^2\mu}}\right)^{\frac{1}{2}} \exp\left(\frac{\frac{-\pi N_2^2\rho_1}{4\sqrt{N_0}\sin^2\mu}}{1+\frac{(4-\pi)N_2\rho_1}{2\sqrt{N_0}\sin^2\mu}}\right) d\mu \tag{8.34}$$

$$\zeta = \int_0^{\pi/2}\left(\frac{1}{1+\frac{(4-\pi)N_1\left(\sqrt{2\rho_2}+\sqrt{\rho_1}\right)}{2\sqrt{N_0}\sin^2\mu}}\right)^{\frac{1}{2}} \exp\left(\frac{\frac{-\pi N_1^2\left(\sqrt{2\rho_2}+\sqrt{\rho_1}\right)}{4\sqrt{N_0}\sin^2\mu}}{1+\frac{(4-\pi)N_1\left(\sqrt{2\rho_2}+\sqrt{\rho_1}\right)}{2\sqrt{N_0}\sin^2\mu}}\right) d\mu \tag{8.35}$$

$$\psi = \int_0^{\pi/2}\left(\frac{1}{1+\frac{(4-\pi)N_1\left(\sqrt{2\rho_2}-\sqrt{\rho_1}\right)}{2\sqrt{N_0}\sin^2\mu}}\right)^{\frac{1}{2}} \exp\left(\frac{\frac{-\pi N_1^2\left(\sqrt{2\rho_2}-\sqrt{\rho_1}\right)}{4\sqrt{N_0}\sin^2\mu}}{1+\frac{(4-\pi)N_1\left(\sqrt{2\rho_2}-\sqrt{\rho_1}\right)}{2\sqrt{N_0}\sin^2\mu}}\right) d\mu \tag{8.36}$$

8.4.2 Blind Transmission

The channel phases between each RIS element and receiver are not available at the RIS for precompensation in a blind transmission method.

8.4.2.1 Outage Probability Analysis of Blind RIS-AP-NOMA

The detailed probability of outage expressions for blind RIS-aided NOMA user 2 and user 1 are derived by [42]

$$P_2^B = 1 - \exp\left\{-\left(\frac{D_2}{\left(\beta_2 - \beta_1 D_2\right)\delta_2^2 N_2 \kappa}\right)\right\} \tag{8.37}$$

$$P_1^B = 1 - \exp\left\{-\frac{1}{\delta_1^2 N_1}\left(\max\left\{\frac{D_2}{\left(\beta_2 - \beta_1 D_2\right)\kappa}, \frac{D_1}{\beta_1 \kappa}\right\}\right)\right\} \tag{8.38}$$

where δ_2^2 and δ_1^2 are average channel gains experiences by user 2 and user 1, respectively.

8.4.2.2 ABER Analysis of Blind RIS-AP-NOMA

The received signal of user 1 is given by,

$$y_1 = \underbrace{\left[\sum_{i=1}^{N/2} h_i\right]}_{P} x_s + w_1 \tag{8.39}$$

where $P \sim C\mathcal{N}\left(0, N_1\right)$. Then Γ_1 becomes

$$\Gamma_1 = |P|^2 \kappa \tag{8.40}$$

The received signal of user 2 is given by,

$$y_2 = \underbrace{\left[\sum_{i=(N/2)+1}^{N} h_i\right]}_{Q} x_s + w_2 \tag{8.41}$$

where $Q \sim C\mathcal{N}\left(0, N_2\right)$. Then Γ_2 becomes

$$\Gamma_2 = |Q|^2 \kappa \tag{8.42}$$

The MGF of received SNR is expressed by [24],

$$M_{\Gamma}(t) = \left(\frac{1}{1 - tN\kappa}\right) \tag{8.43}$$

For blind RIS–AP scheme, ASEP is obtained using [24]

$$p_e^B = \frac{1}{\pi}\int_0^{\pi/2}\left(\frac{1}{1 + \frac{N\kappa}{\sin^2\mu}}\right)\mathrm{d}\mu \tag{8.44}$$

From (8.44) and (8.30), the expression for ABER of user 2 is obtained as

$$p_2^B(\mathrm{e}) = \frac{1}{2\pi}\int_0^{\pi/2}\left(\frac{1}{1+\dfrac{N_2\left(\sqrt{\rho_2}+\sqrt{\rho_1/2}\right)}{\sqrt{N_o}\,\sin^2\mu}}\right)\mathrm{d}\mu + \frac{1}{2\pi}\int_0^{\pi/2}\left(\frac{1}{1+\dfrac{N_2\left(\sqrt{\rho_2}-\sqrt{\rho_1/2}\right)}{\sqrt{N_o}\,\sin^2\mu}}\right)\mathrm{d}\mu \tag{8.45}$$

From (8.44) and (8.32), the expression for ABER of user 1 is obtained as in (8.46).

$$P_1^B(e) = \frac{1}{4\pi}\left[\int_0^{\pi/2}\left(\frac{1}{1+\dfrac{N_1\rho_1}{\sqrt{N_0}\sin^2\mu}}\right)d\mu.\{4-\varphi-\eta\}-\varphi\right] \tag{8.46}$$

where,

$$\varphi = \int_0^{\pi/2}\left(\frac{1}{1+\dfrac{N_1\left(\sqrt{2\rho_2}+\sqrt{\rho_1}\right)}{\sqrt{N_0}\sin^2\mu}}\right)d\mu \tag{8.47}$$

$$\eta = \int_0^{\pi/2}\left(\frac{1}{1+\dfrac{N_1\left(\sqrt{2\rho_2}-\sqrt{\rho_1}\right)}{\sqrt{N_0}\sin^2\mu}}\right)d\mu \tag{8.48}$$

8.5 Discussions on Simulations

The performance of the proposed system is validated using numerical simulations in this section. Table 8.1 lists the parameters for numerical simulations.

8.5.1 Outage Analysis

Figure 8.3 shows the outage performance of smart RIS-AP-NOMA user 2 for different values of N. The results indicate that a higher SNR leads to improved outage performance. Moreover, increasing N reduces the SNR requirement. Table 8.2 displays the SNR requirement for the smart RIS-AP-NOMA user 2 to meet the target outage for various values of N. The use of smart RIS enables perfect phase cancellation, which results in diversity and array gain in the system. As a result, the smart RIS-AP-NOMA system can achieve the target outage even

Table 8.1 Parameters for numerical simulations.

Parameters	Values
Block length	10^7
Target data rate of user 2 ($\tilde{D}_2$)	1 b/s/Hz
Target data rate of user 1 ($\tilde{D}_1$)	1 b/s/Hz
Power fractions (β_1, β_2)	0.1,0.9
RIS elements (N)	32, 64, 128, 256, and 512
Mean channel gain between user 1 and AP (δ_1^2)	1
Mean channel gain between user 2 and AP (δ_2^2)	1
Modulation orders (M)	2, 4
Target outage probability	10^{-4}
Target ABER	10^{-6}
Number of users	2

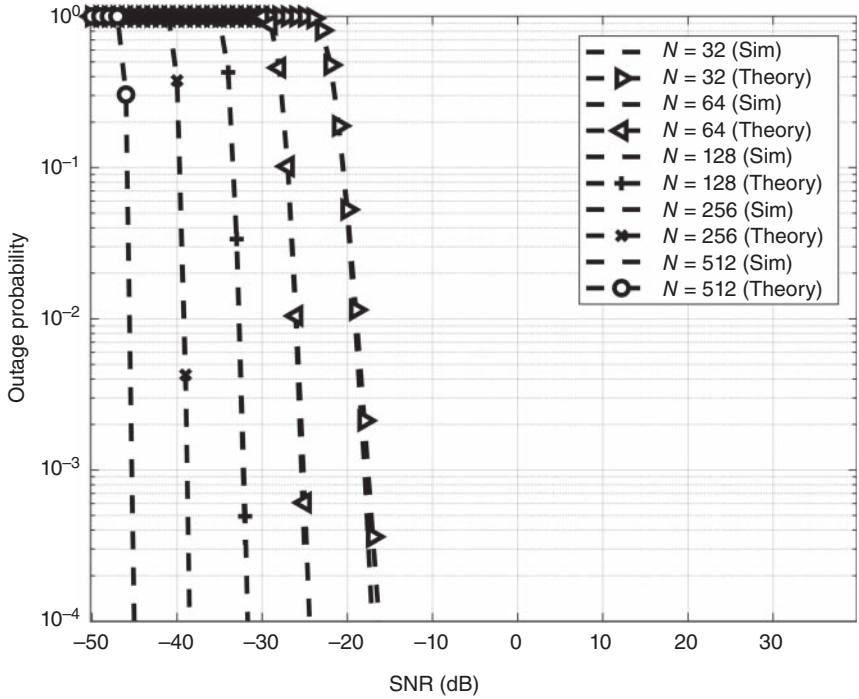

Figure 8.3 Outage performance of smart RIS-AP-NOMA user 2 for different values of N.

Table 8.2 SNR requirement (in dB) of smart and blind RIS-AP-NOMA users for various N to attain target outage.

	Smart RIS-AP-NOMA		Blind RIS-AP-NOMA		SNR gain of smart over blind RIS	
N	User 2	User 1	User 2	User 1	User 2	User 1
32	~ -17	~ -8	~ 29	~ 38	~ 46	~ 46
64	~ -25	~ -15	~ 26	~ 35	~ 51	~ 50
128	~ -32	~ -23	~ 23	~ 32	~ 55	~ 55
256	~ -39	~ -30	~ 20	~ 29	~ 59	~ 59
512	~ -45	~ -36	~ 17	~ 26	~ 62	~ 62

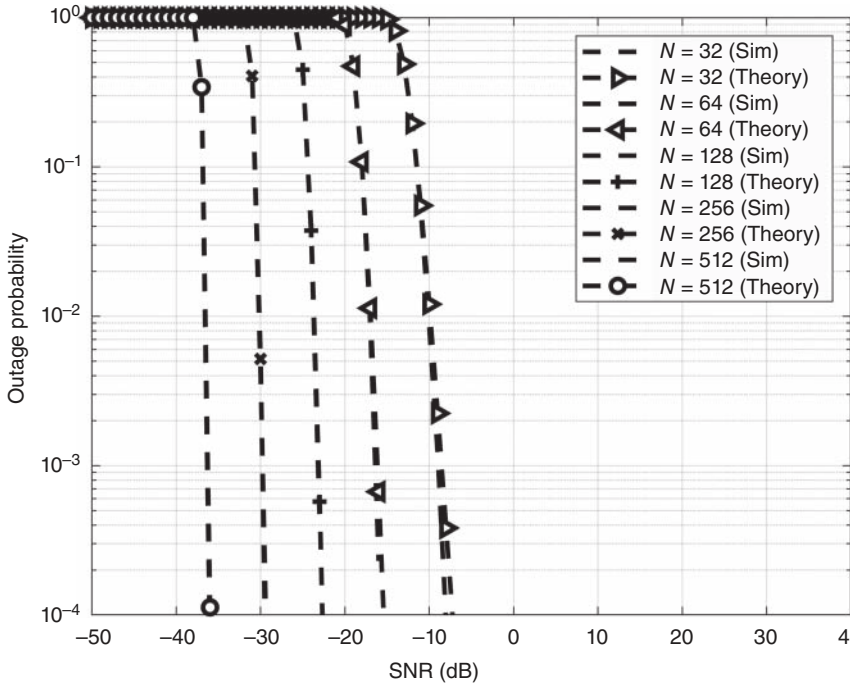

Figure 8.4 Outage performance of smart RIS-AP-NOMA user 1 for different values of N.

at negative SNR values. Theoretical outage curves for smart RIS-AP-NOMA user 2 are plotted based on (8.14). The accuracy of the derived closed-form outage expressions is validated through simulations.

Figure 8.4 shows that smart RIS-AP-NOMA user 1 also exhibits a similar trend. Theoretical outage curves for smart RIS-AP-NOMA user 1 are plotted based on

(8.23). Compared to user 1's outage performance, user 2's outage performance is superior because a higher power fraction is allocated to user 2 to maintain system fairness.

In Figure 8.5, we see the outage performance of blind RIS-AP-NOMA user 2 at different values of N. The results indicate that an increased SNR leads to better outage performance. Furthermore, increasing N reduces the SNR requirement. Table 8.2 displays the SNR requirement of blind RIS-AP-NOMA user 2 to meet the target outage at various N values. Blind RIS does not perform phase cancellation, only achieving array gain. Consequently, to achieve the target outage, blind RIS-AP-NOMA user 2 requires more SNR than smart RIS-AP-NOMA user 2. Theoretical outage curves for blind RIS-AP-NOMA user 2 are plotted based on (8.37) and the accuracy of the derived closed-form outage expressions is validated through simulations.

In Figure 8.6, the blind RIS-AP-NOMA user 1 trend is similar to blind RIS-AP-NOMA user 2. Theoretical outage curves for blind RIS-AP-NOMA user 1 are plotted based on (8.38). User 2 exhibits superior outage performance compared to user 1 because a higher power fraction is allocated to user 2 to maintain

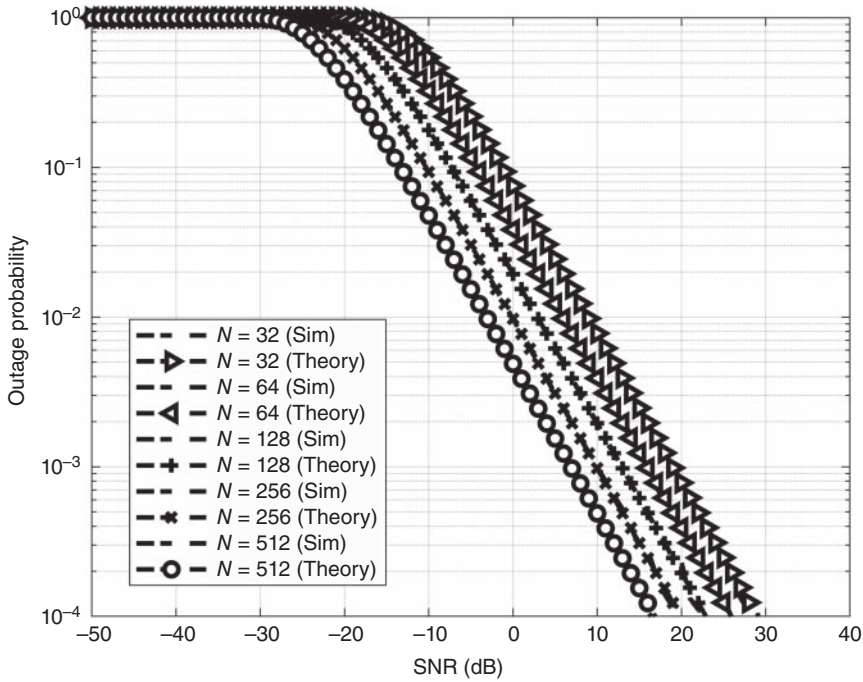

Figure 8.5 Outage performance of blind RIS-AP-NOMA user 2 for different values of N.

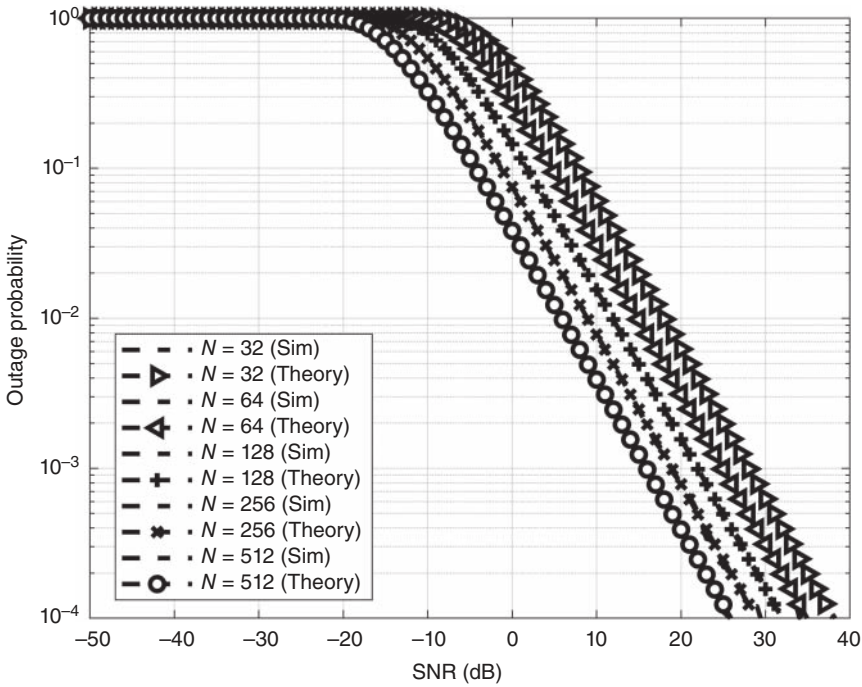

Figure 8.6 Outage performance of blind RIS-AP-NOMA user 1 for different values of *N*.

system fairness. The SNR requirement of smart and blind RIS-AP-NOMA users for various N is tabulated in Table 8.2.

Figure 8.7 compares user 2's outage performance between NOMA, blind RIS-AP-NOMA and smart RIS-AP-NOMA systems. The RIS-aided systems use $N = 32$. The continuous phase cancellation in a smart RIS-AP-NOMA system provides diversity and array gain, eventually achieving the target outage probability at ~ -17 dB. Whereas blind RIS-AP-NOMA attains only array gain, which reaches target outage at ~ 29 dB. The conventional NOMA requires ~ 40 dB to reach the target outage. It shows that smart RIS-AP-NOMA outperforms blind RIS-AP-NOMA and conventional NOMA by ~ 46 dB and ~ 58 dB respectively. And blind RIS-NOMA performs ~ 12 dB than the conventional NOMA.

Figure 8.8 compares user 1's outage performance between NOMA, blind RIS-AP-NOMA and smart RIS-AP-NOMA systems. The RIS-aided systems use $N = 32$. The continuous phase cancellation in a smart RIS-AP-NOMA system provides diversity and array gain, eventually achieving the target outage probability at ~ -8 dB. Whereas blind RIS-AP-NOMA attains only array gain, which reaches target outage at ~ 38 dB. The conventional NOMA requires ~ 50 dB to

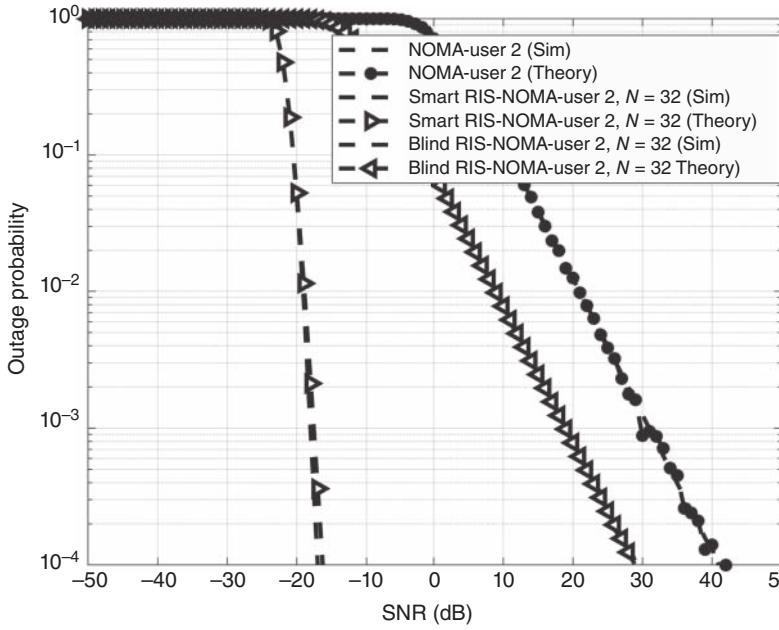

Figure 8.7 Comparison of outage of user 2 for NOMA, blind RIS-AP-NOMA and smart RIS-AP-NOMA systems.

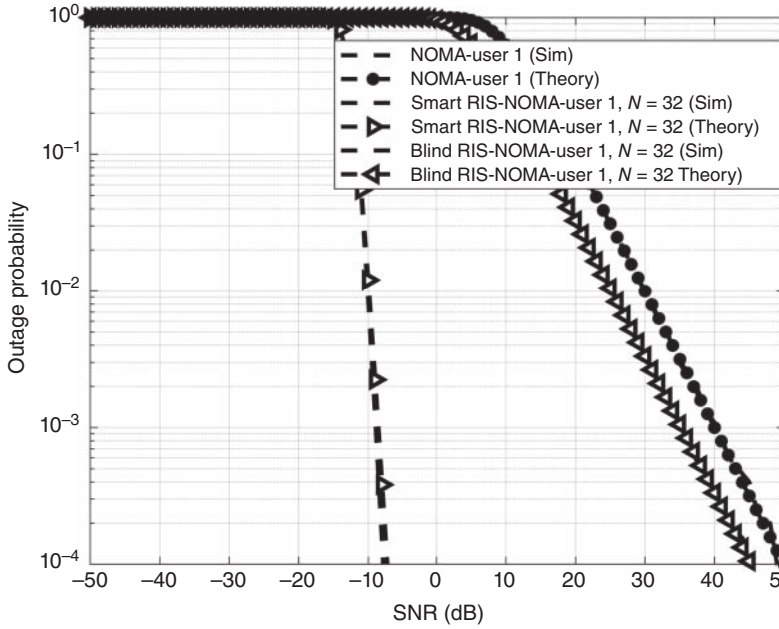

Figure 8.8 Comparison of outage of user 1 for NOMA, blind RIS-AP-NOMA and smart RIS-AP-NOMA systems.

reach the target outage. It shows that smart RIS-AP-NOMA outperforms blind RIS-AP-NOMA and conventional NOMA by ∼46 dB and ∼58 dB, respectively. And blind RIS-NOMA performs ∼12 dB than the conventional NOMA. The higher power fraction allocated to user 2 results in better outage performance than user 1.

8.5.2 ABER Analysis

Figure 8.9 depicts the ABER performance of smart RIS-AP-NOMA user 2. The RIS in a smart transmission system is aware of the channel phases. For $N = 32$, $N = 64$, $N = 128$, $N = 256$, $N = 512$, an SNR gain of ∼−18 dB, ∼−34 dB, ∼−46 dB, ∼−58 dB, ∼−71 dB is required to attain the target ABER. Smart transmission through RIS-AP-NOMA has a superior performance than blind transmission. For example, if $N = 512$, blind transmission necessitates an SNR of ∼60 dB, but smart transmission necessitates an SNR of ∼−71 dB. The channel phases are unknown to RIS in blind transmission. As a result, SNR maximization is

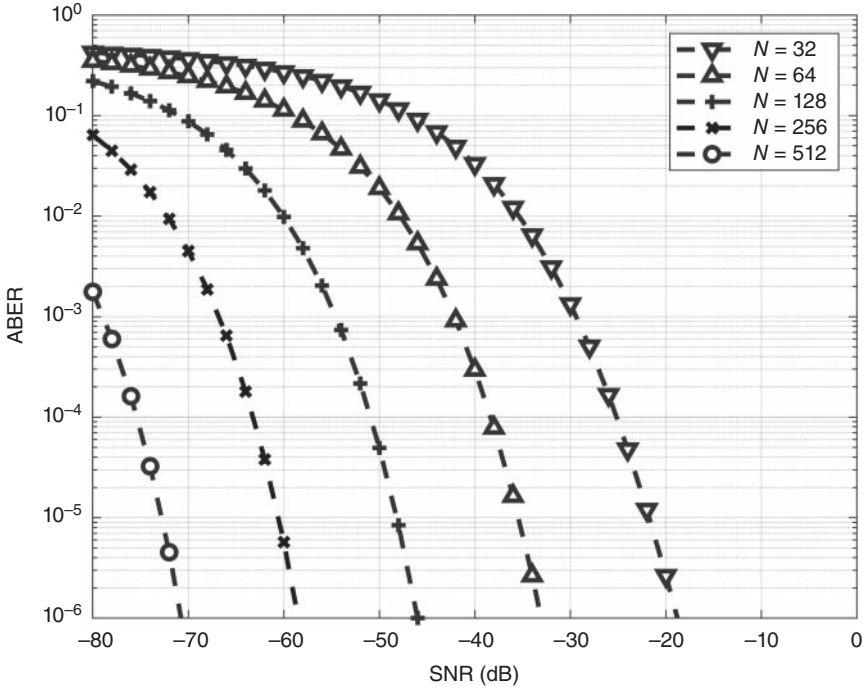

Figure 8.9 ABER performance of a smart RIS-AP-NOMA user 2.

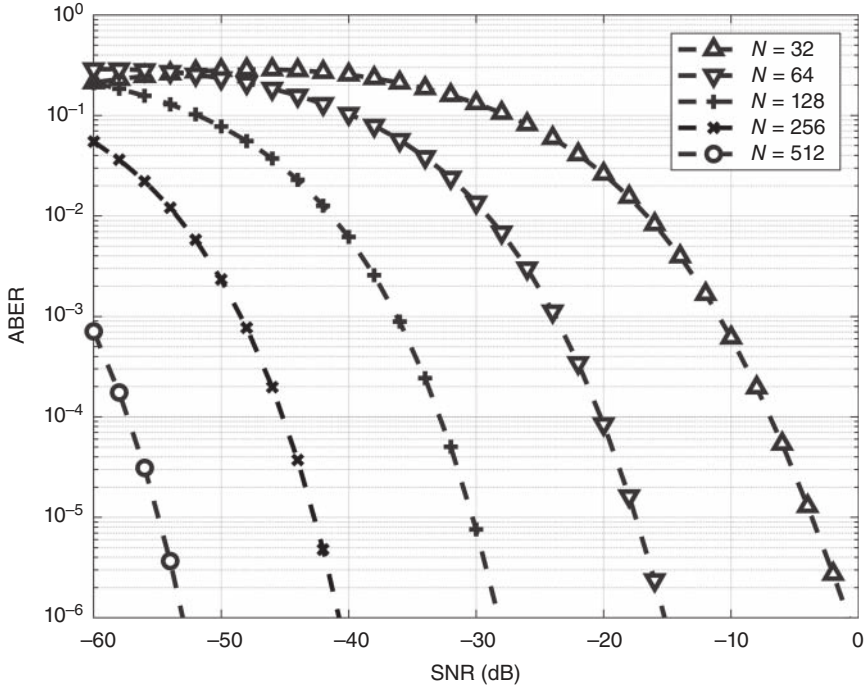

Figure 8.10 ABER performance of a smart RIS-AP-NOMA user 1.

not an option. As a result, blind transmission performs poorly as compared to smart transmission through RIS. Figure 8.10 depicts the ABER performance of smart RIS-AP-NOMA user 1. $N = 32$, $N = 64$, $N = 128$, $N = 256$, $N = 512$ systems require SNRs of ~ -1 dB, ~ -15 dB, ~ -28 dB, ~ -41 dB, and ~ -53 dB, respectively, to reach the target ABER. The SNR gain grows as N increases. We can see from Figures 8.9 and 8.10 that the user 2's ABER performance is better than the user 1's. For $N = 512$, user 1 and user 2 require an SNR of ~ -71 dB and ~ -53, dB respectively. It is because we allocate the user 2 more power. The SNR requirements of smart RIS-AP-NOMA user 1 and user 2 for varied N are shown in Table 8.3.

Figure 8.11 shows the ABER performance of a blind RIS-AP-NOMA user 2. The channel phases are unknown to RIS in a blind transmission system. $N = 32$, $N = 64$, $N = 128$, $N = 256$, $N = 512$ systems require SNR of $\sim$84 dB, $\sim$78 dB, $\sim$72 dB, $\sim$66 dB, $\sim$60 dB, respectively, to reach the target ABER. There is a rise in SNR gain as N grows. Figure 8.12 shows the ABER performance of a blind RIS-AP-NOMA user 1. $N = 32$, $N = 64$, $N = 128$, $N = 256$, $N = 512$ systems require SNRs of $\sim$103 dB, $\sim$97 dB, $\sim$91 dB, $\sim$85 dB, and $\sim$79 dB, respectively,

Table 8.3 SNR requirement (in dB) of smart and blind RIS-AP-NOMA users for various N to attain target ABER.

	Smart RIS-AP-NOMA		Blind RIS-AP-NOMA		SNR gain of smart over blind RIS	
N	User 2	User 1	User 2	User 1	User 2	User 1
32	∼−18	∼−1	∼84	∼103	∼102	∼104
64	∼−34	∼−15	∼78	∼97	∼112	∼112
128	∼−46	∼−28	∼72	∼91	∼118	∼119
256	∼−58	∼−41	∼66	∼85	∼124	∼126
512	∼−71	∼−53	∼60	∼79	∼131	∼132

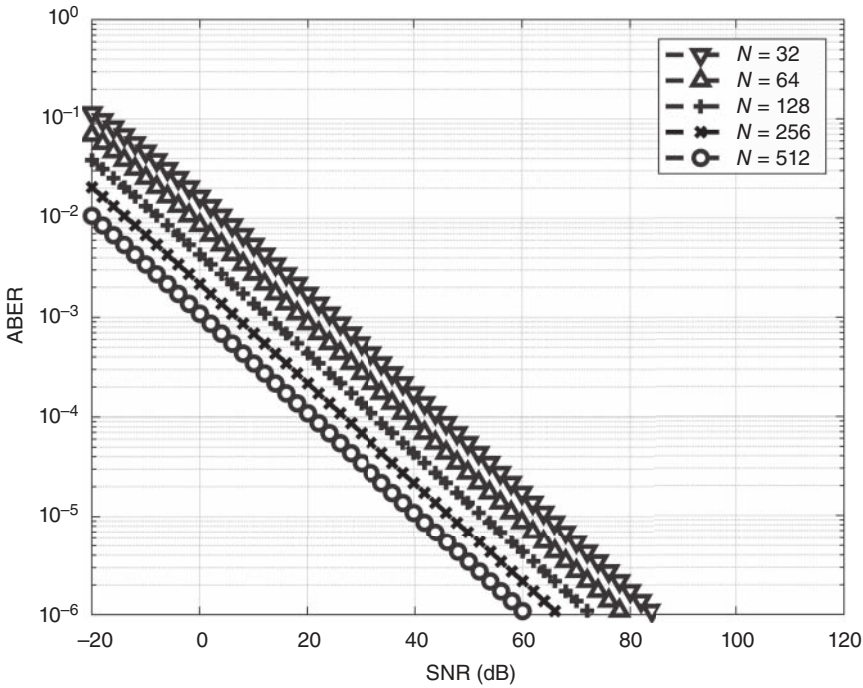

Figure 8.11 ABER performance of a blind RIS-AP-NOMA user 2.

to reach the target ABER. The SNR gain grows as N increases. Figures 8.11 and 8.12 show that the user 2's ABER performance is superior to that of the user 1. The reason for this is that we allocate the user 2 more power. For example, the user 2 with $N = 32$ requires an SNR of ∼84 dB, but the user 1 requires ∼103 dB to reach the target ABER.

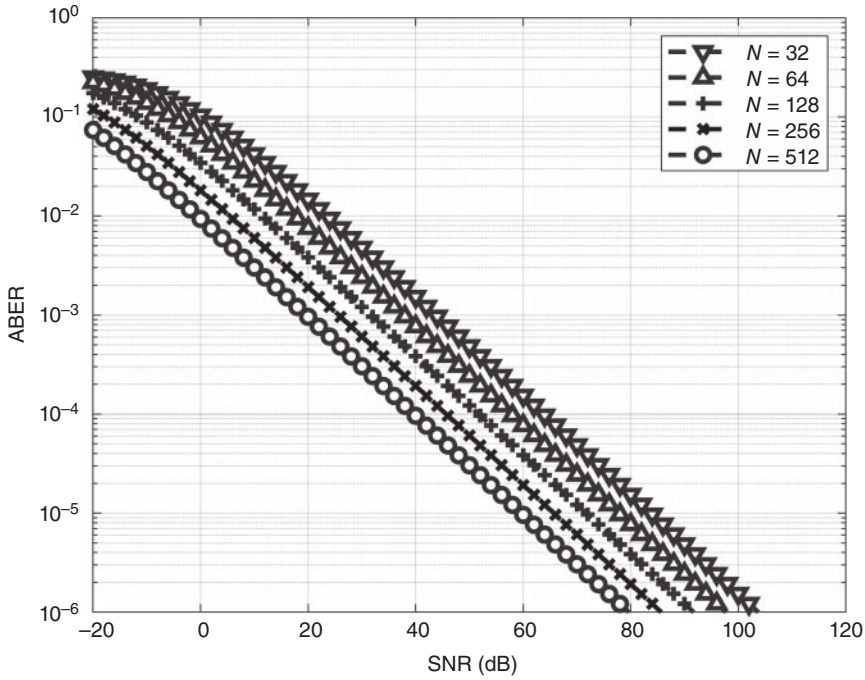

Figure 8.12 ABER performance of a blind RIS-AP-NOMA user 1.

Figure 8.13 compares the user 2's ABER performance of the proposed smart RIS-AP-NOMA and blind RIS-AP-NOMA with conventional NOMA. The proposed RIS systems are assumed to have $N = 32$. Similarly, Figure 8.14 compares the user 1's ABER performance of the proposed smart RIS-AP-NOMA and blind RIS-AP-NOMA with conventional NOMA. Due to array and diversity gain benefits, smart RIS-AP-NOMA outperforms conventional NOMA. The conventional NOMA user 2 requires an SNR of ∼13 dB to achieve the target ABER, but the smart RIS-AP-NOMA user 2 requires an SNR of ∼−18 dB. As a result, the smart RIS-AP-NOMA user 2 outperforms the conventional NOMA user 2 by ∼31 dB. In comparison to conventional NOMA user 1, smart RIS-AP-NOMA user 1 has a gain of ∼25 dB. At low-SNR levels, blind RIS-AP-NOMA outperforms conventional NOMA; however, at high SNR values, conventional NOMA outperforms blind RIS-AP-NOMA.

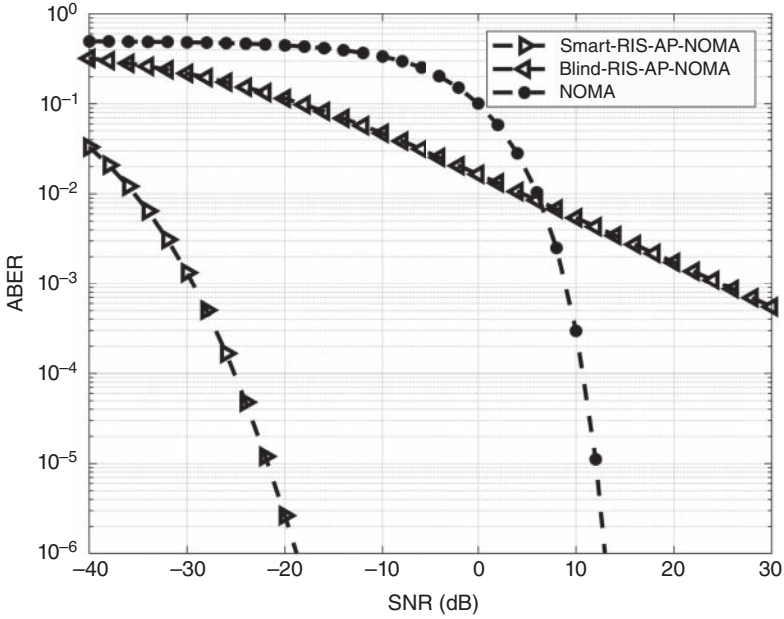

Figure 8.13 ABER comparison of conventional NOMA, smart and blind RIS-AP-NOMA user 2.

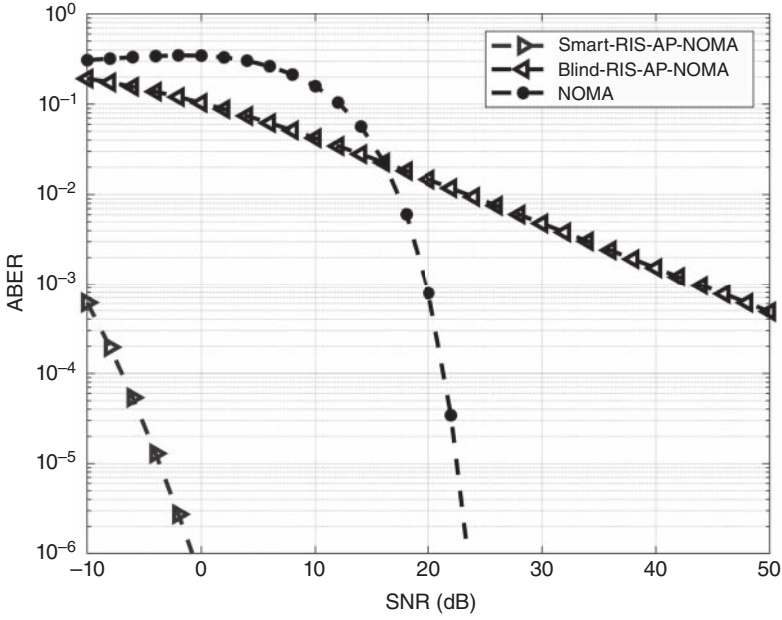

Figure 8.14 ABER comparison of conventional NOMA, smart and blind RIS-AP-NOMA user 1.

8.6 Conclusions

The analytical outage and ABER expressions of RIS-AP-NOMA for both smart and blind transmissions are developed in this chapter. Because of the addition of RIS, NOMA now provides outstanding reliability even at very low SNR conditions. For both smart and blind transmission methods, it is discovered that increasing N enhances the SNR gains. The proposed system has great reliability even at negative SNRs since the channel impacts are pre-compensated at RIS in smart transmission. There is no diversity advantage from blind transmission. However, at low SNR, there is a substantial improvement over the standard NOMA system due to the array gain. The increase in PA enhances the SNR gains.

When compared to conventional NOMA, the proposed smart RIS-AP-NOMA user 1 attains the target outage with $\sim$58 dB SNR gain and target ABER with $\sim$25 dB SNR gain. In the case of user 2, the proposed system achieves target outage with $\sim$58 dB SNR gain and target ABER with $\sim$31 dB SNR gain. The proposed systems may be a viable option for next-generation networks because of its appealing features. The ABER performance of NOMA users can be increased further if the powers are assigned optimally. The proposed systems can be expanded to ordered NOMA and cooperative NOMA systems.

References

1 Imam-Fulani, Y.O., Faruk, N., Sowande, O.A. et al. (2023). 5G frequency standardization, technologies, channel models, and network deployment: advances, challenges, and future directions. *Sustainability* 15 (6): 5173.

2 Van Nguyen, M.-S., Do, D.-T., Phan, V.-D. et al. (2022). Ergodic performance analysis of double intelligent reflecting surfaces-aided NOMA—UAV systems with hardware impairment. *Drones* 6 (12): 408.

3 Imoize, A.L., Adedeji, O., Tandiya, N., and Shetty, S. (2021). 6G enabled smart infrastructure for sustainable society: opportunities, challenges, and research roadmap. *Sensors* 21 (5): 1709.

4 Basar, E., Di Renzo, M., De Rosny, J. et al. (2019). Wireless communications through reconfigurable intelligent surfaces. *IEEE Access* 7: 116753–116773.

5 Wang, C.-X., You, X., Gao, X. et al. (2023). On the road to 6G: visions, requirements, key technologies and testbeds. *IEEE Communications Surveys & Tutorials* 25 (2): 905–974.

6 Jiang, F., Abrardo, A., Keykhoshravi, K. et al. (2023). Two-timescale transmission design and RIS optimization for integrated localization and communications. *IEEE Transactions on Wireless Communications* 22 (12): 8587–8602.

7 Jalaja, R.R.U., Thirumavalavan, V.C., Velmurugan, P.G.S., and Thiruvengadam, S.J. (2021). Spatially correlated dual hop RIS aided next generation wireless systems: an outage perspective. *IEEE Access* 9: 56127–56139.

8 Huang, C., Zappone, A., Alexandropoulos, G.C. et al. (2019). Reconfigurable intelligent surfaces for energy efficiency in wireless communication. *IEEE Transactions on Wireless Communications* 18 (8): 4157–4170.

9 Liu, R., Li, M., Luo, H. et al. (2023). Integrated sensing and communication with reconfigurable intelligent surfaces: opportunities, applications, and future directions. *IEEE Wireless Communications* 30 (1): 50–57.

10 Hemanth, A., Umamaheswari, K., Pogaku, A.C. et al. (2020). Outage performance analysis of reconfigurable intelligent surfaces-aided NOMA under presence of hardware impairment. *IEEE Access* 8: 212156–212165.

11 Arzykulov, S., Nauryzbayev, G., Tsiftsis, T.A., and Maham, B. (2019). Performance analysis of underlay cognitive radio nonorthogonal multiple access networks. *IEEE Transactions on Vehicular Technology* 68 (9): 9318–9322.

12 Chen, S., Sun, S., Kang, S., and Ren, B. (2019). Pattern division multiple access (PDMA). *Multiple Access Techniques for 5G Wireless Networks and Beyond*, 451–492. Springer.

13 Do, D.-T., Le, A.-T., and Lee, B.M. (2020). Noma in cooperative underlay cognitive radio networks under imperfect SIC. *IEEE Access* 8: 86180–86195.

14 Do, D.-T., Van Nguyen, M.-S., Jameel, F. et al. (2020). Performance evaluation of relay-aided CR-NOMA for beyond 5G communications. *IEEE Access* 8: 134838–134855.

15 Han, Z., Yue, X., Dai, B. et al. (2023). Reconfigurable intelligent surface assisted unified NOMA framework. *IEEE Transactions on Vehicular Technology* 72 (8): 10617–10632.

16 Li, X., Li, J., Liu, Y. et al. (2019). Residual transceiver hardware impairments on cooperative NOMA networks. *IEEE Transactions on Wireless Communications* 19 (1): 680–695.

17 Ding, J. and Cai, J. (2019). Two-side coalitional matching approach for joint MIMO-NOMA clustering and BS selection in multi-cell MIMO-NOMA systems. *IEEE Transactions on Wireless Communications* 19 (3): 2006–2021.

18 Zheng, B., Wu, Q., and Zhang, R. (2020). Intelligent reflecting surface-assisted multiple access with user pairing: NOMA or OMA? *IEEE Communications Letters* 24 (4): 753–757.

19 Cui, T.J., Qi, M.Q., Wan, X. et al. (2014). Coding metamaterials, digital metamaterials and programmable metamaterials. *Light: Science & Applications* 3 (10): –e218.

20 Di Renzo, M. and Song, J. (2019). Reflection probability in wireless networks with metasurface-coated environmental objects: an approach based on random spatial processes. *EURASIP Journal on Wireless Communications and Networking* 2019 (1): 1–15.

21 Tang, W., Li, X., Dai, J.Y. et al. (2019). Wireless communications with programmable metasurface: transceiver design and experimental results. *China Communications* 16 (5): 46–61.

22 Liaskos, C., Nie, S., Tsioliaridou, A. et al. (2018). A new wireless communication paradigm through software-controlled metasurfaces. *IEEE Communications Magazine* 56 (9): 162–169.

23 Wu, Q. and Zhang, R. (2019). Towards smart and reconfigurable environment: intelligent reflecting surface aided wireless network. *IEEE Communications Magazine* 58 (1): 106–112.

24 Basar, E. (2019). Transmission through large intelligent surfaces: a new frontier in wireless communications. *2019 European Conference on Networks and Communications (EuCNC)*, 112–117. IEEE.

25 Di Renzo, M., Debbah, M., Phan-Huy, D.-T. et al. (2019). Smart radio environments empowered by reconfigurable AI meta-surfaces: an idea whose time has come. *EURASIP Journal on Wireless Communications and Networking* 2019 (1): 1–20.

26 Han, Y., Tang, W., Jin, S. et al. (2019). Large intelligent surface-assisted wireless communication exploiting statistical CSI. *IEEE Transactions on Vehicular Technology* 68 (8): 8238–8242.

27 Abumarshoud, H., Mohjazi, L., Dobre, O.A. et al. (2021). LiFi through reconfigurable intelligent surfaces: a new frontier for 6G? *arXiv preprint arXiv:2104.02390*.

28 Lin, S., Chen, F., Wen, M. et al. (2021). Reconfigurable intelligent surface-aided quadrature reflection modulation for simultaneous passive beamforming and information transfer. *IEEE Transactions on Wireless Communications* 21 (3): 1469–1481.

29 Pan, C., Ren, H., Wang, K. et al. (2021). Reconfigurable intelligent surfaces for 6G systems: principles, applications, and research directions. *IEEE Communications Magazine* 59 (6): 14–20.

30 Basar, E. and Poor, H.V. (2021). Present and future of reconfigurable intelligent surface-empowered communications [perspectives]. *IEEE Signal Processing Magazine* 38 (6): 146–152.

31 Pan, Y., Wang, K., Pan, C. et al. (2022). Sum-rate maximization for intelligent reflecting surface assisted terahertz communications. *IEEE Transactions on Vehicular Technology* 71 (3): 3320–3325.

32 Xu, J., Yuen, C., Huang, C. et al. (2023). Reconfiguring wireless environments via intelligent surfaces for 6G: reflection, modulation, and security. *Science China Information Sciences* 66 (3): 130304.

33 Fu, M., Zhou, Y., and Shi, Y. (2019). Intelligent reflecting surface for downlink non-orthogonal multiple access networks. *2019 IEEE Globecom Workshops (GC Wkshps)*, 1–6. IEEE.

34 Ding, Z. and Poor, H.V. (2020). A simple design of IRS-NOMA transmission. *IEEE Communications Letters* 24 (5): 1119–1123.

35 Hou, T., Liu, Y., Song, Z. et al. (2020). Reconfigurable intelligent surface aided NOMA networks. *IEEE Journal on Selected Areas in Communications* 38 (11): 2575–2588.

36 Chauhan, A., Ghosh, S., and Jaiswal, A. (2022). RIS partition-assisted non-orthogonal multiple access (NOMA) and quadrature-NOMA with imperfect SIC. *IEEE Transactions on Wireless Communications* 22 (4): 4371–4386.

37 Zheng, A., Ni, W., Wang, W., and Tian, H. (2023). Enhancing NOMA networks via reconfigurable multi-functional surface. *IEEE Communications Letters* 27 (4): 1195–1199.

38 Yang, Z., Liu, Y., Chen, Y., and Al-Dhahir, N. (2021). Machine learning for user partitioning and phase shifters design in RIS-aided NOMA networks. *IEEE Transactions on Communications* 69 (11): 7414–7428.

39 Khaleel, A. and Basar, E. (2021). A novel NOMA solution with RIS partitioning. *IEEE Journal of Selected Topics in Signal Processing* 16 (1): 70–81.

40 Aldababsa, M., Khaleel, A., and Basar, E. (2022). STAR-RIS-NOMA networks: an error performance perspective. *IEEE Communications Letters* 26 (8): 1784–1788.

41 Kumaravelu, V.B., Imoize, A.L., Castillo Soria, F.R. et al. (2023). RIS-assisted fixed NOMA: outage probability analysis and transmit power optimization. *Future Internet* 15 (8): 249.

42 Kumaravelu, V.B., Selvaprabhu, P., Han, D.S. et al. (2023). Blind reconfigurable intelligent surface-aided fixed non-orthogonal multiple access for intelligent vehicular networks. *EURASIP Journal on Wireless Communications and Networking* 2023 (1): 83.

43 Velmurugan, P.G.S., Thiruvengadam, S.J., Kumaravelu, V.B. et al. (2023). Performance analysis of full duplex bidirectional machine type communication system using IRS with discrete phase shifter. *Applied Sciences* 13 (12): 7128.

44 Thirumavalavan, V.C. and Jayaraman, T.S. (2020). BER analysis of reconfigurable intelligent surface assisted downlink power domain NOMA system. *2020 International Conference on COMmunication Systems & NETworkS (COMSNETS)*, 519–522. IEEE.

45 Kara, F. and Kaya, H. (2018). BER performances of downlink and uplink NOMA in the presence of SIC errors over fading channels. *IET Communications* 12 (15): 1834–1844.

9

Convergence of RIS with Emerging Wireless Technologies

Mehmet Bilim[1], Nuri Kapucu[2], Yasin Kabalcı[1], and Vinoth Babu Kumaravelu[3]

[1]Department of Electrical and Electronics Engineering, Niğde Ömer Halisdemir University, Nigde, Turkey
[2]Department of Electrical and Electronics Engineering, Hitit University, Corum, Turkey
[3]Department of Communication Engineering, School of Electronics Engineering, Vellore Institute of Technology, Vellore, India

9.1 Introduction

The innovative concept of data transmission through reconfigurable intelligent surfaces (RISs) is envisioned as a hopeful and exciting solution to the persistent issues in wireless communications. The software-controlled shaping of electromagnetic waves offers the potential to make radio communication channels more efficient and facilitate data transmission, making RIS one of the key components of sixth-generation (6G) technology. 6G communication systems are expected to provide faster data rates, lower latency, and higher capacity than previous wireless communication technologies. So, RIS can be used to improve signal coverage and quality in 6G networks in order to meet the high speed and low-latency requirements. 6G and beyond technologies will have the ability to meet the requirements for a connected world with ubiquitous wireless connection for all. This may bring improvements in device-to-device (D2D) communications, and it is possible to support for a massive number of simultaneous connections.

9.1.1 Key Contributions of the Chapter

There are several technologies that are crucial in enabling 6G systems, such as non-orthogonal multiple access (NOMA), spatial modulation (SM), small cells, massive multiple-input multiple-output (MIMO), millimeter-wave (mmW) communication, visible light communication (VLC), terahertz (THz) communication,

Reconfigurable Intelligent Surfaces for 6G and Beyond Wireless Networks, First Edition.
Edited by Agbotiname Lucky Imoize, Vinoth Babu Kumaravelu, and Dinh-Thuan Do.

and unmanned aerial vehicle (UAV). These systems may face some challenges in the implementation stage of 6G networks. At this stage, RIS can provide important solutions to overcome some difficulties of 6G enabling technologies. In addition, detailed examinations of the combined use of RIS and these next-generation communication system studies are presented.

Since RISs make it possible to reshape the wireless propagation environment, it provides optimization for the performance of NOMA [1]. RIS units can be utilized in massive MIMO systems to improve the signal quality and enable efficient beamforming [2]. With the use of RISs in SM systems, spectral efficiency, energy efficiency, coverage, and reliability can be enhanced, and interference can be mitigated [3]. In urban areas, it is very important to deploy small cells in proximity to users to increase coverage and capacity, which can be assisted by RISs to maintain a seamless connection [4]. In addition, mmW, VLC, and THz communication systems suffer from path loss and blockage, which can be prevented with the aid of RIS deployment in the wireless environment [5]. Since UAVs in urban areas are mostly subject to blockages when communicating with a user or a base station (BS) in the ground, RIS units placed on the flat surfaces of buildings can be used to maintain the transmission between UAVs and users/BSs [6]. The use of all these studies together with RIS attracts the attention of researchers as an important research topic for next-generation communication systems.

9.1.2 Chapter Organization

In this chapter, RIS deployment in the aforementioned 6G enabling technologies is discussed. Challenges, solutions, and advantages are comprehensively presented in more detail in Section 9.2. In Section 9.3 of this chapter, an analytical framework is introduced for the performance analysis of RIS-assisted wireless communication systems. It is mentioned which parameters affect the analytical analysis in the context of mathematical and probabilistic treatment, and some general formulas are also presented for common performance measures such as outage probability (OP), error probability, and capacity. The chapter concludes in Section 9.4.

9.2 RIS-Assisted Wireless Communication Systems

In this section, major RIS-supported system structures that have advantages for next-generation communication systems are discussed. These system structures can be specified as NOMA, Massive MIMO, SM, small cell network, mmW communications, VLC, THz communications, and UAV communications, respectively. Illustrative figures containing RIS-aided wireless communication systems are shown for various scenarios that are practically possible in our daily lives.

In addition, this section explains the advantages and disadvantages of RIS-aided wireless communications alongside solutions for the challenges that can be encountered in these systems.

9.2.1 RIS–NOMA

To meet the escalating demands for higher data rates and increased spectral efficiency in wireless communication networks, combining NOMA with RIS stands as a promising approach. NOMA, renowned for its capacity to accommodate multiple users on the same time-frequency resource, has been a key player in enhancing spectral efficiency. RISs, with their ability to reshape the wireless propagation environment, offer a unique opportunity to further optimize and customize the performance of NOMA [1, 7–12]. This section provides a thorough examination of the principles, advantages, and applications of RIS-assisted NOMA, shedding light on its potential to redefine the landscape of wireless communication.

NOMA has emerged as a transformative paradigm in multiple access techniques, challenging the conventional orthogonal multiple access methods [13]. The core principle of NOMA involves the simultaneous allocation of the same time-frequency resource to multiple users, differentiating them through varying power levels. This non-orthogonal approach enables improved spectral efficiency by exploiting the diversity in channel conditions among users. NOMA's ability to serve multiple users concurrently positions it as a pivotal technology to address the burgeoning demands of contemporary wireless communication systems.

RISs represent a cutting-edge technology designed to manipulate and control the wireless propagation environment. Consisting of numerous passive or active reflecting elements, RISs can alter the amplitude and phase of incident electromagnetic waves. The reconfigurability of these surfaces allows for dynamic adjustments, enabling precise control over signal propagation, interference mitigation, and beamforming. By intelligently modifying the wireless channel characteristics, RISs offer a powerful tool to enhance the performance of wireless communication systems.

The integration of RISs with NOMA introduces a novel approach to address the challenges and limitations of existing wireless communication networks. RISs can be strategically placed within the communication environment to enhance the signals' quality and improve the overall system performance. By leveraging the dynamic capabilities of RISs, NOMA can benefit from enhanced channel conditions, reduced interference, and improved coverage, ultimately leading to a more efficient and reliable communication network [8]. In the RIS-assisted NOMA framework, the combination of these technologies introduces a dynamic interplay between the intelligent surfaces and multiple access techniques. The reflecting

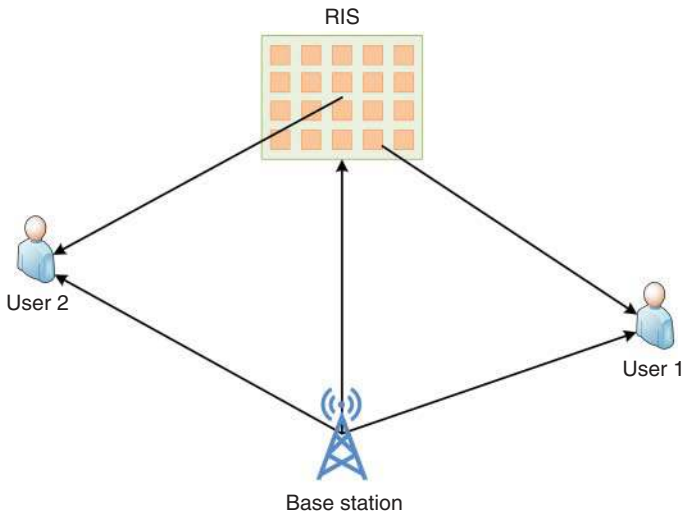

Figure 9.1 Visual depiction of a network model featuring a two-user setup in an RIS-aided NOMA network.

elements of the RIS are intelligently configured to optimize the signals' path and distribution, thereby enhancing the performance of NOMA. The power allocation in NOMA can be further refined by considering the reconfigurable nature of the intelligent surfaces, adapting to the varying channel conditions and user requirements in real time. In Figure 9.1, a two-user NOMA system assisted by the RIS technology is illustrated. This figure visualizes the wireless communication based on the NOMA technique between the users and the BS with the aid of RIS.

The integration of RISs with NOMA offers several key advantages that contribute to the overall improvement of wireless communication systems. One notable advantage is the ability to mitigate interference through precise control over signal reflections. By strategically positioning the RIS elements, interference from other users or external sources can be minimized, resulting in a cleaner and more reliable communication link [14]. Additionally, the adaptability of RISs enables dynamic optimization, allowing the system to respond to changing environmental conditions and user requirements effectively. The versatility of RIS-assisted NOMA opens up new avenues for applications across various scenarios in wireless communication networks. In dense urban environments with high user density, RISs can be deployed to alleviate interference and enhance the overall network capacity. In indoor environments, RISs can improve coverage and connectivity, especially in areas with challenging propagation conditions. Furthermore, RIS-assisted NOMA holds promise for future 6G networks, where the demand for ultra-reliable and low-latency communication is paramount.

While the integration of RISs with NOMA presents a compelling opportunity, several challenges and considerations must be addressed for practical implementation. The design and deployment of RISs require careful consideration of the network topology, user distribution, and environmental conditions. Additionally, the dynamic nature of wireless channels and user mobility necessitate adaptive algorithms for optimal RIS configuration. Moreover, issues related to power consumption, cost, and scalability must be carefully evaluated to ensure the feasibility of deploying RIS-assisted NOMA in real-world scenarios [1, 8, 14, 15].

The exploration of RIS-assisted NOMA opens up new possibilities for research opportunities and avenues for further investigation. Future research endeavors may focus on developing advanced algorithms for dynamic RIS configuration, considering machine learning and artificial intelligence techniques to adapt to changing network conditions. Additionally, investigating the integration of RISs with other emerging technologies, such as massive MIMO and edge computing, can further enhance the overall performance and capabilities of wireless communication networks. As wireless communication networks evolve toward 6G and beyond, the integration of intelligent surfaces with advanced multiple access techniques is poised to play a pivotal role in shaping the future of communication technologies. Figure 9.1 shows a visual depiction of a network model featuring a two-user setup in an RIS-aided NOMA network.

9.2.2 RIS–Massive MIMO

The landscape of wireless communication is continuously evolving, driven by the ever-increasing demand for higher data rates, improved spectral efficiency, and enhanced system capacity. Among the transformative technologies at the forefront of this evolution are massive MIMO systems and RISs. Massive MIMO systems, with their ability to utilize a large number of antennas at the BS, have emerged as a key enabler for meeting these demands. Concurrently, RISs, comprising intelligent reflecting elements, offer the ability to dynamically control and manipulate the wireless propagation environment [16]. This section explores the integration of RISs with Massive MIMO, aiming to leverage the combined advantages of these technologies for the enhancement of wireless communication systems.

Massive MIMO, a key innovation in wireless communication, harnesses the power of spatial diversity by deploying a large number of antennas at the BS. Unlike traditional MIMO systems, which typically use a few antennas, massive MIMO leverages the simultaneous transmission and reception of signals from multiple antennas. This technique exploits the spatial diversity of the communication channel, improving spectral efficiency and enhancing the system's overall capacity. Massive MIMO mitigates the effects of fading and interference, providing robust and reliable communication in dense user environments. The deployment of numerous antennas allows for efficient beamforming, enabling targeted

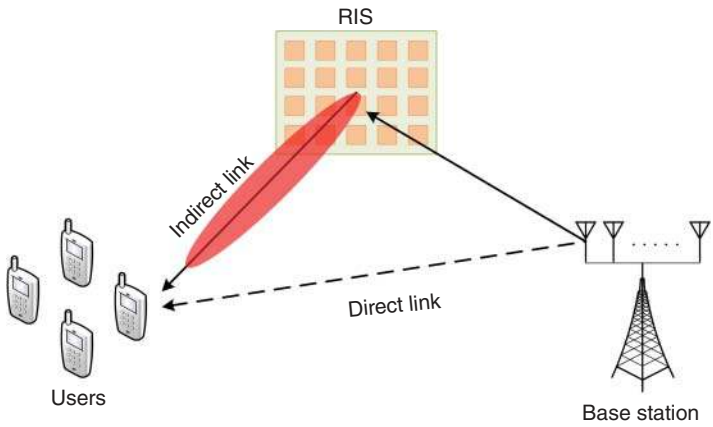

Figure 9.2 Illustration for RIS-aided massive MIMO system.

communication and enhancing the quality of service [17, 18]. An RIS-aided massive MIMO communication system is illustrated in Figure 9.2 where the *BS* has *multiple* antennas, whereas users are equipped with a single antenna.

The integration of RISs with massive MIMO introduces a novel approach to optimize the performance of wireless communication networks. RISs can be strategically deployed in the environment to enhance the signals' quality and enable more efficient beamforming. By dynamically adjusting the reflecting elements, RISs facilitate adaptive control over the wireless channel, offering a complementary solution to the capabilities of massive MIMO. The integration of these technologies represents a synergistic approach to address the challenges and enhance the capabilities of wireless communication networks. In the RIS-assisted massive MIMO framework, the reflecting elements of the RIS are strategically deployed within the communication environment. These elements work in tandem with the massive array of antennas in the MIMO system to provide an additional layer of control over the wireless propagation environment. The dynamic adjustment of the RIS elements complements the spatial diversity offered by massive MIMO, contributing to improved signal quality, reduced interference, and enhanced overall network efficiency. The advantages of RIS-assisted massive MIMO can be sorted out as follows [2, 19].

1) One of the primary advantages of RIS-assisted massive MIMO is the enhancement of coverage and reliability. The dynamic control over signal propagation provided by the RIS contributes to more effective beamforming and coverage expansion. This is particularly beneficial in scenarios where traditional infrastructure may face challenges, such as in indoor environments or areas with high user density.

2) RIS-assisted massive MIMO contributes to improved spectral efficiency by leveraging the spatial diversity of massive MIMO and the adaptive control capabilities of RISs. This results in a more efficient utilization of the available frequency spectrum, enabling higher data rates and accommodating a larger number of users simultaneously.
3) The intelligent reflecting elements of the RIS play a crucial role in mitigating interference. By dynamically adjusting the phase and amplitude of reflected signals, RISs can minimize the impact of interference from other users or external sources. This leads to a cleaner and more reliable communication link, especially in densely populated urban areas where interference is a common challenge.
4) RIS-assisted massive MIMO enables adaptive beamforming, allowing the system to dynamically adapt to changing channel conditions and user requirements. The combined capabilities of massive MIMO and RISs provide a level of adaptability that enhances the system's resilience to varying environmental factors, such as user mobility and changing propagation conditions.

RIS-assisted massive MIMO holds significant promise across various applications and scenarios in wireless communication networks. In urban environments with high user density, the deployment of RISs can alleviate interference and enhance overall network capacity. In indoor scenarios, such as stadiums or shopping malls, RIS-assisted massive MIMO can improve coverage and connectivity. Moreover, the integration of these technologies is particularly relevant in scenarios where traditional infrastructure deployment is challenging, such as remote or underserved areas.

The versatility of this combined approach opens up a myriad of applications across different scenarios in wireless communication networks. In densely populated urban environments with high user density, RISs can be strategically deployed to alleviate interference and enhance the overall capacity of the network. The dynamic control over signal paths and adaptive beamforming capabilities contribute to improved connectivity and user experience. Another application is that RIS-assisted massive MIMO is particularly beneficial in indoor environments, such as stadiums, shopping malls, or large conference venues. The integration of RISs enhances coverage and connectivity, addressing challenges related to signal propagation in confined spaces. In remote or challenging areas where traditional infrastructure deployment may be impractical, RIS-assisted massive MIMO may provide a flexible solution for this case. The adaptive nature of RISs allows for dynamic optimization of communication links, making it possible to establish reliable connections in areas with difficult propagation conditions [14, 15, 17, 18].

While the integration of RISs with massive MIMO holds great promise, several challenges and considerations must be addressed for practical implementation.

The integration of two advanced technologies introduces a level of complexity that requires careful consideration. The design and deployment of RIS-assisted massive MIMO systems necessitate sophisticated algorithms for intelligent configuration, coordination, and management of both technologies. The dynamic nature of wireless channels and user mobility poses challenges in dynamically configuring the reflecting elements of the RIS. Efficient algorithms must be developed to adaptively adjust the RIS configuration in real time, considering the changing communication environment. The deployment of a large number of antennas in massive MIMO and the additional reflecting elements in RISs may lead to increased power consumption. Balancing the energy efficiency of the system while maintaining performance is a crucial consideration for practical implementations. The cost of deploying and maintaining RIS-assisted massive MIMO systems is a significant consideration. Evaluating the cost-effectiveness and scalability of such systems is essential for widespread adoption, especially in the context of evolving wireless communication standards.

Advancing intelligent algorithms for the dynamic configuration of RIS-assisted massive MIMO systems represents a promising research direction. Machine learning and artificial intelligence techniques can be leveraged to optimize system performance, adapt to changing conditions, and enable autonomous decision-making. Exploring the integration of these systems with emerging technologies such as network slicing and edge computing can further enhance the capabilities of communication networks. This integration can support diverse communication services with varying requirements, including ultra-reliable, low-latency communication and enhanced mobile broadband. In addition, standardization efforts and the development of interoperability standards are crucial for the widespread adoption of combination. Establishing common frameworks and interfaces will facilitate the seamless integration of these technologies into existing and future communication networks.

9.2.3 RIS–SM

Spatial modulation represents a paradigm shift in MIMO communication by intelligently utilizing the spatial dimensions for enhanced data transmission. Unlike traditional MIMO schemes, where all antennas transmit simultaneously, SM selects a subset of antennas for signal transmission, effectively encoding information in both the spatial and signal domains. This approach reduces the complexity associated with traditional MIMO, as it only requires the activation of a limited number of antennas at any given time. By exploiting spatial diversity, SM improves spectral efficiency and system capacity, making it an attractive solution for next-generation wireless networks.

The integration of RISs with SM offers a synergistic approach to address the challenges and opportunities in modern wireless communication. In the RIS-assisted SM framework, the collaboration between these two technologies occurs through the RIS's dynamic control of reflecting elements. The SM scheme, which intelligently selects active antennas for data transmission, benefits from the additional control provided by the RIS in shaping the wireless channel. By adjusting the phase and amplitude of reflected signals, RISs contribute to the optimization of signal paths, interference mitigation, and overall enhancement of SM performance. This integration leverages both technologies' strengths to create a more flexible and adaptive communication system. Figure 9.3 illustrates a communication system aided by the RISs. Within this framework, user equipment transmits information to an access point (AP) with the support of the RIS. The advantages of RIS-assisted SM can be summarized as follows [3, 20–23].

1) SM inherently enhances spectral efficiency by transmitting information in both spatial and signal domains. The addition of RISs provides an extra layer of adaptability, enabling further optimization of communication links. The dynamic control over the wireless propagation environment allows for real-time adjustments to enhance spectral efficiency, accommodating the varying needs of different communication scenarios.
2) RIS-assisted SM contributes to improved coverage and reliability by optimizing signal paths and mitigating interference. The dynamic adjustment of reflecting elements allows for targeted signal distribution, extending coverage

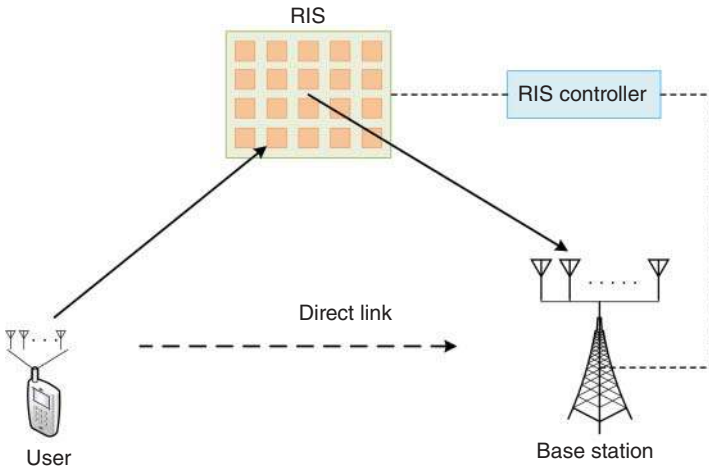

Figure 9.3 A communication system for uplink transmission that integrates SM with the support of RISs.

in challenging environments such as urban areas or locations with obstacles. This, in turn, enhances the reliability of communication links, providing a more robust and consistent user experience.

3) One of the significant advantages of RIS-assisted SM is its capability to mitigate interference. The dynamic control over reflecting elements enables the system to intelligently manage and minimize interference from other users or external sources. This interference mitigation contributes to a cleaner and more reliable communication link, especially in scenarios with high user density or coexisting wireless systems.
4) The adaptability of RISs introduces opportunities for energy-efficient communication. By optimizing signal paths and distribution, RIS-assisted SM allows for targeted energy consumption, activating specific reflecting elements based on real-time channel conditions. This can lead to energy savings, contributing to the sustainability of wireless communication networks.
5) The versatility of RIS-assisted SM extends to various applications and scenarios within wireless communication networks. In densely populated urban environments with high user density, RIS-assisted SM can optimize coverage, enhance spectral efficiency, and mitigate interference. The dynamic control over the wireless propagation environment allows the system to adapt to the unique challenges of urban communication, providing improved connectivity and user experience [20]. Another application scenario is particularly beneficial in indoor deployments, such as shopping malls, airports, or office buildings. The adaptability of RISs enables precise control over signal paths, reducing multipath fading and improving coverage in confined spaces, where traditional MIMO systems may face challenges. The RIS-assisted SM holds promise for Internet of Things (IoT) networks, where efficient use of spectrum and energy is crucial. The adaptability of RISs aligns well with the dynamic and diverse communication requirements of IoT devices, providing an intelligent solution for optimizing connectivity and energy consumption [21]. In mmW communication, where propagation is highly sensitive to obstacles and atmospheric conditions, the combination can offer dynamic adjustments to overcome challenges. The precise control over the wireless channel enables the system to easily adapt to changing conditions, ensuring reliable communication in mmW frequency bands, and holds great promise for fifth-generation (5G) and future generations of wireless communication [22].

While the integration of RISs with SM presents compelling advantages, several challenges and considerations must be addressed for practical implementation. The dynamic configuration of reflecting elements in real-time poses challenges in terms of algorithm complexity and signaling overhead. Efficient algorithms must be developed to adaptively adjust the RIS configuration, coordinating with SM requirements and considering changing channel conditions. Accurate channel

state information (CSI) is crucial for the successful implementation of SM. The integration of RISs introduces additional complexities in acquiring CSI due to the dynamic nature of the reflecting elements. Robust and efficient methods for CSI acquisition in RIS-assisted SM scenarios are essential.

The deployment of RISs and the associated hardware bring additional complexity to the overall system. Ensuring the cost-effectiveness and scalability of RIS-assisted SM systems while considering the hardware requirements is a critical consideration for practical implementation.

Advancing machine learning and artificial intelligence techniques for the dynamic configuration and optimization of these combined systems are promising research directions. These intelligent algorithms can adapt to changing network conditions, enhancing system performance and efficiency. Exploring cooperative communication strategies, where multiple RISs collaborate to optimize SM performance, presents an intriguing research opportunity. Cooperative schemes can leverage the distributed intelligence of multiple RISs to enhance coverage, reliability, and spectral efficiency.

9.2.4 RIS–Small Cell Networks

Small cell networks are a pivotal component of modern mobile communications, especially in urban areas with high user density. These networks consist of small BSs, or cells, deployed in proximity to users to enhance coverage and capacity. Small cells play a crucial role in offloading traffic from macrocells, improving data rates, and ensuring a consistent user experience in crowded urban environments. However, challenges such as interference and optimal resource utilization persist, prompting the exploration of innovative solutions like the integration of RISs. In the RIS-assisted small cell network, the collaboration between RISs and small cell BSs is orchestrated to optimize the wireless environment. The intelligent reflecting elements of the RISs strategically are adjusted based on the communication requirements and network conditions. This collaboration aims to improve signal paths, mitigate interference, and enhance the overall efficiency of small-cell networks, especially in challenging urban scenarios. Therefore, integrating RISs with small cell networks offers many advantages, addressing critical challenges and ushering in a new era of urban connectivity [4, 24, 25]. The macro base station (MBS) broadcasts the signal to the macro user. At the same time, the RIS communicates the information obtained from the wired backhaul to multiple micro users by seamlessly integrating it into the incident MBS signals, as illustrated in Figure 9.4.

One of the primary advantages of RIS-assisted small cell networks is the effective mitigation of interference. The dynamic adjustment of reflecting elements by RISs allows for intelligent interference management, minimizing the impact

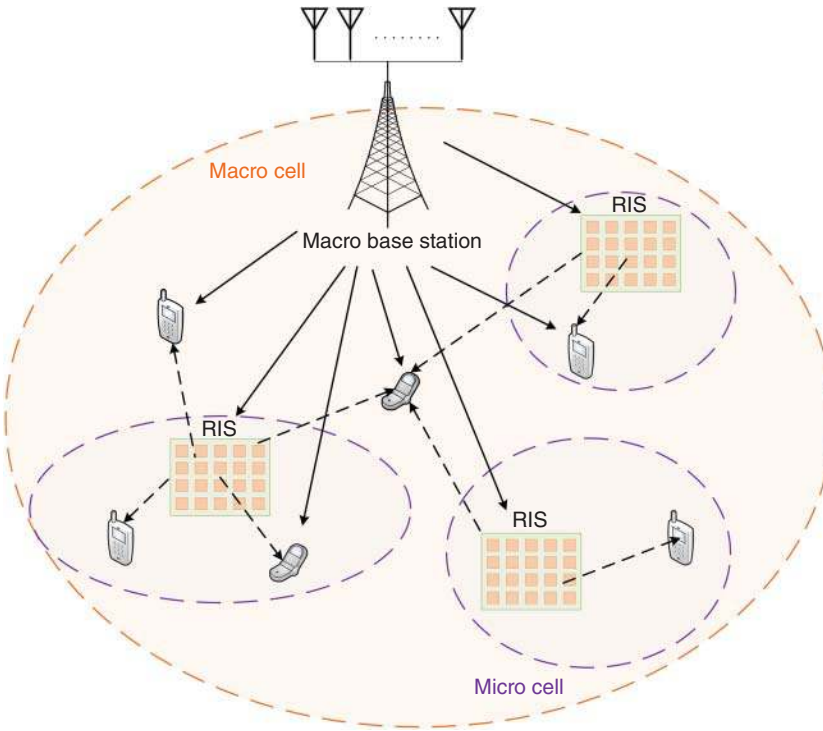

Figure 9.4 An illustrative scenario demonstrating the application of a small cell network assisted by RISs.

of interference from neighboring cells or external sources. This results in cleaner and more reliable communication links, enhancing the overall quality of service. RIS-assisted small cell networks contribute to enhanced coverage and connectivity in urban environments. By optimizing signal paths and distribution, RISs address coverage gaps, especially in areas with obstacles or challenging propagation conditions. This is crucial for providing reliable and seamless connectivity to users in diverse urban settings. The integration of RISs introduces a new level of adaptability to spectral efficiency in small-cell networks. By dynamically adjusting the wireless environment, RIS-assisted systems optimize the use of available frequency resources. This leads to increased spectral efficiency, enabling higher data rates and supporting the growing demand for bandwidth-intensive applications in urban areas. RIS-assisted small cell networks support more efficient resource allocation. The reflecting elements can be intelligently configured to prioritize specific users or adapt to changing user densities. This adaptability ensures optimal resource utilization, enhancing the overall capacity of the network and accommodating the varying demands of urban users [4, 24].

The versatility of RIS-assisted small cell networks extends to various applications and scenarios within urban wireless communication networks. In urban hotspots such as shopping districts, parks, or transportation hubs, RIS-assisted small cell networks can enhance connectivity and data rates. The adaptability of RISs allows for precise control over signal paths, optimizing coverage and ensuring a consistent user experience in high-traffic urban areas. In the context of smart cities, where connected devices and sensors play a crucial role in urban management, RIS-assisted small cell networks can optimize connectivity for IoT devices. The intelligent adjustment of the wireless environment supports the seamless integration of smart city applications, contributing to efficient urban operations. In densely populated residential areas, RIS-assisted small cell networks can alleviate challenges associated with interference and coverage gaps. The adaptability of RISs ensures that communication links are optimized, providing reliable and high-speed connectivity to residents in multi-family dwellings and high-rise buildings. In venues such as stadiums, arenas, or concert halls, where user density can spike during events, RIS-assisted small cell networks can ensure robust and reliable connectivity. The dynamic adjustment of reflecting elements caters to the changing communication demands, offering an enhanced user experience in crowded environments.

While the integration of RISs with small cell networks holds great promise, several challenges and considerations must be addressed for practical implementation. Effectively coordinating the deployment and operation of RISs with small cell BSs requires robust synchronization mechanisms. Ensuring seamless collaboration between RISs and small cell networks is essential for optimizing the overall performance, especially in scenarios with dynamic user mobility. The dynamic configuration of reflecting elements in real-time introduces challenges related to algorithm complexity and signaling overhead. Efficient algorithms must be developed to adaptively adjust the RIS configuration, coordinating with small cell communication requirements and considering varying channel conditions. Accurate CSI is crucial for the successful implementation of RIS-assisted small cell networks. The dynamic nature of the reflecting elements adds complexity to acquiring reliable CSI, requiring robust methods for estimation and feedback. The deployment of RISs in conjunction with small cell networks introduces additional hardware and infrastructure costs. Ensuring the cost-effectiveness and scalability of RIS-assisted small cell networks is critical for widespread adoption, especially in the context of urban deployments with varying scales.

Considering the integration of RIS-assisted small cell networks with edge computing architectures can further enhance the efficiency of data processing. This integration can support real-time analysis at the network edge, reducing latency and improving the responsiveness of small cell networks, especially in urban scenarios with diverse application requirements. In addition, exploring cooperative

networking strategies, where multiple RIS-assisted small cell networks collaborate to optimize performance, presents an intriguing research opportunity. Cooperative schemes can leverage the distributed intelligence of multiple RISs to enhance coverage, reliability, and spectral efficiency in complex urban environments.

9.2.5 RIS-mmW Communications

Wireless communication systems have been restricted in a frequency band ranging from hundreds of megahertz up to early gigahertz (GHz) region. In this area, wavelengths are between a few centimeters and a meter. To date, this aforementioned frequency spectrum has been almost fully utilized by some wireless communication systems during time periods of heavy usage. Hence, new and forthcoming wireless mobile technologies need a lot more bandwidth to operate and meet the requirements of 6G systems [26]. In order to meet the requirements of the latest wireless mobile communication systems, it has become an obligation to use the spectrum between 30 and 300 GHz, which is called the mmW band, where the wavelength of a signal ranges from 1 to 10 mm. More than 90% of the radio spectrum falls in the mmW band, and it contains many unlicensed bands that can be utilized to reduce crowding in low-frequency regions.

There are two major trends that have spurred the use of mmW bands. First, with the development of complementary metal oxide semiconductors and digital signal processing technologies, it is possible to produce low-cost radio-frequency (RF) circuits. Thus, these developments in combination with very small mmW signal wavelength enable many small antennas to be placed in a very small area, which makes possible fabricated on the skin of a mobile phone, in the BS, or in a chip [5]. Second, the latest generation of wireless mobile communications, such as 5G and 6G evolved toward smaller radii to meet high data rate requirements and seamless connectivity with the aid of femtocell and picocell. Especially, cell sizes have been in the range of 100–200 m in radii, which corresponds to mmW range, and it is possible to utilize the mmW band for 6G [5].

However, despite the benefits of mmW communications, there are some challenges such as path loss and blockage effects with realizing the transmission at mmW frequencies. Since free space omnidirectional path loss between transmitter and receiver increases with the square of the frequency, the path loss is much larger at mmW frequency bands. Path loss can be avoided with the use of beamforming schemes in which the radiated power is focused on direct targets [5, 27, 28]. The blockage effects at mmW frequencies easily occur due to many outdoor obstructions such as a building, a tree, a car and even a part of the human body. At this point, RIS can be considered as a promising solution to solve the blocking effect by adding a new link to supply the present communication system. RISs are placed on the facades of a building to receive the signal from BS or user

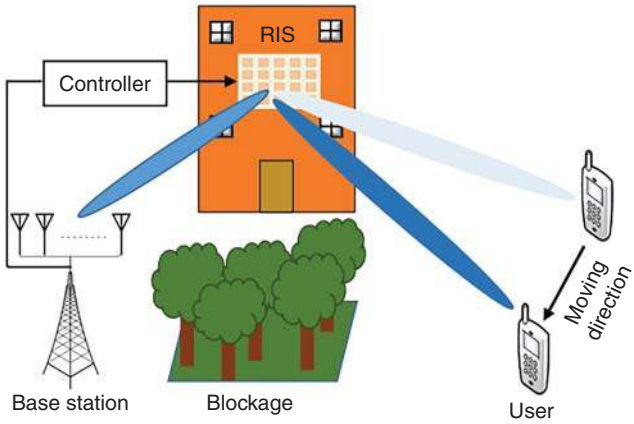

Figure 9.5 RIS-aided mmW transmission with beamforming.

and then, the received signal can be sent from RIS to target receiver. Reflection of the received signals by RIS is made only passively, it provides energy-efficient transmission by reducing the power consumption without additional noise since RIS has passive characteristics [29]. In Figure 9.5, a transmission between a BS and a moving user at mmW frequency is illustrated where beamforming is used to combat path loss, and the blockage effect is avoided by using RIS placed on a building. In this figure, oval-shaped lines represent beams for the illustration purpose of beamforming in mmW communications. Figure 9.5 shows that the beam from the RIS unit follows the moving user to seamlessly maintain the mmW communications. RIS is sensitive to the blockage effects and mmW communication is limited by range due to large path loss, so it is very important to determine the optimal placement, orientation, and configuration of RIS elements.

This case needs to be carefully taken care of to improve the signal quality and coverage area since it poses a major challenge and sophisticated algorithms are required that consider the dynamic nature of mmW channels. In addition, the sensitivity of mmW communications to the blockage makes the line-of-sight (LoS) more important for maintaining the transmission. When the LoS link is unavailable, phase shift adjustment in the RIS unit is required for proper reflection towards blocked users. In uncertain environments like this, phase shift optimization at RIS and BS beamforming schemes are the challenges to deal with [30].

9.2.6 RIS–VLC

VLC technology is a way of communication in which visible light emitted by light-emitting diodes (LEDs) is used to transmit data. The frequency spectrum in

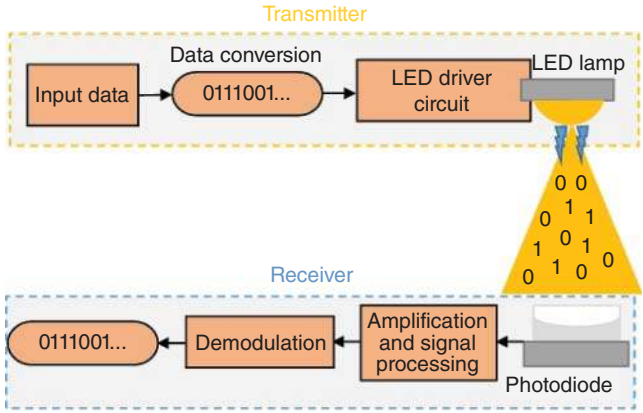

Figure 9.6 Block diagram illustration of VLC system model.

VLC systems ranges from 400 to 800 THz. Unlike RF systems using antennas in lower THz bands, VLC technology relies on the intensity of light. So, modulating the intensity of the emitted light by LEDs at high speeds is the fundamental of this technology. The modulated light intensity is converted into a voltage signal by photodiode and then, it is processed by a signal processing unit before demodulation [31, 32]. A block diagram for VLC systems is illustrated in Figure 9.6.

In this figure, LED lamp emits the light and the light is collected by a photodiode. Specifically, the transmitter, where the data conversion is made, and the receiver, which makes signal processing before demodulation, are shown in Figure 9.6. The spectrum resources offered by VLC technology are more than that of RF communications, and hence, the requirement of higher bandwidth for a higher data rate can be provided for 6G systems. Since the VLC systems do not interfere with RF communications, hence it can be considered as a good complementary system for indoor RF communications [33]. In addition, visible light cannot penetrate through walls, so this technology offers a higher level of security in comparison to traditional RF systems [34]. VLC technique has several important applications, such as light fidelity (Li-Fi) [35], indoor positioning [36] and underwater wireless communications [37].

Despite several benefits, VLC technology has some drawbacks, like limited range and sensitivity to LoS blockage. A clear LoS link between the light source and photodetector is essential in a VLC system to successfully transmit data. However, a clear LoS link does not always exist, and it is not guaranteed owing to the presence of obstacles and different users. To overcome this challenge, non-LoS path can be assisted by RIS units that help the maintenance of transmission [38]. Hence, the coverage of the VLC system can be extended with the use of RIS by overcoming

obstacles. Adaptive adjustments of RIS elements via dynamic control improve the reliability of the VLC channel in varying environments.

In an RIS-assisted VLC system, mirror array sheets (MASs) or metasurface arrays are deployed to form an RIS unit. The MAS is composed of several mirrors in a way of arrangement, and each mirror has an angular orientation for properly focusing the light beam. Each of the individual mirrors has a mechanical control system to make orientation of mirrors. There are two angles known as the yaw and the roll angles in every individual mirror. When the number of elements in the MAS are increased, the beam direction control is more critical which makes dimensionality and complexity higher. Different from MAS, meta-materials are used to produce metasurface arrays. Metasurface arrays have much complexity and they are more expensive in comparison with the MAS. Owing to the light attenuation, MASs are generally well fitted for indoor applications of RIS-aided VLC, while metasurface arrays can be considered for outdoor RIS-assisted VLC systems with proper selection of case material for metasurface arrays in the RIS [31, 39]. In Figure 9.7, the use of RIS in VLC systems is shown for an indoor scenario.

There are two RIS units that are placed onto different walls of an office or a room. There are some blockages between users and the LED light source, so the VLC communications are maintained with two RIS units according to the location of the blockages in Figure 9.7. Device orientation is a major challenge that needs to be effectively combated to overcome blockage in LoS link and another major problem is the location of the VLC receiver, which is also important for the existence of a clear LoS path. It is crucial to find the optimal orientation of MAS elements which is vital to use its full benefits. Another orientation challenge is to assign RIS elements to APs or users to determine which elements serve which APs and users. This issue is important because the VLC link is affected by the geometric

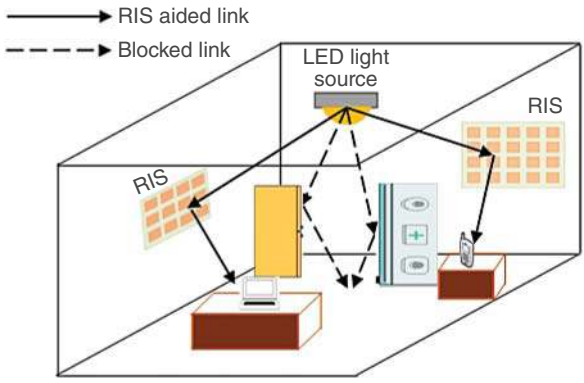

Figure 9.7 An RIS-assisted indoor VLC system illustration.

locations of AP and user nodes. Another orientation problem is the positioning of RIS arrays, so the position of RIS arrays needs to set accordingly for receiving more optic signals.

9.2.7 RIS–THz Communications

5G communication systems use spectrum above 6 GHz called as mmW frequencies to meet high data rate requirements for 5G. In 6G wireless communication systems, it is aimed to make possible the use of THz frequencies (0.1–10 THz) to achieve even ultra-high data rates. However, the use of THz bands results in great path attenuation, so the THz spectrum is appropriate for short-range communications. Specifically, from 275 GHz to 3 THz frequency range, which is not allocated for a specific purpose is the applicable THz frequency spectrum for mobile communications. The capacity enhancement can be achieved with the addition of THz band to mmW band in 6G cellular communications. With this addition, it is possible to increase the total capacity almost 11 times when compared to the capacity of only mmW spectrum [40–43].

Due to shorter THz wavelength between 0.03 and 3 mm and reduction of antenna aperture, THz signals are more directional and anti-eavesdropping abilities compared to mmW. Despite these, higher propagation loss is one of the major challenges that limit communication range as mentioned before. In addition, molecular absorption of water vapor and oxygen molecules causes molecular absorption, and it also makes a significant contribution to path loss [44, 45].

Fortunately, RIS is an encouraging technology to enhance the effective communication range by increasing the propagation distance. For this reason, RIS can be used to combat distance problems in THz communications. At the same time, it is possible to mitigate blockage in the LoS path by deploying RIS units as it is used in mmW and VLC systems for improving coverage areas in indoor and outdoor communication scenarios. Since appropriate RIS configuration enables beamforming in which the THz signal is directed towards particular receivers and hence, the coverage area can be optimized. Another benefit of RIS usage in THz communications is the interference mitigation by reflecting THz waves away from undesired directions and it provides improvements in the total signal-to-noise ratio (SNR). With the reflection from RIS elements, diversity, and communication reliability can be improved as the reflected signals is controlled in RIS technology.

9.2.8 RIS–UAV Communications

UAVs are a class of aircrafts or known as drones that are controlled remotely or an autonomous program without a human being in the vehicle. Nowadays,

UAV communications have a crucial role in wireless communication systems. UAVs are commonly utilized for rapid networking thanks to small size and flexibility where the areas are disabled for communication. Thus, they can be used as aerial platforms for data collection, APs or relays. When signals are not always available from BSs due to mountains and desert regions, UAVs can also be used to create ad-hoc networks [6, 46–48]. Some applications of UAV-aided wireless communications envisioned for 6G are listed as below [6, 46]:

1) Wireless sensor networks, caching-aided wireless networks, cloud radio access networks, emergency networks, cognitive radio networks
2) D2D communications
3) Vehicle-to-everything communications
4) IoT
5) Mobile edge computing
6) Virtual reality and augmented reality
7) Hologram
8) Intelligent transportation
9) Smart city

UAVs are the key part of the three-dimensional (3D) heterogeneous network architectures which will become common applications in 6G, so 3D seamless communications will be facilitated in this manner. However, using UAVs for communication purpose in urban areas has some difficulties where the transmission path between the UAVs and the users/BSs can be subject to blockages such as buildings, trees, cars, etc. Fortunately, maneuverability and high mobility are the important advantages of UAVs to operate at low cost and provide LoS path acting as a mobile aerial BS for helping users on the ground [6, 49]. RIS technology can be integrated into UAV-assisted wireless communication systems to combat non-LoS conditions. In Figure 9.8, an urban scenario is shown where the users and the BSs communicate with the assistance of RIS-aided UAVs. A user near a building communicates with a BS with the help of RIS and UAV, which is shown by solid lines (user-RIS-UAV-BS direction) and vice versa represented with dashed lines (BS-UAV-RIS-user direction) in an outdoor scenario.

However, the scenario illustrated in Figure 9.8 considers the case in which RIS is placed on the side wall of the building, and the mobility of the RIS is ignored. As it is considered in [49], the RIS can be mounted onto the UAV to be able to make possible RIS having mobility. Hence, the RIS can be used as a mobile relay moving with UAV to support mobile communications in urban areas. This case is demonstrated in Figure 9.9. A user in a car park and a moving car on the road communicate with a BS via a flying UAV, which has an RIS unit mounted on it. Solid lines represent the direction of UAV, and the dashed lines are used for the direction from UAV.

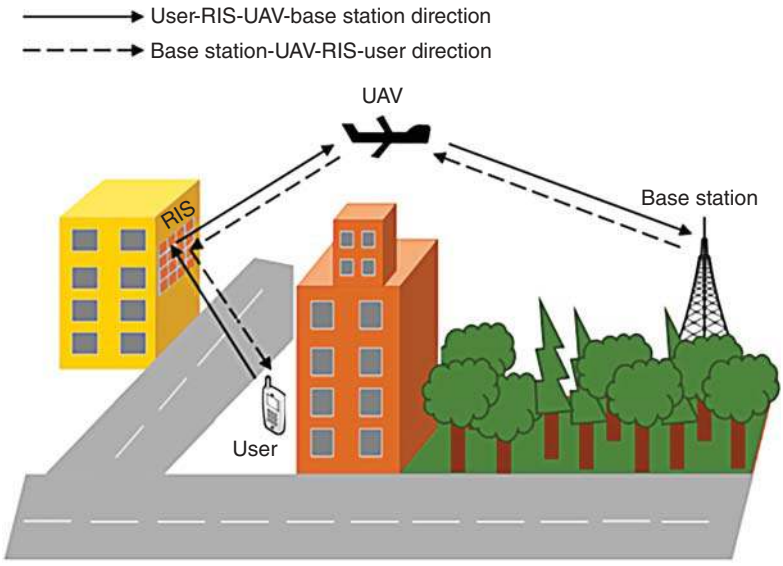

Figure 9.8 RIS-assisted UAV communications between a user and a BS.

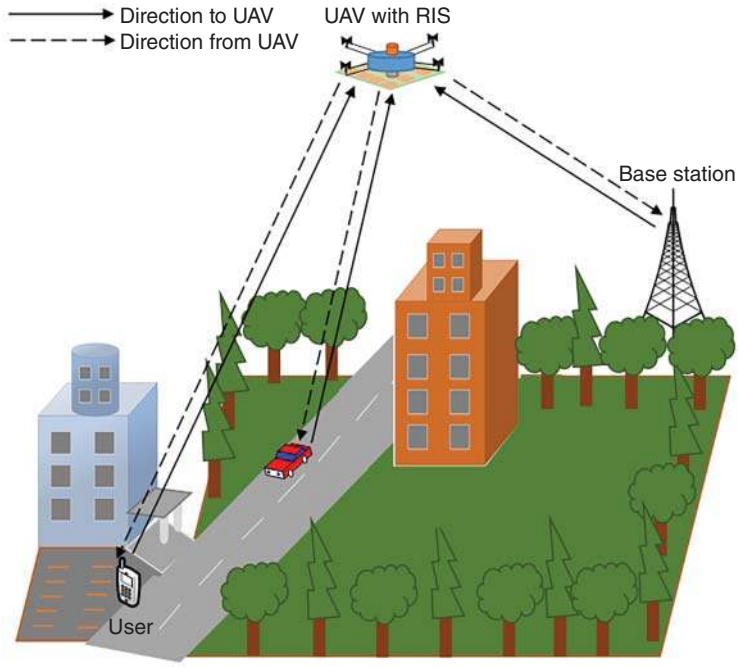

Figure 9.9 An RIS mounted onto a UAV to act as a mobile relay to communications between a user and a BS.

In particular, RIS-assisted UAV communications enable LoS channels with a high probability and can be used in flexible deployment scenarios by providing cost-effective solutions to support high data rates in mobile communications for remote areas and emergency cases. However, using UAVs brings several challenges, such as size, power limitations, and weight. So, designing antennas must take these constraints into account. In addition, the mobility of the UAV-assisted RISs also causes channel variations that needs to be solved to maintain a clear transmission. Since UAVs move fast and sway randomly, it is difficult to properly adjust the beam for tracking channel [6].

9.3 Theoretical Analysis of RIS-Assisted Systems

In this section, general concepts for theoretical analysis are emphasized. Some key points such as system model, modulation technique and fading scenario that affect and change the analytical analysis are mentioned as a guide. Then, general formulas for OP, error probability, and capacity analysis are presented and explained in an analytical framework.

9.3.1 Some Key Points for Theoretical Analysis

Recently, RIS-assisted wireless communication systems have been extensively studied, and it has become popular. Therefore, the development of theoretical analysis for RIS-assisted communication systems is crucial. As known, researchers typically first establish the theoretical analysis of a system and subsequently attempt to implement the system. If the results obtained from theoretical analyses are not satisfactory, the system does not perform practical applications. Then, the system is modified, and modified system models are reconsidered. Looking at the overall landscape of RIS-assisted wireless communication systems, it can be observed that, similar to cooperative communication systems, RIS structures play a relay-like role and assist in achieving more successful information transfer between source and destination nodes [50–53]. In this regard, the importance of RIS structures is highly significant for such wireless communication systems. In cooperative systems, a relay is a secondary user tasked with facilitating the transfer of information between the source and destination. The relay employs two fundamental methods, namely, decode-and-forward and amplify-and-forward, to carry out this information transfer. In these systems, the secondary user serving as a relay consumes energy, and there is also a security vulnerability due to the presence of another user in the system. On the other hand, RISs are surfaces containing electromagnetic materials that can be electronically controlled by devices inherent in their structure. In other words, they are not

any user in the system. If an RIS-assisted system is used, there is no security issue because the function performed by the RIS is directly analogous to that of a relay. Each reflective element on the RIS successfully facilitates communication by relaying the signal it receives from the source to the destination, functioning as if it were multiple relays. Additionally, the abundance of reflective elements on RIS enhances system performance without affecting energy consumption in the system [51]. The passive transmission of reflective elements is a significant advantage of the RIS. For all these reasons, it is considered that RIS structures will be utilized in the design and architecture of next-generation wireless systems [54–56].

Typically, in the development of theoretical analyses for RIS-assisted wireless communication systems, the probability density function (PDF) or cumulative distribution function (CDF) expressions for the received instantaneous SNR or the instantaneous signal-to-noise-plus-interference ratio (SINR) at the destination node are utilized [51, 57, 58]. The system model addressed here is also highly important. The theoretical analyses in the considered system model vary according to the diversity of the system. By diversity, it means the structure of the system model and the different arrangements in the system. For example, it includes how RIS-assisted is adopted in the system, the variations in fading channel structures among wireless system nodes (such as Rayleigh, Nakagami, and Rician, etc.), different modulation schemes employed in the system (like SM, index modulation [IM], spatial shift keying [SSK]), and various protocol types used by system users (such as NOMA or sparse code multiple access [SCMA]). In addition to these, the inclusion or exclusion of perfect or imperfect CSI, as well as the consideration of phase and path losses in RIS transmission, further differentiates the theoretical analyses. Due to all these different arrangements mentioned, there are numerous examples of theoretical analyses of RIS-assisted wireless communication systems in the literature [57–73].

In [57], two different system models named dual-hop RIS-assisted and RIS-assisted transmit scheme were considered in a Rayleigh fading channel environment. The PDF and CDF expressions for these setups were derived, and utilizing these, analyses were performed by deriving OP, average bit error rate, and average capacity expressions. In another study, [60], which conducted an analysis in Rayleigh fading, the SNR coverage probability for RIS-assisted single-input single-output communications has been presented. The studies in [57, 60] were conducted considering Rayleigh fading. As known, in theoretical studies, Rician and Nakagami-m fading are also commonly used similarly to Rayleigh fading. Studies examining RIS-assisted communication systems using these fading channels can be found in [58, 61–64]. In the study [58], OP, average

symbol error rate, and ergodic achievable rate analyses were presented for an RIS-assisted dual-hop communication system over Nakagami-*m* fading channels. In [61], the cascaded RIS system structure was considered over Nakagami-*m* fading. By utilizing the end-to-end instantaneous SNR expression, the OP expression for the system was derived. In [62], the two-way full-duplex RIS-assisted communication system model was analyzed with both Rician and Nakagami-*m* fading. As a result of the analysis, OP and ergodic capacity results were demonstrated. In [63], OP, approximate bit error rate, and average capacity expressions for an RIS-assisted downlink communication system over Nakagami-*m* fading were proposed. As a different system model, [64] presented a structure with two relays, where one relay is adapted to a powerline communication system, providing communication to the source, and the other relay provides UAV-based RIS-assisted dual-hop communication. In the UAV-based RIS-assisted part, fading is considered as Rician. OP and average bit error rate (BER) analyses for this system structure have been provided.

The type of fading is a significant factor in theoretical analysis, but the protocols used in the system also contribute to the differentiation of theoretical analysis. For example, the system that will be integrated with the RIS [59, 65–67] leads to changes in the theoretical analysis of these structures. In [65], the ergodic rate analysis of the simultaneously transmitting and reflecting (STAR) RIS-assisted NOMA system has been approximately conducted based on the PDF of the instantaneous SNR. In [66], an RIS-assisted cooperative NOMA system structure is considered in a downlink scenario. In this study, detailed presentations of both precise and asymptotic OP expressions, as well as achievable rate analysis, have been provided. In [59], the study focuses on the RIS-assisted power domain NOMA system structure, proposing total sum rate, OP, and average BER analyses based on instantaneous SINR. In [67], it is emphasized that the RIS-assisted SCMA system model will be fundamental for future-generation wireless communication systems. An optimization study has been presented based on appropriate theoretical analyses for the considered system model.

On the other hand, the new types of modulation used by nodes in RIS-assisted systems also differentiate theoretical analyses. Examples of such new modulation types include IM, SM, and SSK. The use of those aforementioned modulation techniques enhances system performance but, as expected, also increases system complexity. On the other hand, studies in the literature have widely presented RIS-assisted IM, SM, or SSK applications [68, 69]. In [68], the study investigates the effects of IM in an RIS-assisted system based on SM and SSK applications. Accordingly, exact closed-form expressions for the probability of erroneous receive antenna index detection were obtained. In [69], RIS-assisted SSK with

passive beamforming and RIS-assisted SSK with Alamouti space–time block coding scenarios have been considered. Bit error probability expressions were derived for both considered system models. In [70], the study proposed the average BER and ergodic capacity analysis of the RIS-assisted SSK system model. Then, the reflection phase modulation was also considered in this study. In addition, the CSI condition is another factor that differentiates theoretical analysis in RIS-assisted communication. Theoretical analyses vary between imperfect CSI and perfect CSI scenarios. It is known that in real-world applications, imperfect CSI is observed. Therefore, addressing this condition is an important issue for practical implementations. There are some studies in the literature [71–73] that examine RIS-assisted communication systems with imperfect CSI, conducting theoretical analyses in these scenarios. In [71], OP and ergodic capacity analyses were presented for the two-way full-duplex RIS-assisted communication system under imperfect CSI conditions. In [72], a robust transmission design was conducted for an RIS-assisted communication system under imperfect CSI conditions, and OP analysis was performed. In the uplink scenario, the achievable rate analysis of the STAR RIS-assisted NOMA system under imperfect CSI conditions has been thoroughly explained by the authors of [73].

As mentioned earlier, all these variations within RIS-assisted systems alter theoretical analyses, consequently impacting analytical results. In the latter part of this chapter, an attempt is made to provide a general framework for basic theoretical analyses, taking into account the brief literature review given above. Accordingly, starting with the fundamental features of the RIS-assisted system, a set of theoretical rules is presented under three subheadings: OP, error probability, and capacity analysis.

9.3.2 Outage Probability

In general, OP defines the likelihood of falling below a threshold value. In other words, it represents the probability of not transmitting when the instantaneous SNR is below a certain threshold and transmitting when it is above that threshold. Therefore, it is a crucial performance evaluation metric in wireless communications. Especially in theoretical analyses, it is frequently examined for various communication systems. Assuming γ_{th} as the threshold for the instantaneous SNR, the OP is defined as follows:

$$OP = \Pr(\gamma \leq \gamma_{th}) \tag{9.1}$$

Given that there is a condition "$\leq$," and considering that this is a probabilistic expression, it corresponds to the CDF based on probability theory. Therefore, by substituting the value of γ_{th} into the overall CDF expression of the system, the total OP can be obtained. Consequently, it is necessary to find the CDF expression

depending on the instantaneous SNR of RIS-assisted communication systems. When considering the RIS effect, the maximum value of the instantaneous SNR at the receiver is addressed with $\gamma = \left[\left(\sum_{i=1}^{N} h_i g_i\right)^2 E_s\right] / N_0$ [51], where N is the number of reflecting surface elements, h_i and g_i are identically distributed random variables related to the channel attenuation, N_0 is the noise power, and E_s is the average power of the transmitted signals. For instance, in [57], PDF and CDF expressions related to the instantaneous SNR for RIS-assisted communication systems are provided. The study in [57] considers two different RIS-assisted system structures. The first scenario involves an RIS-assisted dual-hop communication system, and the second one utilizes the RIS structure as a source node using an RF signal generator. In the first scenario, there is a single source node, a destination node, and the RIS structure serving as a passive relay for signal transmission. Accordingly, the PDF and CDF expressions based on the instantaneous SNR for this system are given as follows [57]:

$$f_\gamma(\gamma) \approx \frac{2W^{a+b}\gamma^{\left(\frac{a+b}{2}-1\right)}}{\Gamma(a)\Gamma(b)} K_{a-b}(2W\sqrt{\gamma}) \tag{9.2}$$

$$F_\gamma(\gamma) \approx \frac{1}{\Gamma(a)\Gamma(b)} G_{1,3}^{2,1}\left[W^2\gamma \,\middle|\, \begin{matrix} 1 \\ b, a, 0 \end{matrix}\right], \tag{9.3}$$

where $W = \sqrt{ab/(\overline{\gamma}\,\Omega)}$, a and b shaping parameters. $\overline{\gamma}$ and Ω are the average SNR and the mean power, respectively. $K_v(\cdot)$ is the modified v-order Bessel function of the second kind [74, eq. (8.432)] and $\Gamma(\cdot)$ is the Gamma function [74, eq. (8.310.1)]. $G_{\cdot,\cdot}^{\cdot,\cdot}[\cdot]$ is the Meijer's G-function defined in [74, eq. (9.301)]. In the second scenario, the RIS structure acts as a source node in the form of an RF signal generator. The PDF and CDF expressions for this scenario are also derived in [57] and they are as follows:

$$f_\gamma(\gamma) \approx \frac{\gamma^{(N-1)} e^{-\frac{\gamma}{B\overline{\gamma}}}}{(B\overline{\gamma})^N (N-1)!} \tag{9.4}$$

$$F_\gamma(\gamma) \approx 1 - e^{-\frac{\gamma}{B\overline{\gamma}}} \sum_{k=0}^{N-1} \frac{\gamma^k}{(B\overline{\gamma})^k k!}, \tag{9.5}$$

where N is number of reflecting elements in RIS and $B = 1 + (N-1)\Gamma^2\left(\frac{3}{2}\right)$. The PDF and CDF expressions given in Eqs. (9.2)–(9.5) are obtained for the Rayleigh fading channel case. Additionally, they are derived considering the previously described RIS-assisted system scenarios. In the literature, the equations from (9.2) to (9.5) have been utilized to analyze various system structures and theoretical analyses have been conducted for new RIS-assisted system models. The OP expressions in these studies vary depending on the different features of the systems mentioned in the literature review section.

9.3.3 Error Probability

The concept of average bit error probability (ABEP) is a crucial and extensively studied evaluation metric for a communication system. In this section, we aim to provide a general framework for the theoretical analysis of ABEP in an RIS-assisted communication system. Generally, two fundamental approaches are employed for ABEP: one based on PDF and the other on CDF. As implied by their names, these analyses and theoretical expressions are derived using the total PDF or CDF expressions of the system. Starting with the first approach, the overall PDF expression for an RIS-assisted wireless communication system is obtained by adhering to the basic principles of probability theory. Subsequently, using the expression in Eq. (9.6), the ABEP expression is derived. Therefore, the PDF-based error expression approach for ABEP is as follows:

$$ABEP = \int_0^\infty p(e\,|\gamma\,) f_\gamma(\gamma) d\gamma, \tag{9.6}$$

where $p(e|\gamma)$ is the conditional error probability and this expression varies depending on the modulation type used. $f_\gamma(\gamma)$ is the PDF of the instantaneous SNR expression at the receiver for the considered system model. On the other hand, the CDF-based ABEP expression is as follows [75]:

$$ABEP = \frac{r^p}{2\Gamma(p)} \int_0^\infty \gamma^{p-1} e^{-r\gamma} F_\gamma(\gamma) d\gamma, \tag{9.7}$$

where r and p are modulation parameters, and for example, $r = 1$ and $p = 0.5$ for binary phase shift keying modulation, respectively. Through the expressions given in (9.6) or (9.7), either PDF- or CDF-based approaches are preferred for the ABEP. Depending on which function, namely PDF or CDF is obtained, the appropriate formula in (9.6) or (9.7) can be used to find ABEP expression. These derivations can be performed through the necessary mathematical manipulations with the help of relevant handbooks or online solution centers such as Wolfram [76].

9.3.4 Capacity Analysis

Another important performance metric is the average channel capacity (ACC). Channel capacity takes into account the maximum achievable transmission rate of the considered system. In addition, just like in the theoretical analyses of ABEP, both PDF-based and CDF-based approaches are used for the ACC. Here again, it is necessary to obtain the total PDF or total CDF expressions for the RIS-assisted communication system, as mentioned earlier. In this way, theoretical analyses of the ACC are conducted, and expressions for ACC can be derived. The expression for ACC analysis with a PDF-based approach is as follows:

$$ACC = \frac{BW}{2} \int_0^\infty \log_2(1+\gamma) f_\gamma(\gamma) d\gamma, \tag{9.8}$$

where BW is the bandwidth of the system. On the other side, in the CDF-based approach, a similar process to that of ABEP is followed by deriving the total CDF expression. Therefore, the expression for ACC is as follows:

$$ACC = \frac{1}{\ln(2)} \int_0^{\infty} (1+\gamma)^{-1} F_{\gamma,c}(\gamma) d\gamma, \tag{9.9}$$

where $F_{\gamma,c}(\gamma)$ is the complementary CDF function for the considered system. Ultimately, the CDF or PDF expressions for instantaneous SNR or instantaneous signal to noise and interference ratio (SNIR) of RIS-assisted communication systems should be derived first. After this stage, depending on whether the PDF-based or CDF-based approaches provided for OP, ABEP, and ACC are preferred, these expressions are substituted, and the necessary mathematical solutions or manipulations are performed to obtain the final expressions. The theoretical analyses of such systems (OP, ABEP, ACC, etc.) are pivotal steps for the evaluation and realization of practical applications, given the anticipated potential of RIS-assisted communication systems for future-generation wireless communication systems.

9.4 Conclusions

This chapter is an excellent resource for anyone interested in RIS structures and their convergence with emerging wireless technologies in the literature. The chapter provides detailed explanations on how RIS structures can be used in conjunction with NOMA, SM, small cells, massive MIMO, mmW communication, VLC, THz communication, UAVs, and more. The chapter elaborates on the characteristics, advantages, and system performance evaluations of these structure systems. Additionally, the final section of the chapter offers a comprehensive examination of how theoretical assessment metrics in communication systems, such as OP, ABEP, and capacity analyses, are applied in RIS structures. This chapter is a must-read for anyone looking to gain a deeper understanding of RIS structures and their applications in modern communication systems. In summary, the advantages and disadvantages of RIS-supported system structures, theoretical analysis, and starting points have been explained in detail, and a book chapter has been created that will provide good guide information for RIS-supported system structures for researchers.

References

1 Zhang, Z., Xiao, Y., Ma, Z. et al. (2019). 6G wireless networks: vision, requirements, architecture, and key technologies. *IEEE Vehicular Technology Magazine* 14 (3): 28–41. https://doi.org/10.1109/MVT.2019.2921208.

2 Dai, J.Y., Cheng, Q., and Cui, T.J. (2022). IRS hardware architectures. In: *Intelligent Reconfigurable Surfaces (IRS) for Prospective 6G Wireless Networks* (ed. M.A. Imran, L. Mohjazi, L. Bariah, et al.), 83–98. Wiley.

3 Wu, M., Lei, X., Zhou, X. et al. (2021). Reconfigurable intelligent surface assisted spatial modulation for symbiotic radio. *IEEE Transactions on Vehicular Technology* 70 (12): 12918–12931. https://doi.org/10.1109/TVT.2021.3121698.

4 Wang, J., Liang, Y.-C., Pei, Y., and Shen, X.S. (2021). Reconfigurable intelligent surface for small cell network. *2021 IEEE Global Communications Conference (GLOBECOM)*, 1–6. Madrid: IEEE. https://doi.org/10.1109/GLOBECOM46510.2021.9685214.

5 Rangan, S., Rappaport, T.S., and Erkip, E. (2014). Millimeter-wave cellular wireless networks: potentials and challenges. *Proceedings of the IEEE* 102 (3): 366–385. https://doi.org/10.1109/JPROC.2014.2299397.

6 Xiao, Z., Zhu, L., Liu, Y. et al. (2022). A survey on millimeter-wave beamforming enabled UAV communications and networking. *IEEE Communication Surveys & Tutorials* 24 (1): 557–610. https://doi.org/10.1109/COMST.2021.3124512.

7 Xiao, Y., Shi, G., Li, Y. et al. (2020). Toward self-learning edge intelligence in 6G. *IEEE Communications Magazine* 58 (12): 34–40. https://doi.org/10.1109/MCOM.001.2000388.

8 Pan, C., Ren, H., Wang, K. et al. (2021). Reconfigurable intelligent surfaces for 6G systems: principles, applications, and research directions. *IEEE Communications Magazine* 59 (6): 14–20. https://doi.org/10.1109/MCOM.001.2001076.

9 Wu, C., Liu, Y., Mu, X. et al. (2021). Coverage characterization of STAR-RIS networks: NOMA and OMA. *IEEE Communications Letters* 25 (9): 3036–3040. https://doi.org/10.1109/LCOMM.2021.3091807.

10 Wu, Q. and Zhang, R. (2020). Towards smart and reconfigurable environment: intelligent reflecting surface aided wireless network. *IEEE Communications Magazine* 58 (1): 106–112. https://doi.org/10.1109/MCOM.001.1900107.

11 Xue, N., Mu, X., Liu, Y., and Chen, Y. (2024). NOMA assisted full space STAR-RIS-ISAC. *IEEE Transactions on Wireless Communications* 23 (8): 8954–8968. https://doi.org/10.1109/TWC.2024.3357349.

12 Li, X., Tian, Z., He, W. et al. (2024). Covert communication of STAR-RIS aided NOMA networks. *IEEE Transactions on Vehicular Technology* 73 (6): 9055–9060. https://doi.org/10.1109/TVT.2024.3349543.

13 Chen, G., Wu, Q., Chen, W. et al. (2023). IRS-aided wireless powered MEC systems: TDMA or NOMA for computation offloading? *IEEE Transactions on Wireless Communications* 22 (2): 1201–1218. https://doi.org/10.1109/TWC.2022.3203158.

14 Ding, Z., Lv, L., Fang, F. et al. (2022). A state-of-the-art survey on reconfigurable intelligent surface-assisted non-orthogonal multiple access networks.

Proceedings of the IEEE 110 (9): 1358–1379. https://doi.org/10.1109/JPROC.2022.3174140.

15 Fu, S., Wang, Y., Feng, X. et al. (2023). Reconfigurable intelligent surface assisted non-orthogonal multiple access network based on machine learning approaches. *IEEE Network* 1–8. https://doi.org/10.1109/MNET.004.2300271.

16 Chien, T.V., Ngo, H.Q., Chatzinotas, S., and Ottersten, B. (2022). Reconfigurable intelligent surface-assisted massive MIMO: favorable propagation, channel hardening, and rank deficiency [lecture notes]. *IEEE Signal Processing Magazine* 39 (3): 97–104. https://doi.org/10.1109/MSP.2021.3128352.

17 Björnson, E., Hoydis, J., and Sanguinetti, L. (2017). Massive MIMO networks: spectral, energy, and hardware efficiency. *FNT in Signal Processing* 11 (3–4): 154–655. https://doi.org/10.1561/2000000093.

18 Marzetta, T.L., Larsson, E.G., and Yang, H. (2016). *Fundamentals of Massive MIMO*. Cambridge University Press.

19 Kazim, J.R., Rains, J., Imran, M.A., and Abbasi, Q.H. (2022). Application and future direction of RIS. In: *Intelligent Reconfigurable Surfaces (IRS) for Prospective 6G Wireless Networks* (ed. M.A. Imran, L. Mohjazi, L. Bariah, et al.), 171–188. Wiley.

20 Li, Q., Wen, M., Li, J. et al. (2023). Interplay between reconfigurable intelligent surfaces and spatial modulation: new application paradigms. *IEEE Wireless Communications* 30 (1): 126–133. https://doi.org/10.1109/MWC.011.2100143.

21 Zhang, Q., Liang, Y.-C., and Poor, H.V. (2021). Reconfigurable intelligent surface assisted MIMO symbiotic radio networks. *IEEE Transactions on Communications* 69 (7): 4832–4846. https://doi.org/10.1109/TCOMM.2021.3070043.

22 Ma, Y., Liu, R., Li, M., and Liu, Q. (2020). Passive information transmission in intelligent reflecting surface aided MISO systems. *IEEE Communications Letters* 24 (12): 2951–2955. https://doi.org/10.1109/LCOMM.2020.3013943.

23 Liu, C., Yu, F., Shi, Z. et al. (2024). RIS-assisted precoding spatial modulation: optimal design and performance analysis. *IEEE Access* 12: 4399–4412. https://doi.org/10.1109/ACCESS.2023.3349371.

24 Wang, J., Liang, Y.-C., Pei, Y., and Shen, X. (2023). Reconfigurable intelligent surface as a micro base station: a novel paradigm for small cell networks. *IEEE Transactions on Wireless Communications* 22 (4): 2338–2351. https://doi.org/10.1109/TWC.2022.3211191.

25 Li, Z., Hu, H., Zhang, J., and Zhang, J. (2021). Enhancing indoor mmWave wireless coverage: small-cell densification or reconfigurable intelligent surfaces deployment? *IEEE Wireless Communications Letters* 10 (11): 2547–2551. https://doi.org/10.1109/LWC.2021.3106821.

26 Andrews, J.G., Buzzi, S., Choi, W. et al. (2014). What will 5G be? *IEEE Journal on Selected Areas in Communications* 32 (6): 1065–1082. https://doi.org/10.1109/JSAC.2014.2328098.

27 Du, H., Zhang, J., Cheng, J., and Ai, B. (2021). Millimeter wave communications with reconfigurable intelligent surfaces: performance analysis and optimization. *IEEE Transactions on Communications* 69 (4): 2752–2768. https://doi.org/10.1109/TCOMM.2021.3051682.

28 Hong, W., Jiang, Z.H., Yu, C. et al. (2021). The role of millimeter-wave technologies in 5G/6G wireless communications. *IEEE Journal of Microwaves* 1 (1): 101–122. https://doi.org/10.1109/JMW.2020.3035541.

29 Wang, P., Fang, J., Zhang, W. et al. (2022). Beam training and alignment for RIS-assisted millimeter-wave systems: state of the art and beyond. *IEEE Wireless Communications* 29 (6): 64–71. https://doi.org/10.1109/MWC.006.2100517.

30 Alsenwi, M., Abolhasan, M., and Lipman, J. (2022). Intelligent and reliable millimeter wave communications for RIS-aided vehicular networks. *IEEE Transactions on Intelligent Transportation Systems* 23 (11): 21582–21592. https://doi.org/10.1109/TITS.2022.3190101.

31 Aboagye, S., Ndjiongue, A.R., Ngatched, T.M.N. et al. (2023). RIS-assisted visible light communication systems: a tutorial. *IEEE Communication Surveys & Tutorials* 25 (1): 251–288. https://doi.org/10.1109/COMST.2022.3225859.

32 Jiang, W., Han, B., Habibi, M.A., and Schotten, H.D. (2021). The road towards 6G: a comprehensive survey. *IEEE Open Journal of the Communications Society* 2: 334–366. https://doi.org/10.1109/OJCOMS.2021.3057679.

33 Shen, P. and Lu, L. (2023). Reconfigurable intelligent surface enabled spatial modulation for visible light communications. *IEEE Photonics Journal* 15 (5): 1–12. https://doi.org/10.1109/JPHOT.2023.3302409.

34 Chen, C., Huang, S., Abumarshoud, H. et al. (2023). Frequency-domain channel characteristics of intelligent reflecting surface assisted visible light communication. *Journal of Lightwave Technology* 41 (24): 7355–7369. https://doi.org/10.1109/JLT.2023.3299520.

35 Haas, H., Yin, L., Wang, Y., and Chen, C. (2016). What is LiFi? *Journal of Lightwave Technology* 34 (6): 1533–1544. https://doi.org/10.1109/JLT.2015.2510021.

36 Li, Y., Ghassemlooy, Z., Tang, X. et al. (2018). A VLC smartphone camera based indoor positioning system. *IEEE Photonics Technology Letters* 30 (13): 1171–1174. https://doi.org/10.1109/LPT.2018.2834930.

37 Ata, Y., Abumarshoud, H., Bariah, L. et al. (2023). Intelligent reflecting surfaces for underwater visible light communications. *IEEE Photonics Journal* 15 (1): 1–10. https://doi.org/10.1109/JPHOT.2023.3235916.

38 Aboagye, S., Ngatched, T.M.N., Dobre, O.A., and Ndjiongue, A.R. (2021). Intelligent reflecting surface-aided indoor visible light communication systems. *IEEE Communications Letters* 25 (12): 3913–3917. https://doi.org/10.1109/LCOMM.2021.3114594.

39 Saifaldeen, D.A., Ciftler, B.S., Abdallah, M.M., and Qaraqe, K.A. (2022). DRL-based IRS-assisted secure visible light communications. *IEEE Photonics Journal* 14 (6): 1–9. https://doi.org/10.1109/JPHOT.2022.3178852.

40 Akyildiz, I.F., Kak, A., and Nie, S. (2020). 6G and beyond: the future of wireless communications systems. *IEEE Access* 8: 133995–134030. https://doi.org/10.1109/ACCESS.2020.3010896.

41 Chowdhury, M.Z., Shahjalal, M., Ahmed, S., and Jang, Y.M. (2020). 6G wireless communication systems: applications, requirements, technologies, challenges, and research directions. *IEEE Open Journal of the Communications Society* 1: 957–975. https://doi.org/10.1109/OJCOMS.2020.3010270.

42 Kumar, M.H., Sharma, S., Deka, K., and Bhatia, V. (2022). Intelligent reflecting surface assisted terahertz communications. *2022 IEEE International Conference on Signal Processing and Communications (SPCOM)*, 1–5. Bangalore: IEEE. https://doi.org/10.1109/SPCOM55316.2022.9840765.

43 Xue, Q., Ji, C., Ma, S. et al. (2024). A survey of beam management for mmWave and THz communications towards 6G. *IEEE Communication Surveys & Tutorials* 26 (3): 1520–1559. https://doi.org/10.1109/COMST.2024.3361991.

44 Xun, W., Liu, Y., Ni, Y. et al. (2022). A survey on terahertz communication theory assisted by intelligent reflecting surface and device-to-device technologies. *2022 IEEE 22nd International Conference on Communication Technology (ICCT)*, 678–682. Nanjing: IEEE. https://doi.org/10.1109/ICCT56141.2022.10073033.

45 Huang, C., Yang, Z., Alexandropoulos, G.C. et al. (2021). Multi-hop RIS-empowered terahertz communications: a DRL-based hybrid beamforming design. *IEEE Journal on Selected Areas in Communications* 39 (6): 1663–1677. https://doi.org/10.1109/JSAC.2021.3071836.

46 Zhang, L., Zhao, H., Hou, S. et al. (2019). A survey on 5G millimeter wave communications for UAV-assisted wireless networks. *IEEE Access* 7: 117460–117504. https://doi.org/10.1109/ACCESS.2019.2929241.

47 Yang, L., Meng, F., Zhang, J. et al. (2020). On the performance of RIS-assisted dual-hop UAV communication systems. *IEEE Transactions on Vehicular Technology* 69 (9): 10385–10390. https://doi.org/10.1109/TVT.2020.3004598.

48 Ren, H., Zhang, Z., Peng, Z. et al. (2023). Energy minimization in RIS-assisted UAV-enabled wireless power transfer systems. *IEEE Internet of Things Journal* 10 (7): 5794–5809. https://doi.org/10.1109/JIOT.2022.3150178.

49 Yu, Y., Liu, X., and Leung, V.C.M. (2022). Fair downlink communications for RIS-UAV enabled mobile vehicles. *IEEE Wireless Communications Letters* 11 (5): 1042–1046. https://doi.org/10.1109/LWC.2022.3154822.

50 Wu, Q. and Zhang, R. (2019). Intelligent reflecting surface enhanced wireless network via joint active and passive beamforming. *IEEE Transactions on Wireless Communications* 18 (11): 5394–5409. https://doi.org/10.1109/TWC.2019.2936025.

51 Basar, E., Di Renzo, M., De Rosny, J. et al. (2019). Wireless communications through reconfigurable intelligent surfaces. *IEEE Access* 7: 116753–116773. https://doi.org/10.1109/ACCESS.2019.2935192.

52 Zhang, Z. and Dai, L. (2021). A joint precoding framework for wideband reconfigurable intelligent surface-aided cell-free network. *IEEE Transactions on Signal Processing* 69: 4085–4101. https://doi.org/10.1109/TSP.2021.3088755.

53 Bilim, M. (2023). Performance analysis of RIS-assisted wireless networks in the presence of imperfect phase errors. *AEU - International Journal of Electronics and Communications* 171: 154923. https://doi.org/10.1016/j.aeue.2023.154923.

54 Huang, C., Zappone, A., Alexandropoulos, G.C. et al. (2019). Reconfigurable intelligent surfaces for energy efficiency in wireless communication. *IEEE Transactions on Wireless Communications* 18 (8): 4157–4170. https://doi.org/10.1109/TWC.2019.2922609.

55 Tang, W., Chen, M.Z., Chen, X. et al. (2021). Wireless communications with reconfigurable intelligent surface: path loss modeling and experimental measurement. *IEEE Transactions on Wireless Communications* 20 (1): 421–439. https://doi.org/10.1109/TWC.2020.3024887.

56 Huang, C., Mo, R., and Yuen, C. (2020). Reconfigurable intelligent surface assisted multiuser MISO systems exploiting deep reinforcement learning. *IEEE Journal on Selected Areas in Communications* 38 (8): 1839–1850. https://doi.org/10.1109/JSAC.2020.3000835.

57 Yang, L., Meng, F., Wu, Q. et al. (2020). Accurate closed-form approximations to channel distributions of RIS-aided wireless systems. *IEEE Wireless Communications Letters* 9 (11): 1985–1989. https://doi.org/10.1109/LWC.2020.3010512.

58 Ni, Y., Zhao, H., Liu, Y. et al. (2023). Analysis of RIS-aided communications over Nakagami-*m* fading channels. *IEEE Transactions on Vehicular Technology* 72 (7): 8709–8721. https://doi.org/10.1109/TVT.2023.3234643.

59 Chauhan, A., Ghosh, S., and Jaiswal, A. (2023). RIS partition-assisted non-orthogonal multiple access (NOMA) and quadrature-NOMA with imperfect SIC. *IEEE Transactions on Wireless Communications* 22 (7): 4371–4386. https://doi.org/10.1109/TWC.2022.3224645.

60 Cui, Z., Guan, K., Zhang, J., and Zhong, Z. (2021). SNR coverage probability analysis of RIS-aided communication systems. *IEEE Transactions on Vehicular Technology* 70 (4): 3914–3919. https://doi.org/10.1109/TVT.2021.3063408.

61 Zhakipov, Z., Rabie, K.M., Li, X., and Nauryzbayev, G. (2023). Accurate approximation to channel distributions of cascaded RIS-aided systems with

phase errors over Nakagami-*m* channels. *IEEE Wireless Communications Letters* 12 (5): 922–926. https://doi.org/10.1109/LWC.2023.3251647.

62 Li, S., Yan, S., Bariah, L. et al. (2023). IRS-assisted full duplex systems over Rician and Nakagami fading channels. *IEEE Open Journal of Vehicular Technology* 4: 217–229. https://doi.org/10.1109/OJVT.2022.3233857.

63 Selimis, D., Peppas, K.P., Alexandropoulos, G.C., and Lazarakis, F.I. (2021). On the performance analysis of RIS-empowered communications over Nakagami-*m* fading. *IEEE Communications Letters* 25 (7): 2191–2195. https://doi.org/10.1109/LCOMM.2021.3073981.

64 Chen, S., Yang, L., Zhu, Q. et al. (2023). On the performance of the UAV RIS-assisted dual-hop PLC-RF systems. *IEEE Transactions on Vehicular Technology* 72 (8): 11035–11040. https://doi.org/10.1109/TVT.2023.3261559.

65 Zhao, B., Zhang, C., Yi, W., and Liu, Y. (2022). Ergodic rate analysis of STAR-RIS aided NOMA systems. *IEEE Communications Letters* 26 (10): 2297–2301. https://doi.org/10.1109/LCOMM.2022.3194363.

66 Gu, X., Zhang, G., Zhuo, B. et al. (2023). On the performance of cooperative NOMA downlink: a RIS-aided D2D perspective. *IEEE Transactions on Cognitive Communications and Networking* 9 (6): 1610–1624. https://doi.org/10.1109/TCCN.2023.3306354.

67 Al-Nahhal, I., Dobre, O.A., Basar, E. et al. (2022). Reconfigurable intelligent surface optimization for uplink sparse code multiple access. *IEEE Communications Letters* 26 (1): 133–137. https://doi.org/10.1109/LCOMM.2021.3120560.

68 Dash, S.P., Mallik, R.K., and Pandey, N. (2022). Performance analysis of an index modulation-based receive diversity RIS-assisted wireless communication system. *IEEE Communications Letters* 26 (4): 768–772. https://doi.org/10.1109/LCOMM.2022.3147804.

69 Li, Q., Wen, M., Wang, S. et al. (2021). Space shift keying with reconfigurable intelligent surfaces: phase configuration designs and performance analysis. *IEEE Open Journal of the Communications Society* 2: 322–333. https://doi.org/10.1109/OJCOMS.2021.3057118.

70 Singh, U., Bhatnagar, M.R., and Bansal, A. (2022). RIS-assisted SSK modulation: reflection phase modulation and performance analysis. *IEEE Communications Letters* 26 (5): 1012–1016. https://doi.org/10.1109/LCOMM.2022.3157055.

71 Vu, T.-H. and Kim, S. (2023). Performance analysis of full-duplex two-way RIS-based systems with imperfect CSI and discrete phase-shift design. *IEEE Communications Letters* 27 (2): 512–516. https://doi.org/10.1109/LCOMM.2022.3231290.

72 Peng, Z., Chen, Z., Pan, C. et al. (2022). Robust transmission design for RIS-aided communications with both transceiver hardware impairments and imperfect CSI. *IEEE Wireless Communications Letters* 11 (3): 528–532. https://doi.org/10.1109/LWC.2021.3135413.

73 Li, Q., El-Hajjar, M., Sun, Y. et al. (2023). Achievable rate analysis of the STAR-RIS-aided NOMA uplink in the face of imperfect CSI and hardware impairments. *IEEE Transactions on Communications* 71 (10): 6100–6114. https://doi.org/10.1109/TCOMM.2023.3287995.

74 Gradshtein, I. and Ryzhik, I. (2007). *Table of Integrals, Series, and Products*, 7e. Academic Press.

75 Ansari, I.S., Al-Ahmadi, S., Yilmaz, F. et al. (2011). A new formula for the BER of binary modulations with dual-branch selection over generalized-K composite fading channels. *IEEE Transactions on Communications* 59 (10): 2654–2658. https://doi.org/10.1109/TCOMM.2011.063011.100303A.

76 Wolfram (2024). The Wolfram functions site. http://functions.wolfram.com (accessed 01 February 2024).

10

A Survey on RIS for 6G–IoT Wireless Positioning and Localization

Vivek Menon Unnikrishnan[1], Poongundran Selvaprabhu[1], Nivetha Baskar[1], Vinoth Kumar Chandra Babu[1], Rajeshkumar Venkatesan[1], Vinoth Babu Kumaravelu[1], Sunil Chinnadurai[2], and Agbotiname Lucky Imoize[3]

[1]*Department of Engineering (Enzo Ferrari), University of Modena and Reggio Emilia, Modena, Italy*
[2]*Department of Electronics and Communication Engineering, School of Engineering and Sciences, SRM University-AP, India*
[3]*Department of Electrical and Electronics Engineering, Faculty of Engineering, University of Lagos, Lagos, Nigeria*
[4]*Department of Electrical Engineering and Information Technology, Ruhr University, Bochum, Germany*

10.1 Introduction

As fifth-generation (5G) networks continue to roll out globally, efforts are underway in both industry and academia to go beyond this technology and to conceptualize the sixth-generation (6G) networks, reflecting the exponential growth in global mobile traffic, which is expected to surpass five zettabyte/month by 2030 [1, 2]. According to [3], this upsurge in traffic is anticipated to coincide with an increase in worldwide mobile subscriptions, reaching 17.1 billion by 2030. The impending Internet of Vehicles systems and industrial Internet of Things (IoT) will impose heightened demands on communication systems, necessitating reliability, throughput, and delay improvements. Expanding coverage stands as a pivotal and formidable challenge in IoT deployment, alongside critical concerns regarding privacy/security, energy efficiency, and achieving widespread connectivity on a large scale. Consequently, as the utilization of IoT continues to advance, the evolving demands and constraints of 5G underscore the imperative need for the development of 6G [4, 5].

The escalating need for location-based amenities like self-driving vehicles, medical monitoring, and precise positioning indoors and outdoors has sparked a burgeoning interest in pervasive positioning. To accomplish this objective,

Reconfigurable Intelligent Surfaces for 6G and Beyond Wireless Networks, First Edition.
Edited by Agbotiname Lucky Imoize, Vinoth Babu Kumaravelu, and Dinh-Thuan Do.

the development of top-tier localization techniques is imperative. Such techniques would not only enhance the quality and efficiency of communication across the various layers of the network but also cater to the diverse necessities of the new-age commercial and industrial sectors that are highly dependent on location-based services [6]. The forthcoming 6G wireless network aims to enable communication among individuals, mobile gadgets, machinery, and objects. Additionally, it will seamlessly incorporate communication, localization, sensing, control, and computing functionalities to facilitate the swift, highly dependable, and energy-efficient transmission of data and the precise localization of individuals and devices. Thus, improved accuracy, ultralow latency, improved reliability, energy efficiency, multidimensional positioning, and ubiquitous coverage are the trends that reflect the evolving requirements and expectations for location-based services in the era of 6G wireless communication and driving innovation and advancements in positioning technologies.

With the advancements in each generation of wireless communication systems, positioning accuracy is also said to improve. The upcoming 6G is envisioned to have a remarkable localization precision of 1 cm in three-dimensional scenarios [7]. Furthermore, the 6G is anticipated to extend to the terahertz (THz) band, where the 6G THz elevated frequency transmission is remarkably susceptible to environmental obstructions. Also, line-of-sight (LoS) signal transmission is prone to obstruction, and non-LoS (NLoS) propagation results in measurement errors. Despite numerous works attempting to address multipath and NLoS effects, they often operate under the supposition that the wireless domain is unrestrainable. However, with the increasing need for wireless networks, solely focusing on enhancement at the transmission and reception ends may prove insufficient for meeting future network demands. To address this, the notion of smart/intelligent radio environments has been proposed. Therefore, to promote the realization of the vision of the smart radio environment, the current focus is given to the key enabling technology termed reconfigurable intelligent surface (RIS) [8].

RIS refers to planar surfaces comprising a vast array of reflective elements designed to precisely direct signals from transmitters to designated receivers, effectively manipulating the wireless environment. RIS technology offers a compact, lightweight, and highly adaptable solution at a relatively low cost. Importantly, they can seamlessly blend into current network infrastructures without necessitating alterations to hardware or standards, requiring only adjustments to communication protocols. This versatility facilitates their deployment in diverse settings, whether fixed or mobile, including applications involving human subjects. Henceforth, the RIS will be positioned to contribute the advancement of the interconnected 6G network, spanning space, air, ground, and underwater domains, thereby advancing the IoT paradigm [9]. The work in [10] compares RIS with other related technologies, and it was identified that multiple-input

multiple-output (MIMO) is the closest technology to RIS, but there are significant differences between the two concerning their source, energy usage, hardware complexity, and cost. As RIS employs an extensive array of passive reflective components and can be deemed predominantly passive, energy usage is significantly minimized. Furthermore, RIS provides benefits such as cost reduction and exceptionally minimal power usage. Sections 10.2 and 10.3 will provide a comprehensive elucidation of RIS attributes pertinent to wireless positioning and localization. Even with the entirety of these benefits, rendering RIS an enticing technology for aiding in sensing, communication and simultaneous wireless information and power transfer (SWIPT) within the context of 6G, it remains imperative to explore the potential applications and technical hurdles associated with RIS-supported localization [11].

Regarding high-precision positioning, RIS possesses the capability to establish virtual LOS connections, effectively addressing NLOS challenges. Additionally, they exhibit the cognitive ability to control and manage the transmission of electromagnetic waves, enabling them to steer the signal accurately toward the intended user location. RIS operations can be handled by a swiftly responsive field-programmable gate array, ensuring compliance with the stringent latency demands of 6G positioning. Furthermore, in the localization arena, RISs efficacy can be attributed to its provision of novel channel degrees of freedom and its cost-effectiveness in hardware. Thus, it is evident that a comprehensive exploration of RIS application in 6G positioning is required.

Lately, there has been a surge in interest in wireless localization using RIS. RIS can function in two distinct modes: reflector mode or receiver mode. When functioning as a receiver, RIS is provided with sensing circuits or radio frequency (RF) chains, allowing it to receive emitted signals and extend the continuous surface beyond the traditional massive antenna array [12]. Conversely, in reflector mode, RIS serves as an additional anchor, facilitating localization through time and angle-based techniques [13]. Furthermore, reconfiguring the coefficients of RIS to obtain various received signal strength (RSS) maps presents another effective strategy.

10.1.1 Key Contributions of the Chapter

In this chapter, it becomes evident that a plethora of research and review articles are available within the realms of RIS, 6G, and the IoT. Nevertheless, there is a notable scarcity of surveys that methodically examine the utilization of RIS for wireless positioning and localization in the context of 6G–IoT. Hence, we were motivated to conduct a comprehensive study into the application of RIS for wireless positioning and localization in the realm of 6G–IoT. The following are the key contributions that have emerged from this chapter.

i) The function of RIS in wireless positioning and localization is delineated. The attributes of RIS that are appropriate for wireless positioning and its application in IoT networks are presented.
ii) The chapter elaborates extensively on the principles of localization, encompassing time of arrival (ToA)/time difference of arrival (TDoA), angle of arrival (AoA)/angle of departure (AoD), RSS, and hybrid measurements. Subsequently, it explores a range of algorithms for localization aided by RIS.
iii) The cutting-edge research on positioning and localization, comprising RIS-assisted millimeter-wave (mm-wave) positioning systems, RIS for near-field, indoor, outdoor, and far-field localization, and RIS for THz communication, is elaborated in detail.
iv) Finally, the prospective obstacles and forthcoming avenues of research linked with RIS-assisted 6G–IoT for wireless positioning and localization are outlined.

10.1.2 Chapter Organization

Section 10.2 explores the role of RIS-assisted IoT networks in wireless positioning and localization in which a comprehensive examination of the RIS characteristics suitable for wireless positioning and localization, an overview of related works on RIS-assisted IoT networks and an in-depth exploration of the system model for the RIS-supported radio localization are illustrated. Following this, Section 10.3 delves into the localization principles and the various RIS-assisted localization algorithms. Then, in Section 10.4, the cutting-edge research on positioning and localization with the assistance of RIS in 6G–IoT is illustrated in detail by explaining the cutting-edge technologies such as RIS-assisted mm-wave positioning systems, RIS for indoor localization, near-field localization, outdoor, far-field localization, and RIS integration in THz communication. Section 10.5 discusses the potential challenges, such as challenges in acquiring parameters related to the position, impediments due to unavoidable near-field positioning, challenges encountered by the nodes in motion of the RIS-aided 6G–IoT localization and wireless positioning, and so on. Finally, Section 10.6 outlines prospective research avenues for RIS-aided 6G–IoT in positioning and localization, concluding our discourse in this chapter.

10.2 Role of RIS-Assisted IoT Networks in Wireless Positioning and Localization

In this section, the characteristics that make RIS appropriate for wireless positioning and localization are discussed first. Subsequently, the crucial challenges that hinder the full potential of 6G–IoT are presented, and how RIS offers a promising

solution to this challenge is delineated. Furthermore, an in-depth exploration of the system model for RIS-supported radio localization is exemplified.

10.2.1 RIS Characteristics Suitable for Wireless Positioning and Localization

The RIS holds strong potential for engineering applications due to its ability to customize wireless environments. The following are some of the traits that make RIS appropriate for wireless positioning and localization.

i) **Reconfigurable and intelligent:** The RIS offers a notable advantage in its ability to customize wireless environments. Constructed with dynamic meta-atoms, this surface can undergo reconfiguration following manufacturing and deployment within the environment. RIS configuration enables each element to continuously adjust the incident signals' amplitude, frequency, phase, and polarization in real time through programming. Moreover, it possesses the capability to implement precise alterations to influence radio waves, efficiently managing the environment of propagation.
ii) **Quasi-passive:** RIS achieves passive manipulation of electromagnetic waves through the modulation of the physical attributes of artificial electromagnetic materials. However, it requires some energy consumption for its regulation process.
iii) **Focusing energy:** The RIS technology is characterized by its adaptability and ability to reconfigure its properties to meet various requirements and scenarios. This adaptability allows for real-time manipulation of electromagnetic waves, enabling the attainment of specific objectives. RIS can direct the electromagnetic waves accurately and precisely toward designated user targets. This precision is invaluable for applications necessitating targeted communication or energy delivery, as it optimizes resource utilization and mitigates interference with other users or signals [14].
iv) **Expanding coverage area:** Beyond the 6 GHz threshold, the transmission of mm-wave over long distances faces significant challenges due to severe signal attenuation and blocking, resulting in degraded positioning performance for users at the cell edges. RIS technology overcomes these hurdles by intelligently redirecting signals and establishing a flexible virtual LoS link in areas of limited coverage or blind spots in which direct LoS communication is impractical or inadequate. This coverage expansion, particularly beneficial for mm-wave communications impacted by indoor congestion, thus enhances the overall connectivity and performance [15].
v) **Reduced manufacturing cost:** In practical RIS implementation, its components typically consist of inexpensive materials, namely, reflective elements, small-scale antennas, and diodes.

vi) **Reduced power consumption:** The passive nature of RIS networks and their minimal reliance on active components result in reduced power consumption, rendering them well-suited for diverse applications requiring energy-efficient wireless communication solutions.
vii) **Economical and ease of deployment:** RIS can be effortlessly installed and removed from various locations, such as buildings, roofs, partitions, and exterior walls, resulting in minimal positioning and maintenance expenses. Furthermore, integrating RIS into existing communication networks typically necessitates a change in network protocol, thus eliminating the need for hardware adjustments. As a result, deploying and integrating RIS into wireless networks can be achieved at a lower overall cost. Likewise, RIS is easily scalable and deployable across various surfaces within wireless propagation environments through its two-dimensional planar structure.
viii) **Programmable software control:** RIS offers the flexibility of programmable physical attributes, enabling real-time and dynamic adjustments of electromagnetic responses.
ix) **Broadband response:** RIS demonstrates versatility by functioning across different frequency bands, including mm-wave, microwave, THz, and visible light bands.

10.2.2 RIS-Assisted IoT Networks

The IoT network links many appliances for communication and data exchange, facilitating applications, such as smart homes, healthcare, and industrial automation. Despite its rapid evolution, several challenges hinder realizing its full potential [16]. The following are the two crucial challenges associated.

i) **Limited range:** Many low-power IoT devices face constraints in operational range, necessitating efficient power management for densely deployed networks.
ii) **Spectrum scarcity:** The dearth of available radio spectrum constrains the efficacy of IoT networks.

Emerging technologies such as backscatter communication and SWIPT have been developed to tackle these challenges and manage energy limitations [17, 18]. In contrast, cognitive radio (CR) addresses spectrum scarcity. However, these solutions can partially satisfy the requirements of future 6G–IoT networks, which require improved energy harvesting, data integrity, throughput, energy, spectrum efficiency, and extended operational ranges. Also, as discussed earlier, evolving requirements for location-based services in the 6G wireless communication era emphasize improved accuracy, ultralow latency, improved reliability, energy efficiency, multidimensional positioning, and ubiquitous coverage, driving

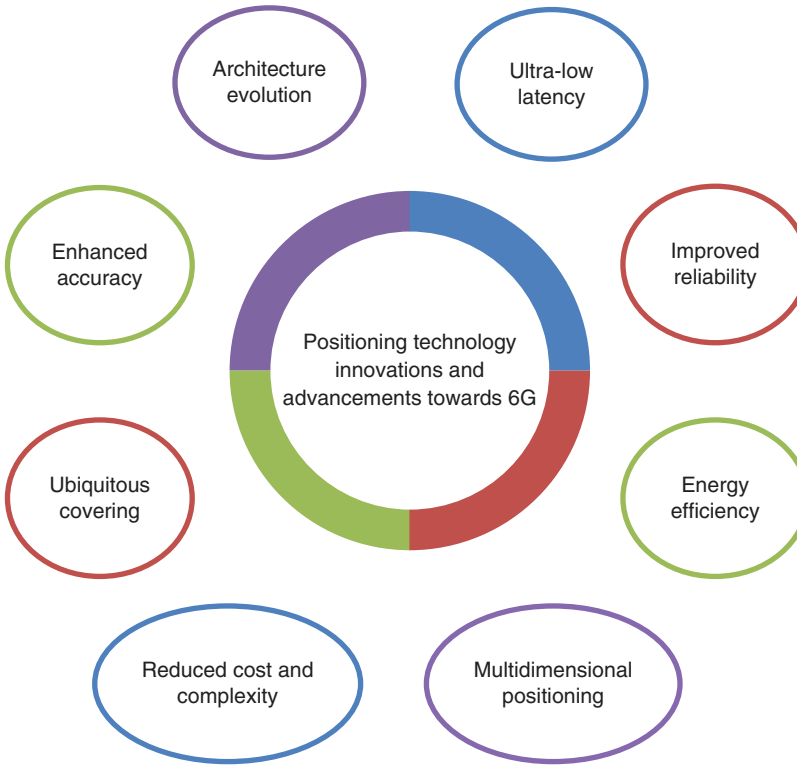

Figure 10.1 Positioning technology innovations and advancements toward 6G.

innovations in positioning technologies. Figure 10.1 showcases the most recent technological advancements and improvements in the realm of positioning technology, specifically with regard to the advancements being made toward 6G. Furthermore, RIS offers a promising solution to enhance system performance by combining signals to amplify the RSS. Thus, in the realm of 6G technology applications, RISs have recently garnered significant research attention. The RIS surfaces comprise arrays of passive scattering components arranged in artificial planar configurations, with individual components featuring an electronic circuit that enables software-defined reflection of impinging electromagnetic waves. The flexibility inherent in RISs makes them a promising solution for bolstering the design and optimization of wireless systems. Through assisting in signal propagation, channel modeling, and procurement, RISs pave the way for developing intelligent radio environments, which are advantageous for 6G-based applications.

Indeed, RIS presents numerous beneficial applications in the realm of 6G–IoT networks. As an illustration, it can simultaneously enhance signals from operating

base stations (BSs) in multicell IoT networks, reducing intercell interference among multiple IoT devices [19]. Resembling the paramount importance of RIS, one of its vital applications is augmenting the data offloading rates for IoT systems. Notably, the magnitude of the offloaded data to edge servers depends significantly on the channel gain of offloading links. RISs can be strategically positioned to establish virtual array gain and facilitate reflection-based beamforming gain, which can be leveraged for computation offloading links. This utilization of RISs facilitates efficient data offloading to edge servers, where processing occurs in a time-effective manner compared to conventional offloading methods. Furthermore, RIS-aided 6G–IoT applications are actively explored across different sectors, including smart buildings, vehicle-to-vehicle networks, and aiding RF sensing for human posture recognition systems [20]. Recently, researchers have explored integrating RISs into backscatter communication, SWIPT, and CRs to unlock the potential of 6G–IoT networks. This integration harnesses the advantages of RISs to overcome limitations and enhance the overall efficiency and performance of IoT systems.

RIS-assisted localization is vital for achieving high localization performance in intelligent interactive IoT networks. Within intelligent interaction contexts, RIS optimizes signal propagation for various communication types, such as interactions between individuals, individuals and machines, and machine-to-machine communication. Also, RIS is crucial in achieving precise location information and minimizing errors in tele-presentation and telecontrol technologies [21]. RIS significantly enhances the capture of real-time environment and the transmission of critical information by providing advanced signal optimization and calibration technologies, making it a game changer for telesurgery applications, where the quality and accuracy of information are critical for success. RIS also enhances reliability and data rates in wireless brain–computer interface applications, thus ensuring seamless patient tracking and monitoring across locations [22].

The application of RIS in IoT communication showcases their capabilities in IoT positioning. Additionally, the four-layer network architecture envisaged for 6G is highlighted, emphasizing its goal of delivering widespread connectivity across various environments, including space, air, ground, and underwater networks, to support emerging IoT sectors. Figure 10.2 shows the emerging applications of RIS in 6G. The space network tier encompasses satellites, which researchers have investigated for IoT services [23]. The air network tier incorporates flying BSs like high-altitude platforms and unmanned aerial vehicles (UAVs), which have seen increasing use in various IoT applications [24]. Meanwhile, the underwater network tier involves autonomous underwater vehicles (AUV) and submarines aimed at establishing underwater IoT connectivity [25]. Table 10.1 provides a concise overview of some related works of RIS-aided 6G–IoT using the four-layered network architecture.

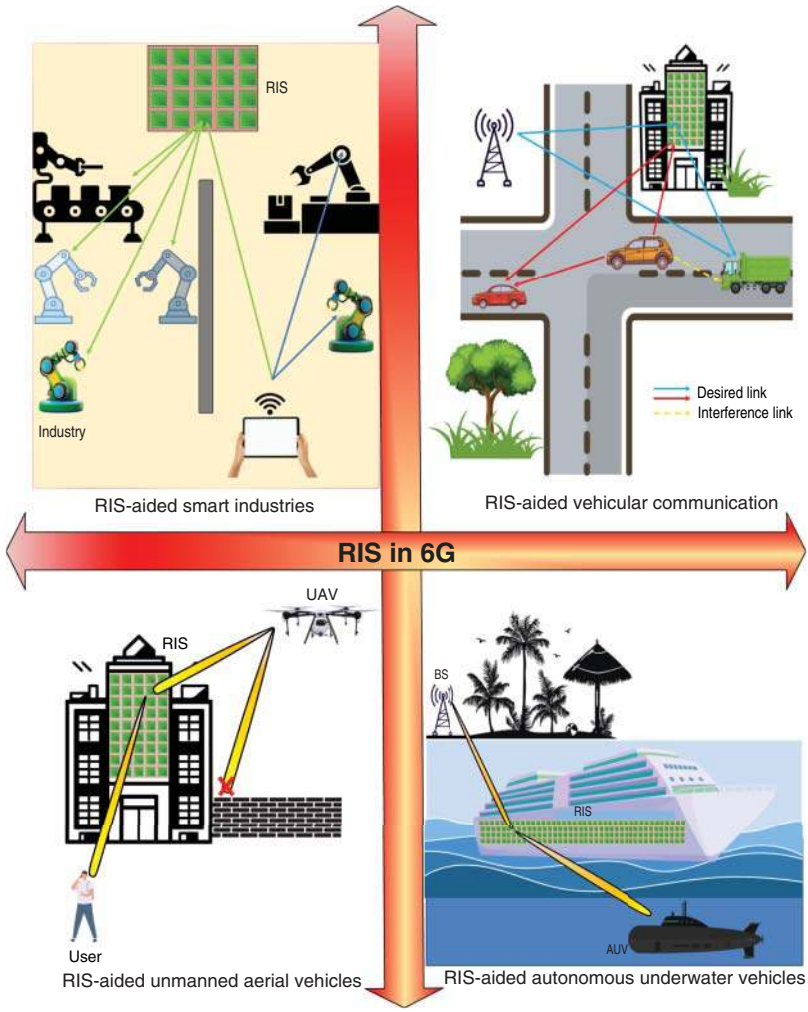

Figure 10.2 Emerging applications of RIS in 6G.

10.2.3 RIS for Wireless Positioning and Localization

To illustrate the coordinated operation of RIS and BS for user equipment (UE) positioning and localization, we can examine the RIS-supported radio localization setting depicted in Figure 10.3. The scenario involves a multiantenna BS with M_B antennas situated at (x_B, y_B, z_B). The RIS, which features M_R reflecting elements, is centered at (x_R, y_R, z_R), while the UE is located at (x_U, y_U, z_U), equipped with M_U antennas. Also, in the given settings, it is worth noting that two propagation

Table 10.1 Related works of RIS-aided 6G–IoT using the four-layered network architecture.

References	Network tier type	Research summary
Tekbıyık et al. [26].	Space network tier	The authors of this work presented a framework outlining the use of RIS technology to enhance the energy efficiency of IoT in low Earth orbit (LEO) satellites. They advocate that using RIS units integrated into satellites alleviates path losses associated with long distances in the transmission of signals. Furthermore, studies indicate that using RIS can significantly boost downlink rates by up to 10^5 times and enhance achievable uplink rates for IoT networks.
Ranjha and Kaddoum [27].	Air network tier	In this work, the authors utilize a UAV and an RIS to disseminate brief, ultrareliable, low-latency communication messages among terrestrial IoT devices. Furthermore, the authors demonstrate through simulations that by appropriately positioning the UAV in a strategic location and raising the number of antenna elements in the RIS, it is possible to achieve ultrahigh communication reliability, indicating significant performance improvements for RIS.
Mursia et al. [28]	Ground network tier	This work introduced an approach to enhance access to extensive IoT networks employing mm-wave technology by optimizing both the BS precoding technique and RIS parameters. Through simulation outcomes, this work demonstrated an improvement in the sum-rate performance gain.
Kisseleff et al. [29]	Underwater network tier	In this work, the authors delve into the potential applications, deployment tactics, and design attributes of RIS devices within IoT networks designed for demanding environments like underwater scenarios. Additionally, the RIS configurations for underwater settings are discussed in depth, considering the deployment location. The three RIS configurations for underwater environments include fixed RIS on the ground or shore, RIS mounted on AUV, and RIS placed below the water's surface.

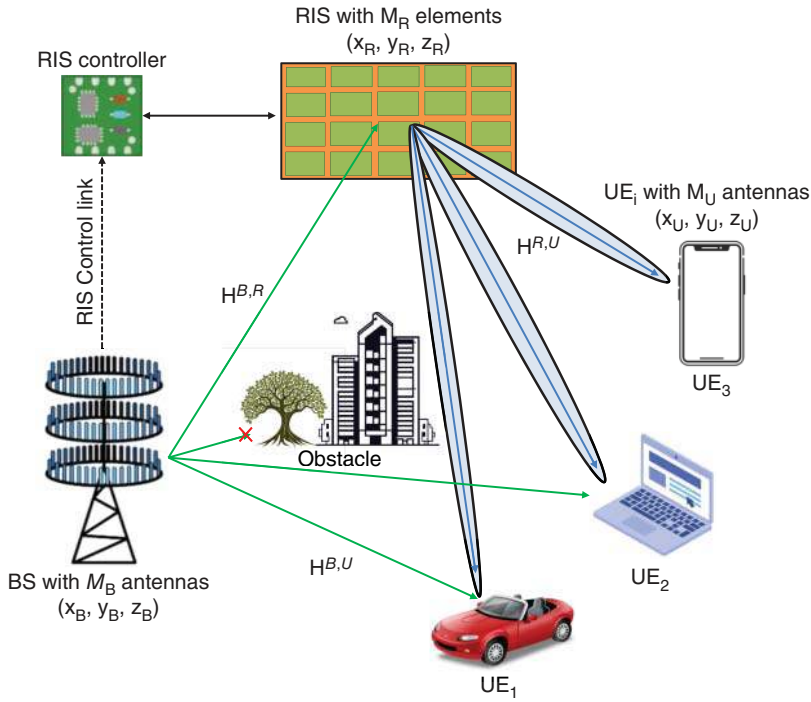

Figure 10.3 RIS-aided localization network.

paths are at play – one path is direct from the BS to the UE. The other path is reflected, passing through the RIS before reaching the UE. Furthermore, we take into account the standard channel model and represent the received signal and channel model in the frequency domain. Specifically, we consider N samples that are separated by an interval of Δf. For a given frequency $n \in 0, \ldots, (N-1)$ and symbol $k \in 0, \ldots, (K-1)$, the UE receives a signal that is represented in Eq. (10.1).

$$Rx_{n,k} = H_{n,k} Tx_{n,k} + n_{n,k} \tag{10.1}$$

Here, the signal received at the UE can be characterized by $Rx_{n,k}$, and the signal transmitted by the BS can be represented by $Tx_{n,k}$, and $n_{n,k}$ represents the additive Gaussian noise. Also, $H_{n,k} = H^D_{n,k} + H^R_{n,k}$ represents the complete channel response considering both the direct and reflected paths from the RIS. Likewise, the channel responses of the direct path, $H^D_{n,k} \in \mathbb{C}^{M_B \times M_D}$, are accompanied by the RIS incident and reflected channel response, denoted by $H^R_{n,k}$. This response is further broken down into $H^{B,R}_{n,k} \in \mathbb{C}^{M_B \times M_R}$, the channel response of the path between the BS and the RIS, and $H^{R,U}_{n,k} \in \mathbb{C}^{M_R \times M_U}$, the channel response from the RIS to the UE. These collective responses are denoted as $H^R_{n,k}$. Additionally, the channel

response linked with the direct and reflected path has been elaborated in [30]. To determine a UEs position, we use the information (orientation, position, and clock bias information) obtained from the received signal $Rx_{n,k}$. The methodology involves three stages: Initially, we estimate the channel parameters such as TOA, AOA, and AOD. Then, we extract the LOS and RIS path parameters. Ultimately, we localize the UE based on the information obtained from the preceding two stages. Moreover, in wireless communication systems, localization typically relies on the presence of multiple BSs to operate effectively. However, it is worth noting that using RIS technology can significantly reduce the infrastructure needs for localization while providing added benefits such as enhanced energy efficiency, streamlined deployment, and reduced maintenance expenses.

10.2.4 Hardware Design of RIS-Assisted 6G–IoT System

RISs stand out as thin layers of electromagnetic metamaterials engineered to manipulate radio waves, enabling tailored customization of the wireless environment to meet specific system needs [31]. While RIS structures typically consist of multiple layers, the composition of each layer may vary depending on the type, including reflective, refractive, and hybrid configurations. The outermost layer features a two-dimensional array of RIS elements designed to engage with incoming signals directly. Positioned beneath is a middle layer, typically constructed of a plate, for instance, a copper plate, serving to prevent the leakage of signal energy. Lastly, the innermost layer consists of a printed circuit that interfaces with the 6G RIS controller, facilitating meticulous regulation of the phase shifts linked with the RIS elements [32].

Thus, the hardware design of RIS-assisted 6G–IoT entails the development of proficient and robust RIS structures capable of augmenting wireless communication and positioning capabilities in the 6G epoch [33, 34]. These structures comprise arrays of passive reflective components, such as antennas or metamaterial elements, managed by programmable hardware elements. Central to the hardware design lies the configuration of the intelligent surface, encompassing the layout and setup of the passive components alongside the control mechanism. These passive components are strategically positioned to reflect and regulate incoming electromagnetic waves, thus shaping the propagation environment [35]. The hardware elements tasked with governing the intelligent surface wield significant influence over its functionality. Typically encompassing phase shifters, amplifiers, and controllers, these components facilitate precise adjustment of the phase and magnitude of the reflected signals. Moreover, alongside the passive components and control hardware, the design may integrate sensing and communication modules for acquiring environmental data and exchanging control

signals with other network entities. These modules empower the RIS to adapt to evolving conditions and optimize its operational efficiency in real time [36].

Moreover, advancing RIS hardware technologies hold the potential to enhance both spectrum efficiency and energy efficiency in 6G–IoT networks [37, 38]. Specifically, ensuring seamless connectivity in 6G–IoT networks presents a multi-faceted challenge, as the escalating number of devices strains available bandwidth

Table 10.2 Related works of RIS for outdoor and far-field localization.

References	Research summary
Wymeersch et al. [40]	In this work, the authors comprehensively examine radio localization and mapping facilitated by RIS technology. They contend that RISs offer significant advantages for localization and mapping endeavors, including enhanced precision and broader geographical reach under the condition that suitable models and algorithms are devised. Additionally, the authors suggest that as we transition into the era of post-5G communications, it is pertinent to explore localization techniques that extend beyond the capabilities of current and forthcoming generations of wireless technology.
Chen et al. [10]	Building upon RISs inherent capabilities to enhance the radio localization of IoT devices, this study provides a comprehensive overview of RIS applications in 6G–IoT wireless positioning. While the research extensively addresses various aspects of RIS utilization for 6G–IoT wireless positioning, it falls short of thoroughly examining the fundamental principles of localization.
Basharat et al. [16]	In this work, the authors conducted a thorough and methodical examination of the latest advancements in RISs, which are widely acknowledged as potent tools for enhancing 6G wireless networks. Additionally, the research briefly explores the synergies between RIS and other communication technologies, such as IoT. While the study provides comprehensive coverage of various aspects of RIS applications in 6G networks, it is essential to note that the fundamental concept of RIS localization within the context of 6G–IoT has yet to be addressed, indicating a potential area for further research.
Proposed work	This survey is not just a theoretical exploration but a practical guide to RIS applications for wireless positioning and localization in the context of 6G–IoT, encompassing almost all the topics in terms of localization principles, the range of algorithms for localization aided by RIS, cutting-edge research on positioning and localization, the prospective obstacles, and forthcoming avenues of research linked with RIS-assisted 6G–IoT for wireless positioning and localization.

resources, necessitating heightened spectrum efficiency [39]. Concurrently, optimizing energy usage is a critical imperative for mobile 6G–IoT devices, given the widening gap between signal processing circuit power consumption and device battery capacity. Furthermore, the dense proliferation of devices within 6G–IoT networks engenders substantial inter-device interference, posing potential limitations on network capacity. Nevertheless, the maturing hardware capabilities of RIS offer a promising solution to surmount these challenges, affirming its pivotal role in shaping the future landscape of 6G–IoT networks. Hence, the hardware of RIS enhances the spectrum efficiency of 6G–IoT networks, with each RIS element contributing an additional communication link, thereby facilitating spatial diversity gain. Likewise, the utilization of these channels does not necessitate additional energy-consuming hardware, leading to an enhancement in energy efficiency through increased data rates.

10.2.5 Related Works

Numerous survey articles are individually available in the domains of RIS, 6G, wireless positioning, and localization. However, there is a limitation in the survey articles specifically addressing RIS localization in 6G–IoT, given its emergent nature. Therefore, this study aims to bridge this gap by presenting a comparative analysis, illustrated in Table 10.2, between our proposed survey and other recent surveys in the realm of RIS-assisted 6G–IoT wireless positioning and localization.

10.3 Localization Principles and RIS-Aided Localization Algorithms

In this section, we delve into the foundational aspects of localization, comprising three key components: measurements, reference systems, and estimation algorithms. Initially, we discuss these components in detail. Following that, we comprehensively explain the commonly utilized measurements, such as ToA, TDoA, AoA, AoD, RSS, and hybrid measurements. Subsequently, we illustrate various localization algorithms assisted by RIS, including simultaneous localization and mapping (SLAM), geometry-based location estimation algorithms, fingerprinting, and Kalman filters.

10.3.1 Localization Principles

The localization principles pertain to the fundamental techniques and methodologies utilized in ascertaining the spatial position or location of objects, devices, or users in a specific environment [41]. The radio localization systems consist of three

crucial elements: measurements, reference systems, and estimation algorithms. The measurements, commonly involving ToA, TDoA, AoA, AoD, and RSS, are gathered from radio signals dispatched between the source and destination via the process of estimating the channel. The reference system encompasses a series of anchors, including scatterers, reflectors, gadgets, and other relevant entities, that possess predetermined positions and geometric interconnections to the objectives of interest. Ultimately, estimation algorithms contribute to building a mathematical association between the measurements obtained and the location of the targets and references involved. Based on the varied classes of measurements, there exist several rudimentary principles of localization that can be classified into categories such as ToA/TDoA, AoA/AoD, RSS, and hybrid measurements. Figure 10.4 illustrates the basic principles of localization and the localization algorithms that RIS assists.

10.3.1.1 Time of Arrival/Time Difference of Arrival

ToA and TDoA are methods that hinge on measurements of the time taken for signal propagation between the target and anchors. Essentially, these techniques are based on time and are used to determine the target's location. To be specific, ToA measures the time a signal travels from a transmitter (anchor) to a receiver (target) [42]. The distance can be calculated based on the speed of the signal. Consider a scenario where M anchors are available for aiding in positioning. Let the n^{th} anchor be located at coordinates (x_n, y_n). Thus, the following Eq. (10.2) can represent the distance between the target and the n^{th} anchor

$$d_n = c\tau_n, \qquad n = 1, 2, \ldots M. \tag{10.2}$$

Here, the value of τ_n represents the ToA for an event, while the speed of light is denoted by c. Furthermore, the ToA method for localization is known to have a significant drawback, i.e., the need for stringent synchronization. This is because the ambiguity regarding the beginning time can cause time offsets in ToA measurements, which limits its practical use. Hence, it is primarily employed in global navigation satellite systems (GNSSs), including global positioning systems (GPSs), where advanced synchronization control and clock calibration systems exist to ensure increased precision.

One potential approach to mitigate synchronization expenses is to leverage TDoA, which signifies the difference or disparity in ToA measurements [43]. Therefore, TDoA is a technique for determining a target's location. It works by analyzing the time disparities between the signals received from multiple anchors instead of calculating the absolute duration of the signal transmission. The constant differential distance between the designated entity and any pair of anchors enables the determination of the target's position on a hyperbolic curve, with the two anchors serving as focal points. This mathematical relationship

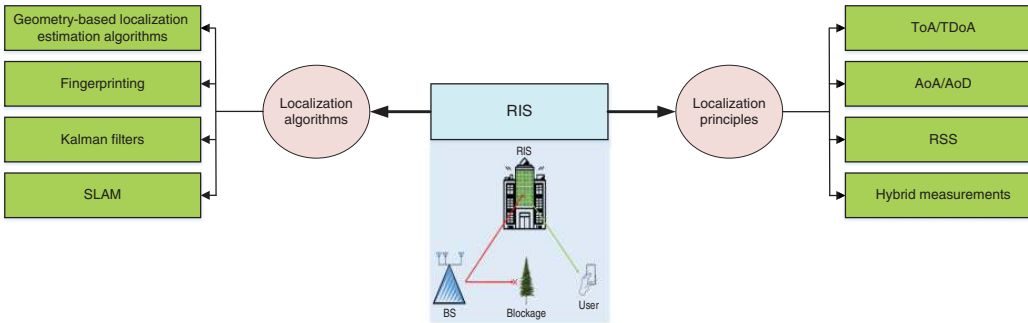

Figure 10.4 Fundamental localization principles and the RIS-aided localization algorithms.

makes TDoA a highly accurate and reliable method for pinpointing the location of a target.

$$\Delta d_n = d_n - d_0 \tag{10.3}$$

In Eq. (10.3), the benchmark anchor is denoted by the subscript 0. Consequently, the intersection of the hyperbolas is calculated to obtain the target position. Unlike other methods, the TDoA-based system does not require detecting signal transmission time. This leads to a noteworthy decrease in synchronization prerequisites between the target and anchors, as achieving synchronization among anchors is relatively more straightforward than that between the target and anchors. Nevertheless, the subtraction of ToA measurements in TDoA-based positioning introduces correlated noise, a crucial aspect that warrants consideration.

10.3.1.2 Angle of Arrival/Angle of Departure

Angular measurements offer localization data that complements temporal measurements, utilizing the directional information from nearby anchors rather than their distances. The AoA is a method used to determine the angle of a signal as it arrives at a receiver. This technique typically involves using an antenna array to triangulate the position of the signal. Analogously, the AoD is akin to AoA but instead concentrates on the angle at which a signal leaves a transmitter. Furthermore, in 5G networks, implementing massive antenna arrays has paved the way for introducing AoA- and AoD-based positioning strategies. These advanced techniques allow for more precise and accurate positioning of devices, enhancing the network's overall performance.

10.3.1.3 Received Signal Strength

Alternative approaches may be required when measurements based on time and angle are not readily available. One such approach is RSS-based localization, which involves converting radio signals into a position estimate [44]. This can be achieved by leveraging distance information obtained through methods such as ToA and TDoA or by contrasting calculated RSS values with RSS fingerprints to determine the probable location. To be precise, RSS computes the separation or spatial gap between the sender and receiver using the power of the received signal or signal strength. Also, it is noted that with an increase in the distance separating the devices, the signal tends to weaken. Furthermore, in cases where the environment is subject to change or the propagation framework is unknown, the RSS-based localization strategy can be used to generate a received power map. This map matches the RSS measurement to the stored RSS fingerprint, making it an effective method for localization. Moreover, fingerprinting has the drawback of reduced precision, requiring database restoration in case of environmental

changes. Nonetheless, implementing RSS fingerprinting localization in hardware is more straightforward and cost-effective than time or angle-based approaches, making it a significant consideration in indoor localization. In reality, positioning technologies based on RSS have broader network applications that can achieve positioning accuracy at the meter level.

10.3.1.4 Hybrid Measurements

As aforementioned, time-based techniques necessitate stringent synchronization, whereas angle-based methods require an antenna array. Nevertheless, both approaches offer superior accuracy and are more cost-effective than RSS approaches. In contrast, RSS techniques are simpler to obtain and do not need dedicated hardware. However, the data derived from RSS for measuring range is imprecise, and the signal strength measurements are vulnerable to the impact of channel states. Numerous algorithms that employ hybrid measurements are presented to enhance accuracy. These solutions have been shown to have superior noise resilience compared to using individual measurements. Thus, hybrid measurement merges numerous types of measurements to boost accuracy and reliability. That is, hybrid approaches harness the strengths of different methods to achieve a more precise outcome. In [45], the authors proposed a constrained total least squares methodology to tackle the challenge of localizing targets in three dimensions utilizing hybrid TDoA–AoA measurements. Later in [46], the authors proposed a high-speed algorithm that effectively mitigates errors associated with NLoS in TDOA–AOA hybrid localization. This algorithm is particularly well-suited for real-time applications where expeditious and accurate localization is critical.

10.3.2 RIS-Aided Localization Algorithms

Model-based and learning-based approaches are the two categories associated with RIS-aided localization algorithms. Model-driven approaches encompass inferential- or physics-guided approaches, including SLAM, geometry-based location estimation algorithms, fingerprinting, and Kalman filters. Meanwhile, the learning-driven approaches are data-centric, employing machine learning (ML) algorithms like neural networks to comprehend and delineate the correlation among signals aided by RIS and the position of the receiver. The benefits of model-driven strategies over data-driven methodologies are manifold. These approaches are underpinned by performance constraints that provide robust guarantees of efficiency and dependability. They depend on established signal processing strategies and generally entail lower intricacy compared to data-driven techniques. Below is a brief discussion of some frequently utilized model-driven strategies in RIS-assisted localization.

10.3.2.1 Geometry-Based Location Estimation Algorithms

Geometry-based techniques for UE localization depend on TOA and AOA calculations or an amalgamation of these two to calculate the UEs two-dimensional or three-dimensional location. Unlike conventional systems, where these methods necessitate calculations from numerous BSs to ascertain the UE location, geometry-based approaches facilitate UE location estimation with the assistance of an individual BS and an RIS [47]. The location estimation process implicates developing an objective function that integrates geometric data and addresses an optimization issue incorporating geometric limitations. Noteworthy features of geometry-centered localization methods include their independence from training requirements, theoretical analyzability, and scalability across diverse environmental settings.

10.3.2.2 Fingerprinting

The fingerprinting method involves building a database that maps the characteristics of the signal received at different positions in a given setting [48]. The database holds technical details unique to each location, such as signal amplitude patterns, RSS, or channel state information (CSI) [49]. Also, to localize a device, multiple points in the environment are measured for their RSS and signal characteristics with the help of RIS. These measures are then cross-referenced with a fingerprint database to ascertain the most similar match. Here, RISs are deeply involved in the manipulation of the wireless channel to improve the accuracy and consistency of measurements. The reflected signal is optimized by altering the reflection coefficients associated with RIS elements, which results in the measurements obtained becoming more accurate and consistent. Nevertheless, the environmental factors that fingerprinting depends on can effectively change with time in case of any changes in the RIS configuration, which can potentially cause degradation of the location estimations accuracy. Environmental stability in employing RIS in fingerprinting calls for a constant RIS configuration during fingerprinting and the location estimation is performed post-fingerprinting. This would have accounted for any phase shift or perturbation of the signal taking place in the RIS system, which was seen to remain the same with the changes in time. In addition, many methodologies could have been used to match the fingerprints, ranging from pattern matching to ML and deep learning (DL) algorithms, to weigh the most optimal correlation among the calculated signals and fingerprints found within a database [50]. It can estimate the location of the device with which this matched fingerprint was associated.

10.3.2.3 Kalman Filters

The Kalman filter is an iterative estimation algorithm specially crafted for the optimal fusion of dynamic frameworks with noisy measurements to estimate a

system state. Within the field of localization, the Kalman filter has RIS-assisted measurements using RSS or ToA, enhancing the precision of the device's position by leveraging the preceding state estimate and motion dynamics [51]. Utilizing the Kalman filter-centered strategy has the potential to substantially alleviate the negative influences resulting from multipath, noise, and other propagation phenomena on the accuracy of localization. This is accomplished by revising the state estimate iteratively while integrating RIS-aided dimensions. Regardless of its ubiquitous utilization in localization tasks, the Kalman filtering strategy possesses numerous drawbacks. The system's linearity and the Gaussian noise assumption may not be valid in complicated real-life environments. In addition, the initial or starting state that the filter mandates may not be precisely known, and any mistakes therein can spread, leading to imprecision in estimating the state. Likewise, the assumption of constant process and measurement noise covariances, a prerequisite for Kalman filters, is often unmet in real-world situations. Moreover, model discrepancies and outliers can considerably impact their performance. The extended Kalman filter [52] could be a favorable remedy to tackle the nonlinear challenges encountered by the Kalman filter.

10.3.2.4 Simultaneous Localization and Mapping

SLAM is a well-known technique for position estimation of a device while concurrently generating a comprehensive map of its environments. This method involves the careful placement of the RISs in the environment so as to enable the change of the wireless channel, thus resulting in the improvement of the quality of reception of the signal. The device estimates metrics like RSS or ToA at different RIS-aided locations throughout the SLAM process [53]. Such measurements, in conjunction with the locations of the RISs that are known, help position the UE and create a complete map of the surrounding terrain. The pivotal role played by RISs in heightening the precision and dependability of localization and mapping endeavurs is underscored by their ability to optimize the quality of received signals. That is, such an approach has the edge in precise localization, even in intricate environments wherein multipath propagation and NLoS situations could prevail. Further, using RISs within the environment can dynamically change the reflection coefficients to the environment to enhance the strength and resilience of the SLAM-empowered localization framework.

10.4 State-of-the-Art Research on Positioning and Localization with the Assistance of RIS in 6G–IoT

This section extensively explores the forefront research advancements in positioning and localization leveraging RIS technology within the domain of 6G–IoT.

Specifically, it delves into research endeavors encompassing various facets of positioning and localization, including RIS-supported mm-wave positioning systems, RIS applications in near-field, indoor, outdoor, and far-field localization, and RIS integration for THz communication.

10.4.1 Potential of RIS-Assisted Positioning

RIS can efficiently reconstruct radio signals and alter their inherent characteristics, including direction and polarization, by interacting with the surrounding environment. This transformation of the wireless channel into an intelligent transmission framework enables RIS to manage signal propagation intelligently. Furthermore, there is a possibility of focusing energy within three-dimensional space for transmitting and receiving purposes, using novel communication, sensing, and electromagnetic environment control capabilities. The authors in [40] developed suitable models and algorithms where RISs are utilized to enhance the precision of positioning and extend physical coverage, thus promoting positioning tasks.

The potentiality and inception of RIS localization can be outlined in three points. Initially, the RISs significantly larger surface area offers a notable advantage compared to traditional MIMO positioning approaches. RIS leverages the complete continuous surface for both transmitting and receiving radio signals. Additionally, with the growth in the surface area of the RIS, the Cramer-Rao lower bound (CRLB) for terminal device positioning decreases. Second, measuring both phase and amplitude ensures that RIS localization remains cost-effective.

Third, an efficient online scheme for optimizing the phase configuration of wireless RIS using DL techniques has been introduced [54]. This scheme aims to focus transmission energy accurately on the intended user position, maximizing signal strength. Leveraging the elevated focusing capacity of enormous RIS sizes enables accurate estimation of mobile terminal positions, facilitating improved precision ranging and radio localization. Figure 10.5 depicts the cutting-edge technologies that are employed in RIS-aided 6G–IoT networks. A detailed explanation of these technologies will be provided in Sections 10.4.2–10.4.6.

10.4.2 RIS-Assisted mm-Wave Positioning System

Research on positioning using signals in the mm-wave band and MIMO systems is extensive due to the wide bandwidth and high-temporal resolution offered by the mm-wave spectrum and the increased spatial resolution provided by enormous arrays of antenna featuring exceedingly narrow beams in the angular domain [55–57]. Studies [58] indicate that it is possible to attain accurate positioning using a single BS. RIS is integrated into the mm-wave MIMO localization setup as reflective elements, presuming a direct LOS path is present between the BS and

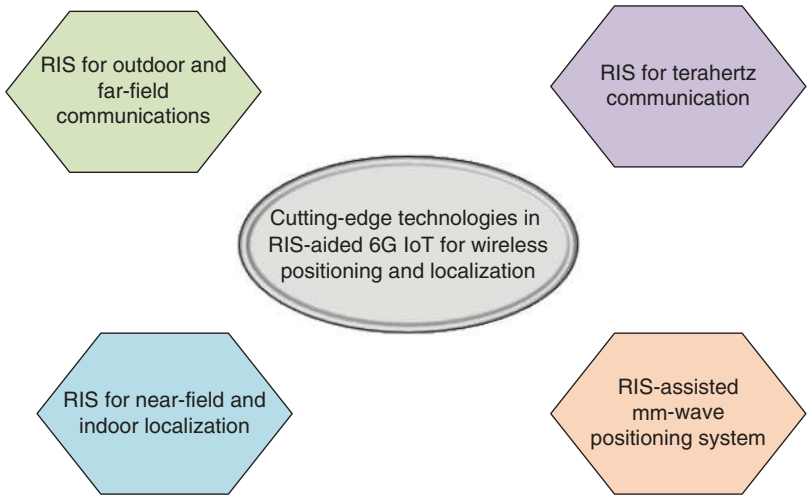

Figure 10.5 State-of-the-art technologies in RIS-aided 6G–IoT networks.

the mobile station. Through derivation of the Fisher information matrix (FIM), the system establishes the CRLB for the standard deviation of positioning and orientation estimation errors. This analysis demonstrates the superiority of the RIS-aided mm-wave MIMO positioning framework over traditional methods. However, research into positioning under conditions of obscured LOS is still limited. As a continuation of the aforementioned localization setup, the authors have further investigated adaptive beamforming techniques for RIS-assisted mm-wave MIMO localization. This work's critical distinction lies in treating the direct path attenuation among the BS as well as the mobile station as an obstruction. Utilizing a hierarchical codebook (HCB) and feedback from the receiver, the author proposes an adaptive phase-shifter design. This design aims to maximize the phase value of individual RIS units, thereby enhancing positioning accuracy and data rate performance. This study is of great importance in exploring practical approaches for coordinated positioning and communication strategies.

The authors of [59] investigated a multiuser location algorithm utilizing an HCB. Simulation outcomes achieved across different signal-to-noise ratio (SNR) scenarios showcase the efficacy of the proposed approach in facilitating multiuser localization within the mm-wave MIMO radar framework, given the utilization of an appropriate HCB design. However, it is crucial to emphasize that realizing this potential hinges upon implementing an appropriate HCB design. Later in [60], the authors address the challenge of signal obstruction prevalent in mm-wave MIMO communication environment by introducing a technique enabling concurrent beam training and positioning. This approach entails estimating the AoD channel

parameter through beam training, which is then leveraged by the mobile terminal to ascertain its location. Subsequently, the obtained information on the position assists in fine-tuning the parameters for beam training. Simulation outcomes demonstrate that this proposed method achieves centimetre-level positioning accuracy for multiple users.

10.4.3 RIS for Indoor Localization

RIS can help determine the position of objects or devices within indoor environments. RIS surfaces are embedded with a large number of small elements capable of modifying electromagnetic wave propagation characteristics. It can control the reflection, refraction, and diffraction of electromagnetic waves to optimize signal propagation. By adjusting the properties of electromagnetic waves, RIS can amplify signals and reduce signal degradation, leading to improved accuracy in localization.

RIS can be placed strategically indoors to optimize signal coverage and enhance localization performance. Technologies like Wi-Fi or Bluetooth-based positioning systems are commonly used for indoor localization. RIS can reduce the effects of multipath propagation, where signals take multiple paths to reach a receiver, causing signal distortion and errors in localization. Through focusing signals and reducing interference, RIS can improve the ratio of useful signals to background noise, resulting in more accurate localization. Moreover, RIS can enable more precise localization by directing signals toward specific areas or devices within the indoor space.

In indoor environments, GPS signals can be unreliable due to obstructions and obstacles that degrade signal quality. However, RIS offers a promising solution. By strategically deploying RIS elements, mitigating the effects of signal attenuation and multipath propagation caused by obstacles is possible. Consequently, RIS can enhance communication reliability and assist in achieving high-precision positioning for users within indoor spaces where GPS signals alone can be insufficient. The authors of [61] utilize ultra-wideband (UWB) positioning along with RIS technology. Manipulating the reflection phases of each RIS unit, multipath signals can be labeled and processed more efficiently within the range of 0 to 2π. This innovative indoor localization approach integrates the capability of RIS to characterize multipath channels with the increased multipath resolution of UWB technology. The presented scheme's CRLB suggests that RIS can achieve precise positioning even with only one access point. Additionally, as the scheme necessitates just an individual access point and inexpensive RIS components, it presents a highly precise and cost-efficient option for indoor localization.

The authors in [62] introduced a framework for indoor positioning which utilizes RIS. They also proposed a new formula to determine the optimal RIS

configuration for enhanced precision in indoor positioning. The present formula is designed to minimize the probability of incorrect positioning. Moreover, an iterative approach is adopted to optimize the system's configuration and ensure an effective resolution of the problem. Numerical results demonstrate that the presented approach greatly reduces positioning errors in contrast to methods lacking RIS assistance. Furthermore, it highlights the effectiveness of RIS technology in indoor positioning.

In [63], a DL approach is introduced for the real-time optimization of RIS configurations in indoor communication networks. The approach uses a fingerprint database of coordinates to train a deep neural network (DNN) capable of mapping user location data to the optimal phase settings for the RIS. This optimization aims to maximize RSS at the desired location. The results of simulations performed in three-dimensional indoor circumstances have indicated that the method proposed, which relies on DNNs, consistently improves the achievable throughput in different scenarios at the specific user location aimed for.

In [64], the author introduces and assesses an ML approach designed for wireless fingerprinting localization within environments enhanced by RIS. This method integrates standard components like k-nearest neighbors (k-NN) localization and genetic algorithms, capitalizing on RIS abilities to establish an adaptable and intelligent radio landscape. The findings demonstrate the efficacy of this approach in achieving precise localization accuracy without requiring numerous access nodes or extensive fingerprint grid samples. The study underscores the potential of RIS and advanced radio environments in achieving sub-meter localization precision. Furthermore, it suggests that future investigations examine highly complex systems, including mixed LoS and NLoS circumstances, elevated frequencies, numerous RIS components, and considerable RIS implementations.

10.4.4 RIS for Near-Field Localization

RIS-assisted near-field localization for 6G–IoT involves leveraging RIS to enhance localization accuracy and reliability in close proximity scenarios. Near-field localization refers to determining the position of devices or objects within the Fraunhofer distances, which are typically within a few meters. A dual-phased localization approach is presented for pinpointing the transmitter's position using an RIS functioning as a lens operating within the mm-wave frequency range. This method demonstrates the capability to achieve localization accuracy at the decimeter level within the near-field region [65]. The authors [66] presented a model for regional localization aided by RIS, encompassing phase optimization and location inference. Findings indicate that the model exhibits exceptional efficacy, delivering near-peak performance in localization tasks. In [67], a comprehensive framework is formulated, which covers both near-field and far-field

configurations. It introduces an SNR-driven phase optimization algorithm for reflecting RIS, aiming to mitigate CRLB. Compared to traditional systems lacking RIS, this method notably diminishes both position error bound (PEB) and directional error bounds. Achieving accurate localization in real-world settings is a complex task necessitating consideration of various factors. Situations involving LoS obstructions are particularly crucial and demand attention in near-field localization studies assisted by RIS. Overlooking these scenarios could impede the efficacy of RIS-supported localization techniques. Therefore, addressing LoS obstruction scenarios is imperative for optimal performance in real-world environments.

In the work [68], authors explored localization and CSI estimation within a sub-THz system employing an RIS in the near-field. They proposed a collective channel estimation and localization scheme tailored explicitly for near-field scenarios, demonstrating exceptional performance compared to conventional methods typically applied in far-field conditions, particularly regarding localization accuracy and CSI estimation root mean square error. The research underscores the significance of acknowledging near-field phenomena and angle separations among UE to achieve precise localization utilizing a single RIS panel. Moreover, when employing a more extensive RIS panel with a greater number of elements, it becomes imperative to consider the spherical wavefront characteristics to prevent any deterioration in performance.

An algorithm for localization relying on TOA was proposed in [69]. The outcomes obtained from this algorithm demonstrate that high localization accuracy can be maintained even in situations with significant blockages in the near-field region of RIS. Furthermore, the algorithm operates in two steps, and its efficacy has been demonstrated through rigorous testing. The findings support the TOA-based algorithm's feasibility for accurate localization in complex environments. In [70], the authors present a simplified near-field localization technique named approximation mismatched maximum likelihood, leveraging the Jacobi–Anger expansion and integrating RIS amplitude. They also suggest an iterative enhancement strategy to update both positioning and RIS amplitude framework parameters, utilizing the outcome as the starting estimate. Simulations indicate the effectiveness of this method, with the iterative algorithm approaching the CRLB for localization accuracy asymptotically.

In [71], the authors analyzed RIS-enabled asynchronous localization of UE through PEB and equivalent fisher information (EFI). Results show the feasibility of UE localization employing near-field spherical wavefront modeling, albeit with diminishing EFI over distance. The study underscores disparities in performance among spatial and power gain within the BS–RIS channel. Additionally, caution was advised against employing the SNR-maximizing focusing control strategy for RIS in positioning functionalities. In the work [72], the authors investigated

the potential of a holographic RIS (HRIS) in achieving more precise mm-wave near-field localization. By considering antenna radiation patterns, they derived both the FIM and CRLB. Theoretical results indicate that the position determination accuracy could be enhanced with larger HRIS. To further improve results, they proposed an iterative entropy regularization approach to optimize HRIS phases and diminish the worst-case CRLB.

10.4.5 RIS for Outdoor and Far-Field Localization

RISs show great potential in outdoor and far-field localizations within 6G–IoT network scenarios. Conventional localization in outdoor environments and far-field scenarios usually entails difficulties such as signal attenuation, multipath propagation, and physical barriers. RISs present innovative solutions to these problems by actively controlling the wireless channel to boost the accuracy as well as dependability of localization. One of the most essential benefits of RIS-aided localization in the outdoor environment is the ability to counteract signal attenuation across extensive distances. Through strategic placement along the communication path, RISs can compensate for signal loss and uphold signal strength, thereby extending the coverage of wireless networks in outdoor settings. This is especially useful for cases where devices are dispersed across expansive areas, such as asset tracking, environmental monitoring, and precision agriculture. Moreover, RISs can potentially alleviate the influences of multipath propagation in far-field scenarios. At the far-field, RISs can mitigate the influences of multipath interference and raise the received signals spatial resolution by controlling the reflected signals phase and amplitude. Thus, accurate localization of IoT devices is facilitated, even in environments characterized by intricate propagation patterns.

Furthermore, RIS-assisted localization in outdoor and far-field scenarios opens avenues for collaborative localization schemes. Through integration with established localization technologies like GNSS or cellular networks, RISs can increase localization accuracy and resilience through hybrid positioning methods. This may include helping to localize GNSS receivers with extra positioning data or mitigating multipath effects, especially in complex urban or obstructed environments. In summary, localization with RIS assistance is among the essential enabling techniques for far-field and outdoor applications within the 6G–IoT networking domain. Table 10.3 presents an outline of various research works in the domain of RIS for outdoor and far-field localization.

10.4.6 RIS for THz Communication

Assistance from RIS is necessary for accurate localization and positioning, which are crucial in making the most of THz communication for 6G–IoT networks. RIS

Table 10.3 Related works of RIS for outdoor and far-field localization.

References	Research summary
Zhang et al. [73]	In this work, the authors present a novel approach employing RIS to improve outdoor localization based on RSS fingerprinting using a single BS. The proposed approach leverages RISs controllable phase shifts to generate distinguishable RSS values at identical locations. Furthermore, to optimize the localization accuracy, the proposed approach employs a localization error minimization algorithm that utilizes the generated RSS fingerprints.
Yildirim et al. [74]	The authors of this work have highlighted the prospective advantages of using RIS to model and examine indoor and outdoor utilizations in upcoming wireless networks that operate on various frequencies. Furthermore, this work has yielded significant insights regarding error performance and attainable data rates, even when the system is not ideal, such as when there are range limitations in phase adjustment or when the channel phase estimation at the RISs is inaccurate.
Emenonye et al. [75]	The authors of this work devised a Bayesian framework to tackle localization challenges in RIS-assisted systems, examining uncertainties in both near- and far-field settings. In addition, this study yielded the Bayesian equivalent FIM (EFIM), which sheds light on the limitations in correcting RIS orientation deviation in far-field situations when the phase offset is unknown, while this phase offset did not influence near-field cases. Moreover, EFIM analysis was established to show the importance of having prior knowledge about RIS location for effective localization across various RIS sizes and propagation conditions. Numerical analysis further demonstrated the information degradation occurring when employing the far-field model to interpret signals received in near-field propagation scenarios.
He et al. [76]	The authors introduced the notion of a partially linked receiving RIS (R-RIS) engineered to detect and pinpoint users generating electromagnetic waveforms in this work. The hardware design of the proposed R-RIS comprises subarrays of meta-atoms that utilize waveguides to route waveforms toward reception RF chains for the estimation of both channel and signal parameters. With a particular emphasis on far-field scenarios, the work proposes a three-dimensional localization approach that relies on narrowband signaling and AoA estimates, leveraging meta-atoms phase configuration.

significantly enhances the dependability and performance of localization and positioning systems in THz-based communication environments by improving signal propagation, enabling precise beamforming, mitigating multipath effects, and facilitating adaptive localization algorithms. In [77], the authors present a comprehensive study on integrating intelligent reflecting surfaces with THz communication. Furthermore, this work delves into the core technologies, promising applications, and potential hurdles posed by the combination of intelligent reflecting surfaces and THz communication in the context of 6G communication systems. In a subsequent work [78], the authors investigated the capabilities of the 6G THz network regarding localization, focusing on contrasting it with 5G mm-wave localization systems. Additionally, this work offers guidance regarding developing effective and feasible localization algorithms tailored for MIMO systems comprising RIS-assisted arrays of subarrays, shedding light on potential avenues for further investigation.

10.5 Potential Challenges of RIS-Aided 6G–IoT for Wireless Positioning and Localization

RIS has been gaining traction in the field of IoT due to its ability to improve positioning accuracy and localization. However, implementing RIS-based localization in the context of 6G–IoT presents several challenges. As with any emerging technology, certain technical hurdles need to be overcome. Below are some of the critical challenges associated with RIS-based localization in 6G–IoT. Figure 10.6 schematically depicts the impediments of RIS-based localization in 6G–IoT.

10.5.1 Challenges in Acquiring Parameters Related to the Position

The traditional methods used for estimating the channel can provide solely the numerical values of parameters associated with position, including ToA and AoA. However, the indices are ambiguous or lack clarity, and we cannot determine if a particular ToA/AoA is associated with the BS or a specific RIS. As mobile communications in the future are likely to leverage mm-wave, THz, and even advanced frequency bands, the channel response is expected to exhibit sparsity in the angle domain and will predominantly rely on the geometric association among devices and their surroundings. Consequently, acquiring position-related metrics can be resolved more effectively by utilizing compressive sensing approaches [79], as they are closely linked to each other.

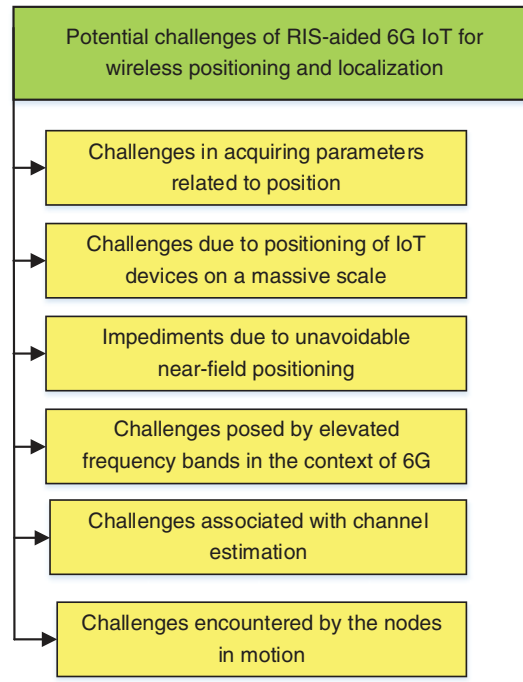

Figure 10.6 Challenges of RIS-based localization in 6G–IoT.

10.5.2 Positioning of IoT Devices on a Massive Scale

Multitarget positioning, while useful, has limitations and can only be effective for a small number of targets. As more and more IoT devices are being used, it is anticipated that the upcoming 6G–IoT devices will facilitate a larger number of positioning requirements compared to the current 5G devices. This implies that positioning-dependent devices in a wide range of indoor and outdoor IoT applications, including smart homes and smart cities, will evolve more robustly. Furthermore, to enhance the usability of RIS for the IoT, it is essential to conduct further research on its capability to support multiuser localization. Likewise, the design of network architectures must be restructured to facilitate the integration of ultramassive machine-type communications. Also, for the purpose of positioning a massive scale of users in the upcoming 6G systems, it is imperative to establish rational protocols for localization and RIS beamforming.

10.5.3 Impediments Due to Unavoidable Near-Field Positioning

With the proliferation of carrier frequencies in 6G, near-field localization is unavoidable in upcoming 6G networks. In the near-field scenario, the phase

of the spherical wave exhibits nonlinearity concerning incident angles and distances of individual paths. The proximity between BS–RIS and RIS–UE in RIS-assisted IoT systems results in elliptical equiphase surfaces. This elliptical characteristic, differing from the assumptions made for far-field scenarios, causes significant performance degradation when conventional technology is directly applied to the near-field. Integrating RIS into the IoT localization framework necessitates reassessing the channel model, considering elliptical phase surfaces. This integration also demands the precise focusing of beams for users at varying angles and distances [80]. Furthermore, as the size of the RIS and the frequency of the carrier increase, it is more probable for transceivers to be positioned in the near-field. Therefore, this poses a challenge in the context of indoor localization and IoT positioning applications.

10.5.4 Challenges Posed by Elevated Frequency Bands in the Context of 6G

As we move toward the next generation of wireless communication, 6G, there will be a shift toward transmitting higher frequency signals. However, these high-frequency signals are more susceptible to obstructions in the propagation environment, which requires a greater focus on NLOS positioning. Most current indoor positioning studies assume LOS conditions, which are unsuitable for 6G–IoT indoor applications. To address this, we need to design a system model that accounts for real-world NLOS positioning scenarios. Additionally, the rise in frequency also impacts the dimensions of the RIS element. As we move toward more elevated frequency bands, significant manufacturing and integration challenges are posed that require us to develop innovative solutions to adapt to these changes. It is worth discussing whether novel hardware configurations and operational principles are necessary to overcome this challenge.

10.5.5 Challenges Associated with Channel Estimation

RIS has arisen as a prospective technology for enhancing wireless positioning and localization. However, the effectiveness of RIS depends heavily on the accuracy of the CSI available for RIS optimization [81]. The CSI can be obtained by converting position-related information into partial or statistical CSI [82]. Thus, to fully utilize the benefits of RIS, it is essential to have perfect knowledge of CSI. However, achieving this is not easy due to the limitations of signal reception and processing in reflecting state or limitations on the quantity of RF chains when RIS acts as a transceiver. Therefore, the most formidable impediment in the practical implementation of RIS still pertains to channel estimation. Consequently, in 6G–IoT RIS-assisted positioning, channel estimation techniques usually involve high

training overheads or complex computations, which become even more challenging when dealing with large RIS setups. Therefore, developing low-complexity but near-optimal channel estimation methods is essential to address these challenges.

10.5.6 Challenges Encountered by the Nodes in Motion

Further attention is required in the area of RIS localization, particularly in relation to the mobile or moving nodes [83]. Consideration should be given to factors such as the dynamic modeling of channels, Doppler effects due to the velocity of the node, and the influence of channel instabilities on localization accuracy, and trajectories should be planned accordingly. These impediments warrant discussion and in-depth analysis to ensure optimal performance is achieved. Also, the process of optimization of signal reflection and transmission in an RIS primarily entails the manipulation of the electromagnetic characteristics of its constituent elements. The optimization process for RIS can be a bottleneck, especially for high-mobility applications. This can prompt obsolete or inadequate arrangements that degrade or nullify the performance of the system. Thus, this delay in controlling the RIS is a significant limitation that hinders the complete utilization of RIS technology in high-mobility applications, including but not limited to drones, driverless vehicles and supersonic trains.

In addition to these challenges, RIS-based localization in 6G–IoT faces several other significant issues. One prominent issue in RIS optimization is the need for practical algorithms that can meet low target position criteria. Additionally, there is a lack of standardization across RIS systems, further complicating the optimization process [84]. Another issue is the absence of RIS control mechanisms based on location that can guarantee reliability and accuracy while maintaining low latency. Furthermore, the successful implementation of RIS technology in 6G–IoT localization applications faces significant challenges due to the constraints in RIS hardware and the susceptibility of individual RIS elements, known as pixels, to malfunction [85]. Notably, the challenges involved in this regard are intricate design requirements, slower processing speeds, and elevated energy consumption, all of which must be tackled to guarantee dependable and effective performance. Likewise, the process of achieving accurate and efficient calibration of RIS technology is a notable challenge that must be tackled for its broader implementation.

10.6 Future Research Directions

The development of 6G–IoT wireless positioning and localization with the aid of RIS has garnered much attention from researchers lately. As such, numerous

avenues of exploration have been identified for future research. Below are some of the directions being pursued.

10.6.1 RIS-Aided Joint Sensing and Communication

In recent years, there has been an emergence in the importance of positioning aided by RIS technology, making it increasingly significant for RIS to perform joint sensing and communication in the context of the IoT [86]. In the long run, positioning and communication services integration necessitates the availability of sensing capabilities, including localization and imaging, which can be leveraged to improve communication performance. At the same time, it requires a more profound integration of architectures and waveforms to achieve seamless coordination between the two domains [87]. Furthermore, the RIS is distinguished by its exceptional capability to manipulate reflected electromagnetic waves artificially. This unique capability of RIS holds remarkable potential for merging positioning and communication. The concept of merging location and communication by name refers to the use of identical hardware architectures and algorithms for both processes. This strategy aids in reducing the expenses associated with deploying the location network. Nevertheless, the combined design of RIS to aid communication and positioning has yet to receive much attention in research. In the context of positioning, the process of transmitting signaling and packets of data intended for positioning purposes can cause interference with communication channels, reducing communication data's transmission efficiency. In order to push the boundaries of joint sensing and communication, future research should focus on exploring the protocols associated with transmission, network architecture, and theoretical boundaries associated with the fundamental information. This should be coupled with the advancements in high-frequency signal processing technology and the design of coding, modulation, and beamforming for RIS-aided systems.

10.6.2 Artificial Intelligence-Empowered Strategies for RIS-Assisted Localization

Data-driven approaches are becoming more prevalent in the era of artificial intelligence (AI), supplanting model-based signal processing due to their superior algorithmic robustness [88]. In light of this, the development of AI-guided approaches for radio localization enhanced by RIS have the potential to enhance radio localization performance significantly [89]. AI-powered RIS control can expand the design possibilities of these surfaces, making it an essential area of study [90]. Likewise, the implementation of ML- and AI-based algorithms in RIS, active RIS, and simultaneos transmitting and reflecting (STAR)–RIS-supported networks is anticipated to have a significant impact in the near future.

10.6.3 Distributed RIS

An effective strategy to enhance the overall localization performance is to split the total extensive RIS into more diminutive components and disperse them at a predetermined distance. This approach surpasses the reliability of centralized approaches, resulting in a heightened average localization performance [91]. Furthermore, the distributed operation of RIS is particularly beneficial in disaster scenarios. The incorporation of numerous RIS patches, readily detachable from the comprehensive RIS, enhances connectivity and effectively mitigates the infrastructure fragmentation resulting from disasters. Deploying RIS in a distributed manner can lead to heightened intricacy, as each individual patch of the RIS must be intelligent, and there may be significant feedback overhead. Additionally, any RIS design should consider the need for detachable functionalities.

10.6.4 Positioning and Localization of Users Inside the Tunnel

Autonomous vehicles fitted with network access units and sensors are poised to undertake a significant role in forthcoming intelligent transportation structures, which are a crucial component of smart cities. However, in a highway tunnel, GPS signal strength is typically weak, posing a persistent challenge for achieving accurate positioning. The attainment of precise positioning is paramount for forthcoming autonomous vehicles, as it directly influences optimal safety and security measures. Furthermore, efficient rescue work during tunnel accidents heavily relies on the precise location tracking of personnel and vehicles. This highlights the critical importance of accurate positioning systems in such scenarios. Thus, by installing RIS on the walls or ceiling of a tunnel, it becomes possible to accurately track the location of personnel or vehicles inside the tunnel [92, 93]. That is, RIS holds the capability to enhance the strength of received signals through the strategic reuse of signals in environments with multipath propagation, consequently resulting in improved performance for positioning. Nevertheless, the application of RIS encounters a challenge in practical scenarios, primarily due to the swift mobility of vehicles. Ensuring instantaneous assistance for vehicle positioning necessitates an RIS controller equipped with swift computational abilities to dynamically modify the reflected beam's direction. This specific requirement must be thoroughly addressed in the current literature on RIS positioning. In instances where a vehicle is in motion within a tunnel, the RIS must dynamically estimate the channel as the target user moves, simultaneously devising a suitable phase shifter. Exploring the feasibility of relying solely on channel-state statistics becomes crucial when perfect CSI is not readily accessible.

10.6.5 Installation and Optimization of Radio Localization with RIS

The prevailing body of literature primarily revolves around formulating theoretical frameworks, with minimal or no substantive initiatives dedicated to practical explorations into radio localization's design and deployment facets with RIS. Consequently, there exists a substantial void that demands scrutiny concerning the practical viability of methodologies advocated in the literature. Achieving peak performance in communication parameters, precision of localization/sensing, and coverage hinges on optimizing RIS quantity and placement. Furthermore, verifying that the refined deployment of RIS indeed confers advantages over conventional BS deployments is imperative, particularly regarding total energy usage and coordination endeavors. This optimization procedure encompasses precisely calibrating the position along with the orientation of the RIS, coupled with its synchronization with BSs.

10.6.6 Focusing of Beams in Near-Field

Challenges and opportunities arise in the transmission of electromagnetic wave signals when it comes to 6G systems, especially in the context of the near-field. While far-field plane waves are restricted in directing the energy of the beam to a particular angle, this becomes a limitation in densely populated user scenarios within the same angle domain due to interference. In contrast, the wavefront in the near-field differs from the one in the far-field. It provides additional resolution in the range domain, enabling the beam to focus its energy at a precise angle and distance. Consequently, it can potentially enhance the precision of location identification in situations where multiple users are present.

In the field of RIS-aided 6G–IoT wireless positioning and localization, there are several research trends to keep an eye on in the future. One is the need to validate and test RIS-aided prototypes for multiuser scenarios. Another trend is optimizing RIS reflection for more realistic scenarios with partial or imperfect CSI or hardware imperfections [94]. Furthermore, integrating RIS with other emerging technologies like blockchain [95] and quantum computing [96] is expected to gain traction in the future. Quantum communication for channel estimation is a promising area of research in this regard.

10.7 Conclusions

The advancements of the 6G wireless communication system introduce novel positioning requirements and present unique challenges. Thus, leveraging RIS to enhance the radio localization of IoT devices emerges as a prospective avenue for

study. This chapter initially elucidates the role of RIS-aided 6G–IoT networks in wireless positioning and localization. Moreover, it expounds on the characteristics of RIS that render it conducive to wireless positioning and localization, illustrating RIS-assisted IoT networks and RIS for wireless positioning and localization through a system model. Subsequently, the chapter delves extensively into localization principles, encompassing ToA/TDoA, AoA/AoD, RSS, and hybrid measurements. It then explores various algorithms for localization aided by RIS. Following this, it elaborates in detail on cutting-edge research about positioning and localization, encompassing RIS-assisted mm-wave positioning systems, RIS for indoor, near-field, outdoor, and far-field localization, as well as RIS for THz communication. Finally, the prospective obstacles and forthcoming avenues of research linked with RIS-assisted 6G–IoT for wireless positioning and localization are outlined. Thus, this section presents a comprehensive state-of-the-art survey covering nearly all aspects of RIS-aided 6G–IoT for wireless positioning and localization, anticipated to provide valuable insights and guidance for researchers in this domain.

References

1 Vaezi, M., Azari, A., Khosravirad, S.R. et al. (2022). Cellular, wide-area, and non-terrestrial IoT: a survey on 5G advances and the road toward 6G. *IEEE Communications Surveys & Tutorials* 24 (2): 1117–1174.

2 De Lima, C., Belot, D., Berkvens, R. et al. (2021). Convergent communication, sensing and localization in 6G systems: an overview of technologies, opportunities and challenges. *IEEE Access* 9: 26902–26925.

3 Wang, Z., Zhang, J., Du, H. et al. (2024). A tutorial on extremely large-scale MIMO for 6G: fundamentals, signal processing, and applications. *IEEE Communications Surveys & Tutorials* 26 (3): 1560–1605.

4 Guo, F., Yu, F.R., Zhang, H. et al. (2021). Enabling massive IoT toward 6G: a comprehensive survey. *IEEE Internet of Things Journal* 8 (15): 11891–11915.

5 You, X., Wang, C.-X., Huang, J. et al. (2021). Towards 6G wireless communication networks: vision, enabling technologies, and new paradigm shifts. *Science China Information Sciences* 64: 1–74.

6 Trevlakis, S.E., Boulogeorgos, A.-A.A., Pliatsios, D. et al. (2023). Localization as a key enabler of 6G wireless systems: a comprehensive survey and an outlook. *IEEE Open Journal of the Communications Society* 4: 2733–2801.

7 Strinati, E.C., Barbarossa, S., Gonzalez-Jimenez, J.L. et al. (2019). 6G: the next frontier: from holographic messaging to artificial intelligence using subterahertz and visible light communication. *IEEE Vehicular Technology Magazine* 14 (3): 42–50.

8 Liu, R., Wu, Q., Di Renzo, M., and Yuan, Y. (2022). A path to smart radio environments: an industrial viewpoint on reconfigurable intelligent surfaces. *IEEE Wireless Communications* 29 (1): 202–208.

9 Liu, Y., Liu, X., Mu, X. et al. (2021). Reconfigurable intelligent surfaces: principles and opportunities. *IEEE Communications Surveys & Tutorials* 23 (3): 1546–1577.

10 Chen, R., Liu, M., Hui, Y. et al. (2022). Reconfigurable intelligent surfaces for 6G IoT wireless positioning: a contemporary survey. *IEEE Internet of Things Journal* 9 (23): 23570–23582.

11 Liu, Y., Liu, E., Wang, R., and Geng, Y. (2021). Reconfigurable intelligent surface aided wireless localization. *ICC 2021-IEEE International Conference on Communications*, 1–6. IEEE.

12 Yildirim, I., Kilinc, F., Basar, E., and Alexandropoulos, G.C. (2021). Hybrid RIS-empowered reflection and decode-and-forward relaying for coverage extension. *IEEE Communications Letters* 25 (5): 1692–1696.

13 Tang, X., Lan, X., Zhai, D. et al. (2021). Securing wireless transmissions with RIS-receiver coordination: passive beamforming and active jamming. *IEEE Transactions on Vehicular Technology* 70 (6): 6260–6265.

14 Vaca-Rubio, C.J., Ramirez-Espinosa, P., Kansanen, K. et al. (2021). Assessing wireless sensing potential with large intelligent surfaces. *IEEE Open Journal of the Communications Society* 2: 934–947.

15 Sang, J., Yuan, Y., Tang, W. et al. (2022). Coverage enhancement by deploying RIS in 5G commercial mobile networks: field trials. *IEEE Wireless Communications* 31 (1): 172–180.

16 Basharat, S., Khan, M., Iqbal, M. et al. (2022). Exploring reconfigurable intelligent surfaces for 6G: state-of-the-art and the road ahead. *IET Communications* 16 (13): 1458–1474.

17 Galappaththige, D.L., Rezaei, F., Tellambura, C., and Herath, S. (2022). RIS-empowered ambient backscatter communication systems. *IEEE Wireless Communications Letters* 12 (1): 173–177.

18 Pan, C., Ren, H., Wang, K. et al. (2020). Intelligent reflecting surface aided MIMO broadcasting for simultaneous wireless information and power transfer. *IEEE Journal on Selected Areas in Communications* 38 (8): 1719–1734.

19 Menon, V. and Selvaprabhu, P. (2022). A novel tri-staged RIA scheme for cooperative cell edge users in a multi-cellular MIMO IMAC. *IEEE Access* 10: 117141–117156.

20 Nguyen, D.C., Ding, M., Pathirana, P.N. et al. (2021). 6G Internet of Things: a comprehensive survey. *IEEE Internet of Things Journal* 9 (1): 359–383.

21 Nasralla, M.M., Khattak, S.B.A., Rehman, I.U., and Iqbal, M. (2023). Exploring the role of 6G technology in enhancing quality of experience for m-health multimedia applications: a comprehensive survey. *Sensors* 23 (13): 5882.

22 Hassouna, S., Jamshed, M.A., Rains, J. et al. (2023). A survey on reconfigurable intelligent surfaces: wireless communication perspective. *IET Communications* 17 (5): 497–537.

23 Vivek, M.U. and Selvaprabhu, P. (2022). Role of telecommunication technologies in microgrids and smart grids. In: *Smart Grids and Microgrids: Technology Evolution* (ed. P. Prabhakaran, U. Subramaniam, S.M. Krishna, et al.), 325–364. Wiley.

24 Pogaku, A.C., Do, D.-T., Lee, B.M., and Nguyen, N.D. (2022). UAV-assisted RIS for future wireless communications: a survey on optimization and performance analysis. *IEEE Access* 10: 16320–16336.

25 Zhao, L. and Bai, Y. (2024). Unlocking the ocean 6G: a review of path-planning techniques for maritime data harvesting assisted by autonomous marine vehicles. *Journal of Marine Science and Engineering* 12 (1): 126.

26 Tekbıyık, K., Kurt, G.K., and Yanikomeroglu, H. (2021). Energy-efficient RIS-assisted satellites for IoT networks. *IEEE Internet of Things Journal* 9 (16): 14891–14899.

27 Ranjha, A. and Kaddoum, G. (2020). URLLC facilitated by mobile UAV relay and RIS: a joint design of passive beamforming, blocklength, and UAV positioning. *IEEE Internet of Things Journal* 8 (6): 4618–4627.

28 Mursia, P., Sciancalepore, V., Garcia-Saavedra, A. et al. (2020). RISMA: reconfigurable intelligent surfaces enabling beamforming for IoT massive access. *IEEE Journal on Selected Areas in Communications* 39 (4): 1072–1085.

29 Kisseleff, S., Chatzinotas, S., and Ottersten, B. (2021). Reconfigurable intelligent surfaces in challenging environments: underwater, underground, industrial and disaster. *IEEE Access* 9: 150214–150233.

30 Wymeersch, H. and Seco-Granados, G. (2022). Radio localization and sensing–Part I: fundamentals. *IEEE Communications Letters* 26 (12): 2816–2820.

31 Zeng, S., Zhang, H., Di, B. et al. (2021). Reconfigurable intelligent surfaces in 6G: reflective, transmissive, or both? *IEEE Communications Letters* 25 (6): 2063–2067.

32 Zhang, H., Di, B., Bian, K. et al. (2022). Toward ubiquitous sensing and localization with reconfigurable intelligent surfaces. *Proceedings of the IEEE* 110 (9): 1401–1422.

33 Imoize, A.L., Obakhena, H.I., Anyasi, F.I. et al. (2022). Reconfigurable intelligent surfaces enabling 6G wireless communication systems: use cases and technical considerations. *2022 5th Information Technology for Education and Development (ITED)*, 1–7. IEEE.

34 Kumaravelu, V.B., Imoize, A.L., Castillo Soria, F.R. et al. (2023). RIS-assisted fixed NOMA: outage probability analysis and transmit power optimization. *Future Internet* 15 (8): 249.

35 Imoize, A.L., Adedeji, O., Tandiya, N., and Shetty, S. (2021). 6G enabled smart infrastructure for sustainable society: opportunities, challenges, and research roadmap. *Sensors* 21 (5): 1709.

36 Kumaravelu, V.B., Selvaprabhu, P., Han, D.S. et al. (2023). Blind reconfigurable intelligent surface-aided fixed non-orthogonal multiple access for intelligent vehicular networks. *EURASIP Journal on Wireless Communications and Networking* 2023 (1): 83.

37 Mondal, A., Al Junaedi, A.M., Singh, K., and Biswas, S. (2022). Spectrum and energy-efficiency maximization in RIS-aided IoT networks. *IEEE Access* 10: 103538–103551.

38 Li, X., Zhu, Q., Yu, T., and Chen, Y. (2023). Active RIS assisted spectrum sharing: able to achieve energy-efficient notable detection performance gains. *IEEE Transactions on Vehicular Technology* 72 (9): 11668–11684.

39 Imoize, A.L., Obakhena, H.I., Anyasi, F.I. et al. (2022). Spectral efficiency bounds of cell-free massive MIMO assisted UAV cellular communication. *2022 IEEE Nigeria 4th International Conference on Disruptive Technologies for Sustainable Development (NIGERCON)*, 1–5. IEEE.

40 Wymeersch, H., He, J., Denis, B. et al. (2020). Radio localization and mapping with reconfigurable intelligent surfaces: challenges, opportunities, and research directions. *IEEE Vehicular Technology Magazine* 15 (4): 52–61.

41 Liaskos, C., Mamatas, L., Pourdamghani, A. et al. (2022). Software-defined reconfigurable intelligent surfaces: from theory to end-to-end implementation. *Proceedings of the IEEE* 110 (9): 1466–1493.

42 Wu, S., Zhang, S., and Huang, D. (2019). A TOA-based localization algorithm with simultaneous NLOS mitigation and synchronization error elimination. *IEEE Sensors Letters* 3 (3): 1–4.

43 Dai, Z., Wang, G., Jin, X., and Lou, X. (2020). Nearly optimal sensor selection for TDOA-based source localization in wireless sensor networks. *IEEE Transactions on Vehicular Technology* 69 (10): 12031–12042.

44 Huang, S., Wang, B., Zhao, Y., and Luan, M. (2022). Near-field RSS-based localization algorithms using reconfigurable intelligent surface. *IEEE Sensors Journal* 22 (4): 3493–3505.

45 Xu, Z., Li, H., Yang, K., and Li, P. (2023). A robust constrained total least squares algorithm for three-dimensional target localization with hybrid TDOA–AOA measurements. *Circuits, Systems, and Signal Processing* 42 (6): 3412–3436.

46 Kim, J. (2023). Suppression of NLOS errors in TDOA-AOA hybrid localization. *Wireless Networks* 29 (2): 657–667.

47 Jiang, H., He, R., Ruan, C. et al. (2021). Three-dimensional geometry-based stochastic channel modeling for intelligent reflecting surface-assisted UAV

MIMO communications. *IEEE Wireless Communications Letters* 10 (12): 2727–2731.

48 Wu, T., Pan, C., Pan, Y. et al. (2023). Fingerprint-based mmWave positioning system aided by reconfigurable intelligent surface. *IEEE Wireless Communications Letters* 12 (8): 1379–1383.

49 Menon, V.U. and Selvaprabhu, P. (2022). Blind interference alignment: a comprehensive survey. *International Journal of Communication Systems* 35 (8): e5116.

50 Wang, Y., Ho, I.W.-H., Zhang, S., and Wang, Y. (2023). Intelligent reflecting surface enabled fingerprinting-based localization with deep reinforcement learning. *IEEE Transactions on Vehicular Technology* 72 (10): 13162–13172.

51 Yu, D., Zheng, G., Shojaeifard, A. et al. (2023). Kalman filter based channel tracking for RIS-assisted multi-user networks. *IEEE Transactions on Wireless Communications* 23 (4): 3856–3869.

52 Ammous, M. and Valaee, S. (2022). Positioning and tracking using reconfigurable intelligent surfaces and extended Kalman filter. *2022 IEEE 95th Vehicular Technology Conference:(VTC2022-Spring)*, 1–6. IEEE.

53 Yang, Z., Zhang, H., Zhang, H. et al. (2022). MetaSLAM: wireless simultaneous localization and mapping using reconfigurable intelligent surfaces. *IEEE Transactions on Wireless Communications* 22 (4): 2606–2620.

54 Huang, C., Alexandropoulos, G.C., Yuen, C., and Debbah, M. (2019). Indoor signal focusing with deep learning designed reconfigurable intelligent surfaces. *2019 IEEE 20th International Workshop on Signal Processing Advances in Wireless Communications (SPAWC)*, 1–5. IEEE.

55 Gao, P., Lian, L., and Yu, J. (2022). Wireless area positioning in RIS-assisted mmWave systems: joint passive and active beamforming design. *IEEE Signal Processing Letters* 29: 1372–1376.

56 Menon, U.V., Challa, N.R., and Bagadi, K. (2019). Lenstra Lenstra lovász (LLL) assisted likelihood ascent search (LAS) algorithm for signal detection in massive MIMO. *2019 International Conference on Vision Towards Emerging Trends in Communication and Networking (ViTECoN)*, 1–4. IEEE.

57 He, J., Jiang, F., Keykhosravi, K. et al. (2022). Beyond 5G RIS mmWave systems: where communication and localization meet. *IEEE Access* 10: 68075–68084.

58 Wu, Q., Zhang, S., Zheng, B. et al. (2021). Intelligent reflecting surface-aided wireless communications: a tutorial. *IEEE Transactions on Communications* 69 (5): 3313–3351.

59 Čišija, E., Ahmed, A.M., Sezgin, A., and Wymeersch, H. (2021). RIS-aided mmWave MIMO radar system for adaptive multi-target localization. *2021 IEEE Statistical Signal Processing Workshop (SSP)*, 196–200. IEEE.

60 Wang, W. and Zhang, W. (2021). Joint beam training and positioning for intelligent reflecting surfaces assisted millimeter wave communications. *IEEE Transactions on Wireless Communications* 20 (10): 6282–6297.

61 Ma, T., Xiao, Y., Lei, X. et al. (2020). Indoor localization with reconfigurable intelligent surface. *IEEE Communications Letters* 25 (1): 161–165.

62 Zhang, H., Zhang, H., Di, B. et al. (2021). Metalocalization: reconfigurable intelligent surface aided multi-user wireless indoor localization. *IEEE Transactions on Wireless Communications* 20 (12): 7743–7757.

63 Zhou, H., Erol-Kantarci, M., Liu, Y., and Poor, H.V. (2023). A survey on model-based, heuristic, and machine learning optimization approaches in RIS-aided wireless networks. *IEEE Communications Surveys & Tutorials* 26 (2): 781–823.

64 Nguyen, C.L., Georgiou, O., Gradoni, G., and Di Renzo, M. (2021). Wireless fingerprinting localization in smart environments using reconfigurable intelligent surfaces. *IEEE Access* 9: 135526–135541.

65 Abu-Shaban, Z., Keykhosravi, K., Keskin, M.F. et al. (2021). Near-field localization with a reconfigurable intelligent surface acting as lens. *ICC 2021-IEEE International Conference on Communications*, 1–6. IEEE.

66 Luan, M., Wang, B., Zhao, Y. et al. (2021). Phase design and near-field target localization for RIS-assisted regional localization system. *IEEE Transactions on Vehicular Technology* 71 (2): 1766–1777.

67 Pan, C., Zhou, G., Zhi, K. et al. (2022). An overview of signal processing techniques for RIS/IRS-aided wireless systems. *IEEE Journal of Selected Topics in Signal Processing* 16 (5): 883–917.

68 Pan, Y., Pan, C., Jin, S., and Wang, J. (2023). RIS-aided near-field localization and channel estimation for the terahertz system. *IEEE Journal of Selected Topics in Signal Processing* 17 (4): 878–892.

69 Keykhosravi, K., Seco-Granados, G., Alexandropoulos, G.C., and Wymeersch, H. (2022). RIS-enabled self-localization: leveraging controllable reflections with zero access points. *ICC 2022-IEEE International Conference on Communications*, 2852–2857. IEEE.

70 Ozturk, C., Keskin, M.F., Wymeersch, H., and Gezici, S. (2023). RIS-aided near-field localization under phase-dependent amplitude variations. *IEEE Transactions on Wireless Communications* 22 (8): 5550–5566.

71 Ceniklioglu, B., Tubail, D.A., Canbilen, A.E. et al. (2022). Error analysis of the joint localization and synchronization of RIS-assisted mm-Wave MISO-OFDM under the effect of hardware impairments. *IEEE Open Journal of the Communications Society* 3: 2151–2161.

72 Gan, X., Huang, C., Yang, Z. et al. (2022). Near-field localization for holographic RIS assisted mmWave systems. *IEEE Communications Letters* 27 (1): 140–144.

73 Zhang, H., Zhang, H., Di, B. et al. (2021). RSS fingerprinting based multi-user outdoor localization using reconfigurable intelligent surfaces. *2021 15th International Symposium on Medical Information and Communication Technology (ISMICT)*, 167–172. IEEE.

74 Yildirim, I., Uyrus, A., and Basar, E. (2020). Modeling and analysis of reconfigurable intelligent surfaces for indoor and outdoor applications in future wireless networks. *IEEE Transactions on Communications* 69 (2): 1290–1301.

75 Emenonye, D.-R., Dhillon, H.S., and Buehrer, R.M. (2023). RIS-aided localization under position and orientation offsets in the near and far field. *IEEE Transactions on Wireless Communications* 22 (12): 9327–9345.

76 He, J., Fakhreddine, A., Vanwynsberghe, C. et al. (2023). 3D localization with a single partially-connected receiving RIS: positioning error analysis and algorithmic design. *IEEE Transactions on Vehicular Technology* 72 (10): 13190–13202.

77 Chen, Z., Ma, X., Han, C., and Wen, Q. (2021). Towards intelligent reflecting surface empowered 6G terahertz communications: a survey. *China Communications* 18 (5): 93–119.

78 Chen, H., Sarieddeen, H., Ballal, T. et al. (2022). A tutorial on terahertz-band localization for 6G communication systems. *IEEE Communications Surveys & Tutorials* 24 (3): 1780–1815.

79 ElMossallamy, M.A., Zhang, H., Song, L. et al. (2020). Reconfigurable intelligent surfaces for wireless communications: principles, challenges, and opportunities. *IEEE Transactions on Cognitive Communications and Networking* 6 (3): 990–1002.

80 Rinchi, O., Elzanaty, A., and Alouini, M.-S. (2022). Compressive near-field localization for multipath RIS-aided environments. *IEEE Communications Letters* 26 (6): 1268–1272.

81 Baskar, N. and Selvaprabhu, P. (2023). Selective interference alignment and neutralization in coordinated multipoint using multiuser MIMO. *International Journal of Communication Systems* 36 (13): e5547.

82 Yang, P., Yang, L., and Wang, S. (2021). Performance analysis for RIS-aided wireless systems with imperfect CSI. *IEEE Wireless Communications Letters* 11 (3): 588–592.

83 Odeyemi, K.O., Owolawi, P.A., and Olakanmi, O.O. (2020). Reconfigurable intelligent surface assisted mobile network with randomly moving user over Fisher-Snedecor fading channel. *Physical Communication* 43: 101186.

84 Tang, W., Dai, J.Y., Chen, M.Z. et al. (2020). MIMO transmission through reconfigurable intelligent surface: system design, analysis, and implementation. *IEEE Journal on Selected Areas in Communications* 38 (11): 2683–2699.

85 Ozturk, C., Keskin, M.F., Sciancalepore, V. et al. (2024). RIS-aided localization under pixel failures. *IEEE Transactions on Wireless Communications* 23 (8): 8314–8329.

86 Xu, Y., Li, Y., Zhang, J.A. et al. (2023). Joint beamforming for RIS-assisted integrated sensing and communication systems. *IEEE Transactions on Communications* 72 (4): 2232–2246.

87 Guo, T., Li, X., Mei, M. et al. (2023). Joint communication and sensing design in coal mine safety monitoring: 3D phase beamforming for RIS-assisted wireless networks. *IEEE Internet of Things Journal* 10 (13): 11306–11315.

88 Ajani, T.S., Imoize, A.L., and Atayero, A.A. (2021). An overview of machine learning within embedded and mobile devices–optimizations and applications. *Sensors* 21 (13): 4412.

89 Jadhav, H.K. and Kumaravelu, V.B. (2023). Deep learning-assisted transmit antenna classifiers for fully generalized spatial modulation: online efficiency replaces offline complexity. *Applied Sciences* 13 (8): 5134.

90 Wang, J., Tang, W., Han, Y. et al. (2021). Interplay between RIS and AI in wireless communications: fundamentals, architectures, applications, and open research problems. *IEEE Journal on Selected Areas in Communications* 39 (8): 2271–2288.

91 Zhao, Y., Xu, W., You, X. et al. (2022). Cooperative reflection and synchronization design for distributed multiple-RIS communications. *IEEE Journal of Selected Topics in Signal Processing* 16 (5): 980–994.

92 Baskar, N. and Selvaprabhu, P. (2024). Performance analysis of successive di-state full-duplex cooperative wireless cellular networks. *Alexandria Engineering Journal* 91: 139–151.

93 Chen, C. and Pan, C. (2021). Blocking probability in obstructed tunnels with reconfigurable intelligent surface. *IEEE Communications Letters* 26 (2): 458–462.

94 Peng, Z., Chen, Z., Pan, C. et al. (2021). Robust transmission design for RIS-aided communications with both transceiver hardware impairments and imperfect CSI. *IEEE Wireless Communications Letters* 11 (3): 528–532.

95 Selvaprabhu, P. (2023). An examination of distributed and decentralized systems for trustworthy control of supply chains. *IEEE Access* 11: 137025–137052.

96 Narottama, B. and Aïssa, S. (2023). Modular quantum machine learning for channel estimation in STAR-RIS assisted communication systems. *2023 IEEE 34th Annual International Symposium on Personal, Indoor and Mobile Radio Communications (PIMRC)*, 1–6. IEEE.

11

Security and Privacy Issues in RIS-Based Wireless Communication Systems

Nivetha Baskar[1], Poongundran Selvaprabhu[1], Vivek Menon Unnikrishnan[1], Vinoth Kumar Chandra Babu[1], Vinoth Babu Kumaravelu[1], Vetriveeran Rajamani[2], Sunil Chinnadurai[3], and Md. Abdul Latif Sarker[4]

[1] *Department of Engineering (Enzo Ferrari), University of Modena and Reggio Emilia, Modena, Italy*
[2] *Department of Micro and Nano Electronics, School of Electronics Engineering, Vellore Institute of Technology, Vellore, Tamil Nadu, India*
[3] *Department of Electronics and Communication Engineering, School of Engineering and Sciences, SRM University-AP, India*
[4] *Department of Electronics and Information Engineering, Jeonbuk National University, Jeonju, Korea*

11.1 Introduction

Reconfigurable intelligent surfaces (RISs) or intelligent reflecting surfaces (IRSs) have brought about a significant change in the traditional wireless communication by turning them into smart radio networks. These networks are capable of providing high data rates with power efficiency at an affordable cost. They have been a game-changer for beyond fifth-generation (B5G) and sixth-generation (6G) networks. A RIS is a planar surface consisting of a vast number of reflective elements that can alter the amplitude and phase of incoming signals using intelligent control [1]. RISs can dynamically reconfigure wireless propagation channels to enhance signal power for intended users. RISs can effectively manipulate the wireless propagation environment to optimize signal coverage, mitigate interference, and improve overall system performance by strategically adjusting the phase and amplitude of reflected signals [2]. This capability enables RISs to significantly enhance the capacity, reliability, and efficiency of wireless communication systems in diverse environments and scenarios [3]. The deployment of RISs in B5G and 6G networks holds great promise for addressing the ever-increasing demands for high-speed, reliable, and ubiquitous connectivity [4]. Leveraging the unique capabilities of RIS technology, network operators and service providers can unlock new opportunities for delivering advanced services

Reconfigurable Intelligent Surfaces for 6G and Beyond Wireless Networks, First Edition.
Edited by Agbotiname Lucky Imoize, Vinoth Babu Kumaravelu, and Dinh-Thuan Do.

and applications, ranging from ultra-fast internet access to immersive multimedia experiences and mission-critical communication services [5]. The existing body of research provides the robust evidence demonstrating the significant performance improvements offered by RISs in various applications of 6G networks. Numerous studies have highlighted the effectiveness of RISs in enhancing the performance of communication systems operating in terahertz (THz) and millimeter-wave (mmWave) communications frequency bands [6, 7]. Additionally, RISs have been shown to improve communication reliability and efficiency in device-to-device (D2D) network scenarios [8, 9]. In this context, RISs enable unmanned aerial vehicles (UAVs) to have better connectivity and coverage, leading to improved data transmission and control capabilities [10]. Similarly, in satellite communications, RISs help optimize signal propagation and mitigate interference, enhancing communication reliability [11]. Furthermore, RISs play a crucial role in integrated sensing and communication (ISAC) networks, facilitating efficient data collection, processing, and transmission for various sensing applications [12]. In Internet of things (IoT) deployments, RISs enable intelligent signal routing and optimization, enhancing connectivity and communication efficiency [13]. Despite the significant advancements in wireless networks, B5G and 6G technologies are still vulnerable to various security threats. These threats include pilot contamination attacks, pilot spoofing attacks, jamming, environment reconfiguration attacks (ERAs), and eavesdropping, which can significantly impact the confidentiality, availability, and integrity of communication systems in these advanced networks. To mitigate these privacy and security concerns, researchers have proposed different approaches to address the unique characteristics and requirements of 6G networks. Some of these approaches include:

- **Physical key generation:** Utilizing physical properties of communication channels to generate secure cryptographic keys, ensuring secure communication between network entities.
- **RIS deployment:** Leveraging RISs to reshape wireless environments and enhance communication security by controlling signal propagation, mitigating interference, and improving signal confidentiality.
- **Artificial noise generation:** Introducing artificial noise into communication channels to obfuscate transmitted signals and prevent eavesdroppers (EAVs) from intercepting sensitive information.
- **Frequency hopping:** Employing frequency hopping techniques to dynamically switch between different frequency channels, making it difficult for attackers to jam or eavesdrop on communication links.

Among these approaches, RISs have emerged as a promising solution for enhancing security in B5G and 6G networks. RISs offer the capability to intelligently control signal propagation and optimize wireless environments without imposing significant costs or complexity on network infrastructure. Through strategically

deploying RISs, network operators can mitigate security threats, improve communication reliability, and enhance overall network performance.

11.1.1 Key Contributions of the Chapter

The following are the significant contributions of this chapter:

- **Identification of privacy and security concerns:** This chapter identifies and explores the significant privacy and security concerns associated with implementing RIS technology in wireless communication systems. This recognition is crucial for understanding the risks and challenges of deploying RIS-based networks.
- **Comprehensive analysis of issues:** It offers a comprehensive analysis of the multifaceted landscape of privacy and security issues, covering aspects such as data leakage, location privacy, user profiling, surveillance, unauthorized access, data tampering, signal jamming, infrastructure vulnerabilities, and regulatory compliance.
- **Proposed solutions and strategies:** The chapter proposes solutions and strategies for various attacks to address the identified privacy and security challenges, including implementing robust encryption, authentication mechanisms, intrusion detection systems, and adherence to privacy and security regulations. This proactive approach is essential for mitigating risks and ensuring the integrity and confidentiality of data in RIS-enabled networks.
- **Focus on physical layer security:** It highlights the importance of incorporating physical layer security measures into RIS deployments to enhance the confidentiality and integrity of wireless communication. This emphasis on physical layer security is significant for safeguarding against eavesdropping and unauthorized access, contributing to the overall resilience of RIS-assisted networks.
- **Identification of future research directions:** This chapter identifies future research directions and challenges in leveraging the benefits of RIS technology for physical layer security and covert communications. This recognition underscores the ongoing need for innovation and advancement in the field to address emerging threats and maximize the potential of RIS-enabled networks.

11.1.2 Chapter Organization

Section 11.2 presents the related works on ensuring security and privacy in 6G applications assisted by RIS. Section 11.3 introduces the security and privacy perspectives in RIS-assisted 6G applications. Section 11.4 describes the various threats and attacks in RIS-supported wireless systems, while Section 11.5 covers the secure physical layer networks for RIS-assisted systems, and Section 11.6 concludes the chapter with a discussion of future directions.

11.2 Related Work

The section represents a subset of the research efforts aimed at addressing security and privacy concerns in RIS-assisted wireless communication systems, and they offer valuable insights into the challenges and potential solutions in this emerging area of research. Table 11.1 lists various literature works on security and privacy perspectives in RIS-assisted wireless communication systems.

Table 11.1 Related works on security and privacy issues in RIS-assisted wireless communication systems.

References	Research summary
Hossain et al. [14]	This research analyzes the security performance of mixed dual-hop RIS-aided networks against eavesdropping. It evaluates secrecy capacity, outage probability, and ensures positive secrecy capacity to understand the implications of security threats and performance capabilities.
Kaveh et al. [15]	This article explores the effect of RIS technology on physical layer security in smart grid communications. An RIS, smart meter, and eavesdropper are considered to create a smart environment. The objective is to improve physical layer security performance in terms of secrecy outage probability and average secrecy capacity.
Lin et al. [16]	This study analyzed four security-reliability trade-off (SRT) schemes: random jammer selection (RJS), optimal jammer selection (OJS), multiple jammers (MJ), and non-jamming (NJ) found that RJS, OJS, and MJ perform better than NJ in terms of SRT. Moreover, the author conducted a secrecy gain analysis, which showed that the three aforementioned schemes are superior. Finally, simulations revealed significant SRT benefits of RJS, OJS, and MJ compared to the conventional NJ scheme.
Porambage et al. [17]	The author discusses 6G network security, including key performance indicators and potential threats. Furthermore, this study examines privacy and security challenges with 6G requirements and applications and provides insights into ongoing standardization efforts and research projects. Finally, the author explores security considerations for enabling technologies like physical layer security, distributed AI/ML, visible light communication (VLC), THz, and quantum computing.
Khalid et al. [18]	The article provides a comprehensive overview of employing RIS within the realm of physical layer security for 6G-IoT networks, focusing on eavesdropping and jamming attacks. It explores the fundamental principles, hardware architecture, and various design strategies leveraging RIS, including resource allocation, beamforming, artificial noise, and cooperative communication. Furthermore, it addresses research challenges such as RIS modeling, channel modeling, optimization, machine learning, and recent advancements like simultaneously transmitting and reflecting intelligent surface (STAR)-RIS and malicious RIS.

11.3 Ensuring Security and Privacy in 6G Applications Assisted by RIS

The integration of RIS, with a keen focus on privacy and security and exploring its vast range of applications in the field of 6G networks presents an exciting opportunity for the development of advanced wireless communication systems. Though it is a complex and multifaceted task, it is a critical venture that promises to bring significant advancements in the field.

11.3.1 RIS Operation

The operation of an RIS involves dynamic adjustments of electromagnetic properties to enable RIS to actively influence and enhance wireless communication by adapting to the changing conditions of the communication environment [19]. This operation involves real-time adaptability to varying communication conditions, enhancing signal quality, and improving overall performance in diverse environments [20, 21]. Various security attacks on RIS-assisted wireless communication systems are illustrated in Figure 11.1.

1. **Wave Interaction**
   - RIS comprises a surface embedded with numerous small elements, including antennas or reflecting elements.

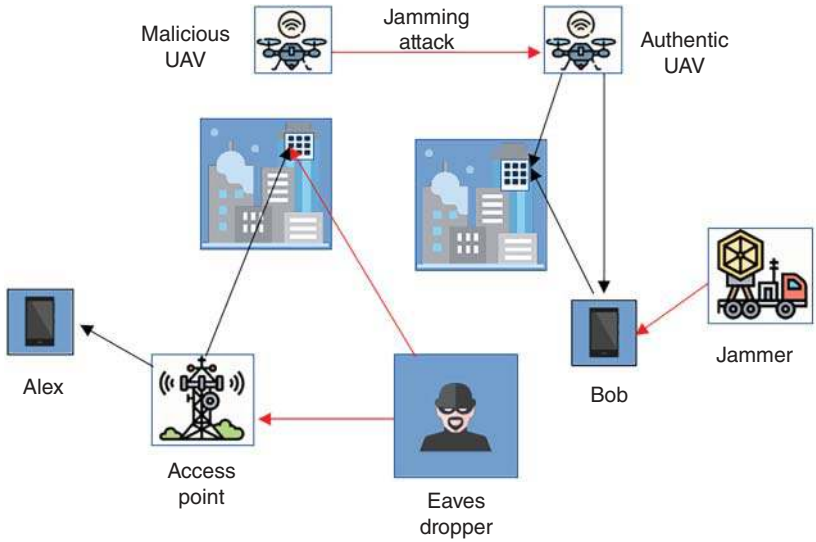

Figure 11.1 Security attacks on RIS-assisted wireless communication systems.

- These elements interact with incident electromagnetic waves, influencing their characteristics, such as phase, amplitude, or polarization.

2. **Phase Control**
   - A fundamental function of RIS is to manage the phase of incoming electromagnetic waves.
   - Through precise adjustments to the phase of reflected or transmitted waves, RIS can strategically create constructive or destructive interference patterns, thereby shaping the overall communication environment.
3. **Smart Surface Adaptation**
   - RIS undergoes continuous adaptation by dynamically adjusting its configuration in response to real-time environmental conditions, user requirements, or network demands.
   - Adaptive algorithms process feedback from the environment or user devices, leading to dynamic reconfiguration of RIS elements for optimal wireless communication.
4. **Beamforming and Steering**
   - RIS facilitates beamforming by strategically concentrating signal energy in specific directions to enhance communication links.
   - RIS optimizes signal strength and quality by steering beams toward intended receivers, effectively mitigating interference and countering multipath effects for improved overall performance.
5. **Channel State Information Feedback**
   - RIS employs feedback mechanisms, such as channel state information (CSI), to gain insights into the prevailing state of the wireless channel.
   - This feedback provides valuable information to the RIS, allowing it to assess the effectiveness of its adjustments and optimize its configuration dynamically for enhanced communication performance.
6. **Collaboration with Base Stations**
   - RIS collaborates with base stations (BSS) within cellular networks to augment coverage and capacity.
   - Coordination with BSs entails sharing information about channel conditions, enabling the RIS to adapt its configuration to complement and optimize the existing network infrastructure. This collaborative approach contributes to improved overall network performance.
7. **Interference Mitigation**
   - RIS is a tool for mitigating interference by intelligently manipulating signals through reflection or refraction, thereby minimizing unwanted effects from nearby transmitters.
   - Through dynamic adaptation to the communication environment, RIS enhances signal quality and effectively reduces interference, improving overall communication performance.

8. **Integration with 5G/6G Networks**
   - RIS is purposefully designed to integrate seamlessly with existing (5G) and future (potentially 6G) wireless communication standards.
   - This integration emphasizes interoperability and coordinated functionality to harness the full potential of RIS within advanced communication environments, ensuring optimal performance and compatibility with evolving network technologies [22].
9. **Dynamic Optimization Algorithms**
   - RIS employs intelligent algorithms for dynamic optimization, considering factors such as signal-to-noise ratio, interference levels, and user quality of service (QoS) requirements.
   - These algorithms dynamically adjust RIS parameters and continuously adapt to changing communication conditions, thus ensuring optimal performance in diverse, evolving wireless environments.
10. **Energy Efficiency**
    - In RIS operation, there is a focus on incorporating energy-efficient strategies, mainly when the surface operates with limited resources.
    - Using energy-aware algorithms aims to achieve a harmonious balance between enhancing performance and conserving energy, thereby ensuring sustainable and efficient RIS operation.

11.3.2 Security and Privacy Perspectives on RIS

Security in RIS implementation entails safeguarding against unauthorized access, malicious manipulation, and interception of wireless communication signals [23]. Privacy concerns arise due to the potential for unintended disclosure of sensitive information during signal manipulation by RIS. Since RIS can alter signal characteristics, there is a risk of unintentional leakage or interception, compromising user privacy [24]. Integrating security and privacy considerations into RIS design and implementation processes, the full potential of wireless communications can be realized while ensuring confidentiality and integrity.

- **Encryption:** Implement an end-to-end encryption process to protect the confidentiality of communication over RIS. This process ensures that data transmitted between devices and through the RIS remains secure and inaccessible to unauthorized entities.
- **Authentication:** Establish robust authentication protocols for devices interacting with the RIS. This protocol prevents unauthorized access and ensures that only legitimate devices can communicate with the RIS. Utilize methods such as digital certificates and biometric authentication for enhanced security.
- **Access control:** Implement robust access control mechanisms to regulate which devices or users can interact with the RIS. This implementation includes

defining permissions, user roles, and restrictions to prevent unauthorized RIS configuration or data manipulation.

- **Regular Security Audits:** Conduct frequent security audits to identify and address potential vulnerabilities in the RIS infrastructure. Regular assessments help stay ahead of evolving security threats and ensure continuous improvement in the security posture of the 6G network.
- **Updates and Patching:** Keep the RIS system up-to-date with the latest security patches and updates. However, it is essential to address any known vulnerabilities and protect against exploits that could compromise the security of the RIS.
- **Industry Collaboration:** Engage with industry experts and collaborate to share insights and best practices related to RIS security. Staying informed about the latest security trends and solutions is crucial in developing effective strategies to safeguard the 6G network.
- **Adherence to Standards:** Ensure compliance with established security standards and protocols relevant to RIS in 6G. Adhering to recognized standards provides a baseline for security measures and facilitates interoperability with other secure systems.
- **Network Segmentation:** Employ network segmentation to isolate critical components of the 6G infrastructure. However, it limits the impact of potential security breaches, preventing attackers from moving laterally within the network.
- **Monitoring and Incident Response:** Implement robust monitoring systems to detect anomalous activities and potential security incidents. Develop a well-defined incident response plan to mitigate and recover from security breaches effectively.

11.3.3 Various Applications of RIS in 6G from Security and Privacy Perspective

The section provides a structured overview of the applications of RIS in 6G networks and the associated security and privacy challenges, highlighting the need for comprehensive strategies to address these concerns and foster the development of secure and privacy-preserving communication systems.

- **THz and mmWave**: In the first application, RISs are crucial in overcoming communication challenges, particularly in THz and mmWave systems. THz frequencies encounter signal propagation challenges, and RIS can optimize their path [6]. Meanwhile, mmWave signals are susceptible to interference. RIS can mitigate interference by adjusting reflected signals and improving reliability and security [25]. RISs effectively extend coverage and mitigate path loss issues associated with these high-frequency bands through a strong line-of-sight (LOS)

channel between transmitter and receiver. Additionally, RISs can improve the rank and power of wireless channels. This can lead to better spatial diversity, particularly for outdoor systems. Moreover, it mitigates interference, improves security through secure beamforming, and safeguards against unauthorized access and eavesdropping in high-frequency communication, thus making it pivotal for future technologies like 6G and IoT. Viewing security and privacy attacks from the perspective of non-terrestrial networks empowered by RIS are illustrated in Figure 11.2.

- **Cell Edge:** In the second application, a network aided by RIS is described, with users positioned at the cell periphery facing interference from neighboring BSs and experiencing significant signal attenuation from their own BS [26]. Here, RIS is crucial in enhancing communication system security by effectively countering eavesdropping and mitigating jamming interference. However, challenges arise at the cell edge due to non-line-of-sight (NLOS) communication channels and potentially malicious multiple antenna jamming treads introducing replayed or falsified signals that disrupt transmissions.
- **D2D:** Ensuring security and privacy in D2D applications within RIS networks is crucial. The interaction between devices in close proximity raises potential vulnerabilities, including the risk of unauthorized access, eavesdropping, and data interception [27]. Protecting sensitive information becomes paramount, necessitating robust encryption mechanisms and secure authentication protocols [28]. Additionally, the dynamic nature of RIS introduces challenges in managing access control and preventing malicious activities. Addressing these concerns is essential for ensuring the secure and private operation of D2D applications within RIS networks.
- **IoT Networks:** The fourth application uses RIS to optimize energy consumption in IoT networks with budget constraints. RIS technology optimizes the propagation environment for IoT devices by adjusting signal paths [29]. This optimization helps to overcome obstacles such as signal attenuation, interference [30], and multipath fading, resulting in more reliable communication between IoT devices. In the meantime, it reduces power losses that occur over long distances by using passive beamforming in RIS. However, IoT networks aided by RIS are vulnerable to coordinated attacks orchestrated by enhanced adversarial vehicles and malicious jammers (MJs) can undermine system performance. MJs can interfere with both RISs and BSs, complicating the decoding of transmitted information within the network.
- **NOMA:** The fifth application focuses on 6G non-orthogonal multiple access (NOMA) systems. RIS can assist NOMA systems in maximizing spectral efficiency, increasing the number of served users, and enhancing communication rates [31]. RIS can help NOMA systems achieve better spectral efficiency, serve more users, and improve communication rates. "However, RIS-assisted

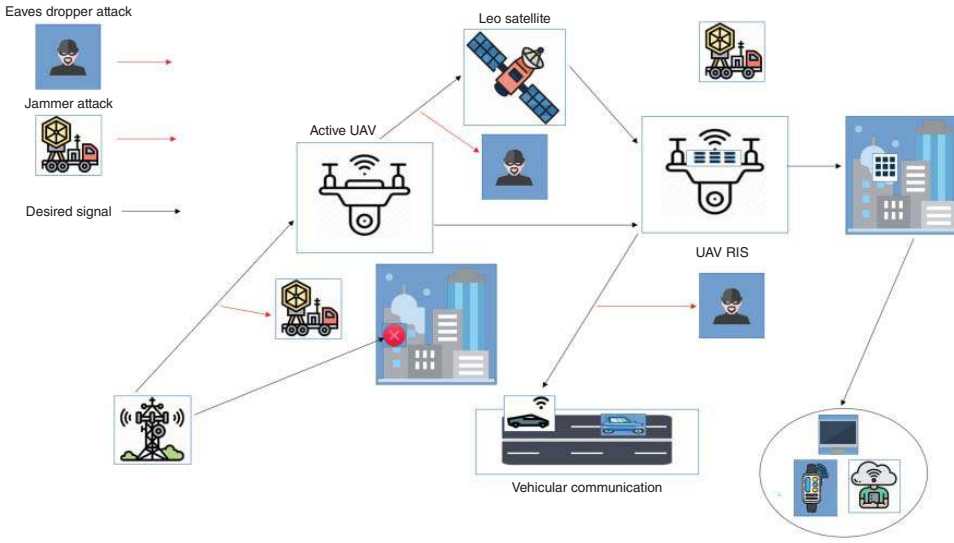

Figure 11.2 Security attacks on RIS-assisted wireless communication systems.

NOMA networks face security challenges from both internal and external eavesdropping threats." High-power users are vulnerable to eavesdropping; internal EAVs can compromise their info due to interference cancellation [32]. Moreover, integrating NOMA techniques into RIS networks offers promising opportunities to address the growing demand for high-capacity, efficient, and secure wireless communication systems.

- **Cognitive Radio:** Cognitive radio (CR) enables dynamic spectrum access by allowing RIS to select optimal frequency bands intelligently based on real-time spectrum availability and user demands. CR algorithms continuously monitor the spectrum and adapt RIS parameters such as phase shifts and reflection coefficients to operate in the most efficient frequency bands [33]. Additionally, CR performs spectrum sensing to detect idle or underutilized frequency bands. RIS networks can use this information to adjust their reflective properties to enhance signal strength and quality in the selected frequency bands. CR algorithms consider various QoS metrics, such as throughput, latency, and reliability. Moreover, RIS networks can adapt their reflective properties to meet QoS requirements by optimizing signal coverage, multipath diversity, and interference levels [34].
- **Multi-access edge computing:** In the seventh application, multi-access edge computing (MEC) brings computing resources closer to the network edge, enabling low-latency processing and content delivery. Through deploying MEC servers near RIS nodes, latency-sensitive applications can leverage the RIS's ability to optimize signal propagation paths, reducing communication delays [35]. MEC allows offloading computational tasks from end-user devices to nearby edge servers for efficient execution. Meanwhile, integrating MEC with RIS networks can optimize communication paths and signal coverage to facilitate seamless offloading of data and computation-intensive tasks, improving overall system performance. Moreover, RIS nodes can assist in content delivery by optimizing signal reflections to direct traffic toward MEC-enabled servers hosting cached content, enhancing user experience and network efficiency.
- **UAV:** In the eighth application, UAV can serve as aerial BSs or relays, providing enhanced connectivity and coverage in areas with limited infrastructure [36]. RIS nodes can adjust their reflective properties dynamically to optimize signal propagation paths between UAVs and ground terminals, mitigating signal blockage and improving link reliability. UAV-mounted RIS units can enhance on-demand signal and beamforming capabilities for mobile communication devices. However, adjusting their reflective properties in real time can optimize signal strength and quality for UAV-to-ground and UAV-to-UAV communication links, thus facilitating seamless mobility and handover. RIS networks can minimize co-channel interference [37], maximize spatial reuse, and enhance overall spectral efficiency in UAV communication systems. UAV–RIS networks

can enhance security and privacy by implementing secure communication protocols and dynamic signal encryption, protecting sensitive data, and preventing unauthorized access or interception.

- **SWIPT:** Simultaneous wireless information and power transfer (SWIPT) enables simultaneous transmission of both information and power in the same frequency band. Integrating RIS with SWIPT networks can optimize signal reflections to ensure minimal interference between power and information signals, thus maximizing spectral efficiency and communication reliability [38]. Additionally, RIS nodes can assist in optimizing the timing and power allocation for energy harvesting and information transmission, ensuring efficient utilization of harvested energy and maximizing communication throughput [39]. Moreover, RIS nodes can implement secure communication protocols and authentication mechanisms to ensure the integrity and confidentiality of data transmission and power transfer operations.

11.4 Various Threats and Attacks in RIS-Supported Wireless Systems

The section provides a structured overview of the various threats and attacks in RIS-supported wireless systems, along with potential countermeasures and defense strategies to address these security challenges effectively.

11.4.1 Pilot Contamination Attack

Pilot contamination is a significant threat in RIS networks, particularly in systems where multiple users share the same pilot resources. This contamination can arise from interference between reflected signals and the pilot signals of other users, resulting in adverse effects such as decreased spectral efficiency, increased interference levels, and a degraded signal-to-interference-plus-noise ratio (SINR) [40]. Also, it can result in inaccurate channel estimation, leading to suboptimal beamforming, precoding, and resource allocation. Malicious attackers could exploit this vulnerability by manipulating the phase shifts of RIS elements to intentionally corrupt the pilot signals of specific users. Additionally, adversaries can engage in eavesdropping on legitimate users' (LUs') pilot signals and subsequently inject interference [41] into the RIS-aided reflections to exacerbate the contamination. Moreover, these threats underscore the critical need for robust security measures within RIS networks to safeguard their performance and integrity. Various attacks on RIS-assisted wireless communication systems are illustrated in Figure 11.3. Mitigation strategies for pilot contamination attack:

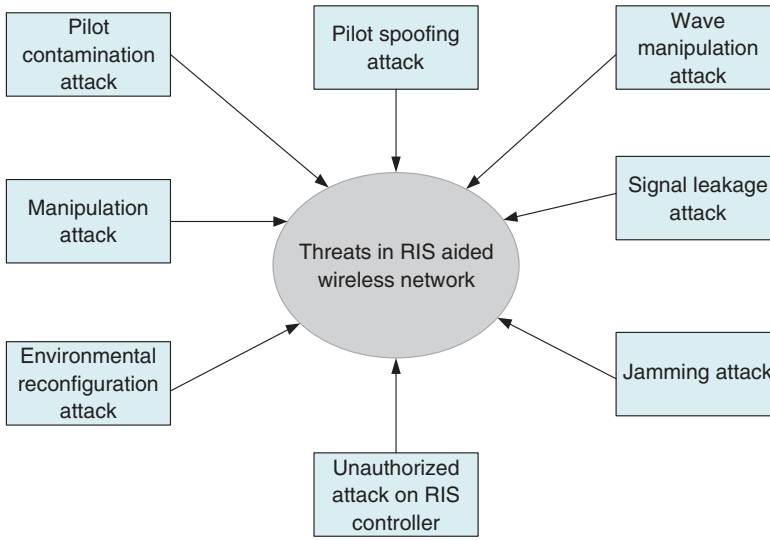

Figure 11.3 Threats and attacks in RIS-aided wireless network system.

- **Randomized pilot allocation:** Employ randomized pilot allocation schemes to reduce the likelihood of pilot contamination by dynamically assigning pilot sequences to users.
- **Pilot decontamination techniques:**Utilize advanced signal processing techniques such as pilot decontamination algorithms to mitigate the effects of pilot contamination.
- **Secure RIS control:** Implement secure control mechanisms to prevent malicious entities from unauthorized manipulating RIS phase shifts and configurations.
- **Physical layer security:** Utilize physical layer security techniques such as artificial noise injection to protect pilot signals from eavesdropping and tampering.

11.4.2 Pilot Spoofing Attack

Pilot spoofing can be particularly detrimental in an RIS network due to the complex interactions between the RIS elements and user equipment. Attackers generate fake pilot signals or alter existing ones to mislead receivers about channel conditions or user identities. This type of attack can severely disrupt communication protocols and compromise network performance [42]. Also, it can exploit the reconfigurable nature of RIS elements to manipulate the propagation environment and amplify the effects of pilot spoofing. Furthermore altering the phase shifts of RIS elements, attackers can enhance the propagation of spoofed pilot

signals and make them appear more authentic to receivers. A pilot spoofing attack involves engaging in active eavesdropping by deploying indistinguishable training sequences to manipulate channel estimation during the pilot training sequence, potentially resulting in unauthorized access to or interception of intended data. Although this necessitates detailed knowledge of the pilot sequence, using random sequences can aid in detecting such attacks. The emergence of RISs and real-time programmable features in wireless channels creates possibilities for conducting pilot spoofing more efficiently. Through embedding RIS control methods seamlessly into communication protocols, malicious individuals can manipulate wireless channels, potentially introducing threats such as the obliteration of the interchange between uplink and downlink channels, thus posing additional risks to legitimate communication. Moreover, the RIS adds complexity to the communication channel, exacerbating the impact of pilot spoofing and making it harder to detect and mitigate fake signals. Countermeasures for pilot spoofing attacks:

- Mitigating pilot spoofing attacks in RIS networks requires a multifaceted approach.
- Techniques such as robust authentication mechanisms, secure channel estimation algorithms, and anomaly detection methods can help identify and mitigate spoofed pilot signals.
- Additionally, implementing encryption and authentication protocols for pilot signals can enhance the security of RIS networks and protect against spoofing attacks.

11.4.3 Jamming Attack

Cooperative jamming serves as a strategic approach to counter eavesdropping and jamming attacks to bolster communication security. This technique involves the transmission of information signals by the primary station to authorized users while concurrently emitting a jamming signal by a relay node to disrupt the communication channel. Unlike traditional jamming methods, cooperative relaying or jamming enhances network security by creating a secure connection between end nodes [43]. Common cooperative relaying strategies include decode-and-forward and amplify-and-forward. These methods effectively mitigate the impact of eavesdropping and jamming attacks, thus reinforcing the overall security of the communication network. Furthermore, RIS can dynamically adjust the phase and amplitude of its reflecting elements to create focused beams toward the LR while simultaneously steering nulls toward the jamming source. Mitigation strategies for jamming attack:

- The dynamical adaptation of the beamforming pattern, pattern allows RIS to effectively mitigate the effects of the jamming signal.

- Additionally, intelligent algorithms integrated within the RIS network can detect patterns or anomalies indicative of jamming signals. Upon detection, the RIS can dynamically reconfigure its reflecting elements to counteract the jamming signal or inform the communication system to adjust its transmission strategy accordingly.
- Through intelligently manipulating the phase and amplitude of the reflecting elements, the RIS can create destructive interference at the receiver's location, effectively neutralizing the jamming signal.
- Employing frequency hopping or spread spectrum techniques with RIS can make it more challenging for jammers to disrupt communication. Meanwhile, by spreading the signal over multiple frequencies or rapidly switching between frequencies, the impact of jamming can be reduced, as the jammer would need to target a broader spectrum.

11.4.4 Environment Reconfiguration Attack

The ERA represents a novel form of jamming attack on modern wireless networks. Unlike traditional jamming techniques involving actively emitting jamming signals, ERA leverages an RIS to rapidly manipulate the electromagnetic propagation environment. By exploiting the RIS, adversaries can swiftly alter the environment in a way that disrupts legitimate communications for legitimate receivers (LRs). The key advantage of ERA lies in its utilization of the RIS to reflect existing legitimate signals, granting the adversary significant leverage over conventional jamming methods. This approach obviates the need for the adversary to emit jamming signals actively, thereby reducing the risk of detection while still achieving disruption of wireless communications. In [44], the authors proposed an innovative approach to investigate the effectiveness of ERA using orthogonal frequency division multiplexing (OFDM) modulation. They also introduced an optimization algorithm aimed at enhancing the jamming effectiveness of ERA, which can have significant practical applications. The research findings showed that even a small RIS could significantly degrade the data rates in the wireless network. This suggests that ERA poses a considerable threat to wireless communication systems, as it can cause substantial degradation in performance with minimal resources. The utilization of OFDM modulation in this context likely allowed for a detailed analysis of the attack's impact on communication quality and throughput, given OFDM's widespread use in modern wireless communication systems.

11.4.5 Manipulation Attack

The author Alakoca et al. [45] has proposed a new method called the RIS-aided manipulation attack, which aims to improve the security of wireless communication systems by reducing the key generation rate. In this scenario, Eve utilizes

a technique that involves quickly altering the phase of the RIS to exert control over the wireless environment. The frequency response coefficient likely served as a metric to gauge the impact of the manipulated wireless environment on the critical generation process, allowing for a detailed analysis of the attack's effectiveness. This study sheds light on the potential security risks of emerging wireless technologies by exploring how RIS can manipulate the wireless environment. The findings can help guide the future development of more secure wireless communication systems. It underscores the need for robust security measures to mitigate the impact of such attacks on key generation processes and overall network security. The author Acharjee and Chattopadhyay [46] proposed a slewing rate detection process based on path separation to counter RIS-enabled manipulation attacks and reduce the critical generation rate in wireless communication systems. This process involves identifying and separating the affected path in the time domain. A flexible quantization method is then implemented to speed up key generation. Simulation results demonstrated successful detection of the attacked path. The authors recognized that their process requires further refinement and improvement in future studies. This implies that while the initial results are encouraging, there is room for enhancement and optimization to strengthen the effectiveness of the proposed countermeasure. The introduction of this countermeasure highlights the ongoing efforts in the research community to develop robust defense mechanisms against emerging threats in wireless communication security, such as manipulation attacks facilitated by RIS. Continued research and refinement of such techniques are crucial to ensuring the resilience and security of wireless communication systems against evolving attack vectors.

11.4.6 Signal Leakage and Interference Attack

In the study, author Wang et al. [47] introduced the concept of an illegal reconfigurable intelligent surface (IRIS), which involves the unauthorized or malicious use of an RIS. The authors conducted an investigation to address the security concerns raised by the deployment of IRIS, with a particular focus on interference and signal leakage. Their findings could help mitigate potential security risks and ensure a safe and effective deployment of IRIS technology. Interference refers to the disruption or degradation of legitimate wireless communications caused by the presence of the IRIS. This could result from the IRIS's intentional manipulation of the electromagnetic environment to interfere with authorized transmissions. Signal leakage involves the unintentional or unauthorized transmission of signals by the IRIS, which could lead to privacy breaches or unauthorized access to sensitive information. This leakage could occur due to improper configuration or control of the IRIS, allowing signals to be transmitted beyond intended boundaries. Through examining these security issues associated with the presence of an IRIS, the author

sheds light on the potential risks and vulnerabilities introduced by unauthorized manipulation of RIS technology in wireless communication systems. Addressing these security concerns is crucial to safeguarding the integrity, confidentiality, and reliability of wireless communications in the presence of such threats. Signal leakage, in the context of an IRIS, refers to a scenario where the IRIS is exploited by an EAV to enhance the data rate of eavesdropped transmissions and improve the amount of data leaked to the EAV [48]. Unlike traditional wireless systems, where an IRIS can reflect environmental signals, in this scenario, the EAV utilizes the IRIS to reflect the environmental signal and collect transmission signals that were not received earlier. Passively enhancing the communication quality of illegal links and degrading the performance of primary legitimate systems without emitting additional radio frequency (RF) signals, the IRIS facilitates signal leakage, making it challenging to detect and prevent. The ability of an EAV to wiretap can be improved by capturing more legal signals leaked from the access point. This is the main focus of signal leakage. This differs from RIS-based jamming, which involves reducing the signal power received by the LU through the destructive addition of signals from the RIS and access point. While both techniques involve manipulation of the wireless environment through the use of RIS, their objectives and effects on communication differ significantly [49]. The use of RISs for improving physical layer security performance poses challenges in achieving satisfactory system performance due to the legitimate system's need for more control over IRIS-aided interference links. Mitigating interference from IRIS is nearly impossible, which can severely impede channel estimation and data transmission processes.

11.4.7 Unauthorized Access and Attacks on RIS Controller

The susceptibility of RISs to various incident signals from different network nodes, including those generated and transmitted by malicious users, underscores the importance of implementing proper identification systems for RISs within a network. Malicious signals transmitted to LUs via RISs without such identification systems can significantly impact decision-making processes. For instance, consider a scenario where false information about traffic is transmitted to an ambulance via an RIS. This misinformation could lead to delays or inappropriate routing decisions, potentially worsening the patient's condition. Similarly, in a tactical network, unauthorized personnel using RISs could complicate tactical situations by transmitting misleading or disruptive signals [50]. Implementing robust identification and authentication mechanisms for RISs within a network is crucial to mitigate the risk of unauthorized access and manipulation. Through ensuring the authorized entities can control and interact with RISs, the network can enhance its resilience against malicious attacks and unauthorized interference,

safeguarding the integrity and reliability of communications and decision-making processes. Indeed, intruders can target the tunable chips of RISs as another avenue for attack. These chips play a crucial role in RISs by allowing the reconfiguration of signal phase and amplitude, thereby influencing the propagation of signals to their intended destinations. The objective of the adversary is to manipulate tunable chips' parameters to divert information-carrying signals from their original path. Through altering the phase and amplitude of signals using compromised tunable chips, the attacker can disrupt communication links, degrade signal quality, or even redirect sensitive information to unintended destinations. Protecting the integrity and security of tunable chips within RISs is essential for ensuring the reliability and confidentiality of wireless communication systems. Implementing robust authentication, encryption, and tamper-resistant measures can help mitigate the risk of unauthorized access and manipulation of these critical components. Continuous monitoring and detection mechanisms can also help identify and promptly respond to potential attacks on tunable chips.

11.5 Secure Physical Layer Networks for RIS-Assisted System

The research on security threats related to RISs is indeed still in its early stages, and only a few studies have focused on addressing potential countermeasures for these threats. However, the importance of understanding and mitigating these security risks is becoming increasingly recognized as RIS technology gains traction in wireless communication systems.

11.5.1 RIS-Assisted Wireless Network

The author Mei and Zhang [51] utilized a semi-definite programming relaxation technique to demonstrate cooperative beamforming and jamming in the presence of EAVs with imperfect CSI. The objective was to maximize energy efficiency (EE) in such scenarios. The proposed technique improved EE even when the CSI was imperfect, enhancing the robustness of cooperative jamming and beamforming systems against eavesdropping attacks. In [52], an optimization algorithm was presented for RIS phase shift and beamforming design in wireless networks. The optimization framework aimed to maximize the secrecy rate, which denotes the rate at which confidential data can be transmitted, even in the presence of EAVs [53]. The simulation results obtained from this study indicate that the proposed model has successfully achieved a higher secrecy rate. Thus, indicating improved security and confidentiality in communication, even in the presence of EAVs. This underscores the potential of RIS technology to improve the security

of wireless communication systems by mitigating eavesdropping threats through intelligent signal manipulation. These studies highlight the ongoing efforts in the research community to develop advanced techniques and algorithms for improving the security and performance of RIS-enabled wireless communication systems, particularly in challenging scenarios involving EAVs and imperfect CSI. The author Do et al. [54] introduced an Alternating optimization technique to enhance the secrecy rate in a downlink multiple-input single-output broadcast network with multiple EAVs. The proposed technique achieved a higher secrecy rate while enhancing the physical layer security. Using RISs in such scenarios can improve the security and confidentiality of wireless communications by mitigating the impact of EAVs. In another study [55], a combination of semidefinite programming relaxation and policy gradient descent techniques was proposed to achieve a higher secrecy rate while minimizing transmission power in a RIS–MISO model. Simulations were conducted under both rank-one and rank–rank channel scenarios, and the results indicated improvements in physical layer security performance, transmission power efficiency, and secrecy rate. This study suggests that leveraging RIS technology can enhance the efficiency and security of wireless communication systems, particularly in scenarios where secrecy and reliability are paramount. Overall, these studies demonstrate the potential of advanced optimization techniques and algorithms to exploit the capabilities of RISs in improving the security and performance of wireless networks, especially in the presence of EAVs and practical constraints. Continued research in this area is essential for further refining and validating these techniques, ultimately contributing to developing more robust and secure wireless communication systems.

11.5.2 RIS-Aided ISAC

In ISAC networks, the transmitted signal typically contains both sensing and communication signals, which potential intruders can intercept [55]. This introduces security concerns, as unauthorized interception of these signals can compromise the confidentiality, integrity, and reliability of the communication and sensing processes in the network. Addressing the interception threat in ISAC networks requires the development of robust security mechanisms and protocols to safeguard transmitted signals from unauthorized access and manipulation. Techniques such as encryption, authentication, and intrusion detection can help mitigate the risk of signal interception and ensure the confidentiality and integrity of communication and sensing data. Through addressing the security challenges associated with signal interception in ISAC networks, the deployment of RISs can realize their full potential in enhancing network capacity and target sensing capability while maintaining the security and privacy of transmitted information.

Continued research and development efforts in this area are essential to ensure the resilience and security of ISAC networks in real-world deployment scenarios. The work in [12] is notable for developing a physical layer security network framework by employing Artificial Noise at the transmitting nodes. The authors formulated an optimization problem as fractional programming to simultaneously minimize the SINR at radar targets and maximize the secrecy rate in the ISAC network. The numerical results of this study demonstrated that the proposed framework achieved the highest secrecy rate. However, it is essential to note that the model assumed perfect CSI and precise knowledge of the target location at the BS. This assumption cannot hold in practical scenarios, particularly in the presence of RISs, which can introduce additional complexities and challenges. RISs in ISAC networks can impact the propagation environment and introduce uncertainties in CSI estimation and target localization. As a result, traditional physical layer security techniques developed for conventional ISAC networks cannot directly apply in the presence of RISs. Addressing these challenges requires developing new physical layer security techniques that account for the unique characteristics and capabilities of RISs. This study can incorporate advanced signal processing algorithms, adaptive modulation and coding schemes, and robust optimization frameworks that can adapt to varying environmental conditions and uncertainties in CSI and target localization.

11.5.3 RIS-Assisted Non-Terrestrial Network

In the context of next-generation communication networks, achieving ubiquitous and user-focused connectivity for 6G networks entails orchestrating both terrestrial and non-terrestrial networks. This integration aims to leverage the unique capabilities of non-terrestrial frameworks, such as UAVs and satellites, for enhancing connectivity, coverage, and capacity. From a physical layer security perspective, addressing security challenges in non-terrestrial networks, specifically UAV and satellite communications, is crucial due to their susceptibility to various threats, including eavesdropping, jamming, spoofing, and physical attacks. Securing communications in these networks is essential to protect sensitive information, ensure confidentiality, integrity, and availability of data, and maintain the overall reliability and resilience of the network.

i. **UAV networks**: In this study, Khalili et al. [56] introduced an iterative method for resilient design, aiming to optimize the flight path of UAVs and the phase adjustment of RIS in the presence of an EAV. The framework involving UAVs aided by RIS resulted in an enhanced secrecy rate during transmission, thereby bolstering security at the physical layer. This approach highlights the potential of integrating RISs and UAVs to boost the security and performance of wireless communication frameworks, particularly in scenarios where eavesdropping

threats are prevalent. Similarly, the author in [56] presented three algorithms: S-procedure, sequential convex approximation, and semidefinite relaxation aimed at improving physical layer security and secrecy rate in the network. These algorithms enhance the efficiency of users' transmitting power, manipulation of RIS beamforming, and the flight path of UAVs while accounting for the presence of EAVs amidst imperfect CSI. The proposed techniques provide robust solutions for optimizing system parameters to mitigate eavesdropping threats and enhance communication security in wireless networks.

Furthermore, the researchers in [57] introduced a convex approximation method to optimize the manipulation of RIS phase shifts and the flight paths of UAVs amidst the existence of EAVs. This approach leverages convex optimization techniques to optimize RIS phase shifts and UAV trajectories efficiently, thereby improving communication security and performance in the presence of EAVs. These studies highlight the importance of developing advanced optimization techniques and algorithms to enhance physical layer security and secrecy rate in wireless communication networks, particularly in scenarios involving UAVs, RISs, and EAVs. By leveraging these techniques, optimizing system parameters effectively and mitigating security risks is possible, thereby ensuring the confidentiality and integrity of wireless communication systems.

ii. **Satellite networks:** The author in [58] devised an alternating optimization method to reduce the SINR at the EAV while maintaining dependable signal strength for both satellite and terrestrial network users. Decreasing the SINR at the EAV constrains the maximum interference experienced by the satellite user, thereby ensuring dependable communication for users in the terrestrial network. Simulation results from this study demonstrated a higher secrecy gain and a significant reduction in the SINR at the EAV, highlighting the effectiveness of the proposed technique in enhancing security and reliability in satellite communication systems.

In a separate investigation concerning the incorporation of RISs into the space-air-ground-integrated network (SAGIN), the authors Chen et al. [59] observed that integrating RISs with SAGIN could result in notable enhancements in connectivity, wireless coverage, and physical layer security. By deploying RISs strategically within the SAGIN infrastructure, it becomes feasible to improve signal propagation, alleviate interference, and improve the overall performance of the network. This integration of RISs with SAGIN offers promising opportunities for optimizing network resources, enhancing communication security, and enabling various applications and services in diverse environments. Overall, the studies conducted by these authors underscore the importance of advanced optimization techniques and innovative network architectures in improving security, reliability, and performance in satellite communication systems and integrated network environments.

11.5.4 RIS-Assisted Covert Communication

The author in [60] introduced a penalty successive convex approximation (PSCA) algorithm for designing the RIS reflecting coefficient and transmit power in covert communication scenarios. This algorithm was designed to optimize RIS parameters while considering the lack of Willie's instantaneous CSI and global CSI, which are typically required for covert communication techniques. The results showed that RIS-assisted networks have the potential to surpass conventional networks regarding covert communication. Through leveraging the PSCA algorithm to optimize RIS parameters, such as reflecting coefficients and transmit power, RIS-assisted networks can achieve improved efficacy in covert communication, surpassing traditional networks [61]. This finding underscores the capacity of RIS technology to enhance the security and confidentiality of communication systems, particularly in scenarios where covert communication is required. By intelligently manipulating the propagation environment, RISs can help mitigate the risk of eavesdropping and interception, enabling more secure and covert communication. In this research [62], a one-dimensional exploration technique was suggested to enhance the optimal reflection amplitude of RIS and the transmit power in covert networks with RIS assistance. The approach presumed the presence of statistical CSI for Willie worldwide. The computational outcomes indicated that the proposed method attained superior covert capability compared to situations where the RIS method was not utilized. This investigation underscores the efficacy of utilizing RIS technology to advance covert communication in wireless networks. Likewise, numerous additional research endeavours have introduced RIS-supported architectures for covert communication within NOMA networks [63, 64]. These frameworks aim to optimize RIS parameters, such as reflection coefficients and transmit powers, to enhance the covertness and security of communication in NOMA networks. Through intelligently manipulating the wireless propagation environment, RISs can help conceal transmitted signals and mitigate the risk of eavesdropping and interception, thereby enabling covert communication in NOMA networks.

11.6 Conclusions and Future Scope

In conclusion, the RISs technology has undeniably revolutionized wireless communication, offering unprecedented opportunities for advancement. However, its implementation raises substantial security and privacy concerns from signal manipulation and potential vulnerabilities. This research has thoroughly examined the multifaceted landscape of these issues, highlighting privacy risks, such as data leakage and surveillance, alongside security challenges, including

unauthorized access and data tampering. Addressing these concerns demands a robust strategy encompassing encryption, authentication, and regulatory compliance. Additionally, integrating physical layer security measures enhanced the confidentiality and integrity of communication, bolstering resilience against threats. While numerous challenges remain for future research, it is evident that safeguarding individual privacy and system security is essential for maximizing the transformative potential of RIS technology in wireless communication networks. Finally, this chapter offers valuable insights into the evolving landscape of RIS technology, emphasizing the need for a holistic approach to address security and privacy concerns while harnessing its transformative capabilities.

References

1 Zheng, B., You, C., Mei, W., and Zhang, R. (2022). A survey on channel estimation and practical passive beamforming design for intelligent reflecting surface aided wireless communications. *IEEE Communications Surveys & Tutorials* 24 (2): 1035–1071.

2 Özdogan, Ö., Björnson, E., and Larsson, E.G. (2019). Intelligent reflecting surfaces: physics, propagation, and pathloss modeling. *IEEE Wireless Communications Letters* 9 (5): 581–585.

3 Kumaravelu, V.B., Selvaprabhu, P., Han, D.S. et al. (2023). Blind reconfigurable intelligent surface-aided fixed non-orthogonal multiple access for intelligent vehicular networks. *EURASIP Journal on Wireless Communications and Networking* 2023 (1): 83.

4 Kumaravelu, V.B., Imoize, A.L., Castillo Soria, F.R. et al. (2023). RIS-assisted fixed NOMA: outage probability analysis and transmit power optimization. *Future Internet* 15 (8): 249.

5 Pan, C., Ren, H., Wang, K. et al. (2020). Intelligent reflecting surface aided MIMO broadcasting for simultaneous wireless information and power transfer. *IEEE Journal on Selected Areas in Communications* 38 (8): 1719–1734.

6 Ning, B., Chen, Z., Chen, W. et al. (2021). Terahertz multi-user massive MIMO with intelligent reflecting surface: beam training and hybrid beamforming. *IEEE Transactions on Vehicular Technology* 70 (2): 1376–1393.

7 Lin, T., Yu, X., Zhu, Y., and Schober, R. (2022). Channel estimation for IRS-assisted millimeter-wave MIMO systems: sparsity-inspired approaches. *IEEE Transactions on Communications* 70 (6): 4078–4092.

8 Ni, Y., Liu, Y., Wang, J. et al. (2021). Performance analysis for RIS-assisted D2D communication under Nakagami-m fading. *IEEE Transactions on Vehicular Technology* 70 (6): 5865–5879.

9 Wang, R., Wen, X., Xu, F. et al. (2023). Joint particle swarm optimization of power and phase shift for IRS-aided D2D underlaying cellular systems. *Sensors* 23 (11): 5266.

10 Jiao, S., Fang, F., Zhou, X., and Zhang, H. (2020). Joint beamforming and phase shift design in downlink UAV networks with IRS-assisted NOMA. *Journal of Communications and Information Networks* 5 (2): 138–149.

11 Hong, S., Pan, C., Ren, H. et al. (2020). Artificial-noise-aided secure MIMO wireless communications via intelligent reflecting surface. *IEEE Transactions on Communications* 68 (12): 7851–7866.

12 Yang, X., Wei, Z., Liu, Y. et al. (2024). RIS-assisted cooperative multicell ISAC systems: a multi-user and multi-target case. *IEEE Transactions on Wireless Communications* 23 (8): 8683–8699.

13 Das, S.K., Benkhelifa, F., Sun, Y. et al. (2023). Comprehensive review on ML-based RIS-enhanced IoT systems: basics, research progress and future challenges. *Computer Networks* 224: 109581.

14 Hossain, T., Shabab, S., Badrudduza, A.S.M. et al. (2022). On the physical layer security performance over RIS-aided dual-hop RF-UOWC mixed network. *IEEE Transactions on Vehicular Technology* 72 (2): 2246–2257.

15 Kaveh, M., Yan, Z., and Jäntti, R. (2023). Secrecy performance analysis of RIS-aided smart grid communications. *IEEE Transactions on Industrial Informatics* 20 (4): 5415–5427.

16 Lin, S., Zou, Y., Li, B., and Wu, T. (2022). Security-reliability trade-off analysis of RIS-aided multiuser communications. *IEEE Transactions on Vehicular Technology* 72 (5): 6225–6237.

17 Porambage, P., Gür, G., Osorio, D.P.M. et al. (2021). The roadmap to 6G security and privacy. *IEEE Open Journal of the Communications Society* 2: 1094–1122.

18 Khalid, W., Rehman, M.A.U., Van Chien, T. et al. (2023). Reconfigurable intelligent surface for physical layer security in 6G-IoT: designs, issues, and advances. *IEEE Internet of Things Journal* 11 (2): 3599–3613.

19 Imoize, A.L., Obakhena, H.I., Anyasi, F.I. et al. (2022). Reconfigurable intelligent surfaces enabling 6G wireless communication systems: use cases and technical considerations. *2022 5th Information Technology for Education and Development (ITED)*, 1–7. IEEE.

20 Tang, W., Dai, J.Y., Chen, M.Z. et al. (2020). Design and implementation of MIMO transmission through reconfigurable intelligent surface. *2020 IEEE 21st International Workshop on Signal Processing Advances in Wireless Communications (SPAWC)*, 1–5. IEEE.

21 Li, H., Cai, W., Liu, Y. et al. (2021). Intelligent reflecting surface enhanced wideband MIMO-OFDM communications: from practical model to reflection optimization. *IEEE Transactions on Communications* 69 (7): 4807–4820.

22 Imoize, A.L., Obakhena, H.I., Anyasi, F.I. et al. (2022). Spectral efficiency bounds of cell-free massive MIMO assisted UAV cellular communication. *2022 IEEE Nigeria 4th International Conference on Disruptive Technologies for Sustainable Development (NIGERCON)*, 1–5. IEEE.

23 de Araújo, G.T., de Almeida, A.L.F., and Boyer, R. (2021). Channel estimation for intelligent reflecting surface assisted MIMO systems: a tensor modeling approach. *IEEE Journal of Selected Topics in Signal Processing* 15 (3): 789–802.

24 Dong, L. and Wang, H.-M. (2020). Secure MIMO transmission via intelligent reflecting surface. *IEEE Wireless Communications Letters* 9 (6): 787–790.

25 Li, J. and Hong, Y. (2022). Design of an intelligent reflecting surface aided mmWave massive MIMO using X-precoding. *IEEE Access* 10: 69428–69440.

26 Zhou, T., Xu, K., Xia, X. et al. (2020). Achievable rate optimization for aerial intelligent reflecting surface-aided cell-free massive MIMO system. *IEEE Access* 9: 3828–3837.

27 Nivetha, B., Selvaprabhu, P., Menon, U.V. et al. (2024). 6G vision on edge artificial intelligence. In: *Towards Wireless Heterogeneity in 6G Networks*, 127–157. CRC Press.

28 Gu, X., Zhang, G., Zhuo, B. et al. (2023). On the performance of cooperative NOMA downlink: a RIS-aided D2D perspective. *IEEE Transactions on Cognitive Communications and Networking* 9 (6): 1610–1624.

29 Sagir, B., Aydin, E., and Ilhan, H. (2023). Deep-learning-assisted IoT-based RIS for cooperative communications. *IEEE Internet of Things Journal* 10 (12): 10471–10483.

30 Baskar, N. and Selvaprabhu, P. (2023). Selective interference alignment and neutralization in coordinated multipoint using multiuser MIMO. *International Journal of Communication Systems* 36 (13): e5547.

31 Vivek, M.U. and Selvaprabhu, P. (2022). Role of telecommunication technologies in microgrids and smart grids. In: *Smart Grids and Microgrids: Technology Evolution*, 325–364. Wiley Online Library.

32 Selvaprabhu, P. (2023). An examination of distributed and decentralized systems for trustworthy control of supply chains. *IEEE Access* 11: 137025–137052.

33 Zhang, L., Wang, Y., Tao, W. et al. (2020). Intelligent reflecting surface aided MIMO cognitive radio systems. *IEEE Transactions on Vehicular Technology* 69 (10): 11445–11457.

34 Menon, V. and Selvaprabhu, P. (2022). A novel tri-staged RIA scheme for cooperative cell edge users in a multi-cellular MIMO IMAC. *IEEE Access* 10: 117141–117156.

35 Yang, Y., Gong, Y., and Wu, Y.-C. (2022). Intelligent-reflecting-surface-aided mobile edge computing with binary offloading: energy minimization for IoT devices. *IEEE Internet of Things Journal* 9 (15): 12973–12983.

36 Pogaku, A.C., Do, D.-T., Lee, B.M., and Nguyen, N.D. (2022). UAV-assisted RIS for future wireless communications: a survey on optimization and performance analysis. *IEEE Access* 10: 16320–16336.

37 Baskar, N. and Selvaprabhu, P. (2024). Performance analysis of successive di-state full-duplex cooperative wireless cellular networks. *Alexandria Engineering Journal* 91: 139–151.

38 Gong, S., Yang, Z., Xing, C. et al. (2020). Beamforming optimization for intelligent reflecting surface-aided SWIPT IoT networks relying on discrete phase shifts. *IEEE Internet of Things Journal* 8 (10): 8585–8602.

39 Rajak, S., Muniraj, I., Elumalai, K. et al. (2022). Energy efficient hybrid relay-IRS-aided wireless IoT network for 6G communications. *Electronics* 11 (12): 1900.

40 Menon, V.U. and Selvaprabhu, P. (2022). Blind interference alignment: a comprehensive survey. *International Journal of Communication Systems* 35 (8): e5116.

41 Dassanayake, J.K., Gunasinghe, D., and Baduge, G.A.A. (2023). Secrecy rate analysis and active pilot attack detection for IRS-aided massive MIMO systems. *IEEE Transactions on Information Forensics and Security* 19: 2664–2679.

42 Chai, L., Bai, T., and Bai, L. (2022). RIS-aided robust secure beamforming design against pilot spoofing attack. *2022 14th International Conference on Wireless Communications and Signal Processing (WCSP)*, 944–949. IEEE.

43 de Sena, A.S., Kibiłda, J., Mahmood, N.H. et al. (2024). Malicious RIS versus massive MIMO: securing multiple access against RIS-based jamming attacks. *IEEE Wireless Communications Letters* 13 (4): 989–993.

44 Staat, P., Elders-Boll, H., Heinrichs, M. et al. (2022). Mirror, mirror on the wall: wireless environment reconfiguration attacks based on fast software-controlled surfaces. *Proceedings of the* 2022 *ACM on Asia Conference on Computer and Communications Security*, 208–221.

45 Alakoca, H., Namdar, M., Aldirmaz-Colak, S. et al. (2022). Metasurface manipulation attacks: potential security threats of RIS-aided 6G communications. *IEEE Communications Magazine* 61 (1): 24–30.

46 Acharjee, S.S. and Chattopadhyay, A. (2022). Controller manipulation attack on reconfigurable intelligent surface aided wireless communication. *2022 IEEE International Symposium on Information Theory (ISIT)*, 1247–1252. IEEE.

47 Wang, Y., Lu, H., Zhao, D. et al. (2022). Wireless communication in the presence of illegal reconfigurable intelligent surface: signal leakage and interference attack. *IEEE Wireless Communications* 29 (3): 131–138.

48 Elhoushy, S., Ibrahim, M., and Hamouda, W. (2021). Exploiting RIS for limiting information leakage to active eavesdropper in cell-free massive MIMO. *IEEE Wireless Communications Letters* 11 (3): 443–447.

49 Salem, A., Wong, K.-K., and Chae, C.-B. (2023). Impact of phase-shift error on the secrecy performance of uplink RIS communication systems. *IEEE Transactions on Wireless Communications* 23 (7): 7376–7391.

50 Hu, L., Li, G., Luo, H., and Hu, A. (2021). On the RIS manipulating attack and its countermeasures in physical-layer key generation. *2021 IEEE 94th Vehicular Technology Conference (VTC2021-Fall)*, 1–5. IEEE.

51 Mei, W. and Zhang, R. (2021). Multi-beam multi-hop routing for intelligent reflecting surfaces aided massive MIMO. *IEEE Transactions on Wireless Communications* 21 (3): 1897–1912.

52 Wang, Z., Liu, L., Zhang, S., and Cui, S. (2022). Massive MIMO communication with intelligent reflecting surface. *IEEE Transactions on Wireless Communications* 22 (4): 2566–2582.

53 Song, W., Rajak, S., Dang, S. et al. (2022). Deep learning enabled IRS for 6G intelligent transportation systems: a comprehensive study. *IEEE Transactions on Intelligent Transportation Systems* 24 (11): 12973–12990.

54 Do, H., Lee, N., and Lozano, A. (2022). Line-of-sight MIMO via intelligent reflecting surface. *IEEE Transactions on Wireless Communications* 22 (6): 4215–4231.

55 Chen, X., Shi, J., Yang, Z., and Wu, L. (2021). Low-complexity channel estimation for intelligent reflecting surface-enhanced massive MIMO. *IEEE Wireless Communications Letters* 10 (5): 996–1000.

56 Khalili, A., Monfared, E.M., Zargari, S. et al. (2021). Resource management for transmit power minimization in UAV-assisted RIS HetNets supported by dual connectivity. *IEEE Transactions on Wireless Communications* 21 (3): 1806–1822.

57 Liu, X., Liu, Y., and Chen, Y. (2020). Machine learning empowered trajectory and passive beamforming design in UAV-RIS wireless networks. *IEEE Journal on Selected Areas in Communications* 39 (7): 2042–2055.

58 Ren, H., Zhang, Z., Peng, Z. et al. (2022). Energy minimization in RIS-assisted UAV-enabled wireless power transfer systems. *IEEE Internet of Things Journal* 10 (7): 5794–5809.

59 Chen, C.-W., Tsai, W.-C., Wong, S.-S. et al. (2022). WMMSE-based alternating optimization for low-complexity multi-IRS MIMO communication. *IEEE Transactions on Vehicular Technology* 71 (10): 11234–11239.

60 Liu, Q., Fu, M., Li, W. et al. (2022). RIS assisted ambient backscatter communication for SAGIN IoT. *IEEE Internet of Things Journal* 10 (11): 9375–9384.

61 Cao, Y., Lv, T., and Ni, W. (2022). Two-timescale optimization for intelligent reflecting surface-assisted MIMO transmission in fast-changing channels. *IEEE Transactions on Wireless Communications* 21 (12): 10424–10437.

62 Jiang, H., Ruan, C., Zhang, Z. et al. (2021). A general wideband non-stationary stochastic channel model for intelligent reflecting surface-assisted MIMO

communications. *IEEE Transactions on Wireless Communications* 20 (8): 5314–5328.

63 Chen, X., Zheng, T.-X., Dong, L. et al. (2021). Enhancing MIMO covert communications via intelligent reflecting surface. *IEEE Wireless Communications Letters* 11 (1): 33–37.

64 Pan, C., Ren, H., Wang, K. et al. (2020). Multicell MIMO communications relying on intelligent reflecting surfaces. *IEEE Transactions on Wireless Communications* 19 (8): 5218–5233.

12

AI and ML Techniques for Intelligent Power Control in RIS-Empowered Wireless Communication Systems

Ammar Summaq[1], Mukkara Prasanna Kumar[1], Sunil Chinnadurai[1], Poongundran Selvaprabhu[2], Vinoth Babu Kumaravelu[2], and Agbotiname Lucky Imoize[3,4]

[1] *Department of Electronics and Communication Engineering, School of Engineering and Sciences, SRM University-AP, India*
[2] *Department of Communication Engineering, School of Electronics Engineering, Vellore Institute of Technology, Vellore, Tamil Nadu, India*
[3] *Department of Electrical and Electronics Engineering, Faculty of Engineering, University of Lagos, Lagos, Akoka, Nigeria*
[4] *Department of Electrical Engineering and Information Technology, Ruhr University, Bochum, Germany*

12.1 Introduction

Reinforcement learning (RL) and its extension, DRL, utilize deep neural networks (DNN) to address decision-making tasks in dynamic environments. DRL focuses on long-term objectives and consists of two main components: the agent and the environment, which interact to generate control actions [1]. DRL methods like deep Q-networks (DQN), Actor-Critic (A3C), and deep proximal policy optimization (DPPO) are effective for handling high-dimensional problems but encounter challenges in dealing with complex objective functions [2]. Various approaches exist to tackle power allocation and control problems, including optimized performance, game theory, and machine learning [3]. Optimization-based algorithms, such as a difference of convex programming and Lagrangian multiplier, have been explored to address these challenges [4]. DRL methods, such as DQN, A3C, and DPPO, utilize policy or DNN approximation functions to learn effective policies by maximizing rewards during environmental interactions [5]. However, handling the complex objective functions involved in DRL remains challenging, necessitating investigation into optimization algorithms like stochastic gradient descent, RMSprop, and Adam [6]. Resource management problems in wireless communication, including caching, transmission scheduling, spectrum access,

Reconfigurable Intelligent Surfaces for 6G and Beyond Wireless Networks, First Edition.
Edited by Agbotiname Lucky Imoize, Vinoth Babu Kumaravelu, and Dinh-Thuan Do.

and power management, are often modeled as Markov decision processes (MDPs) [7]. DRL approaches, such as DQN and DL transmission scheduling mechanisms, have been proposed to address these issues [8–10]. Despite advances in DRL-based resource management research, ongoing and high-dimensional challenges continue to exist in wireless communication networks. To address this, DRL algorithms based on the actor–critic framework, such as A3C and DPPO, have been proposed for power control in continuous domains, aiming to improve network convergence [11]. In the realm of power control in wireless communication systems, DRL algorithms optimize transmit power levels to adapt to dynamic environmental conditions, interference, and user demands. Notable DRL algorithms like DQN approximate the optimal action-value function using DNNs, facilitating effective policy learning through iterative updates based on interactions with the environment [12]. However, several challenges remain for DRL algorithms in power control within wireless communication systems:

- **Complexity of the environment:** Wireless communication environments are intricate, with factors like varying channel conditions, interference, and device mobility. Designing DRL algorithms capable of effective learning in such dynamic and uncertain environments remains challenging.
- **High-dimensional state and action spaces:** State and action spaces in wireless systems can be extensive, encompassing information about channel conditions, traffic load, and interference levels. Training DRL algorithms to navigate these high-dimensional spaces efficiently demands sophisticated exploration strategies.
- **Non-stationarity:** Wireless environments exhibit non-stationarity, with characteristics changing over time due to user behavior and network topology shifts. Adapting DRL algorithms to handle these changes and continuously update policies in real time poses a significant challenge.
- **Sample efficiency:** Training DRL algorithms for power control typically requires collecting many samples from environmental interactions. Improving sample efficiency to learn effective power control policies with limited data is crucial for practical deployment in wireless communication systems.
- **Generalization and robustness:** DRL algorithms must generalize well across diverse scenarios and remain robust to environmental variations. Ensuring the transferability and applicability of learned policies across different real-world settings remains a critical challenge.

Addressing these challenges necessitates advancements in algorithmic techniques, training methodologies, and realistic simulation environments that accurately capture the complexities of wireless communication systems. Leveraging domain knowledge and incorporating expert guidance into DRL algorithms

can enhance their performance and durability in real-world scenarios. This chapter explores a proposed methodology to tackle these challenges through cooperative deep reinforcement learning (DRL) systems.

12.1.1 Motivation of the Chapter

RL and its advanced form, DRL, offer powerful approaches to decision-making in complex environments. Particularly in time-variant dynamic systems, DRL's ability to handle high-dimensional state and action spaces makes it well-suited for generating efficient control actions. In wireless communication systems, DRL algorithms like DQN can optimize transmit power levels, responding to dynamic environmental conditions and user demands. Despite their potential, DRL algorithms face challenges like complex environments, high-dimensional state spaces, non-stationary, sample efficiency, and robustness. Addressing these challenges requires advancements in algorithms, training methodologies, and realistic simulation environments, leading to more effective power control strategies in wireless communication systems.

12.1.2 Objectives and Contributions of the Chapter

This chapter explores the transformative potential of leveraging AI and Machine Learning (ML) techniques, specifically DRL, to enhance the performance of RIS-empowered wireless communication systems, with a primary focus on power control objectives. **The key contributions of this chapter endeavor include:**

- **Innovative methodologies:** Introducing novel methodologies that harness DRL algorithms, we will mention in the future as **Deep Reinforcement Learning Master and Slave DRL (M-S)** to optimize RIS configurations for effective power control.
- **Real-time adaptability:** Recognizing the critical importance of achieving real-time accuracy, the chapter proposes AI and ML-based approaches to overcome the challenges of dynamic wireless environments.
- **Efficiency enhancement:** By integrating AI and ML techniques, the chapter aims to enhance the efficiency and adaptability of RIS-integrated wireless systems, particularly in terms of power control objectives. This includes minimizing energy consumption while maximizing EE through intelligent transmit power adjustments.
- **Interdisciplinary collaboration:** This chapter bridges the domains of wireless communication, AI, and ML. It highlights the significance of collaborative efforts in developing innovative solutions to address the evolving demands of wireless networks.

12.1.3 Chapter Organization

The rest of this chapter is organized as follows: Section 12.1 provides an introduction to the convergence of RIS technology, AI, and ML in wireless communication systems, with a focus on power control objectives. Section 12.2 reviews existing literature on RIS technology, AI, and ML applications in wireless communication, identifying research gaps. In Section 12.3, RL algorithms for RIS-assisted scenarios are explored, discussing how DRL trains agents for sequential decision-making. Section 12.4 elaborates on the methodology for enhancing RIS design using ML for power control, including algorithmic frameworks and practical implementations. Following the methodology, Section 12.5 presents the results and analysis, detailing the outcomes of applying DRL-M algorithms for RIS optimization with a focus on optimization joint beamforming and phase shift for maximize the sum rate with discussions on performance metrics and real-world implications. Subsequently, Section 12.6 delves into the limitations encountered during the survey process. Section 12.7 discusses critical lessons learned from the survey, highlighting insights with implications for future research and practice. Finally, Section 12.8 provides the conclusion and future scope, summarizing expected benefits, addressing challenges and limitations, and outlining future research directions in advancing RIS-enabled wireless communication systems, particularly concerning power control objectives. Through this structured approach, the chapter aims to offer original insights and practical solutions for advancing RIS-enabled wireless communication systems, particularly in the realm of power control.

12.2 Related Work

This section represents a subset of the research efforts aimed at AI and ML techniques for intelligent power control in RIS-empowered wireless communication systems. It offers valuable insights into the challenges and potential solutions in this emerging area of research. In this study [13], a practical model for RIS phase shift is introduced, combining reflection amplitude and phase shift to optimize the sum rate in an RIS-assisted multiple input single output (MISO) interference channel scenario. Leveraging DRL, the proposed algorithm effectively configures digital beamforming and analogy phase shift matrices, outperforming benchmark schemes regarding achievable sum rate. Addressing performance bottlenecks in orthogonal frequency division multiplexing (OFDM) systems, another paper [14] proposes intelligent resource allocation through RL

in RIS-enhanced setups. By jointly optimizing subcarrier allocation, base station beamforming, and Intelligent Reconfigurable Surfaces (IRS) phase shift, the proposed scheme, combining DQN and DDPG, achieves significant transmission rate improvements over benchmark schemes, with considerations for spectrum sharing. Furthermore, a novel approach to multi-cell power allocation is explored in [15], utilizing DRL to maximize overall network capacity. Introducing a wireless resource mapping method and a deep-Q-full-connected-network (DQFCNet), this approach outperforms traditional methods like water-filling and Q-learning, exhibiting faster convergence and improved stability in simulations. Another paper [16] presents a multi-hierarchical interpretable strategy for power system dispatch and operation using the graph deep Q-network (GDQN) model. By combining an improved sample-balanced deep Shapley additive explanation (SE-DSHAP) approach with a subgraph explainer, this approach provides intuitive and comprehensive explanations for decision-making in complex power systems, aiding operators in achieving efficient and accurate control. Finally, Xu et al. [17] proposes a hierarchical depth deterministic strategy gradient (H-DDPG) framework for resource allocation in downlink CF-mMIMO systems, optimizing AP clustering and power allocation. Operating on different timescales, the framework cooperatively enhances EE by utilizing two-layer control networks, with numerical results demonstrating improvements in convergence speed, spectral efficiency (SE), and EE. Furthermore, the research presented in [18] focuses on mobile edge computing (MEC), which enables offloading computation tasks from mobile devices to edge servers, which is vital for latency-sensitive applications. Despite challenges from communication links, reconfigurable intelligent surfaces (RISs) show promise in enhancing network capabilities. This chapter presents a novel computation offloading algorithm for RIS-empowered MEC networks, optimizing delay, energy consumption, and operator costs through an MDP and deep deterministic policy gradient (DDPG), yielding significant performance improvements over traditional methods. Building upon the research in [19] introduces a DRL method to enhance secrecy energy efficiency (SEE) in B5G mobile systems employing RIS. Through joint optimization of phase shifts, orientations, beamforming, and RIS locations using the advantage actor-critic (A2C) algorithm, the proposed approach significantly boosts SEE, showcasing its efficacy for future RIS-enabled communication systems. In a related study [20], the authors explore a RIS-assisted secure symbiosis radio (SR) network, where the RIS acts as a secondary transmitter to ensure primary transmitter (PTx) security while transmitting its information. By jointly optimizing PTx beamforming and RIS phase shifts using proximal policy optimization (PPO), significant secrecy EE gains (up to 22%) are achieved against eavesdroppers, demonstrating the

efficacy of the proposed approach for robust and secure communication in practical scenarios. The paper in [21], a symbiotic RIS-assisted MEC system that optimizes user offloading, HAP beamforming, and RIS beamforming jointly is examined to minimize hybrid access point (HAP) energy consumption. It presents a framework called optimization-driven hierarchical deep deterministic policy gradient (OH–DDPG) demonstrating substantial performance improvements compared to conventional methods in reducing overall energy consumption and enhancing learning efficiency and reliability. The study in [22] delves into a multi-RIS-assisted integrated satellite-unmanned aerial vehicle-terrestrial network (IS-UAV-TN) system, tackling transmission path obstacles and dynamic unmanned aerial vehicles (UAVs) communication challenges. By deploying RIS on UAV and leveraging non-orthogonal multiple access (NOMA) protocols, a multi-objective optimization problem is devised to minimize UAV energy consumption and maximize system rate addressed through a DDPG-based algorithm for online trajectory control. Simulation results underscore the efficacy of RIS and multi-UAV co-optimization in enhancing system performance and communication tasks in IS-UAV-TNs. The authors in [23] present a wireless-powered sensor network coordinated by a multi-antenna access point (AP), aiming to minimize average age-of-information (AoI) through joint node scheduling and transmission control strategies. By leveraging an RIS to enhance channel conditions, a hierarchical DRL framework optimizes AoI, showing significant reduction and controllable fairness among sensor nodes. Finally, the work in [24] explores sub-connected active RIS-assisted communication systems under imperfect Channel State Information (CSI) to maximize EE through joint optimization of transmit precoders and RIS beamforming matrices using DRL-based methods like DDPG, PPO, and modified PPO. It demonstrates improved convergence and robustness compared to traditional techniques and analyzes system parameters' impact on performance. In Table 12.1, we present a comprehensive summary of recent research efforts focusing on AI and ML techniques for intelligent power control in RIS-empowered wireless communication systems. Each paper listed in the table addresses specific objectives related to optimization, resource allocation, and system performance improvement using various methodologies, including DRL and optimization algorithms. This table provides valuable insights into the advancements made in this field and serves as a basis for identifying gaps and opportunities for further research.

Table 12.2 presents a summary of related literature on AI and ML Techniques in RIS-Empowered wireless communication systems. The contribution and limitations are presented briefly.

Table 12.1 Research efforts on AI and ML techniques.

Paper	Objective	Method	Results
[13]	Develop a deep learning approach to improve channel estimation efficiency	DL-based predictive beamforming (DLPB) algorithm Proposed LA-CLNet and ICSI-aware fully connected neural network (IA-FNN) for predictive beamforming and transmit beamforming design	The suggested scheme can nearly reach the same sum-rate performance as the DL technique with the full ICS. The predictive RIS phase shift matrix used in the DLPB method is far more successful than the nonpredictive and random RIS phase shift matrices used in the other two methods.
[14]	The issue of resource allocation in RIS-assisted OFDM systems through collaboratively optimizing the beamforming of the BS	A hybrid multiple deep Q networks (MDQN)-DDPG framework-based algorithm	Outperforms benchmark schemes regarding achievable sum rate
[15]	Multi-cell power allocation optimization	Uses DRL to maximize overall network capacity through wireless resource mapping method and DQFCNet	Outperforms traditional methods like water-filling and Q-learning, exhibiting faster convergence and improved stability
[16]	Power system dispatch optimization	Integrates GDQN model with SE-DSHAP method and subgraph explainer	Provides intuitive and comprehensive explanations for decision-making in complex power systems, aiding operators in achieving efficient and accurate control
[17]	Resource allocation optimization in CF-mMIMO systems	Proposes H-DDPG framework for AP clustering and power allocation optimization	Improvements in convergence speed, SE, and EE

(Continued)

Table 12.1 (Continued)

Paper	Objective	Method	Results
[18]	Computation offloading optimization in MEC networks	Develops a novel algorithm for RIS-empowered MEC networks optimization using a Markov decision process and DDPG	Significant performance improvements over traditional methods in optimizing delay, energy consumption, and operator costs
[19]	Enhancement of SEE in B5G mobile systems	Uses DRL to optimize phase shifts, orientations, beamforming, and RIS locations	Significantly boosts SEE, showcasing efficacy for future RIS-enabled communication systems
[20]	Secure SR network optimization	Joint optimization of PTx beamforming and RIS phase shifts using PPO	Achieves significant secrecy energy efficiency gains against eavesdroppers, demonstrating robust, and secure communication
[21]	Energy consumption minimization in symbiotic RIS-assisted MEC system	Introduces OH-DDPG framework for joint optimization of user offloading, HAP beamforming, and RIS beamforming	Substantial performance improvements in reducing overall energy consumption and enhancing learning efficiency
[22]	System rate maximization in multi-RIS-assisted IS-UAV-TN system	creates a multi-objective optimization problem to minimize UAV energy consumption and maximize system rate.	DDPG-based algorithm demonstrates efficacy in enhancing system performance and communication tasks
[23]	AoI minimization in wireless-powered sensor network	Uses hierarchical DRL framework to optimize AoI through joint node scheduling and transmission control strategies	Significant reduction in AoI and controllable fairness among sensor nodes
[24]	EE maximization in active RIS-assisted communication systems	Joint optimization of transmit precoders and RIS beamforming matrices using DRL-based methods	Improved convergence and robustness compared to traditional techniques.

Table 12.2 Limitation of related work.

References	Contribution	Limitations
He et al. [13]	DRL for optimizing sum rate in RIS-assisted MISO	Testing real-world implementations with actual measured data is necessary.
Chang et al. [14]	Reinforcement learning for resource allocation in IRS setups	Impact on latency needs to be highlighted.
Zhu et al. [15]	DRL for multi-cell power allocation	Hardware constraints are not discussed.
Liu et al. [16]	Graph-based DRL for power system dispatch	Interaction with dynamic systems needs to be expanded.
Xu et al. [17]	H-DDPG for resource allocation in downlink CF-mMIMO	Feedback mechanisms require further discussions.
Mnih et al. [18]	DDPG for computation offloading in RIS-empowered MEC	Energy consumption analysis require further discussions.
Mismar et al. [19]	A2C for enhancing SEE in RIS-enabled B5G systems	Security considerations needs to be highlighted.
Zhang et al. [20]	PPO for secure communication in RIS-assisted SR networks	Channel estimation accuracy needs to be highlighted.
Wu et al. [21]	OH-DDPG for energy-efficient RIS-assisted MEC	Mobility management is not covered.
Zhang et al. [22]	DDPG for multi-RIS-assisted IS-UAV-TN systems	Hardware synchronization needs to be highlighted.
Zhang et al. [23]	Hierarchical DRL for AoI optimization in wireless sensor networks	Energy harvesting efficiency is not captured.
Tan et al. [24]	DRL-based methods for active RIS-assisted communication	Interference management are not covered.

12.3 DRL Algorithms for RIS-Assisted Wireless Communication Systems

In the context of wireless communication systems assisted by RIS, DRL algorithms play a vital role in optimizing system performance and resource allocation. By leveraging DRL, these systems can adaptively adjust beamforming, phase shifting, and power control strategies to enhance communication efficiency and reliability in dynamic environments. This section provides an overview of DRL fundamentals and its application in wireless communication, and our proposed algorithm for

intelligent power control setting the stage for exploring specific algorithms tailored for RIS-assisted systems.

12.3.1 Deep Reinforcement Learning Fundamentals

DRL is a branch of machine learning that specializes in teaching agents how to make decisions in sequence within settings to accomplish particular objectives. Unlike traditional supervised or unsupervised learning, where models are trained on labeled datasets, DRL agents learn by interacting with their environment through trial and error [25]. DRL combines deep learning techniques, like neural networks, with RL algorithms to handle high-dimensional state and action spaces. The fundamental components of DRL include an agent, which takes actions based on observed states, an environment, which provides feedback to the agent based on its actions, and a reward signal, which guides the agent toward desirable outcomes [26], as shown in Figure 12.1. Through repeated interactions with the environment, DRL agents learn to maximize cumulative rewards by discovering optimal strategies or policies. In Figure 12.1, the agent, representing the RIS controller, receives states $s(t)$ and rewards $r(t)$ as input from the environment. Based on these inputs and the optimal policy, the agent takes actions to maximize cumulative rewards. This process involves training to learn and improve its decision-making abilities over time. Successful DRL algorithms like DQN [27], PPO [28], and DDPG have found applications in diverse domains [29], from robotics to finance by iteratively improving strategies through interactions with the environment and feedback mechanisms. **Algorithm 12.1** outlines the general procedure for training a DRL agent. Each step in the algorithm serves a specific purpose, such as interacting with the environment, updating the agent's

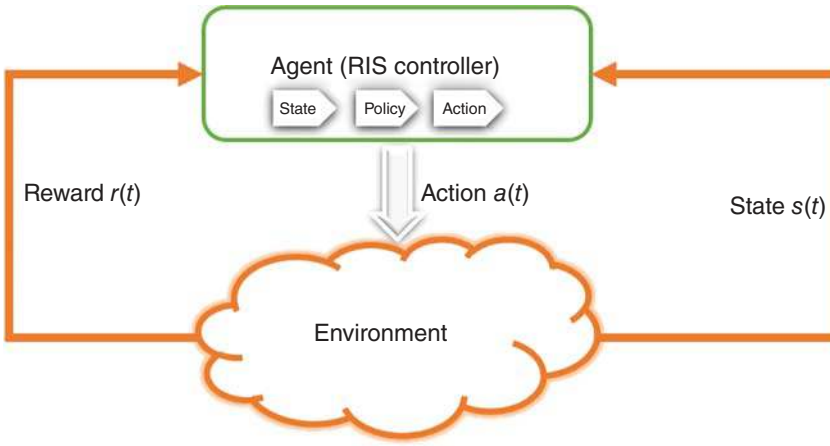

Figure 12.1 Deep reinforcement learning (DRL).

Algorithm 12.1: Deep Reinforcement Learning

Initialization:

Initialize neural network parameters θ representing the Agent's policy and value function.

Initialize environment and set initial state s.

Set hyperparameters (e.g., learning rate α, discount factor γ, exploration rate ϵ).

Repeat until convergence or maximum iterations:

Receive current state s from environment.

Select action a based on current state and agent's policy: $a = \pi(s, \theta)$.

Execute action a in environment: $s', r = \text{Env}(s, a)$.

Save the memory buffer containing the experience tuple (s, a, r, s').

Sample mini-batch of memories stored in a buffer.

Compute target values for each experience tuple using the Bellman equation

$$y_t = r_t + \lambda Q'(S_{t+1}, \pi'(S_{t+1}|\theta'_\mu)|\theta'_Q).$$

Compute loss function: Loss = Mean Squared Error of (target, predicted value)

$$L(\theta_Q) = \frac{1}{H}\sum_{t\in T}(y(t) - Q(s(t), a(t)|\theta_Q))^2$$

Compute gradients of loss relative to the parameters of the neural network

$$\nabla_\theta \text{Loss} : L_i(\theta_i) = \left[r_j + \Gamma \max_{(a_{j+1})} Q(s_{j+1}, a_{j+1}; \theta_{i-1}) - Q(s_j, a_j; \theta_i)\right]^2.$$

Update parameters of neural network using gradient descent:

$$\theta = \theta - \alpha \cdot \nabla_\theta \text{Loss}.$$

Exploration–Exploitation:

Adjust exploration strategy based on current policy (e.g., epsilon-greedy).

Policy Update:

Update the Agent's policy based on learned value function (e.g., policy gradients)

$$\nabla_{\theta_\mu} J \approx \mathbb{E}_{S_t\sim\rho^\pi}\left[\nabla_a Q(S, a|\theta^Q)\Big|_{S=s_t, a=a_t} \nabla_{\theta_\mu}\pi(S|\theta_\mu)\Big|_{S=s_t}\right].$$

Evaluation:

Periodically evaluate the Agent's performance on the validation set or in the environment.

Convergence Check:

Check convergence criteria (e.g., target average reward, stability).

Termination:

Terminate training when convergence criteria are met or after maximum iterations.

policy, or monitoring convergence to guide the learning process toward optimal performance [30, 31].

Two stages are involved in assessing the DRL algorithm: training and testing within the DRL framework. Initially, the framework is constructed with a simulated environment and user agents. The environment generates training and testing data, simulating user–agent interaction with the system, which provides feedback on the sum rate. TensorFlow is utilized to build and train DNNs for each user agent in the DDPG algorithm. During training (outlined in Algorithm 12.1), user agents interact with the environment over multiple RL tasks, each episode starting from a random initial state and ending after a predefined number of steps. Experience tuples are stored in buffers, and actor–critic networks are updated using mini-batches of experiences. After training, each user agent independently learns a dynamic computation policy. In the testing stage, user agents load their parameters of the trained network and randomly interact with an initialized environment, selecting actions based on the actor network's output [32].

12.3.2 Applications of DRL in Wireless Communication

DRL has gained prominence in wireless communication due to its ability to optimize system parameters and improve performance metrics adaptively. In wireless communication systems, DRL algorithms can be employed for various tasks as shown in Figure 12.2, including resource allocation [33, 34], power

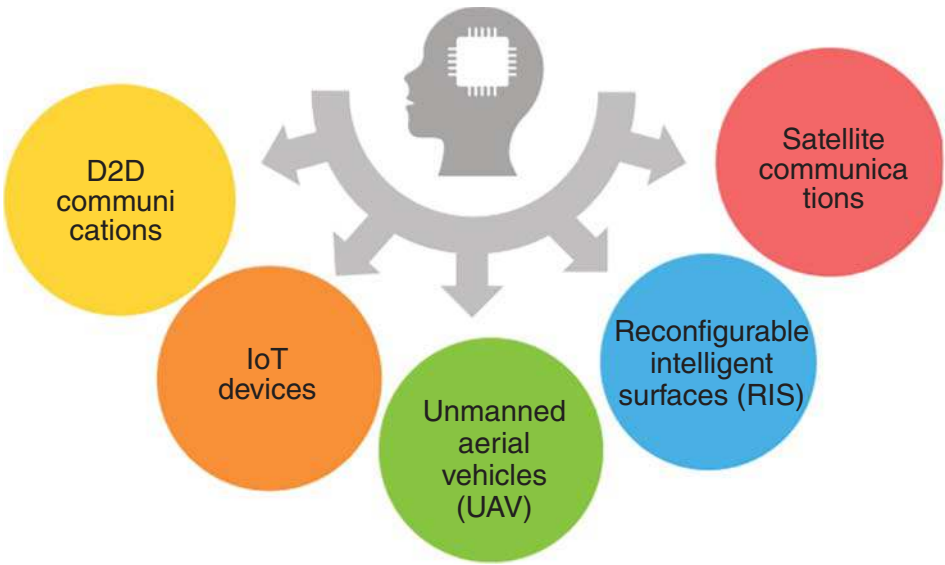

Figure 12.2 Applications of DRL in wireless communication.

control [35, 36], beamforming [37, 38], and channel estimation. By formulating wireless communication problems using MDP [39, 40], DRL agents can learn to make intelligent decisions based on observed channel conditions, traffic patterns, and system requirements. DRL-based approaches have been successfully applied to address challenges such as spectrum management [41], interference mitigation [42], and energy efficiency [43] in wireless networks. The versatility of DRL enables its application across different wireless communication scenarios, including cellular networks, IoT devices [44], UAV [45], RIS [46], satellite communications [47], and D2D communications [48]. Through ongoing research and development, DRL continues to advance the state-of-the-art in wireless communication, offering novel solutions to complex optimization problems and enabling the realization of next-generation wireless networks.

12.3.3 Integrating DRL with RIS for Enhanced Wireless Communication

We consider an MISO system with a BS, a reflecting RIS, and multiple users. The BS has M antennas and communicates with K users. The RIS has N reflecting elements and a microcontroller. Data streams are transmitted from the BS to users via the RIS. Channel matrices from BS to RIS (H_1) and RIS to users ($h_{k,2}$) are assumed known. The received signal at user k is

$$y_k = h_{k,2}^T \Phi H_1 W x + w_k \tag{12.1}$$

where x contains data streams, W is the BS's beamforming matrix, Φ is the RIS phase shift matrix, and w_k is noise. The sum rate C is used to evaluate system performance, with

$$R_k = \log_2(1 + \rho_k) \tag{12.2}$$

where R_k is the data rate of the k_{th} user, and ρ_k the SINR at the k_{th} user. We aim to maximize C by optimizing W and Φ, subject to power constraints. We propose a DRL method for optimization that leverages CSI. The optimization problem can be formulated as:

$$\max_{W,\Phi} \quad C(W, \Phi, h_{k,2}, H_1) \tag{12.3}$$

$$\text{s.t.} \quad \text{tr}\{WW^H\} \leq P_t \tag{12.4}$$

$$|\phi_n| = 1 \quad \forall n = 1, 2, \ldots, N \tag{12.5}$$

The following constraint is taken into consideration to maintain the transmission power at the BS:

$$E\left\{\text{tr}\{Wx(Wx)^H\}\right\} \leq P_t \tag{12.6}$$

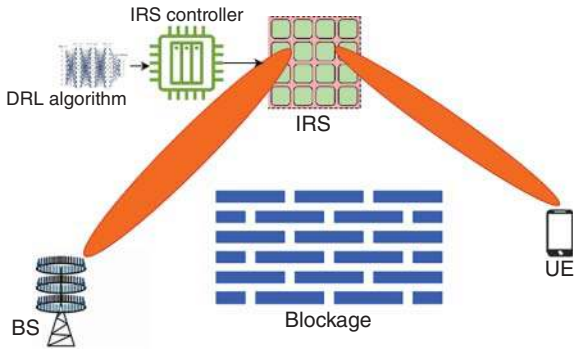

Figure 12.3 Integrating DRL with RIS for enhanced wireless communication.

where P_t is the total transmission power allowed at the BS, the optimization problem is non-convex and non-trivial due to the non-convex objective function and constraint. Exhaustive search is infeasible, especially for large-scale networks. Instead of seeking optimal solutions, algorithms are crafted to discover suboptimal solutions through alternating optimization methods. This entails solving for suboptimal W while keeping Φ fixed in each iteration and reciprocally solving for suboptimal Φ while holding W constant until convergence. Instead of tackling the intricate optimization problem directly through mathematical means, we approach the sum rate optimization issue with advanced DRL techniques to attain viable solutions for W and Φ. In DRL based wireless communication systems, the RIS play a crucial role by acting as intelligent reflectors or transceivers that can adaptively manipulate electromagnetic waves. RIS enhances wireless communication by dynamically controlling the propagation environment to optimize signal transmission and reception [49]. In DRL-based wireless systems, RIS serve as active components that interact with the environment, enabling agents, as shown in Figure 12.3 the agent represents the RIS controller learn optimal policies for adjusting their configurations based on observed states and rewards. By intelligently reflecting, refracting, or absorbing radio waves, RIS can mitigate channel impairments, enhance signal strength, reduce interference, and improve system performance [50]. RIS's ability to reconfigure their reflective properties in real time makes them well-suited for integration with DRL algorithms, allowing for adaptive and efficient wireless communication in diverse scenarios.

12.3.4 DRL Algorithms to Optimize RIS

Various DRL algorithms have been proposed and applied to optimize the operation of RIS in wireless communication systems. DQN [51], PPO [52], DDPG [53], and other RL algorithms can be tailored to address specific challenges in RIS optimization. These algorithms learn to adjust the phase shifts or beamforming weights of RIS elements to maximize communication performance metrics such as throughput, SINR, or EE. In Figure 12.4, the DRL-based optimization of RIS is depicted,

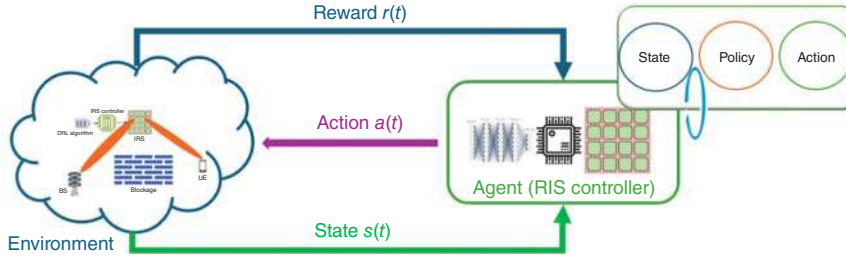

Figure 12.4 DRL algorithms for RIS optimization.

which involves formulating the problem as a MDP. In this framework, the state represents the current conditions, the action corresponds to the configuration of RIS elements, and the reward reflects the system's performance. The agent receives the reward $r(t)$ and the state $s(t)$ as input from the environment and then determines the action (joint optimization of beamforming and phase shifting), aiming to maximize the reward [54]. Through iterative interactions with the environment and receiving feedback, DRL agents can learn effective strategies for RIS adaptation, leading to improved SE, coverage, and reliability in wireless communication systems.

12.4 Proposed Method for Intelligent Power Control

The methodology involves implementing a hierarchical cooperative DRL system with two interconnected networks, as shown in Figure 12.5, DRL-M and DRL-S, and we will mention it in the future as **Deep Reinforcement Learning Master and Slave DRL (M-S),** and in this figure, we brief the propose of the architecture

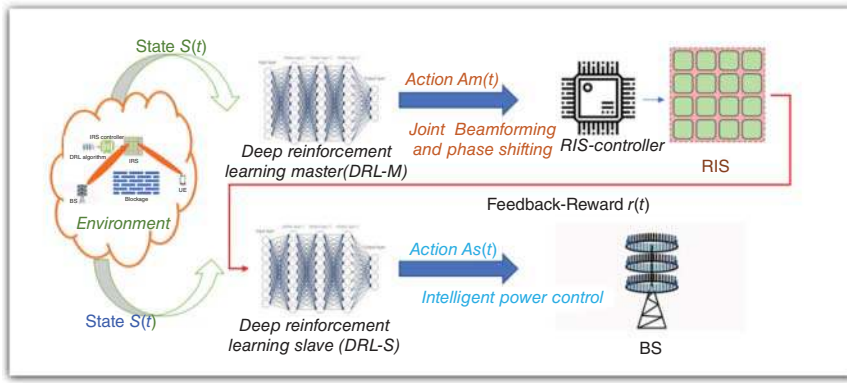

Figure 12.5 The proposed DRL(M-S) algorithm architecture.

algorithm and the object of each one from these two DRL networks, DRL-M and DRL-S:

- **DRL-M (Master) network:** This network receives channel information as input and produces joint actions represented by the transmit beamforming matrix (W) and the phase shift matrix (Φ). The aim of DRL-M is to enhance overall system performance by considering metrics like sum rate (R) and SINR.
- **DRL-S (Slave) network:** Operating in tandem with DRL-M, this network takes reward feedback from DRL-M as input and outputs actions for adjusting transmit power (a_S) to optimize EE. DRL-S aims to minimize energy consumption or maximize EE through transmit power adjustments.

  The DRL-M network takes the state from the environment as input, and the output will be the action $Am(t)$ taken by the agent (RIS-Controller). This action involves joint beamforming (from BS) and phase shifting (from RIS) to maximize the reward (sum rate) and, therefore, enhance overall system performance. On the other hand, DRL-S receives the state from the environment, and the feedback reward (from DRL-M) as input, and the output will be the action $As(t)$ that is taken by the agent (BS) to control the transmit power intelligently, adjusting it accordingly based on the feedback reward (increasing or reducing power transmission). By leveraging DRL-M and DRL-S networks, this approach aims to optimize system performance and EE, thereby contributing to the advancement of RIS-integrated wireless systems and offering robust solutions to power control complexities in dynamic environments.

Figure 12.6 illustrates the collaborative operation of the proposed DRL (M-S) algorithm in a dynamic environment. First, the DRL-M algorithm serves as the master algorithm, optimizing the action of joint beamforming and phase-shifting, an action conducted by the agent (RIS controller) to maximize the reward represented by the sum rate. Subsequently, this reward is fed as feedback to the DRL-S algorithm, the slave algorithm. DRL-S observes changes in this reward to

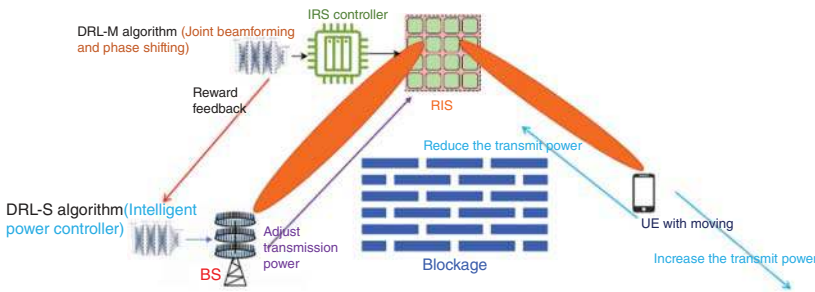

Figure 12.6 The collaborative operation of the proposed DRL (M-S) algorithm in a dynamic environment.

implement intelligent power control. In a dynamic environment, as users move closer to the RIS, the power received by these users strengthens, and due to that, **the signal-to-noise ratio (SNR) will increase (via Eq. (12.2))**, leading to an increase in the reward (which is fed back to DRL-S). Conversely, as users move away from the RIS, the power received weakens, decreasing the reward. DRL-S utilizes this reward as input and adjusts its actions based on these changes in this reward. Accordingly, DRL-S takes suitable action by the BS to control power transmission until the desired reward is achieved. When the feedback reward increases, indicating stronger received power, the BS takes action to reduce power transmission until the desired reward is achieved. Conversely, when the feedback reward (from DRL-M) decreases, indicating weaker received power, the BS adjusts its actions to increase power transmission until the desired reward is attained. This collaborative process can ensure intelligent power control in a dynamic environment. The optimization problem for adjusting transmit power based on rewards from DRL-M and updating EE parameters can be expressed as follows: **Objective:** Control the transmit power to maximize the EE of the system, defined as the ratio of achievable data rate (R) to the total power consumption($\sum_{n=1}^{N} P_n$)

$$\max_{EE} \quad \frac{R}{\sum_{n=1}^{N} P_n} \tag{12.7}$$

$$P_n \leq P_{\max_n}, \quad \forall n \in N \tag{12.8}$$

where P_n transmit power of the system for the user, and the transmit power P_n should not exceed a certain maximum value dictated by hardware constraints.

- The steps of the DRL (M-S) algorithm for intelligent power controller execution are as follows:
  i) **Initialization:** Set up the system by initializing the experience replay memory (M), training and target actor and critic network parameters, and the transmit beamforming matrix (W) and phase-shift matrix (Φ).
  ii) **DRL-M execution:** Iterate over episodes, collecting and preprocessing channel information for each episode. Within each episode, iterate over time steps to:
    - Obtain joint actions from the actor-network based on the current state.
    - Observe new states and instant rewards and store experiences in the replay memory.
    - Update the critic and actor networks through stochastic gradient descent (SGD) based on the training loss functions.
    - Periodically update target networks and set inputs for the next time step.
  iii) **DRL-S execution:** During the execution specific to DRL-S, the algorithm iterates over episodes, focusing on collecting and preprocessing reward feedback from DRL-M. Within each episode, the following steps are taken:

- **Observation of rewards from DRL-M:** Rewards received from DRL-M are observed, and power adjustment actions are determined based on this feedback and the current system parameters.
- **Adjustment of transmit power:** Transmit power (P) is adjusted based on the calculated actions. If the received reward increases (when the user moves close to RIS), the Algorithm reduces the transmit power until the desired reward level is achieved. Conversely, if the reward decreases (when the user moves far from RIS), the transmit power increases until the desired reward level is attained.
- **Update of energy efficiency parameters:** Energy efficiency-related parameters are updated to reflect the changes in transmit power and the corresponding feedback rewards received.

These steps will ensure that the transmit power is dynamically adjusted to optimize EE levels, thereby contributing to the overall enhancement of the system's performance. **Algorithm 12.2** presents the hierarchical cooperative DRL (M-S) system, detailing the coordinated execution of the DRL-M (Master) and DRL-S (Slave) networks. Each step in the algorithm contributes to optimize system performance and EE by iteratively adjusting transmit beamforming, phase shift, and power control actions based on environment feedback and learned policies.

Algorithm 12.2: The Proposed DRL (M-S) Algorithm

DRL-M (Master) Network:
Input: Channel information ($H1, h_{k,2}, \forall k$)
Output: Joint action $a_M = \{W, \Phi\}$ (Transmit beamforming matrix, Phase shift matrix)
Goal: Maximize overall system performance, considering sum rate (R) and SINR.
DRL-S (Slave) Network:
Input: Reward feedback (r) from DRL-M
Output: Transmit Power adjustment action a_S (for EE)
Goal: Minimize energy consumption or maximize EE using transmit power (P) adjustments.
Algorithm Execution:
Initialize:
Experience replay memory M with size D.
Training actor network parameters θ_{train_a}.
Target actor network parameters $\theta_{target_a} = \theta_{train_a}$.
Training critic network parameters θ_{train_c}.
Target critic network parameters $\theta_{target_c} = \theta_{train_c}$.
Transmit beamforming matrix W.
Phase shift matrix Φ.

for episode $= 0, 1, 2, \ldots, N-1$ **do**
  Collect and preprocess $H(n)_1, h(n)_{k,2}, \forall k$ for the nth episode to derive the initial state $s(0)$.
  for $t = 0, 1, 2, \ldots, T-1$ **do**
    Obtain action $a(t) = \{W(t), \Phi(t)\} = \pi(\theta_{train_a})$ from the actor network.
    Observe the new of state $s(t+1)$ given action $a(t)$.
    Observe the instant of reward $r(t+1)$.
    save the experience $(s(t), a(t), r(t+1), s(t+1))$ in the replay memory.
    Obtain the Q value function as $Q = q(\theta_{train_c}|s(t), a(t))$ from the critic network.
    Sample random mini-batches of size W of experiences from replay memory M.
    Construct the loss function $\ell(\theta_{train_c})$ for training the critic network.
    Perform stochastic gradient descent (SGD) on training critic network to obtain $\Delta\theta_{train_c}\ell(\theta_{train_c})$.
    Perform SGD on target critic network to obtain $\Delta a_q(\theta_{target_c}|s(t), a)$.
    Perform SGD on training actor-network to obtain $\Delta\theta_{train_a}\pi(\theta_{train_a}|s(t))$.
    Update the training of critic network θ_{train_c}.
    Update the training of actor network θ_{train_a}.
    Every U steps, update the target critic network θ_{target_c}.
    Every U steps, update the target actor network θ_{target_a}.
    Set input to DNN as $s(t+1)$.
  end for
end for
for episode$_S = 0, 1, 2, \ldots, N_S - 1$ **do**
  Collect and preprocess reward feedback $r_S(n)$ from DRL-M for the nth episode.
  for $t_S = 0, 1, 2, \ldots, T_S - 1$ **(DRL-S specific steps) do**
    Observe reward $r_S(t_S)$ from DRL-M.
    Determine action $a_S(t_S)$ based on $r_S(t_S)$ and current energy efficiency parameters.
    Adjust transmit power P based on $a_S(t_S)$.
    if $r_S(t_S)$ increases **then**
      Reduce P until reaching desired r_S.
    end if
    if $r_S(t_S)$ decreases **then**
      Increase P until reaching desired r_S.
    end if
    Update energy efficiency-related parameters.
    Set input to DNN as $s_S(t_S + 1)$.
  end for
end for

- The following steps thoroughly elucidate the process of this Algorithm, providing a comprehensive understanding of its execution.
  1) **Define DRL-M (Master) network:**
     - **Actor-network:** $a_M = \text{Actor}(s; \theta_a)$
       - **Inputs:** State s representing channel information
       - **Outputs:** Joint action a_M comprising transmit beamforming matrix and phase shift matrix
       - **Parameters:** θ_a representing the weights of the actor-network
     - **Critic network:** $Q = \text{Critic}(s, a_M; \theta_c)$
       - **Inputs:** State s and action a_M
       - **Output:** Q-value representing the expected cumulative reward
       - **Parameters:** θ_c representing the weights of the critic network
  2) **Define DRL-S (Slave) network:**
     - **Network:** $a_S = \text{Network}(r_S)$
       - **Inputs:** Reward feedback r_S from DRL-M
       - **Output:** Transmit power adjustment action a_S
  3) **Initialize parameters:**
     - Experience Replay Memory Size: D
     - Number of Episodes for DRL-M: $N_{episodes}$
     - Number of Episodes for DRL-S: N_S
     - Number of Steps per Episode for DRL-M: T
     - Number of Steps per Episode for DRL-S: T_S
     - Mini-batch Size for Experience Replay: W
     - Desired Reward Level for DRL-S: $r_{desired}$
  4) **Algorithm execution for DRL-M:**
     - Loop Over Episodes for DRL-M:
       - Collect and preprocess channel information: s
       - Loop Over Time Steps per Episode:
         * Obtain action from DRL-M actor-network: $a_M = \text{Actor}(s; \theta_a)$
         * Observe new state, reward, and store experience
         * Sample mini-batch from experience replay memory
         * Train critic network for DRL-M: $Q = \text{Critic}(s, a_M; \theta_c)$
         * Train actor network for DRL-M: $\theta_a \leftarrow \theta_a + \alpha_a \nabla_{\theta_a} J(\theta_a)$
         * Update target networks for DRL-M: $\theta_{target_a} \leftarrow \theta_a$, $\theta_{target_c} \leftarrow \theta_c$
  5) **Algorithm execution for DRL-S:**
     - Loop Over Episodes for DRL-S:
       - Collect reward feedback from DRL-M: r_S
       - Loop Over Time Steps per Episode for DRL-S:
         * Determine action from DRL-S based on reward feedback: $a_S = \text{Network}(r_S)$
         * Adjust transmit power based on action from DRL-S:

- If $r_S > r_{desired}$: Reduce transmit power
- If $r_S < r_{desired}$: Increase transmit power
- Otherwise, maintain transmit power at the desired level

* Update energy efficiency parameters

6) **End of Algorithm:** The algorithm execution concludes after completing all episodes for both DRL-M and DRL-S.

12.5 Results and Analysis

In this section, we present simulation results to validate the efficacy of the proposed scheme in a RIS–MISO system with the BS's antenna count $M = 8$, $K = 8$ users, and RIS elements $N = [8, 32]$. In the simulations, the channel matrix H_1 and $h_{k,2}$ are randomly generated following the Rayleigh distribution. As for the DRL parameters, each Actor is trained in a DNN to approximate its action-value function. The DRL architecture comprises three hidden layers with contain 256, 256, and 512 neurons, respectively. Rectified linear units (ReLUs) are activation functions for the first two hidden layers, while the function used for the last layer is hyperbolic tangent. We update the weights θ using the adaptive moment estimation (Adam) algorithm, as it requires only first-order gradients with minimal memory to attain the optimum. Simulation parameters are outlined in Table 12.3.

To gain a deeper insight into the efficacy of our proposed DRL (M-S) based approach, first, we analyze the DRL-M performance under varying transmit power (P_t). Figure 12.7 illustrates the impact of different P_t values, specifically $P_t = 0$ dB,

Table 12.3 The simulation parameters.

Parameter description	Value
The learning rate to update the parameters of the target actor network.	0.0001
The learning rate to update the parameters of the target critic network.	0.0001
The learning rate to update the parameters of the training critic network.	0.0001
The learning rate to update the parameters of the training actor network.	0.0001
Decaying rate to update the parameters of the critic network.	0.00001
Decaying rate to update the parameters of the actor network.	0.00001
The size of the buffer used for experience replay.	50 000
Number of episodes	4000
The total number of steps within each episode.	20 000
Discounted rate for future reward	0.90
of experiences included in the mini-batch.	16

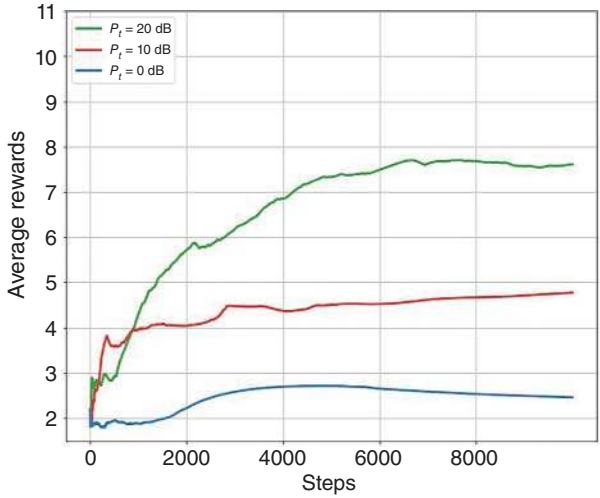

Figure 12.7 Rewards over time steps at $P_t = 0$, $P_t = 10$ dB and $P_t = 20$ dB, respectively.

$P_t = 10$ dB and $P_t = 20$ dB on the rewards obtained over time steps. Through simulations, it becomes evident that the rewards tend to converge as the number of time steps increases. Notably, convergence occurs more rapidly under low SNR conditions ($P_t = 0$ dB, $P_t = 10$ dB) than high SNR conditions ($P_t = 20$ dB). This phenomenon arises from the wider dynamic range of rewards at higher SNR levels, leading to increased fluctuations and slower convergence.

12.6 Discussions

The hierarchical cooperative DRL (M-S) System will demonstrate its effectiveness in improving system performance and EE.

12.6.1 Performance Enhancement with DRL-M

- **Maximized system performance:** The DRL-M network successfully optimized joint beamforming and phase shift actions (a_M) to maximize overall system performance. The system significantly improved communication reliability and SE by considering metrics such as sum rate (R).
- **Efficient resource allocation:** One of the key advantages of DRL-M is its capability to dynamically adjust beamforming and phase shift strategies in response to changing channel conditions. This adaptability ensures robust communication links even in challenging environments, enhancing system reliability.

12.6.2 Energy Efficiency Optimization with DRL-S

- **Minimized energy consumption:** The DRL-S network will optimize EE through transmit power adjustments, aiming to minimize energy consumption while maintaining reliable communication links. By dynamically adjusting transmit power based on feedback from DRL-M, the system will achieve significant energy savings without compromising performance.
- **Adaptive power control:** DRL-S will demonstrate adaptive power control capabilities, effectively adjusting transmit power levels based on real-time feedback and EE parameters. This adaptive approach will ensure optimal power utilization, allowing the system to operate efficiently under varying conditions and traffic loads.

12.6.3 Synergistic Cooperation Between DRL-M and DRL-S

- **Complementary optimization:** The hierarchical cooperative framework is expected to facilitate seamless information exchange between DRL-M and DRL-S, enabling collaborative decision-making for optimal system performance and EE. The feedback loop between the two networks will ensure synchronized operation and mutual reinforcement, resulting in superior overall results.

12.7 Limitations of the Survey

In conducting this survey, certain limitations were encountered that need to be acknowledged. These limitations include:

- **Lack of comprehensive coverage:** The survey may not have encompassed every aspect or study of intelligent power control with RIS in dynamic environments. Some relevant works may have been inadvertently omitted.
- **Scope restrictions:** The survey may have been constrained by limitations in scope, such as focusing on specific types of intelligent power control techniques or excluding certain types of studies.

Despite these limitations, efforts were made to ensure the thoroughness and accuracy of the survey.

12.8 Critical Lessons Learned

Through conducting this survey, several critical lessons were learned that have implications for future research and practice. These lessons include:

- **Importance of interdisciplinary approaches:** Intelligent power control with RIS in dynamic environments requires interdisciplinary collaboration between researchers in wireless communications, machine learning, and signal processing to address complex challenges effectively.
- **Need for real-world validation:** While theoretical studies and simulations provide valuable insights, there is a critical need for empirical validation of intelligent power control techniques in real-world dynamic environments to assess their practical feasibility and performance.
- **Continuous adaptation and optimization:** Dynamic wireless communication environments necessitate adaptive and optimized power control strategies that can quickly respond to changing conditions and uncertainties, highlighting the importance of ongoing research in this area.
- **Consider practical constraints:** Practical considerations, such as hardware limitations, regulatory constraints, and EE requirements, must be considered when designing and implementing intelligent power control systems with RIS.

These critical lessons underscore the importance of continued research and innovation in intelligent power control with RIS in dynamic environments. This will address existing challenges and advance the state-of-the-art.

12.9 Conclusion

The proposed hierarchical cooperative Deep Reinforcement Learning (DRL system, DRL (M-S), is anticipated to play a pivotal role in optimizing system performance and EE in wireless communication systems integrated with RIS. The system is poised to address the intricate challenges of power control in dynamic environments by harnessing interconnected networks, DRL-M and DRL-S. DRL-M optimizes system performance by adjusting transmit beamforming and phase shift strategies, while DRL-S will intelligently regulate power transmission based on feedback from DRL-M. This hierarchical collaborative framework is envisioned to significantly elevate the adaptability and resilience of RIS-enabled wireless networks, heralding a future characterized by scalable, cost-effective, and energy-neutral connectivity solutions.

12.10 Future Scope

Our future aim is to implement the proposed algorithm DRL (M-S) to achieve the desired results. Our plan involves diligently following the steps outlined in the algorithm and leveraging appropriate tools and resources to ensure its

successful execution. Through careful analysis, we aim to obtain meaningful results that validate the effectiveness of the proposed approach. Looking ahead, we envision significant progress in applying cooperative DRL systems to enhance RIS-integrated wireless communication. To achieve this, future research endeavors may refine DRL algorithms by introducing more sophisticated reward mechanisms or adaptive learning strategies. These enhancements aim to expedite convergence and elevate overall system performance. Moreover, there is potential for extending the framework to encompass multi-agent scenarios or diverse network environments, such as heterogeneous setups. This expansion could provide valuable insights into the scalability and adaptability of the proposed approach, thereby broadening its applicability to various real-world scenarios. Furthermore, practical implementations and experimental validations will play a crucial role in substantiating the effectiveness and viability of the proposed methodology in real-world settings. By conducting such empirical studies, we can gain valuable insights into the performance and practicality of cooperative DRL-based solutions across different operational conditions. In essence, the future outlook presents numerous opportunities for refining and deploying cooperative DRL-based solutions to effectively address the evolving challenges and requirements of RIS-enabled wireless systems. By capitalizing on these opportunities, we can continue to drive innovation and advancements in wireless communication technologies.

References

1 Dong, H., Dong, H., Ding, Z. et al. (2020). *Deep Reinforcement Learning*. Springer.

2 Van Hasselt, H., Guez, A., and Silver, D. (2016). Deep reinforcement learning with double q-learning. *Proceedings of the AAAI conference on artificial intelligence*, volume 30.

3 Wang, Y. and Zou, S. (2022). Policy gradient method for robust reinforcement learning. *International Conference on Machine Learning*, 23484–23526. PMLR.

4 Naparstek, O. and Cohen, K. (2018). Deep multi-user reinforcement learning for distributed dynamic spectrum access. *IEEE Transactions on Wireless Communications* 18(1): 310–323.

5 Lillicrap, T.P., Hunt, J.J., Pritzel, A. et al. (2015). Continuous control with deep reinforcement learning. *arXiv preprint arXiv:1509.02971*.

6 Mnih, V., Badia, A.P., Mirza, M. et al. (2016). Asynchronous methods for deep reinforcement learning. *International Conference on Machine Learning*, 1928–1937. PMLR.

7 Schulman, J., Wolski, F., Dhariwal, P. et al. (2017). Proximal policy optimization algorithms. *arXiv preprint arXiv:1707.06347*.

8 Fang, F., Zhang, H., Cheng, J., and Leung, V.C.M. (2016). Energy-efficient resource allocation for downlink non-orthogonal multiple access network. *IEEE Transactions on Communications* 64(9): 3722–3732.

9 Zhang, H., Yang, N., Long, K. et al. (2018). Secure communications in NOMA system: subcarrier assignment and power allocation. *IEEE Journal on Selected Areas in Communications* 36(7): 1441–1452.

10 Zhang, H., Huang, S., Jiang, C. et al. (2017). Energy efficient user association and power allocation in millimeter-wave-based ultra dense networks with energy harvesting base stations. *IEEE Journal on Selected Areas in Communications* 35(9): 1936–1947.

11 Recht, B., Re, C., Wright, S., and Niu, F. (2011). Hogwild!: a lock-free approach to parallelizing stochastic gradient descent. *Advances in Neural Information Processing Systems 24 (NIPS 2011)*.

12 Kingma, D.P. and Ba, J. (2014). Adam: a method for stochastic optimization. *arXiv preprint arXiv:1412.6980*.

13 He, Y., Zhang, Z., Yu, F.R. et al. (2017). Deep-reinforcement-learning-based optimization for cache-enabled opportunistic interference alignment wireless networks. *IEEE Transactions on Vehicular Technology* 66(11): 10433–10445.

14 Chang, H.-H., Song, H., Yi, Y. et al. (2018). Distributive dynamic spectrum access through deep reinforcement learning: a reservoir computing-based approach. *IEEE Internet of Things Journal* 6(2): 1938–1948.

15 Zhu, H., Cao, Y., Wei, X. et al. (2018). Caching transient data for Internet of Things: a deep reinforcement learning approach. *IEEE Internet of Things Journal* 6(2): 2074–2083.

16 Liu, C.H., Chen, Z., Tang, J. et al. (2018). Energy-efficient UAV control for effective and fair communication coverage: a deep reinforcement learning approach. *IEEE Journal on Selected Areas in Communications* 36(9): 2059–2070.

17 Xu, Z., Tang, J., Yin, C. et al. (2019). Experience-driven congestion control: when multi-path TCP meets deep reinforcement learning. *IEEE Journal on Selected Areas in Communications* 37(6): 1325–1336.

18 Mnih, V., Kavukcuoglu, K., Silver, D. et al. (2015). Human-level control through deep reinforcement learning. *Nature* 518(7540): 529–533.

19 Mismar, F.B., Evans, B.L., and Alkhateeb, A. (2019). Deep reinforcement learning for 5G networks: joint beamforming, power control, and interference coordination. *IEEE Transactions on Communications* 68(3): 1581–1592.

20 Zhang, J., Zhang, H., Zhang, Z. et al. (2021). Deep reinforcement learning-empowered beamforming design for IRS-assisted MISO interference channels. *2021 13th International Conference on Wireless Communications and Signal Processing (WCSP)*, 1–5. IEEE.

21 Wu, W., Yang, F., Zhou, F. et al. (2022). Intelligent resource allocation for IRS-enhanced OFDM communication systems: a hybrid deep reinforcement learning approach. *IEEE Transactions on Wireless Communications* 22(6): 4028–4042.

22 Zhang, Y., Kang, C., Ma, T. et al. (2018). Power allocation in multi-cell networks using deep reinforcement learning. *2018 IEEE 88th Vehicular Technology Conference (VTC-Fall)*, 1–6. IEEE.

23 Zhang, K., Zhang, J., Xu, P. et al. (2023). A multi-hierarchical interpretable method for DRL-based dispatching control in power systems. *International Journal of Electrical Power & Energy Systems* 152: 109240.

24 Tan, F., Deng, Q., and Liu, Q. (2024). Energy-efficient access point clustering and power allocation in cell-free massive MIMO networks: a hierarchical deep reinforcement learning approach. *EURASIP Journal on Advances in Signal Processing* 2024(1): 18.

25 Zhang, X., Wu, W., Liu, S., and Wang, J. (2023). An efficient computation offloading and resource allocation algorithm in RIS empowered MEC. *Computer Communications* 197: 113–123.

26 Razaq, M.M., Song, H., Peng, L., and Ho, P.-H. (2024). Optimizing secrecy energy efficiency in RIS-assisted MISO systems using deep reinforcement learning. *Computer Communications* 217: 126–133.

27 Li, B., Liu, W., and Xie, W. (2024). Joint resource allocation and beamforming design for RIS-aided symbiotic radio networks: a DRL approach. In: *Digital Communications and Networks*. Elsevier.

28 Zhao, S., Liu, Y., Gong, S. et al. (2023). Computation offloading and beamforming optimization for energy minimization in wireless-powered IRS-assisted MEC. *IEEE Internet of Things Journal* 10(22): 19466–19478.

29 Guo, K., Wu, M., Li, X. et al. (2023). Deep reinforcement learning and NOMA-based multi-objective RIS-assisted IS-UAV-TNs: trajectory optimization and beamforming design. *IEEE Transactions on Intelligent Transportation Systems* 24(9): 10197–10210.

30 Gong, S., Cui, L., Gu, B. et al. (2023). Hierarchical deep reinforcement learning for age-of-information minimization in IRS-aided and wireless-powered wireless networks. *IEEE Transactions on Wireless Communications* 22(11): 8114–8127.

31 Sharma, V., Paul, A., Singh, S.K. et al. (2024). Robust transmission for energy-efficient sub-connected active RIS-assisted wireless networks: DRL versus traditional optimization. *IEEE Transactions on Green Communications and Networking* 8(4): 1902–1916.

32 Huang, C., Mo, R., and Yuen, C. (2020). Reconfigurable intelligent surface assisted multiuser MISO systems exploiting deep reinforcement learning. *IEEE Journal on Selected Areas in Communications* 38(8): 1839–1850.

33 Zhang, H., Wang, H., Li, Y. et al. (2023). DRL-driven dynamic resource allocation for task-oriented semantic communication. *IEEE Transactions on Communications* 71(7): 3992–4004.

34 Hazarika, B., Singh, K., Biswas, S., and Li, C.-P. (2022). DRL-based resource allocation for computation offloading in IOV networks. *IEEE Transactions on Industrial Informatics* 18(11): 8027–8038.

35 Luo, L., Zhang, J., Chen, S. et al. (2022). Downlink power control for cell-free massive MIMO with deep reinforcement learning. *IEEE Transactions on Vehicular Technology* 71(6): 6772–6777.

36 Xiang, H., Yang, Y., He, G. et al. (2022). Multi-agent deep reinforcement learning-based power control and resource allocation for D2D communications. *IEEE Wireless Communications Letters* 11(8): 1659–1663.

37 Al-Eryani, Y. and Hossain, E. (2022). Self-organizing mmWave MIMO cell-free networks with hybrid beamforming: a hierarchical DRL-based design. *IEEE Transactions on Communications* 70(5): 3169–3185.

38 Dong, H., Hua, C., Liu, L. et al. (2023). Optimization-driven DRL based joint beamformer design for IRS-aided ITSN against smart jamming attacks. *IEEE Transactions on Wireless Communications* 23(1): 667–682.

39 Reyes, R.R. and Bauschert, T. (2021). Towards DRL-based routing and spectrum assignment in optical networks: lessons to be learned from Markov decision processes. *2021 IEEE Latin-American Conference on Communications (LATINCOM)*, 1–6. IEEE.

40 El Hamdani, S., Loudari, S., Novotny, S. et al. (2021). A Markov decision process model for a reinforcement learning-based autonomous pedestrian crossing protocol. *2021 3rd IEEE Middle East and North Africa COMMunications Conference (MENACOMM)*, 147–151. IEEE.

41 Han, R., Li, H., Apaza, R. et al. (2022). Deep reinforcement learning assisted spectrum management in cellular based urban air mobility. *IEEE Wireless Communications* 29(6): 14–21.

42 Dahal, M. and Vaezi, M. (2023). Multi-agent deep reinforcement learning for multi-cell interference mitigation. *2023 57th Annual Conference on Information Sciences and Systems (CISS)*, 1–6. IEEE.

43 Ghomri, B.I.-d., Bendimerad, M.Y., and Bendimerad, F.T. (2024). DRL-driven optimization for energy efficiency and fairness in NOMA-UAV networks. *IEEE Communications Letters* 28(5): 1048–1052.

44 Wu, J., Wang, H., Shi, Z., and Pan, S. (2023). DRL-based scheduling scheme with age of information for real-time IoT systems. *China Conference on Wireless Sensor Networks*, 219–230. Springer.

45 Zhu, Y., Li, M., Liu, Y. et al. (2022). DRL-based joint beamforming and BS-RIS-UE association design for RIS-assisted mmWave networks. *2022 IEEE Wireless Communications and Networking Conference (WCNC)*, 345–350. IEEE.

46 Zhao, J., Yu, L., Cai, K. et al. (2022). RIS-aided ground-aerial NOMA communications: a distributionally robust DRL approach. *IEEE Journal on Selected Areas in Communications* 40(4): 1287–1301.

47 Huang, J., Yang, Y., Yin, L. et al. (2022). Deep reinforcement learning-based power allocation for rate-splitting multiple access in 6G LEO satellite communication system. *IEEE Wireless Communications Letters* 11(10): 2185–2189.

48 Ron, D. and Lee, J.-R. (2021). DRL-based sum-rate maximization in D2D communication underlaid uplink cellular networks. *IEEE Transactions on Vehicular Technology* 70(10): 11121–11126.

49 Lin, J., Zout, Y., Dong, X. et al. (2020). Deep reinforcement learning for robust beamforming in IRS-assisted wireless communications. *GLOBECOM 2020 - 2020 IEEE Global Communications Conference*, 1–6. https://doi.org/10.1109/GLOBECOM42002.2020.9322372.

50 Imoize, A.L., Obakhena, H.I., Anyasi, F.I. et al. (2022). Reconfigurable intelligent surfaces enabling 6G wireless communication systems: use cases and technical considerations. *2022 5th Information Technology for Education and Development (ITED)*, 1–7. IEEE.

51 Dong, H., Ding, Z., Zhang, S. and Chang, H. (2020). *Deep Reinforcement Learning*. Springer.

52 Zai, A. and Brown, B. (2020). *Deep Reinforcement Learning in Action*. Manning Publications.

53 Li, S.E. (2023). Deep reinforcement learning. In: *Reinforcement Learning for Sequential Decision and Optimal Control*, 365–402. Springer.

54 Feng, K., Wang, Q., Li, X., and Wen, C.-K. (2020). Deep reinforcement learning based intelligent reflecting surface optimization for MISO communication systems. *IEEE Wireless Communications Letters* 9(5): 745–749. https://doi.org/10.1109/LWC.2020.2969167.

13

An Overview of Channel Modeling and Propagation Measurements in IRS-Based Wireless Communication Systems

Mukkara Prasanna Kumar[1], Ammar Summaq[1], Sunil Chinnadurai[1], Vinoth Babu Kumaravelu[2], Poongundran Selvaprabhu[2], Agbotiname Lucky Imoize[3], and Gaurav Jaiswal[4]

[1] *Department of Electronics and Communication Engineering, School of Engineering and Sciences, SRM University-AP, India*
[2] *Department of Communication Engineering, School of Electronics Engineering, Vellore Institute of Technology, Vellore, India*
[3] *Department of Electrical and Electronics Engineering, Faculty of Engineering, University of Lagos, Lagos, Nigeria*
[4] *SW/Test Validation Engineer in Wi-Fi-Bluetooth Coex, NXP Semiconductor, Pune, India*

13.1 Introduction

The intelligent reflecting surface (IRS) is a novel electromagnetic (EM) structure that has the potential to revolutionize wireless communication systems by overcoming the constraints of traditional techniques [1]. IRS employs several passive components, separating it from more conventional technologies like massive multiple input multiple output (MIMO) or relay and providing advantages like less power consumption and low cost. An overview of IRS technology, including its benefits, features, and operation over current systems, and potential applications in wireless communication [2]. The comprehensive understanding of 5G examines various technological aspects [3]. It includes a systematic evaluation of candidate enabling technologies, discussions of 5G's evolution, and advancements in wireless mobile networks. The historical overview of wireless communication standards and context for understanding 6G's goals and needs [2]. It also explores the key technologies proposed to support 6G and introduces potential applications like multisensory extended reality and digital replication. The optimization of channel capacity in an IRS-assisted indoor millimeter-wave (mmWave) communication system is explored [4]. This system model focuses on two-dimensional (2D) propagation scenarios, explicitly considering the propagation. The advancement of IRS-assisted communications

Reconfigurable Intelligent Surfaces for 6G and Beyond Wireless Networks, First Edition.
Edited by Agbotiname Lucky Imoize, Vinoth Babu Kumaravelu, and Dinh-Thuan Do.

necessitates thoroughly comprehending the inherent channel characteristics. The IRS assists in modeling wireless propagation channels in indoor wireless communication systems [5]. The framework utilizes ray tracing to calculate transmission paths power delay profile (PDP). While numerous research outcomes have been on path loss modeling of IRS systems [1, 4, 6–26], investigations into multipath small-scale statistical channel modeling are still in their early stages. Moreover, channel modeling for IRS-assisted unmanned aerial vehicle (UAV) mmWave communications remains unexplored. By segmenting the substantial IRS into tiles [27] devised a statistical channel model, although this approach disregarded the practical orientation angle of the IRS. Although it was designed for sub-6 GHz terrestrial communication scenarios, a three-dimensional (3D) nonstationary channel model was developed by Jiang et al. [28] for IRS-assisted MIMO systems. The various MIMO channel models are used in wireless communication systems. The physical, analytical, and standardized models are the three primary categories. The MIMO channel is described by physical models using real-world characteristics. Analytical models focus on the statistical aspects of the MIMO channel based on collected data. Standardized models offer a common framework for radio systems, signal processing, and multiple access techniques [29]. While linear models based on log distance are commonly used for predicting path loss in wireless cellular networks, more advanced nonlinear models are required for accurate estimation, especially in complex microcellular environments. Conventional models typically have a root mean square error ranging from 8 to 12 dB, which exceeds the acceptable error limit of 0–6 dB. Therefore, there is a growing need for machine learning-based path loss prediction models that can provide more precise estimates [30]. In [31], the cascaded line-of-sight (LoS) MIMO channel incorporates IRS to facilitate communication between a transmitter and a receiver equipped with uniform linear arrays (ULAs). The IRS reflects electromagnetic waves to establish LoS links between the transmitter and receiver. This model takes into account the wavefront's curvature on various IRS reflecting components. Spatial multiplexing can only be achieved via the IRS-assisted MIMO channel using the cascaded LoS links. The 3D wideband channel model for communication systems assisted by IRS and UAVs [32] takes into consideration the IRS reflecting elements radiation pattern and aperture area. In contrast to specular reflectors, each IRS element is considered as an anomalous reflector, allowing for joint beamforming of signals in desired directions. The IRS-assisted link path loss is calculated and verified against real outdoor measurements. It is based on the square of the aperture area of the IRS reflecting components. Furthermore, Basar and Yildirim [33] introduced a statistical channel model for IRS-assisted mmWave communications, albeit with limitations confined to narrowband stationary systems. According to [28], the time-varying features of IRS-assisted MIMO communications are examined

by splitting the channel between mobile transmitters and receivers into three subchannels. The results indicate low correlations in the space domain within the IRS-assisted communication system. However, the derivation of IRS phase shifts is not provided by this study; instead, it simply takes into account the placements of the IRS in the channel model. A thorough wideband nonstationary channel model that considers realistic discrete phase shifts and cluster evolution in the space domain is presented in [22–24] for IRS-assisted MIMO communication. In comparison to continuous phase shifts, discrete phase shifts do not affect the time correlation, according to this study's investigation of IRS's impacts on the time and spatial correlation functions. Nevertheless, these models present limitations with ideal assumptions that are challenging to satisfy, rendering them incapable of accurately describing the statistical properties of IRS propagation channels. Under the assumption of isotropic scattering, the channel model for IRS-aided communications [34] demonstrated that, for a linear IRS with half-wavelength spacing, but not for a rectangular IRS, the subchannels between the transmitter-IRS and IRS-receiver could be characterized by uncorrelated Rayleigh fading. Nevertheless, the concept was limited to devices with a single antenna. A statistical channel model was developed by Najafi et al. [27] by dividing the large IRS into tiles and taking into account the effects of unit number and polarization. This model incorporated the tile responses to derive the channel response. However, this approach relies on simplistic channel models and overlooks practical aspects of IRS deployment.

13.1.1 Key Contributions of the Chapter

The following are the significant contributions of this chapter:

- **IRS technology and its benefits**: This chapter provides information about the importance of IRS technology in wireless communication systems. IRS technology is a promising technique for improving performance. It employs passive reflecting components like programmable reflectors or meta-surfaces to modify electromagnetic waves. By intelligently modifying the phase and amplitude of reflected signals, IRS can efficiently manage signal propagation, reduce interference, and enhance coverage and capacity in wireless networks.
- **Focus on channel modeling and propagation measurements**: It offers information on the importance of channel modeling and propagation measurements, which are essential for developing and enhancing wireless communication systems. Channel modeling involves developing mathematical models of wireless channel behavior, including the impacts of fading, interference, and signal propagation. In contrast, propagation measurements use field measurements and experiments to empirically characterize real-world wireless

channels. Measurements of propagation gather data about signal strength, multipath fading, and other propagation phenomena, which help explain how wireless channels behave in various environments.

- **IRS channel modeling**: It highlights the importance of IRS channel modeling for developing a mathematical model that accurately represents the behavior of wireless channels and is enhanced through IRS technology. These models aim to represent the impact of beamforming, phase shifting, and signal reflection that the IRS provides on the overall channel characteristics. When modeling an IRS channel, factors such as the size and location of the IRS elements, the characteristics of the incident signals, and environmental factors that impact signal propagation are considered.
- **Identification of future research directions**: This section identifies important directions for further research and potential challenges of IRS channel modeling and propagation measurement techniques. Considering the importance of accurate channel models in optimizing the performance of IRS-enabled communication systems, more research is required to improve current modeling techniques.

13.1.2 Chapter Organization

The chapter is organized as follows: Section 13.2 presents the related works on channel modeling for wireless communication systems. Section 13.3 introduces the IRS technology and its fundamental principles. Section 13.4 describes channel modeling and propagation measurements for communication systems. Section 13.5 introduces IRS channel modeling. Section 13.6 delves into the limitations of the Survey. Section 13.7 discusses the critical lessons learned. Section 13.8 describes the potential challenges of propagation measurements and channel modeling. Section 13.9 presents the conclusion and future research directions.

13.2 Related Work

The section represents a subset of the research efforts aimed at addressing channel modeling concerns in wireless communication systems, and they offer valuable insights into the challenges and potential solutions in this emerging area of research. Table 13.1 lists various literature works on channel modeling perspectives in wireless communication systems.

Table 13.1 Related works on channel modeling for wireless communication systems.

References	Summary
Sun et al. [24]	This work examines the influence of practical discrete IRS phase shifts on channel properties, including spatial cross-correlation function, temporal auto-correlation function, and local Doppler spread. The results show that the IRS significantly impacts channel behavior by improving stability and separating the entire channel.
Dovelos et al. [35]	This article presents an IRS-assisted channel model for THz band communication. Plate scattering and molecular absorption procedures specific to THz bands are essential components of the path loss model employed. Simulation results show that IRS significantly improves energy efficiency (EE) in MIMO systems, especially for beam focusing and near-field applications.
Sánchez et al. [19]	The study offers the concept of the keyhole MIMO channel, in which each element of the IRS symbolizes a keyhole, to create a channel with one degree of freedom (DoF). By this, the IRS-MIMO channel is modeled by adding the contributions from every IRS element and ignoring the direct transmitter–receiver channel. A methodology for channel estimation is presented that uses single value decomposition (SVD) to estimate each cascaded channel connection separately. This method improves the correctness of the channel model by taking into account the IRS component's phase and amplitude responses.
Sun et al. [23]	This study analyzed the channel characteristics of IRS-assisted near-field communication under various conditions of local scatterers. The proposed 3D IRS-assisted MIMO channel model considers LoS, single-bounced (SB) at IRS, and double-bounced (DB) modes, where radio waves reflect from the IRS and scatterers close to the receiver. It is based on a cylindrical model. The authors used this model to examine important statistical characteristics of shoot and bounce ray (SBR) and DB propagation, including the Doppler power spectrum and the time-frequency-space correlation function. Simulation results indicated that factors like the number of IRS elements, horizontal and vertical locations of the IRS, distribution of surrounding scatterers, and receiver movement significantly affect channel characteristics. They calculated the channel capacities of SB and DB modes, demonstrating that large IRS sizes and appropriate IRS locations can substantially enhance the channel capacity of IRS-assisted communication.
Xiong et al. [36]	The authors developed a comprehensive 3D wideband non-stationary MIMO geometry-based stochastic model (GBSM) to characterize the small-scale fading of IRS-assisted wireless communication channels. By representing the IRS as a virtual cluster, they have generalized and modeled the complex channel impulse response (CIR) using proposed formulas. They have also verified the equivalence between end-to-end and cascaded modeling of IRS channels and proposed a low-complexity solution to derive the time-varying IRS reflection phases. Through simulations, the modeled approach accurately captures the physical propagation properties of practical IRS-assisted wireless communication channels, enabling validations of algorithms, system designs, and performance evaluations.

13.3 IRS Technology and Its Fundamental Principles

IRS-assisted communication systems, utilizing passive reflecting elements, can significantly improve wireless channel quality and extend coverage. This technology manipulates wireless signals for enhanced performance, deploying small, low-cost reflecting elements in diverse environments to create a controllable wireless environment. IRS reflects electromagnetic waves from a base station in desired directions, providing alternative wireless paths, as shown in Figure 13.1. These elements adjust phase and amplitude, allowing signal manipulation for beamforming and interference cancellation [37]. IRS can enhance signal strength, coverage, and capacity and mitigate interference. It has the potential to revolutionize wireless communication, offering cost-effective and energy-efficient solutions for applications like 5G [38]. IRS technology involves programmable passive units for smart radio environments in wireless communications [23]. It manipulates the wireless channel by adjusting signal phase shifts. A proposed 3D wideband nonstationary end-to-end channel model considers physical properties like unit numbers, sizes, orientations, and configurations. The model describes the channel using virtual LoS, single-bounced non-line-of-sight (NLoS), and double-bounced NLoS components [36]. The path-loss model considers electromagnetic phenomena and is validated through experimental measurements using a developed IRS prototype. Each unit cell can change the reflection phase based on the required IRS configuration [39]. By software-controlled phase adjustment, IRS technology optimizes system metrics like energy efficiency, transmit power, and achievable rate. IRS, typically in a software-controlled uniform planar array, offers intelligence through software-controlled phase adjustment of reflecting elements [40].

13.3.1 Benefits of the IRS in Terms of Coverage, Capacity, and Energy Efficiency

IRS technology improves coverage by manipulating radio waves and adjusting phase shifts for better signal propagation. It increases capacity by managing

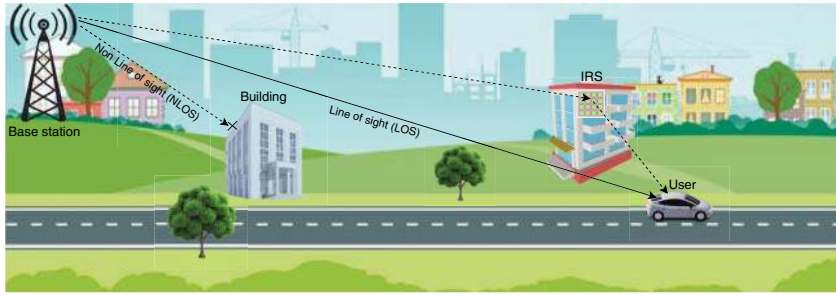

Figure 13.1 An IRS-aided wireless communication system.

spectrum resources and mitigating interference, contributing to energy efficiency in wireless communication systems.

1) **Coverage Enhancement**
   - IRS manipulates radio waves to optimize reflections, substantially improving wireless coverage. Through field trials, IRS showcases its ability to enhance communication coverage in both indoor and outdoor settings.
2) **Capacity Improvement**
   - By adjusting the phase shift of reflected waves, IRS enhances wireless channel quality, resulting in increased capacity. Validated pathloss models and radiation patterns through simulations and field-trial measurements provide a foundation for ongoing research in IRS-assisted communications.
3) **Energy Efficiency**
   - IRS optimizes radio resource usage, leading to improved energy efficiency. By manipulating radio waves, IRS boosts received signal power, reducing the need for high transmit power. This energy-saving approach enhances overall system efficiency.

     IRS technology extends coverage outdoors and indoors, addressing various environments and needs. It manages interference, enhances MIMO spatial channels, and offers multiple wireless propagation paths, improving signal strength, coverage, and system efficiency. Experimental validation ensures reliable performance. IRS technology stands out in coverage, capacity, and energy efficiency. Intelligent radio wave manipulation improves coverage by enhancing the signal-to-noise ratio (SNR) in diverse environments. Software-controlled phase adjustment optimizes system metrics, increasing capacity in wireless communication systems. IRS enhances energy efficiency by fine-tuning transmit power and reducing interference, ensuring resource-efficient utilization.

13.4 Channel Modeling and Propagation Measurements for Communication Systems

Channel modeling involves the creation of mathematical models that accurately represent the transmission and reception of signals between transmitters and receivers. These models are essential for predicting various parameters, such as signal strength and phase shifts, which are key to the effective performance of communication systems. To ensure the accuracy of these models, it is crucial to gather real-world data through propagation measurements. These measurements are conducted in various scenarios and environments, providing valuable insights into how signals behave in real-world conditions, such as indoor and outdoor locations, LoS, and NLoS conditions, and across a range of frequency bands. The important points of channel modeling and propagation measurement are explained below.

13.4.1 Importance of Accurate Channel Modeling

In wireless communication applications, accurate channel modeling is fundamental for understanding channel behavior, predicting performance, and designing efficient communication systems. It facilitates the evaluation of factors such as interference, fading, and noise impact on the channel. Essential for simulating and testing wireless communication systems, accurate channel modeling ensures reliability and performance and aids in the development of advanced technologies like 5G and beyond. Accurate channel modeling is crucial for advancing the IRS and optimizing its impact on communication systems. This modeling is instrumental in understanding the potential improvements in wireless channel quality and coverage that can be achieved through the IRS. In addressing key factors such as pathloss, radiation pattern, mirror beam effect, and multipath effects, accurate channel modeling guides in developing theoretical models and measurement techniques. It is particularly significant in designing optimized IRS phase-shift configurations to eliminate mirror beam effects and provide insights into IRS physical properties and performance limitations. The importance of accurate channel modeling extends to various wireless communication contexts, including MIMO systems. It guides the design and optimization of communication systems by offering insights into channel characteristics and performance limitations. For IRS in both indoor and outdoor scenarios, accurate channel modeling helps optimize system performance. It enables the correlation analysis between transmitter-IRS and IRS-receiver channels, generating line of sight (LOS) and non-line of sight (non-LOS) channel coefficients. This information is vital for system design and optimization, allowing assessment of the received SNR in noisy environments. In indoor scenarios, accurate channel modeling identifies weak coverage areas, devises strategies for network improvement, and determines IRS placement. Considering indoor layout and user occupancies, it offers a realistic representation of communication channels. This modeling evaluates rate gains, assesses IRS placement effectiveness, and calculates path loss for the cascaded channel, optimizing IRS phase angle configurations [41]. For IRS-empowered wireless networks, accurate channel modeling delves into electromagnetic wave propagation on IRS and optimizes their spatial placement. Realistic models considering near-field EM propagation and interactions in the IRS circuitry are crucial. This modeling estimates channel gains at IRS elements, studies path loss models, and enables the design of networking schemes empowered by the IRS for ultra-reliable and ultra-high-rate communications. Accurate channel modeling predicts wave propagation in multipath radio environments to analyze IRS-enabled connections. It accounts for mutual coupling between IRS unit cells, multipath effects, and the variability of IRS scattering properties.

13.4.2 Nonstationary Nature of Wireless Channels and its Impact

Wireless channels exhibit a nonstationary nature, characterized by variations in their characteristics over time and space. This dynamic behavior is influenced by mobility, environmental conditions, and interference, posing challenges for IRS-assisted communication systems. Understanding and modeling this nonstationary nature is crucial for optimal system design and performance.

13.4.2.1 Dynamic Impact on IRS-Assisted Communication

The dynamic nature of wireless channels significantly impacts IRS-assisted communication systems. Changes in the wireless channel introduce variations in path loss, signal strength, and overall communication link quality. Accurate channel modeling techniques consider these dynamic aspects, providing insights into IRS performance limitations and optimization strategies. Field trials and measurements validate theoretical models, shedding light on the impact of nonstationary wireless channels on IRS-assisted communications.

13.4.2.2 Challenges Posed by Nonstationary Channels

Inherent nonstationarity in wireless channels, attributed to object movement, environmental changes, and interference, results in signal strength, fading, and interference variations. Accurate modeling of nonstationary wireless channels is crucial for comprehending and predicting their behavior, enabling the development of efficient signal processing algorithms to mitigate fading and interference effects.

13.4.2.3 Time-Varying Channel Conditions

The nonstationary nature of wireless channels leads to time-varying channel conditions, which cause fluctuations in signal strength, increased error rates, and reduced overall system capacity. Adaptive techniques, including adaptive modulation and coding, channel estimation, and diversity schemes, dynamically adjust transmission parameters based on current channel conditions, mitigating the impact of nonstationary channels.

13.4.2.4 Variability in Indoor Environments

In indoor scenarios, the nonstationary nature of wireless channels is influenced by walls, furniture, and architectural elements. This variability results in signal strength, interference, and multipath propagation fluctuations, impacting the quality and reliability of wireless communication. Accurate modeling is essential for understanding and optimizing communication system performance in indoor scenarios.

13.4.2.5 Mitigation Strategies Using IRS Placement

The strategic placement of the IRS can mitigate the impact of nonstationary channels. These surfaces enhance network coverage and improve coverage rates in challenging areas. Accurate modeling, considering the indoor layout, user occupancies, and realistic channel models, allows for evaluating rate gains and the effectiveness of IRS placement approaches.

13.4.2.6 Impact on Throughput, Latency, and Reliability

The nonstationary nature of wireless channels, leading to fluctuations in signal strength, multipath fading, and time-varying channel conditions, significantly impacts the performance of wireless communication systems. Parameters such as throughput, latency, and reliability are affected. Accurate modeling of non-stationary channels is crucial for optimizing the design and performance of wireless communication systems, including those empowered by the IRS.

13.4.3 Channel Sounders and Measurement Campaign

A channel sounder measures a communication channel's properties, and the measurement campaign involving real-world data collection in various scenarios validates channel models. Below is a detailed explanation of channel sounders and measurement campaigns.

13.4.3.1 Channel Sounders

A channel sounder is a system used to measure the properties of a communication channel. It typically consists of a fast data acquisition unit, a transmitter, and a receiver. As the frequency of operation increases, the equipment required becomes more expensive and challenging to design. This includes high-performance signal generators, arbitrary waveform generators, digitizers, power amplifiers, phase-stable cables, high-gain antennas, and low-noise amplifiers. Designing a mmWave channel sounder with features like an extensive dynamic range, wide bandwidth, quick measuring speed, long continuous record time, extended measurable distance, and support for multiple channels presents significant challenges. The channel impulse response (CIR) or channel transfer function (CTF) can be obtained by measuring the frequency or time domain channel parameters.

- **Frequency domain channel sounders**: A frequency domain channel sounder, often implemented with a vector network analyzer (VNA), is a precise tool that employs multi-tone signals across a broad frequency range to analyze the channel. This method allows precise frequency sweeping over a wide bandwidth with synchronized hardware [42]. The measured parameter,

S21, represents the CTF and can be converted to the CIR. However, this approach is primarily suitable for indoor measurements due to limitations in measurable distance caused by high-frequency cable attenuation [43]. Additionally, obtaining a snapshot of the channel can be time-consuming, making it more suitable for quasi-stationary environments where channel variations are minimal. Efforts to extend the dynamic range and measurable distance of VNA-based channel sounders include integrating additional up-converters and down-converters to reduce cable losses and using signal generators to increase the distance between transmitter and receiver [44]. Cable connections allow for frequency control and reference clock synchronization between the signal generator and VNA. Moreover, employing electronic to optical (E/O) and optical to electronic (O/E) converters allows for longer optical fiber cables with lower loss. Custom-designed frequency domain channel sounders have also been developed. For instance, a digital frequency sweep channel sounder was created using multi-tone signals for a 2×2 MIMO channel analysis [18]. Another channel sounder measured a 24×24 MIMO channel using unmodulated multi-tone signals [17], while another employed multi-tone sounding signals for an 8×2 antenna array analysis on both transmitter and receiver sides [45].

- **Time domain channel sounders**: The Time domain channel sounders operate by transmitting pseudo-noise (PN) sequences or short pulses from the transmitter and recording the received signals at the receiver using a sampling oscilloscope. These signals are cross-correlated to produce the CIR. This method is implemented with commercial off-the-shelf (COTS) hardware or custom-designed components, and it offers efficient data compression and high bandwidth for real-time recording and fast post-processing [46]. One common technique, known as the swept time-delay cross-correlation sounder, utilizes the PN sequences for pulse compression, resulting in an improved SNR [16, 47]. Wideband correlation techniques have recently been developed that allow high-speed analog to digital converters (ADCs) to directly sample without the requirement for waveform copying [48]. In time domain channel sounders, transmitter and receiver units can be separated, making them suitable for outdoor measurements to quickly capture many samples [49]. However, the component's bandwidth or sampling speed limits the maximum signal bandwidth. UVA and rotated directional antenna (RDA) methods are commonly used to gather angular domain information [44]. These methods involve scanning directional antennas or shifting omni-directional antennas to characterize angular information. One drawback is that the channel must remain static during measurements. Additionally, some channel sounders support MIMO channel measurements using real antenna arrays [8].

Table 13.2 Transmission over several networks.

References	Network architecture	Fading channel	Performance metric	Summary
Li et al. [50]	NOMA	Nakagami-m	Secure outage probability	Investigated the effects of in-phase and quadrature-phase imbalance on single-input multiple-output (SIMO)–NOMA systems.
Cao et al. [51]	NOMA	Rayleigh	Secure outage probability	Full duplex Jam scheme, employing a multi-antenna full-duplex relay and jamming, significantly enhances secrecy performance in downlink NOMA systems by effectively mitigating eavesdropping threats.
Xie et al. [52]	NOMA	Rician	Secure outage probability	Secrecy performance in the half-duplex relay scenario, in the presence of an eavesdropper, can be enhanced through power allocation coefficient optimization in NOMA schemes, as verified through simulations.
Xu et al. [53]	Vehicular network	N-Nakagami	Strictly positive secrecy capacity (SPSC), secure outage probability, average secrecy capacity (ASC)	Investigations have been conducted on the secrecy performance of mobile vehicular networks. Using Monte Carlo simulations, exact closed-form formulations were developed and validated for the probabilities of SPSC, secure outage probability, and ASC.

Zhao et al. [54]	DF Relay network	Generalized-k	Secure outage probability	The study indicates how different relay systems behave regarding secrecy outage probability (SOP) and asymptotic secrecy outage probability (ASOP). It also develops a fast code rate calculation method based on the derived expressions, indicating characteristics such as diversity order and slope consistency with varying SNR.
Yadav [55]	Cognitive radio sensor network (CRSN)	α-μ	secure outage probability	These authors examined a CRSN's secrecy performance during α-μ fading. Through simulations, exact and asymptotic secrecy outage probability expressions are generated and verified.
Bayat and Çolak [56]	Cognitive radio DF relay network	Rayleigh	secure outage probability, Strictly Positive Secrecy Capacity	The study examines the secrecy outage probability of a dual-hop DF underlay cognitive radio network system under slow Rayleigh fading channels. It indicates that co-channel interference (CCI) and primary network interference affect system performance, and consistent analytical and simulation findings emphasize the need to account for primary network interference.
Song et al. [21]	mmWave communication	Nakagami-m	Secure outage probability, secrecy capacity	It introduces an adaptive transmission scheme, utilizes stochastic geometry to derive secrecy metrics, and identifies the best power allocation for increased secrecy throughput. These findings have implications for the guard zone radius of sector secrecy and potential applications in complex scenarios like UAVs and non-orthogonal multiple access (NOMA).

13.4.3.2 Measurement Campaign

Measurement campaigns involving real-world data collection in various scenarios validate channel models. Simulation-based measurements, using software tools and channel models, analyze propagation characteristics in different scenarios, aiding the understanding of parameter impacts on channel behavior. Measurement campaigns examine wireless channels, focusing on the efficiency of the communication systems and how signals move through the environment. In order to collect real-world data, several efforts are required to set up equipment across several places. Several parameters are essential to analyze in a wireless communications measurement campaign to collect data for channel modeling and define the radio channel's behavior. Table 13.2 presents various networks with different fading channels and performance metrics.

13.5 IRS Channel Modeling

In communication systems, channel modeling for the IRS utilizes mathematical representations to describe the propagation of signals inside these configurations, aiming to capture the complex interactions between the IRS, the environment, and transmitted signals. These models provide significant insights into signal behavior and system performance by considering various aspects such as phase shifting, attenuation, scattering, reflection, and multipath propagation. Various pathloss and channel models are described below for comprehensive channel modeling. Figure 13.2 explains the different channel models and briefly discusses the information on the channel models. Figure 13.2 shows three channel models:

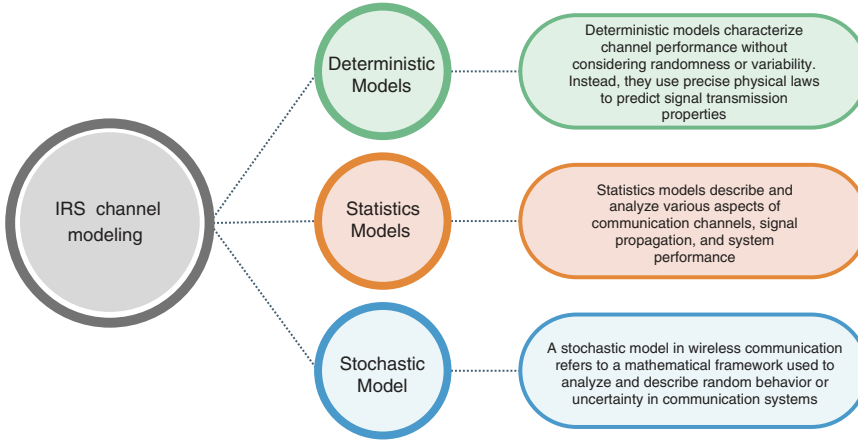

Figure 13.2 Different models for channel modeling.

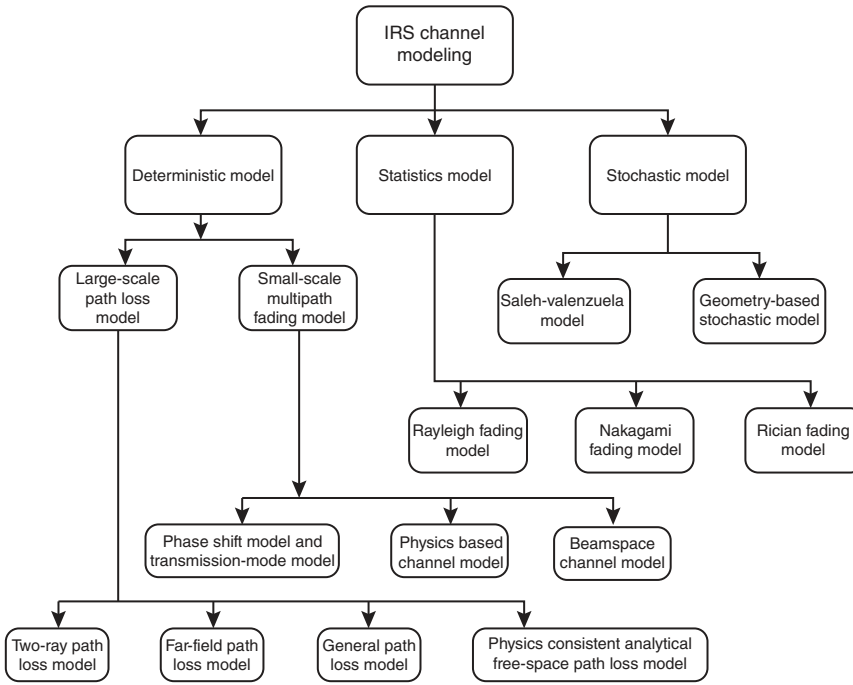

Figure 13.3 Detailed information about the different channel models.

the deterministic channel model, the statistics channel model, and the stochastic channel model.

Figure 13.3 shows the depth of this channel modeling. The Deterministic channel model has a large-scale path loss model and a small-scale multipath fading model. The large-scale path loss model has a two-ray path loss model, far-field path loss model, general path loss model, and physics-consistent analytical free-space path loss model. The small-scale multipath fading model has phase shift and transmission-mode channel models, physics-based channel models, and beamspace channel models. The statistics channel model has the Rayleigh fading channel model, the Nakagami fading channel model, and the Rician fading channel model. The stochastic model has the Saleh–Valenzuela model and the geometry-based stochastic model.

13.5.1 Deterministic Models

In wireless communication, deterministic models characterize channel performance without considering randomness or variability. Instead, they use precise mathematical equations or physical laws to predict signal transmission properties.

These models assume a perfect understanding of the environment and how electromagnetic waves behave. They work well when the channel environment is clear and does not change much, like when there is a direct LOS between sender and receiver or in controlled indoor spaces. However, they may not be as reliable in dynamic or complex situations where randomness and change are important.

13.5.1.1 Large-Scale Path Loss Models

In wireless communication systems, large-scale path loss models represent the attenuation of the signal's strength as it travels over a distance. These models describe the signal power loss resulting from different factors, such as multipath fading, shadowing, and free-space loss. The transmitted signal in wireless communication systems attenuates as it travels in the medium. The path loss models are covered in detail in the following survey.

To better understand the operation of the IRS, [57] examined the two-ray path loss approach, comprising a ray with LoS and a ground-reflected ray.

$$P_r \approx (Q+1)^2 P_t \left(\frac{\lambda}{4\pi d_{tr}} \right)^2 \tag{13.1}$$

The received power denoted by P_r, is directly proportional to the square of the number of elements in the IRS is denoted by Q, and inversely proportional to the square of the distance between the transmitter and receiver, denoted by d_{tr}. Thus, the path loss can be mitigated as the number of elements in the IRS increases.

In [6], a far-field path loss model for IRS communications utilizing physical optics techniques has been presented. The analysis revealed several elements on the surface, all of which function as diffuse scatterers. Nevertheless, when combined, all of these elements can beamform the signal with a particular beamwidth and in the desired direction. The mathematical expression for the far-field path loss was as follows:

$$PL = \frac{\left(4\pi d_1 d_2\right)^2}{G_t G_r (ab)^2 \cos^2\theta_i \text{sinc}\left(\frac{\pi b}{\lambda} \left(\sin\theta_s - \sin\theta_r \right) \right)} \tag{13.2}$$

The sampling function is represented by the equation sinc(x) = sin(x)/x, and the dimensions of the rectangle IRS are indicated by the variables a and b. The antenna gains of the transmitter and receiver are denoted by G_t and G_r, respectively. Furthermore, d_1 and d_2 represent the distances between the transmitter and receiver to the IRS. The angles of incidence, desired reflection angle, and observed reflection angle are denoted as θ_i, θ_r, and θ_s, respectively. When observing at the desired reflection angle, i.e., $\theta_s = \theta_r$. Simplified, the path loss model is:

$$PL = \frac{\left(4\pi d_1 d_2\right)^2}{G_t G_r (ab)^2 \cos^2\theta_i} \tag{13.3}$$

Inversely proportional to the square of the product of distances d_1 and d_2, the received power is directly proportional to the square of the IRS area. This differs from the assertion made in [57], which suggested that the power obtained would be proportional to $\frac{1}{(d_1+d_2)^2}$. This assumption may be valid for an IRS of infinite size, where the IRS functions as a mirror. However, it is likely to be inaccurate in a far-field setup.

A general path loss model for IRS-assisted communication was presented in [26]. The formulation of this model is as follows:

$$PL = \frac{64\pi^3}{G_t G_r G d_x d_y \lambda^2} \times \left| \sum_{m=1}^{M} \sum_{n=1}^{N} \frac{\sqrt{F_{n,m}^{combine}}\Gamma_{n,m}}{r_{n,m}^t r_{n,m}^r} e^{\frac{-j2\pi\left(r_{n,m}^t + r_{n,m}^r\right)}{\lambda}} \right|^{-2|} \tag{13.4}$$

where d_x and d_y represent each element size along the x-axis and y-axis, respectively, m and n denote the number of elements along the x-axis and y-axis, respectively. G stands for one element's gain. $F_{n,m}^{combine}$. $\Gamma_{n,m}$ demonstrate each element's normalized power radiation pattern and how it influences the power of the received signal. $\Gamma_{n,m}$ represents the reflection coefficient of each element with amplitude A and phase ϕ, and $r_{n,m}^t$ and $r_{n,m}^r$ signify the distances from the transmitter and receiver to each element. This highlights the relationship between the received power and various factors, including the antenna size, gains, number, specific electromagnetic properties of elements, and the distances traveled.

A physics-consistent analytical free-space path loss model for IRS was introduced, leveraging a vector-based extension of Green's theorem [58]. This model applies to 2D homogenized metasurfaces and is characterized by a computable integral dependent on various factors such as transmission distances, radio wave polarization, surface dimensions, and intended surface transformation. The closed-form expressions were obtained for both far-field and near-field deployment scenarios. A path loss model for THz communication systems aided by the IRS was presented in [59]. This model considers the unique characteristics of the THz band and IRS. Specifically, it explains the relationship between various IRS specifications, including element size, number of elements, phase shift, radiation pattern, reflection coefficient, and transmission parameters such as frequency band, transmitter–receiver distance, and THz-specific parameters. In [60] presented a path loss model for IRS communications based on radar cross-section (RCS). The distances between the transmitter and receiver and the IRS, the angles in the transmitter-IRS-receiver triangle, and each element's effective area and reflection coefficient were all related to the received power.

Furthermore, channel measurements were performed in various scenarios to confirm the suggested model in both near-field and far-field environments.

13.5.1.2 Small-Scale Multipath Fading Models

Small-scale multipath Fading Models describe the rapid fluctuations in signal strength caused by the constructive and destructive interference of multiple signal paths arriving at the receiver. Some small-scale channel models have been proposed for communication supported by the IRS. These consist of the phase shift model and transmission-mode model, physics-based channel model, geometry-based stochastic model, and beamspace channel model [61].

- **Phase Shift Model and Transmission-Mode Model**: The three cascading subchannels are described by the phase shift model: the direct transmitter-receiver channel, the transmitter-IRS channel, and the IRS-receiver channel [27]. However, this model has two drawbacks. First, the number of scatterers, which is usually fewer than the number of IRS elements, limits the ranks of the transmitter-IRS matrix and the IRS-receiver matrix. Second, it does not account for the physical properties of the IRS, polarization, incident angles, and reflected angles. To address these drawbacks, the transmission-mode model was proposed. The large IRS is divided into tiles by this model, which also calculates the tile response function. After that, it selects multiple transmission modes for each tile by dividing the low-rank channel matrices. Each transmission mode is associated with a specific sequence of phase shifts that the tile's unit cells apply to an incoming electromagnetic wave.
- **Physics-Based Channel Model**: For IRS communications, a physics-based channel model was presented in [62]. The multipath propagation of signals is examined in this model, it considers the scattering environment and the IRS as a single entity. The combined channel contains a specular component from the IRS LoS connection and a scattered component from the NLoS direct link. The model takes into account M IRS multipath components (MPCs) and N MPCs for the scattering environment while analyzing channel information. It suggests that a Rician distribution can effectively approximate the wireless channel aided by the IRS. In [11, 12], far-field situations with holographic MIMO small-scale fading, a spatially stationary channel model was introduced. This concept describes an array with many antennas in a small area, like the IRS configuration. The small-scale fading was described by a zero-mean, correlated Gaussian scalar random field that is spatially stable and obeys the Helmholtz equation in the frequency domain, which is equal to the scalar wave equation in the time domain. For IRS-assisted free-space optical systems, an analytical channel model based on the Huygens–Fresnel principle was presented in [63]. This model accounts for various effects, including the phase

shift configuration of the IRS, the influence of IRS size, the positions of the source, and the nonuniform power distribution of Gaussian beams.

- **Beamspace Channel Model**: In [64], a beamspace channel model was introduced for IRS communications. This model considers the IRS as a controllable scattering cluster reflecting its MPCs, in contrast to the phase shift paradigm. It is constructed using the expanded Saleh Valenzuela (SV) channel architecture. Additionally, an antenna segmentation approach was proposed to integrate the IRS into the developed far-field model, highlighting the characteristics of its MPCs and demonstrating their controllability.

13.5.2 Statistics Models

Several statistical models are used in wireless communication systems to characterize different aspects of the communication channel. Some statistical models include the following.

13.5.2.1 Rayleigh Fading Model

Rayleigh fading is a statistical model commonly used in wireless communication systems to describe how multipath propagation affects the received signal. The assumption is that the transmitter and receiver do not have a strong line-of-sight connection. However, the signal travels through several reflected paths, each with a unique phase and amplitude, finally reaching the receiver. In this model, the strength of the received signal follows a Rayleigh distribution, showing the likelihood of the signal envelope having a particular strength. Fading describes unexpected changes in signal strength that occur over time due to reflections, diffractions, and scattering in the surrounding environment. Rayleigh fading is applicable in urban or suburban areas with many obstacles, reflective surfaces, and indoor or outdoor settings where direct paths are blocked. Relay stations and IRS are essential for strengthening wireless communication networks under Rayleigh fading scenarios when signals fluctuate rapidly due to multipath propagation. IRS technology manipulates signal propagation by strategically reflecting signals, reducing the impact of fading. By changing the phase shifts of its elements, IRS can improve received signal strength and reduce fading by reflecting the signals toward the receiver. Additionally, the IRS can create multiple reflected paths, enhancing reliability in fading channels. Relay stations that perform decode and forward operations compensate for signal loss resulting from fading, particularly when long distance or obstructed paths. They create additional transmission paths, reducing fading effects and improving link reliability. The hybrid relay-IRS system is a combination of IRS and relay. The hybrid relay-IRS system satisfies high data rates and more extended distance coverage specifications [14]. As shown in Figure 13.4, the hybrid relay-IRS system architecture consists of

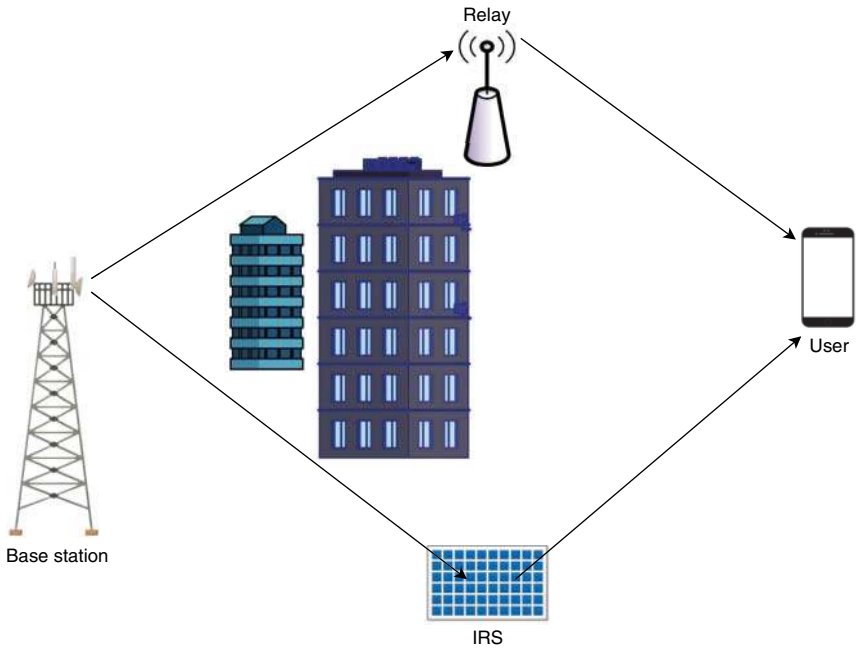

Figure 13.4 System model: hybrid relay-IRS-aided system model.

four main parts: the base station, relay, IRS with N elements, and mobile user. A half-duplex relay uses the Decode and Forward (DF) protocol to overcome the base station's limited coverage area. Moreover, with its reflective capabilities, the IRS improves transmission from the source to the destination by strategically manipulating signal reflections. In this scenario, the base station sends signals to the relay, which can transmit signals to the mobile user. The transmission from the base station to the mobile user follows a half-duplex DF protocol involving two-time slots. Signals are transmitted from the base station to the relay in the first slot. Then, in the second slot, the relay decodes the signal and forwards it to the mobile user. Additionally, the base station sends signals to the IRS, which then reflects these signals to the destination. The IRS comprises N discrete elements, and the user receives the signals reflected by the IRS.

The EE versus user distance is shown in Figure 13.5 for three different types of wireless networks: hybrid relay-IRS-aided, relay-aided, and IRS-aided. Plotting shows that the hybrid relay-IRS network EE performs better than the IRS-aided and relay-aided networks. This suggests that employing a hybrid relay-aided IRS is more effective in covering longer distances. Remarkably, at 700 m, the EE of the hybrid relay-IRS-aided network and the relay network achieve 7.11 and 7.36 bits/Joule, respectively.

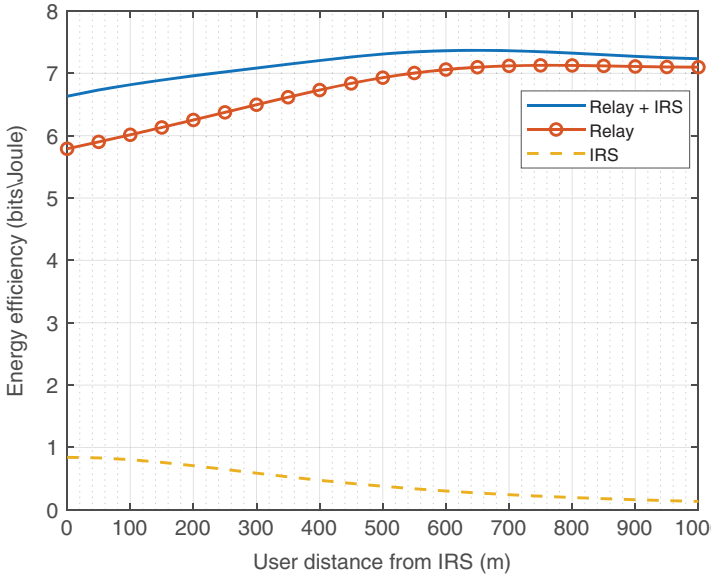

Figure 13.5 EE versus user distance.

13.5.2.2 Rician Fading Model

In Rician fading, the received signal comprises a strong LoS component and scattered multipath components. Two essential factors are required for the Rician fading model to operate effectively: K is the Rician factor, and σ, which stands for the multipath components standard deviation. The Rician factor K indicates the ratio of the power of the dominant LoS component to that of the scattered multipath components. In comparison to the scattered multipath, a greater value of K denotes a stronger LoS component, whereas a lower value denotes a weaker LoS component with more multipath effects. When there is a direct LoS between the transmitter and the receiver, such as in rural or urban locations with few obstacles, the Rician fading model is frequently used. Here, consider in Figure 13.6 the Rician fading at the base station, the users, and the IRS. The IRS stands out as a leading solution and offers hope for meeting future generation requirements at the Rician fading scenario. Figure 13.6 shows that combining IRS with MIMO could significantly improve spectral efficiency and capacity, and by adding these, a small amount of complexity is added. When combined, IRS and MIMO may perform various tasks that improve overall system performance. IRS-assisted MIMO systems resolve many of the issues with conventional MIMO configurations. IRS–MIMO performance is enhanced by optimizing transmitter/receiver precoding matrices, phase shifts, and neural network algorithms, among other techniques.

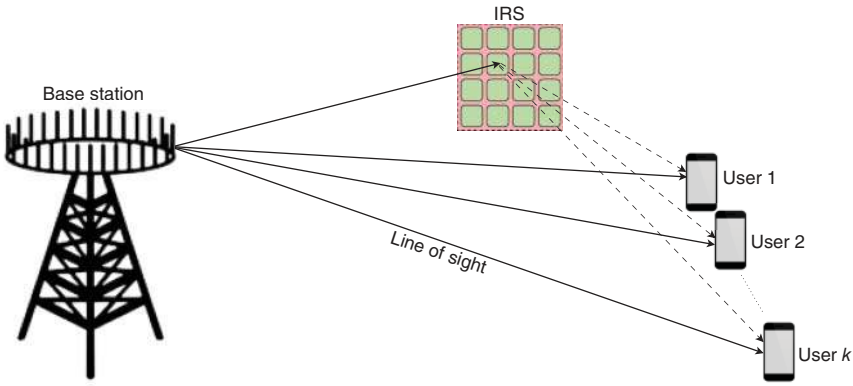

Figure 13.6 System model: IRS-assisted MIMO system model.

13.5.2.3 Nakagami Fading Model

The Nakagami fading model is an essential statistical method for characterizing changes in signal strength during transmission in wireless communication systems. The received signal strength in the model is governed by two key parameters: m and Ω. The parameter m, also known as the fading parameter, plays a significant role in shaping the distribution and determining the severity of fading. Higher m values result in less severe fading, resembling a Gaussian distribution, while lower values indicate more fading. The range of signal strength variations is determined by the second parameter, Ω, often known as the scale parameter, which governs the signal's diversity or spread. This adaptable model effectively represents different fading situations that arise in wireless environments. For example, the Nakagami model simplifies to a Rayleigh distribution when $m = 1$. This distribution is frequently observed in NLoS situations such as urban multipath fading. Conversely, when m is greater than 1, the model suggests a Rician distribution, familiar in LoS scenarios with a dominating direct path. The Nakagami fading model provides adaptability. It enables switching between Rayleigh and Rician distributions and adjusting m according to different scenarios. This flexibility allows the model to capture a range of propagation circumstances from LoS to NLoS scenarios, which is important for real-world observations. In the Intelligent Transportation System (ITS) model depicted in Figure 13.7, the transportation network operates in two different scenarios. The cooperative IRS-relay network supports the ITS [15], the IRS and relay transmit the signal from the base station to the intelligent vehicles, ensuring seamless connectivity with high data rates. The multiple IRS blocks instead of relays are deployed within the ITS. This deployment aims to enhance the network's coverage area and EE.

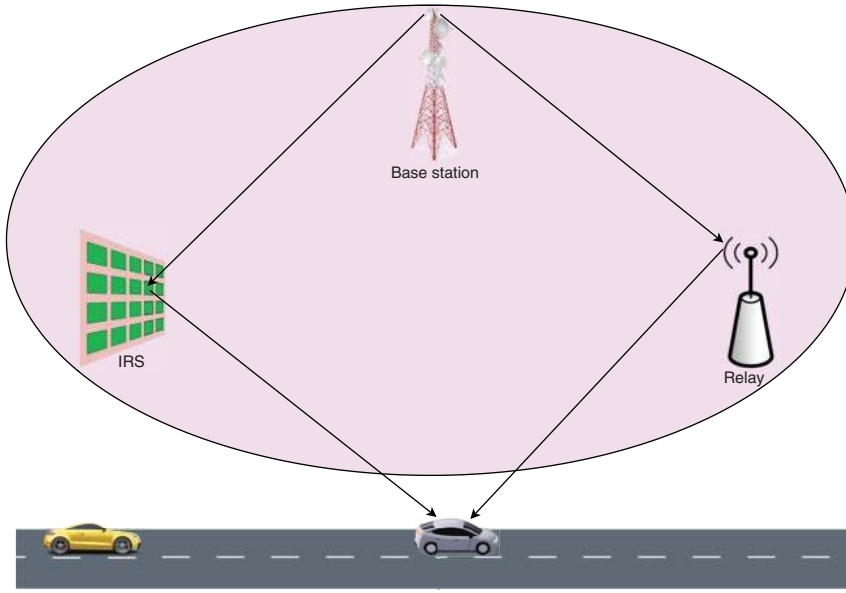

Figure 13.7 System model: cooperative relay-IRS aided ITS model.

Figure 13.8 explores the EE versus SNR for cooperative IRS-relay and multi-IRS-aided ITS. In the multi-IRS scenario, all IRS blocks employ a fixed number of elements set to $N = 400$. The results indicate that the multi-IRS-aided ITS exhibits superior EE performance across all SNR values. Specifically, at SNR = 110 dBm, the network aided by 4-IRS blocks demonstrates the highest EE at 64.23 bits/Joule, surpassing the conventional IRS, relay, and cooperative IRS-relay network with an EE of 46.44 bits/Joule. This analysis underscores the potential of multi-IRS configurations to enhance ITS performance by reducing power consumption and hardware costs in specific scenarios.

13.5.3 Stochastic Model

In channel modeling, stochastic models combine deterministic and statistical methods to provide an in-depth understanding of wireless propagation scenarios. These models incorporate randomness and deterministic features to provide an adaptable framework for analyzing complex propagation environments. Stochastic models offer a distinct advantage in channel modeling by providing a probabilistic representation of channel behavior, effectively capturing wireless channel's inherent unpredictability and uncertainty. This approach evaluates the system's performance in various scenarios while considering factors such as multipath propagation, shadowing, and interference. Stochastic models facilitate

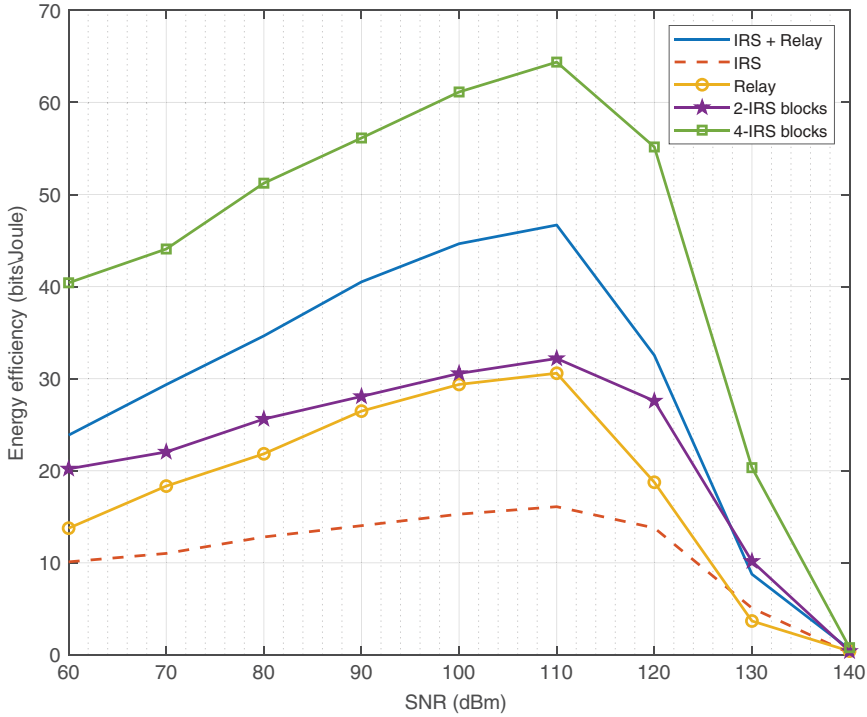

Figure 13.8 EE versus SNR.

the design and optimization of robust communication systems in real-world situations by providing an exhaustive overview of channel characteristics and maintaining a balance between predictability and randomness. Some stochastic models include the following.

13.5.3.1 Saleh–Valenzuela-Based Model

The SV based model often represents channel impulse response in indoor environments [44]. The foundational premise is that signals come gradually in clusters, with inter-arrival periods distributed exponentially and delays distributed according to a Poisson distribution. The characteristics of these clusters include parameters such as arrival rates and cluster power decay rates. The adjustments made to this model for usage in IEEE standards such as 802.15.3c and 802.11ad [44] consider precursor and postcursor decay rates within each cluster.

13.5.3.2 Geometry-Based Stochastic Model

5G and 6G channel modeling applications have extensively used the GBSM technique, as evidenced by the proposed channel models in [65]. In [33], an

open-source SimIRS channel simulator was introduced for IRS-assisted communication. The setup involves a 3D geometry with an IRS mounted on the xz-plane, representing physical channel characteristics. The model accounts for indoor and outdoor wireless environments at mmWave frequencies, adopting practical aspects from 5G channel models. Operating frequency and environmental factors determine the number of clusters and their locations. Two types of distributions are used for clusters and scatterers: Poisson and uniform. When the receiver is close to the IRS, they may share the same clusters. It is easy to calculate the array response vectors for the IRS and transmitter using departure/arrival angles. However, if angles are random for the transmitter, they must be calculated using trigonometry for the IRS. Receiver array response vectors can have randomly distributed arrival angles. This simulator's channel model is versatile, catering to various indoor and outdoor scenarios and operating across different frequency bands, including the mmWave band. It is similar to the 3GPP cluster channel model and consists of realistic path loss and shadowing models, IRS element gains, transmitter/receiver units, array responses of IRS, LoS probabilities between terminals, and environmental characteristics across various scenarios and frequency bands. However, it is worth noting that this model is primarily suited for far-field scenarios. Furthermore, in [66], the SimIRS channel simulator was leveraged to offer insights into the performance optimization of IRS-assisted smart radio environments (SREs). The study investigated the effects of IRS positioning, the rotation of IRS in single and multi-IRS environments, and the number of reflecting elements. The findings underscored the critical importance of these factors in achieving capacity and reliability enhancements in SREs.

Table 13.3 provides information about the IRS literature. It includes information about which model is used for IRS channel modeling, how many devices are involved, which metrics are found, and the summary of the article.

- **IRS–NOMA**: The combination of NOMA and IRS technology presents a promising solution to address the challenges of future-generation networks. Integrating IRS with NOMA networks holds significant potential to meet the data rate requirements of 6G networks. By leveraging NOMA with IRS, a novel approach emerges to address the demanding needs of low latency, massive connectivity, and high data rates in future networks. Traditionally, user's channel conditions were considered fixed, determined solely by their propagation environment. However, the IRS offers the opportunity to intelligently adjust the user's propagation environment to support NOMA applications, resulting in considerable performance improvements. Specifically, incorporating IRS with NOMA provides more flexibility in system design, particularly when users have similar channel gains. This flexibility allows for transitioning from a channel condition-based NOMA approach to a quality-of-service (QoS)-based

Table 13.3 IRS literature.

References	Channel	Devices	Metrics	Summary
de Souza Junior and Abrao [67]	Nakagami	IRS, two users	Outage Probability	The study examines the cooperative simultaneous wireless information and power transfer (SWIPT)–NOMA system with IRS assistance in Nakagami-*m* fading. For cell-edge devices, the cell-center device acts as an full duplex (FD)–DF relay. The energy harvesting, outage probability, and achievable rate have been calculated using closed-form expressions. For cell-edge devices, IRS improves data rate; residual self-interference reduction is crucial.
Arzykulov et al. [68]	Nakagami	One/two IRS, source, destination	Outage Probability, Spectral Efficiency, bit error ratio (BER)	The article investigates dual-hop FD relaying networks assisted by IRS and gives precise mathematical derivations for BER, average spectral efficiency, and outage probability. The channel shape parameter and IRS elements determine system diversity order; a higher *N* value improves system efficiency.
Bhowal and Aïssa [69]	Indoor, outdoor reciprocal	IRS, one pair transceiver	Symbol Error Rate, Outage Probability, Ergodic Capacity	The study focuses on residual self-interference (SI) and hardware limitations in IRS-assisted FD MIMO bidirectional D2D communication in indoor and outdoor settings. Using a realistic channel model, it derives tractable formulas for outage probability, average symbol error probability, and channel capacity. According to validation using Monte Carlo simulations, the system performs better in indoor circumstances than in outdoor ones, across a range of self-interference levels, hardware impairments, and IRS setups.
Nguyen et al. [70]	Rayleigh reciprocal	IRS, two terminals	Symbol Error Rate, Ergodic Capacity	The article examines IRS-assisted wireless systems, focusing on FD terminal hardware and inadequate SI cancelation. It analyzes the performance of the IRS-aided FD-hardware impairments system with other configurations and develops closed-form formulas for ergodic capacity (EC) and symbol error rate (SER). The results show that residual SI and hardware impairments have a considerable impact and that modulation orders and SNR have an impact on EC and SER.

Nguyen et al. [71]	Rayleigh Reciprocal	*N* IRS, two terminals	Outage Probability, Ergodic Capacity	The study investigates the advantages of utilizing many IRS in future wireless networks, with an emphasis on improving coverage and system performance. By examining a bidirectional FD system assisted by multiple IRS, the study obtains equations for outage probability and EC under cooperative communication with residual SI in Rayleigh fading channels. Numerical results illustrate the impact of residual SI, showing saturation of outage probability and EC at high SNR values and demonstrating that larger IRS configurations might lead to better EC.
Peng et al. [9]	Rician	IRS, *K* pairs of devices	Outage Probability	The study examines the cooperative SWIPT–NOMA system with IRS assistance in Nakagami-*m* fading. For cell-edge devices, the cell-center device acts as an FD–DF relay. The energy harvesting, outage probability, and achievable rate have been calculated using closed-form expressions. For cell-edge devices, IRS improves data rate; residual self-interference reduction is crucial.
Kudumala et al. [72]	Spatially Correlated Rician	IRS, *K* full duplex user-pairs	Optimize sum- rate	The article investigates a multi-pair FD two-way communication system with IRS assistance, considering hardware limitations, electromagnetic interference (EMI), and spatially correlated Rician channels. It derives the attainable sum rates approximate closed-form equation and validates it with an ergodic equivalent.
Papazafeir et al. [7]	Correlated Rayleigh	STAR-IRS, two half duplex (HD) users	Optimize sum rate	In order to account for spatial correlation at the STAR–IRS, this study examines the sum rate of an FD communication system assisted by STAR–IRS. Only large-scale statistics are used to develop closed-form formulas for achievable downlink and uplink rates. Numerical simulations demonstrate that the low-overhead optimization approach performs better than reflecting-only IRS and HD systems.
Peng et al. [10]	Rician	IRS, one base station (BS), multiple users	Maximize-Minimum user rate	An IRS is used in a multiuser FD two-way communication network to improve user fairness. By optimizing the IRS reflection coefficients and the BS precoding matrix, the suggested approach achieves excellent communication performance at a low computational complexity.

NOMA approach. In NOMA systems, successive interference cancellation (SIC) is crucial in mitigating interference. The selection of the SIC decoding order is based on the user's channel state information (CSI) and their QoS requirements. IRS enhances the design flexibility of NOMA networks, enabling the relaxation of constraints typically encountered in multiple-antenna NOMA setups.

The IRS–NOMA system allocates more power to users with weaker channels. User 1 is positioned near the base station, while user 4 is the farthest away. Users 2 and 3 are situated between users 1 and 4, with user 2 closer to user 1 than user 3, as shown in Figure 13.9. Thus, the channel gains follow the order: $h_{SU4} < h_{SU3} < h_{SU2} < h_{SU1}$. In IRS–NOMA, superposition coding at the transmitter and SIC at the receiver combine data signals in the power domain. Four users, denoted as user 1, user 2, user 3, and user 4, aim to communicate simultaneously on the same frequency. Each user's desired data is represented as x_1, x_2, x_3, and x_4, respectively. Before adding x_1, x_2, x_3, and x_4, each data signal is weighted differently regarding power. It is important to ensure that the sum of the weights of power (a_1, a_2, a_3, and a_4) equals 1. Table 13.4 compares NOMA and orthogonal multiple access (OMA) with different specifications. Table 13.5 shows the literature on the performance of NOMA networks. It provides information on which fading channel is used, the type of the NOMA link, like downlink or uplink, and the article's contribution. Table 13.6 provides information on IRS-NOMA literature. It provides information on which fading channel is used, which type of NOMA link, characterization, and metrics of the article.

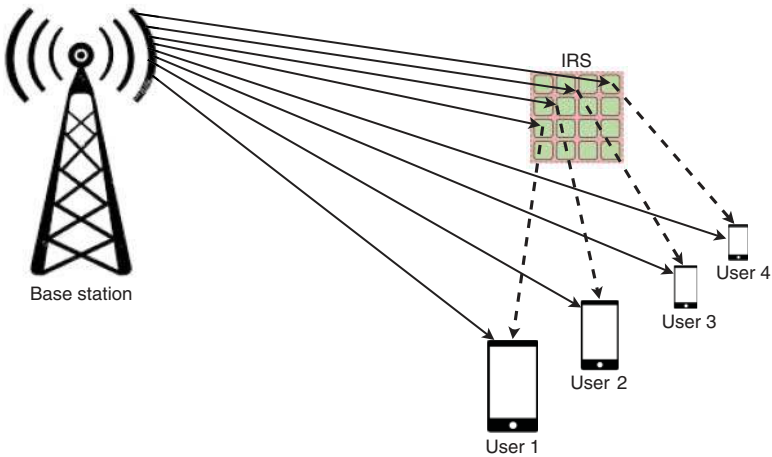

Figure 13.9 IRS-NOMA communication system. Source: Kriang/Adobe Stock Photos.

Table 13.4 Comparison of NOMA and OMA techniques.

Specification	NOMA	OMA
User connectivity	High	Low
System throughput	Larger	Smaller
Energy consumption	High	Low
Receiver complexity	High	Low

Table 13.5 Literature on NOMA networks performance.

References	Fading channel	Type of NOMA link	Contribution
Ding et al. [73] and Timotheou and Krikidis [74]	Rayleigh	Downlink	Evaluation of power distribution techniques and the impacts of user pairing in a network.
Zhang et al. [75]	Rayleigh	Uplink	Outage probability and sum rate analysis.
Liu et al. [76]	Rayleigh	Downlink and uplink	Power allocation analysis.
Ali et al. [77]	Rayleigh	Uplink	Power allocation and outage analysis using statistical CSI scheduling at base station.
Ding et al. [78]	α-μ, Nakagami-m	Downlink	Cooperative relaying functionality in the NOMA network.
Sharma et al. [20]	$\kappa-\mu$ and $\eta-\mu$	Downlink	Sum rate analysis and Outage probability.
ElHalawany et al. [79]	Shadowed $\kappa-\mu$	Downlink	Outage probability, Bit Error Rate, and average achievable rate.
Kumar et al. [80, 81]	$\alpha-\mu$ and shadowed $\kappa-\mu$	Downlink	Analyzing rates effectively.
Alqahtani and Alsusa [82]	α-η-μ	Downlink	Outage probability and sum rate analysis.
Rabie et al. [13]	Fisher–Snedecore	Downlink	Asymptotic analysis and ergodic capacity analysis.
Agarwal et al. [83]	$\kappa-\mu$, Rayleigh, Nakagami-m/q/ log-normal, Rician, Nakagami-lognormal, $\eta-\mu$	Downlink and uplink	Outage probability analysis.

Table 13.6 Performance evaluation of IRS-assisted NOMA networks.

References	Fading channel	Type of NOMA link	Characterization	Parameter metrics
Yuan et al. [84]	Rayleigh	Downlink	Exact and asymptotic expressions	Outage probability and ergodic rate.
Di Renzo and Song [85]	Rayleigh	Downlink	Closed-form expression	Outage probability.
Thirumaval and Jayaraman [86]	Rayleigh	Downlink	Closed-form expression	Bit error rate.
Mu et al. [87]	Rayleigh	Downlink	Analytical and asymptotic expressions	Secrecy Outage probability.
Ding et al. [88]	Rayleigh	Downlink	Approximated and upper bound expression	Outage probability.
Hou et al. [89]	Rayleigh	Downlink	Closed-form expression	Outage probability and ergodic rate.
Cheng et al. [90]	Nakagami-m	Downlink and Uplink	Closed-form expression	Outage probability and ergodic rate.
Tahir et al. [25]	Nakagami-m	Downlink and Uplink	Closed-form expression	Outage probability.
Tang et al. [91]	Nakagami-m	Downlink	Closed-form expression	Secrecy outage probability, ASC.

13.6 Limitations of the Survey

It is important to highlight the limitations that occurred when conducting this research. Among these limitations are:

- **Limitations on Scope**: Due to the broad scope of the topic, the survey may not cover all methods currently used for channel modeling and propagation measurement.
- **Lack of Data on IRS Channel Measurements**: Since IRS channel measurements and experiments are still in their early stages, comprehensive data on the topic are lacking. Further investigation and gathering of information are required in this field.

  Despite these drawbacks, an attempt was made to ensure the survey's accuracy and completeness.

13.7 Critical Lessons Learned

Through conducting this survey, several critical lessons were learned.

- **Enhanced Propagation Paths**: The capacity of IRS to optimize propagation paths by intelligently reflecting signals, therefore overcoming obstructions and expanding coverage range, particularly in NLOS conditions.
- **Dynamic Adaptability**: The IRS configuration's dynamic adaptability enables real-time adaptation to changing user requirements and environmental conditions, optimizing system performance.
- **Simplified Signal Processing**: Compared to standard MIMO systems, IRS-assisted systems require simpler channel estimation techniques, so signal processing complexity can often be reduced using IRS technology.

13.8 Potential Challenges of Propagation Measurements and Channel Modeling

- **Frequency-Selective Fading**: Frequency-selective fading effects in IRS-assisted communication systems, where different signal frequencies experience varied levels of attenuation or enhancement, require advanced modeling techniques to be incorporated into channel models.
- **Path Loss Variation**: Path loss in IRS-assisted channels varies significantly based on IRS element configurations, reflection angles, and the distances between the transmitter, IRS, and receiver. Developing models that capture path loss variations in diverse scenarios is crucial for optimizing system performance.
- **Nonstationarity and Time-Varying Nature**: The dynamic nature of UAV movement and the environment introduces nonstationarity and time-varying characteristics to the channel. Accurately capturing these variations in the IRS channel model is essential for realistic performance evaluation.
- **Complexity of IRS Systems**: Due to the large number of passive elements involved, accurately modeling the complex interactions among IRS elements, incident waves, and reflected waves is challenging.
- **Cluster-Based Modeling**: Challenges are in proper modeling clustering and scatterers in the channel for capturing multipath characteristics accurately in IRS-assisted communications.
- **Accuracy and Generality**: Traditional channel models may lack the accuracy and generality to describe realistic IRS-assisted UAV communication environments. Developing models that are both accurate and adaptable to various scenarios is a crucial challenge.

13.9 Conclusion and Future Scope

In this chapter, we provided a comprehensive review of channel modeling and propagation measurements in IRS-based wireless communication systems. This chapter has extensively examined the transformative impact of IRS within the area of 6G wireless communication, highlighting their pivotal role in reshaping network intelligence and efficiency. The IRS is an essential mechanism for improving communication capacities regarding coverage, energy efficiency, and capacity by manipulating radio waves. The chapter also discussed the different IRS channel models and complex issues related to channel modeling and propagation measurements in wireless environments. In contrast to conventional channel modeling techniques, IRS channel modeling represents a significant improvement. This chapter's comprehensive overview is valuable for academics and industry professionals in wireless communication. This chapter contributes to the fundamental knowledge necessary for developing and implementing cutting-edge wireless communication systems. To improve the accuracy and efficiency of channel modeling for IRS systems, future research will focus on developing dynamic IRS channel modeling, which accurately captures the time-varying characteristics of IRS-assisted communication channels, advanced propagation measurement techniques, which will allow for the accurate characterization of IRS-enabled communication channels, and machine learning algorithms, which will predict IRS-assisted channel characteristics based on user mobility patterns, environmental parameters, and historical channel data. These research paths will assist in developing accurate and reliable channel models for IRS-assisted communication systems, which will improve the performance and efficiency of future wireless networks.

References

1 Shi, E., Zhang, J., Chen, S. et al. (2022). Wireless energy transfer in RIS-aided cell-free massive MIMO systems: opportunities and challenges. *IEEE Communications Magazine* 60 (3): 26–32.

2 Imoize, A.L., Obakhena, H.I., Anyasi, F.I. et al. (2022). Reconfigurable intelligent surfaces enabling 6G wireless communication systems: use cases and technical considerations. *2022 5th Information Technology for Education and Development (ITED)*, 1–7. IEEE.

3 Imam-Fulani, Y.O., Faruk, N., Sowande, O.A. et al. (2023). 5G frequency standardization, technologies, channel models, and network deployment: advances, challenges, and future directions. *Sustainability* 15 (6): 5173.

4 Perović, N.S., Di Renzo, M., and Flanagan, M.F. (2020). Channel capacity optimization using reconfigurable intelligent surfaces in indoor mmWave environments. *ICC 2020 - 2020 IEEE International Conference on Communications (ICC)*, 1–7. IEEE.

5 Farashahi, M., Seet, B.-C., and Li, X. (2024). Framework for propagation modeling of IRS-assisted communication based on ray tracing. *Physical Communication* 63: 102301.

6 Özdogan, Ö., Björnson, E., and Larsson, E.G. (2019). Intelligent reflecting surfaces: physics, propagation, and pathloss modeling. *IEEE Wireless Communications Letters* 9 (5): 581–585.

7 Papazafeir, A., Kourtessis, P., and Krikidis, I. (2022). STAR-RIS assisted full-duplex systems: impact of correlation and maximization. *IEEE Communications Letters* 26 (12): 3004–3008.

8 Papazian, P.B., Gentile, C., Remley, K.A. et al. (2016). A radio channel sounder for mobile millimeter-wave communications: system implementation and measurement assessment. *IEEE Transactions on Microwave Theory and Techniques* 64 (9): 2924–2932.

9 Peng, Z., Li, T., Pan, C. et al. (2021). RIS-aided D2D communications relying on statistical CSI with imperfect hardware. *IEEE Communications Letters* 26 (2): 473–477.

10 Peng, Z., Zhang, Z., Pan, C. et al. (2021). Multiuser full-duplex two-way communications via intelligent reflecting surface. *IEEE Transactions on Signal Processing* 69: 837–851.

11 Pizzo, A., Marzetta, T., and Sanguinetti, L. (2020). Holographic MIMO communications under spatially-stationary scattering. *2020 54th Asilomar Conference on Signals, Systems, and Computers*, 702–706. IEEE.

12 Pizzo, A., Sanguinetti, L., and Marzetta, T.L. (2022). Fourier plane-wave series expansion for holographic MIMO communications. *IEEE Transactions on Wireless Communications* 21 (9): 6890–6905.

13 Rabie, K., Makarfi, A.U., Kharel, R. et al. (2020). On the performance of non-orthogonal multiple access over composite fading channels. *arXiv preprint arXiv:2004.07860*.

14 Rajak, S., Muniraj, I., Elumalai, K. et al. (2022). Energy efficient hybrid relay-IRS-aided wireless IoT network for 6G communications. *Electronics* 11 (12): 1900.

15 Rajak, S., Muniraj, I., Selvaprabhu, P. et al. (2024). A novel energy efficient IRS-relay network for ITS with Nakagami-m fading channels. *ICT Express* 10 (3): 507–512.

16 Rappaport, T.S., MacCartney, G.R., Samimi, M.K., and Sun, S. (2015). Wideband millimeter-wave propagation measurements and channel models for

future wireless communication system design. *IEEE Transactions on Communications* 63 (9): 3029–3056.

17 Saito, K., Takada, J.-I., and Kim, M. (2017). Dense multipath component characteristics in 11-GHz-band indoor environments. *IEEE Transactions on Antennas and Propagation* 65 (9): 4780–4789.

18 Salous, S., Feeney, S.M., Raimundo, X., and Cheema, A.A. (2015). Wideband MIMO channel sounder for radio measurements in the 60 GHz band. *IEEE Transactions on Wireless Communications* 15 (4): 2825–2832.

19 Sánchez, J.D.V., Urquiza-Aguiar, L., Paredes, M.C.P., and López-Martínez, F.J. (2021). Expectation-maximization learning for wireless channel modeling of reconfigurable intelligent surfaces. *IEEE Wireless Communications Letters* 10 (9): 2051–2055.

20 Sharma, P., Kumar, A., and Bansal, M. (2020). Performance analysis of downlink NOMA over η—μ and κ—μ fading channels. *IET Communications* 14 (3): 522–531.

21 Song, Y., Yang, W., Xiang, Z. et al. (2019). Secure transmission in mmWave wiretap channels: on sector guard zone and blockages. *Entropy* 21 (4): 427.

22 Sun, G., He, R., Ma, Z. et al. (2021). A 3D geometry-based non-stationary MIMO channel model for RIS-assisted communications. *2021 IEEE 94th Vehicular Technology Conference (VTC2021-Fall)*, 1–5. IEEE.

23 Sun, G., He, R., Ai, B. et al. (2022). A 3D wideband channel model for RIS-assisted MIMO communications. *IEEE Transactions on Vehicular Technology* 71 (8): 8016–8029.

24 Sun, Y., Wang, C.-X., Huang, J., and Wang, J. (2021). A 3D non-stationary channel model for 6G wireless systems employing intelligent reflecting surfaces with practical phase shifts. *IEEE Transactions on Cognitive Communications and Networking* 7 (2): 496–510.

25 Tahir, B., Schwarz, S., and Rupp, M. (2020). Analysis of uplink IRS-assisted NOMA under Nakagami-m fading via moments matching. *IEEE Wireless Communications Letters* 10 (3): 624–628.

26 Tang, W., Chen, M.Z., Chen, X. et al. (2020). Wireless communications with reconfigurable intelligent surface: path loss modeling and experimental measurement. *IEEE Transactions on Wireless Communications* 20 (1): 421–439.

27 Najafi, M., Jamali, V., Schober, R., and Poor, H.V. (2020). Physics-based modeling and scalable optimization of large intelligent reflecting surfaces. *IEEE Transactions on Communications* 69 (4): 2673–2691.

28 Jiang, H., Ruan, C., Zhang, Z. et al. (2021). A general wideband non-stationary stochastic channel model for intelligent reflecting surface-assisted MIMO communications. *IEEE Transactions on Wireless Communications* 20 (8): 5314–5328.

29 Imoize, A.L., Ibhaze, A.E., Atayero, A.A., and Kavitha, K.V.N. (2021). Standard propagation channel models for MIMO communication systems. *Wireless Communications and Mobile Computing* 2021: 1–36.

30 Isabona, J., Imoize, A.L., Ojo, S. et al. (2022). Development of a multilayer perceptron neural network for optimal predictive modeling in urban microcellular radio environments. *Applied Sciences* 12 (11): 5713.

31 Zhang, M. and Yuan, X. (2023). Intelligent reflecting surface aided MIMO with cascaded LoS links: channel modeling and full multiplexing region. *IEEE Transactions on Wireless Communications* 23 (2): 1184–1198.

32 Lian, Z., Su, Y., Wang, Y. et al. (2023). A novel geometry-based 3-D wideband channel model and capacity analysis for IRS-assisted UAV communication systems. *IEEE Transactions on Wireless Communications* 22 (8): 5502–5517.

33 Basar, E. and Yildirim, I. (2021). Reconfigurable intelligent surfaces for future wireless networks: a channel modeling perspective. *IEEE Wireless Communications* 28 (3): 108–114.

34 Björnson, E. and Sanguinetti, L. (2020). Rayleigh fading modeling and channel hardening for reconfigurable intelligent surfaces. *IEEE Wireless Communications Letters* 10 (4): 830–834.

35 Dovelos, K., Assimonis, S.D., Ngo, H.Q. et al. (2021). Intelligent reflecting surfaces at terahertz bands: channel modeling and analysis. *2021 IEEE International Conference on Communications Workshops (ICC Workshops)*, 1–6. IEEE.

36 Xiong, B., Zhang, Z., Jiang, H. et al. (2021). A statistical MIMO channel model for reconfigurable intelligent surface assisted wireless communications. *IEEE Transactions on Communications* 70 (2): 1360–1375.

37 Zheng, P., Ding, J., Fei, D. et al. (2023). Field trial measurement and channel modeling for reconfigurable intelligent surface. *Digital Communications and Networks* 9 (3): 603–612.

38 Xiong, B., Zhang, Z., Jiang, H. et al. (2022). A 3D non-stationary MIMO channel model for reconfigurable intelligent surface auxiliary UAV-to-ground mmWave communications. *IEEE Transactions on Wireless Communications* 21 (7): 5658–5672.

39 Jeong, J., Oh, J.H., Lee, S.Y. et al. (2022). An improved path-loss model for reconfigurable-intelligent-surface-aided wireless communications and experimental validation. *IEEE Access* 10: 98065–98078.

40 Basar, E., Yildirim, I., and Kilinc, F. (2021). Indoor and outdoor physical channel modeling and efficient positioning for reconfigurable intelligent surfaces in mmWave bands. *IEEE Transactions on Communications* 69 (12): 8600–8611.

41 Issa, M. and Artail, H. (2021). Using reflective intelligent surfaces for indoor scenarios: channel modeling and RIS placement. *2021 17th International Conference on Wireless and Mobile Computing, Networking and Communications (WiMob)*, 277–282. IEEE.

42 Järveläinen, J., Haneda, K., and Karttunen, A. (2016). Indoor propagation channel simulations at 60 GHz using point cloud data. *IEEE Transactions on Antennas and Propagation* 64 (10): 4457–4467.

43 Chen, J., Yin, X., Cai, X., and Wang, S. (2017). Measurement-based massive MIMO channel modeling for outdoor LoS and NLoS environments. *IEEE Access* 5: 2126–2140.

44 Wu, X., Wang, C.-X., Sun, J. et al. (2017). 60-GHz millimeter-wave channel measurements and modeling for indoor office environments. *IEEE Transactions on Antennas and Propagation* 65 (4): 1912–1924.

45 Bas, C.U., Wang, R., Sangodoyin, S. et al. (2017). 28 GHz microcell measurement campaign for residential environment. *GLOBECOM 2017 - 2017 IEEE Global Communications Conference*, 1–6. IEEE.

46 MacCartney, G.R. and Rappaport, T.S. (2017). A flexible millimeter-wave channel sounder with absolute timing. *IEEE Journal on Selected Areas in Communications* 35 (6): 1402–1418.

47 Hur, S., Baek, S., Kim, B. et al. (2016). Proposal on millimeter-wave channel modeling for 5G cellular system. *IEEE Journal of Selected Topics in Signal Processing* 10 (3): 454–469.

48 Ai, B., Guan, K., He, R. et al. (2017). On indoor millimeter wave massive MIMO channels: measurement and simulation. *IEEE Journal on Selected Areas in Communications* 35 (7): 1678–1690.

49 Zhao, X., Li, S., Wang, Q. et al. (2017). Channel measurements, modeling, simulation and validation at 32 GHz in outdoor microcells for 5G radio systems. *IEEE Access* 5: 1062–1072.

50 Li, X., Zhao, M., Zhang, C. et al. (2019). Security analysis of multi-antenna NOMA networks under I/Q imbalance. *Electronics* 8 (11): 1327.

51 Cao, Y., Zhao, N., Pan, G. et al. (2019). Secrecy analysis for cooperative NOMA networks with multi-antenna full-duplex relay. *IEEE Transactions on Communications* 67 (8): 5574–5587.

52 Xie, W., Yang, J., Liu, X. et al. (2020). Secrecy performance analysis of the NOMA system on high-speed railway. *Security and Communication Networks* 2020: 1–6.

53 Xu, L., Yu, X., Wang, H. et al. (2020). Physical layer security performance of mobile vehicular networks. *Mobile Networks and Applications* 25: 643–649.

54 Zhao, H., Liu, Z., Yang, L., and Alouini, M.-S. (2019). Secrecy analysis in DF relay over generalized-K fading channels. *IEEE Transactions on Communications* 67 (10): 7168–7182.

55 Yadav, S. (2020). Secrecy performance of cognitive radio sensor networks over α-μ fading channels. *IEEE Sensors Letters* 4 (9): 1–4.

56 Bayat, E. and Çolak, S.A. (2021). Secrecy capacity analysis of an underlay cognitive radio network in the presence of co-channel and primary network interference. *Electrica* 21 (1): 105–114.

57 Basar, E., Di Renzo, M., De Rosny, J. et al. (2019). Wireless communications through reconfigurable intelligent surfaces. *IEEE Access* 7: 116753–116773.

58 Danufane, F.H., Di Renzo, M., De Rosny, J., and Tretyakov, S. (2021). On the path-loss of reconfigurable intelligent surfaces: an approach based on Green's theorem applied to vector fields. *IEEE Transactions on Communications* 69 (8): 5573–5592.

59 Boulogeorgos, A.-A.A. and Alexiou, A. (2021). Pathloss modeling of reconfigurable intelligent surface assisted THz wireless systems. *ICC 2021-IEEE International Conference on Communications*, 1–6. IEEE.

60 Wang, Z., Tan, L., Yin, H. et al. (2021). A received power model for reconfigurable intelligent surface and measurement-based validations. *2021 IEEE 22nd International Workshop on Signal Processing Advances in Wireless Communications (SPAWC)*, 561–565. IEEE.

61 Huang, J., Wang, C.-X., Sun, Y. et al. (2022). Reconfigurable intelligent surfaces: channel characterization and modeling. *Proceedings of the IEEE* 110 (9): 1290–1311.

62 Xu, J. and Liu, Y. (2021). A novel physics-based channel model for reconfigurable intelligent surface-assisted multi-user communication systems. *IEEE Transactions on Wireless Communications* 21 (2): 1183–1196.

63 Ajam, H., Naja, M., Jamali, V., and Schober, R. (2021). Channel modeling for IRS-assisted FSO systems. *2021 IEEE Wireless Communications and Networking Conference (WCNC)*, 1–7. IEEE.

64 Alayasra, M. and Arslan, H. (2021). IRS-enabled beam-space channel. *IEEE Transactions on Wireless Communications* 21 (6): 3822–3835.

65 Wu, S., Wang, C.-X., Alwakeel, M.M., and You, X. (2017). A general 3-D non-stationary 5G wireless channel model. *IEEE Transactions on Communications* 66 (7): 3065–3078.

66 Toumi, M. and Aijaz, A. (2021). System performance insights into design of RIS-assisted smart radio environments for 6G. *2021 IEEE Wireless Communications and Networking Conference (WCNC)*, 1–6. IEEE.

67 de Souza Junior, W. and Abrao, T. (2022). RIS-aided cooperative FD-SWIPT-NOMA outage performance in Nakagami-m channels. *arXiv preprint arXiv:2204.01900*.

68 Arzykulov, S., Nauryzbayev, G., Celik, A., and Eltawil, A.M. (2022). RIS-assisted full-duplex relay systems. *IEEE Systems Journal* 16 (4): 5729–5740.

69 Bhowal, A. and Aïssa, S. (2022). Performance evaluation of RIS-assisted full-duplex MIMO bidirectional communications with a realistic channel model. *2022 International Wireless Communications and Mobile Computing (IWCMC)*, 83–88. IEEE.

70 Nguyen, T.N., Thang, N.N., Nguyen, B.C. et al. (2022). Intelligent-reflecting-surface-aided bidirectional full-duplex communication system with imperfect self-interference cancellation and hardware impairments. *IEEE Systems Journal* 17 (1): 1352–1362.

71 Nguyen, B.C., Hoang, T.M., Tran, P.T. et al. (2021). Cooperative communications for improving the performance of bidirectional full-duplex system with multiple reconfigurable intelligent surfaces. *IEEE Access* 9: 134733–134742.

72 Kudumala, S.R., Dubey, A.K., Gupta, P. et al. (2022). Hardware impaired RIS assisted multipair FD communication with spatial correlation. *IEEE Communications Letters* 26 (9): 2200–2204.

73 Ding, Z., Fan, P., and Poor, H.V. (2015). Impact of user pairing on 5G nonorthogonal multiple-access downlink transmissions. *IEEE Transactions on Vehicular Technology* 65 (8): 6010–6023.

74 Timotheou, S. and Krikidis, I. (2015). Fairness for non-orthogonal multiple access in 5G systems. *IEEE Signal Processing Letters* 22 (10): 1647–1651.

75 Zhang, N., Wang, J., Kang, G., and Liu, Y. (2016). Uplink nonorthogonal multiple access in 5G systems. *IEEE Communications Letters* 20 (3): 458–461.

76 Liu, Y., Derakhshani, M., and Lambotharan, S. (2017). Outage analysis and power allocation in uplink non-orthogonal multiple access systems. *IEEE Communications Letters* 22 (2): 336–339.

77 Ali, M.S., Tabassum, H., and Hossain, E. (2016). Dynamic user clustering and power allocation for uplink and downlink non-orthogonal multiple access (NOMA) systems. *IEEE Access* 4: 6325–6343.

78 Ding, Z., Peng, M., and Poor, H.V. (2015). Cooperative non-orthogonal multiple access in 5G systems. *IEEE Communications Letters* 19 (8): 1462–1465.

79 ElHalawany, B.M., Jameel, F., Da Costa, D.B. et al. (2019). Performance analysis of downlink NOMA systems over κ-μ shadowed fading channels. *IEEE Transactions on Vehicular Technology* 69 (1): 1046–1050.

80 Kumar, V., Cardiff, B., Prakriya, S., and Flanagan, M.F. (2020). Effective rate of downlink NOMA over κ-μ shadowed fading with integer fading parameters. *2020 IEEE International Conference on Communications Workshops (ICC Workshops)*, 1–7. IEEE.

81 Kumar, V., Cardiff, B., Prakriya, S., and Flanagan, M.F. (2020). Delay violation probability and effective rate of downlink NOMA over α-μ fading channels. *IEEE Transactions on Vehicular Technology* 69 (10): 11241–11252.

82 Alqahtani, A.S. and Alsusa, E. (2020). Performance analysis of downlink NOMA system over α-η-μ generalized fading channel. *2020 IEEE 91st Vehicular Technology Conference (VTC2020-Spring)*, 1–5. IEEE.

83 Agarwal, A., Chaurasiya, R., Rai, S., and Jagannatham, A.K. (2020). Outage probability analysis for NOMA downlink and uplink communication systems with generalized fading channels. *IEEE Access* 8: 220461–220481.

84 Yuan, Z., Yu, G., Li, W. et al. (2016). Multi-user shared access for Internet of Things. *2016 IEEE 83rd Vehicular Technology Conference (VTC Spring)*, 1–5. IEEE.

85 Di Renzo, M. and Song, J. (2019). Reflection probability in wireless networks with metasurface-coated environmental objects: an approach based on random spatial processes. *EURASIP Journal on Wireless Communications and Networking* 2019 (1): 99.

86 Thirumaval, V.C. and Jayaraman, T.S. (2020). BER analysis of reconfigurable intelligent surface assisted downlink power domain NOMA system. *2020 International Conference on COMmunication Systems & NETworkS (COMSNETS)*, 519–522. IEEE.

87 Mu, X., Liu, Y., Guo, L. et al. (2020). Exploiting intelligent reflecting surfaces in NOMA networks: joint beamforming optimization. *IEEE Transactions on Wireless Communications* 19 (10): 6884–6898.

88 Ding, Z., Schober, R., and Poor, H.V. (2020). On the impact of phase shifting designs on IRS-NOMA. *IEEE Wireless Communications Letters* 9 (10): 1596–1600.

89 Hou, T., Liu, Y., Song, Z. et al. (2020). Reconfigurable intelligent surface aided NOMA networks. *IEEE Journal on Selected Areas in Communications* 38 (11): 2575–2588.

90 Cheng, Y., Li, K.H., Liu, Y. et al. (2021). Downlink and uplink intelligent reflecting surface aided networks: NOMA and OMA. *IEEE Transactions on Wireless Communications* 20 (6): 3988–4000.

91 Tang, Z., Hou, T., Liu, Y. et al. (2022). Physical layer security of intelligent reflective surface aided NOMA networks. *IEEE Transactions on Vehicular Technology* 71 (7): 7821–7834.

14

Deep Reinforcement Algorithms in RIS-Empowered Wireless Communication Systems

Dang Ngoc Thien Nguyen

Tran Dai Nghia High School for the Gifted, Ho Chi Minh City, Vietnam

14.1 Introduction

Reconfigurable intelligent surface (RIS) is a brand new concept that enables every surface in a propagation environment to be used effectively to control the environment for efficient transmission and to exploit the scattering waves [1]. Structure-wise, RIS is a planar array consisting of a large number of low-cost passive reflecting elements with reconfigurable phase shifts, each of which can be dynamically tuned via a software controller to reflect the incident signals. Hence, the constructive signals can be combined and the interference can be suppressed by tuning the phase shifts of reflecting elements adaptively. Experiments regarding RIS have demonstrated the energy efficiency and strengthened throughput in various systems [2].

Therefore, it can be seen that RIS is very much at the forefront of revolutionizing telecommunications and will remain so as more solutions are created to further improve its capabilities [3–5]. Specifically, RIS is a surface made up of low-cost and low-energy controllable elements, where each element can be tweaked accordingly. Hence, RIS has a variety of functionalities, e.g., reflection [6] and absorption, and total control over wireless transmission is achievable [7], making it viable to be installed practically anywhere. Moreover, there are two types of RIS elements, passive and active: the former can reflect signal without additional calculation and low energy while the latter takes computational power and more energy, but they strengthen the signal in return.

Reconfigurable Intelligent Surfaces for 6G and Beyond Wireless Networks, First Edition.
Edited by Agbotiname Lucky Imoize, Vinoth Babu Kumaravelu, and Dinh-Thuan Do.

Despite its tremendous potential in revolutionizing telecommunications, RIS are not without certain limitations. One of the challenges faced by RIS technology is its susceptibility to common errors, such as CE errors or reflected waves that are delayed and phase-shifted [8]. These errors can degrade the performance of RIS systems, especially in dynamic and highly complex propagation environments. To address these challenges and enhance the capabilities of RIS, researchers and engineers have explored the integration of machine learning techniques. Specifically, deep learning (DL), reinforcement learning (RL), and deep reinforcement learning (DRL) have shown promise in compensating for the inherent limitations of RIS and optimizing their performance.

DL algorithms have been employed to mitigate the impact of CE errors and enhance the accuracy of channel estimation in RIS systems [9]. These algorithms can learn complex mappings between the received signals and the channel characteristics, enabling more accurate estimation and compensation of channel distortions. RL techniques have been utilized to optimize the phase shifts of RIS elements dynamically. RL algorithms can learn optimal policies for adjusting the phase shifts in real time, considering dynamic channel conditions and system objectives [10]. This approach enables adaptive and efficient utilization of the RIS for achieving desired performance metrics, such as maximizing the received signal strength or minimizing interference. DRL algorithms have been applied to optimize the configuration of RIS elements and adaptively control the reflection patterns based on the environment and system requirements [11]. This integration of DL and RL leverages the strengths of both techniques, enabling RIS to learn and adapt to complex wireless environments effectively.

14.1.1 Contributions

The environment is rapidly changing, demanding adaptive technology, namely DRL. In regards to recent surveys on RL; such as [12, 13], which only discussed general knowledge of RL without extending its scope; this chapter expands on different algorithms such as deep Q networks (DQNs) and deep deterministic policy gradient (DDPG) as well as DRL algorithms. Due to the limited number of surveys that are based on DRL applications in RIS, this work helps with that problem by providing information regarding DRL algorithms for the optimization of RIS technology to overcome various wireless communication problems. The main contributions are as follows:

- We study the foundations of DRL, as well as its inner parts. We then discuss those components and how they complement each other in the product that is

DRL. Moreover, we provide algorithms, like deep Q learning, that could assist in understanding the frameworks – that are DL and RL.
- We present the system model of a standard DRL-based system and examples of DRL-based systems for RIS-assisted wireless communication networks from prior works. The structures and functionalities of each work are also given to give insight into the systems.
- Demonstrate relevant algorithms and the impact they have on the RIS-assisted systems, which, more specifically, are the algorithms to train deep neural networks (DNN) and the algorithm to optimize action dependent on the phase shift.

14.1.2 Chapter Organization

The rest of this chapter is organized as follows. Section 14.2 introduces DRL and its components: DL and RL, as well as discusses algorithms made using these frameworks. Section 14.3 reviews papers regarding DRL usage in RIS environment. Section 14.4 presents the conclusion and possible works in the future.

14.2 Related Works

DRL techniques have been leveraged to enhance energy efficiency in RIS-assisted communication systems. Tham et al. [14] introduced a DRL-based approach for secrecy energy-efficient unmanned aerial vehicle (UAV) communication with RIS. By formulating the energy-efficient communication problem as a MDP, the proposed DRL agent learns optimal policies for UAV trajectory design and RIS phase configuration, considering both secrecy and energy efficiency objectives. The results demonstrated significant improvements in energy efficiency while maintaining secure communication links. Similarly, Lee et al. [15] proposed a DRL framework for energy-efficient networking with RIS. The DRL agent optimizes the transmission power allocation and RIS phase shifts to maximize the energy efficiency of the overall communication system. The design showed promising results in terms of energy savings and improved spectral efficiency. Sun et al. [16] proposed a DRL-based plot for cell-free multi-access edge computing (MEC) servers. Furthermore, Peng and Wang [17] focused on energy harvesting RIS for UAV applications using robust DRL. The proposed method enables the UAV to learn adaptive policies for optimizing the RIS configuration and UAV trajectory to maximize energy harvesting efficiency. The results highlighted the effectiveness of the robust DRL scheme in achieving energy-efficient UAV

Table 14.1 Energy efficiency works summary.

References	Scope	Advantages	Disadvantages
Sun et al. [16]	Energy minimization in multi-RIS cell-free MEC networks	Reviews RIS phase shifts and MEC server association for optimization	Specific to multi-RIS cell-free MEC networks
Lee et al. [15]	Energy-efficient networking in RIS systems	Addresses the critical issue of RIS networks' energy efficiency	Limited to energy optimization, lacking in other performance metrics
Peng and Wang [17]	Energy harvesting in RIS UAV systems	Remarks the importance of energy harvesting in RIS UAV systems; take into account RIS configuration's optimization and UAV trajectory	Specific to UAV systems using RIS

communication with the assistance of RIS. Below is a table regarding the scope, along with the pros and cons of each study presented.

Regarding Table 14.1, it's worth noting that while these studies provide valuable insights and contributions in their respective areas, they may have limitations in terms of the specific scenarios they consider and the metrics they optimize. Further research may be needed to explore the applicability of these approaches in different contexts and to address additional performance objectives. Other than works related to energy efficiency, there have been few survey papers to address DRL usage in RIS settings, but not without certain limitations. Below is a table noting the different aspects of those survey papers.

As can be seen in Table 14.2, prior survey papers on the subject of RIS are without flaws. While two papers focus on RIS–UAV systems, our chapter considers works that are based on standard wireless communication networks, instead. Furthermore, our chapter goes over specific algorithms and explain their functionality as well as structure. The algorithms mentioned are also accompanied by explanation and results gathered from simulations presented in their respective papers.

Table 14.2 Survey papers summary.

References	Scope (system model)	Machine learning (ML) methodology	Advantages	Limitations
Nguyen et al. [18]	RIS–UAV system	DRL	Discusses how DRL can be employed to enhance the performance of RIS-UAV systems; focuses on RIS–UAV communication networks; explores various deployment strategies and system configurations	Delve deep into recent studies and concepts surrounding DRL in RIS-UAV without extensive experimental validation or real-world implementation examples; acknowledges the challenges of deploying RIS–UAV networks without addressing potential hurdles
Pogaku et al. [13]	RIS–UAV system	DRL	Provides a survey on RIS-empowered UAV systems considering multiple contexts such as optimization, communication techniques and DRL; real life implementations of such systems; branches out to different RIS systems (e.g., non-orthogonal matching pursuit (NOMA)); future directions of RIS–UAV systems	Focuses mainly on RIS-UAV systems; mentions specific algorithms but does not go in depth regarding impacts on their respective systems
Faisal and Choi [19]	RIS wireless system	ML	Concise overview of RIS architecture and brief introduction to ML, with different ML techniques; ML techniques' applications are also presented along with equations; includes multiple RIS system types and ML algorithms; acknowledges future direction and key challenges in deploying ML in RIS	Scope is limited to ML
Our work	RIS wireless system	DRL; RL; DL	Explanations for DL, RL, DRL algorithms in detail; presented multiple relevant algorithms along with their advantages and disadvantages; included two algorithms and their respective function and impact on system	Lacking in analytical and numerical simulation results, and fluid presentation of content; some figures are basic, not having much of an impact; doesn't expand on algorithms' equations

14.3 What is Deep Reinforcement Learning?

This section provides a comprehensive exploration of the fundamental components that constitute DRL, which combines the fields of DL and RL. DL focuses on the development and utilization of artificial neural networks to process complex data representations and learn hierarchical features through multiple layers of abstraction [20]. On the other hand, RL revolves around the interaction of an agent with an environment, where the agent learns to make sequential decisions in order to maximize a notion of cumulative reward [21].

Within DRL, DL plays a crucial role in enabling the agent to process high-dimensional sensory inputs, such as images or raw sensor data, and extract meaningful representations that facilitate decision-making [20]. RL, on the other hand, provides the theoretical framework for learning optimal decision-making policies through interaction with an environment [21]. It encompasses concepts like MDPs, value functions, and policy optimization algorithms. To implement DRL, specific algorithms have been created by combining DL and RL techniques. One notable example is the DDPG algorithm [22]. DDPG utilizes deep neural networks to approximate both the actor and critic functions, enabling it to handle continuous action spaces and provide efficient policy updates.

To enhance the understanding of DRL, this section incorporates visual aids such as figures, tables, and equations. These visual representations help illustrate key concepts, architectures, and mathematical formulations employed in DRL research [23, 24]. Additionally, an algorithmic description is included to provide a step-by-step explanation of the processes involved in DRL, aiding readers in grasping the material [25].

14.3.1 Deep Learning

DL was built to simulate the complex decision-making power of the human brain [26], or rather teach computers to process data in a way that is inspired by the human brain. Examples of deep learning can be seen in everyday objects, such as our phones' ability to recognize faces, language translation, or, most notably, ChatGPT. What differentiates DL from other learning is the number of hidden layers it uses, giving it the name "deep." A usual machine learning algorithm would consist of an neural network (NN) with at minimum three layers: the input, the hidden layer, and the output layer. A DL algorithm goes beyond that, with anything more than three layers being called a DNN, which is discussed in Section 14.3.1.1.

14.3.1.1 Deep Neural Networks

As previously mentioned, a Deep Neural Network (DNN) typically has more than three layers in its architecture. This allows it to learn complex datasets more efficiently. However, a higher number of layers can also increase the time complexity. To train a DNN, various algorithms have been developed, including a straightforward one presented later in this section. Nevertheless, this algorithm may be difficult to comprehend without the knowledge of the equations involved, so it is recommended to refer to eq. (5) and eq. (16–20) in [1] to better understand the algorithm. Figure 14.1 illustrates the structure of a DNN, consisting of three parts: the input, hidden layers (which can have even more layers than what is shown in the figure), and the output. In this figure, $R(.)$ and $I(.)$ represent the real and imaginary parts of a complex-valued quantity, while h_p and g_p are part of the phase adjustment information.

$$f_{train}^{i} = [R(h_p)I(h_p)R(g_p)I(g_p)]_{1\times 4} \tag{14.1}$$

Equation (14.1) represents the training data for Figure 14.1, in which the output is the diagonal phase matrix for each RIS including the adjusted phase angles by RIS reflecting elements [1].

As can be inferred in its title, Algorithm 14.1 employs DNN to estimate channel characteristics and optimize the cooperative communication process, which are trained on a dataset consisting of CSI and corresponding transmit power levels. The trained DNNs are then used to predict the optimal transmit power levels for

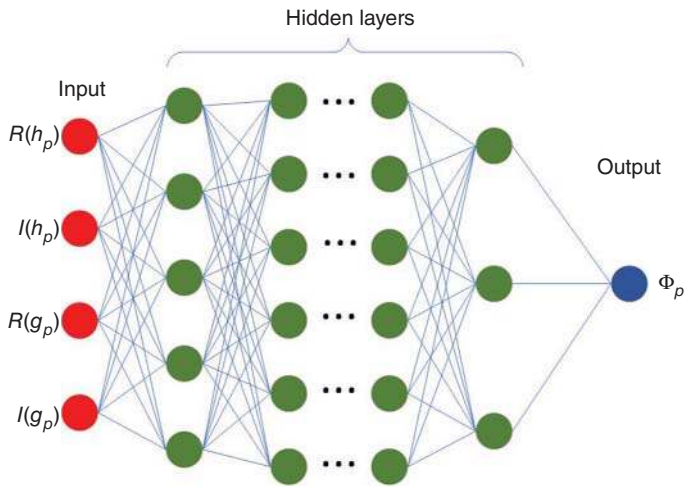

Figure 14.1 Deep neural network.

Algorithm 14.1: Theoretical training algorithm for DNN at *pth* relay (R_p) (DNN_R – *CRIS*).

Input: Channel state information (CSI) data – $j_{p,n}$ (incoming channel) and $k_{p,n}$ (outgoing channel)

Output: Trained DNN at R_p – $\mathbf{W}_k$ and $\mathbf{b}_k$: the weight and bias vectors, respectively.

Initialization: Initialize DNN parameters – $\mathbf{W}_k$, $\mathbf{b}_k$, and loss function $L(\Omega)$ where Ω signifies the training parameter set with $\mathbf{W}_k$, $\mathbf{b}_k$ values.

LOOP Procedure

1: **for** $i = 1$ to s **do**
2: `Pre-process CSI - Separate real and imaginary parts of` $j_{p,n}$ `and` $k_{p,n}$ `and rearranged to generate a feature vector`
3: `Compute the theoretical adjusted phase vector` $\Theta_{p,n}$ `maximizing instantaneous signal-to-noise-ratio (SNR).`
4: `Pre-process phase data in step 3 - Separate real and imaginary parts of said data and rearrange them, generating the output vector`
5: **end for**
6: Generate the training data – Concatenate feature and output vectors to form training data set
7: Until $L(\Omega)$ is minimized, keep training the DNN
8: **return** Trained DNN at R_p

cooperative communications. The algorithm is meant to be used in a cooperative RIS (CRIS) environment; in other words, an environment with multiple RIS elements. The CRIS component optimizes the phase shifts of the RIS elements based on the predictions from the DNN_R component to enhance the overall signal quality and coverage. During training, the weights and biases are optimized to minimize the different between predicted and actual transmit power levels. Results in [1] presents that Algorithm 14.1 can effectively maximize reflected signals and return satisfactory performance compared to non-DNN systems. The system exhibits low system complexity. The authors stated that utilizing maximum ratio combining (cophasing all paths and summed with optimal weighting to maximize SNR at combiner output) could further extend the performance of the system. Although the results are promising, it should be remembered that the CSI is perfectly known and upcoming studies regarding similar scenarios with imperfect or blind CSI would be challenging.

To fully understand Figure 14.2, the author established the relay as R, with L being the number of relays in total. That said, the RIS are managed and configured by an IoT controller, which hosts the DNN software and controls the RIS. The IoT network can be thought of as a gateway for inputting signals to the DNN and managing the RIS-based relay for further functionality; for example, activation/deactivation, troubleshooting, and software updates. Each RIS is considered an IoT device where the existing IoT platforms and communication protocols can be deployed [1].

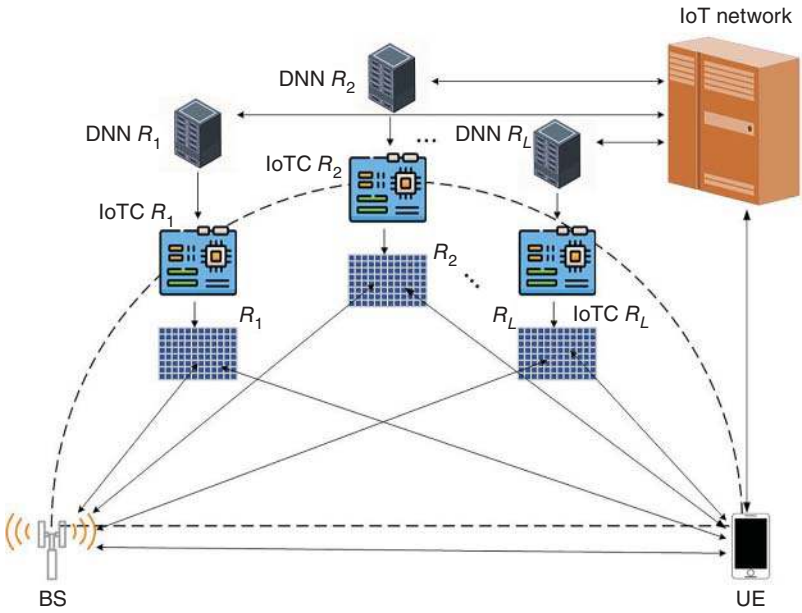

Figure 14.2 DNN in RIS-empowered wireless systems.

14.3.1.2 Autoencoders

Autoencoders, another algorithm that uses DL, are trained to uncover latent variables of the input data (the ones that can't be directly observed but inform the way data is distributed). A few examples of their uses can be denoising images and image compression. Their structure is quite different from "conventional" neural networks, despite also having three layers. According to Figure 14.3, the first is the *encoder*: which consists of layers that encode a compressed representation of the input data through reducing its dimension. The number of nodes of the encoder progressively gets smaller so that as data flows through, it gets compressed by "squeezing" through the decreasing dimensions. The most compressed version of this data is in the middle, called the *bottleneck* (or latent space), and is both the output layer of the *encoder* and the input layer of the *decoder*. The goal of the *bottleneck* is to learn a good but compressed version of the input data. Last is the *decoder*, which, by contrast to the *encoder*, has progressively more nodes that decompress the data through the *bottleneck* back to its original form. In other words, this version is then compared to the original input to measure the effectiveness of the autoencoder; the difference between the two versions is called the *reconstructionerror*. The point of autoencoders is to minimize the dimensions of data while keeping its crucial qualities by learning a compressed version of it.

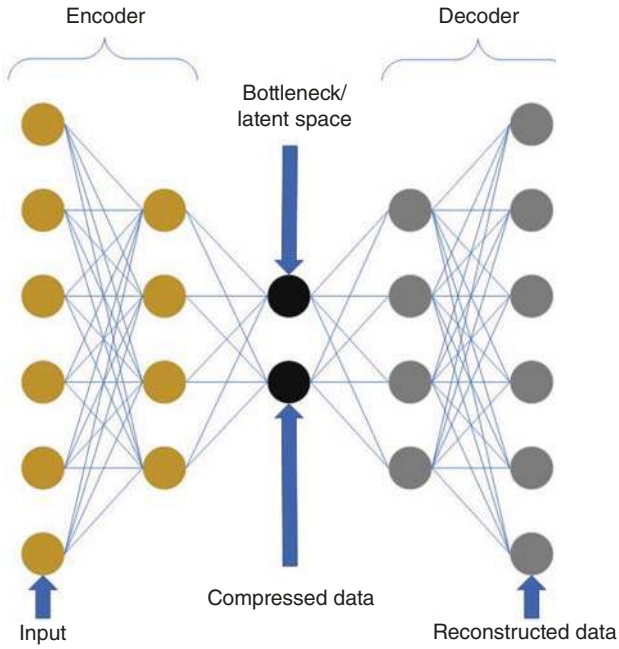

Figure 14.3 Autoencoder structure.

14.3.2 Reinforcement Learning

In short, RL can be understood as a framework based on the principle of interacting with surrounding elements to improve performance by trial and error; in other words, it learns by adjusting actions based on feedback to maximize the reward, minimize the penalty [21].

14.3.2.1 Deep *Q* Network

DQN can be boiled down to being the combination of RL and DNN. It was formed after a classic RL algorithm was strengthened, *Q*-Learning with DNNs. *Q*-Learning is a model-free and off-policy, which generally means estimating the total discounted future reward as if it was following a greedy policy (constantly performs the action that is believed to yield the highest expected reward) even though it is not following such a policy, RL algorithm to return the value of a specific action in a state (the information an agent has about the environment). It is based on the idea of a *Q*-function (state-action value function) of a certain policy. It measures the expected return or discounted sum of rewards from a state by taking a particular action and following a policy thereafter, which is the *Q*-value. Essentially, *Q*-Learning creates a matrix for an agent to refer to maximize its reward. With the

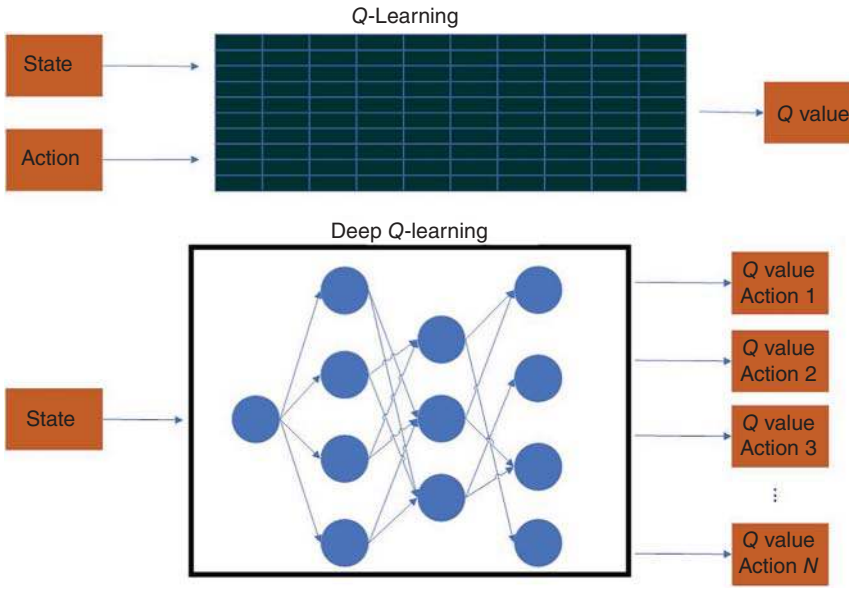

Figure 14.4 *Q*-Learning versus deep *Q*-learning.

highest action-value $Q^*(S, A)$, where S is the state and A is the action, the optimal action can be computed using,

$$A^*(S) = \arg\max_a Q^*(S, A) \tag{14.2}$$

That said, an approximator to $Q^*(S, A)$ is needed, and one key part in helping us solve for it is exactly Eq. (14.2) which is delved into in Section 14.3.2.2.

Continuing where we left off: however, it loses potency as the number of states and actions in an environment increase, leading to the creation of Deep *Q*-Learning (DQL) which utilizes DNNs to calculate all possible actions stemming from one initial state, and use that to determine the optimal action. Figure 14.4 demonstrates this:

Despite DQL being the upgraded version, it still has limitations, such as having difficulty converging to the correct *Q*-function due to it being non-linear and having multiple local minima. A few techniques have been proposed to address this, most prominently being experience relay: storing its experiences and using it to update the *Q*-function, making the learning process more stable.

14.3.2.2 Deep Deterministic Policy Gradient

Despite being presented in the RL section, in essence, DDPG is a combination of DL and RL. Similar to DQN, it is an model-free, off-policy RL algorithm and is

motivated by the same Q-function as DQN, but is mainly used for continuous control which can utilize large function approximators such as NNs [27]. In Eq. (14.1), $Q^*(S, A)$ can be described by recapping the Bellman equation; which for those that don't know, states the following, "the value of a state-action pair is equal to the expected immediate reward plus the discounted value of the best action to take in the next state";

$$Q^*(S, A) = \underset{S' \sim P}{\mathrm{E}}[r(S, A) + \Upsilon \max_{A'} Q_*(S', A')] \tag{14.3}$$

with $r(S, A)$ signifying the expected reward for taking action A at state S, and $S' \sim P$ is shorthand for the next state, S' being sampled by the environment. As mentioned above in Section 14.3.2.1, Eq. (14.2) is the integral part in solving for the approximator to $Q^*(S, A)$. Suppose the approximator is a NN $Q_\Theta(S, A)$, with parameters Θ and a set, B, of transitions, (S, A, R, S', D), where D indicates whether S' is terminal. A mean-squared Bellman error function can help in showing how close $Q_\Theta(S, A)$ is to satisfying Eq. (14.2):

$$L(\Theta, B) = \underset{(S,A,R,S',D) \sim B}{\mathrm{E}}[(Q_\Theta(S, A) - (r + \Upsilon(1 - d) \max_{A'} Q_\Theta(S', A')))^2] \tag{14.4}$$

$(1 - d)$ makes use of a convention where *True* is 1 and *False* is 0. Therefore, if S' is terminal, the Q-function can determine that the agent gets no additional rewards after the current state. Below is a model for the DDPG-based distributed training decentralized execution (DTDE) algorithm [28].

Figure 14.5 features two new networks, actor and critic. Actor–critic is also a RL algorithm that involves both policy and value based methods, which can minimize the limitations when each is used individually. The "actor" learns a policy to make decisions, in this case it's $a'(t + 1)$, explores the action space to maximize the reward; to do that, it has to continuously refine the policy to adapt to the environment. The "critic" evaluates the actor's actions and provides feedback (policy gradient); by doing so, it guides the actor towards actions that has higher expected gain, leveraging the performance of the learning process. Having said that, the remainder explains the figure presented above. In the online execution stage, the BS executes action $a(t)$ according to its current state s_t, which is obtained from user equipments (UEs) and its trained policy. In the offline stage, the authors separately set the parameters of networks and the replace buffer. Based of the current state $s(t)$ and the policy $\pi_k(a|s)$, the BS chooses action $a(t)$ added a random noise which decays for exploration and then gets the reward $r(t)$ and the new state $s(t + 1)$. The experience $(s(t), a(t), r(t), s(t + 1))$ then is stored into the replay buffer. After initializing the learning process, the BS randomly picks a mini-batch experience to train.

14.3.3 Deep Reinforcement Learning

DRL is the combination of RL and DL. Over the past half-century, DRL has achieved remarkable results in various domains, including traffic-related

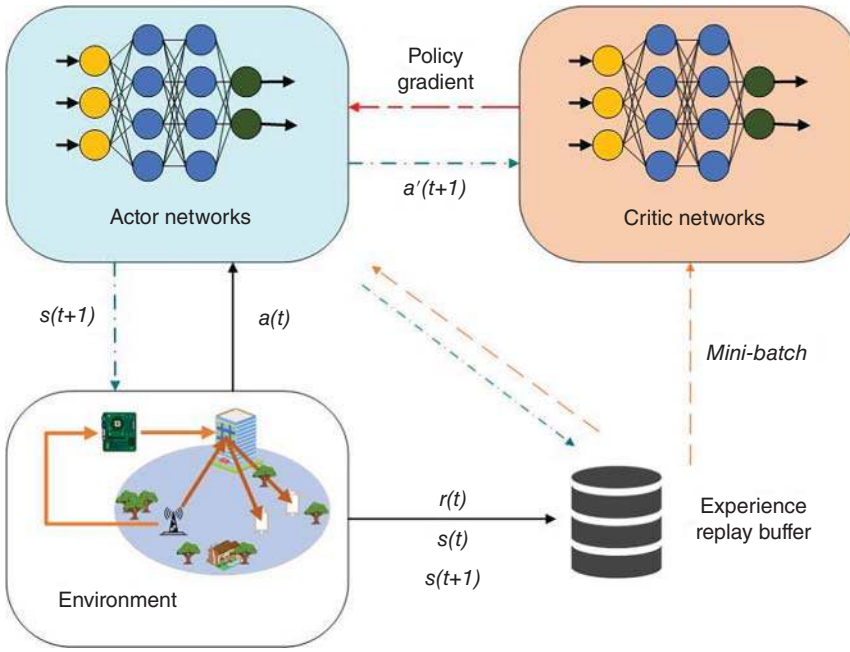

Figure 14.5 DDPG-based DTDE algorithm.

problems [29, 30], robotics [31], cybersecurity [32], and communications/networking [33]. A key motivation behind DRL is the vision of creating systems that can adapt and learn in the real world. While current artificial intelligence (AI) algorithms excel at specific tasks, combining multiple tasks can overwhelm these algorithms. DRL aims to create an "artificial general intelligence" system that can handle any given task or learn how to solve it. DRL has emerged as a crucial component in advancing AI [34]. The basic function of DRL involves an agent interacting with an environment, performing actions, and receiving rewards or punishments based on its performance. Figure 14.6 provides an overview of this process. For example, consider a scenario where a car is heading towards a brick wall, representing the state of the environment. The agent, which is typically a deep neural network (DNN), can choose between continuing to drive or stopping altogether to avoid a crash. If it chooses to continue driving, it receives a punishment of −1 point, indicating a negative outcome. On the other hand, if it decides to stop, it receives a reward of +1 point, indicating a positive outcome. These rewards and punishments guide the DNN's learning process.

Through repeated interactions with the environment, the DNN adjusts its internal weights to optimize its decision-making. By assigning higher weights to actions that lead to rewards and lower weights to actions that result in punishments, the DNN gradually improves its performance on the given task. This iterative learning

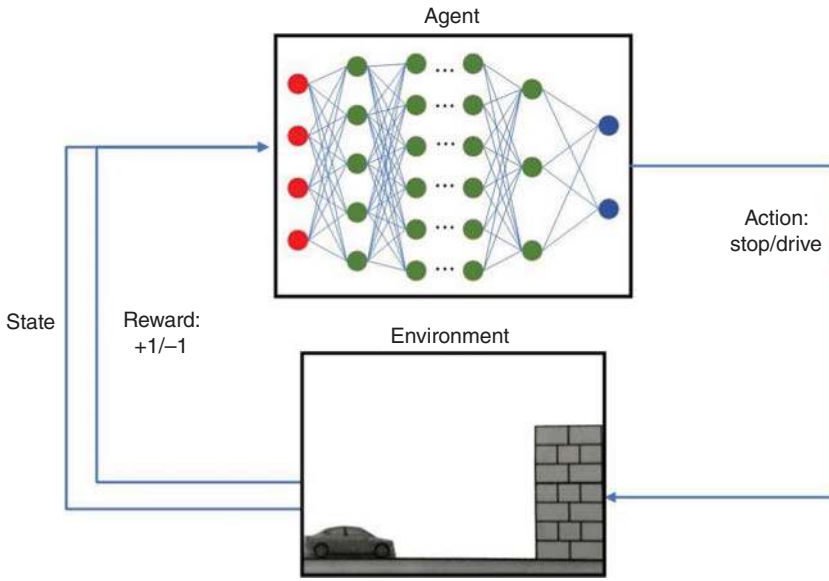

Figure 14.6 Deep reinforcement learning example.

Table 14.3 Technique comparison in terms of performance in RIS.

Technique	Advantages	Disadvantages
DL	Able to learn complex data patterns; scalable model; handling missing and sequential data; predictive modeling; feature extraction; generalization; versatility	Large amount of training data; high computational cost; training complexity
RL	Impromptu error correction; training data gained through environmental interaction; adaptive	Dependent on reward function; hard to debug; requires a large number of environmental interaction to learn viable policies; difficulty converging to optimal solution
DRL	Handling dynamic adaption problems in complicated environments and beamforming design problems [35]; building knowledge about channels without knowing its model and mobility pattern; autonomous knowledge acquisition	Requires high computational power compared to DL and RL; can easily memorize specific scenarios, leading to poor performance on unseen tasks; hyperparameter sensitivity

process, often referred to as training, allows the DNN to become better over time. Table 14.3 below is made to summarize the advantages and disadvantages of DL, RL, and DRL.

Table 14.3 provides an overview of the machine learning techniques that can be used to support RIS performance. There have been several works addressing the RIS performance by utilizing these techniques but quite a few proved to be impractical, unfit for real life deployment. With RIS promising breakthroughs in telecommunication, it is fundamental to resolve current problems and strive for a superior system.

14.4 Deep Reinforcement Learning Algorithms for RIS-Empowered Wireless Communication Systems

Current data rates are climbing exponentially due to the continuous upstaging number of users brought by the Internet of Things (IoT), which demands wireless communication networks to extend their capacity [35, 36]. Despite this, contemporary iterative algorithms have huge computational complexity which results in major processing delays [35]. Therefore, machine learning is used, more specifically DRL, because of its ability to swiftly solve a variety of problems, including real-time dynamic optimization problems [37] and non-convex optimization problems [38]. As the title suggests, this section introduces DRL-based algorithms and go into detail about their modeling as well as functionality.

14.4.1 General System Model

In [35], López-Lanuza et al. based their scheme on mmWave multi-user multiple-input-single-output (MU-MISO). However, [39, 40] were different, proposing a system for multi-hop and factory automation scenarios, accordingly. The others based their system on standard wireless communication networks [1, 36, 37].

Here in Figure 14.7 – which can be explained further in [35] and [2] – the BS, connected to the MEC server, stores the DRL-based algorithm to simultaneously design the hybrid active beamformer at the BS and the passive beamformer at the RIS through the link $H_{B,R}$; furthermore, the data is offloaded at the MEC server to train the DRL model; doing this helps reduce latency and brings forth real-time performance to high-bandwidth applications. From there, the RIS transmits the signal to the user equipments (UE), with the link named $H_{R,UE}$. For the LoS and nLoS, it means line-of-sight and non-LoS, which essentially equates to whether or not there is a clear connection between the transmitter and receiver.

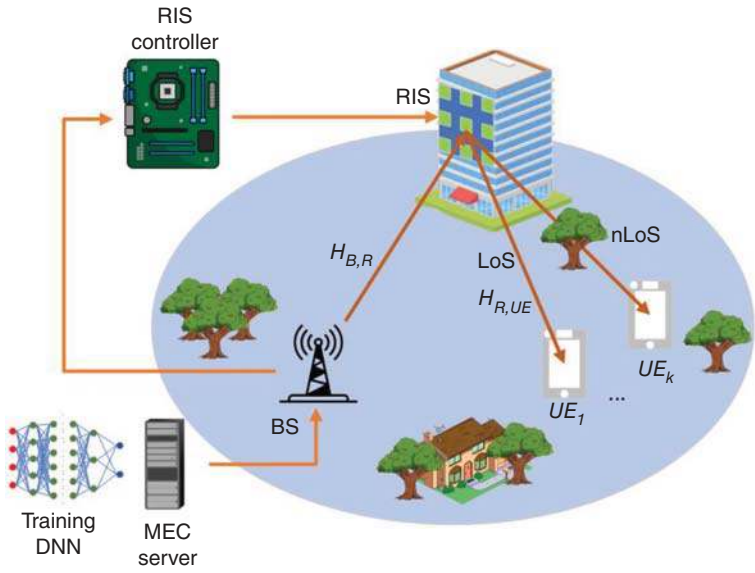

Figure 14.7 System model for RIS-empowered edge DRL system.

14.4.2 RIS-Empowered Wireless Networks DRL Algorithms Structure

To start, we feature a few systems' components and their purpose inside their respective network,

As can be seen in Table 14.4, each paper approaches the problem using a variety of structures and algorithms, such as the aforementioned DDPG algorithm in [38]. In the paper, DDPG is specifically employed to optimize the channel estimation process in RIS-aided wireless networks. Referring back to Section 14.3.2.2, a DDPG algorithm consists of an actor and a critic network. The actor observes the state and executes an action; the critic evaluates the action. In this scenario, the state representation includes the received signal strength information from the RIS elements and the phase shifts applied by the RIS. The action representation involves determining the optimal phase shifts to be applied by the RIS elements for channel estimation. The reward function is defined based on the accuracy of channel estimation and the utilization of resources, such as transmit power and time slots. The algorithm is trained using an offline learning process, where the training data is generated using a channel model and real-world measurements. The actor and critic networks are updated iteratively using gradient-based optimization techniques to maximize the expected cumulative reward. The performance is then evaluated through simulations, comparing the proposed approach to traditional estimation methods, such as least squares estimation.

Table 14.4 Detailed build and inner-workings of models.

System's References	Structure	Functionality/ability
López-Lanuza et al. [37]	Flexible and scalable DL-based unsupervised learning model that can obtain the best phase shift in any situation	Able to handle multi-carrier waveforms and large-size RIS, considering both continuous and discrete phase shifts; use clustering to reduce complexity while upholding performance
Zhu et al. [35]	DRL-based algorithm to design hybrid beamformer (BF) at BS and passive BF at RIS	Utilize a soft actor–critic (SAC) algorithm to obtain a maximum entropy based DRL algorithm to explore more stochastic policies, in turn design active analog precoder and passive BF
Kim et al. [38]	Federated learning using DRL to provide reward gains for robots within the RIS-empowered indoor wireless networks, as well as employing a DDPG to optimize the robots' deployments, RIS's phase shifts and power allocation policy for users	Another federated learning (FL) model with local training and regular global model update to enable cross-learning among the robots to improve training efficiency
Naderializadeh et al. [41]	Scalable multi-agent DRL to resolve distributed user scheduling and downlink power control	Performs joint optimization of user selection and power control decisions; able to manage resource and mitigate interference
Sagir et al. [1]	Two DNN-empowered cooperative RIS models. One model for investigating the potential of RIS installation as an IoT-based relay element in a next-gen cooperative network using DL techniques. The other one is made to reduce the maximum likelihood complexity at a destination, it is merged with DNN-empowered phase optimization	Control each RIS in the system and optimize the phase adjustments in real time, maximizing the reflected signals
Huang et al. [39]	Distributed learning algorithm to employ a deep cascade forward back-propagation network (DCBN) in each relay node to resolve RIS coefficients optimization problem. Based on the results, introduce the proximal-policy-optimization (PPO) algorithm with the clipping method to obtain solutions for joint optimization of routing and power allocation	Learn and evaluate the long-term benefit of different environments based on results from DCBN to train corresponding solutions of DRL-based joint routing and power allocation strategy
Hashemi et al. [40]	DRL algorithm named twin-delayed deep deterministic policy gradient (TD3)	Maximize total finite blocklength (FBL) rate of actuators (AC) in factory environment based on signal-to-interference-plus-noise ratio (SINR) and achievable rate in FBL regime identified for each AC in terms of the phase shift configuration matrix at the RIS

14.4.2.1 DRL Algorithm For Phase-Shift Action

Following this is be a section on a DRL algorithm aimed at optimizing RIS phase shifts. Again, explanations for the equations related to the algorithm would be too long as there are an abundant of variables the authors established; therefore, we are not able to present them here. However, it is highly suggested the equations be looked at to fully understand the algorithm. The equations are eq. (12–17) in [42].

In the sections above, we mentioned "phase shift" a number of times but didn't put an explanation on what it actually is. It is when data is transmitted by changing carrier signal's phase. It's a type of digital modulation, carried out by varying the sine and cosine functions at various time intervals. To retrieve the original data we use a demodulator. One phase shift plan is to use symbol-masking at the post-symbol mapper, which increases the amount of bit information per symbol. A few advantages phase shifting presents are improved bandwidth efficiency, reduced power consumption and fitness with high data rates. Another mentioned technique is beamforming, which makes use of multiple antennas to sent out and direct the same signal towards a single device. The resulting benefit from this

Algorithm 14.2: DRL algorithm to determine the optimal action corresponding to the optimal phase shift.

Initialization: P_α (parameter of actor network) and P_c (parameter of critic network) with random weights, experience replay with memory D, soft update coefficient σ, discount factor $p \in (0, 1]$, learning rate L_r, $P_A \leftarrow P_a$ and $P_C \leftarrow P_c$;

repeat
  Collect the channels of the k-th episode;
  Randomly input $\varsigma_{pm} \forall m = 1, ..., M_p$;
  Compute beamforming w_j using eq. (12) (for $\bar{j} = 3 - j \forall j \in \{1, 2\}$)
  Input policy network representation $\vartheta \sim CN(0, 0.1)$;
  repeat
    Acquire $a(t) = \alpha(s(t)|P_\alpha) + \vartheta$ from the actor network and reshape it;
    Loop Line 4;
    Observe the new state $s(t+1)$ given $a(t)$;
    Store $(s(t), a(t), r(t), s(t+1))$ in D - with the $r(t)$ being the reward of executing $a(t)$;
    Sample a mini-batch M_B transitions $(s(h), a(h), r(h), s(h+1))$ randomly from D;
    Calculate the target value from eq. (13);
    Update critic with eq. (14);
    Update actor with eq. (15);
    Update the target NNs using eq. (16) and eq. (17);
  until t = T (amount of batches D can store);
until k = K (number of episodes);

Output: Optimal action that corresponds to the optimal block matrix containing the RIS' phase shifts.

technique is high directivity (a straight narrow beam connecting transmitter and receiver, high gain in wanted directions and low gain in unwanted ones).

The DRL algorithm [42] is proposed for the environment of RIS-assisted full-duplex (FD) transmission. It aims to optimize the beamforming and phase shifting actions of the RIS elements in order to improve the system's performance. The author considered two RIS configurations: single RIS and distributed RIS. Extensive simulations revealed that the DRL-based distributed RIS configuration outperforms the single RIS configuration in terms of sum rate and energy efficiency, mostly due to the collaborative optimization of multiple RIS elements. Based on the results, the algorithm provides a significant improvement in the sum-rate for the single and distributed RIS schemes compared to the random RIS phase shifts in all scenarios. Furthermore, the algorithm yields a complexity reduction percentage up to 40% for the range from 20 to 60 programmable reflecting elements (PRE) compared to the DRL and it saturates at 57% when the number of PRE is very large. Additionally, through the simulations, it is found that distributed significantly better than single RIS, with sum-rate almost doubling, 11 bits per second/Hz and 6 bits per second/Hz, respectively (numbers are rounded) [42].

14.5 Limitations and Key Takeaways

In this section, we summarize what is wrote in the upper sections and point out certain limitations that are present, afterwards are the key points you, as readers, should take away from this chapter.

14.5.1 Limitations

A few limitations we have in this chapter includes

- Missing simulation results and comparison between the systems' results.
- Equations are not included with algorithms.
- Section 14.4 requires an expansion in terms of content, system models and algorithms being used in those systems.

Simulation results are not presented as we aren't able to access and run the programs to return results in charts, as they would require permission from the papers' authors. Equations are referred back to the original paper as they require the whole paper to understand, and presenting that in our chapter would inefficient and unrealistic. Currently, there are only a few papers regarding DRL in RIS environment, and even less papers that are "good" and relevant. Due to this, Section 14.4 is quite underdeveloped.

14.5.2 Key Takeaways

We believe our chapter is helpful when it comes to immediate information regarding ML techniques in RIS scenarios, such as DRL, and a lesson on algorithms in use. While the chapter focuses on RIS wireless communication systems, some of the cited papers can inform about other types of networks in use, such as NOMA and multiple-input-multiple-output. Our chapter can help in building foundational knowledge to work up into higher levels, as most of the chapter is basic knowledge when it comes to machine learning usage in RIS.

14.6 Conclusion

In this chapter, we have highlighted the efficacy of DRL algorithms in enhancing RIS-empowered communication networks. We explored DRL-based algorithms for RIS-empowered communication networks. We began by delving into the components that constitute DRL and examining conventional algorithms derived from these components. Our exploration has revealed that DRL algorithms significantly contribute to RIS technology in several ways. First, they enable the optimization of combination policies by leveraging the observation of reward functions. DRL algorithms adapt to unforeseen environments by employing RL and DNN. Finally, they facilitate resource allocation in network environments. Further research can focus on developing more advanced DL techniques and DNN architectures. This could involve investigating novel architectures, such as recurrent neural networks or attention mechanisms, to capture temporal dependencies and improve the modeling of complex RIS-enabled communication scenarios. One aspect researchers could touch on is network-specific optimization, which involves designing algorithms that consider the unique characteristics of RIS, such as the impact of different RIS configurations and the number of reflecting elements.

References

1 Sagir, B., Aydin, E., and Ilhan, H. (2023). Deep-learning-assisted IoT-based RIS for cooperative communications. *IEEE Internet of Things Journal* 10 (12): 10471–10483. https://doi.org/10.1109/JIOT.2023.3239818.

2 Huang, S., Wang, S., Wang, R. et al. (2021). Reconfigurable intelligent surface assisted mobile edge computing with heterogeneous learning tasks. *IEEE Transactions on Cognitive Communications and Networking* 7 (2): 369–382. https://doi.org/10.1109/TCCN.2021.3056707.

3 Yang, S., Lyu, W., Xiu, Y. et al. (2023). Active 3D double-RIS-aided multi-user communications: two-timescale-based separate channel estimation via Bayesian

learning. *IEEE Transactions on Communications* 71 (6): 3605–3620. https://doi.org/10.1109/TCOMM.2023.3265115.

4 Dampahalage, D., Manosha, K.S., Rajatheva, N., and Latva-Aho, M. (2022). Supervised learning based sparse channel estimation for RIS aided communications. *ICASSP 2022 – 2022 IEEE International Conference on Acoustics, Speech and Signal Processing (ICASSP)*, 8827–8831. https://doi.org/10.1109/ICASSP43922.2022.9746793.

5 Schroeder, R., He, J., and Juntti, M. (2021). Passive RIS vs. hybrid RIS: a comparative study on channel estimation. *2021 IEEE 93rd Vehicular Technology Conference (VTC2021-Spring)*, 1–7. https://doi.org/10.1109/VTC2021-Spring51267.2021.9448802.

6 He, J., Nguyen, N.T., Schroeder, R. et al. (2021). Channel estimation and hybrid architectures for RIS-assisted communications. *2021 Joint European Conference on Networks and Communications & 6G Summit (EuCNC/6G Summit)*, 60–65. https://doi.org/10.1109/EuCNC/6GSummit51104.2021.9482600.

7 Nakul, M., Rajoriya, A., and Budhiraja, R. (2024). Variational learning algorithms for channel estimation in RIS-assisted mmWave systems. *IEEE Transactions on Communications* 72 (1): 222–238. https://doi.org/10.1109/TCOMM.2023.3324652.

8 Masini, B.M., Silva, C.M., and Balador, A. (2020). The use of meta-surfaces in vehicular networks. *Journal of Sensor and Actuator Networks* 9 (1): 15.

9 O'shea, T. and Hoydis, J. (2017). An introduction to deep learning for the physical layer. *IEEE Transactions on Cognitive Communications and Networking* 3 (4): 563–575.

10 Wu, Q. and Zhang, R. (2019). Towards smart and reconfigurable environment: intelligent reflecting surface aided wireless network. *IEEE Communications Magazine* 58 (1): 106–112.

11 Di Renzo, M., Zappone, A., Debbah, M. et al. (2020). Smart radio environments empowered by reconfigurable intelligent surfaces: how it works, state of research, and the road ahead. *IEEE Journal on Selected Areas in Communications* 38 (11): 2450–2525.

12 Kisseleff, S., Chatzinotas, S., and Ottersten, B. (2021). Reconfigurable intelligent surfaces in challenging environments: underwater, underground, industrial and disaster. *IEEE Access* 9: 150214–150233. https://doi.org/10.1109/ACCESS.2021.3125461.

13 Pogaku, A.C., Do, D.T., Lee, B.M., and Nguyen, N.D. (2022). UAV-assisted RIS for future wireless communications: a survey on optimization and performance analysis. *IEEE Access* 10: 16320–16336. https://doi.org/10.1109/ACCESS.2022.3149054.

14 Tham, M.-L., Wong, Y.J., Iqbal, A. et al. (2023). Deep reinforcement learning for secrecy energy-efficient UAV communication with reconfigurable intelligent surface. *2023 IEEE Wireless Communications and Networking Conference (WCNC)*, 1–6. https://doi.org/10.1109/WCNC55385.2023.10118891.

15 Lee, G., Jung, M., Kasgari, A.T.Z. et al. (2020). Deep reinforcement learning for energy-efficient networking with reconfigurable intelligent surfaces. *ICC 2020 – 2020 IEEE International Conference on Communications (ICC)*, 1–6. https://doi.org/10.1109/ICC40277.2020.9149380.

16 Sun, M., Ni, W., Xu, X., and Tao, X. (2024). Deep reinforcement learning for energy minimization in multi-RIS-aided cell-free MEC networks. *ICASSP 2024 – 2024 IEEE International Conference on Acoustics, Speech and Signal Processing (ICASSP)*, 9011–9015. https://doi.org/10.1109/ICASSP48485.2024.10447551.

17 Peng, H. and Wang, L.-C. (2023). Energy harvesting reconfigurable intelligent surface for UAV based on robust deep reinforcement learning. *IEEE Transactions on Wireless Communications* 22 (10): 6826–6838. https://doi.org/10.1109/TWC.2023.3245820.

18 Nguyen, T.-H., Park, H., and Park, L. (2023). Recent studies on deep reinforcement learning in RIS-UAV communication networks. *2023 International Conference on Artificial Intelligence in Information and Communication (ICAIIC)*, 378–381. https://doi.org/10.1109/ICAIIC57133.2023.10067052.

19 Faisal, K.M. and Choi, W. (2022). Machine learning approaches for reconfigurable intelligent surfaces: a survey. *IEEE Access* 10: 27343–27367. https://doi.org/10.1109/ACCESS.2022.3157651.

20 Bengio, Y., Goodfellow, I., and Courville, A. (2017). *Deep Learning*, vol. 1. Cambridge, MA: MIT Press.

21 Sutton, R.S. and Barto, A.G. (1999). Reinforcement learning: an introduction. *Robotica* 17 (2): 229–235.

22 Lillicrap, T.P. (2015). Continuous control with deep reinforcement learning. *arXiv preprint arXiv:1509.02971*.

23 Mnih, V. (2013). Playing atari with deep reinforcement learning. *arXiv preprint arXiv:1312.5602*.

24 Li, Y. (2017). Deep reinforcement learning: an overview. *arXiv preprint arXiv:1701.07274*.

25 Silver, D., Huang, A., Maddison, C.J. et al. (2016). Mastering the game of Go with deep neural networks and tree search. *Nature* 529 (7587): 484–489.

26 Arnold, L., Rebecchi, S., Chevallier, S., and Paugam-Moisy, H. (2011). An introduction to deep learning. *European Symposium on Artificial Neural Networks (ESANN)*.

27 Nair, A., McGrew, B., Andrychowicz, M. et al. (2018). Overcoming exploration in reinforcement learning with demonstrations. *2018 IEEE International Conference on Robotics and Automation (ICRA)*, 6292–6299. https://doi.org/10.1109/ICRA.2018.8463162.

28 Li, L., Yang, Y., Bao, L. et al. (2023). Deep reinforcement learning-based downlink beamforming and phase optimization for RIS-aided communication system. *IEEE Wireless Communications Letters* 12 (12): 2263–2267. https://doi.org/10.1109/LWC.2023.3318212.

29 Kiran, B.R., Sobh, I., Talpaert, V. et al. (2022). Deep reinforcement learning for autonomous driving: a survey. *IEEE Transactions on Intelligent Transportation Systems* 23 (6): 4909–4926. https://doi.org/10.1109/TITS.2021.3054625.

30 Haydari, A. and Yılmaz, Y. (2022). Deep reinforcement learning for intelligent transportation systems: a survey. *IEEE Transactions on Intelligent Transportation Systems* 23 (1): 11–32. https://doi.org/10.1109/TITS.2020.3008612.

31 Zhao, W., Queralta, J.P., and Westerlund, T. (2020). Sim-to-real transfer in deep reinforcement learning for robotics: a survey. *2020 IEEE Symposium Series on Computational Intelligence (SSCI)*, 737–744. https://doi.org/10.1109/SSCI47803.2020.9308468.

32 Nguyen, T.T. and Reddi, V.J. (2023). Deep reinforcement learning for cyber security. *IEEE Transactions on Neural Networks and Learning Systems* 34 (8): 3779–3795. https://doi.org/10.1109/TNNLS.2021.3121870.

33 Luong, N.C., Hoang, D.T., Gong, S. et al. (2019). Applications of deep reinforcement learning in communications and networking: a survey. *IEEE Communications Surveys & Tutorials* 21 (4): 3133–3174. https://doi.org/10.1109/COMST.2019.2916583.

34 Arulkumaran, K., Deisenroth, M.P., Brundage, M., and Bharath, A.A. (2017). Deep reinforcement learning: a brief survey. *IEEE Signal Processing Magazine* 34 (6): 26–38. https://doi.org/10.1109/MSP.2017.2743240.

35 Zhu, Y., Bo, Z., Li, M. et al. (2022). Deep reinforcement learning based joint active and passive beamforming design for RIS-assisted MISO systems. *2022 IEEE Wireless Communications and Networking Conference (WCNC)*, 477–482. https://doi.org/10.1109/WCNC51071.2022.9771666.

36 Xu, J., Ai, B., and Quek, T.Q.S. (2023). Toward interference suppression: RIS-aided high-speed railway networks via deep reinforcement learning. *IEEE Transactions on Wireless Communications* 22 (6): 4188–4201. https://doi.org/10.1109/TWC.2022.3224009.

37 López-Lanuza, G., Chen-Hu, K., and Armada, A.G. (2022). Deep learning-based optimization for reconfigurable intelligent surface-assisted communications. *2022 IEEE Wireless Communications and Networking Conference (WCNC)*, 764–769. https://doi.org/10.1109/WCNC51071.2022.9771876.

38 Kim, K., Tun, Y.K., Munir, M.S. et al. (2023). Deep reinforcement learning for channel estimation in RIS-aided wireless networks. *IEEE Communications Letters* 27 (8): 2053–2057. https://doi.org/10.1109/LCOMM.2023.3280821.

39 Huang, C., Chen, G., Tang, J. et al. (2022). Machine-learning-empowered passive beamforming and routing design for Multi-RIS-assisted multihop networks. *IEEE Internet of Things Journal* 9 (24): 25673–25684. https://doi.org/10.1109/JIOT.2022.3195543.

40 Hashemi, R., Ali, S., Taghavi, E.M. et al. (2022). Deep reinforcement learning for practical phase shift optimization in RIS-assisted networks over short packet communications. *2022 Joint European Conference on Networks and Communications & 6G Summit (EuCNC/6G Summit)*, 518–523. https://doi.org/10.1109/EuCNC/6GSummit54941.2022.9815804.

41 Naderializadeh, N., Sydir, J.J., Simsek, M., and Nikopour, H. (2021). Resource management in wireless networks via multi-agent deep reinforcement learning. *IEEE Transactions on Wireless Communications* 20 (6): 3507–3523. https://doi.org/10.1109/TWC.2021.3051163.

42 Faisal, A., Al-Nahhal, I., Dobre, O.A., and Ngatched, T.M. (2022). Deep reinforcement learning for RIS-assisted FD systems: single or distributed RIS? *IEEE Communications Letters* 26 (7): 1563–1567. https://doi.org/10.1109/LCOMM.2022.3170061.

15

Examining Physical Layer Security for RIS-Aided Wireless Communication Systems

Tuan Minh La[1], Hieu Tri Nguyen[2], and Khoi Nguyen Phan[3]

[1] *High School for Gifted Student, Hanoi University of Science, Hanoi City, Vietnam*
[2] *Nguyen Sieu High School, Hanoi City, Vietnam*
[3] *British International School, Ho Chi Minh City, Vietnam*

15.1 Introduction

In a wireless communicating environment, it is broadcast nature for every surrounding user to receive the signal from the transmitter, including the main receiver and also the unauthorized ones. Therefore, securing the transmission is a vitally important but complicated and tough procedure, especially applied to the Internet of Things (IoT) and in the environment of a fifth-generation 5G wireless network along with a futuristic 6G network, with abundant connected devices. In that setting, physical layer security (PLS) techniques have emerged as a potential solution to fill in the important position [1].

In recent years, the reconfigurable intelligent surface (RIS) has attracted much consideration as a promising technology for the next-generation network's wireless channel environment. An RIS is a software-controlled planar electromagnetic (EM) metasurface with a large number of nearly passive components, which could be controlled by a microcontroller to alter the amplitude and phase of the reflected signal. The RIS technology provides the ability to renovate transmission environments into intelligent ones, enhancement of the received signals' quality at the destination, mitigate power consumption, alleviate undesired interference, and increase the PLS, which will be considered afterward [2–5].

In parallel, NOMA has also appeared promising in the field of IoT, especially for the forthcoming future 6G era. NOMA provides the ability to achieve massive connectivity using the same resource by optimally and fairly allocating power among users along with power multiplexing. Eventually, NOMA is capable of outperforming conventional orthogonal multiple access (OMA) techniques, due to the capability of serving multiple users at the same time using the same resource [6–8].

Reconfigurable Intelligent Surfaces for 6G and Beyond Wireless Networks, First Edition.
Edited by Agbotiname Lucky Imoize, Vinoth Babu Kumaravelu, and Dinh-Thuan Do.

15.1.1 Motivation

PLS can serve as a standalone security measure or be combined with other technological techniques to safeguard simple 6G-IoT devices. However, their efficacy might diminish in adverse propagation conditions due to the reliance on noise and fading variations in wireless channels. To bolster security in 6G-IoT networks, RIS offers dynamically controlled channels, presenting a promising solution. RIS technology can optimize PLS advantages by leveraging channel propagation characteristics, spatial diversity, beamforming, and cooperative communications. Consequently, RIS-aided PLS designs hold potential for enhancing security in both 5G and 6G networks. However, implementing RIS-aided PLS solutions necessitates precise configuration and placement of RIS, adherence to strict hardware requirements, and coordination among elements. Despite these challenges, such solutions can be tailored to specific design scenarios and communication objectives, allowing for a balance between security performance and implementation complexity.

15.1.2 Chapter Contribution

Our work contributes significantly to the advancement of 6G-IoT wireless networks by presenting a comprehensive framework for designing and implementing PLS solutions using RISs. In addition, we design robust security measures such as beamforming algorithms and artificial noise generation schemes, leveraging RIS capabilities to enhance network resilience against eavesdropping and jamming attacks. Overall, our contributions facilitate the development of secure and reliable 6G-IoT wireless networks by providing a holistic approach that combines theoretical insights, practical implementation strategies, empirical validation, and a roadmap for future research. Moreover, we added a mathematical analysis of PLS and RIS in an implemented network, further validating the efficacy of these solutions and demonstrating improvements in security metrics such as secrecy rate and outage probability, thereby establishing the practical viability of our proposed framework.

15.1.3 Chapter Organization

The rest of this chapter is organized as follows. Section 15.3 introduces approaches to implementing RIS into PLS as well as gives results of studies associated. Section 15.4 gives fundamentals of PLS and RIS. Section 15.5 provides specific analysis of plain RIS-assisted PLS. Section 15.6 presents a mathematical analysis of the RIS-aided NOMA network applied in PLS. Section 15.7 concludes the study and summarizes the result.

15.2 Related Works

PLS for RIS-aided wireless communication systems has been studied in several ways. By managing channel gains and improving outage and total capacity performance, RIS-assisted NOMA systems may increase EE, coverage, and resource allocation fairness. Physical layer security methods like channel coding, power optimization, and boundary techniques can improve secrecy capacity and SNR differentials between legitimate receivers and eavesdroppers, reducing eavesdropping risks. With its programmable and passive reflecting parts, RIS technology is a key component of 6G networks, improving spectrum and EE. Mobile edge computing (MEC) and NOMA convergence reduce power consumption and offload delays, facilitating future wireless communication systems' high data throughput and low latency. These studies demonstrate how RIS transforms next-generation wireless network security and performance.

This section provides brief information on approaches that have been taken into practical use and/or are in experimentation and provides promising results, along with a summarization of eventual results.

15.2.1 RIS-Aided Physical Layer Security

The RIS provides significant performance advantages and compatibility with PLS methods by its exceptional characteristics of high-precision beamforming, full-band response, superior power gain, financial effectiveness, high level of energy and spectral efficiency, etc. Specifically, the transmitter communicates with the receiver over a vulnerable communication link, while the RIS is deployed at a strategic location to exploit the characteristics of the wireless channel. Limiting the information extracted by the eavesdropper by improving the signal-to-inference-plus-noise ratio (SINR) at the receiver and degrading the eavesdropper's abilities to receive information, the RIS–PLS protects against eavesdropper and jamming and secures the communication. These advantages could be applied to key 6G technologies, device-to-device (D2D) communications, and especially the industrial IoT [9–11].

15.2.2 RIS-Aided NOMA Networks

As mentioned in Section 15.1, RIS and NOMA appear promising in researchers' vision of developing PLS, particularly in the field of 6G networks and the IoT, therefore systems applying both of these technologies intelligibly appeared. In the proposed system, RIS is utilized to enhance the coverage performance of NOMA by collaboratively transmitting signals to users located in obstructed or challenging communication environments, such as the "dead zone" caused by

obstructions between the base station (BS) and users. By leveraging the advantages of both NOMA and RIS, such as increased spectral efficiency and improved coverage, the system aims to address the challenges of next-generation wireless networks like 6G. The integration of RIS with NOMA allows for non-orthogonal transmission at the transmitting end, enabling the system to multiplex multiple users' signals based on their power levels. This approach helps eliminate multi-access interference (MAI) through successive interference cancellation (SIC) at the receiver, leading to improved spectral efficiency. Additionally, RIS technology can passively reflect received signals to users, thereby enhancing the EE of the system [12].

15.2.3 Double-Faced Active RIS

Alongside superior characteristics, RIS suffers from prominent drawbacks of attenuation in signal reflection due to the multiplicative nature of the fading loss of the cascaded channels and half-space-restricted transmission. In order to overcome these, RIS architectures emerged renovations called active-RIS [13, 14] and its two editions, active reflecting-only RIS [13, 14] and active refracting-only RIS [15]. These inventions can magnify the signals when they "reflect/refract" the impinging EM waves due to their amplifiers into the conventional reflecting elements, resulting in significantly better performance of RIS in coverage and spectral efficiency. Moreover, to resolve RIS problems thoroughly, researchers proposed a novel model called double-faced active (DFA)–RIS, which fulfills the desire for full space transmission [3].

15.2.4 STAR–RIS Assisted NOMA Networks

Researchers also bring up another application of RIS to deal with these drawbacks, which is called STAR–RIS-assisted NOMA networks. Differing from RIS and active-RIS, STAR-RIS allows independent adjustment of the surface's electrical and magnetic impedance, enabling control over both transmitted and reflected signals (Table 15.1). This capability offers advantages of full-space smart radio environment (SRE) coverage and increased degrees of freedom for system design over reflecting-only C-RIS-NOMA systems, leading to improved spectral efficiency and better mitigation of co-channel interference in NOMA networks, specifically assisting PLS in 6G networks and IoT [6, 16].

Table 15.1 Summary of RIS-aided wireless approaches.

References	Scope (System model)	Advantages	Limitations
Khalid et al. [9]	RIS	• Successfully improved the secrecy rate significantly when positioned accurately. • Can be further analyzed and renovated.	• Complexity in analyzing the functions of the RIS in different hardware implementations. • Path loss and multipath fading. • Half-space restricted transmission.
Zhang et al. [12]	RIS-aided NOMA	• Improvement in the number of reflecting elements of RIS or transmit antennas. • Outperformed RIS in improving the secrecy rate.	• Drawbacks of RIS still remain.
Guo et al. [3]	Double-faced active RIS	• Successfully compensate the severe fading loss and achieve full-space coverage simultaneously. • Outperformed RIS in improving the secrecy rate.	• Rely on complex mathematical models, leading to the limitation in flexibility.
Zhang et al. [6]	STAR–RIS Assisted NOMA	• Successfully compensate the severe fading loss and achieve full-space coverage simultaneously. • Outperformed RIS in improving the secrecy rate.	• Contain potential performance degradation and operating complication. • Rely on complex mathematical models, leading to the limitation in flexibility.

15.3 Fundamentals of PLS, RIS, and IoT

In this section, we discuss the fundamentals of FL, RIS, and IoT. Thus, diving into its advantages and compare to alternative modes of connection.

15.3.1 RIS

Abovecited, RIS (reconfigurable intelligent surface) is known for its promising technology for the future, revolutionizing telecommunication in all aspects. Using an array of reflectors on its surface, RIS can easily stimulate the EM wave and forward the incident wave with amplified strength. RIS essentially works in three steps: receiving, processing, and reconfiguring the incoming signal. Moreover, RIS can help increase a wave's traveling distance and bandwidth [17].

15.3.1.1 RIS Configuration

Figure 15.1 illustrates the RIS configuration, comprising three layers and a controller with the following components:

- **Outer layer:** Consists of flexible, discrete, subwavelength-sized elements. Utilizes diode arrays (e.g., PIN or varactor diodes) to control EM reflection. Voltage settings alter diode states, thereby adjusting tunable elements.
- **Middle layer:** Contains a copper backplane to prevent signal leakage.
- **Inner layer:** Hosts a control circuit board that adjusts reflection coefficients (amplitude and phase), connecting the RIS controller to reflecting elements, receiving and transmitting voltage signals.

15.3.1.2 How RIS Operates

In simple terms, RIS essentially operates by exploiting the superposition of in-phase waves [5], resulting in a phenomenon called constructive interference. When multiple transverse waves travel in the same direction, this additional event can result in an increase in total amplitude, therefore increasing the EM

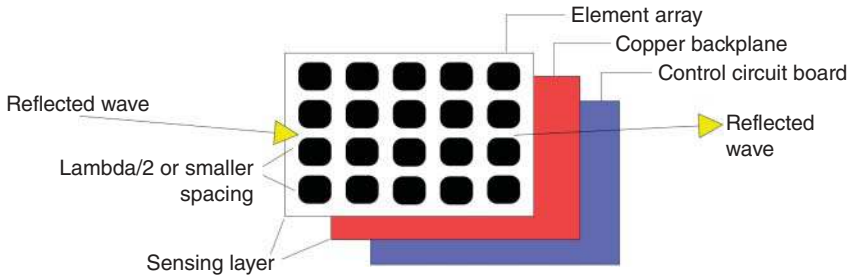

Figure 15.1 Schematic of an RIS.

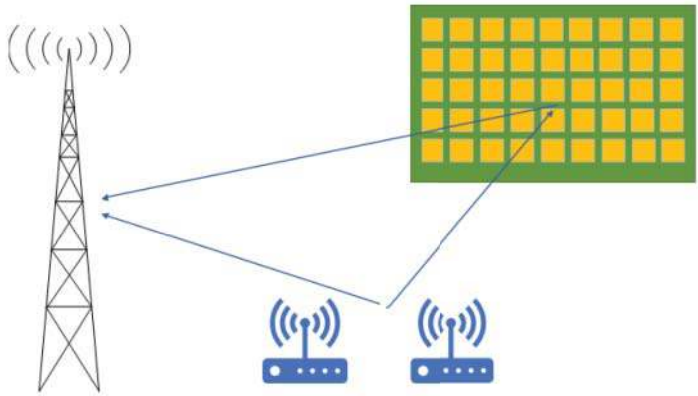

Figure 15.2 Uplink RIS-aided wireless system.

intensity, as shown in Figure 15.2. To be able to stimulate, RIS contains multiple reflective elements on its screen, which are calculated using a complex algorithm to determine the reflective angle strategically. This change in direction has taken elements such as phase difference, amplitude, and wavelength of the incoming wave [4, 18].

Due to this enhancement in the wave signal, RIS ensures constant constructive interference from the target location to the signal receiver. This method not only helps boost the initial weak signal that has been distorted/blocked by obstacles but also helps maintain a stable connection [4].

15.3.1.3 Advantages of RIS

There are several benefits when it comes to putting RIS into practice since it is at the forefront of future communications. To start with, one of RIS's major advantages is its ability to reduce energy waste when it comes to wireless networks and communications [19].

Since the RIS method of elongating signal connections does not require considerable energy to operate, this means these passive element carriers are significantly more power efficient than traditional relay systems, mostly leveraging the properties of EM waves [6]. Moreover, this also enables RIS to support the development of sustainable communication infrastructures. Additionally, RIS increases signal coverage and quality by reflecting signals to directed locations [20]. This makes it possible for RIS to function in a variety of settings, including those where obstacles frequently block signal propagation both indoors and out.

As RIS provides efficient performance in both environments, this technique can easily bolster indoor connections and support the initial infrastructure system without any extended modes of modification. This budget-free solution not only

increases the nature of wireless communications but also aids the exponential demand for connectivity among users [21]. Table 15.2 presents how RIS can perform better than related transmission techniques in terms of main features.

15.3.1.4 How RIS can be Applied on IoT

With RIS being the forerunner of our future's technology, its integration with the IoT can revolutionize the way telecommunications operate with unparalleled range and connection. Responsible for solving communication issues and extending coverage, RIS can greatly bolster IoT in various aspects, such as connectivity and range. First, deploying RIS infrastructures can enhance connections in IoT networks. RIS is especially helpful in places with lots of obstacles or signal problems, like mountainous areas, because it can improve the overall quality of connections by smartly using signal reflection and redirection techniques to lower signal loss. RIS's capacity to modify its reflecting qualities may enhance signal routes, leading to a more dependable and robust IoT connection. The use of RIS technology has the potential to greatly augment the coverage area of communication signals, thereby facilitating the extension of the range of IoT devices. RISs may function as signal enhancers by precisely manipulating EM radiation. This facilitates communication between devices located at longer distances. This feature is particularly advantageous in extensive implementations of the IoT, such as smart cities, industrial environments, and agricultural sectors, where a wider range of connectivity is necessary to provide uninterrupted data transmission and real-time monitoring.

Furthermore, RIS-aided PLS solutions can be applied to various emerging technologies, including mmWave/sub-THz communications, visible light communications, vehicular communications, UAV communications, integrated sensing and communication, Industrial IoT, SWIPT, NOMA, and D2D communications. Despite the promising potential of RIS in enhancing PLS performance, further research is needed to explore its capabilities, limitations, and effective implementation in diverse network topologies and application scenarios. This includes understanding the complexity of design solutions and additional control variables to optimize RIS-aided PLS in future networks.

15.3.2 Physical Layer Security of RIS in the Context of IoT Applications

Despite RIS's promising opportunity to look forward to, this revolutionary wireless system still requires multiple sets of challenges that require further research and solutions.

Table 15.2 RIS compared to other modes of transmission techniques.

Feature	RIS	Traditional relays	MIMO
Functionality	Manipulate electromagnetic waves for signal optimization.	Amplify and forward or decode and forward signals.	Use multiple antennas to transmit and receive signals.
Energy Efficiency	High, as it passively reflects signals without the need for power amplification.	Lower, as it requires power to amplify signals.	Moderate to high, depending on the algorithm and system design.
Deployment cost is potentially lower, due to the passive nature and no need for dedicated power sources.	Higher, because of the active components and power requirements.	High, due to the complexity and number of antennas required.	
Complexity	Low to moderate, mainly in the control software.	Moderate, due to the need for signal processing and power management.	High, due to the signal processing and management of multiple antennas.
Latency is very low, as it does not process the signal, just alters its propagation path.	Moderate, due to processing and forwarding delays.	Low to moderate, depending on the processing efficiency.	
Scalability	High, as it can easily be integrated into various environments without extensive modification.	Moderate, limited by power and hardware requirements.	High, but may be limited by interference and signal processing capabilities.
Application scope	Suitable for enhancing signal coverage and efficiency in dense urban areas.	Commonly used for range extension and overcoming dead zones.	Widely used for high data rate transmission and multipath management.
Privacy and security are enhanced, due to the lack of signal interception and decoding capabilities.	Potential vulnerabilities, as signals are amplified or decoded.	Enhanced through spatial multiplexing and signal encoding techniques.	

Source: Zhang et al. [6]; Renzo et al. [20]; Liaskos et al. [21].

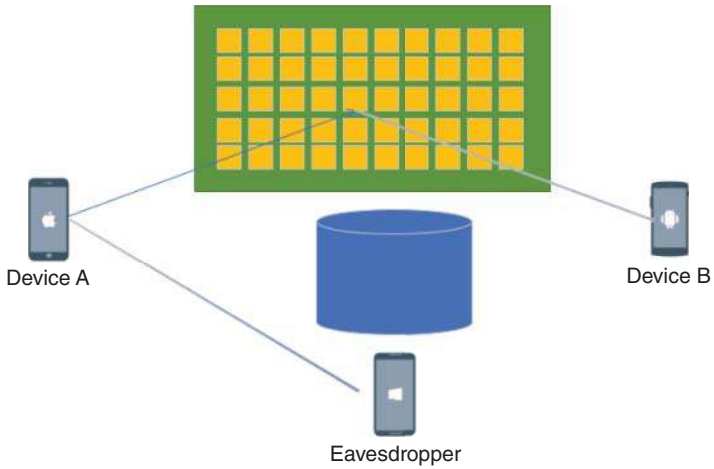

Figure 15.3 Eavesdropping model.

15.3.2.1 PLS and RIS

One of the most problematic problems is about eavesdropping risks when RIS is taken into account. In circumstances when the RIS sends signals to designated receivers, there is the possibility that eavesdroppers may intercept certain parts of these signals, as shown in Figure 15.3. This risk becomes greater if there is no obstruction in the direct path between the source of the signal and the eavesdropper. These signals may be captured and decoded by eavesdroppers that are placed within the signal route, even if these are not the intended targets. In order to mitigate this susceptibility, attention to details of the design and implementation of RIS is crucial, especially with regard to how they direct and regulate signals in diverse contexts.

The consequences of eavesdropping in RISs are considered to have a tremendous effect on the system's reliability. When transporting sensitive data such as user information or model training weights, eavesdroppers can easily gain access to these data by exploiting the systems' weaknesses. After analyzing the intercepted data from the receiver, the eavesdropper can gain various types of insights into the training dataset progress. As a result, hackers use this sensitive information to do illegal activities such as intellectual property theft. This not only affects the system adversely but also leads to less liability from users to the newly implemented system [22].

PLS mechanisms can be employed to safeguard communication between RIS nodes and the central server. For instance, artificial noise injection techniques can be utilized to intentionally introduce random interference into the communication channel, masking the transmitted data and making it difficult for

eavesdroppers to extract meaningful information [23]. Beamforming technologies, which let RIS nodes focus transmission beams on intended recipients while reducing leakage to unauthorized receivers, can also make FL communications more private [24]. Additionally, channel coding techniques can be used to send data in a way that adds redundancy and error correction, making it more resistant to mistakes made by eavesdroppers or attempts to change it [25]. PLS techniques can add another layer of defense against eavesdropping attacks by using the randomness and multipath properties of wireless channels. These techniques can be used in addition to traditional cryptographic methods to make FL-enabled RIS deployments safer overall.

15.3.2.2 PLS for RIS on IoT

Applying PLS techniques to RIS within the IoT ecosystem offers a promising approach to enhance data confidentiality and integrity while mitigating security risks. RIS, equipped with the capability to manipulate EM waves, can leverage PLS mechanisms to secure wireless communication channels and protect transmitted data from eavesdropping and interception. One key aspect of PLS for RIS on IoT involves exploiting the unique properties of the wireless propagation environment to establish secure communication links. By dynamically configuring the reflection coefficients of RIS elements, RIS can shape the wireless channel and create secure transmission paths between IoT devices and gateways. For example, RIS can adjust the phase and amplitude of the reflected signals to constructively interfere with the desired receiver while inducing destructive interference at unintended locations, thus thwarting eavesdropping attempts [26]. Also, RIS-enabled beamforming techniques can make IoT communications more private by guiding transmission beams to the right people and preventing them from getting to people who are not supposed to see them. By changing the phase and amplitude of reflected signals on the fly, RIS can direct transmission beams with high directional gain toward real IoT devices. This makes it much less likely that someone will intercept the signal [27]. Furthermore, channel coding and modulation schemes tailored for RIS-enabled IoT deployments can enhance data confidentiality and integrity. RIS can add redundancy and error correction to transmitted data by using error-correcting codes and modulation techniques that are optimized for the wireless channel. This makes it more resistant to errors caused by eavesdropping or attempts to alter it [25].

15.4 RIS-Aided PLS

15.4.1 General Notion

RIS exhibits numerous unique characteristics, including high-precision beamforming, rapid deployment, limited control messages, real-time configuration,

affordable complexity, full-band response, full-duplex (FD) transmission, superior power gain without imposing thermal noise, cost-effectiveness, and high energy and spectral efficiency. These attributes render RIS an ideal candidate for implementing and enhancing PLS methods. In a straightforward RIS-aided PLS design, the transmitter (Tx) communicates with the receiver (Rx) over a vulnerable communication link, while the RIS is strategically deployed to exploit wireless channel characteristics. By improving the signal-to-interference-plus-noise ratio (SINR) at the Rx and/or degrading the eavesdropper, the RIS can mitigate eavesdropping and jamming attacks. Optimal adjustment of deployment location, number of elements, and reflection coefficients for the RIS can effectively protect the Rx from such attacks. RIS-based PLS solutions find application in various emerging technologies, including mmWave/sub-THz communications, visible light communications, vehicular communications, unmanned aerial vehicle (UAV) communications, integrated sensing and communication, Industrial IoT, simultaneous wireless information and power transfer (SWIPT), NOMA, and device-to-device (D2D) communications. Research efforts have demonstrated improved PLS performance under controlled channel gain through RIS in various scenarios, systems models, methodologies, and optimization problems. However, despite extensive research, the study and evaluation of RIS-aided PLS in 6G-IoT networks are still in the early stages. Further investigation is needed for the design and implementation of RIS-aided PLS under variable network topologies and novel application scenarios. This includes understanding the capabilities and limitations of design solutions, their effective implementations, inherent complexity, and additional control variables.

15.4.2 Design Solution

In complex situations, the use of RIS for enhancing PLS has proven more effective than traditional multiple-input multiple-output (MIMO) methods. This is particularly evident when the receiver (Rx) requires a higher secrecy rate, the eavesdropper or jammer has more antennas or better channel conditions, or when they are situated close to the transmitter (Tx). In such scenarios, conventional methods like large-scale antenna arrays or spatial beamforming may not provide adequate secrecy. Additionally, securing transmissions through a combination of methods, such as transmit beamforming with artificial noise (AN) or cooperative methods can be challenging. However, utilizing RIS to control the strength and direction of reflected signals, along with signal processing and optimization for both Tx and Rx, offers unique security advantages. A well-configured RIS can optimize the radio environment under difficult propagation conditions, improving the effectiveness of wireless channels for secure communications regardless of node numbers, locations, or channel conditions. For instance, in situations where nodes are closely

spaced or the propagation environment lacks scattering, assuming independent observations becomes unreliable due to correlated channels. In such cases, relying solely on one secure technique may not provide complete protection against all attacks. Hence, employing a strategy that combines different RIS-assisted PLS solutions can offer significant security enhancements [9, 28, 29].

15.4.2.1 RIS-Based Secure Resource Management

RIS offers a strategic approach to secure resource management in wireless communication scenarios. By effectively utilizing network resources like bandwidth, time, and power, RIS ensures secure transmissions. Techniques such as link adaptation based on subcarrier and power allocation, adaptive modulation, and coding exemplify methods to achieve security objectives. Moreover, RIS enables PLS provision by optimizing transmission parameters specifically for the Rx link using independent fading. This optimization inherently provides security against jamming and eavesdropping attacks without requiring additional processing or computation at the Rx. Furthermore, adapting the link between the Tx and Rx via RIS, by adjusting transmission parameters and reflection characteristics, establishes a more secure communication link. This adjustment allows the RIS to steer transmitted signals toward the Rx while nullifying interference from jammers and degrading the signal-to-noise ratio (SNR) at eavesdroppers, as shown in Figure 15.4. The strategic deployment of RIS effectively creates a "secure zone" around the Tx and Rx, making it challenging for eavesdroppers or jammers to intercept or disrupt information transmission. Additionally, RIS-based link adaptation and channel-dependent resource allocation support flexible and scenario-specific secure transmissions, satisfying information security requirements in terms of confidentiality and availability. Adjusting parameters like transmit power, modulation order, number of RIS elements, reflection coefficients, error correction, subcarriers, coding rate, and RF bandwidth based on channel characteristics optimizes secure transmissions. In summary, RIS-based secure resource management optimizes network resources and transmission parameters to ensure secure and efficient wireless communications, providing flexibility and adaptability to different scenarios and channel conditions [9, 30].

15.4.2.2 RIS-Based Secure Beamforming

The spatial dimension of multiple antennas in MIMO systems offers opportunities for reliable information transmission. Beamforming and precoding techniques are utilized to transmit spatially directed signals, exploiting diversity and array gains. Beamforming directs EM energy towards a specific location by adjusting beamforming weights in real time using phase shifters. Precoding involves transmitting multiple symbols simultaneously, shaping the radiation pattern of the antenna array towards Rx. Beamforming focuses on single-user transmission, while

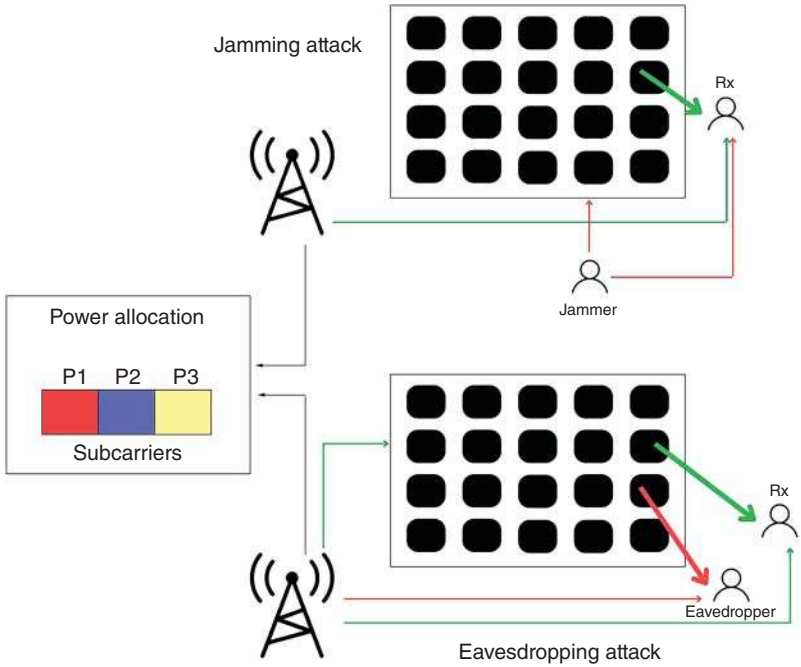

Figure 15.4 RIS-based secure resource allocation.

precoding involves the superposition of different beams for spatial multiplexing of multiple data streams. Signal processing techniques like linear precoding, such as generalized singular value decomposition, zero-force precoding, and dirty-paper precoding, can enhance PLS performance by controlling the directivity or shape of transmitted signals. For instance, the passive beamforming of the RIS can complement the active beamforming of the Tx, enhancing PLS performance. By designing optimal beamforming vectors, the eavesdropping channel can be degraded relative to the legitimate channel, ensuring confidentiality, and enhancing the power of the decoding signal at the Rx, while mitigating the impact of jamming signals to ensure availability, as shown in Figure 15.5. Increasing the number of elements of the RIS can improve the efficiency of secure transmissions compared to increasing the size of the Tx antenna array. Fewer antennas at the Tx can provide a certain degree of secrecy gain when deploying RIS. The higher the number of RIS elements, the fewer antennas are required at the Tx. RIS-based secure beamforming designs enhance PLS performance metrics across different system configurations, including multistream, multiuser, and wideband

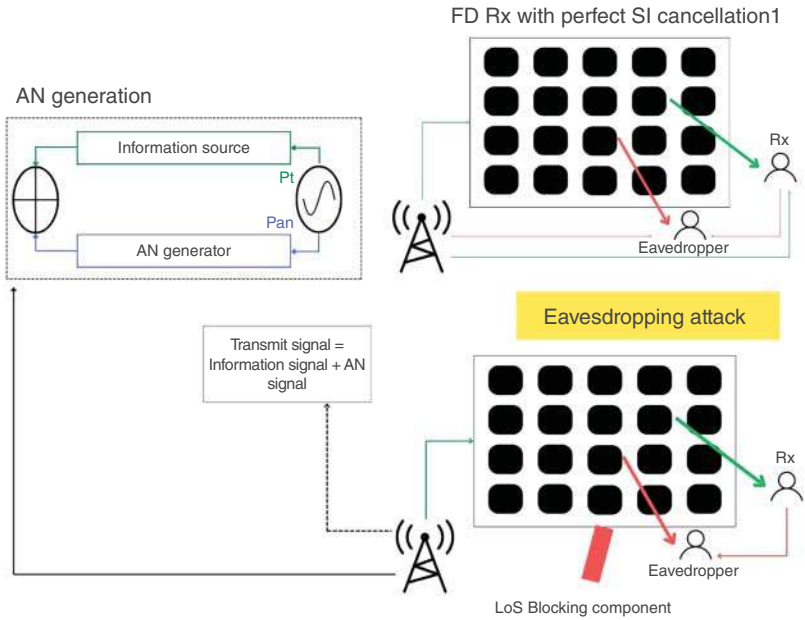

Figure 15.5 RIS-based secure beamforming.

scenarios. However, the choice of technique depends on the rank and security requirements of the transmissions [9, 31].

15.4.2.3 RIS-Based Secure AN Injection

RIS-based secure AN Injection is a method employed to counter eavesdropping attacks in wireless communication, as shown in Figure 15.6. High-powered AN can be emitted by either the Tx or Rx. Specifically, the Tx can emit AN in the same frequency band as the original signal, utilizing the null space in the MIMO channel between the Tx and Rx. Conversely, the Rx can generate AN by adopting in-band FD communications. For example, Mucchi et al. introduced noise deliberately via the Rx using noise-loop modulation while Choi et al. explored AN precoding, adding a known interfering signal to the original signal at the Tx. Isotropic AN is suitable when the channel state information (CSI) of the eavesdropper is unknown, while spatially selective AN is preferable otherwise. However, many studies on AN-based PLS assume knowledge of the eavesdropper's location, which is often impractical. A more realistic approach involves designing AN solely based on information from the Rx. Yet, it's important to acknowledge that even with this approach, attackers with advanced technology or channel knowledge may still intercept the signal. RIS can potentially reflect the AN, increasing interference for the eavesdropper and making signal interception more difficult.

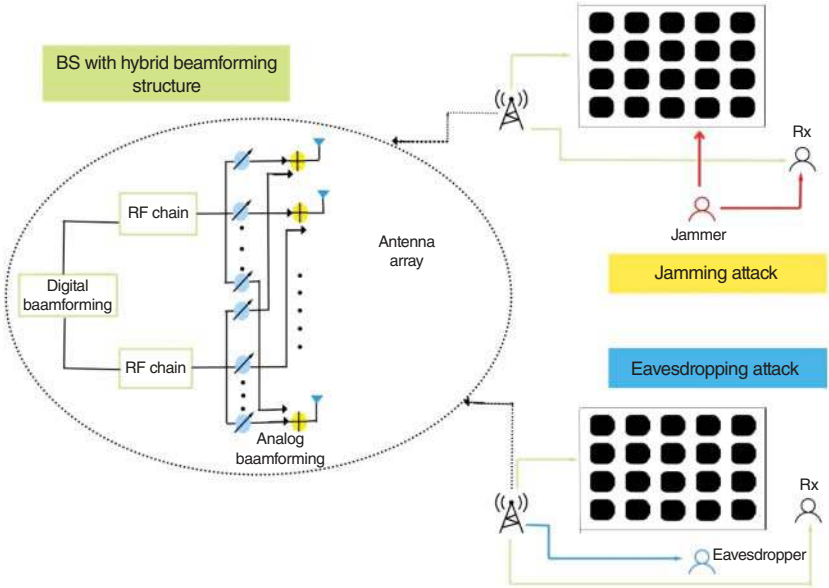

Figure 15.6 RIS-based secure AN injection.

Furthermore, Choi et al. demonstrated improved secrecy with Tx-injected AN when the RIS is near the eavesdropper. Studies indicate that RIS with AN design requires fewer elements and less computational complexity to achieve a certain level of secrecy compared to designs without AN. However, AN injection typically demands more power, consuming additional transmission and circuit power. This necessitates a constrained transmit power to send a confidential message to the Rx while injecting AN simultaneously, potentially disrupting the Rx's decoding ability. RIS can help mitigate this constraint by enabling the Tx to reduce transmit power while maintaining communication performance. The optimization process for RIS-based AN injection entails selecting optimal beams at the Tx/Rx for transmitting/receiving the original signal and injecting AN using real-time CSI, along with designing phase shifts for the RIS. This ensures the efficient and effective deployment of AN to enhance security in wireless communications [32].

15.4.2.4 RIS-Based Secure Cooperative Communications

Cooperative relaying and jamming methods utilize spatial diversity to provide effective security solutions. In cooperative relaying, multiple trusted relays enhance PLS by distributing the benefits of MIMO technology. To improve reception at the Rx against eavesdropping and jamming, relays can be chosen based on their location or using directional antennas. Communication in relay-based networks typically involves two phases: transmission from the Tx to both the

relay and Rx, and then relay retransmission to the Rx. Amplify-and-Forward (AF) and Decode-and-Forward (DF) protocols are commonly used, with AF being simpler but potentially amplifying noise, and DF performing better under certain conditions. Relays can operate in Half-Duplex (HD) or FD mode, and their advantages have been explored in challenging scenarios such as limited backhaul, BS deployment issues, or high throughput needs. However, cooperative relaying presents challenges including relay selection, reliability, power control, and computational complexity. In addition to cooperative diversity, relayed jamming signals can disrupt eavesdroppers. Challenges in cooperative jamming include power allocation and designing jamming signals against multiple eavesdroppers. As shown in Figures 15.7 and 15.8, combining cooperative relaying and jamming

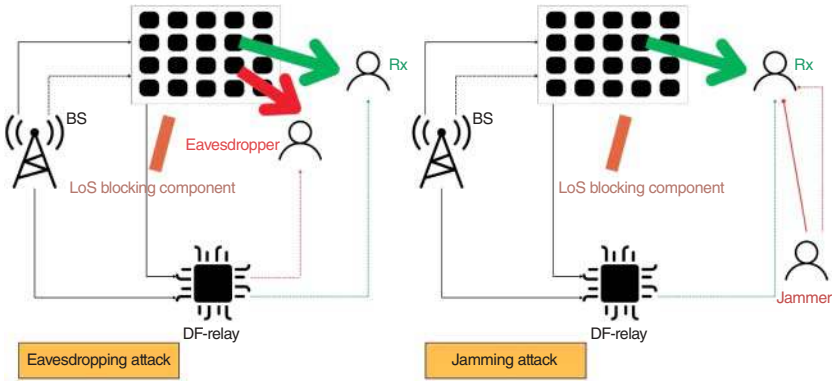

Figure 15.7 RIS-based secure cooperative relaying.

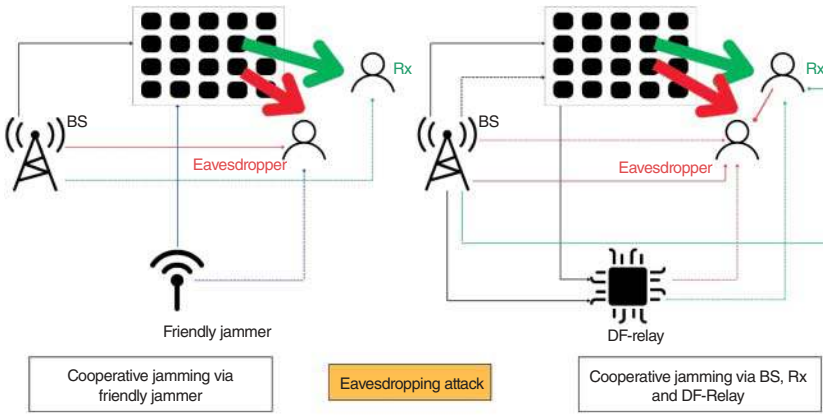

Figure 15.8 RIS-based secure cooperative jamming.

with RIS can further improve PLS by enhancing cooperative diversity. This approach offers a comprehensive strategy to enhance wireless communication security [9, 33, 34].

Noted that improving secrecy performance with RIS-aided PLS faces challenges like complex channel spaces, precise element configuration, strategic RIS placement, and hardware constraints. Robust algorithms are needed to adapt to interference and noise, along with considerations like relay scheduling, AN power allocation, and RIS details. Selecting the right solution depends on tradeoffs between security, hardware complexity, latency, and overhead.

15.5 Mathematical Analysis of PLS in an RIS-Aided NOMA Network

This section presents a system model of an PLS implementation using RIS-aided NOMA, as well as equations used to obtain a closed-form solution of the ergodic secrecy rate (ESR) of the model based on [35]. We can construct a model network consisting of a BS with M antennas, trying to communicate with two users U_A and U_B (with U_B being further away from BS), and an unauthorized eavesdropper U_E. Here, the BS cannot establish direct communication between itself and the users due to obstacles, so an RIS with N reflective elements using the NOMA technique is employed. Additionally, an obstacle exists that prevents communication between the RIS and U_B, so U_A is used to relay signals to and from U_B.

Here, we specify how signals are transferred throughout the network model, as well as obtain equation representations for those signals. The model transmits data from BS to the users in three phases.

15.5.1 First Phase

In the first phase, BS transmits a signal x using p_s power transmission. x is a composite signal made from x_A and x_B, which are data signals meant for U_A and U_B, respectively. A power-splitting factor $a \in [1, 0]$ is used in the calculation of x to distinguish between x_A and x_B signals. A beamforming vector f where $f \in \mathbb{C}^{M\times 1}$ and $||f||^2 = 1$ is used to create a directional signal. The resulting calculation for x is as follows:

$$x = f(\sqrt{ap_s}x_A + \sqrt{(1-a)p_s}x_B) \tag{15.1}$$

The signal received by the RIS in the first phase ($y_{RIS}^{(1)}$) is influenced by the channel between BS and the RIS, represented by $H_{gi} \in \mathbb{C}^{N\times M}$:

$$y_{RIS}^{(1)} = H_{gi}x \tag{15.2}$$

15.5.2 Second Phase

In the second phase, RIS sends its received signal to U_A, which U_E attempts to eavesdrop on. This signal is sent through the channel from the RIS to U_A, represented by $h_{iA} \in \mathbb{C}^{N\times 1}$. This signal is morphed by Φ, a diagonal matrix used to reflect and adjust the signal sent from BS. In addition, an anti-eavesdropping jamming signal is injected by U_B to both U_E and U_A, which is known only to U_A who can eliminate it. This jamming signal is coined x_j, and is sent with power P_j, which U_A receives through $h_{BA} \in \mathbb{C}^{1\times 1}$, the channel from U_B to U_A. Furthermore, U_A receives noise in the form of $n_A^{(2)}$, which is "complex Gaussian noise zero mean and variance (σ_A^2)." In total, U_A receives the following signal in phase 2:

$$y_{U_A}^{(2)} = (h_{iA}^H \Phi H_{gi})x + \sqrt{P_j} x_j h_{BA} + n_A^{(2)} \tag{15.3}$$

In a similar vein, in phase 2, U_E also receives a signal from RIS through the channel $h_{iE} \in \mathbb{C}^{N\times 1}$, as well as a jamming signal from U_B through the channel $h_{BE} \in \mathbb{C}^{1\times 1}$. It is also affected by its own Gaussian noise $n_E^{(2)}$ with variance σ_E^2. The following is the signal received by U_E:

$$y_{U_E}^{(2)} = (h_{iE}^H \Phi H_{gi})x + \sqrt{P_j} x_j h_{BE} + n_E^{(2)} \tag{15.4}$$

15.5.3 Third Phase

In the third phase, U_A acts as a relay that amplifies and forwards the received signal to U_B. As a result, the signal is affected by the gain variable G and is sent through channel $h_{AB} \in \mathbb{C}^{1\times 1}$ (channel from U_A to U_B), with U_B affected by complex Gaussian noise $n_B^{(3)}$ with variance σ_B^2 [35]:

$$y_{U_B}^{(3)} = G h_{AB} y_{U_A}^{(2)} + n_B^{(3)} \tag{15.5}$$

Similarly, U_E receives a signal amplified by gain G that is sent through channel $h_{AE} \in \mathbb{C}^{1\times 1}$, and affected by complex Gaussian noise $n_E^{(3)}$ with variance σ_E^2:

$$y_{U_E}^{(3)} = G h_{AE} y_{U_A}^{(2)} + n_E^{(3)} \tag{15.6}$$

15.5.4 SNR and SINR

From Eqs. (15.3) and (15.4), we can, respectively, deduce the SNR of U_A and the SINR of U_E (since U_A can eliminate the jamming signal from U_2) in phase 2 [35]:

$$\gamma_{U_A}^{(2)} = \frac{\alpha p_s |(h_{iA}^H \Phi H_{gi}) f|^2}{\sigma_A^2} \tag{15.7}$$

$$\gamma_{U_E}^{(2)} = \frac{p_s |(h_{iE}^H \Phi H_{gi}) f|^2}{P_j |h_{BE}|^2 + \sigma_A^2} \tag{15.8}$$

From Eqs. (15.5) and (15.4), we can also deduce the SINR of U_B and U_E in phase 3 respectively [35]:

$$\gamma_{U_B}^{(3)} = \frac{G^2(1-\alpha)p_s|(h_{iA}^H \Phi H_{gi})f|^2|h_{AB}|^2}{G^2(\alpha p_s|(h_{iA}^H \Phi H_{gi})f|^2 + \sigma_A^2)|h_{AB}|^2 + \sigma_B^2} \tag{15.9}$$

$$\gamma_{U_E}^{(3)} = \frac{G^2 p_s|(h_{iA}^H \Phi H_{gi})f|^2|h_{AE}|^2}{G^2(P_j|h_{BA}|^2 + \sigma_A^2)|h_{AE}|^2 + \sigma_E^2} \tag{15.10}$$

15.5.5 Secrecy Rate

We are able to obtain a closed-form expression for figuring out the lower bound of the ESR for this system model. Starting with the *instantaneous sum* secrecy rate (SSR), one can obtain an equation from the total legitimate rate R_L and the total eavesdropping rate R_E [35]:

$$R_s = \frac{2}{3}\max\{0, R_L - R_E\} \tag{15.11}$$

The equations for figuring out R_L and R_E are as follows [35]:

$$R_L = \log_2(1+\gamma_{U_A}^{(2)}) + \log_2(1+\gamma_{U_B}^{(3)}) \tag{15.12}$$

$$R_E = \log_2(1+\gamma_{U_E}^{(2)}) + \log_2(1+\gamma_{U_E}^{(3)}) \tag{15.13}$$

Using (15.12) and (15.13), we can rewrite Eq. (15.11) as follows:

$$\begin{aligned} R_s &= \frac{2}{3}\max\{0, R_L \\ &= \log_2(1+\gamma_{U_A}^{(2)}) + \log_2(1+\gamma_{U_B}^{(3)}) - (\log_2(1+\gamma_{U_E}^{(2)}) + \log_2(1+\gamma_{U_E}^{(3)}))\} \end{aligned} \tag{15.14}$$

From here, one can figure out the closed-form solution to the ESR of this model with further calculations.

15.5.6 Limitations and Implications

This section mainly presents the beginnings of a larger calculation used for obtaining the closed-form solution of the ESR for the system model found in [35]. Here, we identify and present a few key implications and limitations that we think our readers should take away from this chapter.

First, the set of equations presented here does not show the all of the calculations as seen in [35], as the sheer extent of those calculations renders them unrealistic to be fully shown in this section. Additionally, this section does not present the results of the simulation as obtained in [35], for the same reason as above. This

means that this section is not able to be as comprehensive of an analysis as it could be. Readers interested in the full analysis should refer back to the original paper.

Additionally, this analysis is limited to one model of a PLS-aided RIS-NOMA network, based on one paper. As such, other models involving differences in the agents used may not be applicable to this analysis, and any calculations presented here may need to be modified for one's own analysis.

We believe that despite the above limitations, this section still serves to help readers understand the basics of finding solutions for the ESR of PLS in an RIS-NOMA-Aided network. The calculations presented shed light on the mathematics used to determine the effectiveness of the RIS-aided PLS technique. This analysis can act as the foundation for finding the lower bound of the ESR for any future endeavors involving the modeling of RIS-aided PLS networks.

15.6 Limitations and Key Takeaways

When composing a research study that focuses on investigating PLS for RIS-aided wireless communication systems only via current literature, several notable constraints emerge. The lack of software simulations and real-life tests mostly limits the extent and creativity of the study. It is difficult to verify theoretical models, investigate the complex behavior of RIS in many settings, and determine if suggested security improvements are indeed feasible without simulations. Moreover, depending only on theoretical discoveries and previously published literature might result in a possible prejudice since the inferences made are not practically verified. The absence of empirical data hinders the capacity to identify unforeseen problems that may occur in real-world applications, thereby reducing the strength and dependability of the study results. Hence, the work may include an extensive theoretical analysis, but it lacks the practical insights and tangible validation required to make substantial advancements in the subject.

The study discovered that RIS have the ability to adaptively modify the transmission of signals in order to safeguard wireless networks. The research includes a theoretical discussion on Security RIS. In order to avoid unauthorized listening and interference, this paradigm incorporates interactions between RIS and wireless signals. PLS refers to the use of physical properties and techniques to protect communication systems against unauthorized access or interference. The issues faced by RIS include the need for precise channel status information, the complexity of designing the system, and the trade-off between security and other performance metrics such as EE and latency. The article critically examines the integration of RIS (radio interface specification) into research on wireless security frameworks and the following progress made in this area. The paper continues by providing experimental validation, presenting new techniques for setting up

RIS and discussing the integration of machine learning and 5G/6G network collaboration with RIS. These results clarify the possibilities and limits of RIS systems' PLS. In addition, they propose enhancements to research and practice.

15.7 Conclusion

This chapter explores the effectiveness of RIS-aided PLS designs in mitigating eavesdropping and jamming threats. This chapter delves into the foundational principles and hardware architecture of RIS, alongside the security concepts and methodologies of PLS. Various RIS-aided PLS design models are discussed, including RIS-only assisted PLS, RIS combined with NOMA, double-faced active RIS, and STAR–RIS assisted NOMA. Eventually, We present RIS-aided PLS design solutions based on resource allocation, beamforming, and AN, specifically analyzing and simulating RIS-aided PLS model effectiveness. RIS showed promising simulation results but required studies and renovation to maximize its potential.

References

1 Dai, L., Wang, B., Ding, Z. et al. (2018). A survey of non-orthogonal multiple access for 5G. *IEEE Communications Surveys & Tutorials* 20 (3): 2294–2323. https://doi.org/10.1109/COMST.2018.2835558.

2 Khoshafa, M.H., Ngatched, T.M.N., and Ahmed, M.H. (2023). RIS-aided physical layer security improvement in underlay cognitive radio networks. *IEEE Systems Journal* 17 (4): 6437–6448. https://doi.org/10.1109/JSYST.2023.3296012.

3 Guo, Y., Liu, Y., Wu, Q. et al. (2023). Enhanced secure communication via novel double-faced active RIS. *IEEE Transactions on Communications* 71 (6): 3497–3512. https://doi.org/10.1109/TCOMM.2023.3250454.

4 Wu, Q. and Zhang, R. (2020). Towards smart and reconfigurable environment: intelligent reflecting surface aided wireless network. *IEEE Communications Magazine* 58 (1): 106–112. https://doi.org/10.1109/MCOM.001.1900107.

5 Khoshafa, M.H., Ngatched, T.M.N., and Ahmed, M.H. (2021). Reconfigurable intelligent surfaces-aided physical layer security enhancement in D2D underlay communications. *IEEE Communications Letters* 25 (5): 1443–1447. https://doi.org/10.1109/LCOMM.2020.3046946.

6 Zhang, Y., Yang, Z., Cui, J. et al. (2023). STAR-RIS assisted secure transmission for downlink multi-carrier NOMA networks. *IEEE Transactions on Information Forensics and Security* 18: 5788–5803. https://doi.org/10.1109/TIFS.2023.3313353.

7 Liu, Y., Qin, Z., Elkashlan, M. et al. (2017). Nonorthogonal multiple access for 5G and beyond. *Proceedings of the IEEE* 105 (12): 2347–2381. https://doi.org/10.1109/JPROC.2017.2768666.

8 Liu, Y., Mu, X., Liu, X. et al. (2022). Reconfigurable intelligent surface-aided multi-user networks: interplay between NOMA and RIS. *IEEE Wireless Communications* 29 (2): 169–176. https://doi.org/10.1109/MWC.102.2100363.

9 Khalid, W., Rehman, M.A.U., Van Chien, T. et al. (2024). Reconfigurable intelligent surface for physical layer security in 6G-IoT: designs, issues, and advances. *IEEE Internet of Things Journal* 11 (2): 3599–3613. https://doi.org/10.1109/JIOT.2023.3297241.

10 Nguyen, V.-L., Lin, P.C., Cheng, B.C. et al. (2021). Security and privacy for 6G: a survey on prospective technologies and challenges. *IEEE Communications Surveys & Tutorials* 23 (4): 2384–2428. https://doi.org/10.1109/COMST.2021.3108618.

11 Tang, X., Wang, D., Zhang, R. et al. (2021). Jamming mitigation via aerial reconfigurable intelligent surface: passive beamforming and deployment optimization. *IEEE Transactions on Vehicular Technology* 70 (6): 6232–6237. https://doi.org/10.1109/TVT.2021.3077662.

12 Zhang, Z., Zhang, C., Jiang, C. et al. (2021). Improving physical layer security for reconfigurable intelligent surface aided NOMA 6G networks. *IEEE Transactions on Vehicular Technology* 70 (5): 4451–4463. https://doi.org/10.1109/TVT.2021.3068774.

13 Basar, E. and Poor, H.V. (2021). Present and future of reconfigurable intelligent surface-empowered communications [perspectives]. *IEEE Signal Processing Magazine* 38 (6): 146–152. https://doi.org/10.1109/MSP.2021.3106230.

14 Zhang, Z., Dai, L., Chen, X. et al. (2023). Active RIS vs. passive RIS: which will prevail in 6G? *IEEE Transactions on Communications* 71 (3): 1707–1725. https://doi.org/10.1109/TCOMM.2022.3231893.

15 Xie, X., He, C., Ma, X. et al. (2023). Joint precoding for active intelligent transmitting surface empowered outdoor-to-indoor communication in mmWave cellular networks. *IEEE Transactions on Wireless Communications* 22 (10): 7072–7086. https://doi.org/10.1109/TWC.2023.3247906.

16 Zuo, J., Liu, Y., Ding, Z. et al. (2023). Joint design for simultaneously transmitting and reflecting (STAR) RIS assisted NOMA systems. *IEEE Transactions on Wireless Communications* 22 (1): 611–626. https://doi.org/10.1109/TWC.2022.3197079.

17 Björnson, E., Özdogan, Ö., and Larsson, E.G. (2020). Reconfigurable intelligent surfaces: three myths and two critical questions. *IEEE Communications Magazine* 58 (12): 90–96.

18 Wu, Q., Zhang, S., Zheng, B. et al. (2021). Intelligent reflecting surface-aided wireless communications: a tutorial. *IEEE Transactions on Communications* 69 (5): 3313–3351.

19 Hasan, S.R. and Sabuj, S. (2023). A comprehensive review on reconfigurable intelligent surface for 6G communications: overview, deployment, control mechanism, application, challenges, and opportunities. https://doi.org/10.36227/techrxiv.24624420.

20 Di Renzo, M. et al. (2019). Smart radio environments empowered by reconfigurable AI meta-surfaces: an idea whose time has come. *EURASIP Journal on Wireless Communications and Networking* 2019 (1): 1–20.

21 Liaskos, C., Nie, S., Tsioliaridou, A. et al. (2018). A new wireless communication paradigm through software-controlled metasurfaces. *IEEE Communications Magazine* 56 (9): 162–169.

22 Bhagoji, A.N., Chakraborty, S., Mittal, P., and Calo, S. (2019). Analyzing federated learning through an adversarial lens. *International Conference on Machine Learning*, 634–643. PMLR.

23 Melki, R., Noura, H.N., Mansour, M.M., and Chehab, A. (2020). Physical layer security schemes for MIMO systems: an overview. *Wireless Networks* 26 (3): 2089–2111.

24 Zappone, A., Di Renzo, M., and Fotock, R.K. (2023). Surface-based techniques for IoT networks: Opportunities and challenges. *IEEE Internet of Things Magazine* 5 (4): 72–77.

25 Ahmed, J., Nguyen, T.N., Ali, B. et al. (2022). On the physical layer security of federated learning based IoMT networks. *IEEE Journal of Biomedical and Health Informatics* 27 (2): 691–697.

26 Tang, W., Chen, M.Z., Chen, X. et al. (2020). Wireless communications with reconfigurable intelligent surface: path loss modeling and experimental measurement. *IEEE Transactions on Wireless Communications* 20 (1): 421–439.

27 Lyu, B., Hoang, D.T., Gong, S., and Yang, Z. et al. (2020). Intelligent reflecting surface assisted wireless powered communication networks. *2020 IEEE Wireless Communications and Networking Conference Workshops (WCNCW)*, 1–6. IEEE. https://doi.org/10.1109/WCNCW48565.2020.9124775.

28 Gu, X., Duan, W., Zhang, G. et al. (2023). Physical layer security for RIS-aided wireless communications with uncertain eavesdropper distributions. *IEEE Systems Journal* 17 (1): 848–859. https://doi.org/10.1109/JSYST.2022.3153932.

29 Thien, H.T., Tuan, P.-V., and Koo, I. (2022). A secure-transmission maximization scheme for SWIPT systems assisted by an intelligent reflecting surface and deep learning. *IEEE Access* 10: 31851–31867. https://doi.org/10.1109/ACCESS.2022.3159679.

30 Le, C.-B., Do, D.T., Silva, A. et al. (2022). Joint design of improved spectrum and energy efficiency with backscatter NOMA for IoT. *IEEE Access* 10: 7504–7519. https://doi.org/10.1109/ACCESS.2021.3139118.

31 Kaleem, Z., Ali, M., Ahmad, I. et al. (2021). Artificial intelligence-driven real-time automatic modulation classification scheme for next-generation cellular networks. *IEEE Access* 9: 155584–155597. https://doi.org/10.1109/ACCESS.2021.3128508.

32 Guan, X., Wu, Q., and Zhang, R. (2020). Intelligent reflecting surface assisted secrecy communication: is artificial noise helpful or not? *IEEE Wireless Communications Letters* 9 (6): 778–782. https://doi.org/10.1109/LWC.2020.2969629.

33 Jameel, F., Wyne, S., Kaddoum, G., and Duong, T.Q. (2019). A comprehensive survey on cooperative relaying and jamming strategies for physical layer security. *IEEE Communications Surveys & Tutorials* 21 (3): 2734–2771. https://doi.org/10.1109/COMST.2018.2865607.

34 Guo, J., Yu, L., Chen, Z. et al. (2022). RIS-assisted secure UAV communications with resource allocation and cooperative jamming. *IET Communications* 16 (13): 1582–1592. https://doi.org/10.1049/cmu2.12416.

35 Souzani, A., Pourmina, M.A., Azmi, P., and Naser-Moghadasi, M. (2023). Physical layer security enhancement via IRS based on PD-NOMA and cooperative jamming. *IEEE Access* 11: 65956–65967. https://doi.org/10.1109/ACCESS.2023.3290104.

16

RIS-Empowered Terrestrial and Non-terrestrial Wireless Communication Systems

Unwana Macaulay Ekpe

Department of Electrical and Electronic Engineering, Akwa Ibom State University, Ikot Akpaden, Nigeria

16.1 Introduction

Reconfigurable intelligent surfaces (RISs) are surfaces that can be configured to actively or passively modify the wireless propagation channel by reflecting, refracting, and phase-shifting incident electromagnetic waves. This brings about the ability to control the direction, amplitude and polarization orientation of the reflected waves. When RIS is assisted by advanced technologies such as multiple-input multiple-output (MIMO) [1], non-orthogonal multiple access (NOMA) [2], and artificial intelligence (AI) [3], the wireless propagation channel can be controlled in real time, resulting in the creation of steerable beams. This feature can compensate for losses caused by shadowing and large-scale fading, and general enhancement of the wireless propagation channel through interference mitigation techniques. The advantages of using RISs therefore include improved energy and spectral efficiency, cost saving, ease of network expansion, and better cell-edge performance.

Improvement in energy efficiency is made possible by the passive and semi-passive mode of operation of RIS as they do not rely on power-hungry conventional amplify and forward (AF) relaying systems. Achieving improved energy efficiency, however requires a careful tradeoff between the need to frequently obtain channel state information (CSI) and the requirement of timeously acting on such information by adjusting the configuration of the passive RIS elements [4]. It should be noted that spectral efficiency is not always coincident with energy efficiency. Research such as [5] has shown that only active RIS configurations can perform better than line-of-sight (LOS) and AF systems.

The cost savings advantage of RIS is due to their passive nature, enabling them to be easily deployed in existing networks to expand coverage or improve service

Reconfigurable Intelligent Surfaces for 6G and Beyond Wireless Networks, First Edition.
Edited by Agbotiname Lucky Imoize, Vinoth Babu Kumaravelu, and Dinh-Thuan Do.

delivery. RIS can therefore be installed on terrestrial infrastructure such as building facades, indoor walls and ceilings, billboards, vehicles, and street furniture. RIS can also be deployed on non-terrestrial platforms such as aerial vehicles and satellites in low earth orbit (LEO) and geostationary earth orbit (GEO). Based on the motivation for deployment and the available intelligent tuning/control feature, RIS can support full-duplex communications and full-band transmissions in terrestrial, and non-terrestrial environments.

The numerous possible advantages of RIS have made the international telecommunications union (ITU) [6] recognize it as one of the candidate technologies that will be employed to enhance the radio interface of terrestrial communication systems toward the year 2030 and beyond. This recognition is also applicable to non-terrestrial systems, and considerable work has been done to establish the theoretical and practical limits of using RIS in such environments. It is therefore important to present the building blocks of RIS, their controlling mechanisms, and how they can be applied to empower terrestrial and non-terrestrial-based communication systems. These are therefore the major contribution of this chapter.

16.1.1 Chapter Contributions

Having presented basic information on terrestrial and non-terrestrial systems and the role of RIS in such systems, the major contributions of this chapter are as follows:

(a) Metasurfaces have been introduced in easy-to-understand language and some of the mechanisms used in controlling their operation have been presented.
(b) A physics-based model employing a small number of variables to represent RIS-empowered wireless communication systems has been presented. The model covers the fundamental concept of free space loss and presents how the angles of incidence and reflection are applied to describe signal propagation in the presence of RIS.
(c) The important parameters that need to be optimized and the constraints that need to be dealt with in both terrestrial and non-terrestrial RIS-empowered systems have been presented. These parameters include energy efficiency, throughput, and capacity, while the constraints include UAV flight trajectory, signal-to-interference plus noise ratio, and available transmit power.

16.1.2 Chapter Organization

Section 16.1 of the chapter briefly introduces metasurfaces and their control mechanisms while Section 16.2 presents the free space path loss model using variables that are relevant to RIS-based systems before presenting physics-based

channel models that apply to both terrestrial and non-terrestrial RIS-empowered wireless communication systems. Thereafter, a complete system model that takes into cognizance the large-scale and small-scale fading experienced in all wireless communications channels is presented. A discussion on the architecture and the considerations necessary to deploy RIS-empowered systems in the terrestrial environment is presented. Specific considerations on the methodologies for implementing MIMO-assisted and OFDM-assisted terrestrial RIS systems are presented. Following this, RIS-empowered systems for multiple terrestrial users are discussed. Section 16.3 uses the channel models presented for the terrestrial system to discuss aspects of non-terrestrial networks. Specifically, aerial networks involving unmanned aerial vehicles (UAVs) and high-altitude platforms (HAPs) are discussed. Thereafter, networks involving satellites in LEO and GEO are presented before considering a multilayered integrated network that encompasses both terrestrial and non-terrestrial components.

16.2 Metamaterials and Metasurfaces

Metamaterials are subwavelength components fabricated from metals or dielectric materials and are designed to couple resonantly with the electric and/or magnetic components of incident electromagnetic fields [7]. This coupling gives rise to electric permittivity (ε) and/or magnetic permeability (μ) response values that do not exist in nature. When simultaneous negative values are obtained for both permittivity and permeability, the resulting metamaterial is called a double-negative (DNG) metamaterial. Other types of metamaterials include single-negative (SNG) metamaterials, chiral materials, bi-anisotropic media, and linear and nonlinear media.

Permittivity, permeability, and refractive index are properties of bulk three-dimensional (3D) materials and these depend on the size, shape, density, and alignment of the constituent composites. Therefore, synthesizing a metamaterial to achieve desired electromagnetic properties entails engineering such properties to specific geometries. This can be a very complex task in 3D, hence the preference for planar two-dimensional (2D) structures called metasurfaces.

16.2.1 Metasurface Control Mechanisms

The available methods of controlling metasurfaces include mechanical actuation, the use of materials such as graphene and liquid crystals, and the use of electronic devices such as varactor diodes, positive-intrinsic-negative (PIN) diodes, which may depend on field effect transistors (FETs) or micro-electromechanical system-based (MEMS) switches to control state changes. Table 16.1, whose entries

Table 16.1 Comparison of control mechanisms for metasurfaces.

Control method	Controlled component	Advantages	Disadvantages	Applications
Electronic-based	Varactor diodes	Very stable at frequencies ≤ 30 GHz, reliable operation	Exhibit high insertion loss at frequencies > 30 GHz	Used in realizing digitally controlled RIS
	PIN diodes	Mature and stable technology. Suitable for frequencies ≤ 30 GHz	Operation is limited by diode switching frequency. Affected by parasitic reactance. High insertion loss > 30 GHz	Used as beam steerer, absorber, phase shifter, holographic display, and polarization converter
	Schottky diodes	Minimal voltage drop, fast switching speed. Suitable for THz, mm-wave and microwave frequencies	Difficult to fabricate and expensive if the array size is large	Used as a phase shifter for millimeter wave frequencies
Material-based	Graphene	High speed of operation and very stable response. Suitable for THz and near-infrared frequencies	Difficult to achieve uniform material properties. Control of the biasing network requires nonuniform operation	Used as beam steerer, absorber, polarization converter, and digitally controlled RIS
	Liquid crystal	Very low power consumption, low cost, and low complexity. Easy to fabricate and suitable for a very wide range of frequencies (THz, mm-wave, microwave, and visible spectrum)	Non-homogeneous nature of liquid crystal direction of fields. Difficult to achieve impedance matching and biasing	Used as beam steerer, modulator, digitally controlled RIS, and holographic display
	Phase-changing materials such as Vanadium dioxide	Capable of non-volatile reversible phase transition. Suitable for THz to visible frequencies	Imprecise phase transition, nonuniform electrical and optical properties	Used as polarization converter, modulator, beam steerer, absorber

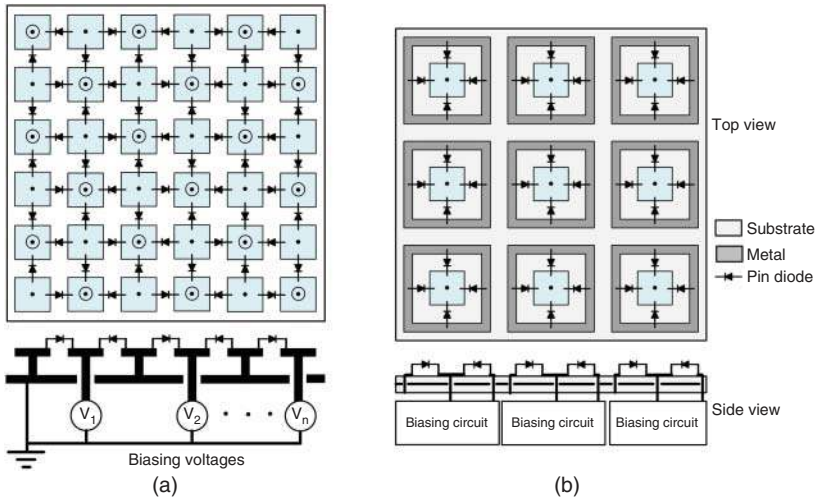

Figure 16.1 Metasurfaces achieved using (a) varactor diodes and (b) PIN diodes.

have been obtained from [8, 9] compares the various methods of controlling metasurfaces and their advantages, disadvantages, and applications.

As shown in Table 16.1, the electronic-based method of control is preferred over others due to its low energy consumption and fast reaction times. Figure 16.1 shows two types of metasurfaces that are controlled by diodes. The diagrams have been generated based on the schematics given in [10] and the metasurfaces shown are controlled by independently tuning the reflection amplitude and phase shift of its elements using different levels of biasing voltages. It should however be noted that continuous tuning is difficult to achieve, therefore, practical systems use discrete voltage levels, and this introduces some loss of accuracy.

16.2.2 Supporting Technologies for the Deployment of RIS

The technologies that can enhance the performance of RIS include orthogonal multiple access techniques such as time division multiple access (TDMA), frequency division multiple access (FDMA), and space division multiple access (SDMA). More recently, there has been an increased drive to implement NOMA techniques with RIS, and this is mainly because such systems rely on receiver-side interference cancellation strategies, and this better suits the passive nature of RIS [11]. Other supporting technologies include MIMO [1], AI, and machine learning (ML) [3]. These technologies are already well advanced, and numerous studies have aimed to bring to reality the communications systems of the future using these technologies [12, 13]. Some other studies have investigated their use in different environments [14–16].

16.3 RIS-Empowered Terrestrial Communication Systems

It has been recognized that the propagation channel for terrestrial RIS-empowered wireless communication is a cascade of at least three subchannels. As shown in Figure 16.2, this comprises the transmitter to the RIS channel, the RIS to the receiver channel, and the direct channel linking the transmitter and receiver. The three subchannels usually span huge distances relative to the wavelength of the propagating signal, therefore traditional large-scale path loss models can adequately describe the characteristics of such channels. Several such models are available in the literature, and some examples are presented in the following subsections.

16.3.1 Free Space Path Loss

A passive reconfigurable intelligent surface aims to achieve an ideal reflection of the incident beam arriving at an angle θ_i, and departing at a desired angle θ_r. Based on an x, y, z reference frame shown in Figure 16.3, the desired reflected wave is described by the following electric and magnetic field distributions.

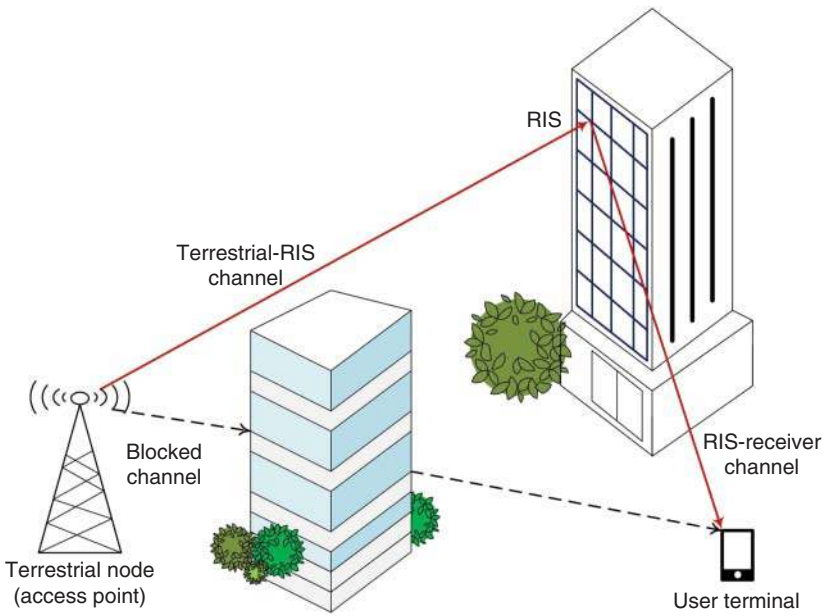

Figure 16.2 Propagation channel of RIS-empowered wireless communication system.

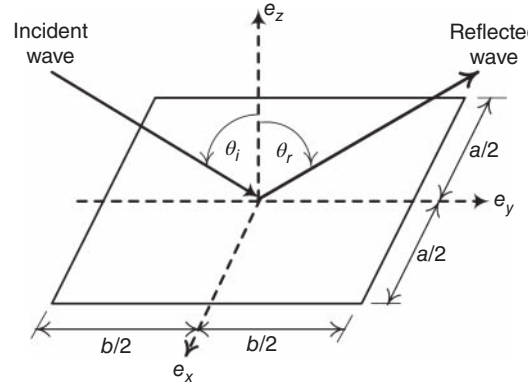

Figure 16.3 An incident wave reflected by an $a \times b$ RIS element.

$$\mathbf{E}_r = E_r e^{-jk(\sin(\theta_r)y + \cos(\theta_r)z)}$$

$$\mathbf{H}_r = -\frac{E_r}{\eta}(\sin(\theta_r)e_z - \cos(\theta_r)e_y)e^{-jk(\sin(\theta_r)y + \cos(\theta_r)z)} \tag{16.1}$$

where η is the characteristic impedance of the surface. Using the diffraction equations given in [17, 18], and following the methodology presented in [19], the superposition of both the incident and reflected electric field is given as,

$$\mathbf{E}_t = E_i e^{-jk\sin(\theta_i)y}\boldsymbol{e}_x + E_r e^{-jk\sin(\theta_r)y}\boldsymbol{e}_x \tag{16.2}$$

This leads to the desired phase of the wanted reflection coefficient being given by,

$$\phi_r(y) = -k\sin(\theta_r)y + k\sin(\theta_i)y \tag{16.3}$$

The dynamic relationship between θ_i, θ_r, and the local reflecting reconfigurable surface, $\phi_r(y)$ is obtained by differentiating (16.3) with respect to y and this results in

$$\frac{d\phi_r(y)}{dy} = k(\sin(\theta_i)y - k\sin(\theta_r)) \tag{16.4}$$

Different values of surface impedance required to reflect an incident wave in a given direction for a characteristic incident angle have been investigated in [19], and it was concluded that phase shifts in practical metasurfaces need to be discretized, and such surfaces must be divided into sub-wavelength-sized elements. Since an incident electric field induces an electric current in the direction of $\boldsymbol{e}_x$ (based on the x, y, z reference frame), this current can be controlled by tuning the surface impedance of each metasurface element to achieve a reflected wave with a main beam steered towards a desired direction, θ_r.

If an RIS is used in reflecting a signal towards the θ_r direction, the squared magnitude of its reflected field when observed from an arbitrary angle, θ_o and at a far-field distance d_2 (see Figure 16.2) can be expressed as,

$$S_{RIS} = \left(\frac{ab}{\lambda}\right)^2 \frac{E_i^2 \cos^2(\theta_i)}{{d_2}^2} \left(\frac{\sin\left(\frac{\pi b}{\lambda}(\sin(\theta_o) - \sin(\theta_r))\right)}{\frac{\pi b}{\lambda}(\sin(\theta_o) - \sin(\theta_r))} \right)^2 \tag{16.5}$$

where E_i^2 is the magnitude of the incident electric field vector, ab represents the combined dimensions of all the elements of the metasurface, and λ represents the wavelength of the propagating wave. The relationship between the electric field strength and the transmit antenna power, P_{tx} and transmit antenna gain, G_{tx} at the RIS surface is given as,

$$E_i^2 = \frac{P_{tx} G_{tx} \eta}{4\pi d_1^2} \tag{16.6}$$

where E_i is measured in volts per meter and η is the efficiency of the transmit antenna. The effective area, A_{rx} of the antenna receiving the reflected RIS signal must be taken into account, and this is given as,

$$A_{rx} = \frac{\lambda^2}{4\pi} G_{rx} \eta \tag{16.7}$$

Analogous to the case of the transmitting antenna, η represents the efficiency with which the antenna receives power within its effective area. If the antenna is located in the far-field region, its effective area dictates the magnitude of the received power, P_{rx}. Therefore, multiplying Eqs. (16.5) and (16.7), we have,

$$P_{rx} = \frac{P_{tx} G_{tx} G_{rx}}{(4\pi)^2} \left(\frac{ab}{d_1 d_2}\right)^2 \cos^2(\theta_i) \left(\frac{\sin\left(\frac{\pi b}{\lambda}(\sin(\theta_o) - \sin(\theta_r))\right)}{\frac{\pi b}{\lambda}(\sin(\theta_o) - \sin(\theta_r))} \right)^2 \tag{16.8}$$

Since maximum observable received power occurs at $\theta_o = \theta_r$, the received signal power at a distance d_2 in the direction, θ_o simplifies to,

$$P_{rx} = \frac{P_{tx} G_{tx} G_{rx}}{(4\pi)^2} \left(\frac{ab}{d_1 d_2}\right)^2 \cos^2(\theta_i) \tag{16.9}$$

Equation (16.9) shows that the received power is directly proportional to the square of the RIS area and inversely proportional to the square of the product of the transmitter-RIS and RIS-receiver distance ($d_1 d_2$).

16.3.2 Complete System Model

In addition to free space loss, propagating electromagnetic waves are also affected by intervening objects such as trees, buildings, and other large and small man-made and natural objects. These objects can cause the waves to be reflected, refracted, diffracted, and/or may allow the waves to be transmitted through. A combination of these mechanisms causes the wavefronts of the propagating signals to travel different distances before reaching a receiver. The wavefronts at the receiver, therefore, arrive with different phases, and as the receiver sums them up, there are random instances of constructive and destructive addition. This causes the resultant sum of the received signal power to fluctuate rapidly. The rapid fluctuation is called small-scale fading or fast fading and is very noticeable when the receiver is moved over distances in the order of a few tens of wavelengths. When there is no direct LOS or dominant propagation path from the transmitter to the receiver, statistical analysis of the small-scale variations of the received signal power generally follows a Rayleigh distribution. On the other hand, when there is an LOS path between a transmitter and a receiver, the received signal power can be adequately characterized by a Rician distribution.

There are many system models in the literature that take into account both the large-scale and small-scale fading of RIS-enabled terrestrial wireless communication systems. One of the well-known models is the open-source geometry-based stochastic (GBS) model presented in [20]. The generic communication environment that the model describes is graphically illustrated in Figure 16.4. Using ellipses and the Cartesian coordinate system, all the angles in the horizontal and vertical direction between the transmitter broadside, scatterers in each of the two scatterer clusters, RIS elements, and receiver broadside are defined by the model. The model also takes into cognizance three subchannels being the transmitter-to-RIS channel, the RIS-to-receiver channel, and the transmitter-to-receiver channel.

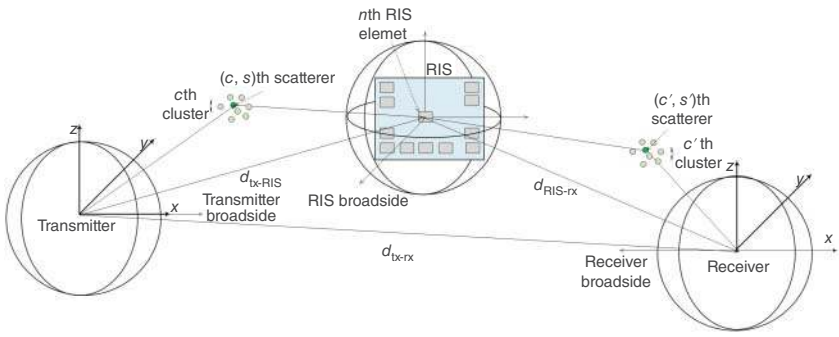

Figure 16.4 Generic 3D model of an RIS-empowered wireless communication system.

In addition to the GBS model, a new channel model that takes into consideration the effects of phase-dependent attenuation caused by the tuned RIS components and the effect this has on the polarization orientation of antennas has been reported in [21]. However, using the GBS model but ignoring the contributions of the scatterers within the clusters, a MIMO system comprising N_{tx} transmit antennas and N_{rx} receive antennas operating in the vicinity of an RIS with N passive reflective elements can be defined as follows

$$\tilde{\mathbf{H}} = \mathbf{H}_{\boldsymbol{d}} + \mathbf{G}\boldsymbol{\Phi}\mathbf{H}_{\mathbf{r}} \tag{16.10}$$

where $\mathbf{H}_{\boldsymbol{d}} \in \mathbb{C}^{N_{rx} \times N_{tx}}$ is a matrix representing the direct LOS or obstructed LOS (OLOS) channel from the terrestrial base station (or access point) to the receiver, $\mathbf{G} \in \mathbb{C}^{N \times N_{tx}}$ is the transmit covariance matrix representing the channel coefficients between the transmitter and the RIS, $\boldsymbol{\Phi}$ is a diagonal matrix that takes care of all the complex reconfigurable responses of the RIS elements and $\mathbf{H}_{\mathbf{r}} \in \mathbb{C}^{N_{tx} \times N}$ is a matrix representing the channel coefficients between the RIS and the receiver.

16.3.3 Architecture and Implementation Considerations for Terrestrial Networks

The dimensions of the metasurface components are subwavelength, and they need to be manufactured to achieve dynamically adjustable permittivity, permeability, and refractive index properties. Shown in Figure 16.5 is a typical architecture of

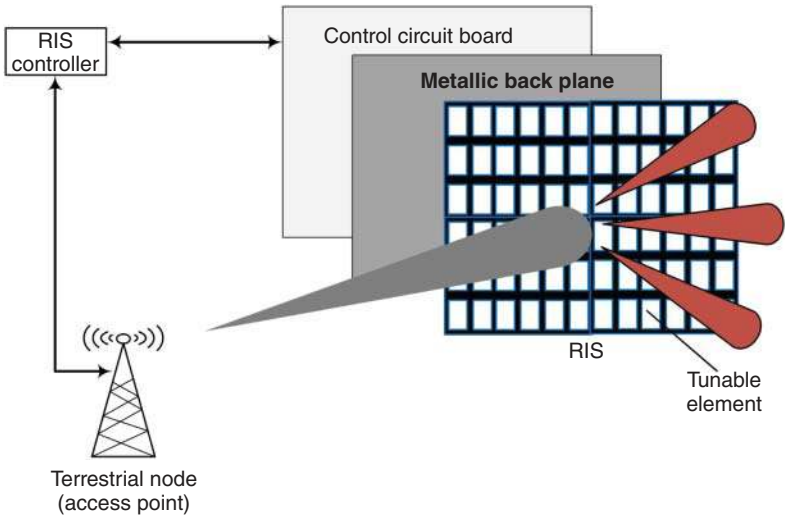

Figure 16.5 Architecture of a reconfigurable intelligent surface.

an RIS, which comprises an outer layer with a large number of tunable metamaterial components, a metallic backplane, and a control circuit board. The metallic backplane, in the case of forward scatter metasurfaces, is included to minimize signal leakage, while the circuit board is responsible for adjusting the properties of the reflecting surface to achieve different levels of reflection amplitudes ($\boldsymbol{\beta} = [\beta_1, \ldots, \beta_N]^T$) and/or phase shifts ($\boldsymbol{\theta} = [\theta_1, \ldots, \theta_N]^T$). A smart controller implemented using a field-programmable gate array (FPGA) enables control of the metasurface in response to desired channel conditions. To achieve this, the controller must communicate with the rest of the wireless communication network system.

For improved control of the reflection properties of the metasurfaces, dedicated sensors can be interlaced with the elements of the RIS to sense the reflection environment and thus reduce the response time and increase the efficiency of the smart controller [22]. This procedure is known as the acquisition of CSI.

To achieve the maximum benefits of RIS, the acquired CSI must be as accurate as possible, and they need to be acquired and acted on within the channel coherence time. The two practical methods of CSI acquisition are the semi-passive and fully passive methods. These are shown in Figures 16.6a,b. The semi-passive method uses sensors that are interlaced with the RIS elements to sample the channel, while the passive method is wholly dependent on pilot signals sent by the terrestrial node or user terminal (UT).

The semi-passive RIS system shown in Figure 16.6a can either operate in channel sensing mode or reflective mode. In channel sensing mode, all the reflecting elements are turned off while the interlaced low-power sensors are turned on to enable them to receive downlink pilot signals from the terrestrial access point and uplink pilot signals from the UTs. The CSI is obtained from the pilot signals, which are embedded within the overall received signal. For example, considering the uplink channel from user k to the access point, the overall received signal is given as,

$$\boldsymbol{y} = \sum_{k=1}^{K} (\mathbf{H}_{d,k} + \mathbf{G}^T \boldsymbol{\Phi} \mathbf{H}_{r,k}) + \boldsymbol{x}_k + \boldsymbol{n} \tag{16.11}$$

where $\mathbf{H}_{d,k}$, $\mathbf{G}^T$, $\boldsymbol{\Phi}$, and $\mathbf{H}_{r,k}$ are as earlier defined in Eq. (16.10) while $\boldsymbol{x}_k \in \mathbb{C}^{N_{tx,UT} \times 1}$ is the transmit signal vector of user k, with $N_{tx,\,UT}$ being the number of its transmit antennas and $\boldsymbol{n} \in \mathbb{C}^{N_{tx,AP} \times 1}$ is an additive Gaussian noise component at the access point, with $N_{tx,\,AP}$ being the number of transmit antennas at the access point.

After the CSI is acquired, the sensors are turned off and the CSI is used in tuning the reflecting elements to enable adequate steering of the downlink and uplink signals. It is worth noting that the transmission protocol, which encompasses both the channel sensing mode and reflection mode, must be completed within the channel coherence time. The protocol requires that UTs and the access point must

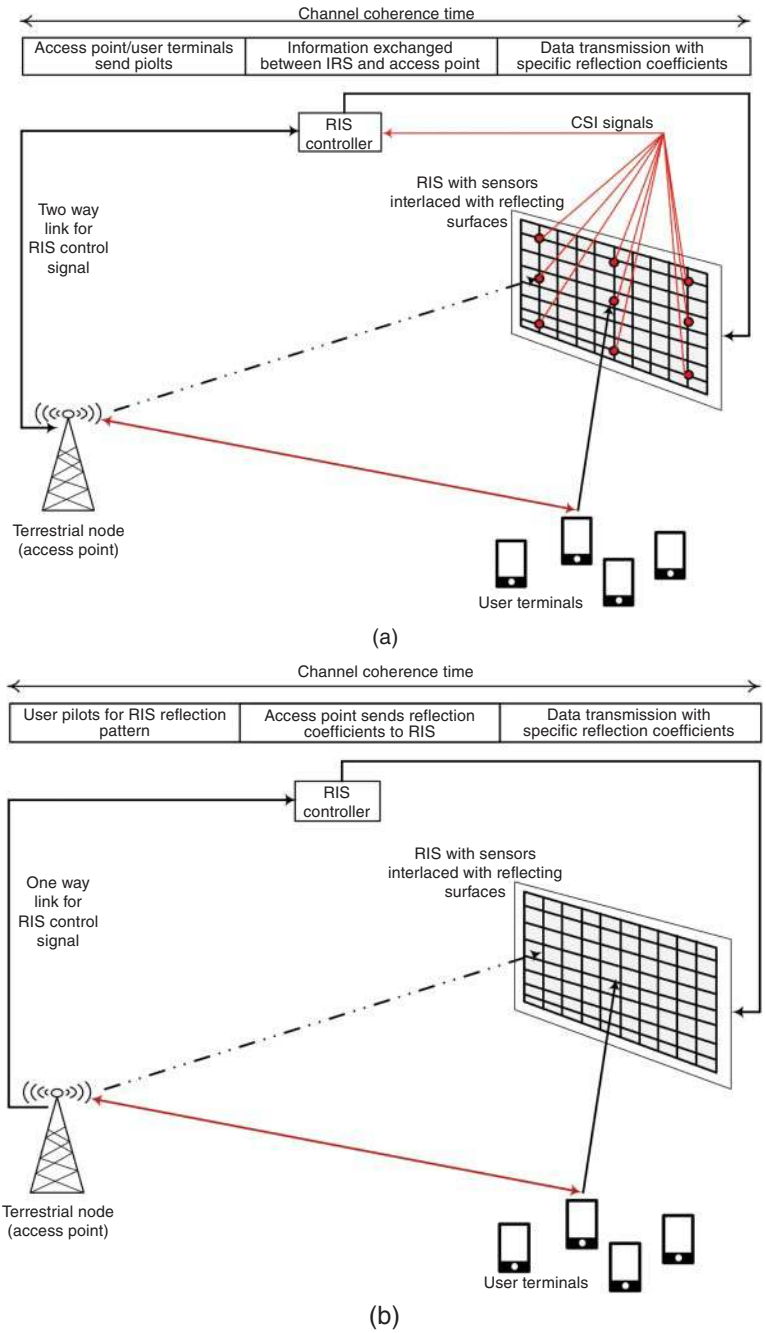

Figure 16.6 Practical methods of acquiring CSI for terrestrial RIS architectures showing (a) semi-passive method and (b) fully passive method.

first transmit orthogonal pilots in the uplink and downlink channels, respectively. Thereafter, information is exchanged between the access point and the RIS controller before the uplink or downlink data is transmitted to reflect off the fully configured RIS. This is a more complex procedure than the fully passive method described as follows.

In the fully passive method shown in Figure 16.6b, there are no sensors mounted on the RIS. This, therefore, means that only the direct channel from the access point to the UT and the cascaded UT-RIS-access point channel can be estimated. Using the uplink channel for illustration, the transmission protocol proceeds by the UT first transmitting orthogonal pilots to the access point. During this transmission, the RIS varies its reflection coefficients based on a predesigned reflection pattern. On receiving the orthogonal pilots, the access point estimates the CSI for the direct channel from the UT to the access point and the CSI for the cascaded UT-RIS-access point channel. The CSI estimates are then sent to the RIS controller through a backhaul link and the received CSI is used in setting unique reflection coefficients for individual UTs as appropriate.

As mentioned in Section 16.2.1, continuous tuning of the RIS is desired but this is difficult to practically achieve because it is a highly complex process. So far, implemented prototype systems resort to discrete and independent tuning of the reflection amplitude and phase shift or joint tuning of both the reflection amplitude and phase shift. There are pros and cons to each of these methods, and examples of practical implementation and modeling of the tuning mechanisms can be, respectively, found in [23, 24]. Recently, a novel system that combines passive and active elements to simultaneously sense and reflect incident electromagnetic waves while making use of the direction of arrival estimation has been reported in [25].

16.3.4 RIS-Empowered Terrestrial MIMO-Based Systems

Since RIS is envisioned to improve the existing terrestrial communication systems, which already employ advanced antenna systems such as multiple-input multiple-output (MIMO) in frequency-flat fading channels, we must consider how RIS can be integrated into such existing systems to enhance their capacity. Based on the RIS-empowered MIMO channel defined in Eq. (16.10), and leveraging on the fact that the RIS must independently or jointly vary the amplitude ($\boldsymbol{\beta}$) and phase ($\boldsymbol{\theta}$) of the reflected wave, we introduce a covariance matrix, $\mathbf{Q}$ to represent this process. Therefore, $\mathbf{Q} \in \mathbb{C}^{N_{tx} \times N_{tx}}$, and considering the possibility of achieving continuous phase shifts and maximum reflection amplitudes of all the RIS elements, the RIS-assisted capacity optimization problem in the terrestrial MIMO channel is presented in [22] as

$$\max_{\mathbf{\Phi},\mathbf{Q}} \log_2 \det\left(\mathbf{I}_{N_{rx}} + \frac{1}{\sigma^2}\tilde{\mathbf{H}}\mathbf{Q}\tilde{\mathbf{H}}^{\boldsymbol{H}}\right) \tag{16.12}$$

Equation (16.12) represents a fundamental capacity limit that RIS-empowered MIMO terrestrial systems would try to achieve, and it is subject to the following conditions:

(a) The value of the phase shift for each RIS element can only range from 0 to 2π,
(b) The amplitude of reflection for all RIS elements must be equal to 1,
(c) The trace of $\mathbf{Q}$ must have a value less than or equal to the total transmit power and
(d) $\mathbf{Q}$ must be a positive semidefinite matrix.

It is worth noting that the capacity limit in Eq. (16.12) is difficult to solve since it is a nonconvex optimization problem. However, some algorithms, such as alternating optimization (AO) [26] and the successive convex approximation (SCA) method [27] have been presented in the literature as capable solutions.

16.3.5 RIS-Empowered Terrestrial OFDM-Based Systems

Orthogonal frequency division multiplexing (OFDM) is usually applied in wideband terrestrial wireless communication systems to counter the effects of frequency-selective fading. Hinged on the consideration that the bandwidth of such a system is always much less than its carrier frequency (i.e., $B \ll f_c$), and its total bandwidth has to be divided into $Q \geq 1$ orthogonal subbands with centralized subcarriers, the rate achievable by a RIS-empowered OFDM-based terrestrial communication system is derived in [22] as,

$$r = \frac{1}{Q}\sum_{q=1}^{Q}\log_2\left(1 + \frac{p_q\left|\boldsymbol{f}_q^H\tilde{\boldsymbol{h}}^d + \boldsymbol{f}_q^H\tilde{\mathbf{G}}^r\boldsymbol{\vartheta}\right|^2}{\tilde{\sigma}^2}\right) \tag{16.13}$$

where p_q represents the power allocated at the transmitter to each orthogonal sub-carrier such that the sum of all sub-carrier powers must be less than or equal to the total transmit power, and the $\tilde{\sigma}^2$ represents the average noise power at each sub-carrier receiver. Also, $\boldsymbol{f}_q^H$ denotes the qth row of the discrete Fourier Transformed $Q \times Q$ matrix, while $\tilde{\boldsymbol{h}}^d = [h^{d^T}, 0, \ldots, 0]^T \in \mathbb{C}^{Q\times 1}$ is a zero-padded time-domain vector representing the transmitter to receiver direct channel, $\tilde{\mathbf{G}}^r = \left[\tilde{g}_1^r, \ldots, \tilde{g}_2^r\right] \in \mathbb{C}^{Q\times N}$ is a matrix containing the results of the convolution of the transmitter to RIS and RIS to receiver channel coefficients $\left(h_n^{r1} \circledast h_n^{r2}\right)$, which have been zero-padded, and $\boldsymbol{\vartheta} = \left[\beta_1 e^{j\theta_1}, \ldots, \beta_N e^{j\theta_N}\right]^T$ is a vector containing the product of the applied amplitude and phase shift coefficients for each of the RIS elements.

It should be noted that maximizing the communication rate for RIS-empowered terrestrial OFDM systems, as presented in Eq. (16.13) would require that phase shifts must be effected on the different subcarriers (when considering frequency domain implementation) or on the different channel taps (if the consideration lies in the time domain). Also, it is necessary to jointly optimize $\boldsymbol{\vartheta}$ and the transmit power allocations for all the subcarriers. As with the MIMO-based system presented in Section 16.3.4, this is a very difficult optimization problem to solve. Fortunately, an efficient SCA-based algorithm has been shown in [12] to be capable of solving this problem.

16.3.6 RIS-Empowered Systems for Multiple Terrestrial Users

To cater to multiple terrestrial users, RIS-empowered communication systems rely on standard multiple access schemes such as TDMA, FDMA, and NOMA. Maximizing the communication rate for each user would entail applying unique coefficients to each of the elements of the RIS reflecting surface. For example, in a TDMA-based system where users are served by orthogonal and nonoverlapping timeslots, the RIS elements need to be tuned as a function of time. However, for FDMA and NOMA-based systems where users are separated by unique frequencies and power levels, respectively, the RIS reflection coefficients must simultaneously, and respectively, be tuned to take care of different frequency responses and power levels. This is much more challenging to implement than the TDMA case.

Despite the implementation difficulties, there are studies in the literature that report on the performance of RIS-empowered multiple access schemes in terrestrial networks. For example, a two-user case scenario was presented in [13], where it was shown that for the same target communication rate, NOMA requires less transmit power at the base station than TDMA except when the users are close to the RIS, and their uplink and downlink communication rates are symmetric. The same study also reports that for all communication rates and configurations, FDMA requires more base station transmit power than both TDMA and NOMA. For other RIS-empowered multiplexing schemes, such as SDMA and rate-splitting multiple access (RSMA), work is ongoing to find optimal rate maximization and interference management solutions. It should be noted that the choice of which multiplexing scheme to adopt depends on how best interference can be managed for a particular type of terrestrial communication system. Also, it is worth pointing out that SDMA and other forms of precoded multiuser schemes function by managing interference at the transmitter, while NOMA systems adopt receiver-side interference management. Finally, RSMA has been reported to be more flexible in its method of interference management and this leads to superior spectral and energy efficiency, flexibility, robustness, and resiliency than the traditional methods [11].

16.4 RIS-Empowered Non-Terrestrial Communication Systems

The concepts of free space path loss and the system model developed for terrestrial networks also apply to non-terrestrial RIS-empowered communication systems. Non-terrestrial networks consist of aerial networks and satellite networks in LEO and GEO. Despite presenting favorable benefits compared to terrestrial networks, non-terrestrial networks are beset with several challenges, such as propagation losses caused by huge distances and attenuation by atmospheric gases, energy limitations due to the size, cost, and launch weight restrictions, and spectral resources limitations due to competing systems. The following subsections consider the different non-terrestrial environments before examining a multilayered integrated network.

16.4.1 Aerial Networks

Aerial systems include RIS-mounted UAVs and HAPs and these are used as platforms to passively relay signals between terrestrial transmitters and ground-based receivers located where there may be no clear and direct LOS path between the transmitter and receiver. These systems are usually deployed to extend network coverage and improve the reliability of communications. An example of this is shown in Figure 16.7, where an RIS-mounted UAV is used to passively reflect

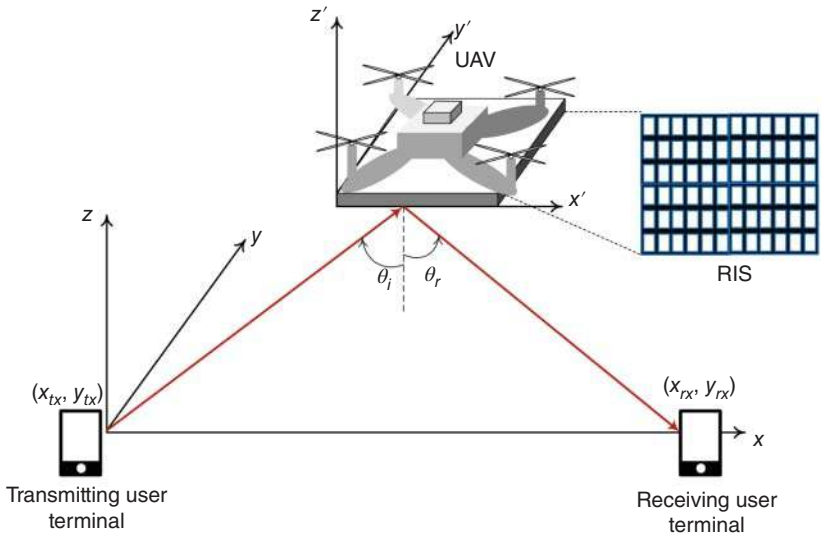

Figure 16.7 Aerial RIS-empowered ground-air-ground communication systems based on the UAV platform.

signals from a land-based transmitter to a land-based receiver located behind obstacles or over the horizon.

The horizontal coordinates of the transmitter and receiver shown in Figure 16.7 are, respectively, given by $W_{tx} = \{x_{tx}, y_{tx}\}^T$ and $W_{rx} = \{x_{rx}, y_{rx}\}^T$. It can be assumed that the trajectory of the UAV while operational is only in the horizontal plane and at a specific height which is usually between 1 and 2 km above sea level. If this is the case, the UAV must also have a finite flying duration represented by T.

Following the description of an RIS-empowered UAV cooperative communication system given in [28], T can be divided into a discrete number of time slots, K. Therefore, $T = K\delta$, where δ the slot width. The coordinate of the RIS-mounted UAV in the horizontal plane during slot n can thus be defined as $l[n] = \{x_u[n], y_u[n]\}^T$, where $n = [1, 2, \ldots, K]$. The approximate flight trajectory should therefore satisfy the following conditions

$$\|l[n+1] - l[n]\|^2 \leq D^2, \quad n = 1, 2, \ldots, K-1 \tag{16.14}$$

$$\|l[1] - l_0\|^2 \leq D^2 \tag{16.15}$$

$$\|l_F - l[K]\|^2 \leq D^2 \tag{16.16}$$

where l_0 and l_F, respectively, represent the initial and final coordinates of the UAV and D represents the maximum flying distance within one time slot and is given as $D = V_{\max}\delta$, where $V_{\max}$ is the maximum flying speed of the UAV. It is important to point out that the UAV has a uniform planar array with characteristics described in Section 16.2.1.

There are at least three optimization problems that need to be dealt with to maximize the throughput of RIS-empowered UAV communication systems. These are power allocation optimization, beamforming maximization, and trajectory optimization. Tractable expressions have been derived in [28] to tackle these problems.

While it is fairly accurate to consider a linear trajectory for UAVs, a stationary or quasistationary circular trajectory is a better representation of RIS-mounted HAPs. The height of a HAP is usually between 10 km and 50 km above sea level, and based on the larger size of HAPs compared to UAVs, more RIS elements can be mounted to achieve better control of the wireless propagation environment. A depiction of an RIS-empowered ground–air–ground communication system mounted on an HAP is shown in Figure 16.8.

The important factors to consider when designing HAP-based RIS systems include expected Doppler shift and the mobility pattern of the RIS elements. These are directly affected by the trajectory of the platform and must be jointly optimized to achieve efficient operation of the HAP-based RIS system. A good example of an attempt at jointly optimizing the Doppler and mobility properties can be found in [29].

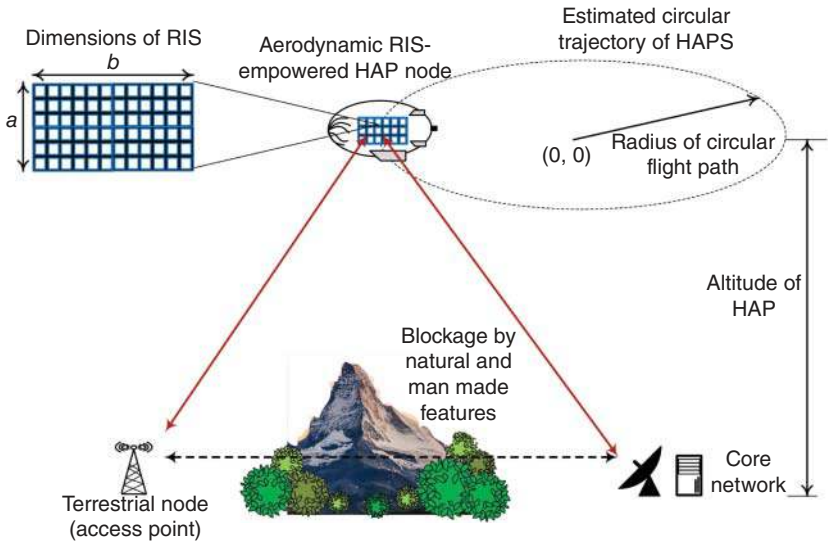

Figure 16.8 Aerial RIS-empowered ground–air–ground communication systems based on the high-altitude platform (HAP).

16.4.2 Orbiting Satellite Networks

Investigation into the use of RIS for LEO satellite systems and other non-terrestrial platforms has been carried out in [14, 15]. This is mainly because of the potential of RIS to increase system capacity, extend network coverage and optimize energy consumption while keeping system complexity low. For RIS to be adapted for use in LEO satellites and other orbiting satellite systems, there must be mechanisms in place for efficient monitoring of user mobility, tracking of satellite ephemeris and obtaining accurate CSI. The data obtained need to be acted on such that the required adaptations to RIS reflection coefficients can be effected in real time.

As indicated in terrestrial systems, NOMA can allow users to share the same frequency and spectral resources while being differentiated by power levels. Therefore, by combining RIS and NOMA in satellite communication systems, available system resources can be more efficiently utilized while also reducing the effect of interference received from other systems/users. Significant research efforts have been made on the use of NOMA for satellite communication systems. For example, Khan et al. [15] investigated a scenario where RIS and NOMA are used but with imperfect successive interference cancellation (being a defining feature of NOMA). This investigated scenario attempts to model what may be experienced in a practical system and is therefore briefly elaborated in the following paragraphs.

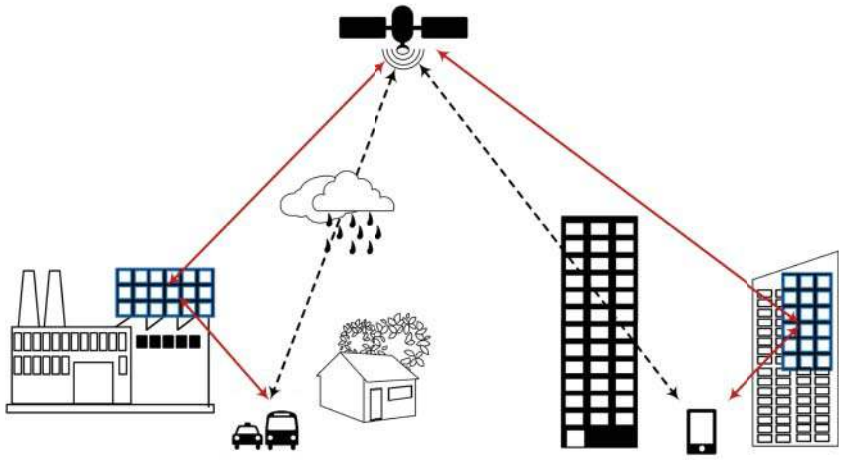

Figure 16.9 RIS-empowered satellite communication system.

Figure 16.9 shows a case where a satellite serves multiple terrestrial users using the NOMA protocol. The users can be located in mountainous regions or in urban street canyons where they experience severe shadowing and large-scale fading due to the frequent OLOS and NLOS conditions. To counteract this, RIS needs to be strategically mounted on mountainsides or building facades to assist in creating strong LOS paths from the satellite to the ground mobile users and vice versa.

Based on the model defined in Eq. (16.10), and using a two-user example, where the users are identified by subscripts i and j, and the satellite is taken as the transmitter, the signal-to-interference plus noise ratio of user i after effecting imperfect successive interference cancellation decoding is given as

$$\gamma_{tx,i} = \frac{P_{tx}\varrho_{tx,i}|h_{tx,i} + \boldsymbol{g}_{tx,m}\boldsymbol{\Phi}\boldsymbol{f}_{m,i}|^2}{\sigma^2 + \left(P_{tx,}\varrho_{tx,j}|h_{tx,i} + \boldsymbol{g}_{tx,m}\boldsymbol{\Phi}\boldsymbol{f}_{m,i}|^2\right)\epsilon} \tag{16.17}$$

where P_{tx} represents the transmit power of the satellite,
$\varrho_{tx,i}$ is the power allocation coefficient for ground user i,
$h_{tx,i}$ is the direct channel gain from the satellite to user i,
$\boldsymbol{g}_{tx,m}$ denotes the channel gain from the satellite to the RIS,
$\boldsymbol{\Phi}$ is a diagonal matrix comprising the complex reconfigurable responses of the RIS elements,
$\boldsymbol{f}_{m,i}$ represents the channel gains from the RIS to the user i,
σ^2 represents the variance of the additive white Gaussian noise, and

ϵ is a parameter inserted to account for the imperfect successive interference cancellation process and is a measure of the difference between the actual and estimated signal of the user.

Equation (16.17) assumes that the direct channel gain of user i is greater than or at best, equal to that of user j ($h_{tx,i} \geq h_{tx,j}$), and without loss of generality, ground user j cannot apply successive interference cancellation to decode its signal when interference from user i is present. Therefore, its signal-to-interference plus noise ratio is given as,

$$\gamma_{tx,j} = \frac{P_{tx}\varrho_{tx,j}|h_{tx,j} + \boldsymbol{g}_{tx,m}\boldsymbol{\Phi}\boldsymbol{f}_{m,j}|^2}{\sigma^2 + \left(P_{tx,}\varrho_{tx,i}|h_{tx,j} + \boldsymbol{g}_{tx,m}\boldsymbol{\Phi}\boldsymbol{f}_{m,j}|^2\right)} \tag{16.18}$$

where the second term in the denominator of Eq. (16.18) is the interference attributed to user i. Therefore, the data rate of user j can be expressed as,

$$R_{tx,j} = \log_2(1 + \gamma_{tx,j}) \tag{16.19}$$

According to [15], to maximize the energy efficiency of the RIS-empowered satellite NOMA system, the following optimization problem must be solved subject to signal-to-interference plus noise constraints, allowable phase shift constraints, available satellite transmit power constraints, and power allocation constraints.

$$\max_{\varrho,\boldsymbol{\Phi}} \frac{\log_2(1 + \gamma_{tx,i}) + \log_2(1 + \gamma_{tx,j})}{P_{tx}(\varrho_{tx,i+tx,j})\nu + p_c} \tag{16.20}$$

where ν has been inserted to account for power amplifier inefficiency and p_c represents the power consumption of the circuit. A similar optimization method but with specific reference to geostationary satellites has been presented in [30].

16.4.3 Multilayered Integrated Networks

Integrated non-terrestrial networks are made up of multiple layers comprising LEO and GEO satellites, and platforms such as UAVs that operate in the low atmosphere and HAPS that operate in the stratosphere. The architecture of such networks makes provision for single-connected operation, fully connected mode, and group-connected operation. In the case of a single connection, the elements of the RIS are not interconnected, and the phase-shift response of the surface is represented by a diagonal matrix. For the fully connected case, the phase shift responses can only be described by a full matrix, while in group connection, the phase shifts are presented in blocks within a matrix and the block in turn must be diagonal.

An integrated multilayered RIS-empowered non-terrestrial network is shown in Figure 16.10 where it can be observed that there are numerous potential applications at different altitudes. RIS is usually included to improve the link

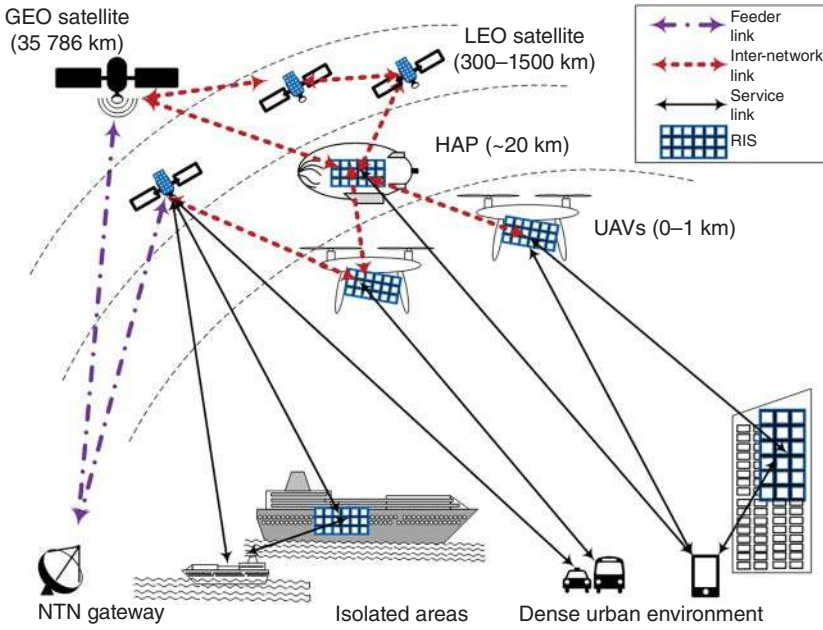

Figure 16.10 Multilayered integrated RIS-empowered NTNs.

budget, enhance signal control and focusing, mitigate the harmful effects of interference, reuse spectral resources, increase energy efficiency and realize green communications, and introduce resiliency and redundancy.

In Figure 16.10, the HAP can act as a relay node for the satellite to the ground terminal or ground RIS link. It can employ the reflective, transmissive, or hybrid type of RIS. A detailed example of where the satellite to HAP link employed optical and radio frequency signals can be found in [31]. Based on the type of RIS employed, the signal received by the HAP can either be passively reflected or amplified and forwarded to the ground-based terminals or RIS. To mitigate the effect of cloud coverage on the HAP to ground terminal link, a UAV relay can be deployed to a position of minimal or negligible cloud coverage to act as a relay and thus maintain a good quality link. This increases the diversity of the communication systems, as shown in Figure 16.11. CSI needs to be feedback to the RIS controllers on board the relay/reflecting and transmitting nodes.

Due to the limited power onboard the UAV in Figure 16.11, its RIS would most likely be a reflector type, and the platform can be deployed based on cloud forecast maps and real-atmospheric condition data. Also, its flight trajectory can be optimized according to Eqs. (16.14)–(16.16). Considering the architectures shown in Figures 16.10 and 16.11, a link-switching scheme and multi-rate communication

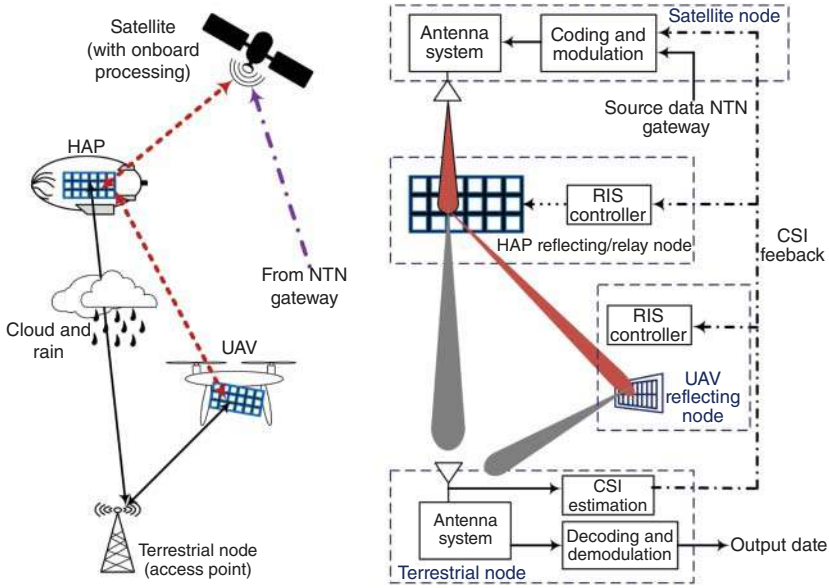

Figure 16.11 Integrated satellite-aerial-terrestrial RIS-empowered communication system pictorial and block diagram.

Table 16.2 Signal routing options for multilayered integrated RIS-empowered NTNs.

Priority order	Link	Description
1	Gateway-satellite-land/ maritime UT	Primary link
2	Gateway-satellite-HAP-land/ maritime UT	Used when cloud cover presents an issue
3	Gateway-satellite-HAP-UAV-land/ maritime UT	Used when the first two strategies are ineffective
4	Gateway-satellite-HAP-UAV-terrestrial RIS-UT	Used when the first three strategies are ineffective

design based on Table 16.2 can be adopted to initiate and maintain ubiquitous communications between a gateway and a UT.

Note that closing a link from a satellite to a ground-based UT is usually difficult because of the nondirectional nature of UT antennas, especially those operating in high-frequency ranges. Therefore, introducing an HAP to focus and direct the signals from the satellite to UT serves a very important function. However, there

are open challenges to the models shown in Figures 16.10 and 16.11, and these include increased hardware complexity, highly dynamic channel conditions, and security/privacy requirements. Fortunately, AI and ML offer exciting opportunities to tackle the challenges in the immediate term and the very near future.

16.5 Lessons Learned and Future Research Direction

The information presented in the chapter reveals that the use of metasurfaces has extended beyond their traditional applications in invisibility cloaking and imaging systems to the arena of wireless communications. However, there are still open problems that need to be solved before developed RIS designs can be transformed into deployable systems for use in terrestrial and non-terrestrial wireless communication systems. The RIS-empowered communication systems of the future must, therefore, meet stringent requirements in terms of spectrum and energy efficiency, capacity, and reliability in all possible use case scenarios. Achieving this requires an in-depth understanding of channel modeling and fundamental knowledge of RIS control mechanisms and the effects of all components of the RIS-empowered systems. Some of the open challenges are elaborated below.

The passive RIS element reflectors must be designed to achieve highly responsive beam steering and interference cancellation in the vicinity of UTs. Therefore, to consistently provide an excellent level of service to all UTs within the passive RIS-empowered network, the RIS reflection coefficients must be jointly designed based on UT and access point transmissions such that end-to-end communication is optimized. Also, since passive RIS-empowered systems do not have radio frequency chains, the acquisition of CSI between the RIS and the receiving access point or UT is extremely difficult to practically achieve. A factor that aggravates this difficulty is the large number of reflecting RIS elements and the associated channel coefficients that need to be realized independently for each UT.

In addition to the problems detailed above, the optimal deployment of RIS elements and structures within a wireless communication network will be significantly different from that of conventional relay systems or AF systems as presently deployed. One of the reasons for this difference is the nature of RIS architectures, which are usually fully passive, semi-passive, or active. Another reason is their intended mode of operation, which may be reflective, transmissive, or hybrid. These different deployment architectures and modes of operation need to be carefully investigated. Finally, on the direction to take to make RIS-empowered systems a reality in the near future, there is a need for systematic studies on the fundamental limits of the algorithms used in CSI determination and design of reflection coefficients. Also, the cost and energy performance and the necessary

engineering trade-offs that need to be made especially for semi-passive RIS operation is an area that needs further study.

16.6 Conclusion

This chapter has presented how RIS is used in terrestrial and non-terrestrial wireless communication systems. Specifically, the building blocks of RIS, metamaterials and metasurfaces were presented, and to understand how these are operated, their control mechanisms have been thoroughly explained. The chapter also presented the free space path loss model before detailing a complete geometry-based system model that can be applied to describe the operation of RIS-empowered communication systems. Using the presented models, the architecture for implementing MIMO-enhanced and OFDM-based RIS-empowered communication systems in the terrestrial environment was presented. For the non-terrestrial environment, RIS-empowered aerial networks comprising UAVs and HAPs were detailed and architectures involving satellites were also presented. Finally, the chapter presented a multilayered integrated RIS-empowered system with both terrestrial and non-terrestrial components functioning to provide ubiquitous wireless communication services.

References

1 Larsson, E.G., Edfors, O., Tufvesson, F., and Marzetta, T.L. (2014). Massive MIMO for next generation wireless systems. *IEEE Communications Magazine* 52 (2): 186–195.
2 Dai, L., Wang, B., Ding, Z. et al. (2018). A survey of non-orthogonal multiple access for 5G. *IEEE Communications Surveys & Tutorials* 20 (3): 2294–2323.
3 Mahmood, M.R., Matin, M.A., Sarigiannidis, P., and Goudos, S.K. (2022). A comprehensive review on artificial intelligence/machine learning algorithms for empowering future IoT toward 6G era. *IEEE Access* 10: 87535–87562.
4 You, L., Xiong, J., Kwan-NG, D.W. et al. (2021). Energy efficiency and spectral efficiency tradeoff in RIS-aided multiuser uplink transmission. *IEEE Transactions on Signal Processing* 69: 1407–1421.
5 Liu, Y., Ma, Y., Li, M. et al. (2022). Spectral efficiency maximization for double-faced active reconfigurable intelligent surface. *IEEE Transactions on Signal Processing* 70: 5397–5412.
6 International Telecommunications Union, Report ITU-R M.2516-0, November 2022. https://www.itu.int/dms_pub/itu-r/opb/rep/R-REP-M.2516-2022-PDF-E.pdf (accessed 2 March 2024).

7 Chen, H., Taylor, A.J., and Yu, N. (2016). A review of metasurfaces: physics and applications. *Reports on Progress in Physics* 79: 1–40.

8 Shafique, K. and Alhassoun, M. (2024). Going beyond a simple RIS: trends and techniques paving the path of future RIS. *IEEE Open Journal of Antennas and Propagation* 5 (2): 256–276.

9 Rana, B., Cho, S.-S., and Hong, I.-P. (2023). Review paper on hardware of reconfigurable intelligent surfaces. *IEEE Access* 11: 29614–29635.

10 Li, A., Singh, S., and Sievenpiper, D. (2018). Metasurfaces and their applications. *Nanophotonics* 7: 989–1011.

11 Clerckx, B., Mao, Y., Jorswieck, E.A. et al. (2023). A primer on rate-splitting multiple access: tutorial, myths, and frequently asked questions. *IEEE Journal on Selected Areas in Communications* 41 (5): 1265–1308.

12 Yang, Y., Zheng, B., Zhang, S., and Zhang, R. (2020). Intelligent reflecting surface meets OFDM: protocol design and rate maximization. *IEEE Transactions on Communications* 68 (7): 4522–4535.

13 Zheng, B., Wu, Q., and Zhang, R. (2020). Intelligent reflecting surface-assisted multiple access with user pairing: NOMA or OMA? *IEEE Communication Letters* 24 (4): 753–757.

14 Lian, X., Yue, X., Li, X. et al. (2022). Reconfigurable intelligent surface assisted non-terrestrial NOMA networks. *Wireless Communications and Mobile Computing* 2022: 1–13.

15 Khan, W.U., Lagunas, E., Mahmood, A. et al. (2023). RIS-assisted energy-efficient LEO satellite communications with NOMA. *IEEE Transactions on Green Communications and Networking* 8: 780–790.

16 Khan, W.U., Mahmood, A., Sheemar, C. et al. (2024). Reconfigurable intelligent surfaces for 6G non-terrestrial networks: assisting connectivity from the sky. *IEEE Internet of Things Magazine* 7 (1): 34–39.

17 Yu, N., Genevet, P., Kats, M.A. et al. (2011). Light propagation with phase discontinuities: generalized laws of reflection and refraction. *Science* 334 (6054): 333–337.

18 Yu, N. and Capasso, F. (2014). Flat optics with designer metasurfaces. *Nature Materials* 13 (2): 139–150.

19 Ozdogan, O., Bjornson, E., and Larsson, E.G. (2020). Intelligent reflecting surfaces: physics, propagation, and pathloss modeling. *IEEE Wireless Communications Letters* 9 (5): 581–585.

20 Basar, E. and Yildirim, I. (2021). Reconfigurable intelligent surfaces for future wireless networks: a channel modeling perspective. *IEEE Wireless Communications* 28 (3): 108–114.

21 Chian, D.-M., Wen, C.-K., Wu, C.-H. et al. (2024). A novel channel model for reconfigurable intelligent surfaces with consideration of polarization and

switch impairments. *IEEE Transactions on Antennas and Propagation* 72 (4): 3680–3695.

22 Wu, Q., Zhang, S., Zheng, B. et al. (2021). Intelligent reflecting surface-aided wireless communications: a tutorial. *IEEE Transactions on Communications* 69 (5): 3313–3351.

23 Wang, X., Xia, D., Li, G. et al. (2023). Design and waveguide measurement of 2-bit reconfigurable amplification metasurface cell. *IEEE Antennas and Wireless Propagation Letters* 22 (9): 2090–2094.

24 Renzo, M.D., Galdi, V., and Castaldi, G. (2023). Modeling the mutual coupling of reconfigurable metasurfaces. *17th European Conference on Antennas and Propagation (EuCAP)*, Florence, Italy, 26–31 March 2023.

25 Luo, C., Hu, J., Xiang, L., and Yang, K. (2024). Reconfigurable intelligent sensing surface aided wireless powered communication networks: a sensing-then-reflecting approach. *IEEE Transactions on Communications* 72 (3): 1835–1848.

26 Bezdek, J.C. and Hathaway, R.J. (2002). Some notes on alternating optimization. *Advances in Soft Computing* 2275 (4): 288–300.

27 Razaviyayn, M. (2014). Successive convex approximation: analysis and applications. PhD thesis. University of Minnesota.

28 Liu, X., Yu, Y., Li, F., and Durrani, T.S. (2022). Throughput maximization for RIS-UAV relaying communications. *IEEE Transactions on Intelligent Transportation Systems* 23 (10): 19569–19574.

29 Azizi, A. and Farhang, A. (2023). RIS meets aerodynamic HAPS: a multi-objective optimization approach. *IEEE Wireless Communications Letters* 12 (11): 1851–1855.

30 Khan, W.U., Lagunas, E., Mahmood, A. et al. (2022). When RIS meets GEO satellite communications: a new sustainable optimization framework in 6G. *IEEE 95th Vehicular Technology Conference: (VTC2022-Spring)*, Helsinki, Finland, 12–22 June 2022.

31 Nguyen, T.V. and Le, H.D.P.A. (2023). On the design of RIS-UAV relay-assisted hybrid FSO/RF satellite-aerial-ground integrated network. *IEEE Transactions on Aerospace and Electronic Systems* 59 (2): 757–771.

17

Energy Efficiency and Optimization of RIS-Based Wireless Communication Systems

Kien Ho[1], Minh Dang Nguyen[2], Minh Tuan Pham[3], Hung Gia Truong[4], and Arjun Chakravarthi Pogaku[5]

[1] *Chu Van An High School, Hanoi City, Vietnam*
[2] *Hanoi Amsterdam for the Gifted, Hanoi City, Vietnam*
[3] *Le Hong Phong High School for the Gifted, Ho Chi Minh City, Vietnam*
[4] *HUS High School for Gifted Students, Hanoi City, Vietnam*
[5] *Department of Electronics and Communications Engineering, Madanapalle Institute of Technology & Science, Madanapalle, India*

17.1 Introduction

Recent reports indicate a significant increase in the usage of wireless devices compared to the past decade [1, 2]. With the introduction of 5G wireless networks to user-ready mobile devices, an unimaginable surge in data traffic has been observed. However, the deployment of fifth generation (5G) is currently limited to a few countries due to its high cost. Despite this limitation, 5G offers immense advantages over its predecessors, including ultra low latency, high data transmission speeds, and enhanced mobile broadband capabilities [3]. Nevertheless, 5G is not the final stage in the evolution of wireless technology. Just as humans continue to evolve over time, technology progresses as well. The next step in this evolutionary line is the development of sixth generation (6G) [3], which is already underway. Although it will take some time to witness the wonders that 6G technologies can achieve, researchers and experts are working diligently to explore its potential. The improved capability of 6G network in terms of bandwidth and latency is expected to empower a wide range of new technologies, such as holographic communication, teleoperated driving, tactile internet, and extended reality applications [4]. It is worth noting that the deployment of wireless technologies like 5G and the future 6G is a complex process that involves various stakeholders, including governments, telecommunication companies, and regulatory bodies. The cost and infrastructure requirements associated

Reconfigurable Intelligent Surfaces for 6G and Beyond Wireless Networks, First Edition.
Edited by Agbotiname Lucky Imoize, Vinoth Babu Kumaravelu, and Dinh-Thuan Do.

with deploying these networks can pose challenges, leading to variations in the availability of these technologies across different countries.

Irrespective of the evolution of wireless networks, several factors are crucial for efficient data transmission and seamless connectivity. One such factor is the efficient usage of the spectrum [5], which becomes increasingly important due to the growing requirements of today's generation. Over time, various techniques have been developed to address these challenges [6], including time division multiple access, frequency division multiple access, code-division multiple access, orthogonal frequency division multiplexing, orthogonal multiple access (OMA), non-orthogonal multiple access (NOMA), and more. Each of these technologies has proven effective in meeting the requirements of its time. However, the continuous development of these techniques plays a pivotal role in the field of telecommunications and wireless communications. Nonetheless, there is an ongoing need for advancements that can further enhance signal transmission through these existing techniques. One such emerging technology is reconfigurable intelligent surfaces (RISs) [7]. RIS is a passive device that utilizes meta-surface reflectors to manipulate radio wave signals based on the position of the receiver. It acts like a mirror surface capable of reflecting and refracting incident waves.

RIS has the potential to revolutionize wireless communications by intelligently shaping the propagation environment [8]. By controlling the phase and amplitude of the reflected signals, RIS can create constructive interference, overcome path loss, and enhance the overall signal strength and quality. This technology offers benefits such as increased coverage, extended range, improved energy efficiency [9], and enhanced spectral efficiency [10]. By deploying RIS in wireless networks, it is possible to mitigate challenges like signal fading, interference, and coverage limitations. RIS can be utilized in various scenarios, including indoor and outdoor environments, to optimize wireless connectivity and enhance communication performance. The full potential and impact of RIS in wireless communications are yet to be fully realized, but its promising capabilities have attracted significant attention from the research community and industry stakeholders.

The authors in [11] studied energy-efficient scheme of STAR–RIS-aided Multiple-Input and Multiple-Output (MIMO)–NOMA networks. In this chapter, the authors focused on the challenges in achieving signal coverage for the sixth generation (6G). Besides that, the chapter also examines about two types of structures: RIS and simultaneous transmitting and reflecting reconfigurable intelligent surface (STAR–RIS). The author investigates NOMA, which is a promising physical layer technique in B5G and 6G to improve spectral efficiency, support massive connectivity, and reduce transmission latency. Moreover, the author wants to focuss on the STAR–RIS-enabled MIMO–NOMA system and its potential for energy efficiency improvement. The authors in [12] explored

power minimization for double cooperative-RIS-assisted uplink NOMA system. In this chapter, the authors focused on the significant role of the RIS. RIS technology plays a crucial role in 6G mobile communication by manipulating phase shifts of reflection elements. RIS has been shown to improve performance in various aspects, such as reducing power consumption, increasing achievable, improving energy efficiency, and enhancing secure communication. The main contributions of this letter are the construction of an uplink (UP) multi user and multi-RIS-aided NOMA system with inter-RIS reflections, which enhances desired signals by jointly designing the phase shifts of multiple RISs. The power efficiency of the system is also enhanced by alternately optimizing the transmit power and the phase shifts. In similar work, the model of sum-rate maximization for STAR–RIS-aided NOMA system with two-way transmission is analyzed in [13]. In particular, the authors developed the maximization for STAR–RIS. The rapid growth of mobile devices and communication data has led to a higher data rate requirement for mobile networks. Therefore, a low-complexity algorithm was used to optimize power and reflection coefficients to maximize sum rate. However, previous transmissions only had one-way links, while the upgraded STAR-RIS operates on both links (downlink and uplink). The study investigates an STAR–RIS-assisted NOMA scheme with two-way communication for the first time. In similar topic, joint beamforming optimization is presented to be applied to RIS-aided wireless networks [14]. In particular, the authors focused on the revolution of wireless networks. The wireless networks approach using RIS to control and improve system performance. RIS can recreates the wireless structures environment by using low-cost passive meta-surface reflection units (RUs) that can adjust the network signal, resulting in cleaner and more reliable received signal. Moreover, the introduction of RIS in 6G systems marks a significant departure from previous generations of wireless communication systems, which focused on improving data rates, latency, and spectral efficiency. The introduction of RIS in 6G systems marks a significant departure from previous generations of wireless communication systems, which focused on improving data rates, latency, and spectral efficiency. These technologies are working together to create a new era of ultra reliable, low-latency communication, capable of supporting a wide range of new and innovative applications. Finally, Table 17.1 summarizes their contributions.

17.1.1 Our Contribution

RIS has been gaining significant momentum in the field of wireless communications. However, it is also important we analyze the energy consumption of the network for the optimized performance delivery [6–9]. In this regard, this chapter mainly focuses on optimizing RIS for various parameters and simulating

Table 17.1 Papers surveyed.

References	System model	Way of communication	Advantages	Disadvantages
[11]	Simultaneously transmitting and reflecting (STAR)–RIS-aided MIMO–NOMA networks	Indoor communication system	• Address the issue of high energy consumption in 6G • Serve the users on both sides of the surface, at its front and back, by simultaneously transmitting and reflecting the incident signal • Freedom in the spatial, frequency, and time domains, resource	• Can only handle discrete actions • Continuous power allocation
[12]	Double cooperative RIS-assisted uplink (UL) NOMA system	Only UL system	• As reducing power consumption • Increasing achievable rate • Improving energy efficiency • Enhancing the ability of secure communication	• Makes the optimization problem more complicated • The coupling effect among different RIS's phase shifts makes the optimization problem more complicated
[13]	STAR–RIS-aided NOMA system with two-way communication	Both UL and downlink (DL) system	• Improve the sum rate compared with several existing method • The STAR–RIS-aided NOMA always outperforms the STAR–RIS-aided NOMA of secure communication	• Transformed to attractable linear program • The UL and the DL transmissions do not interfere with each other
[14]	A new RIS architecture with a single power amplifier	Terahertz and millimeter wave communications systems	• Reducing the bulkiness of the multiple antenna systems as well as the energy consumption • Low cost, simple implementation	• Having the double path loss problem

the performance results in terms of achievable rate. However, as a proven fact, the number of RIS elements does affect the performance of the network, we have compared the performance for number of RIS elements varied. The main contributions are as follows:

- We have deeply studied the architecture of RIS and its transmission channels. An optimization problem was formulated to minimize the UL transmit power as a function of phase shift.
- We reviewed a two RIS system model with Rayleigh fading and formulated a closed form expression of the achievable rate by assuming large number of reflecting elements at both RISs.
- The mathematical analysis can be conducted to demonstrate that constructive combination of signals leads to improved achievable rate, leading to overall enhanced system performance. It also demonstrates the importance in increasing the number of RIS elements.

17.1.2 Chapter Organization

The rest of the chapter is organized as follows. Section 17.2 discusses about the literature on optimization for RIS-based transmission. Section 17.3 discusses about cooperative RIS and defining optimization problem and deriving the formula for optimization. Meanwhile, Section 17.5 discusses about RIS partitioning and developing a two RIS system model. Section 17.6 discusses about simulation results for the RIS model developed in Section 17.5 by deriving the achievable rate formula. This section completely discusses about overall system performance by varying various parameters.

17.2 Optimization for RIS-Based Transmission

In [15], the authors focus on the joint optimization of RIS in wireless communication systems. The chapter examines the optimization problem from both physical and electromagnetic perspectives, considering the physical deployment of RIS elements and their electromagnetic properties. The authors investigate the joint optimization of RIS phase shifts and transmit beamforming to maximize the system performance, such as signal coverage, capacity, or energy efficiency. They also discuss practical constraints, such as hardware limitations and channel estimation errors, and propose solutions to address them. In [16], the authors focus on the optimization of RIS in the context of integrated localization and communication systems. The chapter explores the potential benefits of leveraging RIS for simultaneous localization and communication tasks and addresses the

optimization challenges associated with jointly optimizing the RIS configuration and the localization and communication performance metrics. The authors discuss various optimization frameworks and algorithms, considering factors such as channel estimation, RIS phase shifts, transmit power, and localization accuracy.

In [17], the authors focus on the analysis and optimization of RIS in multi-pair communication scenarios using statistical channel state information (CSI). In the multi-pair system discussed, two devices are communicating with each other with a help of an RIS array, as shown in Figure 17.1. The chapter investigates the use of statistical CSI for RIS-aided multi-pair communication systems where multiple pairs of transmitters and receivers are involved. The authors analyze the achievable rate and outage probability of the communication links and propose optimization algorithms to maximize the overall system performance. They consider practical constraints, such as limited RIS phase shifts and statistical CSI estimation errors, and provide solutions to enhance the performance of RIS-aided multi-pair communication systems. In [18], the authors shift their focus to the analysis and optimization of RIS in multiple-input and multiple-output (MIMO) systems, incorporating statistical CSI. The objective is to leverage RIS to improve the performance of massive MIMO systems by manipulating the wireless propagation environment. The chapter analyzes the achievable rate and outage probability of the RIS-aided massive MIMO systems and introduces optimization algorithms to maximize the overall system performance. The authors consider practical constraints, such as limited RIS phase shifts and statistical CSI estimation errors. In [19], the authors extend the analysis and optimization of RIS in massive MIMO systems by considering the use of zero-forcing (ZF) detectors and accounting for imperfect CSI. The chapter focuses on RIS-aided massive MIMO

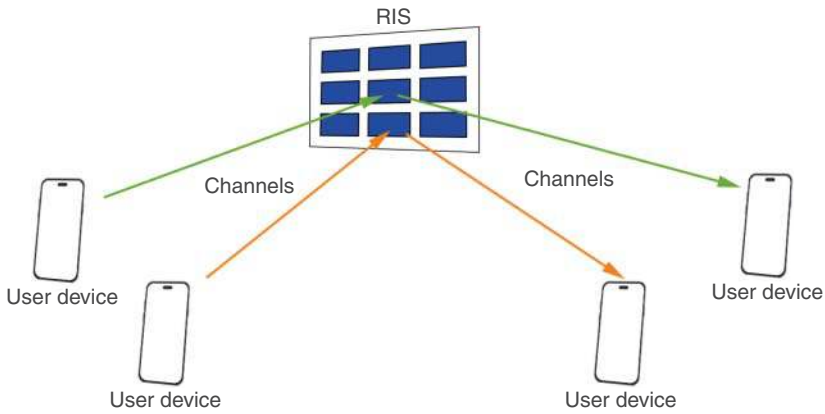

Figure 17.1 RIS-assisted multi-pair communication system diagram.

systems where imperfect CSI is present and investigates the achievable rate and outage probability. The authors propose optimization algorithms to maximize system performance, taking into account the practical limitations of limited RIS phase shifts and imperfect CSI estimation. The findings provide insights into the impact of imperfect CSI and highlight optimization techniques for RIS-aided massive MIMO systems with ZF detectors, offering potential enhancements in system capacity and reliability.

In [20], the authors explore the benefits of RIS in wireless communications through rotation and location optimization. The chapter focuses on leveraging RIS to achieve extra degrees of freedom and enhance system performance. The authors investigate the optimal rotation angles and locations of RIS elements to maximize the achievable rate in RIS-aided wireless communication systems. They propose optimization algorithms that jointly optimize the RIS rotation and location, taking into account practical constraints and CSI. In [21], the authors focus on maximizing the coverage area and signal strength in RIS-assisted wireless communication systems. The authors propose optimization algorithms that jointly optimize the RIS orientation and location, taking into account practical constraints and channel characteristics. By strategically adjusting the orientation and location of the RIS, the authors demonstrate that significant coverage extension can be achieved, thereby improving the overall system performance. In [22], the authors address the joint optimization of location and channel error for beamforming design in multi-RIS-assisted MIMO systems. The chapter focuses on optimizing the beamforming vectors at the transmitters and RIS elements to maximize the achievable rate in the presence of channel estimation errors. The authors propose an optimization framework that jointly optimizes the locations of RIS elements and compensates for channel estimation errors. By considering the impact of both location and channel estimation errors, the proposed approach aims to improve the overall system performance in multi-RIS-assisted MIMO systems. In [23], the authors investigate secure NOMA-based RIS–unmanned aerial vehicle (UAV) networks. The paper focuses on the design of passive beamforming and location optimization strategies to enhance the security of RIS–UAV networks. The authors propose a joint optimization framework that considers the secrecy rate and power allocation in the presence of eavesdroppers. The objective is to maximize the achievable secrecy rate while ensuring power allocation fairness among users. The proposed approach incorporates passive beamforming at the RIS and optimizes the location of the UAV to enhance the overall network security. These studies emphasize the importance of optimizing RIS elements, including rotation, location, and orientation, to improve wireless communication performance, coverage extension, beamforming design, and security in various scenarios.

In [24], the authors focus on energy optimization in a dual-RIS UAV-aided mobile edge computing (MEC)-enabled Internet of Vehicles (IoV) scenario. The chapter aims to optimize the energy consumption of the system by jointly optimizing the transmit power allocation, the UAV trajectory, and the RIS reflection coefficients. The authors propose an optimization framework that considers the trade-off between energy consumption and system performance, taking into account the latency requirements of IoV applications. The findings highlight the potential of dual-RIS UAV-aided MEC-enabled IoV systems in achieving energy-efficient and reliable communication, facilitating the integration of UAVs, RIS, and MEC technologies for future IoV deployments.

In [25], the authors focus on the integration of wireless energy transfer techniques with RIS and cell-free massive MIMO systems to enhance energy efficiency and prolong the operation of wireless networks. The authors discuss the potential benefits, including improved coverage, increased energy harvesting efficiency, and reduced energy consumption, along with the challenges related to energy transfer distance, channel estimation, and interference management. Meanwhile in [26], the authors focus on optimizing the energy efficiency of RIS-assisted wireless-powered communication networks while ensuring a minimum outage probability constraint. The authors propose an optimization framework that jointly optimizes the transmit power allocation, time allocation, and phase shifts at the RIS to maximize the energy efficiency under the outage constraint. In [27], the authors address the challenge of maximizing energy efficiency while ensuring reliable and high-quality communication links between the UAV and multiple ground users. The authors propose an optimization framework that jointly optimizes the UAV trajectory and RIS configuration to minimize the overall energy consumption while satisfying the users' quality-of-service requirements. By considering the dynamic UAV trajectory and the deployment of RIS, the proposed approach aims to enhance the energy efficiency and communication performance of the multi user air-to-ground communication system.

The research articles mentioned above explore various aspects of RIS in wireless communication systems. The chapter investigates joint optimization of RIS elements, including rotation, location, and orientation, to enhance system performance, coverage extension, beamforming design, and security. Each author or article considers practical constraints, such as channel estimation errors and hardware limitations, and proposes optimization algorithms to maximize achievable rates, coverage area, and energy efficiency. These studies emphasize the potential benefits of RIS in different scenarios, including multi-pair communication, massive MIMO, integrated localization and communication systems, wireless power transfer, and UAV-assisted networks, providing valuable insights for optimizing RIS deployment in wireless communication applications.

17.3 Cooperative RIS

17.3.1 System Architecture

We consider a system with two RIS arrays Figure 17.2. Signal from the base station (BS) is reflected by either RIS 1 or RIS 2. While RIS 1 can forward the signal to both user cluster 1 and RIS 2, RIS 2 can only forward the signal to user cluster 2. N_ρ denotes the number of RIS elements; d_{BS,R_ρ} corresponds to the distance between the BS and RIS ρ, $d_{BS,R_1} < d_{BS,R_2}$. Assuming that there is no direct path between each user cluster and the BS, the full list of parameters for the BS, the two RIS arrays and the corresponding user clusters can be summarized in Table 17.2.

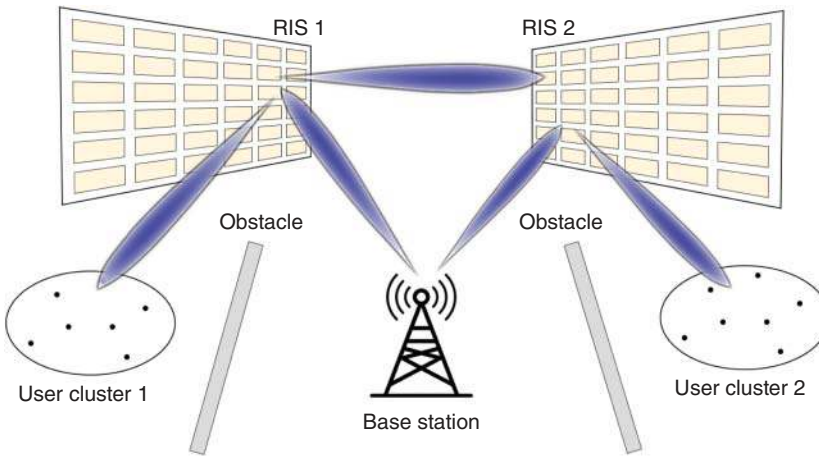

Figure 17.2 The cooperative RIS system discussed.

Table 17.2 Parameters in channel equation of cooperative RIS.

N_ρ	The number of reconfigurable elements in RIS ρ, $N_1 + N_2 = N$
d_{BS,R_ρ}	The distance between the BS and RIS ρ, $d_{BS,R_1} < d_{BS,R_2}$
r_ρ	The radius of the user zone served by RIS ρ
d_{C_ρ}	The distance between center of the user zone served by RIS ρ
$u[\rho, i]$	The channel between the ith user and RIS ρ
$T_{\rho,i}$	The channels between the BS and RIS ρ
D	The channel between RIS 1 and RIS 2
θ_ρ	The phase shift matrix for RIS ρ

Since a user in cluster 1 can receive signal from the BS and reflected by RIS 1, while a user in cluster 2 can receive signal from the BS or RIS 1 and reflected by RIS 2, the equivalent channels from the i_{th} user in cluster ρ can be represented as [28]:

$$h_{1,i} = T_1\theta_1 u_{1,i} \tag{17.1}$$

$$h_{2,j} = T_2\theta_2 u_{2,j} + T_1\theta_1 D\theta_2 u_{2,j}. \tag{17.2}$$

17.3.2 Optimization Problem

The goal of the problem is to minimize UL transmit power. It can be inferred that the channel between users in cluster 1 to the BS is more efficient than that of users in cluster 2. Therefore, the BS will first detect if a user's best channel is in cluster 1, and if true, remove the service from the composite signal by leveraging self-interference cancellation (SIC) operations. With this, the signal-to-interference-plus-noise ratio (SINR) of $u[1,k]$ and $u[2,k]$ are:

$$\gamma_{1,k} = \frac{|h_{1,k}|^2 P_{1,k}}{\sum_{i=k+1}^{K_1} |h_{1,i}|^2 P_{1,i} + \sum_{i=1}^{K_2} |h_{2,i}|^2 P_{1,i} + \sigma^2} \tag{17.3}$$

$$\gamma_{2,k} = \frac{|h_{2,k}|^2 P_{2,k}}{\sum_{i=k+1}^{K_2} |h_{2,i}|^2 P_{2,i} + \sigma^2} \tag{17.4}$$

The optimization problem is formulated as [28]:

$$\begin{aligned} &\mathbf{P_1}: \min: \sum_{\rho=1}^{2} \sum_{k=1}^{K_\rho} P_{\rho,k} \\ &s.t.\ \log_2(1+\gamma_{\rho,k}) \geq C_{\rho,k}^{(th)}, \rho \in \{1,2\} \\ &\phi_{\rho,m} \in \varpi, \forall m = 1, \ldots, N_\rho. \end{aligned} \tag{17.5}$$

Due to the nonconvex and highly coupled nature of problem P_1, we use an alternating optimizations (AOs) to solve the optimization problem. The optimal power control in the problem is going to be expressed as a function of phase shift. With that, we can now solve the problem of optimization regarding only phase shifts. Using the AO method, we would optimize the value of phase shift in ϕ_2 when ϕ_1 is given, and conversely, optimize the value of phase shift ϕ_1 when ϕ_2 is given.

17.3.2.1 Optimal Power as a Function of Phase Shift

For the contradiction that when the problem P_1 gets an optimal solution, equality is achieved for Eq. (17.5). Therefore, we get:

$$\log_2(1+\gamma_{\rho,k}) = C_{\rho,k}^{(th)} \tag{17.6}$$

Define $\tilde{C}_{\rho,k}^{(th)} = 2^{C_{\rho,k}^{(th)}} - 1$. By substituting Eq. (17.6) into (17.4), the transmission power of $u[K_2]$ can be expressed as:

$$P_{2,K_2} = \tilde{C}_{2,K_2}^{(th)} \delta^2 / |h_2, K_2|^2 \tag{17.7}$$

The transmit power of $u[2, K_2 - 1]$ can be derived as:

$$P_{2,K_2} = \tilde{C}_{2,K_{2-1}}^{(th)} \left(\tilde{C}_{\rho,k}^{(th)} + 1 \right) \delta^2 / |h_2, K_{2-1}|^2 \tag{17.8}$$

Accordingly, we can express the transmit power of $u[2, k]$ as:

$$P_{2,k} = \delta^2 \prod_{i=k}^{K_2} \Gamma_{2,i}^{th} / |h_2, K_2|^2 \tag{17.9}$$

where $\Gamma_{2,i}^{th} = \tilde{C}_{2,K_2}^{(th)} + 1$ for $i > k$, and $\Gamma_{2,i}^{th} = \tilde{C}_{2,K_{2-1}}^{(th)} + 1$ for $i = k$.

Similarly, the equation can be adapted for $u[1, k]$ as [28]:

$$\begin{aligned} P_{1,k} &= \left(\sum_{i=1}^{K_2} \delta^2 \prod_{j=i}^{K_2} \Gamma_{2,j}^{th} + \delta^2 \right) \frac{\prod_{i=k}^{K_1} \Gamma_{i,i}^{th}}{|h_1, k|^2} \\ &= \Omega \frac{\delta^2 \prod_{i=k}^{K_1} \Gamma_{1,i}^{th}}{|h_1, k|^2} \end{aligned} \tag{17.10}$$

where $\Omega = 1 + \sum_{i=1}^{k_2} \prod_{j=i}^{K_2} \Gamma_{2,j}^{th}$ and

$$\Gamma_{1,i}^{th} = \begin{cases} \tilde{C}_{1,k}^{(th)} + 1 & \text{if } i > k \\ \tilde{C}_{1,k}^{(th)} & \text{if } i = k \end{cases} \tag{17.11}$$

17.3.2.2 Given θ_1, Optimize θ_2

Since RIS 2 only serves users in cluster 2, problem $\mathbf{P}_1$ can be rewritten into $\mathbf{P}_2$ below:

$$\begin{aligned} &\mathbf{P_2}: \min: \frac{\delta^2 \prod_{i=k}^{K_2} \Gamma_{2,i}^{th}}{|h_2, k|^2} \\ &s.t.\ \phi_{2,m} \in \omega, \forall m = 1, \ldots, N_2 \end{aligned} \tag{17.12}$$

Introducing the cascaded channels $R_{2,k}$, we can further rewrite the optimization problem P_2 and Θ_ρ^T for given phase shift θ_1 as:

$$\begin{aligned} &\mathbf{P_3}: \min_{\Theta_2}: \frac{\delta^2 \prod_{i=k}^{K_2} \Gamma_{2,i}^{th}}{|R_{2,k}\Theta_2|^2} \\ &s.t.\ \phi_{2,m} \in \omega, \forall m = 1, \ldots, N_2 \end{aligned} \tag{17.13}$$

Even with the above optimization, problem P_3 is still nonconvex. However, according to (17.13), the candidate phase shifts are located in a circle with uniform intervals, which means between one phase shift to another is a multiplication with a rotation factor. Using this, the problem could be further optimized such that the optimal solution for the lth phase shift could be obtained by multiplying the optimized phase shift matrix of the $l-1$th iteration with a series of rotational matrices. The above process can be written as shown:

$$\Theta_2^{(l)} = \chi_{N_{2-1}}^{(l)} \times \chi_{N_2}^{(l)} \times \cdots \times \chi_1^{(l)} \Theta_2^{(l-1)}, \tag{17.14}$$

where $\chi_m^{(l)} = diag\{1_{1\times(m-1)}, e^{\sigma\varphi_{2,m}}, 1_{1\times(N_2-m}\}$, which indicates that one phase shift of RIS 2 has been optimized. The other elements of RIS 2 can also be optimized in the same way, and leads us to a rewrite of P_3 into P_4 as shown below:

$$\begin{aligned} &\mathbf{P_4}\colon \min_{\varphi_{2,m}} \; P_B\left(\varphi_{2,m}\right) \\ &s.t.\ \phi_{2,m} \in \omega \end{aligned} \tag{17.15}$$

with

$$P_B(\varphi_{2,m}) = \frac{\delta^2 \prod_{i=k}^{K_2} \Gamma_{2,i}^{th}}{g_k\, \varphi_{2,m}}. \tag{17.16}$$

Now that there is only one optimization in the problem, the optimal solution can be obtained using a search method, and is given as [28]:

$$\varphi_{2,m} = \arg\min_{\varphi_{2,m}} \; P_B(\varphi_{2,m}). \tag{17.17}$$

17.3.2.3 Given θ_2, Optimize θ_1

To optimize phase shift matrix for θ_1 when θ_2 is given, we can convert problem P_1 into problem P_5 as follows:

$$\begin{aligned} &\mathbf{P_5}\colon \min\ \Omega \sum_{k=1}^{K_1} \frac{\delta^2 \prod_{i=k}^{K_1} \Gamma_{1,i}^{(th)}}{|h_1, k|^2} + \sum_{k=1}^{K_2} \frac{\delta^1 \prod_{i=k}^{K_2} \Gamma_{2,i}^{(th)}}{|h_2, k|^2} \\ &s.t.\ \phi_{1,m} \in \omega, \forall m = 1, \ldots, N_1 \end{aligned} \tag{17.18}$$

In this problem, only $h_{1,k}$ and $h_{2,k}$ are the only two variables that relate to our optimization. All other variables can be treated as constants. As mentioned in Section 17.3.1, we introduce the channels $R_{1,k}$, allowing $h_{1,k}$ and $h_{2,k}$ to be rewritten as:

$$\begin{aligned} h_{1,k} &= R_{1,k}\theta_1 \\ h_{2,k} &= R_{2,k}\theta_2 + \tilde{Q}_k\theta_1. \end{aligned} \tag{17.19}$$

In a similar fashion, the l_{th} iteration can be optimized with a sequence from χ_1 to χ_{N_1}. The problem P_5 is further optimized into problem P_6 as:

$$\begin{aligned} &\mathbf{P_6}: \min_{\varphi_{1,m}} \ P_C(\varphi_{1,m}) \\ &s.t. \ \varphi_{1,m} \in \omega \end{aligned} \tag{17.20}$$

with

$$P_C = \Omega \sum_{k=1}^{K_1} \frac{\delta^2 \prod_{i=k}^{K_1} \Gamma_{1,i}^{(th)}}{f_k(\varphi_{1,m})} + \sum_{k=1}^{K_2} \frac{\delta^1 \prod_{i=k}^{K_2} \Gamma_{2,i}^{(th)}}{e_k(\varphi_{1,m})} \tag{17.21}$$

Problem P_6 is an optimization with only one variable $\varphi_{1,m}$. Its solution can be found by searching one-dimensionally, and is expressed as [28]:

$$\varphi_{1,m} = \arg\min_{\varphi_{1,m}} P_C(\varphi_{1,m}). \tag{17.22}$$

17.4 Optimization for RIS-Assisted Beamforming

17.4.1 Beamforming Basics

Beamforming is a key technology in wireless communication systems aimed at enhancing signal transmission and reception. At its core, beamforming involves strategically manipulating the phase and amplitude of signals transmitted or received by an array of antennas to create a directed beam of radio frequency (RF) energy. By adjusting the timing and amplitude of signals across different antennas, beamforming can focus the transmitted energy in a specific direction, thereby increasing signal strength and quality at the intended receiver while reducing interference from other directions. This directional focusing improves the overall efficiency and reliability of wireless communication systems, enabling longer-range transmission, improved coverage, and increased data rates.

There are two main types of beamforming: analog and digital beamforming. Analog beamforming involves adjusting the phase and/or amplitude of RF signals at the antenna level using analog components such as phase shifters or attenuators, offering simplicity and energy efficiency but limited flexibility. Digital beamforming processes signals digitally after conversion to the digital domain, enabling dynamic beamforming, adaptive signal processing, and advanced algorithms but requiring more computational resources and power consumption. Hybrid beamforming combines analog and digital beamforming techniques, utilizing analog beamforming at the RF frontend for coarse beam steering and digital beamforming at the baseband for fine-tuning and optimization, striking a balance between flexibility and efficiency for applications requiring both performance and practicality.

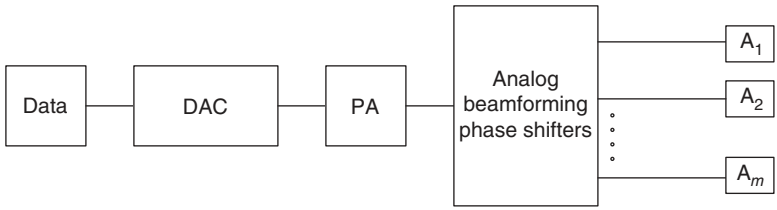

Figure 17.3 A basic analog beamforming model.

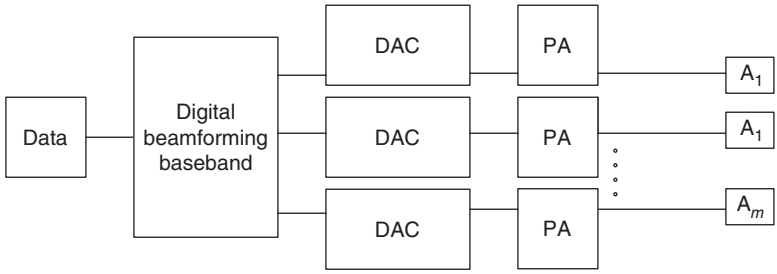

Figure 17.4 A basic digital beamforming model.

Note: In Figures 17.3 and 17.4, PA stands for power amplifier and DAC stands for digital-to-analog converter.

17.4.2 Optimization for RIS-Aided Beamforming Systems

RIS and beamforming can synergistically enhance communication systems by leveraging their respective capabilities. When combined with RIS technology, which consists of a multitude of passive reflecting elements, beamforming gains unprecedented flexibility and adaptability. RIS elements strategically adjust the phase and amplitude of incident RF signals, effectively reshaping the propagation environment. By integrating RIS into the communication system, beamforming algorithms can optimize signal transmission paths, compensate for channel impairments, and mitigate signal blockage and fading effects. This collaboration enables communication systems to achieve significantly improved coverage, higher data rates, enhanced energy efficiency, and better overall performance, making RIS-assisted beamforming a promising solution for next-generation wireless networks. In order to optimize these systems, model enhancements and algorithm enhancements are vital.

17.4.3 Model Enhancements

- **Improve channel models**: Enhancing the accuracy and realism of channel models used in simulations can provide better insights into system behavior and

aid in the development of more robust beamforming and RIS algorithms. A form of improving channel models, 3D spatial models incorporate 3D spatial models for both users and RIS elements, which also capture more realistic propagation effects and enable better optimization of beamforming and RIS configurations.

- **Dynamic environmental models**: Implementing models that account for dynamic environmental factors such as mobility, blockages, and changing interference patterns can enable adaptive beamforming and RIS strategies that respond in real time to changing conditions.
- **Antenna array design**: Optimizing the physical layout and configuration of the antenna array can enhance beamforming performance. This includes considerations such as antenna spacing, array geometry, and the number of antenna elements.
- **RIS deployment strategy**: Improving the deployment strategy of RIS elements can maximize their effectiveness in manipulating signal propagation. This involves determining the optimal placement of RIS elements considering factors such as channel conditions, coverage requirements, and interference mitigation.
- **Hardware upgrades**: Upgrading hardware components such as antennas, RIS elements, and signal processing units can enhance the overall performance and efficiency of the system. This may involve using advanced antenna technologies, higher-resolution RIS elements, and faster signal processing capabilities.
- A table of different types of models: see in Table 17.3

17.4.4 Algorithm Enhancements

- **Beamforming algorithms**: Developing advanced beamforming algorithms that take advantage of RIS capabilities can lead to improved performance. These algorithms may include joint optimization techniques that simultaneously optimize beamforming weights and RIS phase shifts to maximize signal strength, minimize interference, and adapt to changing channel conditions.
- **Channel estimation and prediction**: Enhancing techniques for channel estimation and prediction can improve the accuracy of beamforming and RIS control decisions. This involves developing algorithms that accurately model and predict channel characteristics, enabling proactive adjustments to beamforming and RIS configurations.
- **Dynamic adaptation**: Implementing algorithms that dynamically adapt beamforming and RIS configurations based on real-time feedback and environmental changes can further enhance system efficiency. This includes techniques for adaptive beamforming, learning-based approaches, and cognitive radio principles. Furthermore, this also contain the application and optimization of machine learning techniques in communication systems combining RIS and beamforming, which we will elaborate on in the next part of this section.

Table 17.3 Some RIS-based models.

Model	Specifics	Advantages
Multi-path channel modeling	Incorporates reflections, diffraction, and scattering effects	Provides accurate representations of real-world communication scenarios
Dynamic CSI models	Captures temporal variations in channel conditions, including fading, Doppler shift, and mobility	Enables adaptive beamforming and RIS strategies that respond to changes in the environment over time
Interference modeling	Models co-channel interference, adjacent channel interference, and external interference sources	Aids in designing beamforming and RIS techniques that mitigate interference and improve system performance
Nonlinear effects modeling	Accounts for amplifier distortion, power amplifier nonlinearities, and non-idealities in RIS elements	Improves accuracy of system simulations and enables the design of techniques that mitigate nonlinear distortion effects
Energy harvesting models	Integrates energy harvesting capabilities of RIS elements and user devices into system simulations	Enables optimization of beamforming and RIS configurations to maximize energy harvesting efficiency

17.4.5 The Integration of Deep Reinforcement Learning (DRL) into RIS-Aided Beamforming Systems

Deep reinforcement learning (DRL) offers a powerful approach to optimize the operation of RIS and beamforming in wireless communication systems. By leveraging DRL techniques, the joint optimization of RIS phase shifts and beamforming weights can be achieved in a dynamic and adaptive manner, considering complex interactions between the environment, channel conditions, and system objectives. DRL algorithms, such as deep Q-learning or policy gradient methods, can learn optimal control policies by exploring the vast state-action space of the RIS and beamforming system. These policies can then guide the adjustment of RIS phase shifts and beamforming weights in real time leading to improved communication performance, enhanced coverage, and reduced interference.

Furthermore, DRL can facilitate the design of intelligent algorithms for joint beamforming and RIS control in scenarios where traditional optimization methods may be impractical due to complex and dynamic environments. DRL-based

approaches can adaptively learn to exploit the full potential of RIS technology, such as optimizing signal reflections to mitigate multipath fading, improve signal coverage, and enhance overall system capacity. By continuously learning and adapting to changing conditions, DRL-assisted RIS and beamforming systems can achieve higher efficiency, robustness, and performance, making them well-suited for next-generation wireless networks and emerging communication applications.

In this regard, we will review and condense results of a few studies related to DRL in RIS-aided systems. Then we will infer useful information from these studies as shown in Table 17.4.

17.4.6 Piecewise-DRL

In this section, we want to present how DRL is applied to optimize the RIS-assisted multi-user (MU)–multiple-input, single-output (MISO) communication system.

17.4.6.1 System Architecture

The system in consideration comprises a BS equipped with N_t antennas, M user devices, each equipped with a single antenna, and an $N_{element}$ RIS.

The channel matrix from BS to RIS is denoted as $H_1 \in {}^{N \times N_t}$, which carries the signal that will be manipulated by RIS. H_1 is modeled using Rician fading:

$$H_1 = \sqrt{\frac{\beta}{1+\beta}} H_{LoS} + \sqrt{\frac{1}{1+\beta}} H_{NLoS}. \tag{17.23}$$

The channel matrix from RIS to users is denoted as $H_2 \in {}^{N \times M}$, where the adjustments of RIS shape the effectiveness with which the signals reach users, follows a Rayleigh fading model. Then the signal received by user is denoted as [11]:

$$y = H_2^H \Phi H_1 G_x + \omega, \tag{17.24}$$

where $x \in {}^{M \times 1}$ is the signal transmitted to all users by the BS. $\mathbf{G} \in {}^{N_t \times M}$ is the transmitted precoding matrix, Φ is the RIS phase shift matrix and ω is the additive white Gaussian noise (AWGN). With this the signal received by nth user y_k can be expressed as [11]:

$$y_n = h_{2,n}^H \Phi H_1 g_n l_n + \sum_{x,n=1,\, x \neq n}^{M} h_{2,n}^H \Phi H_1 g_x l_x + \omega_n, \tag{17.25}$$

where g_n is the nth column of G. $h_{2,n}^H \in {}^{N \times 1}$ is the channel vector from the nth user to the RIS. x_k is the signal transmitted to the n_{th} user by the BS. ω_k is the additive white Gaussian noise at the n_{th} user's receiver.

Table 17.4 Some RIS-aided systems relying on machine learning techniques.

Study	Work	Conclusion
[29–35]	On subjects related to deep learning usage in improving multi-carrier systems, RIS, beamforming, MIMO systems and constant false alarm rate (CFAR) detections	The emergence of artificial intelligence (AI) methodologies has led to the gradual integration of deep learning techniques in tackling communication and signal processing challenges
[36]	Enhanced the real-time efficacy of the weighted minimum mean-square error (WMMSE) algorithm by treating it as a nonlinear mapping, employing a deep neural network (DNN) to approximate it	
[37]	A fully connected neural network (NN) was utilized to establish a direct mapping from ideal CSI to the optimal beamforming vector, maximizing transmission rates	
[38]	Proposed a two-stage unsupervised NN for joint beamforming design in MIMO communication setups	Deep learning methods encounter challenges related to their reliance on extensive priori CSI, limiting their applicability to specific systems due to neural networks' weak generalization capabilities
[39, 40]	Utilized DRL frameworks to address mixed integer nonlinear programming (MINLP) problems in communication systems	Demonstration of the effectiveness of DRL in resolving nonconvex optimization challenges
[41, 42]	Investigated the joint optimization of BS beamforming and RIS phase shift matrices using a low-complexity deep Q-network (DQN) approach	
[43]	Employed a DRL-NN framework to concurrently design beam selection and precoding matrices to maximize system sum rates in MIMO communication systems	
[44]	Proposed a soft actor–critic (SAC) algorithm, capable of jointly optimizing the beamforming of multiple BSs and the passive phase shift matrix at the RIS	Able to maximize system sum rates

Then the SINR of n_{th} user can be expressed as:

$$\gamma_n = \frac{|h_{2,n}^H \Phi H_1 g_n|^2}{\sum_{x,n=1,\, x\neq n}^{M} |h_{2,n}^H \Phi H_1 g_x|^2 + \omega_n} \tag{17.26}$$

and the sum rate can be given by:

$$R = \sum_{n=1}^{M} \log(1+\gamma_n) \tag{17.27}$$

17.4.6.2 Optimization Problems

The optimization problem involves jointly optimizing the RIS phase shift matrix ϕ and the transmit precoding matrix G to maximize the system sum rate in an RIS-assisted MU-MISO communication system.

The optimization problem is now formulated as [11]:

$$\begin{aligned} &\mathbf{P_6}\colon \max_{\Phi,G} R = \sum_{n=1}^{M} \log(1+\gamma_k) \\ &\text{s.t. } \Phi(n,n) = e^{j\theta_n}, |e^{j\theta_n}| = 1, \theta_n \in [0,2\pi), \forall n \\ &\text{tr}\{G^H G\} \leq P_{\max}, \end{aligned} \tag{17.28}$$

where $\theta_n \in [0, 2\pi)$ is the phase shift introduced by the nth element of the RIS. $\theta_n \in [0, 2\pi)$ can take any value within $[0, 2\pi)$, ensuring a full 360° phase shift capability.

The optimization aims to jointly determine the RIS phase shifts ϕ and the transmit precoding matrix G to maximize the system sum rate while satisfying the constraints on RIS phase shifts and total transmit power.

17.4.6.3 DDPG for RIS Phase Shift Matrix Optimization

Deep deterministic policy gradient (DDPG) is an actor–critic, model-free algorithm designed specifically to work with continuous action spaces, making it suitable for the complex and continuous nature of beamforming and phase shift adjustments.

The DDPG has two main parts, as shown in Figure 17.5:

- **Actor network** ($\pi(s|\theta^\pi)$): The actor network outputs the action **a** given the state **s** and the parameters θ^π are updated to maximize the expected result.
- **Critic network** $Q(s, a|\theta^Q)$: The critic network estimates the Q-value of the state-action pair. The network parameters θ^Q are updated to minimize the loss between the predicted Q-values and the target Q-values.

The system then maintains a replay buffer of past experiences (s_t, a_t, r_t, s_{t+1}) to break the correlation between consecutive samples and stabilize the training process.

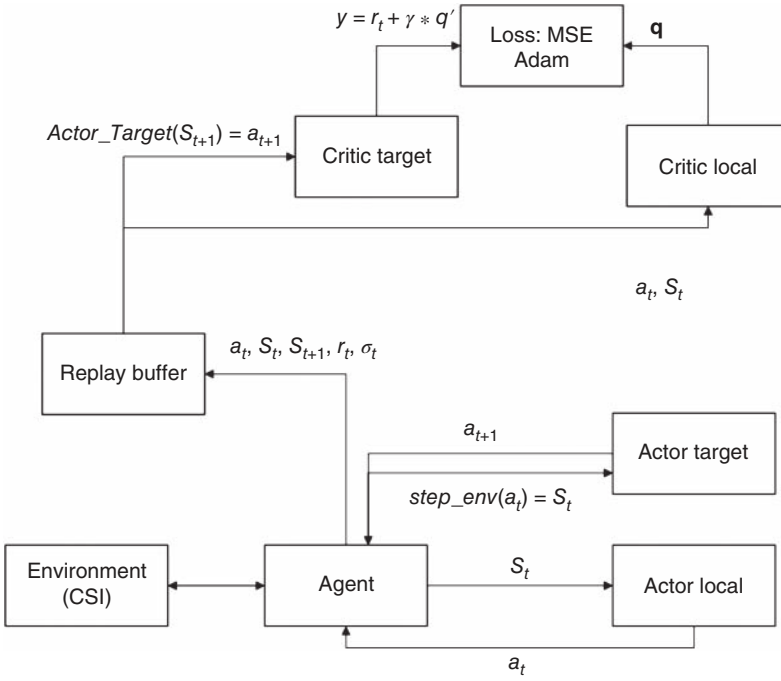

Figure 17.5 DDPG actions discussed.

The training process of the DDPG can be described as follows:

Step 1: Initialization

This step includes initialize the network parameters, replay buffer and the noise process

Step 2: Interaction with the Environment

1) Initialize the environment
2) Execute actions and store experiences
3) Update networks

For more detail information, see [11].

17.4.6.4 NN-WMMSE for Transmit Precoding Matrix Design

A neural network (NN) approximates the Weighted Minimum Mean Square Error (WMMSE) algorithm to reduce computational complexity. The NN-WMMSE algorithm iteratively updates the transmit precoding matrix to maximize the system sum rate so that the DDPG only needs to optimize the Φ.

1) NN design
   - **Network architecture**: Use a NN with several fully connected layers to approximate the WMMSE algorithm's iterative updates.
   - **Normalization**: Include normalization layers to ensure the output precoding matrix G meets the power constraints as in (P_{1c}).
2) Training process
   - Generate training data H_{train}, G_{train} using WMMSE algorithm.
   - Train the network by minimizing the mean square error (MSE) between G_{NN} and G_{WMMSE}.
   - Use backpropagation and gradient descent to optimize the network parameters.

For more detail information, see [11].

17.5 RIS Partitioning

17.5.1 System Topology

The system in consider comprises of a single BS and a RIS array with K reflecting elements, as shown in Figure 17.6. The system uses the Nagasaki-m fading model and adopts a model-based CSI controller. This allows the proposes solution to become the upperbound to practical cases with imperfections and also calculate the most optimal phase shift. To improve performance in a NOMA scheme, RIS is partitioned such that each partition improves the link quality of a distinct user.

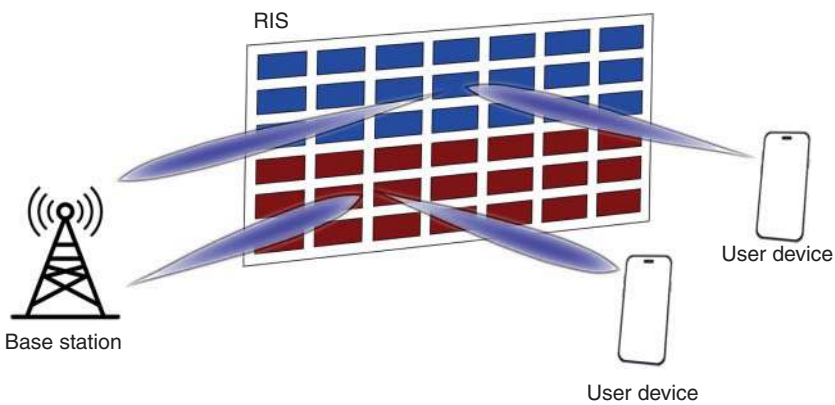

Figure 17.6 A partitioned RIS array.

This approach improves the performance because each user now receives a signal tailored to the specific user's need.

17.5.2 System Architecture

Below, the transmission protocol for a simplistic DL and UL RIS system with two users. It is important, however, to note that it is nontrivial to scale this model to multiple NOMA nodes as the SIC process complexity increases exponentially.

In DL transmission, an approximate representation of the received signal by $U_i, i \in \{1, 2\}$ can be written as [45]:

$$\begin{aligned}\omega = &\left[\alpha_i \sum_{k=1}^{K} g_{i,k} h_k v_i e^{j\eta i,k} + \alpha_r \sum_{k=1}^{K} g_{i,k} h_k v_i e^{j\eta_{r,k}}\right] \\ &\times \sqrt{P_b}\left[\sqrt{B_1} x_1 + \sqrt{B_2} x_2\right] + q_i,\end{aligned} \tag{17.29}$$

where P_b is the transmit power of the BS; K corresponds with the number of RIS element involved; β_1 and β_2 denote the BS power allocation coefficients. The meaning of other parameters in the equation can be found in Table 17.5.

Without loss of generality, we assume that U_1 has a stronger channel. U_1, in this case, will detect and remove U_2 first from the received signal. On the other hand, U_2 also decodes its own message while treating U_1 as an interference, under these circumstances, the generalized SINR for each user can be expressed as [45]:

$$\gamma(\alpha, \beta) = \frac{\beta_i P_b \left|\alpha_i \sum_{k=1}^{K} \Psi_i e^{j\eta_{i,k}} + \alpha_r \sum_{k=1}^{K} \Psi_i e^{j\eta_{r,k}}\right|^2}{\zeta \beta_i P_b \left|\alpha_i \sum_{k=1}^{K} \Psi_i e^{j\eta_{i,k}} + \alpha_r \sum_{k=1}^{K} \Psi_i e^{j\eta_{r,k}}\right|^2 + \delta_i^2}, \tag{17.30}$$

Table 17.5 Parameters in receive signal equation in DL RIS partitioning.

P_b	The transmit power at BS
K_i, K_r	$K_i = [\alpha_i K]$ and $K_r = [\alpha_r K]$, with α_i and α_r being the RIS elements allocation coefficients where $i, r \in 1, 2, i \neq r$ and $\alpha_i + \alpha_r = 1$
K	The number of RIS elements deployed
β_i	The BS power allocation coefficient, $\beta_1 + \beta_2 \leq 1$
$g_{i,k}$	The channel between user i and element of the RIS portion k_{th}
h_k	The channel between RIS portion's k_{th} element and the BS
$d_{i,k}$	The distances of UE_i-RIS RIS–BS links
q_i	The additive white Gaussian noise (AWGN) with variance of δ_i^2
$\eta_{l,k}$	The RIS's phase adjusting coefficient for NOMA user $l, \forall l \in i, r$

where $\alpha = [\alpha_1, \alpha_2]$, $\beta = [\beta_1, \beta_2]$, $\Psi_i = g_{i,k} h_k \psi_i$ and ζ is a decoding variable where

$$\zeta = \begin{cases} 1 & \text{if } i = 2 \\ 0 & \text{if } i = 1 \end{cases}, \tag{17.31}$$

which controls cancellation and decode of interference as explained above.

17.5.3 Optimization Problem

17.5.3.1 Max–Min Fair Regime

The max–min fairness optimization approach focuses on maximizing the lowest data speed for all users across UL and DL. The problem is set up as follow:

$$\begin{aligned} &\max_{\alpha} \left(\min_{i \in 1,2} \gamma(\alpha), \gamma(\alpha) \right) \\ &s.t.\ \alpha_1 + \alpha_2 \leq 1 \end{aligned} \tag{17.32}$$

In the max–min fair regime, the power of the worst-performing transmission should be pushed to its upper limit. The result is a common max–min fair rate for all users in both directions. It is also true that to achieve max–min fairness, the entire RIS has to be utilized ($\alpha_1 + \alpha_2 = 1$), thus reducing the number of RIS portioning variables to one. With this, the problem in (17.32) can be formulated as below:

$$\begin{aligned} &\mathbf{P_5}: \max_{\alpha, R_{th}} R_{th} \\ &C_3^1: \ s.t.\ \gamma(\alpha) \geq \gamma_{th}, i \in 1, 2 \\ &C_3^2: \ \alpha \in [0, 1], \end{aligned} \tag{17.33}$$

where $\gamma_{th} = 2^{R_{th}/B} - 1$. Solving C_3^1 and C_3^2 reveals the optimal RIS portions and max–min fair rates to be $\gamma_1 = \gamma_2 = R_{th}$. The optimal value of α could be obtained when the lower and upper bounds meet each other. However, reaching min–max fairness is not achievable without power control, as the upper bound curve would observe a sudden drop over the frequency spectrum. To alleviate this, power control can be introduced at the BS, and the problem restated as follow:

$$\begin{aligned} &\mathbf{P_6}: \max_{\alpha, \beta, R_{th}} R_{th} \\ &C_4^1: \ s.t.\ \gamma(\alpha, \beta) \geq \gamma_{th}, i \in 1, 2 \\ &C_4^2: \ \alpha \in [0, 1], \beta \in [0, 1] \end{aligned} \tag{17.34}$$

Here, one can have a single power control variable since BS reachs the highest max–min rate possible by using its allowed maximum transmit power. Solving the power control and RIS partitioning problem, we obtain the optimal RIS portion

that yields the UL max–min fair rate:

$$\alpha = -\frac{b_m}{4a_m} + \frac{\pm_t \bar{E}_2 \pm_s \sqrt{-\left[3\bar{A}_1 + 2y_0 \pm_t \frac{2\bar{B}_1}{E_2}\right]}}{2}. \tag{17.35}$$

One can also obtain from Eq. (17.35) the power allocation factor that gives equal DL and UL max–min fair rate [45]:

$$\beta = \frac{-\tilde{B}_2 \pm \sqrt{\tilde{B}_2^2 - 4\tilde{A}_2\tilde{C}_2}}{2\tilde{A}_2}. \tag{17.36}$$

17.6 Simulation Results of Multiple RISs Systems

In this section, we will simulate the performance of the RIS device considering Rayleigh fading with non-line-of-sight communication, as shown in Figure 17.7. In reference to [46], the received signal at the destination has been obtained as:

$$y_D = \sqrt{P}\left(\mathbf{h}_{SI_1}^{\mathbb{R}} T \boldsymbol{\Theta} \mathbf{h}_{I_1 D} + \mathbf{h}_{SI_2}^{\mathbb{R}} T \boldsymbol{\Phi} \mathbf{h}_{I_2 D}\right) x + n_D \tag{17.37}$$

where P is the total transmit power at the source, $\mathbf{h}_{SI_1} \in \mathbb{C}^{N_1}$ is the channel between source and RIS I_1, $\mathbf{h}_{I_1 D} \in \mathbb{C}^{N_1}$ is the channel between RIS I_1 and

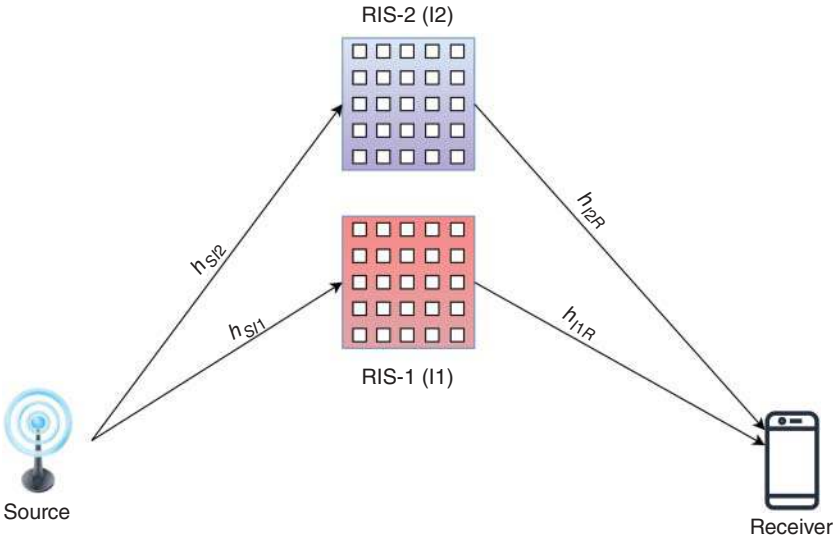

Figure 17.7 System model of two RISs system.

destination, $\mathbf{h}_{SI_2} \in \mathbb{C}^{N_2 \times 1}$ is the channel between source and RIS I_2, $\mathbf{h}_{I_2D} \in \mathbb{C}^{N_2}$ is the channel between intelligent reflecting surface (IRS) I_2 and destination. Note that the CSIs assumed to be known. Moreover, x is the transmitted signal by source, n_D is the circularly symmetric AWGN with zero mean and variance σ_n^2, i.e., $n_D \sim \mathcal{CN}\left(0, \sigma_n^2\right)$. The single antenna source is placed at the origin $(x_s, y_s) = (0, 0)$, the destination at $(x_D, y_D) = (100, 0)$, and the two RISs at $(x_{I_1}, y_{I_1}) = (50, 25)$, $(x_{I_2}, y_{I_2}) = (50, 50)$.

The achievable rate of the device is determined, by assuming a large number of reflecting elements N_1 and N_2 [46], as,

$$\begin{aligned}
\mathbb{E}\left[\tilde{\gamma}_D\right] &= \mathbb{E}\left[\gamma\left(N_1\sqrt{\tilde{\Gamma}_{SI_1D}} + N_2\sqrt{\tilde{\Gamma}_{SI_2D}}\right)^2\right] \\
&= \gamma\left(N_1^2\mathbb{E}\left[\tilde{\Gamma}_{SI_1D}\right] + 2N_1N_2\mathbb{E}\left[\sqrt{\tilde{\Gamma}_{SI_1D}}\sqrt{\tilde{\Gamma}_{SI_2D}}\right]\right. \\
&\quad \left. + N_2^2\mathbb{E}\left[\tilde{\Gamma}_{SI_2D}\right]\right) \qquad (17.38) \\
&\leq \gamma\left(\frac{1}{16}d_{SI_1}^{-\alpha}d_{I_1D}^{-\alpha}\eta^2 N_1\left(16 + (N_1 - 1)\pi^2\right)\right. \\
&\quad + \frac{1}{8}d_{SI_1}^{-\alpha/2}d_{I_1D}^{-\alpha/2}d_{SI_2}^{-\alpha/2}d_{I_2D}^{-\alpha/2} \\
&\quad \eta\zeta\sqrt{\left(16 + (N_1 - 1)\pi^2\right)\left(16 + (N_2 - 1)\pi^2\right)} \\
&\quad \left. + \frac{1}{16}d_{SI_2}^{-\alpha}d_{I_2D}^{-\alpha}\zeta^2 N_2\left(16 + (N_2 - 1)\pi^2\right)\right), \qquad (17.39)
\end{aligned}$$

where $\tilde{\mathbf{h}}_l = \tilde{\mathbf{g}}_l d_l^{-\alpha/2}, l \in SI_1, I_1D, SI_2, I_2D$, where $\tilde{\mathbf{g}}_l$ is the complex-Gaussian small-scale fading channels having zero mean and unit variance, α is the path-loss exponent, and d is the distance between two nodes, either source to RIS or RIS to destination, (η, ζ) are reflection coefficients.

In Figure 17.8, the simulation results demonstrate the relationship between achievable rate and threshold signal-to-noise ratio (SNR). It is evident from the simulation that as the number of RIS elements increases, the performance of the system improves proportionally. This observation indicates that the signals transmitted from multiple RIS devices combine constructively at the destination, resulting in a higher SNR. The constructive combination of the signals leads to an improved achievable rate, thereby enhancing the overall system performance. The simulation results validate the importance of increasing the number of RIS elements in optimizing the wireless communication system.

Figure 17.9 further emphasizes the significance of the number of RIS elements, denoted by N, by exploring its impact on the system performance at different threshold SNRs. The graph reveals that with an increase in N, the system performance experiences a rapid improvement at each threshold SNR. This observation

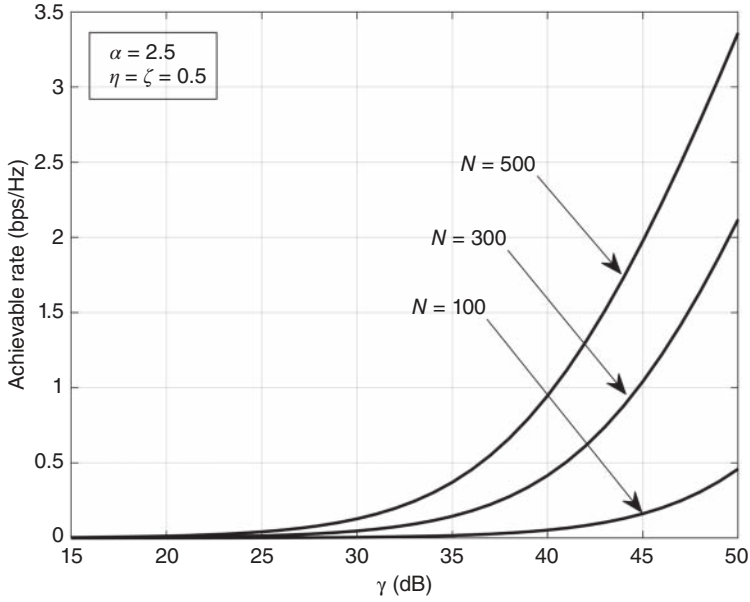

Figure 17.8 Impact on the performance of overall achievable rates by varying the number of RIS over Rayleigh fading channels.

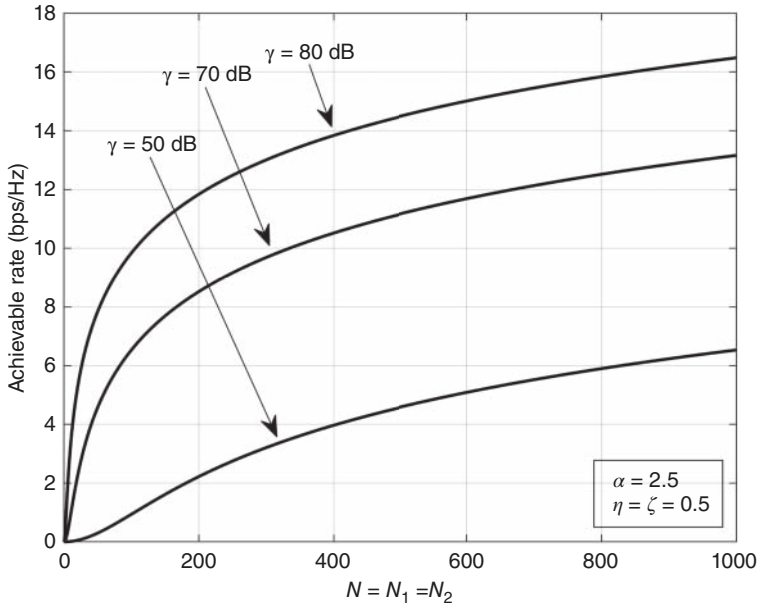

Figure 17.9 Achievable rates versus a different number of reflecting elements under Rayleigh fading channels.

highlights the pivotal role of RIS elements in enhancing the overall system performance, as an increase in their number leads to significant gains in terms of achievable rates and SNR. The results provide quantitative evidence of the positive correlation between the number of RIS elements and system performance, emphasizing the need for a higher number of RIS elements to achieve substantial performance improvements.

These simulation results offer valuable insights into the impact of RIS elements on system performance. The constructive combination of signals transmitted from multiple RIS devices contributes to better SNR and higher achievable rates. Moreover, the findings emphasize that increasing the number of RIS elements yields substantial performance gains. This information is crucial for designing and optimizing RIS-assisted wireless communication systems. By carefully considering the number of RIS elements and their deployment, system designers can effectively exploit the potential benefits of RIS technology and maximize the performance of the wireless communication system.

17.7 Discussion

In this section, we summarize what is discussed in the above sections and discuss the key takeaways from this chapter and limitations that are present.

- The expanded equations above are helpful when it comes to understanding the details of different optimization algorithms to a variety of RIS systems.
- While the equations highlighted focuses on power optimization of RIS-based systems, some of the other cited papers can inform about other types of optimization problems in RIS.
- The chapter can help in building foundational knowledge to work up into higher levels, as most of the chapter is basic knowledge when it comes to energy efficiency and power optimization in RIS systems.

17.8 Conclusion

In this chapter, we have explored the optimization of UL transmit power in wireless communication systems leveraging multiple RIS arrays. Through comprehensive simulations and analysis, we have delved into the intricate interplay between the number of RIS elements and system performance, with a keen focus on achievable rates and SNR. Our findings underscore the pivotal role of RIS technology in enhancing wireless communication systems, revealing a proportional improvement in system performance with an increase in the number of RIS elements.

This enhancement stems from the constructive combination of signals transmitted from multiple RIS devices, leading to heightened SNR and improved achievable rates.

Furthermore, our research underscores the significance of optimizing the deployment of RIS arrays by carefully considering the number of elements. By doing so, system designers can effectively harness the full potential of RIS technology to achieve substantial performance gains. This study provides quantitative evidence of the positive correlation between the number of RIS elements and system performance, emphasizing the necessity of a higher number of RIS elements to fully realize the benefits of RIS-assisted wireless communication systems. These insights are instrumental in guiding future research endeavors and shaping the design and optimization of RIS-based communication systems, ultimately advancing the efficiency and robustness of wireless networks.

References

1 Parasuraman, S., Sam, A.T., Yee, S.W.K. et al. (2017). Smartphone usage and increased risk of mobile phone addiction: a concurrent study. *International Journal of Pharmaceutical Investigation* 7 (3): 125–131. https://doi.org/10.4103/jphi.JPHI_56_17.

2 Pahlavan, K. and Krishnamurthy, P. (2021). Evolution and impact of Wi-Fi technology and applications: a historical perspective. *International Journal of Wireless Information Networks* 28 (6): 1–17. https://doi.org/10.1007/s10776-020-00501-8.

3 Dogra, A., Jha, R.K., and Jain, S. (2020). A survey on beyond 5G network with the advent of 6G: architecture and emerging technologies. *IEEE Access* 9: 67512–67547.

4 Imoize, A.L., Adedeji, O., Tandiya, N., and Shetty, S. (2021). 6G enabled smart Infrastructure for sustainable society: opportunities, challenges, and research roadmap. *Sensors* 21 (5): 1709. https://doi.org/10.3390/s21051709.

5 Joung, J., Ho, C.K., Adachi, K., and Sun, S. (2014). A survey on power-amplifier-centric techniques for spectrum-and energy-efficient wireless communications. *IEEE Communications Surveys & Tutorials* 17 (1): 315–333.

6 Osseiran, A., Braun, V., Hidekazu, T. et al. (2013). The foundation of the mobile and wireless communications system for 2020 and beyond: challenges, enablers and technology solutions. *2013 IEEE 77th Vehicular Technology Conference (VTC Spring)*, 1–5. IEEE.

7 Hemanth, A., Umamaheswari, K., Pogaku, A.C. et al. (2020). Outage performance analysis of reconfigurable intelligent surfaces-aided NOMA under

presence of hardware impairment. *IEEE Access* 8: 212156–212165. https://doi.org/10.1109/ACCESS.2020.3039966.

8 Imoize, A.L., Obakhena, H.I., Anyasi, F.I. et al. (2022). Reconfigurable intelligent surfaces enabling 6G wireless communication systems: use cases and technical considerations. *2022 5th Information Technology for Education and Development (ITED)*, 1–7. https://doi.org/10.1109/ITED56637.2022.10051543.

9 Pogaku, A.C., Do, D.T., Lee, B.M., and Nguyen, N.D. (2022). UAV-assisted RIS for future wireless communications: a survey on optimization and performance analysis. *IEEE Access* 10: 16320–16336. https://doi.org/10.1109/ACCESS.2022.3149054.

10 Pogaku, A.C., Nguyen, N.D., Le, A.T., and Do, D.T. (2022). Enabling cognitive radio in NOMA-assisted reconfigurable intelligent surfaces: outage performance analysis. In: *Advances in Communication, Devices and Networking: Proceedings of ICCDN 2021* (ed. B. Sharma, D.T. Do, S.N. Sur, and C.M. Liu), 569–581. Singapore: Springer Nature Singapore.

11 Fang, F., Wu, B., Fu, S. et al. (2023). Energy-efficient design of STAR-RIS aided MIMO-NOMA networks. *IEEE Transactions on Communications* 71 (1): 498–511.

12 Ma, H. and Wang, H. (2021). Power minimization transmission design for IRS-assisted uplink NOMA systems. *2021 IEEE 94th Vehicular Technology Conference (VTC2021-Fall)*, 1–4.

13 Wang, P., Wang, H., Ma, H. et al. (2023). Sum rate maximization for STAR-RIS aided NOMA system with two-way communication. *IEEE Communications Letters* 27 (10): 2857–2861.

14 Tasci, R.A., Kilinc, F., Basar, E., and Alexandropoulos, G.C. (2022). A new RIS architecture with a single power amplifier: energy efficiency and error performance analysis. *IEEE Access* 10: 44804–44815.

15 Cheng, X., Lin, Y., Shi, W. et al. (2021). Joint optimization for RIS-assisted wireless communications: from physical and electromagnetic perspectives. *IEEE Transactions on Communications* 70 (1): 606–620.

16 Jiang, F., Abrardo, A., Keykhoshravi, K. et al. (2022). Optimization of RIS-aided integrated localization and communication. *arXiv preprint arXiv:2209.02828*.

17 Peng, Z., Li, T., Pan, C. et al. (2021). Analysis and optimization for RIS-aided multi-pair communications relying on statistical CSI. *IEEE Transactions on Vehicular Technology* 70 (4): 3897–3901.

18 Zhi, K., Pan, C., Zhou, G. et al. (2021). Analysis and optimization of RIS-aided massive MIMO systems with statistical CSI. *2021 IEEE/CIC International Conference on Communications in China (ICCC Workshops)*, 153–158. IEEE.

19 Zhi, K., Pan, C., Zhou, G. et al. (2022). Analysis and optimization of RIS-aided massive MIMO with ZF detectors and imperfect CSI. *ICC 2022-IEEE International Conference on Communications*, 219–224. IEEE.

20 Cheng, Y., Peng, W., Huang, C. et al. (2022). RIS-aided wireless communications: extra degrees of freedom via rotation and location optimization. *IEEE Transactions on Wireless Communications* 21 (8): 6656–6671.

21 Zeng, S., Zhang, H., Di, B. et al. (2020). Reconfigurable intelligent surface (RIS) assisted wireless coverage extension: RIS orientation and location optimization. *IEEE Communications Letters* 25 (1): 269–273.

22 Chen, Z., Tang, J., Du, X. et al. (2022). Joint location and channel error optimization for beamforming design for multi-RIS assisted MIMO system. *2022 IEEE 12th Sensor Array and Multichannel Signal Processing Workshop (SAM)*, 181–185. IEEE.

23 Wang, D., Zhao, Y., Lou, Y. et al. (2022). Secure NOMA based RIS-UAV networks: passive beamforming and location optimization. *GLOBECOM 2022 - 2022 IEEE Global Communications Conference*, 3168–3173. IEEE.

24 Michailidis, E.T., Miridakis, N.I., Michalas, A. et al. (2021). Energy optimization in dual-RIS UAV-aided MEC-enabled internet of vehicles. *Sensors* 21 (13): 4392.

25 Shi, E., Zhang, J., Chen, S. et al. (2022). Wireless energy transfer in RIS-aided cell-free massive MIMO systems: opportunities and challenges. *IEEE Communications Magazine* 60 (3): 26–32.

26 Gao, Z., Xu, Y., Wang, Q. et al. (2021). Outage-constrained energy efficiency maximization for RIS-assisted WPCNs. *IEEE Communications Letters* 25 (10): 3370–3374.

27 Yao, Y., Lv, K., Huang, S. et al. (2023). UAV trajectory and energy efficiency optimization in RIS-assisted multi-user air-to-ground communications networks. *Drones* 7 (4): 272. https://doi.org/10.3390/drones7040272.

28 Makin, M., Arzykulov, S., Celik, A. et al. (2023). Optimal RIS partitioning and power control for bidirectional NOMA networks. *IEEE Transactions on Wireless Communications* 23 (4): 3175–3189. https://doi.org/10.1109/TWC.2023.3306048.

29 Choi, J. (2021). Deep reinforcement learning based reconfigurable intelligent surface for FDD massive MIMO systems. *IEEE Transactions on Wireless Communications* 20 (4): 2444–2455.

30 Imran, M.A., Al-Tahir, A., Bakhshi, M.R., and Shakir, M.Z. (2021). Deep reinforcement learning based beamforming for reconfigurable intelligent surfaces in FDD systems. *2021 17th International Wireless Communications & Mobile Computing Conference (IWCMC)*, 797–802.

31 Zhao, Z., Peng, M., Chen, M. et al. (2021). Deep reinforcement learning for reconfigurable intelligent surface aided wireless communications. *IEEE Internet of Things Journal* 8 (7): 5120–5131.

32 Yang, Z. and Zhang, Y. (2021). Beamforming optimization for RIS-aided SWIPT in cell-free MIMO networks. *China Communications* 18 (9): 175–191.

33 Jiang, R., Fei, Z., Cao, S. et al. (2022). Deep learning-aided signal detection for two-stage index modulated universal filtered multi-carrier systems. *IEEE Transactions on Cognitive Communications and Networking* 8 (1): 136–154.

34 Zhao, J., Jiang, R., Wang, X., and Gao, H. (2019). Robust CFAR detection for multiple targets in K-distributed sea clutter based on machine learning. *Symmetry* 11 (12): 1482.

35 Jiang, R., Wang, X., Cao, S. et al. (2019). Deep neural networks for channel estimation in underwater acoustic OFDM systems. *IEEE Access* 7: 23579–23594.

36 Sun, H., Chen, X., Shi, Q. et al. (2018). Learning to optimize: training deep neural networks for interference management. *IEEE Transactions on Signal Processing* 66 (20): 5438–5453.

37 Zhang, S., Zhang, S., Gao, F. et al. (2021). Deep learning optimized sparse antenna activation for reconfigurable intelligent surface assisted communication. *IEEE Transactions on Communications* 69 (10): 6691–6705.

38 Song, H., Zhang, M., Gao, J., and Zhong, C. (2021). Unsupervised learning-based joint active and passive beamforming design for reconfigurable intelligent surfaces aided wireless networks. *IEEE Communications Letters* 25 (3): 892–896.

39 Sutton, R.S. and Barto, A.G. (2018). *Reinforcement Learning: An Introduction*. MIT Press.

40 Luong, N.C., Hoang, D.T., Gong, S. et al. (2019). Applications of deep reinforcement learning in communications and networking: a survey. *IEEE Communications Surveys & Tutorials* 21 (4): 3133–3174.

41 Zhou, Y., Zhou, F., Wu, Y. et al. (2020). Subcarrier assignment schemes based on Q-learning in wideband cognitive radio networks. *IEEE Transactions on Vehicular Technology* 69 (1): 1168–1172.

42 Ji, Z. and Qin, Z. (2020). Reconfigurable intelligent surface enhanced device-to-device communications. *GLOBECOM 2020 - 2020 IEEE Global Communications Conference*, 1–6. IEEE.

43 Hu, Q., Liu, Y., Cai, Y. et al. (2021). Joint deep reinforcement learning and unfolding: beam selection and precoding for mmWave multiuser MIMO with lens arrays. *IEEE Journal on Selected Areas in Communications* 39 (8): 2289–2304.

44 Zhu, Y., Li, M., Liu, Y. et al. (2022). DRL-based joint beamforming and BS-RIS-UE association design for RIS-assisted mmWave networks. *2022 IEEE Wireless Communications and Networking Conference (WCNC)*, 345–350. IEEE.

45 Ma, H., Wang, H., Zhao, H., and Fu, S. (2023). Power minimization for double cooperative-RIS-assisted uplink NOMA system. *IEEE Wireless Communications Letters* 12 (11): 1946–1950. https://doi.org/10.1109/LWC.2023.3301172.

46 Pogaku, A.C., Le, A.T., and Nguyen, N.D. (2023). Ergodic performance analysis of intelligent reflecting surface network with phase errors. *ICT Express* 9 (4): 595–600.

Index

Reconfigurable Intelligent Surfaces for 6G and Beyond Wireless Networks, First Edition.
Edited by Agbotiname Lucky Imoize, Vinoth Babu Kumaravelu, and Dinh-Thuan Do.

WILEY END USER LICENSE AGREEMENT

Go to www.wiley.com/go/eula to access Wiley’s ebook EULA.